Periglacial Landscape Evolution at Lower Mid-Latitudes on Mars: The Thaumasia Highlands

Angelo Pio Rossi
International Space Science Institute, CH-3012, Bern, Switzerland
Stephan van Gasselt
Institut für Geologische Wissenschaften, Freie Universität Berlin, Germany
Monica Pondrelli
IRSPS, Universita' d'Annunzio, Pescara, Italy
Tanja Zegers
RSSD of ESA. ESTEC, NL 2200 AG, Noordwijk, The Netherlands
Ernst Hauber
DLR, Institute for Planetary Research, Berlin, Germany
Gerhard Neukum
Institut für Geologische Wissenschaften, Freie Universität Berlin, Germany

Abstract

We report on the detection of periglacial landforms at high mid-latitudes in the Thaumasia Highland (Mars) that are characterized by lobate to tongue-shaped flow and creep morphologies and which have a close resemblance to terrestrial landforms found in mountainous permafrost regions. It appears that pristine ice-related landforms are best described by small-scale protalus lobes, with few to no distinct impact craters at both HRSC and MOC NA scale. Exposure to solar insulation seems to control the distribution of rock glacier-like landforms, with a preferred occurrence on south-facing slopes. Older, less pristine lineated crater fills, which are commonly considered to represent landforms related to the viscous deformation of ice and debris, show, however, a less systematic distribution of flow directions. Both relatively young landforms are likely related to climatic variations on Mars orbital variations in its recent past and form the youngest witnesses of high obliquity.

Keywords: climate change; Mars; mid-latitudes; periglacial landforms; protalus lobes.

Introduction

Several landforms on Mars have been suggested to be related to the presence of ground ice (Mangold 2003, Squyres 1978, Squyres & Carr 1986), including lobate debris aprons, concentric and lineated crater fill and fretted terrain (Colaprete & Jakosky 1998, Lucchitta 1984, Squyres 1978). These landforms are commonly related to the creep of ice and debris as documented from various latitudes and in a varying geologic context (Crown et al. 2003, Head et al. 2005, 2006, Mangold 2001, Mangold & Allemand 2001, Squyres 1979, van Gasselt et al. 2007).

Large-scale features at the Martian fretted terrain and so-called lobate debris aprons have been primary candidates for periglacial landforms, but the availability of high resolution image and topography data over increasingly large portion of the Martian surface has allowed discovery and exploration of smaller features, comparable in size to terrestrial rock glacier systems. Recent landforms interpreted as glacial or periglacial have been described extensively also at tropical to equatorial latitudes on Mars (Head et al. 2006, Rossi et al. 2000, van Gasselt et al. 2007, 2008) during the last decade.

Also, the presence of ground ice has been indirectly assessed on Mars with non-image data by instruments such as the Neutron Spectrometer onboard 2001 Mars Odyssey spacecraft (Feldman et al. 2004): the large-scale inventory of potential ice-rich deposits in Martian soil indicates regional high abundances of thick bodies of ground ice, especially at mid to high northern latitudes.

Data and Methods

In the present work we used image and topographic data from different sources: MGS (Mars Global Surveyor) MOLA (Mars Orbiter Laser Altimeter) topographic data, MEX (Mars Express) HRSC (High Resolution Stereo Camera), and 2001 Mars Odyssey THEMIS (Thermal Emission Imaging System). In selected areas, we also used THEMIS visible (VIS) and MGS MOC (Mars Orbiter Camera) narrow angle (NA) images. HRSC-derived digital elevation models have been used as well (Gwinner et al. 2005). HRSC data, with their high spatial resolution and large swath, are well complemented by very high resolution MOC NA data. MOLA topography has been used mostly in the form of single profiles (Precision Experiment Data Records, PEDR), in order to avoid any resampling effect introduced during data gridding, because of the small scale (few km) of several of the studied landforms; gridded MOLA Mission Experiment Gridded Data Records (MEGDR) data were used in areas where profiles could not be extracted.

The nomenclature used here is descriptive, trying to avoid genetic terms or implications whenever possible. The

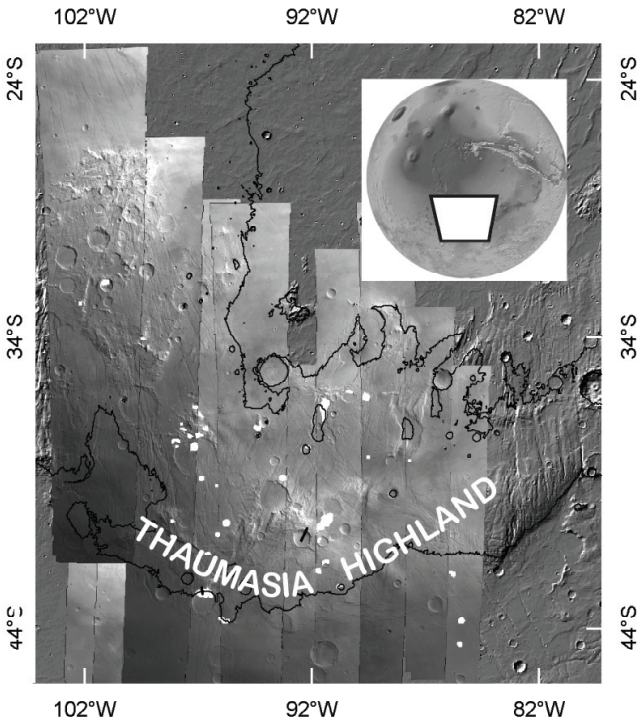

Figure 1. Location of possible periglacial landforms outlined in white, on top of HRSC Nadir Mosaic (Nadir channels from orbits 266, 279, 292, 344, 357, 380, 420, 431, 442, 453, 486, 497, 508, 530, 563) of Thaumasia Highland. The 4000 m altitude contour line is indicated in black; the background is a MOLA topography-based shaded relief.

terminology is similar to the one used by Whalley & Azizi (2003).

Thaumasia Geology and Geomorphology

The Thaumasia region on Mars located in the eastern hemisphere near 35° latitude is well known for its primarily volcanic and complex tectonic history (Fig. 1).

The Thaumasia region on Mars has a rich and complex geological history (Dohm et al. 2001, Dohm & Tanaka 1999). It comprises a tectonic plateau, characterized by high plains and dissected by various graben systems (Grott et al. 2007). In addition several smaller-scaled compressional tectonic features, such as wrinkle ridges (Dohm & Tanaka 1999) indicative of the volcano-tectonic history are observed frequently.

Among younger water-related surface features (Ansan & Mangold 2006), there is also an abundance of geomorphic evidence for cold-climate resurfacing processes such as a variety of periglacial landforms or glacial-like flows. Low latitude glacial or glacial-like morphologies have been described mostly from the northern hemisphere (Head et al. 2006), and recently also from the southern one (Dickson et al. 2006, Rossi et al. 2006),

The Thaumasia region was one of the areas on Mars where work on periglacial and glacial landforms is relatively sparse (Dickson et al. 2006, Rossi et al. 2006) which is predominantly caused by a substantial lack of high resolution data coverage (e.g., MOC) at the time when large-scale mapping efforts were started (Dohm et al. 2001).

Description of Study Area and Landforms

The study area spans in latitude from 25°S to 45°S. The altitude of identified ice-related landforms is more constrained, being in general higher than 4000 m above Mars MOLA datum with elevations as high as 5000 m. (Fig. 1).

Three main kinds of possible ice-assisted creep-related landforms have been found in Thaumasia Highland: lineated crater (and valley) fills, debris aprons, and protalus lobes.

Lineated crater fills

This group of features appears to be very widespread in the study area and was described initially from the northern dichotomy boundary and the southern-hemispheric impact basins (Squyres 1978, 1979).

There is a high abundance of impact craters larger than a few kilometers in diameter that show this peculiar surface texture in Thaumasia Highland.

Lineated crater and valley fills are usually associated to each other and form curvilinear ridges and saddles, usually arranged with slightly concentric to transversal geometries (Figs. 2A, 2C). Longitudinal ridges, similar to the ones present in fretted terrains (Squyres 1978) are usually not observed. Lineations appear as ridges and furrows arranged transversally with respect to the inferred flow direction. The surface texture of lineated fills is relatively rough. Circular to sub-circular features, possibly being degraded small impact craters (Fig. 2C) are visible within the infill. The lack of high-resolution data (e.g., in Fig. 2C) does not allow generalizations over the complete population of lineated craters. Circular to irregular depressions with unclear impact origin are also abundant in crater fills: they show a certain resemblance with thermokarst features (Costard & Kargel 1995).

Lineated and/or curvilinear crater fills on Mars have been interpreted as related to ice flow (Squyres & Carr 1986), or were alternatively attributed to eolian erosion (Zimbelman et al. 1989).

Most lineated fills are showing general slopes consistently with flow directions derived from morphology (Figs. 2A, 2B). The direction of flows in these crater fills shows a correlation to regional slope orientation but little to no connection to local exposure, unlike protalus lobes features as described below.

The actual thickness of these fills in not well constrained, since they appear completely contained within crater rims and no cross-section cuts are visible in the study area.

Debris aprons

Certain craters in the Thaumasia Highland are showing features with a strong resemblance with debris aprons (Colaprete & Jakosky 1998, Squyres 1978, Squyres & Carr 1986) (Fig. 3B). They are isolated or appear superimposed on lineated crater fills. These landforms often show concave upward profiles

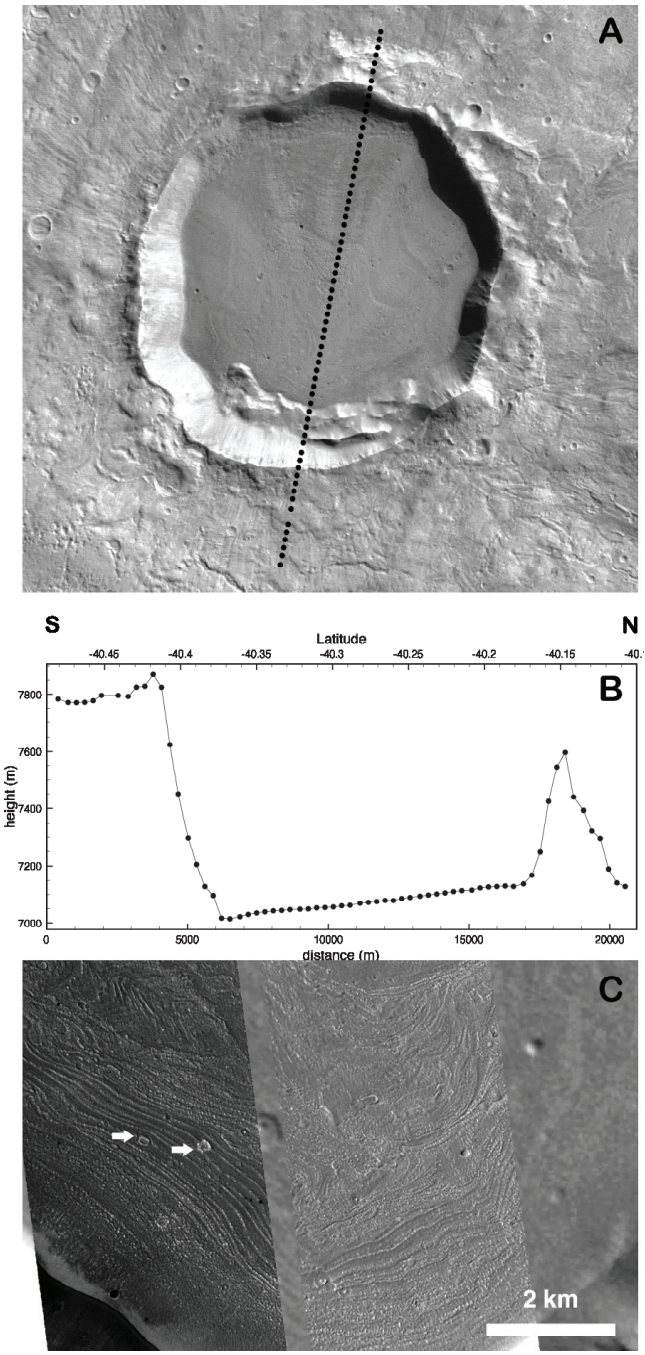

Figure 2. A) HRSC nadir from orbit 442 (north is up), the footprints of MOLA PEDR shots are indicated by black dots; the scene is about 20 km wide. The flow-like lineated crater fill is mainly emanating from the northern part of the crater. B) Portion of MOLA profile from orbit 19873: the lineated crater fill has an almost constant slope of about 0.5° southwards. C) Detail of the morphology of a lineated crater fills at MOC scale (HRSC orbit 508, MOC NA E1200147 and E0501814). Arrows indicate sample deformed (compressed) crater-like features embedded in the crater fill.

on MOLA and HRSC DTM (Gwinner et al. 2005) contrasting to large-scale features observed at the dichotomy boundary which usually are convex upward (Chuang & Crown 2005, Mangold & Allemand 2001, Squyres 1978, van Gasselt et al. 2008). They are characterized by smooth to moderately rough

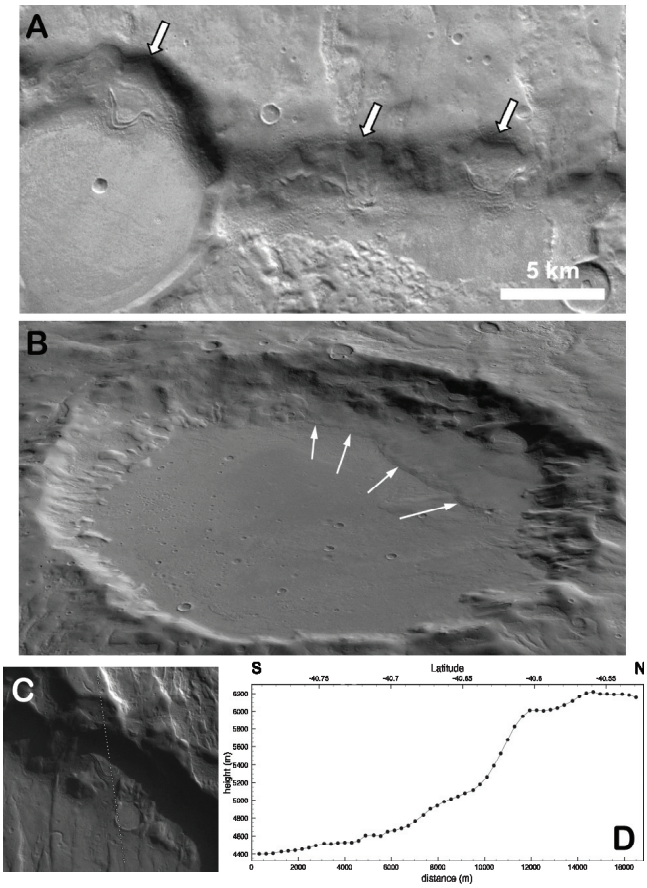

Figure 3. A) Example of well-developed protalus lobes, indicated by arrows (HRSC nadir band from orbit 292, north is up). These lobate forms are developed on crater floors or fills and linear slopes. B) perspective view of HRSC nadir from orbit 453 draped on HRSC stereo-derived DTM (Gwinner et al. 2005). Arrows indicate the edge of a concave debris apron. Small, apparently younger protalus lobes are located on the highest part of the rim, well above the debris apron. C) HRSC nadir from orbit 508, the footprints of MOLA profile shown in 3-D are indicated; the protalus lobe is facing southward and it's largely in shadow; the image is about 25 km wide; the lobate feature is about 5 km long; north is up D) Portion of MOLA PEDR profile from orbit 13002: The protalus lobe in 3C shows a convex upward profile, unlike some debris aprons such as the one in 3B. The inferred thickness for this particular lobe is about 200 m.

surface texture. Both in term of scale, apparent chronology, and degradation level, they appear to be transitional between larger, older lineated crater fills and smaller protalus lobes. They tend to emanate from south-facing slopes, but with a less clear correlation to the general direction of exposure when compared to protalus lobes.

Protalus lobes

Protalus lobes (Whalley & Azizi 2003) are the most common possible periglacial landform which could be found in the study area. They are characterized by multiple lobate concentric ridges. Their width usually exceeds their length (Figs. 3A, 3C), thus forming broad features along footslopes. Their total length is in most cases limited to few kilometers and few of them are just 2 to 3 km long (Fig. 3A).

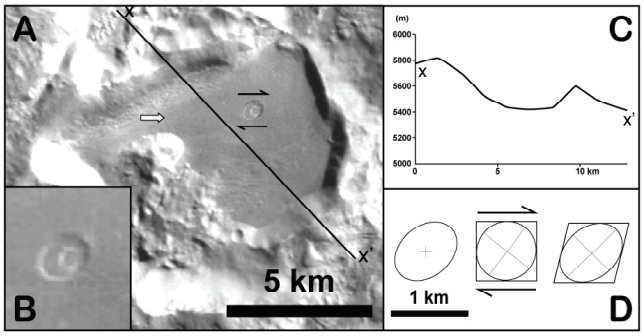

Figure 4. A) Example of possible finite strain of an originally circular impact crater. The black arrows symbolize the simple shear direction, and the white one indicates the directions of linear features in the crater fill with an azimuth consistent with the simple shear inferred by the elliptical crater-like feature; HRSC orbit 497. B) Enlargement of the apparently deformed circular feature (impact crater?) C) Topographic profile across the valley fill imaged in 4A from MOLA gridded topography: the local slope is consistent with the inferred direction of movement and the observed finite strain. D) Strain of a supposed originally circular impact crater under simple shear, hypothesized in this case.

Their texture is moderately rough as observed at scales of HRSC (~15–20 m/pixel resolution) and MOC (~3–5 m/pixel resolution): where high-resolution MOC image data are available, their surface even appears blocky.

Protalus lobes develop preferentially on south-facing slopes, both in case of linear south-facing scarps and northern impact crater rims. The apparent flow direction is from north to south. The correlation between exposure and development for protalus lobes is much stronger than for any other landforms discussed herein.

The impact crater density on these lobate landforms is very scarce: it is the lowest among all morphologies described here. This is also consistent with the observed geometrical relationship between all the different possible periglacial landforms in Thaumasia.

The thickness of protalus lobes can be evaluated using MOLA PEDR profiles: thicknesses range from a few tens of meters up to approximately 200 m (Fig. 3D).

In addition, features similar to protalus ramparts (Whalley & Azizi 2003) have been observed in various parts of Thaumasia Highland (Fig. 3). They appear less widespread than lobes. They tend to develop on top of other larger flow features, such as lineated valley fills.

Morphometric aspects—finite deformation of fills

Both MOLA altrimetric data (single profiles) and HRSC-derived DTM data have been used to characterize the morphology and morphometry of landforms in the Thaumasia Highland.

Crater fills are characterized by very gentle slopes, consistent with the flow direction that could be derived from morphological observations (Fig. 2). The slopes are usually less than one degree. The slopes of crater fills imaged in Fig. 2 are averaging at 0.6 degrees dipping southward. The more convex portion of protalus lobes shows a slope inclination of up to about 7 degrees (Fig. 3D).

Apart from the local disruption and deformation (Fig. 2C), some lineated crater fills show evidence of horizontal deformation/movement. In one case (Fig. 4), it was possible to measure finite deformation of a presently elliptical feature, interpreted as a deformed impact crater (Fig. 4B). Linear features in the crater fill units (Fig. 4A) show a direction consistent with horizontal simple shear, as deduced from the deformation of an original circular impact crater (Fig 4B). The simple shear deformation assumes area conservation on the surface of the fill, which appears to be a reasonable assumption. The assumption of an original circularity of the structure in Fig. 4B is also consistent with the observed crater features (at available resolution), which are ruling out an oblique impact event (an alternative explanation for such an oblique structure), because a hypothetical projectile with a 5–10 degrees incidence angle, needed to produce such an elliptical crater (Gault & Wedekind 1978), would impact on the outer rim before reaching its interior (Fig. 4C).

The finite maximum linear deformation (and linear movement within the fill) of the crater is of about 200 meters. The timescale is not well constrained. Also, the thickness of the deformed fill (and the vertical component of the deformation) is not well constrained.

Relative chronology

Lineated valley/crater fills appear to be the oldest feature among the ones described in the present study. Debris aprons and, later, protalus lobes are characterizing the most recent landscape evolution in the Thaumasia Highland area.

The relative chronology of the landforms in the study area indicates progressive shrinking of landforms confirming the ideas of ice-assisted creep and flow. This view is consistent with considerations of the preservation of morphologies and the local stratigraphic relationships (protalus lobes are clearly postdating lineated crater fills.).

Lineated crater fill units appear often from poorly to slightly altered by crater impacts. At several places, these units have a slightly deflated appearance, which suggests that the present fretted appearance is related partially to erosive effects, also suggesting again an older age of lineated crater/valley fills when compared to protalus ramparts and lobes.

Discussion and Conclusions

Our analysis shows distinct landform development through time in Thaumasia Highland. A generic sequence of periglacial landform development in the study area includes, in chronological order:

a) Large lineated crater fills (areas of ~150–170 km^2), containing possible thermokarst features.
b) Moderate debris aprons (areas of several tens of km^2), with a general "deflated" appearance.
c) Small protalus lobes with little to no impact craters visible at available image resolutions (lengths of ~2–5 km).

d) Locally very small protalus ramparts (several hundred meters to few kilometers in size).

Crater-size frequency analyses to deduce absolute ages will produce unreliable absolute ages due to high degradational effects as well as due to flow deformation of surfaces. The very small size of discovered protalus lobes makes absolute dating even more difficult. Geometrical and stratigraphic relationships are in any case showing a sensibly more recent age of small protalus lobes with respect to lineated crater/valley fills.

Also, the size of these two main groups of landforms is very different: lineated (and sloping) crater fills are large, up to more than 100 km^2, while protalus lobes are usually covering areas of not more than 5–10 km^2.

The flow direction inferred from lineated crater fills show little to no correlation with slope orientation, being more correlated with local and regional topography. On the other hand, mostly concave-upward debris aprons and mostly convex-upward protalus lobes are developed preferentially on south-facing slopes, suggesting a stronger and temporarily closer role of morpho-climatic conditions during their development. This is consistent with previous observations on glacial/periglacial features at mid to low-latitudes (Head et al. 2005).

In the Thaumasia highlands, the dominant concave-upward profile of debris aprons (Mangold & Allemand 2001, Squyres 1978), where present, is indicative of a past scenario involving the melting of ice-cored rock glaciers or debris-covered glaciers (Clark et al. 1994). Contrasting to this, protalus lobes mostly show clear convex-upward profiles (Fig. 3D), which together with their apparent relatively young age is indicating that they might have been active recently or might even be active today.

Although the nature and evolution of such landforms are often controversially discussed, there is observational evidence that the existence and evolution of such landforms is related to climatic variations controlled by the orbital configuration of Mars (Forget et al. 2006, Laskar et al. 2004, Murray et al. 1973, Ward 1974), which was responsible for the deposition of equatorial ice during high-obliquity phases and depletion of an ice reservoir during periods of low obliquities.

The Thaumasia highlands provide the geomorphologic settings necessary for formation of creep-related landforms due to an abundance of high-relief slopes and tectonically dissected terrain allowing accumulation and supply of wall-rock debris at footslopes.

We identified flow and creep morphologies exhibiting a lobate to tongue-like shape and which are characterized by linear to curvilinear ridges and furrows closely resembling large-scale gelifluction lobes or terrestrial rock glaciers and protalus landforms indicative of periglacial environments.

The general lack of impact craters suggests young surface ages. Although water ice is not considered to be stable at equatorial latitudes on Mars today, there are morphologic indicators suggesting re-activation and/or even initial formation of such landforms in the transitional belt between equatorial latitudes and mid-latitudes on Mars during geologically recent times.

Acknowledgments

We thank the HRSC Experiment Teams at DLR Berlin and Freie Universitaet Berlin, as well as the Mars Express Project Teams at ESTEC and ESOC, for their successful planning and acquisition of data as well as for making the processed data available to the HRSC Team. We acknowledge the effort of the HRSC Co-Investigator Team members and their associates who have contributed to this investigation in the preparatory phase and in scientific discussions within the Team.

References

Ansan, V. & Mangold, N. 2006. New observations of Warrego Valles, Mars: Evidence for precipitation and surface runoff. *Planetary and Space Science* 54: 219-242.

Chuang, F.C. & Crown, D.A. 2005. Surface characteristics and degradational history of debris aprons in the Tempe Terra/Mareotis fossae region of Mars. *Icarus* 179: 24-42.

Clark, D.H., Clark, M.M. & Gillespie, A.R. 1994. Debris-covered glaciers in the Sierra Nevada, California, and their impications for snowline reconstructions. *Quaternary Research* 41: 139-153.

Colaprete, A. & Jakosky, B.M. 1998. Ice flow and rock glaciers on Mars. *Journal of Geophysical Research* 103: 5897.

Costard, F.M. & Kargel, J.S. 1995. Outwash plains and thermokarst on Mars. *Icarus* 114: 93-112.

Crown, D.A., McElfresh, S.B.Z., Pierce, T.L. & Mest, S.C. 2003. Geomorphology of debris aprons in the Eastern Hellas region of Mars. *Lun. Planet. Sci. Conf. Abs.* League City, Houston, Tex., USA: Lun. Planet. Inst., 1126. CD-ROM.

Dickson, J.L., Head, J.W., Kreslavsky, M.A. & Marchant, D.R. 2006. Linear Lobate Debris Aprons, Piedmont-like Lobes, and Crater Fill in the Acheron Fossae Graben Region, Mars: Evidence for Debris-covered Glacier Formation and Flow. *37th Annual Lunar and Planetary Science Conference, Volume 37*: 1321.

Dohm, J.M. & Tanaka, K.L. 1999. Geology of the Thaumasia region, Mars: plateau development, valley origins, and magmatic evolution. *Planetary and Space Science* 47: 411-431.

Dohm, J.M., Tanaka, K.L. & Hare, T.M. 2001. *Geologic Map of the Thaumasia Region, Mars*. Map I-2650, Geologic Investigation Series. U.S. Department of the Interior, U.S. Geological Survey.

Feldman, W.C., Prettyman, T.H., Maurice, S., Plaut, J.J., Bish, D.L., Vaniman, D.T., Mellon, M.T., Metzger, A.E., Squyres, S.W., Karunatillake, S., Boynton, W.V., Elphic, R.C., Funsten, H.O., Lawrence, D.J. & Tokar, R.L. 2004. Global distribution of near-surface hydrogen on Mars. *Journal of Geophysical Research (Planets)* 109: 09006, doi: 10.1029/2003JE002160.

Forget, F., Haberle, R.M., Montmessin, F., Levrard, B. & Head, J.W. 2006. Formation of Glaciers on Mars by

Atmospheric Precipitation at High Obliquity. *Science* 311: 368-371.

Gault, D.E. & Wedekind, J.A. 1978. Experimental Studies of Oblique Impact. *Lunar and Planetary Institute Conference Abstracts* 9: 374-376.

Grott, M., Kronberg, P., Hauber, E. & Cailleau, B. 2007. Formation of the double rift system in the Thaumasia Highlands, Mars. *Journal of Geophysical Research (Planets)* 112: 06006, doi: 10.1029/2006JE002800.

Gwinner, K., Scholten, F., Spiegel, M., Schmidt, R., Giese, B., Oberst, J., Jaumann, R., Neukum, G. & Team, H.C.-I. 2005. Hochauflösende Digitale Geländemodelle auf der Grundlage von Mars Express HRSC-Daten: *Photogrammetrie– Fernerkundung–Geoinformation* 5: 387-394.

Head, J.W., Neukum, G., Jaumann, R., Hiesinger, H., Hauber, E., Carr, M., Masson, P., Foing, B., Hoffmann, H., Kreslavsky, M., Werner, S., Milkovich, S., van Gasselt, S. & Co-Investigator Team, T.H. 2005. Tropical to mid-latitude snow and ice accumulation, flow and glaciation on Mars. *Nature* 434: 346-351.

Head, J.W., Marchant, D.R., Agnew, M.C., Fassett, C.I. & Kreslavsky, M.A. 2006. Extensive valley glacier deposits in the northern mid-latitudes of Mars: Evidence for Late Amazonian obliquity-driven climate change. *Earth and Planetary Science Letters* 241: 663-671.

Laskar, J., Correia, A.C.M., Gastineau, M., Joutel, F., Levrard, B. & Robutel, P. 2004. Long term evolution and chaotic diffusion of the insolation quantities of Mars. *Icarus* 170: 343-364.

Lucchitta, B.K. 1984. Ice and debris in the fretted terrain, Mars. *Journal of Geophysical Research* 89: 409.

Mangold, N. 2001. Lobate Debris Aprons as Potential Targets for Ground Ice Detection Analogs to Terrestrial Rock Glaciers. *Conference on the Geophysical Detection of Subsurface Water on Mars*, 7009.

Mangold, N. 2003. Geomorphic analysis of lobate debris aprons on Mars at Mars Orbiter Camera scale: Evidence for ice sublimation initiated by fractures. *Journal of Geophysical Research (Planets)* 108: 8021.

Mangold, N. & Allemand, P. 2001. Topographic analysis of features related to ice on Mars. *Geophysical Research Letters* 28: 407-410.

Murray, B.C., Ward, W.R. & Yeung, S.C. 1973. Periodic insolation variations on Mars. *Science* 180: 638-640.

Rossi, A.P., Komatsu, G. & Kargel, J.S. 2000. Rock Glacier-like Landforms in Valles Marineris, Mars. *Lunar and Planetary Institute Conference Abstracts* 31: 1587.

Rossi, A.P., Chicarro, A.F., Pacifici, A., Pondrelli, M., Helbert, J., Benkhoff, J., Zegers, T., Foing, B. & Neukum, G. 2006. Widespread Periglacial Landforms in Thaumasia Highland, Mars. *37th Annual Lunar and Planetary Science Conference*, *Volume 37*: 1568.

Squyres, S.W. 1978. Martian fretted terrain–Flow of erosional debris. *Icarus* 34: 600-613.

Squyres, S.W. 1979. The distribution of lobate debris aprons and similar flows on Mars. *Journal of Geophysical Research* 84: 8087-8096.

Squyres, S.W. & Carr, M.H. 1986. Geomorphic evidence for the distribution of ground ice on Mars. *Science* 231: 249-252.

van Gasselt, S., Hauber, E. & Neukum, G. 2007. Cold-climate modification of Martian landscapes: A case study of a spatulate debris landform in the Hellas Montes Region, Mars. J*ournal of Geophysical Research (Planets)* 112: 09006, doi: 10.1029/2006JE002842.

van Gasselt, S., Hauber, E., Rossi, A.P. & Neukum, G. 2008. Emplacement of lobate rock glacier landforms and landscape modifications, Mareotis Fossae, Mars. *Proceedings of the Ninth International Conference on Permafrost, Fairbanks, Alaska, June 29–July 3, 2008* (this proceedings).

Ward, W.P. 1974. Climate Variations on Mars, 1, astronomical theory of insulation. *Journal of Geophysical Research* 79: 3375-3386.

Whalley, W.B. & Azizi, F. 2003. Rock glaciers and protalus landforms: Analogous forms and ice sources on Earth and Mars. *Journal of Geophysical Research (Planets)* 108d, doi: 10.1029/2002JE001864.

Zimbelman, J.R., Clifford, S.M. & Williams, S.H. 1989 Concentric crater fill on Mars – an aeolian alternative to ice-rich mass wasting. *19th Lunar and Planetary Science Conference, Houston, TX*. Houston, TX Lunar and Planetary Institute, 397-407.

Stone Frost Mounds in Shallow Bedrock Depressions at Lady Franklin Point, Victoria Island, Nunavut, Canada

Vladislav E. Roujanski
EBA Engineering Consultants Ltd.

Abstract

Unusual terrain features that resemble partially collapsed miniature pingos or stone rings have been recently observed at Lady Franklin Point, Victoria Island, Canada. These features tend to occur in clusters within shallow partially water-filled depressions underlain by frost-shattered flat-lying dolostone bedrock. The mounds are round or oval in shape, 0.5 m to 3 m in diameter, and up to 0.6 m in height. The origin of these mounds is likely associated with frost action. A distinctive central hollow portion of the mounds, partially filled with water, observed in summer at one of the two studied sites is indicative of the seasonal occurrence of an ice core that forms in winter and melts away the following summer. The seasonal formation of an ice core results in doming of the horizontally-lying flat rock fragments. The mounds observed at this site appeared active, and were characterized by loose frost-heaved flat rock fragments and a lack of vegetation. The mounds at another site resembled miniature pingo remnants with a collapsed central portion and well-defined low circular ridge composed of cobble to silt-sized material covered with vegetation. The center was marked by a small shallow depression. At first glance, these features may be viewed as a variety of a frost blister, i.e., a seasonal frost mound. However, unlike a frost blister, which usually develops in finer grained soils and collapses when its ice core melts out, the Lady Franklin Point stone frost mounds remain prominent micro terrain features for a relatively long time because the flat angular fragments of rock do not readily settle back upon melting of the ice core in summer. Therefore, morphologically speaking, the Lady Franklin Point stone frost mounds are a perennial geocryogenic phenomenon.

Keywords: dolostone bedrock; frost action; frost blister; pingo; stone frost mound; stone ring.

Introduction

Lady Franklin Point is an east-west oriented peninsula located on the southwest end of Victoria Island, in the Canadian Arctic (Fig. 1). The peninsula is about 11 km long by 4.5 km wide. The low-lying coastal landscape (the highest point is approximately 15 m above sea level) is dominated by raised beach ridges composed predominantly of gravel- and cobble-sized material with boulders disseminated throughout. Individual ridges are separated by swales or broad level areas dotted with shallow lakes and dry lake depressions. Complexes of the raised beach ridges found in the central part of the peninsula mark former strandlines (Fig. 1).

Over half the peninsula area, mainly the northern portion, is underlain by partially exposed Early Palaeozoic dolostone bedrock: flat-lying and jointed, locally frost-shattered, fractured, frost-jacked, or blanketed by recent marine sediments (mainly gravel and sand) up to 3 m thick. A veneer of glacial clay approximately 0.3 m thick covered by a blanket of marine sand and gravel was encountered at the top of shallow bedrock in one location just north of the existing airstrip. The southern portion of the peninsula consists of low-lying areas underlain by recent lacustrine deposits.

Unusual terrain features that resemble partially collapsed miniature pingos or stone rings were observed in water-filled or partially dried depressions underlain by weathered bedrock. This paper discusses the suggested origin of these landforms and other terrain features found at Lady Franklin Point.

Methods

The descriptions of the permafrost terrain features discussed in this paper are based on ground observations combined with aerial photography and satellite imagery (Google Earth and IKONOS) interpretation.

Stone Frost Mounds

Small distinct mounds were observed at two locations visited by the author of this paper in summers of 2003 and 2004 referred to as Site 1 and Site 2 (Fig. 1). These landforms tend to occur in clusters within shallow, partially water-filled depressions underlain by frost-shattered flat-lying dolostone bedrock (Figs. 2, 3).

The mounds are round or oval in shape, 0.5 m to 3 m in diameter, and up to 0.6 m in height. They resemble partially collapsed miniature pingos (Photos 1 and 2) or stone rings (Photo 3). The formation of pingos is explained in great detail by Mackay (1973, 1979, 1985), Washburn (1973) and others. The origin of stone rings and sorted circles is thoroughly discussed by Washburn (1973), Williams & Smith (1989) and others. The mounds found at Lady Franklin Point are also associated with frost action; however, the mechanism of their formation is different from either pingos or stone rings.

A distinctive central hollow portion of the mounds, partially filled with water, observed in summer of 2003 at Site 1 (Fig. 2, Photos 1 and 2), suggests the seasonal occurrence of an ice core that forms in winter and melts away the following

Figure 1. Location of study sites, Lady Franklin Point, Victoria Island.

summer. The mounds observed at this site appeared active and were characterized by loose frost-heaved flat rock fragments and a lack of vegetation.

A cluster of stone mounds observed at Site 2 in 2003 and 2004 (Fig. 3, Photo 3) is located in a shallow lake depression. The mounds at this site resemble stone rings or miniature pingo remnants with a collapsed central portion and well-defined low circular ridge composed of cobble to silt-sized material. Stones comprising the ridge are lichen-covered with vegetation present both on the ridge and in the central concave area (Photo 3). According to Washburn (1973), the presence of vegetation indicates that the mounds are inactive, which may be associated with drying out of the lake at Site 2.

The formation of the Lady Franklin Point stone mounds is likely the result of frost action. The seasonal formation of an ice core results in doming of the horizontally-lying flat rock fragments. Loose angular pieces of the underlying frost-shattered bedrock are displaced upward by frost jacking and thrusting and undergo some frost sorting. At first glance, these landforms may be viewed as a variety of a frost blister, i.e., a seasonal frost mound. However, unlike a frost blister, which usually develops in finer-grained soils and collapses when its ice core melts out, the Lady Franklin Point stone frost mounds remain prominent micro terrain features for a relatively long time because the flat angular fragments of rock do not readily settle back upon melting of the ice core the following summer. Therefore, morphologically speaking, the Lady Franklin Point stone frost mounds are a perennial geocryogenic phenomenon.

Other Frost-Modified Terrain Features

Linear fractures several hundred meters long and up to 0.5 m wide were observed in several locations within the flat surface of partially exposed dolostone bedrock. The appearance of the fractures suggests that frost action plays an important role in their formation: frost-shattered rock blocks near the ground surface, which form the edges of the fractures, appeared tilted upward by frost jacking and spread out by ice wedging and frost thrusting (Photo 4). The edges of the fractures are slightly raised above the surrounding flat-lying bedrock surface covered by mossy tundra.

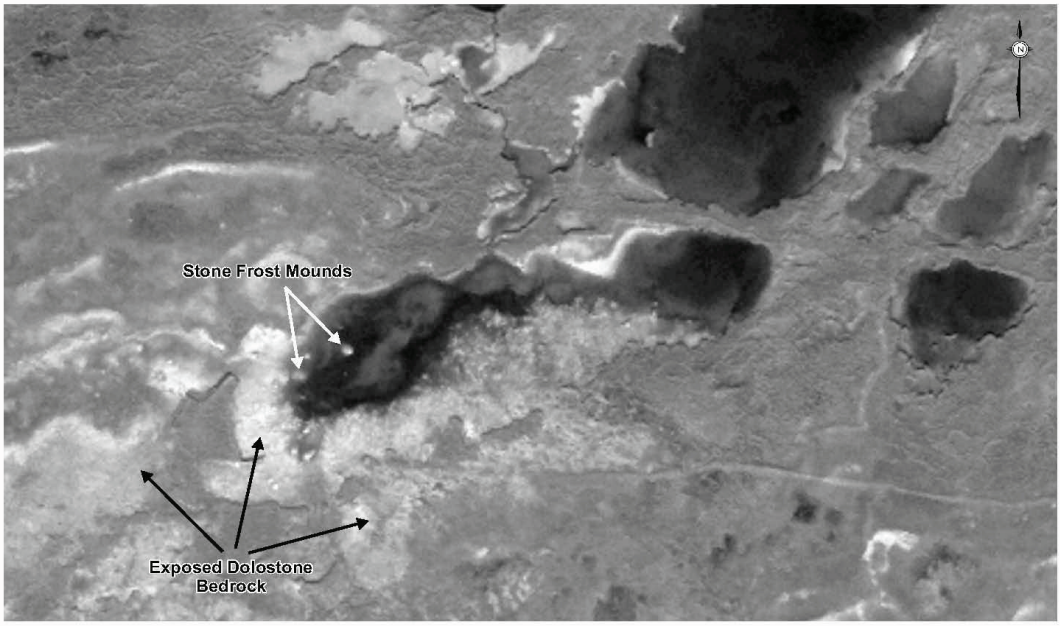

Figure 2. Occurrence of stone frost mounds at Site 1, Lady Franklin Point, Victoria Island.

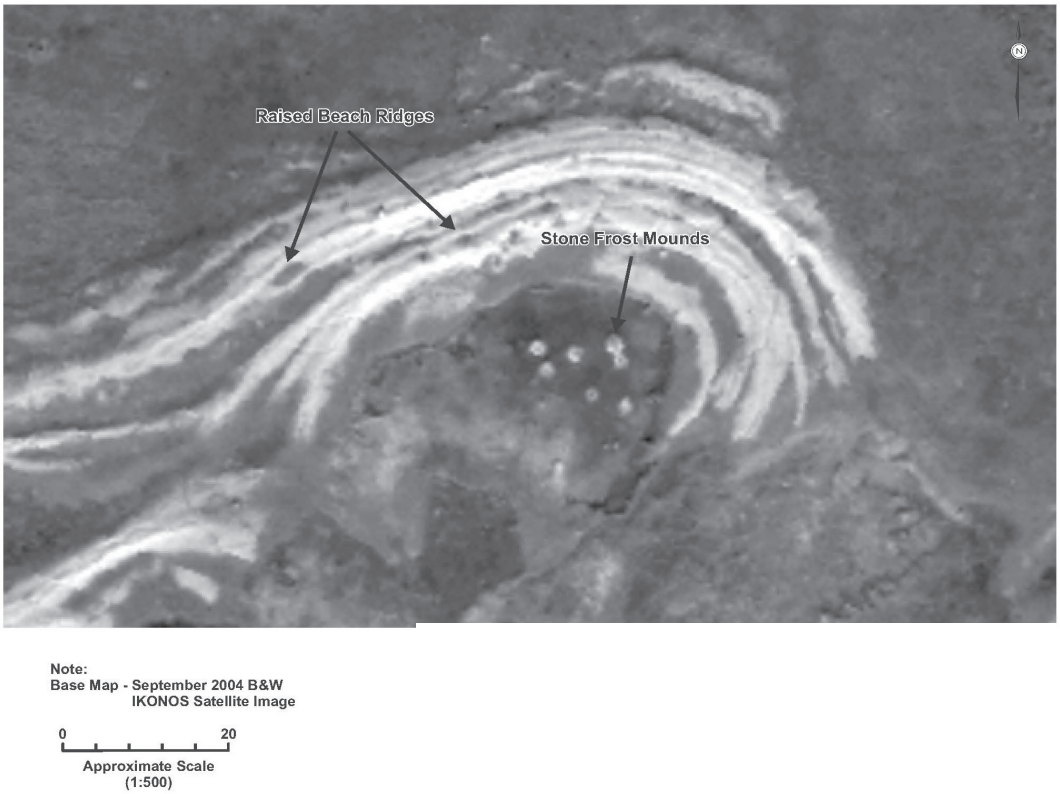

Figure 3. Occurrence of stone frost mounds at Site 2, Lady Franklin Point, Victoria Island.

Photo 1. Site 1. A stone frost mound developed in a shallow water-filled dolostone bedrock depression. Notice hollow central portion of the mound filled with water and a field book for scale. Lady Franklin Point, south Victoria Island. Photo taken August 31, 2003.

Photo 2. Site 1. A stone frost mound developed in a shallow water-filled dolostone bedrock depression. More stone frost mounds in the background. Lady Franklin Point, south Victoria Island. Photo taken August 31, 2003.

Photo 3. Site 2. A cluster of stone frost mounds located in a shallow water-filled dolostone bedrock depression. A raised beach ridge in background. Lady Franklin Point, south Victoria Island. Photo taken August 27, 2003.

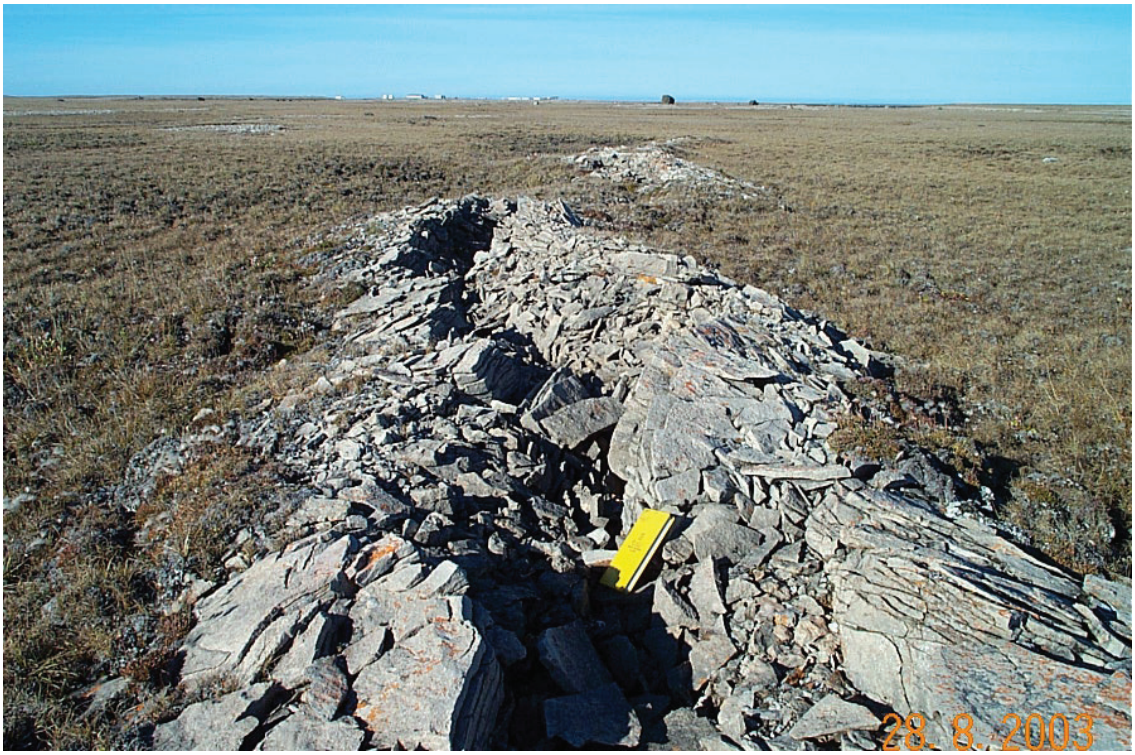

Photo 4. A frost-modified fracture in partially exposed dolostone bedrock. Lady Franklin Point, south Victoria Island. Photo taken August 28, 2003.

Conclusions

Frost action is an important geomorphic process at Lady Franklin Point resulting in unusual terrain features: stone frost mounds and frost-modified fractures in exposed bedrock.

The Lady Franklin Point stone frost mounds result from cycles of seasonal thawing and freezing in the saturated frost-shattered uppermost layer of the flat-lying dolostone bedrock. Thus, they can be considered a seasonal feature. However, morphologically speaking, they are perennial landforms that remain prominent micro terrain features for a relatively long time.

References

Mackay, J.R. 1973. The growth of pingos, western Arctic coast, Canada. *Canadian Journal of Earth Sciences* 10(6): 979-1004.

Mackay, J.R. 1979. Pingos of the Tuktoyaktuk Peninsula area, Northwest Territories. *Geographie Physique et Quaternaire* 33(1): 3-61.

Mackay, J.R. 1985. Pingo ice of the western Arctic coast, Canada. *Canadian Journal of Earth Sciences* 22(10): 1452-1464.

Washburn, A.L. 1973. *Periglacial Processes and Environments* London: Edward Arnold Ltd., 320 pp.

Williams, P.J. & Smith, M.W. 1989. *The Frozen Earth: Fundamentals of Geocryology.* Cambridge: Cambridge University Press, 360 pp.

Arctic Road Research Program: Experiences and Implementation

Seppo M.I. Saarelainen
Senior Research Scientist, Technical Research Centre of Finland VTT, Espoo, Finland

Abstract

In the Arctic Road Research Program, experimental construction was carried out on the Main Road 21 in Kilpisjarvi, Northern Finland, in the years of 1986–87. The aim was to reduce or mitigate various problems caused by cold climate. The themes of test construction were as follows: control of frost-heave damage, reduction of thaw settlements of a road on permafrost, reduction of snow accumulation on the pavement, and control of icing on the pavement. According to the experience gained, frost protection at frost heave sites had functioned according to the design, and the tested materials can be used in the frost protection of road pavements, at least in the conditions of Main Road 21, Kilpisjarvi. The rate of thaw settlement of the road on permafrost had been markedly reduced. Snow accumulation on the pavement had been reduced significantly. Ice accumulation on the pavement was not observed after the experimental repair of the worst sites. The methodical experience and knowledge was seen necessary to implement and apply in the guidelines of pavement planning and design in Finland.

Keywords: design; frost heave; naled control; pavements; permafrost; snow accumulation; test construction.

Introduction

Finland is located between latitudes 60 and 70°N, and the annual mean air temperature varies between +4°C in the south and -3°C in the north. Discontinuous permafrost is found only in Northern Lapland, mainly on peatlands and fjell plateaus. Precipitation is about 350 mm/year, and the terrain is treeless tundra.

The problems are mostly manifested of the maintenance of main roads from Finland to Norway, where winters are long enough to cause problems with excessive frost heaving and naled formation, causing pavement damage and traffic safety problems (Saarelainen & Vaskelainen 1988). Permafrost, lying and thawing under the road, causes settlements, and the open terrain with high wind speeds benefits snow accumulation on the pavement. Further, indications of deficient stability of thawing fjell slopes were detected.

To find a better solution to pavement structures, a test construction program was carried out at Kilpisjarvi, Northern Lapland, at 67°N in the years of 1986–87. (Saarelainen 1993a, 1993b, 1993c, Saarelainen & Vaskelainen 1995, Saarelainen & Onninen 2000). The sites were selected according to the investigations, test pavements were designed according to the site conditions, and after construction, test pavements and structures were monitored, primarily over two years, and later in longer intervals (Fig. 1).

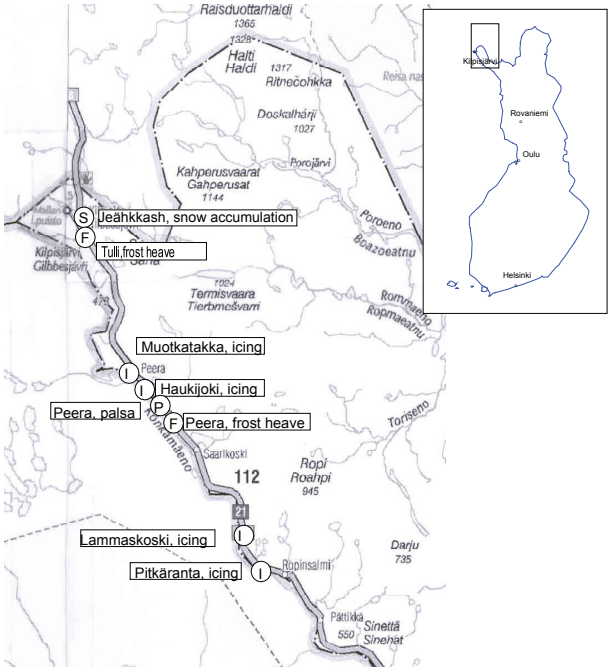

Figure 1. Arctic Road, Kilpisjarvi. Site locations.

Outline of the Problems

Frost heaving

Pavement damage and roughness, resulting from large and uneven frost heaving were found at some road stretches constructed on subgrades of silts and silty tills. The measured normal heaves varied up to 300 mm with seasonal frost penetration up to 3–4 m. At the Kilpisjärvi meteorological station in the period of 1931–1960, the annual average air freezing index was about 43,000 Kh (deg-hours), and the maximum freezing index, occurring once in 10 years, has been about 55,000 Kh (deg-hours).

Thaw settlements

Settlements due to thawing permafrost were found at some peatland sites, which also were characterised with palsa-mounds. The road line, crossing a palsa, had settled about 1.8 m since it was paved in 1982 with a settlement rate of 80 mm/y. The depth of permafrost at the site was about 7–8 m. The frozen subgrade consisted of frozen peat, that was compressed about 70% based on thaw-compression testing. The old road surface prior to paving was dark oiled gravel.

Snow accumulation

Excessive snow accumulation had been met during years in the pavement maintenance in an open mountainous terrain, where wind speed may rise considerably. The snow densities were low due to cold, continuous winters. Accumulation was most severe in road-cuts along the hill slopes. Snow plowing was normally started in December. The traffic suffered also from reduced visibility (white-out) during severe winds and storms. Along the test road, snow depths along the road profile and in transverse sections were measured. The recorded maintenance of snow accumulation started when the measured wind speed exceeded about 5 m/s or after a snowfall of 50 mm.

Naled formation

In cold winters, like in the late 1980s, ice accumulation had been observed, causing expensive maintenance work. Problematic sites were located either on a road section along a hill slope or on a road crossing a watercourse, stream, or river. Indicated problems resulted from disturbance in the winter drainage. Groundwater continued flowing during the winter in the ground below the seasonal frost. If the frost penetrated to or below groundwater level, groundwater was forced onto the ground and snow surface where it froze. In a local natural watercourse, water flow froze from bottom up and formed ice dams that forced the water onto the surface to freeze. In more southern regions, road culverts are filled with ice in wintertime. Ice-filled side ditches and bridge or culvert openings may flood over during quick snowmelt in spring and cause erosion damage and traffic risks on the road.

Solution of the Problems

Frost heaving

At selected sites, test pavements were designed so that the frost heaving in a design winter (maximum once in 10 years) was less than 50 to 70 mm. The design was done applying "Segregation potential concept" (Konrad & Morgenstern 1981)

$$\frac{\partial v_w}{\partial t} = SP\frac{\partial T}{\partial z} \quad (1)$$

where $\frac{\partial v_w}{\partial t}$ is flow of water from unfrozen soil to the freezing zone, $\frac{\partial T}{\partial z}$ is the thermal gradient in the freezing zone, SP is the coefficient of proportionality, segregation potential.

The frost heave was calculated using a layered finite-difference program SSR that solves, in time intervals, a balance equation of heat at the freezing front (Saarelainen 1992). This is based on the surface temperature and thermal properties of the layered horizon and results in calculating the frost penetration and frost heave in time. With the same procedure, the segregation potential (SP) was back-estimated and compared with the estimated frost penetration and

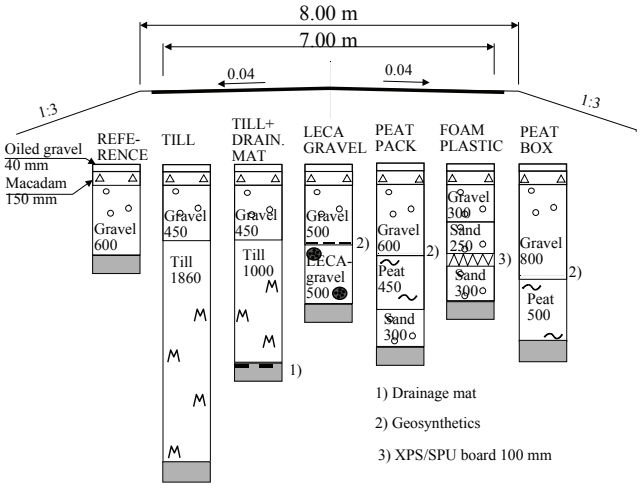

Figure 2. Tulli. The material layers of different frost-protected test pavements.

levelled frost heaving of the old pavement during the winter of 1985–86. The back-estimated segregation potential varied between 0 and 7 mm²/Kh.

The aim of the test pavements was to study the applicability of different frost protection materials, like extruded polystyrene (XPS), LECA-gravel (lightweight expanded clay aggregate), prepacked and dried peat, local dried peat, and a slightly frost-susceptible sandy till. The layer thickness needed in frost protection was determined in the individual design. The frost heaving as well as SP varied along the line greatly, and the structures are not quite comparable with each other. The mechanical design of the pavement was carried out according to the actual road standards (minimum surface modulus during thaw more than about 170 MPa).

Structures with layer thicknesses are illustrated in Figure 2.

The test pavements were constructed in summer 1987. The frost protection materials were transported from southern-central Finland except for the local till and local peat.

Thaw settlements

Permafrost could be seen in the terrain in the form of frost mounds and palsas on peatlands. The average annual air temperature according to long-term climatic observations was about −3°C, and the elevation is about +400 m above sea level. The area is in the discontinuous alpine permafrost zone.

According to temperature profiling and electric soundings, the thickness of palsa below the test site was about 7–8 m. The top layer below the old pavement consisted of frozen peat with ice content about 50–95% by volume and thaw-compression of more than 70% under compressive stress of 25 kPa.

The test pavement contained, besides an overlay of 700 mm of gravel and asphalt, insulation of XPS, underlain with a gravel layer of 500 mm. The thickness of XPS (100 mm) was analysed using an analytic thermal FEM program, ADINA-T. The analysis with a given insulation thickness was conducted over three calendar years with the objective

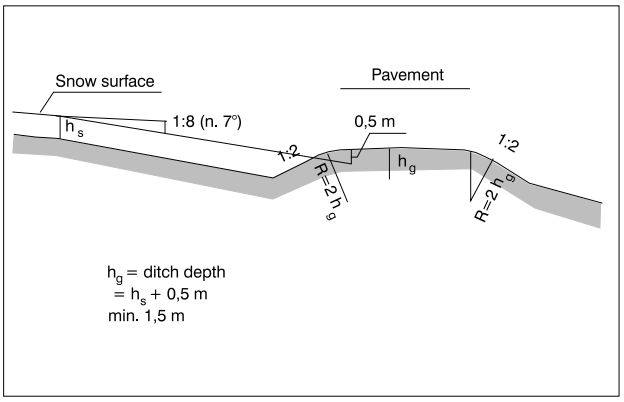

Figure 3. Type transverse profile to prevent snow accumulation on pavement in a sloping terrain.

that the thaw should not penetrate to the underlying frozen and thaw-sensitive subgrade.

The old pavement was removed in autumn 1986, and the new pavement with insulation was constructed in May 1987. The test section was paved in the next summer.

Snow accumulation

To reduce snow accumulation, the new pavement grade was raised above the estimated maximum snow level. The snow level was measured during the previous winter along the road. (Because the observed snow thickness at the Kilpisjärvi meteorological station was maximum occurring once in 10 years, the measured snow surface level at the site corresponded also to a maximum snow level, occurring once in 10 years, see Byalobzhenskiy 1983). Applying the observation statistics of snow thickness from a neighbouring observation station, this interpretation can be done for snow depth observations at a road site. The pavement surface was set 0.2–0.5 m higher than the estimated design snow level. Because the test road was located along a mountain slope, the transverse profile of the road was smoothed with curved shoulders and the upslope ditch was widened to provide a storage area for the accumulation of snow (Fig. 3).

The snow fences installed previously were removed.

Naled formation

Improvement of winter drainage was tested at four sites, two of which were slopes with groundwater icing problems and two with watercourse icing.

The principal improvement at groundwater icing was to collect the water into subsurface drains in the upper terrain below the estimated frost penetration and to drain it into a deep insulated pipe across the road.

The principal improvement at the watercourse icing site was to lead the upstream water flow through the road into a deep insulated pipe installed below the seasonal frost depth.

The drainage installations were constructed in 1987, and no pavement icing needing maintenance measures has been observed since then. Tested approaches have been successfully applied in road maintenance operations in Finnish Lapland since then (Kaitala et al. 2007).

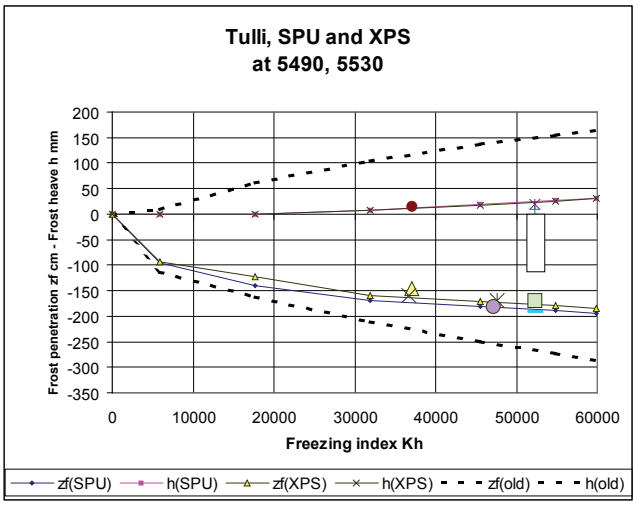

Figure 4. Tulli, the estimated and observed frost penetration (zf) and frost heaving (h) of polyurethane (SPU), and polystyrene (XPS) insulated test pavements.

Experiences after Construction

Frost heaving

The calculated frost heaving and frost penetration vs. freezing index are illustrated in Figure 4 for the test pavement with frost insulation boards. Observed frost heaves and frost penetration of different winters (1987/88, 1988/89, and 1989/90) have also been marked. A reasonable match can be seen that the applied calculation model SSR reasonably estimated actual frost heave and frost penetration, and that the material characteristics applied in the analysis were of correct magnitude.

For different frost protection materials, the following estimated characteristics were summarized in Table 1.

According to the observations, the frost heaving and frost penetration corresponded well to the calculated values. This confirmed the validity of the calculation model, the back-estimated frost-heave parameters (segregation potential), and the insulation properties of the applied materials. A more comprehensive presentation of the test pavements is included in the site reports (Saarelainen 1993, 2002).

Thaw settlements

The settlements were observed along the road centerline. Observations are illustrated in Figure 5. During the first years, the pavement surface was light-coloured, and the maximum annual settlement was about 10 to 20 mm/y. After the road was paved with dark asphalt pavement, the rate of settlement increased to a maximum 30 mm/y.

It is obvious that in these marginal permafrost conditions, thaw can be decreased with thermal insulation and light-coloured surface. For further reduction, active cooling might be useful. The rate of settlement in this actual case was reduced to a level that could be maintained by normal road maintenance.

Table 1. Characteristics of applied frost insulation materials (Saarelainen 2002).

Material	Dry density kg/m^3	Moisture content $w_{vol?}$ %	Frozen thermal conductivity λ_f W/Km Estim.	Obs.
LECA-gravel	300	7	0.2	0.2
Packed peat	300	10	0.5	0.7
SPU	40	4	0.035	0.035
XPS	38	0,4	0.035	0.035
Local peat	200	60	1.0	1.0

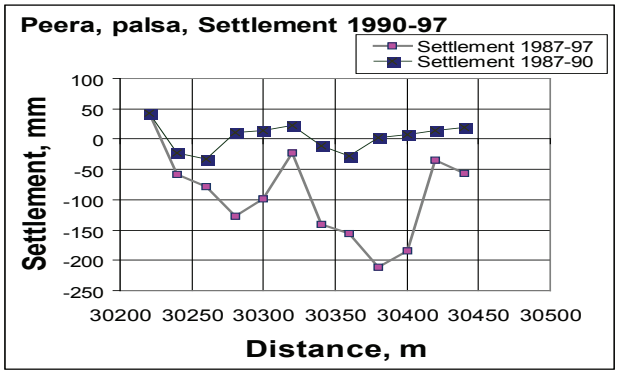

Figure 5. Peera, palsa. Pavement settlements since construction in 1987 until 1990 and 1997.

Snow accumulation

Before repair, snow and ice removal was needed by December. After the road was raised, the wind was observed to keep the pavement free from snow over the winter. In most severe winters with a very thick snow cover, heavy maintenance was still necessary as late as March.

The following recommendations to reduce snow accumulation were seen as appropriate:

- the pavement surface should be raised more than 0.5 m above the maximum design snow level,
- in a sloping terrain, a spare space for snow accumulation should be planned in the cut upslope,
- the pavement shoulders should be rounded to minimize wind turbulence on the road, and
- snow fences may still be necessary to maintain visibility during snowstorms

Naled formation

Ice accumulation in the road ditches was monitored after the repair. The ice accumulation was clearly reduced, and it did not cause any further maintenance effort, although winter temperatures were still severe.

In conclusion, the following recommendations are appropriate:

- Groundwater icing can be reduced with deep drainage in the upper terrain, and draining the water through the road in a deep thawed pipe.
- Surface water icing can be reduced or prevented by leading the water flow in the watercourse into a thermally-insulated deep culvert across the road line. During snowmelt and summer season, water then flows in the open watercourse.
- Icing can be reduced and water flow can be maintained by local heating. The electrical energy needed for heating cables can be produced with a wind generator.

It was also observed that icing problems are induced when a natural watercourse is treated and disturbed by excavation.

Conclusions

The described test construction revealed some extreme road maintenance problems in Finland. The approaches applied in the design and construction were seen as efficient, and they have been later applied elsewhere in Northern Finland. The results in the form of design models and approaches, as well as the design characteristics of insulation materials, may be useful also in other regions in cold climates.

References

Bjalobzenskij, G.V. 1983. Determination of snow cover thickness for snow accumulation design of pavements. *Avtomobilnye dorogi*, 1983, No. 10 (in Russian).

Kaitala, E. & Saarelainen, S. 2007. Improvement of de-icing on the roads at Kittila, Muonio, Enontekio, Inari and Utsjoki. *Proceedings of the Eighth International Symposium on Cold Region Development ISCORD 2007, Sept. 25–27. 2007, Tampere, Finland*, 2 pp.

Konrad, J.-M. & Morgenstern, N.R. 1981. The segregation potential of freezing soil. *Can Geot. Journal* 17: 473-486.

Saarelainen, S. & Vaskelainen, J. 1988. Problems of Arctic road construction and maintenance in Finland. *Proceedings of the Sixth International Conference on Permafrost.* Trondheim: Tapir Publishers, 1466-1471.

Saarelainen, S. 1992. *Modelling frost heaving and frost penetration at some observation sites in Finland. The SSR model.* Espoo: VTT Publications 95, 121pp, http://www.vtt.fi/inf/pdf/publications/1992/P95.pdf

Saarelainen S. 1993a. Repair of a road built on permafrost at Kilpisjarvi, Northern Finland. *Proceedings of the Sixth International Conference on Permafrost, Beijing, China, June 1993*: 539-543.

Saarelainen, S. 1993b. Use of frost insulation in the repair of frost heave damages. *Proc. Int. Symp. on Frost in Geotechnical Engineering, Anchorage, Alaska, June 28th–July 1st 1993:* 113-116.

Saarelainen, S. 1993c. Arctic road construction. Final report of Kilpisjarvi-project in Finnish with English summary. Helsinki. *Tielaitoksen tutkimuksia* 5/1993, 62 pp.

Saarelainen, S. & Kivikoski, H. 1995. Preventing snow accumulation on road pavements. *PIARC, Proc. of International Winter Road Conference, Lulea, Sweden, 1995*.

Saarelainen, S. & Onninen, H. 2000. Long term settlement of a road built on permafrost at Kilpisjarvi, Northern Finland. *Proceedings of the International Workshop on Permafrost Engineering, Longyearbyen, Svalbard, Norway 18–21 June 2000.* Oslo: Norwegian Geotechnical Institute, 129-138.

Saarelainen, S. 2002. *Arctic Road Research Program 1985–1990. Final report.* Helsinki: Finnish Road Administration, Report 21, 89 pp.

Methane Emission from Siberian Wet Polygonal Tundra on Multiple Spatial Scales: Vertical Flux Measurements by Closed Chambers and Eddy Covariance, Samoylov Island, Lena River Delta

Torsten Sachs
Alfred Wegener Institute for Polar and Marine Research, Telegrafenberg A43, 14473 Potsdam, Germany
Michael Giebels
Institute of Geoecology, Technical University Braunschweig, Germany
Christian Wille
Institute of Botany and Landscape Ecology, Ernst Moritz Arndt University of Greifswald, Germany
Lars Kutzbach
Institute of Botany and Landscape Ecology, Ernst Moritz Arndt University of Greifswald, Germany
Julia Boike
Alfred Wegener Institute for Polar and Marine Research, Telegrafenberg A43, 14473 Potsdam, Germany

Abstract

Ecosystem-scale measurements and investigations of the small-scale variability of methane emission were carried out in northern Siberian wet polygonal tundra using the eddy covariance technique during the entire 2006 growing season. Simultaneous closed chamber flux measurements were conducted daily at 15 plots in four differently developed polygon centers and a polygon rim from July–September 2006. Our study site was located in the southern part of the Lena River Delta, characterized by arctic continental climate and comparatively cold, continuous permafrost. Controls on methane emission were identified by applying multi-linear and multi-nonlinear regression models. We found a relatively low growing season average methane flux of 18.7 ± 10.2 mg m^{-2} d^{-1} on the ecosystem scale and identified near-surface turbulence, soil temperature, and atmospheric pressure as the main controls on the growing season variation methane emissions. On the micro-site scale, fluxes showed large spatial variability and were best described by soil surface temperature.

Keywords: closed chambers; eddy covariance; flux; methane; Siberia; tundra.

Introduction

Introduction

Arctic tundra ecosystems cover an area of about 7.34 x 10^{12} m^2 (Reeburgh et al. 1998) and are underlain by permafrost. Despite increased research, especially in connection with the much stated concern of potential increased emission of climate-relevant trace gases from warming or thawing tundra areas, these sensitive high-latitude ecosystems with their complex network of interconnected processes and controls are far from being understood. Vegetation, state of the permafrost, soil texture, hydrology, and many other relevant parameters and consequently also processes controlled by these parameters vary greatly on small spatial scales. This is especially valid for methane emission on various scales from arctic wetlands (Christensen et al. 2000, Kutzbach et al. 2004, Whalen & Reeburgh 1992).

To our knowledge, only four studies reported methane flux data from Arctic tundra on the ecosystem scale using eddy covariance techniques, namely Fan et al. (1992) from western Alaska, Harazono et al. (2006) from northern Alaska, Friborg et al. (2000) from Greenland, and Hargreaves et al. (2001) from Finland. Manuscripts by Wille et al. (2008) and Sachs et al. (2008) reporting data from the Lena River Delta, Siberia, are currently in press.

On the other hand, many studies are available reporting point data using closed chamber methods (Christensen et al. 2000, Kutzbach et al. 2004, Whalen & Reeburgh 1992). While closed chamber methods have multiple inherent problems, such as the exclusion of atmospheric parameters and induced alteration of concentration gradients underneath the chamber, resulting in disturbed fluxes, they are widely used to investigate the small scale variability of methane fluxes. The eddy covariance method does not allow for a spatial resolution high enough to investigate that kind of variability in heterogeneous areas.

We conducted intensive field studies on the ecosystem (1 ha to 1 km^2) and micro-site scales (0.1–100 m^2) using eddy covariance and closed chamber methods simultaneously in order to investigate the temporal and spatial variability of methane emissions. For the first time, methane flux measurements on the ecosystem scale in Arctic Siberian tundra were carried out during an entire growing season from the beginning of June–September 2006, and measurements on the micro-site scale were conducted within the eddy covariance footprint from July–September 2006.

Material and Methods

Study site

The study site was located on Samoylov Island, 120 km south of the Arctic Ocean in the southern central Lena River

Delta (72°22′N, 126°30′E) and is considered representative of the active delta landscape. Over the past ten years, Samoylov Island has been the focus of a wide range of studies on surface-atmosphere gas and energy exchange, soil science, hydrobiology, microbiology, cryogenesis, and geomorphology (Boike et al. 2003, Kutzbach et al. 2004, 2007, Liebner & Wagner 2007, Schwamborn et al. 2002, Wille et al. 2008, Sachs et al. 2008).

Samoylov Island covers an area of about 7.5 km². The western part of the island (3.4 km²) is a modern floodplain with elevations from 1–5 meters above sea level (a.s.l.). The study site is located in the center of the Late-Holocene eastern part (4.1 km²) with elevations from 10–16 meters a.s.l. The surface of the terrace is characterized by wet polygonal tundra with a flat but regular micro-relief caused by the development of low-center ice wedge polygons. The typical elevation difference between depressed polygon centers and elevated polygon rims is up to 0.5 m (Kutzbach 2006). The poorly drained and hence mostly inundated centers are characterized by *Typic Historthels*, while *Glacic* or *Typic Aquiturbels* dominate at the dryer but still moist polygon rims (Soil Survey Staff 1998, Kutzbach et al. 2004). As the summer progresses, these soils typically thaw to a depth of 30–50 cm.

Hydrophytic sedges, as well as mosses, dominate the vegetation in the wet polygon centers (Kutzbach et al. 2004). Polygon rims are dominated by mesophytic dwarf shrubs, forbs, and mosses. Surface classification of aerial photographs taken in 2003 shows that elevated and dryer polygon rims cover approximately 60% of the area surrounding the study site, while depressed and wet polygon centers and troughs cover 40% of the area (G. Grosse pers. comm.. 2005).

The climate in the region is arctic continental climate characterized by very low temperatures and precipitation. Mean annual air temperature at the meteorological station on Samoylov Island was -14.7°C and mean precipitation was 137 mm, ranging from 72–208 mm in a period from 1999–2005 (Boike et al. 2008). Snowmelt and river break-up typically start in the first half of June, and the growing season lasts from mid-June through mid-September. The continuous permafrost in the delta reaches depths of 500–600 m (Grigoriev 1960) and is characterized by very low temperatures between -13°C and -11°C (Kotlyakov & Khromova 2002).

Ecosystem scale flux measurements

In situ ecosystem scale methane fluxes were measured using the eddy covariance (EC) method with a tunable diode laser spectrometer (TGA 100, Campbell Scientific Ltd., USA) for CH_4 analysis. A more detailed description of the technical set-up can be found in Sachs et al. (2008).

The EC system was set up in the center of the eastern part of Samoylov Island and was surrounded by a relatively homogenous fetch of wet polygonal tundra. Larger lakes were located at the periphery of a 600 m radius around the tower. Successful measurements were conducted for 103 days from June 9–September 19, 2006, covering an entire growing season (Sachs et al. 2008).

Additional parameters measured at the eddy covariance system and an automated long-term monitoring station 700 m south of the EC tower include air temperature, relative humidity, incoming and outgoing solar and infrared radiation, photosynthetically active radiation (PAR), barometric pressure, precipitation, and soil temperature data at various depths. Additional daily manual measurements at five sites in close proximity to the tower included thaw depth using a steel probe, soil temperatures in 5 cm depth intervals, water level, and soil moisture using a Theta Probe type ML2x (Delta-T Devices Ltd., Cambridge, UK) where no standing water was present.

The area from which 80% of the cumulative methane flux originated was calculated using a footprint analysis according to Schuepp et al. (1990). The upwind distance of this flux contribution was on average 518 m, the maximum contribution originated from an average distance of 116 m.

Small scale flux measurements

For small-scale flux measurements, five different micro-sites characteristic of the prevalent surface and vegetation features within the eddy covariance fetch were established in close proximity to the flux tower (Fig. 1).

Polygon 1 was a low-center polygon with standing water in the center. The northern side of the polygon rim showed signs of beginning degradation, which might serve as a hydraulic connection to surrounding polygon troughs. Vegetation in the center is dominated by *Drepanocladus revolvens* (100% coverage) and *Carex chordorrhiza* (8% coverage).

Polygon 2 was a high-center polygon with no standing water in the center due to drainage into surrounding thermokarst cracks and troughs. The vegetation was dominated by *Hylocomium splendens* (85% coverage) and *Tomentypnum nitens* (10% coverage).

Polygon 3 was a low-center polygon with a massive rim on the western side and a completely degraded rim on the eastern side, where a large thermokarst crack of more than 2

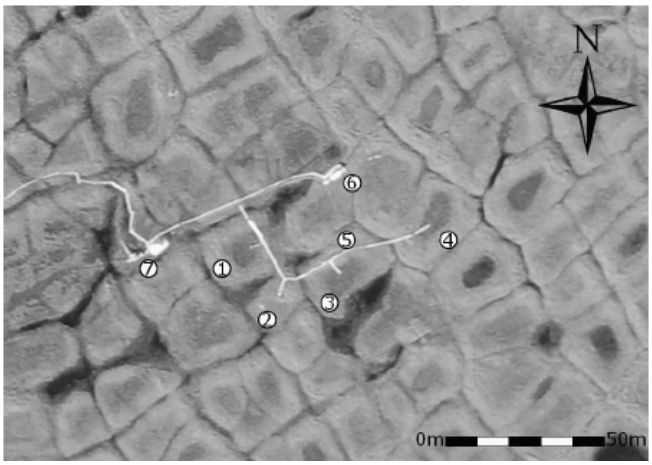

Figure 1. Aerial view of investigation site: 1 – low-center polygon, 2 – high-center polygon, 3 – low-center polygon, 4 – low-center polygon, 5 – rim, 6 – eddy covariance system, 7 – tent for equipment (Photo: J. Boike).

m depth was located. There was standing water in the polygon center and the vegetation was dominated by *Drepanocladus revolvens* (90% coverage), *Carex chordorrhiza* (10% coverage), and *Carex concolor* (10% coverage).

Polygon 4 was a low-center polygon with no apparent rim degradation and no apparent hydraulic connection to surrounding cracks or troughs. It usually maintained the highest water level and was dominated by *Scorpidium scorpidioides* (100% coverage), *Carex chordorrhiza* (8% coverage), and *Carex concolor* (3% coverage).

The polygon rim micro-site was underlain by a massive ice wedge and draining into polygon 3 to the east and the polygon crack to the west. Vegetation was dominated by *Hylocomium splendens* (60% coverage), *Rhytidium rugosum* (30% coverage), and *Carex concolor* (4% coverage).

In each of the four polygon centers and along the rim, three 50 cm x 50 cm PVC chamber collars with a water-filled channel as a seal were inserted 10–15 cm into the active layer. Chambers were made of opaque PVC and clear PVC, respectively, for light and dark measurements. Chamber volume was 12.5 l at the high-center and rim micro-sites and 37.5 l at the other sites, where higher vegetation did not allow for the use of small chambers.

Chamber measurements at all 15 plots were made daily from July 12–September 19, 2006 with both clear and opaque chambers. Sample air was drawn from a port on top of the chamber every 45 s for 8–10 minutes for simultaneous analysis of CO_2, CH_4, and water vapor using a photo-acoustic infrared gas spectrometer Innova 1412 with optical filters UA0982 for CO_2, UA0969 for CH_4, and SB0527 for water vapor (INNOVA AirTech Instruments, Denmark). A membrane pump was connected to two other ports and circulated chamber headspace air through perforated dispersive tubes for mixing.

Due to water interference with the CH_4 optical filter sample air was dried prior to entering the analyzer using 0.3 nm molecular sieve (beads, with moisture indicator; Merck KGaA, Darmstadt, Germany). Temperature and pressure inside the chamber were logged continuously by a MinidanTemp 0.1° temperature logger (Esys GmbH, Berlin, Germany) and the Innova 1412, respectively.

Flux modeling

We used multiple linear regression, as well as regression tree analysis, to identify the main controls on eddy covariance methane fluxes. All analyses were based on daily averages of measured and quality-controlled fluxes and are reported elsewhere in detail (Sachs et al. 2008). A multiplicative exponential regression model modified and extended after Friborg et al. (2000), was set up and fitted to the in situ data for small-scale flux modeling. It can be written as

$$FCH_4 = a \cdot b^{((T-\overline{T})/10)} \cdot c^{(u*-\overline{u*})} \cdot d^{(p-\overline{p})} \quad (1)$$

where a, b, c, and d are fitted parameters, T is the soil temperature at 10 cm depth in a polygon center, u_* is the friction velocity, p is the air pressure, and horizontal bars denote the mean values of the respective variables. A weighting factor of σFCH_4^{-2} was applied during the fitting process, with σFCH_4 being the daily mean of the noise estimates of the hourly flux data points.

For closed chamber measurements, we used multiple linear regression analyses to identify statistically significant controls on methane flux. Data was first tested for multi-collinearity following Schuchard-Ficher (1982) and for parameter significance using a t-test. The regressors were discarded in a stepwise procedure until only independent and significant parameters remained.

Results

Ecosystem-scale methane flux

Mean daily ecosystem methane flux was 18.7 ± 10.17 mg m^{-2} d^{-1} during the study period and showed relatively small seasonal variation (Fig. 2). However, strong variations could be observed, which coincided with pronounced decreases in air pressure and higher wind speed after calm periods.

In the first two weeks of measurements, average daily methane fluxes were already 13.8 mg m^{-2} d^{-1}, with high variability from 5.7 mg m^{-2} d^{-1} to 22.0 mg m^{-2} d^{-1}. Soil temperature was still below 0 °C when measurements started and showed very little variation in the early part of the thawing period. The lowest methane flux was observed during days with relatively high air pressure and low wind speed. Methane fluxes increased to an average of 25.0 mg m^{-2} d^{-1} in the third week. However, this increase was mainly due to an extreme peak on June 27, which coincided with the lowest observed air pressure during the summer and high wind speeds. The last ice from the bottom of ponds and smaller lakes surfaced and melted around this time.

Methane fluxes dropped to an average of 12.3 mg m^{-2} d^{-1} during the calm period at the end of June, and then steadily increased to the highest measured fluxes of on average 35.1 mg m^{-2} d^{-1} in the first week of August, roughly following variations in soil temperature and closely following variations in wind speed. Throughout July, above-average methane fluxes frequently correlated with rapid decreases in air pressure. Until the third week of August, fluxes remained between 17.0 and 20.0 mg m^{-2} d^{-1} and then decreased to less than 13.0 mg m^{-2} d^{-1} during a longer calm high-pressure period at the end of August.

During the first and second week of September, which were characterized by steadily decreasing air pressure, partly strong winds, and rain or snow events, methane fluxes increased to an average of 18.2 mg m^{-2} d^{-1} and 21.6 mg m^{-2} d^{-1}, respectively, despite a decrease in soil temperature and refreezing of the top soil layers and water bodies. By mid-September, all water bodies, except for the large thermokarst lakes, were covered with ice up to 8 cm thick. During the calm high-pressure period after September 13, methane fluxes decreased markedly to below 10.0 mg m^{-2} d^{-1} at the end of the measurement period.

All approaches showed that variation in methane fluxes could best be explained by friction velocity u_* and soil

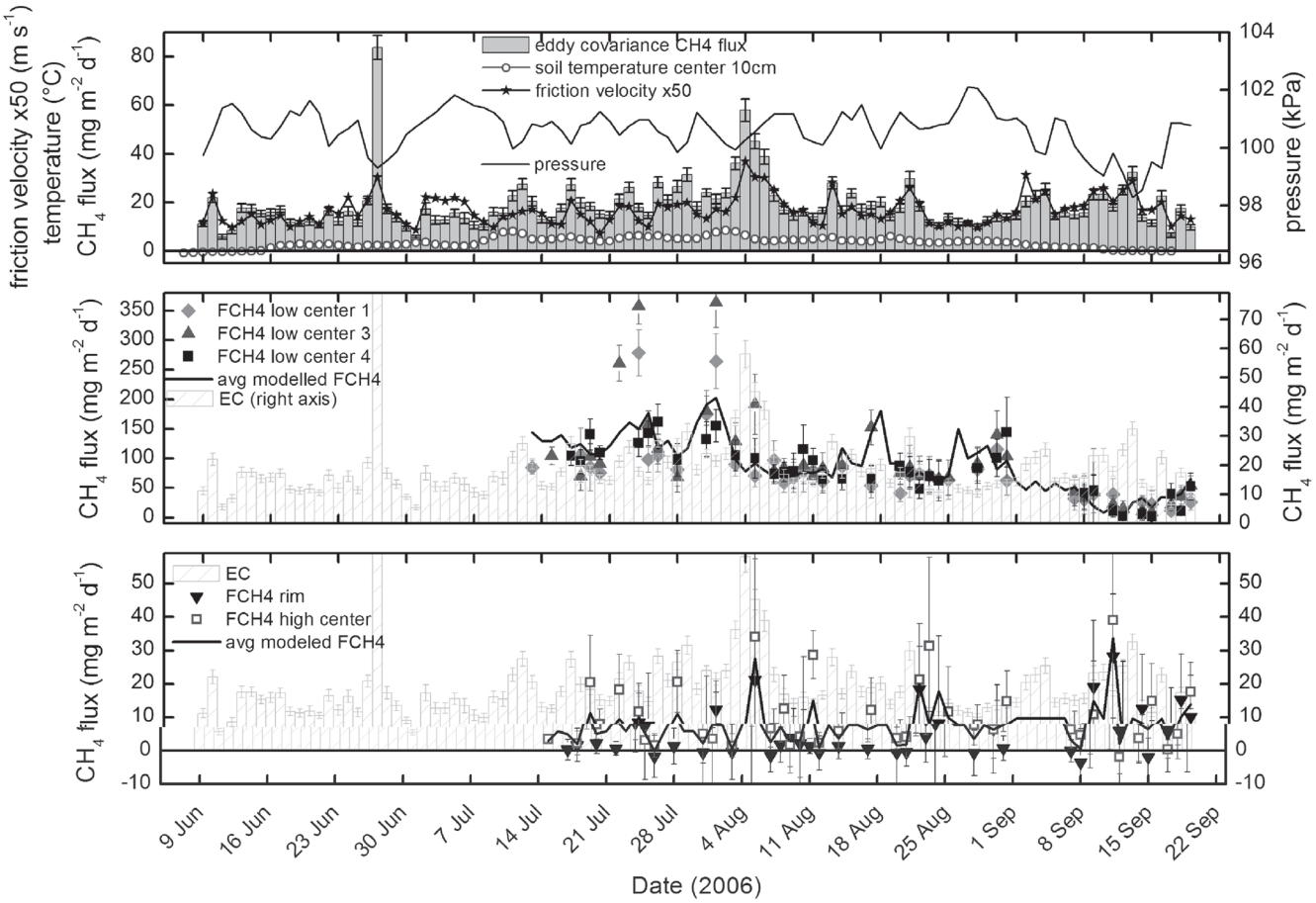

Figure 2. Top panel: Daily averages of eddy covariance methane fluxes and environmental controls during the 2006 growing season. The error bars of the eddy covariance data indicate the daily average noise level. Middle panel: Closed chamber methane fluxes from low center polygons and average modeled chamber flux. Each point represents the average of six flux measurements in the respective polygon. Bottom panel: Closed chamber methane fluxes from a polygon rim and a high center polygon and average modeled chamber flux. Each point represents the average of six flux measurements at the respective site. The error bars of the chamber data indicate the mean standard errors of the flux estimates. In the middle and bottom panel, the eddy covariance fluxes are given as light-grey columns for comparison. Note the different scale of the two y-axes in the middle panel!

temperatures at 10 cm depth in a polygon center and 20 cm depth in a polygon rim, respectively. Friction velocity alone accounted for 57% of the variance in methane emissions and another 3% could be explained by wind speed, which is closely correlated with friction velocity. Soil temperatures on the other hand only explained about 8% of the variance. The best agreement (r^2_{adj} = 0.68) of modeled and measured data was obtained by a model which included an exponential term that accounts for the observed influence of air pressure.

Thaw depth, which increased gradually and without variation throughout the season, did not improve the model, nor did water level, which remained above the soil surface at all times in the polygon centers.

The cumulative methane emission during the 2006 growing season was 1.93 g m^{-2}, which agrees well with the cumulative flux during the same period of a combined 2003 and 2004 dataset that amounted to 1.87 g m^{-2} (Wille et al. 2008). The model underestimated the cumulative measured flux by less than 5%.

Small-scale methane flux

Small-scale methane emission was similar among low-center polygons (Fig. 2) and differed strongly from fluxes at the high-center and rim micro-sites (Fig. 2).

At all three low-center micro-sites, mean daily fluxes in July and August were around 100 mg m^{-2} d^{-1} and decreased at the beginning of September to less than 50 mg m^{-2} d^{-1}, closely following variations in air temperature. When snow started to accumulate between September 10 and 15 during a period of below-zero temperatures, emissions fluctuated below 20 mg m^{-2} d^{-1}. At polygon 4, the seasonal course was less pronounced and variability was less extreme than at polygon 1 and 3, where peak fluxes exceeded 350 mg m^{-2} d^{-1} and were associated with spatial standard deviations of up to ±300 mg m^{-2} d^{-1}, demonstrating a large spatial variability even within micro-sites. These extreme emissions were generally associated with high temperatures.

It was not possible to construct a multidimensional regression model with independent and significant parameters. The predictor variable with the highest

explanatory power within the final one-dimensional model was surface temperature.

At polygon 2 (high center) and at the polygon rim, very low methane concentrations in the closed chamber system frequently caused the analyzer to reach its detection limit, resulting in noisy data and a high exclusion rate during flux calculation. Fluxes that could be calculated were very low throughout the campaign and rarely exceeded 10 mg m^{-2} d^{-1}, which is about 10% of the average fluxes from low-center polygon micro-sites. No seasonal course is evident from the data and no statistically significant correlation with any of the observed environmental parameters was found. Gaps in the time series were filled with monthly average flux values, accounting for the small positive fluxes that were present.

Averaging closed chamber methane fluxes from wet polygon centers and drier sites, respectively, and weighing them according to the distribution of wet (40%) and drier (60%) surfaces classes results in an up-scaled closed chamber flux of 39.11 mg m^{-2} d^{-1}, which is double the eddy covariance flux during the same time period.

Discussion

Discussion

Results from eddy covariance measurements differ from closed chamber data both in terms of the seasonal variation and the identified controls on methane emissions. While ecosystems scale fluxes do not show much of a seasonal course, results from low-center polygon closed chambers show a pronounced decrease of methane emission towards the end of the season, which is more in agreement with most studies and results from deterministic process-based models used for larger scale modeling (Kirschke et al. 2008).

Emission peaks also do not match on the different scales. While ecosystem scale emission peaks usually coincide with high wind speed, low air pressure, and generally "bad weather" conditions, the largest emission from polygon centers as measured by closed chambers occurred during warm and dry days. However, the very weak peaks visible in closed chamber data from the rim and high-center micro-site tend to be more in agreement with eddy covariance emission peaks.

These differences in the seasonal dynamics may partly be explained by the very different hydrological conditions of the investigated micro-sites in combination with the importance of plant-mediated transport of methane (Kutzbach et al. 2004): in the wet polygon centers, water levels were always at or above the soil surface. Here, higher water levels could lead to decreased methane emission, as more vegetation becomes submerged and plant-mediated transport decreases. In addition, higher temperatures likely increase microbial methane production close to the surface. Hence, warm weather and falling water levels could actually increase emissions as long as the water table remains above the surface. At "drier" micro-sites, on the other hand, storm systems with strong precipitation events lead to a temporary increase in anaerobic soil volume and an increase in methane production, while lower temperatures have a negative effect on the activity of methane oxidizing microbes in the upper horizons of the active layer.

However, a large influence on the ecosystem methane flux can also be ascribed to open-water surfaces such as polygon ponds and thermokarst cracks, which were not covered by the closed chamber measurements but were present in the eddy covariance footprint. Diffusive and turbulent gas transfer between water and atmosphere is known to be proportional to the third power of the wind speed (Wanninkhof & McGillis 1999) and observation of methane ebullition (Walter et al. 2006) in the field indicates that water bodies are an important contributor to ecosystem methane efflux. These micro-sites must be included in future small-scale measurements within the eddy covariance footprint in order to more accurately scale chamber flux measurements to larger areas. A more detailed analysis of the small-scale variability and the scaling problems is in preparation.

The discrepancies in the results on the different scales also highlight the need for more non-intrusive and spatially integrating measurements from high-latitude ecosystems to verify and understand the results produced by the eddy covariance method. Larger scale methane emission models that have previously been developed on the basis of closed chamber data only, should incorporate new findings from eddy covariance or other non-intrusive techniques.

Our findings raise the question to which extent methane fluxes in permafrost ecosystems are controlled by near-surface controls including atmospheric boundary layer conditions and vegetation, or by soil characteristics and processes in the deeper active layer including microbial community structure and activity.

Acknowledgments

We would like to thank the members of the joint Russian-German expedition LENA-2006, especially Waldemar Schneider (AWI), Dmitry Yu. Bolshianov (AARI, St. Petersburg), Mikhail N. Grigoriev (Permafrost Institute, Yakutsk), Alexander Y. Derevyagin (Moscow State University), and Dmitri V. Melnitschenko (Hydro Base, Tiksi) for all logistical, travel, and administrative arrangements. We are also grateful to Günther "Molo" Stoof for technical support in the field and to Barnim Thees for valuable input regarding the statistical analysis.

References

Boike, J., Hinzman, L.D., Overduin, P.P., Romanovsky, V., Ippisch, O. & Roth, K. 2003. A comparison of snow melt at three circumpolar sites: Spitsbergen, Siberia, Alaska. *Proceedings of the Eighth International Conference on Permafrost, Zürich, Switzerland*: 79-84 pp.

Boike, J., Wille, C. & Abnizova, A. 2008. The climatology and summer energy and water balance of polygonal tundra in the Lena River Delta, Siberia. *J. Geophys. Res.* (in press).

Christensen, T. R., Friborg, T., Sommerkorn, M., Kaplan, J., Illeris, L., Soegaard, H., Nordstroem, C. & Jonasson, S. 2000. Trace gas exchange in a high-arctic valley 1. Variations in CO_2 and CH_4 flux between tundra vegetation types. *Global Biogeochem. Cycles* 14(3): 701-714.

Fan, S.M., Wofsy S.C., Bakwin P.S., Jacob D.J., Anderson S.M., Kebabian P.L., McManus J.B., Kolb C.E. & Fitzjarrald D.R. 1992. Micrometeorological measurements of CH_4 and CO_2 exchange between the atmosphere and subarctic tundra. *J. Geophys. Res.* 97(D15): 16,627-16,643.

Friborg, T., Christensen T.R., Hansen B.U., Nordstroem C. & Soegaard H. 2000. Trace gas exchange in a high-arctic valley: 2. Landscape CH_4 fluxes measured and modeled using eddy correlation data. *Global Biogeochem. Cycles*, 14(3): 715–724.

Grigoriev, N.F. 1960. The temperature of permafrost in the Lena delta basin – deposit conditions and properties of the permafrost in Yakutia. *Yakutsk*, 2: 97-101.

Harazono, Y., Mano, M., Myiata, A., Yoshimoto, M., Zulueta R.C., Vourlitis G.L., Kwon H. & Oechel W.C. 2006. Temporal and spatial differences of methane flux at arctic tundra in Alaska. *Mem. Natl. Inst. Polar Res.*, Spec. Issue 59: 79-95.

Hargreaves, K.J., Fowler, D., Pitcairn, C.E.R. & Aurela M. 2001. Annual methane emission from Finnish mires estimated from eddy covariance campaign measurements. *Theor. Appl. Climatol.*, 70: 203-213.

Kirschke, S., Guenther, K.P., Wisskirchen, K., Sachs, T. & Dech, S. 2008. Methane Emission from Siberian Wet Polygonal Tundra on Multiple Spatial Scales: Process-based Modeling of Methane Fluxes on the Regional Scale, Lena Delta. (this proceeding)

Kotlyakov, V. & Khromova T. 2002. Permafrost, snow and ice. In: *Land Resources of Russia*. CD-ROM. V. Stolbovoi & I. McCallum (eds.), International Institute of Applied Systems Analysis and the Russian Academy of Science, Laxenburg, Austria.

Kutzbach, L., Wagner D. & Pfeiffer E.-M. 2004. Effect of microrelief and vegetation on methane emission from wet polygonal tundra, Lena Delta, Northern Siberia. *Biogeochemistry* 69: 341-362.

Kutzbach, L. 2006. The exchange of energy, water and carbon dioxide between wet arctic tundra and the atmosphere at the Lena River Delta, Northern Siberia. *Reports on Polar and Marine Research* 541.

Kutzbach, L., Wille, C. & Pfeiffer, E.-M. 2007. The exchange of carbon dioxide between wet arctic tundra and the atmosphere at the Lena River Delta, Northern Siberia. *Biogeosciences* 4: 869-890.

Liebner, S. & Wagner, D. 2007. Abundance, distribution and potential activity of methane oxidizing bacteria in permafrost soils from the Lena Delta, Siberia. *Environmental Microbiology* 9(1): 107-117.

Reeburgh, W.S., King J.Y., Regli S.K., Kling G.W., Auerbach N.A. & Walker, D.A. 1998. A CH_4 emission estimate for the Kuparuk River basin, Alaska. *J. Geophys. Res.* 103(D22): 29,005-29,014.

Sachs, T., Wille, C., Boike, J. & Kutzbach, L. 2008. Environmental controls on ecosystem-scale CH_4 emission from polygonal tundra in the Lena River Delta, Siberia. *J. Geophys. Res.* in press.

Schuchard-Ficher, C., Backhaus, K., Humme, U., Lohrberg, W., Plinke, W. & Schreiner, W. 1982. *Multivariate Analysemethoden. Eine anwendungsorientierte Einführung*. Berlin, Heidelberg, New York: Springer-Verlag, 346 pp.

Schuepp, P.H., Leclerc M.Y., MacPherson J.I. & Desjardins R. L. 1990. Footprint prediction of scalar fluxes from analytical solutions of the diffusion equation. *Boundary-Layer Meteorology* 50(1-4): 355-373.

Schwamborn, G., Rachold, V. & Grigoriev, M.N. 2002. Late Quaternary sedimentation history of the Lena Delta. *Quaternary International* 89: 119-134.

Soil Survey Staff. 1998. *Keys to Soil Taxonomy 8th Edition*. Blacksburg, Virginia: Soil Conservation Service.

Walter, K.M., Zimov, S.A., Chanton, J.P., Verbyla, D. & Chapin III, F.S. 2006. Methane bubbling from thaw lakes as a positive feedback to climate warming. *Nature* 443: 71-75.

Wanninkhof, R. & McGillis, W.R. 1999. A cubic relationship between air-sea CO_2 exchange and wind speed. *Geophysical Research Letters* 26(13): 1889-1892.

Whalen, S.C. & Reeburgh, W.S. 1992. Interannual variations in tundra methane emission: A 4-year time series at fixed sites, *Global Biogeochem. Cycles* 6(2): 139-159.

Wille, C., Kutzbach, L., Sachs, T., Wagner, D. & Pfeiffer, E.-M. 2008. Methane emission from Siberian arctic polygonal tundra: Eddy covariance measurements and modeling. *Global Change Biology* (in press).

Refinement of Physical Land Scheme for Cold-Region Subsurface Hydrothermal Processes and Its Impact on High-Latitude Hydroclimate

Kazuyuki Saito
International Arctic Research Center (IARC), University of Alaska Fairbanks, Fairbanks, USA
Frontier Research Center for Global Change, Japan Agency for Marine-Earth Science and Technology (JAMSTEC), Yokohama, Japan

Abstract

Sensitivity experiments on subsurface and atmospheric hydroclimate were conducted to examine different levels of complexity in a physical terrestrial scheme in a coupled global climate model (GCM). In one-dimensional off-line experiments local impacts were examined for (1) snow cover and the organic layer, (2) soil column depth, and (3) hydrothermal parameterization in which effects of ground ice and unfrozen water under the freezing point are taken into account. The results reaffirmed the crucial role of snow and the organic layer for subsurface thermal regime. A total depth of 20 m was needed for physically-consistent simulation in the cold regions. An on-line simulation coupled with the atmospheric GCM showed the importance of the refined parameterization for better climatology and seasonality of the active layer and the high-latitude hydroclimate. The findings provide a basis for better physical representations in GCMs to investigate the hydroclimate of the Arctic, and on the larger spatial scales.

Keywords: frozen ground; global climate model; hydroclimate; physical land surface scheme.

Introduction

Global climate models (GCMs) are a useful tool to investigate large-scale permafrost and seasonally frozen ground (frozen ground, hereafter), and its impacts on the climate system, where the multiple feedbacks and interactions connect different components within the system. However, the current implementation and performance of physical terrestrial schemes in the state-of-the-art regional/global models still need substantial improvement and optimization on the resolved local physical (and biogeochemical) processes and properties, networking between different climate components, the initial and boundary conditions, and others, to be fully used.

Previous studies have pointed out the importance of a number of factors: (1) snow cover and top organic layer (e.g., Saito et al. 2007, Beringer et al. 2001), (2) total resolved depth of the soil column (Saito et al. 2007, etc.), (3) hydrothermal parameterization of the soil property, namely consideration of both solid and liquid water under the freezing point (e.g., Romanovsky & Osterkamp 2000, Flerchinger & Saxton 1989). Recently, several studies have appeared to examine the importance of those factors using the National Center for Atmospheric Research Land Surface Model (NCAR LSM) (Alexeev et al. 2007, Nicolsky et al. 2007, Yi et al. 2007). In this study, sensitivity experiments were conducted to evaluate the impact of the aforementioned factors using a land surface scheme in a Japanese-developed coupled global climate model. One-dimensional off-line experiments were intended to examine local subsurface hydrothermal impacts. On-line experiments coupled with the atmospheric component investigated the impacts on the high-latitude hydroclimate both below the surface and in the atmosphere.

Methods

Model and data

The numerical model used in the present study was CCSR/NIES/FRCGC MIROC3.2 coupled Atmosphere-Ocean global climate model (K-1 developers 2005), and the physical terrestrial scheme, MATSIRO (Takata et al. 2003). On-line experiments were performed at the horizontal resolution of Triangular 42 truncation (T42; ca. 2.5° by 2.5°).

For the off-line experiments, two different observational forcing datasets, both from the arctic tundra climate zones, were used; one taken at Barrow, AK, for 1990 through 2003 (soil temperatures were available only for the limited periods) provided by the Permafrost Laboratory, Geophysical Institute, University of Alaska Fairbanks (Mölders & Romanovsky 2006), and the other taken at Tiksi, Russia, for 1999 through 2005, provided by the Institute of Observational Research Center for Global Change, Japan Agency for Marine-Earth Science and Technology (JAMSTEC), Japan (H. Yabuki, personal communication). The period analyzed in this paper is from August 2002 to July 2003, since it is the only period during which Barrow and Tiksi observations overlapped.

Experimental conditions of the off-line experiments are summarized in Table 1. In off-line experiments (s4, g4, m4, n4, and o4) impact of snow cover and the top organic layers were examined in a 4 m soil column. Snow amount is prognosticly calculated in the model, thus different amounts of precipitation were applied. Organic soil was specified by prescribing different values of thermal conductivity in the top layer. The original hydrothermal parameterization (C) does not consider the effect of either ground ice or unfrozen water on thermal properties under the freezing point. The refined parameterization (R) took both into account. Detailed explanation of the hydrothermal parameterization is found in Saito (2008). In another set of experiments (C4, C10, C50;

Table 1. Summary of the settings and conditions for the off-line experiments.

Name	Total depth (m)	Depth of soil layer boundaries (m)	Spin-up (year)	Precipitation	Thermal conductivity of top organic layers (W/m/K)[a)]	Thermal param. [b)]
s4	4	0.05, 0.25, 0.50, 1.0, 2.0, 4.0	30	5 times larger than observed	N/A	C
g4				As observed		
m4				No snow		
n4					0.1	
o4					0.025	
C4	4	0.05, 0.25, 0.50, 1.0, 2.0, 4.0	100	As observed	0.1	C
R4						R
C10	10	0.05, 0.25, 0.50, 1.0, 2.0, 3.5, 6.0, 10	100	As observed	0.1	C
R10						R
C50	50	0.05, 0.25, 0.50, 1.0, 2.0, 3.5, 6.0, 9.0, 14, 21, 30, 40, 50	100	As observed	0.1	C
R50						R

a) Specified only in the top layer (5 cm thick). Default value is that of mineral soil. b) Parameterization methods for soil thermal conductivity and heat capacity. C: Conventional, R: Ground ice and unfrozen water. See text for details.

R4, R10, R50), difference in total soil column depth was examined at three different depths (Table 1.).

Four integrations were performed online for combinations of presence/absence of the top organic soil layers in taiga and tundra zones (TOS/NoTOS), and the hydrothermal parameterization in the conventional (C) or refined (R) form. The top organic layer was prescribed only in tundra and taiga regions. The soil column depth was set to 4 m in all cases to focus on the above effects. The model was forced by monthly climatological sea surface temperatures and sea ice concentrations for the period between 1980 and 2000. Ten year outputs after 20-year spin-up were used for analysis.

Results

Near-surface conditions

Annual soil temperature range is shown with depth in Figure 1. Similarly, the seasonal evolution in the near-surface hydrothermal regime is shown in Figure 2. For both sites, Barrow and Tiksi, excessive snow cover led to a smaller annual amplitude and warmer soil temperatures for all layers; in Tiksi, the zero curtain was found below 2.5 m (s4; Figs. 1, 2).

When the snow amount and, therefore, the snow-covered period were more realistically simulated (g4), the thermal regime was closer to the observed. When snow cover was removed, cooling in winter was expectedly enhanced, whereas summer temperatures showed little impact (m4). On the contrary, inclusion of the top organic layer exerted a larger impact in summer than in winter for both areas (n4 and o4). The wetness of the upper soil layers was different with and without the top organic layer; it was kept close to saturation when the organic layer was present (Fig. 2c). With a stronger organic layer effect (o4), freezing and thawing at 20 cm depth occurred at a later time and proceeded more slowly.

Total depth and thermal parameterization

Examination of different total soil column depths showed

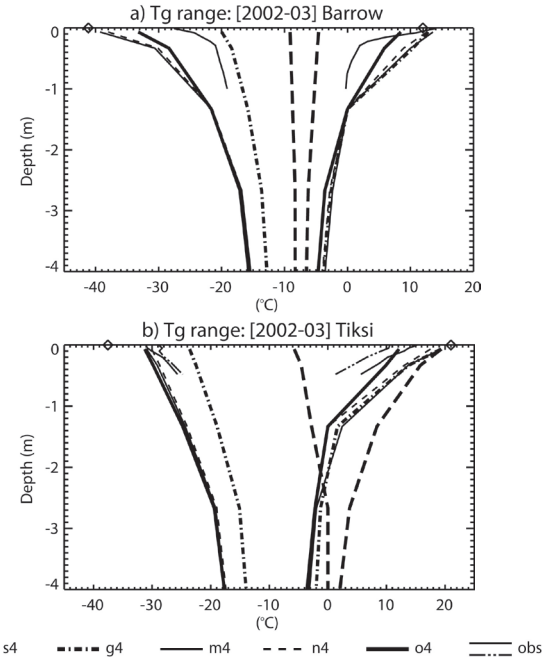

Figure 1. Annual range of soil temperature with depth, simulated for a one-year period from August, 2002 to July, 2003 for a) Barrow and b) Tiksi. Thin lines down to 1 m at Barrow and .48 m (two locations) at Tiksi are the observed values. Thick dashed lines are for experiment s4, and similarly, the thick dot-dashed for g4, the thin solid for m4, the thin dashed for n4, and the thick solid for o4.

that 15 m or below that annual amplitude is almost zero so that the zero heat flux condition at the lower boundary should be justified (Fig. 3). The refined parameterization (solid lines) simulated larger annual amplitude (warmer maximum) of soil temperature between 2 and 10 m. The equilibrated temperature below 15 m was warmer for the R runs by about one degree.

On-line experiments

Figure 4 shows the latitudinal profile of atmospheric and hydrological variables in January and July, averaged over

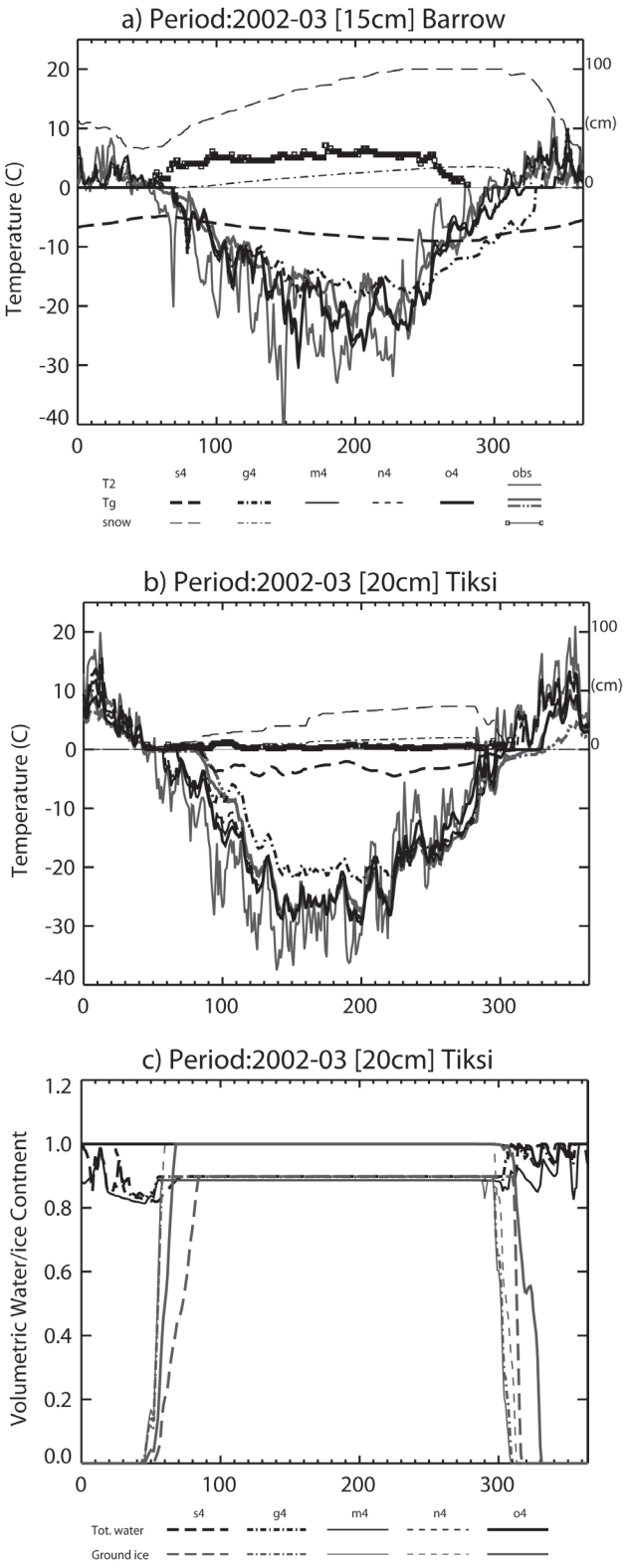

Figure 2. Seasonal evolution of soil temperature at (a) Barrow at the depth of 15 cm, (b) Tiksi at 20 cm depth. Line styles are the same as in Figure 1, except the thin solid gray line for surface air temperature at 2 m [forcing data]. Thinner lines above the 0 level are snow depth, and observed snow depth is shown with box symbols. (c) Seasonal evolution of soil moisture (thick lines) and ground ice content (thin gray lines), both relative to the saturation, at Tiksi; no observations were available for the period.

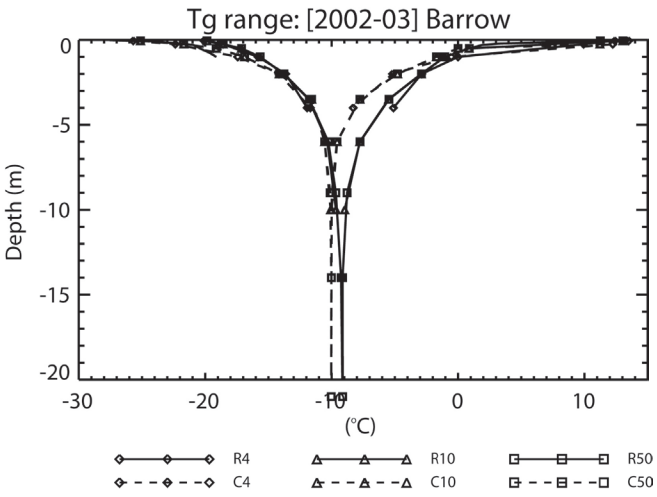

Figure 3. Annual range of soil temperatures, against depth, for different soil column depths (4 m, 10 m, and 50 m), and for the different thermal parameterizations. Dashed lines show the result of the conventional parameterization (C), while solid lines show that of the refined one (R).

land grids (excluding ice-covered areas) in each zonal band. Near-surface hydrologic conditions (i.e., soil moisture content) showed little difference between the four runs in all months (not shown), but subsurface thermal regimes (and ground ice content) differed to a substantial degree by the thermal parameterization (Figs. 4e, 4g). In the R4 runs it was cooler and a substantial amount of ice was retained in the summertime.

As for the atmospheric impact, surface air warmed faster and greater from spring to summer in R4 (Fig. 4a), and, similarly, cooled faster and greater in winter (Fig. 4b). The difference was most apparent in high latitudes. This led to an earlier and larger snow accumulation in winter (not shown), although precipitation did not vary much between the four simulations (Figs. 4c, 4d) in the high-latitudes. It was in the lower latitudes during summer monsoonal period that large precipitation differences were found; wetting of the Tibetan Plateau and drying of coastal China (not shown). The differences were canceled when taking the zonal average in Figure 4d. Land-average total annual runoff did not vary greatly between integrations; however, its seasonal distribution did change between the R4 and C4 runs. During the high-latitude melting season, runoff was greater for the R4 runs due to shallower active layer depth (Fig. 4g). On the contrary, it was smaller in summer because a larger amount of soil moisture was removed to the atmosphere by evapotranspiration (Fig. 4h, cf. Fig. 4b).

Distributions of frozen ground depended on both the organic soil and the hydrothermal parameterization (Fig. 5). The classification of the frozen ground followed the same methodology used in Saito et al. (2007). *Near-surface permafrost* is defined as an area with the maximum active layer thickness shallower than the model soil depth, in this case 4 m, for two consecutive years. Similarly, *seasonally-frozen ground* is defined as an area with its soil experiencing

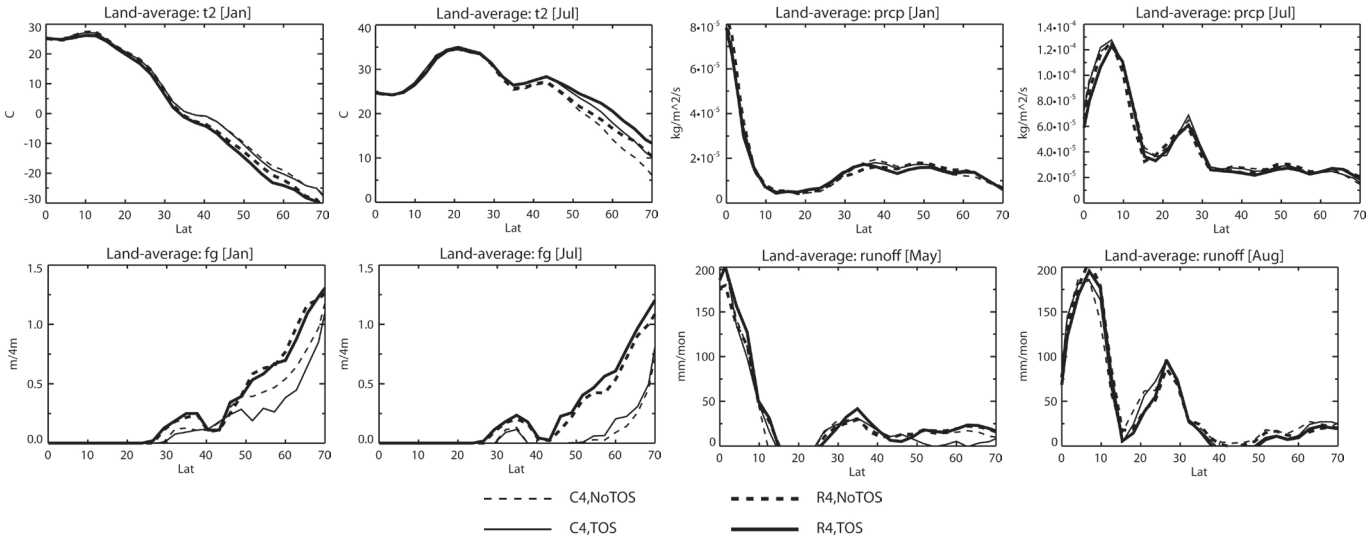

Figure 4. Latitudinal profiles of the a) surface air temperatures (T2), c) precipitation (total of liquid and solid), e) total ground ice amount in the 4 m column, averaged over land grids (except for permanently ice-covered areas) in January. Thick lines show the results by the refined thermal parameterization, whereas the thin lines show the conventional one. Solid lines denote the top-organic-soil (TOS) runs, and dashed lines the no-top-organic-layer (NoTOS) runs. Except for July b), d), and f) are same as a), c), and e). Except for runoff in May and August g) and h) are same as a) and b), respectively.

subfreezing at any time of a year. Distribution of near-surface permafrost (dark shades) is surprisingly different between R4 and C4; in the C4 runs it is very scarce largely due to excessive warming and thawing in summer (Fig. 4f). In contrast the R4 runs overestimated, when compared to the present-day observational estimate (e.g., Fig. 5c in Saito et al. 2007). Seasonally-frozen ground distribution did not differ much between runs and the observations (again, cf. Fig. 5c in Saito et al. 2007) for it is largely determined by surface air temperatures, which did not vary south of 30°N between runs (Figs. 4a, 4b).

Discussion

Weather-regime difference

The impact of snow cover appeared differently in Barrow and Tiksi, although both sites are located in arctic tundra, (Figs. 1, 2). The exaggerated warming in the s4 case for Tiksi likely resulted from warmer summer surface air temperatures (T2), which led to complete thawing down to 4 m in summer and to shallower snow cover climatology in winter. Tiksi's annual T2 range was -37.6°C to 21.0°C, while it was -41.2°C to 12.0°C for Barrow, for the examined period. Average snow depth was 6.7 cm for Tiksi and 23.0 cm for Barrow, although snow covered both sites for about 63% of the period (63.5% for Tiksi, and 62.4% for Barrow). Therefore, snow cover greater than observed had a larger insulation impact in Tiksi than in Barrow. There we also found seasonal differences affected the quality of the simulations: for the early snow accumulation period in Tiksi (days 50–85 in Fig. 2b) soil temperature was simulated best by the g4 run, whereas it was the no snow cover cases (m4, n4 and o4) that simulated the thermal regime best. In Barrow, discrepancies between the simulated and observed thermal regime are large during the snow melt season. Delayed snow melt led to slower subsurface warming (days 260–320 in Fig. 2a). These discrepancies, however, may be due in part to improper snow calculation in the model; it is prone to slower accumulation in the early cold season, greater insulation effects in midwinter, and slower melting in the warming season (Figs. 2a, 2b).

Another source of discrepancy from the observed thermal regime was the depth of the top organic layer. It is about 30 cm in Barrow and more than 50 cm in Tiksi, as inferred by the observed soil temperature profiles (cf. Figs. 1a, 1b). Hence, the prescribed organic layer of 5 cm may have been insufficient.

The experiments showed similar outcomes in Barrow and Tiksi, but also gave different responses in some variables or in different seasons, although both sites are located in the same arctic tundra climate zone. Similar evaluations with observations taken at places with varying weather and bio-climate regimes (not only arctic tundra, but also arctic taiga, high-altitude areas, etc.) will be instrumental to verify the findings in the present study, confirm the generality, and understand the heterogeneity between the regions more quantitatively. Similarly, knowledge of the geographical distribution of depth and physical/ biogeochemical properties of the organic layers, for example, will also be beneficial for more plausible future climate predictions.

Interactions with the atmosphere

Implementation of the physically-based parameterization of the soil hydrothermal properties impacted not only the subsurface but also the near-surface atmosphere. Surface air temperature in high latitudes decreased by about 5°C in winter (zonal average, only over land), and increased about 2°C in summer (Figs. 4a, 4b). Takata (2002) and

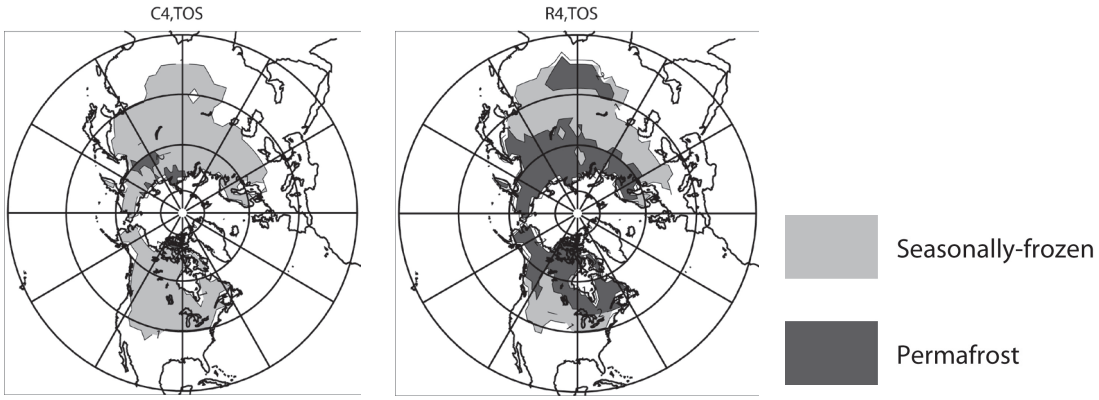

Figure 5. Distribution of near-surface permafrost (dark shades) and seasonally-frozen ground (light shades) simulated with a) the conventional thermal parameterization and b) the refined thermal parameterization. Near-surface permafrost is defined as the areas in which some layers are frozen for more than two consecutive years. Seasonally-frozen ground is defined as the areas in which soil temperatures in any layer is below 0°C at least once a month.

Takata and Kimoto (2000) have previously examined the impact of land processes (including freezing/thawing, but with "conventional" parameterizations) on the atmospheric hydroclimate. They showed changes in the regional-scale atmospheric circulations, and argue that the warming of high-latitude land in summer and the cooling in winter enhance the thermal contrast between the continents and oceans, leading to a stronger monsoonal circulation.

In high latitudes, surface heat fluxes were different between C4 and R4 runs. In the R4 runs, both sensible and latent heat fluxes to the atmosphere were stronger from spring to early summer due to a higher conductivity of heat with ground ice present, and to the near-surface moisture abundance resulting in a warmer near-surface air. From autumn to winter, again because of a higher heat conductivity, downward sensible heat flux (i.e., from the atmosphere to the ground) was stronger in the R4 runs, leading to a cooler air.

Inclusion of the top organic soil (50 cm for taiga and 20 cm for tundra, shown as difference between solid and dashed lines in Fig. 4) further added to the annual amplitude of surface air temperature, but stabilized the annual change in the subsurface ground ice content. This is a reasonable response because the organic layers tend to thermodynamically decouple the atmosphere and the subsurface more efficiently.

Overestimation of the near-surface permafrost in the R4 runs likely resulted from prescribed organic layers being too thick in Central to Western Eurasia, Central to Southern Canada, and the Tibetan Plateau (Fig. 5). On the contrary, the near absence of near-surface permafrost in the C4 runs was primarily due to the warmer T2 in winter with the prescribed sea surface temperature experiments as compared to the coupled ocean runs (Saito et al., 2007). The cause of these differences needs to be investigated further.

Summary and Implications

A series of sensitivity experiments performed off- and on-line in the present study showed the importance of representing complexity for frozen ground simulations. Of crucial importance in the physical terrestrial schemes is physically-based hydrothermal parameterization; that is, consideration of ground ice and unfrozen water under the freezing point. It affects not only subsurface hydrothermal regimes, but also the exchange of energy and water between the soil and the atmosphere. For a physically consistent thermal simulation, a soil column of 20 m or deeper was found necessary. Implementation of these components should be seriously considered when impact of atmospheric warming on frozen ground and its feedback to the atmosphere are to be investigated.

Snow conditions and soil properties (such as top-layer organic soil) need more localized attention. Snow calculations still require a considerable amount of elaboration, on both the atmospheric (cloud formation, advection, radiation, atmospheric thermal and hydrological conditions, etc.), and terrestrial (snow microphysics, radiative properties, thermodynamics, and their regional differences) sides of the GCM. In the current version of the model, the organic soils are only prescribed and do not vary in the course of integrations. This may suffice for short-term simulations, for example, for 30 years. However, one of the anticipated targets in the next Assessment Report of the Intergovernmental Panel for Climate Change (IPCC), is to consider a timescale where the residence timescale of subsurface organic contents in the cold regions matter. For such longer-term simulations, in which 100 or 300 years are targeted, adaptation strategy will be needed to reflect biogeochemical changes in time.

Acknowledgments

This work was partly supported by (1) the Global Environment Research Fund (B-061) of the Ministry of the Environment, Japan, (2) Ministry of Education, Culture, Sports, Science and Technology (MEXT), Japan, and (3) the National Science Foundation under Agreement No. ARC-0327664, USA. All numerical integrations were run on the NEC SX-8 supercomputer at JAMSTEC. The author would

like to thank the Permafrost Laboratory at the Geophysical Institute, University of Alaska Fairbanks, and also the Institute of Observational Research for Global Change, JAMSTEC, for providing observational data.

References

Alexeev, V.A., Nicolsky, D.J., Romanovsky, V.E. & Lawrence, D.M. 2007. An evaluation of deep soil configurations in the CLM3 for improved representation of permafrost. *Geophys. Res. Lett.* 34: L09502, doi:10.1029/2007GL029536.

Beringer, J., Lynch, A.H., Chapin, F.S., III, Mack, M. & Bonan, G.B. 2001. The representation of Arctic soils in the land surface model: the importance of mosses. *J. Climate* 14: 3324-3335.

Flerchinger, G.N. & Saxton, K.E. 1989. Simultaneous heat and water model of a freezing snow-residue-soil system I. Theory and development. *Trans. ASAE* 32: 565-571.

K-1 Model Developers. 2004. K-1 coupled GCM (MIROC) description. Tech. Rep. 1. H. Hasumi & S. Emori (eds.), Cent. for Clim. Syst. Res., Univ. of Tokyo, Kashiwa, Japan. 34 pp.

Molders, N. & Romanovsky, V.E. 2006. Long-term evaluation of the hydro-thermodynamic soil-vegetation scheme's frozen ground/permafrost component using observations at Barrow, Alaska. *J. Geophys. Res.* 111: D04105, doi:10.1029/ 2005JD005957.

Nicolsky, D.J., Romanovsky, V.E., Alexeev, V.A. & Lawrence, D.M. 2007. Improved modeling of permafrost dynamics in a GCM land-surface scheme. *Geophys. Res. Lett.* 34: L08501, doi:10.1029/ 2007GL029525.

Romanovsky, V.E. & Osterkamp, T.E. 2000. Effects of unfrozen water on heat and mass transport processes in the active layer and permafrost. *Permafrost Periglacial Processes* 11: 219-239.

Saito, K., Kimoto, M., Zhang, T.J., Takata, K. & Emori, S. 2007. Evaluating a high-resolution climate model: Simulated hydrothermal regimes in frozen ground regions and their change under the global warming scenario. *J. Geophys. Res.* 112: F02S11, doi:10.1029/ 2006JF000577.

Saito, K. 2007. Cold-region subsurface hydro-thermal sensitivity of physical land scheme in global climate model: idealized off-line evaluation. *Geophys. Res. Lett.* In preparation.

Takata, K. 2002. Sensitivity of land surface processes to frozen soil permeability and surface water storage. *Hydrol. Processes* 16: 2155-2172.

Takata, K. & Kimoto, M. 2000. A numerical study on the impact of soil freezing on the continental-scale seasonal cycle. *J. Meteorol. Soc. Jpn*. 78: 199-221.

Takata, K., Emori, S. & Watanabe, T. 2003. Development of the minimal advanced treatments of surface interaction and runoff. *Global Planet. Change* 38: 209-222.

Yi, S., Woo, M.K. &Arain, M.A. 2007. Impacts of peat and vegetation on permafrost degradation under climate warming. *Geophys. Res. Lett.* 34: L16504, doi:10.1029/2007GL030550.

Zhang, T., Barry, R.G., Knowles, K., Ling, F. & Armstrong, R.L. 2003. Distribution of seasonally and perennially frozen ground in the Northern Hemisphere, in *Proceedings of the 8th International Conference on Permafrost, 21–25 July, 2003, Zurich, Switzerland*, vol. 2, M. Phillips, S.M. Springman & L.U. Arenson, (eds.), Brookfield, VT: A.A. Balkema, 1289-1294.

Portable Shallow Drilling for Frozen Coarse-Grained Material

Tohru Saito
International Arctic Research Center, University of Alaska Fairbanks
Kenji Yoshikawa
Water and Environmental Research Center, University of Alaska Fairbanks

Abstract

We are drilling boreholes for a permafrost outreach program that involves schools in arctic regions. The purpose of the project is to establish permafrost-monitoring stations at schools and have students and teachers participate in gathering data. We drill a 6 m deep borehole for the monitoring stations to measure ground temperatures. There are more than 50 sites established, and many of the schools are located in remote villages in Alaska and Canada. This created a great opportunity and necessity to develop a portable, lightweight, small-diameter drill system. However, permafrost conditions and local geology vary greatly. A portable drill system is strongly affected by the grain size of the frozen materials. The design for the auger and coring bits (mechanical properties) for fine-grained, frozen soils are already well developed. However, frozen gravel, boulders, and glacial sediments are extremely difficult to drill, even when using heavier track-mounted hydraulic drill systems. In our outreach project, we tried to develop a method of drilling through frozen gravel using a portable drill system. This study presents our experiments and an introduction to different techniques for a portable drill system.

Keywords: auger; frozen gravel; percussion drill; portable drill; rotary percussion system.

Introduction

Portable drilling systems were probably developed as percussion systems to find shallow groundwater. Sample percussion systems were established and widely used in Japan as 'Kazusa-hori' in the early 18th century. After the industrial revolution, rotary-type drilling systems became more popular than the traditional percussion systems. Today, there are many more different types of drill systems widely available. Table 1 lists the classification of various drilling systems.

Drilling systems should meet the following conditions to be useful for the permafrost outreach program:

1. Lightweight: All systems should be compact and light enough to carry on a small airplane, helicopter, snowmobile, and small boat to reach remote villages.
2. Portable: The operation should only require one or two persons to start and complete all work to establish the monitoring station.
3. Small diameter hole: The hole should be as small as possible to minimize site disturbance, and the borehole only needs to be large enough to install a 1-inch (25 mm) PVC casing.
4. Versatile: The drill should be able to penetrate different types of frozen ground (materials). Most sites consist of widely different types of sacrificial geology. It is important to be able to adapt to any kind of ground condition to successfully drill at each school.

Drilling techniques for fine-grained soils, such as frozen silt and sand, are well researched and developed, especially by the US Army Corps of Engineers Cold Regions Research and Engineering Laboratory (CRREL) (e.g., Mellor 1976, Lawson & Brockett 1980, Sellmann & Brockett 1986, 1988, Calmels et al. 2005). Sellmann & Mellor (1986) summarized extraordinary work on drill-bit design for frozen fine-grained soils. They concluded that for best performance, the drill bits should (1) stay sharp as long as possible, (2) resist damage from impact with any coarse-grained material, and (3) be large enough to allow penetration at the maximum feasible design rates. Lack of adequate clearance angle between bits and flute is a common problem.

This study focuses on attributes of a portable drilling system for frozen, coarse-grained materials, such as frozen gravel, because this material is one of the most difficult materials to drill and is very common around the study sites. We also need to be able to drill boreholes through these materials in many remote villages.

Table 1. Popular drilling systems used today. Experiments on prototype portable drilling systems are indicated.

type	system	in this study
percussion	rope drill	no
	rod drill	yes
	hammer drill	yes
	down-hole drill (in line drill)	yes
rotary	spindle drill	yes
	rotary table drill	no
	drive head drill	yes
	power swivel drill	yes
	bit rotation (turbo drill, dyne drill, electro drill)	no
other	earth auger	yes
	push casing	yes

Figure 1. Hot water jet system employed for old borehole (left) and prototype lightweight compact disassembled rotary drill with air swivel (right).

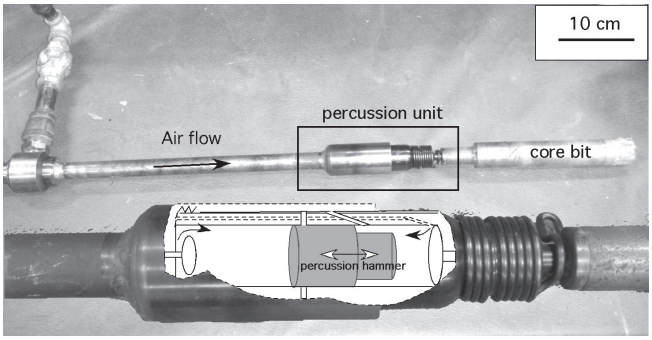

Figure 2. Prototype down-hole drill unit (in-line percussion drill)

Methods

Drilling system

Water jet drill

Water jet (hot water jet) systems (Fig. 1) are widely used for glaciological investigations. This method is definitely effective for boreholes on glaciers, sea ice, and ice rich permafrost. We used a Honda 5HP pressure jet pump with a custom-made nozzle and also tested a hot water jet unit from Kovacs Enterprise Ltd.

Jackhammer

A jackhammer is a powerful tool to break hard, solid material such as rock or ice, but limited drill depth is a weak point of this tool. Usually jackhammers can only dig 1–3 m or less. However, we used a gas-powered Swedish rotation jackhammer (Pionjar 120) that could drill a hole 6 m deep to bedrock, even through granite. The jackhammer was capable of producing two actions: percussion and rotation. By design, percussion is the primary action and rotation is the secondary action. Problems occur when the ground material melts from the drilling. The borehole becomes wet from the thawing silt, and the rotating driving shaft starts to stick to the mud and eventually stops rotating. The wet silty material and melt water generated by the action also absorb the percussion power of the jackhammer. As a result, jackhammers work wonderfully in dry bedrock but not in frozen silty gravel.

Figure 3. Portable hydraulic spindle (rotary) drill with air swivel. This is lightweight unit compared with track rig machine, but it is still heavy (more than 100 kg) to carry around.

Down-hole drill (in-line percussion drill)

It is generally known that shock and vibration action is very efficient for gravel or bedrock drilling to separate each grain (Borisovich 1990). We tried to employ this action in an adaptation with our portable drilling system. We modified the in-line shock actions using an air hammer tool (Aircoworld air hammer: bore diameter 19.05 mm, 4500 blow per minute (RPM), average air consumption 143 cubic meter per minute) (Fig. 2). This unit has about 100 g of weight moving up and down in the cylinder 4500 times per minute controlled by pressurized air. Air is supplied by the air compressor through the ¾-inch steel rod.

Rotary drill and earth auger

Both rotary drills and earth augers use rotation action for drilling. We used three different types of rotary drills: (1) Electric drills are easiest to use and work well in cold temperatures. (2) Mechanical (gasoline powered?) drills (Fig. 1) are probably the most commonly used portable drills, because they are relatively lightweight and strong, but they can be hard to start in colder temperatures. (3) Hydraulic drills are best for deeper boreholes. They are easy to handle and strong, which is why most commercial drillers use this method. Hydraulic systems, however, require many different heavy components that prevent them from converting into a portable system (Fig. 3). Also the hydraulic fluid needs to be kept warm during operation.

Percussion drill

The electric percussion/rotation drill is one of the best portable drill systems. We tried the heavy-duty, electric percussion drill to see if we could drill in permafrost (Fig. 4).

Figure 4. Electric percussion drill with water swivel. This hammer drill has 14A/120V power with 120–250 RPM rotation with impact (energy: 13.3 ft/lb)

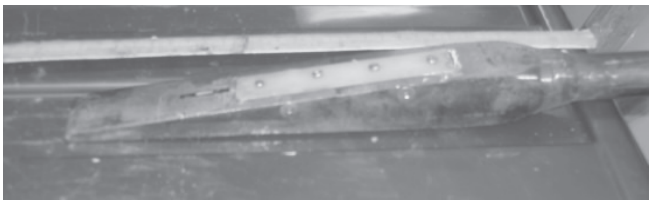

Figure 5. Prototype percussion drill bit with thermistor and electric resistivity contact points (Wenner configuration).

Drill bits

Drill bits are one of the most important components of drilling. We tested many different bits for this experiment. Auger bits with a rotating system are faster and easier to drill. However, this is difficult in a gravel layer. In general, core bits are used for core sampling but can also be used for drilling in gravel layers. We used several different shapes of core bits with carbide or diamond chips.

Drill bit experiment

The drill bit comparison experiment was carried out in an outdoor laboratory using a controlled frozen soil medium, comparing the drill speed in fine-grained soil and coarse-grained material. Auger bits and drills were tested on artificially frozen blocks of frozen ground about 50 cm x 50 cm and 30 cm deep. Time was recorded every 10 cm to compare the speed of the drill with different drill bits.

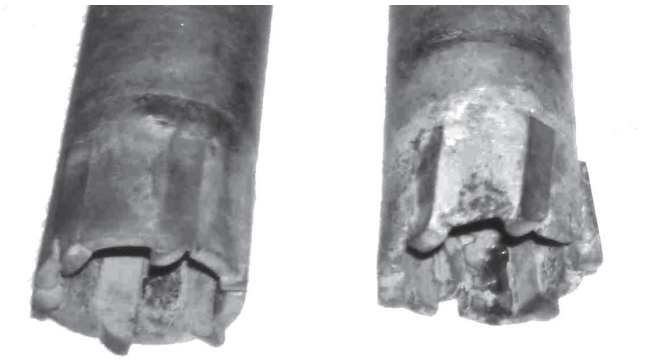

Figure 6. 30 mm diameter core bit for gravel (negative rake angle) (on left) and for silt (positive rake angle) (on right).

Figure 7. Fifty mm-wide auger bit for multi-grained (no rake angle [left]) and for silt (positive rake angle [right]).

Results

In general, the in-line percussion method worked better than just using the rotational drill. Figure 8 shows results from the experiment with the rotational drill using the in-line percussion and without it, in fine and coarse-grained materials. This figure shows that the inline system works well for both (fine- and coarse-grained) materials. However, the benefit of the percussion action is clearer in coarse gravel. The in-line percussion drill system performs 2.2 times more efficiently than using a rotation drill alone (Fig. 8, open dots).

Using water/air is a great way to remove materials (chips) from the borehole and also keep the bit tip clean. The water/air swivel allows pressurized water or air to flow through the tips of the drill bit while the drill is rotating. The chips are then blown out of the borehole. The system requires a large air compressor (>100 CFM) or high-pressure water pump (2 GPM), and it worked great with our portable drill system. This drilling system, therefore, includes three major components when digging the ground: (1) rotation action, (2) high pressure forced water/air - pushing action to remove chips, (3) impact (percussion) action. The swivel effectively blows chips out of the borehole, but working with permafrost

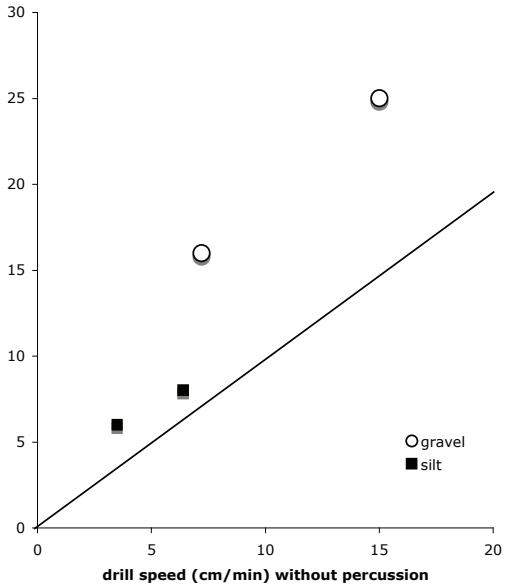

Figure 8. Drill speed performance with/without percussion action (inline) for frozen silt and gravel.

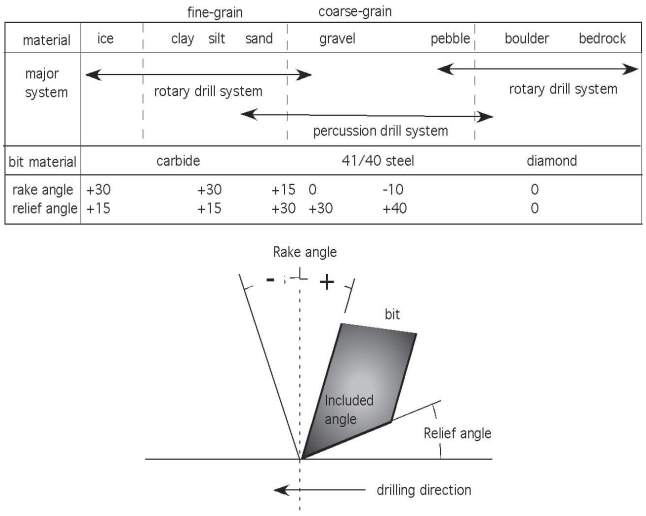

Figure 9. Ideal main drill system and bit properties of portable drill system for different frozen materials. Rake and relief angles for ice and fine-grained soil is after Sellmann & Mellor (1986). The rake and relief angle is the angle between the surface of the permafrost to the carbide bit. The relief angle is to prevent the land from rubbing on the surface of the work being cut.

we would like to keep the study site frozen while we drill. Therefore, a cooling system is needed for the water or air sent through the swivel. If supercooled water or chilled air is used, the system will cause minimal disturbance.

In general, physical theory for effective drilling depends on three major functions: rotation of the bit, down loading, and chip removal. When one of these functions does not work properly, drill speed slows down significantly or even stops. Using the portable drill system in a graveled area, the depth of the cutting blade is significantly smaller than the grain size of the gravel restricting rotation. Also, removing the chips requires water, air, or auger flights to establish a large enough flow pathway. The velocity of the flow pathway is related to the grain size of the chips. Maximum grain size (G:mm) is calculated by the following equation (Mori 1981).

$$G = 0.0055v^2 G_w/(G_s - G_w)$$

where v = velocity(cm/sec), G_s = density of grain, and G_w = density of water. Using this equation, 6–10 mm diameter grains require 40–60 cm/sec of velocity using water. Although this is not an impossible pressure to create, it makes it unlikely to easily convert a portable drill system. Drilling through coarse-grained material clearly exceeds the limit of the physical theory for drilling, and our experience suggests the following conclusions for drilling frozen, coarse materials:

1. Rotation systems do not work properly.
2. Percussion systems aid in removing grain particles
3. Pyramid shaped bits (zero apparent rake) (Fig. 9) work well for removing pebbles, especially when very fine grain material content is present in the matrix.
4. Bentnite works well to keep the wall stable.
5. Diamond core bits work great to drill through any kind of gravel, rock, and boulder, but take longer and generate heat.

Figure 10. Human-powered traditional percussion system using steel rod.

Table 2 shows a summary of our experiments. Percussion action helps to separate each grain and remove the gravel

Table 2. Summary of the portable drilling operation for fine- and coarse-grained frozen materials.

type	system	for fine-grained materials	for coarse-grained materials	benefit	weakness	remarks
percussion	jackhammer	Fair	fair	portable	need weight	Pionjar 120
	jackhammer with rotation	Fair	good	portable	requires 2 people	Pionjar 120
	rod drill	Fair	good	simple	heavy depend on weight of hammer	handmade
	hammer drill	Fair	fair	very portable	weak action	Bosch 14A
	down-hole drill (in-line drill)	Fair	good	efficient	needs air compressor	modified from air hammer
rotary	spindle drill	Good	fair	strong hydraulic system	heavy	hydraulic system
	spindle drill with air	Excellent	good	strong hydraulic system	heavy, need air compressor >100CFM	hydraulic system
	spindle drill with water	Excellent	good	strong hydraulic system	heavy, need water pump and water source	hydraulic system
	drive head drill	Good	fair	portable	weaker action	
	drive head drill with air	Excellent	good	portable	weaker action	
	drive head drill with water	Excellent	good	portable	weaker action	
other	earth auger	Good	fair	portable	only fine grained materials	little beaver
	push casing	Fair	bad	strong hydraulic system	unlike success???	hydraulic system
	water jet	Good	fair	portable	needs water pump and water source	5HP Honda

from the frozen matrix allowing it to move. However, the chips (grain) could not be removed from the borehole because of the grain size. A smaller diameter driving-rod is an essential parameter to successfully drill through coarse-grained material.

Percussion power simply depends on the weight of the hammer (Borisovich 1990). Heavier weights on the driving rod generate greater percussion energy. However, the reality of drilling in remote villages limits the size of a human-powered percussion system to about 30 kg (Fig. 10). Using a smaller diameter rod (12 mm) instead of using heavy weights for percussion can reduce weight and still allow effective drilling. Because of the smaller diameter, the speed of drilling was increased, and the borehole is small enough that the grainy materials can be pushed to the inside wall of the borehole.

Conclusion

The rotating drill is highly effective for fine-grained materials and even in coarse-grained material if the pore space is filled with silt or clay. The percussion system creates an effective action for drilling in coarse grain materials. This is illustrated in Figure 9. Heavier weights on the driving rod generate better percussion energy. However, the reality of drilling in remote villages limits the transport of heavier weights. Using a smaller diameter rod for percussion reduces weight, yet allows effective drilling.

The inline percussion (down-the-hole) drill improved drilling performance with the combination of percussion action and bit rotation. The combined actions are important systems for drilling through the coarse grain permafrost. We still need to design and build an inlinein-line percussion system for heavy-duty use and stronger impact energy in the future.

Acknowledgments

This project was funded by the National Science Foundation EPSCoR program (#0346770, #0701898) and the State of Alaska. We would like to thank the UAF Mechanical Engineering machine shop (Ned Manning and Eric Johansen) for building the prototype in-line percussion system, and Jon Holmgren and Sam Skidmore for developing many prototype bits, and VECO Polar Resources for logistical support.

References

Borisovich, B. 1990. *Drilling in the Permafrost.* pPublished for the Office of Polar Programs, New Delhi: National Science Foundation by Amerind Pub. Co., 318 pp.

Calmels, F., Gagnon, O. & Allard, M. 2005. A portable earth-drill system for permafrost studies. *Permafrost and Periglacial Processes* 16(3): 311-315. DOI: 10.1002/ppp.52

Lawson, D. & Brockett, B. 1980. *Drilling and Coring of Frozen Ground in Northern Alaska.* US Army Cold Regions Research and Engineering Laboratory, CRREL Special Report 80-12, 14 pp.

Mellor, M. 1976. *Mechanics of Cutting and Boring. Part II: Kinematics of Axial Rotation Machines*. US Army Cold Regions Research and Engineering Laboratory, CRREL Report 77-7, 85 pp.

Mori, H. 1981. *Study on the properties of soils in the northern coast of Tokyo Bay using a self-boring pressuremeter.* Soils and Foundations, Japanese Society of Soil Mechanics and Foundation Engineering.

Sellmann, P.V. & Brockett, B. 1986. *Auger Bit for Frozen Fine-grained Soil.* US Army Cold Regions Research and Engineering Laboratory, CRREL Special Report 86-36.

Sellmann, P.V. & Brockett, B. 1988. *Evaluation of Several Auger Bits in Frozen Fine-Grained Soils, Asphalt, and Concrete.* US Army Cold Regions Research and Engineering Laboratory, CRREL Special Report 88-8, 10 pp.

Sellmann, P.V. & Mellor, M. 1986. *Drill Bits for Frozen Fine-gGrained Soil.* US Army Cold Regions Research and Engineering Laboratory, CRREL Special Report, 86-27.

Detection and Enrichment of Ammonia Oxidizers from Permafrost Soils of Siberia

Tina Sanders, Claudia Fiencke
Institute of Soil Science, University of Hamburg, Germany
Eva Spieck
Biocenter Klein Flottbek, University of Hamburg, Germany
Eva-Maria Pfeiffer
Institute of Soil Science, University of Hamburg, Germany

Abstract

Permafrost soils cover about a quarter of the Earth's land surface. The soils are continuously frozen throughout the year, and only the active layer thaws near the surface during the short vegetation period. Microbial life of the polygonal Siberian tundra is influenced by extreme gradients of temperature and moisture. During nitrification, ammonia is oxidized by chemolithoautotrophic nitrifiers, the ammonia (AOB) and nitrite oxidizers (NOB), in two steps via nitrite to nitrate. Cell numbers of nitrifiers and potential activities of AOB were determined in geochemical characterized soil samples of the active layers. Results obtained by MPN-counts showed clearly that higher cell numbers of AOB and activities were found in the upper part of the dryer polygon rims compared to the waterlogged polygon centres. Our results reveal the existence of AOB in permafrost soil, which are well-adapted to the extreme environment.

Keywords: ammonia-oxidizing bacteria; Lena Delta; nitrifiers; nitrification; permafrost; Siberia.

Introduction

Since artic wetland soils are the most important natural source of the climate-relevant trace gas methane, many investigations focused on the microbial C-cycle of permafrost soils. But despite a close connection between C-cycle and N-cycle, the N-cycle is mostly unexplored.

Nitrogen as well as carbon cycling in arctic ecosystems is dominated by physical and biogeochemical controls which are unique to the generally cold-dominated environment. Drastic seasonal fluctuations in temperature, a short growing season, cold soil temperature, and the occurrence of permafrost are some of the obvious physical controls on nitrogen cycling and biological activity. Most of the nitrogen accumulates in the organic substance in response to low soil temperatures, excessive soil moisture, and low soil oxygen concentration (Gersper et al. 1980, Marion & Black 1987, Nadelhoffer et al. 1991, Schimel et al. 1996). Standing crops in tundra vegetation store about two times more nitrogen than temperate grasslands (Van Cleve & Alexander 1981). But through the low N-mineralization rates and lack of N-input by N-fixation and N-pollution, the soils are nitrogen deficient and rely to a large extent on internal recycling (McCown 1978).

N-cycling in the soil is crucial for growth of plants and microorganisms. Imbalances in N-cycling are due to nitrate leaching, nitrogen oxide release, and increase the methane emission (Adamsen & King 1993, Carini et al. 2003). Most of the N-transformations were catalyzed by microorganisms (Fig. 1, Fiencke et al. 2005). Nitrification, the microbiological oxidation of ammonia to nitrate via nitrite, occupies a central position within the terrestrial nitrogen cycle. Aerobic chemolithoautotrophic ammonia (AOB) and nitrite oxidizing (NOB) bacteria represent the most important group of nitrifying bacteria (Fiencke et al. 2005). As a result of nitrate and acid formation, the nitrification process has various direct and indirect implications of soil systems. It increases the loss of soil nitrogen due to leaching of nitrate and volatilization of nitrogen gases directly or by denitrification and therefore, influences the nitrogen supply to plants.

Beside ammonia oxidizing Proteobacteria, it has been mentioned that Archaea (AOA) participate in ammonia oxidation and have been found in different soils and habitats. (Nicol & Schleper 2006, Leininger et al 2006). Some representative of the AOA were enriched and described (Könneke et al. 2005, Hatzenpichler et al. 2008). In some habitats, more archaeal than bacterial genes were detected. (Leininger et al. 2006), but at this moment it is not clear which group of microorganisms dominate in the N-cycle.

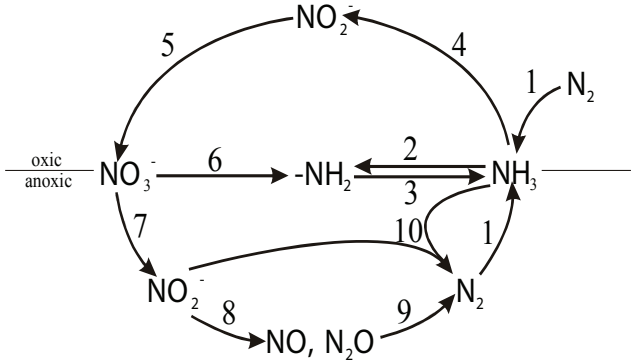

Figure 1. Nitrogen cycle. (1) dinitrogen (N_2) fixation, (2) assimilation of ammonia (NH_3) to amino group ($-NH_2$) of protein, (3) ammonification, (4) ammonia oxidation, (5) nitrite (NO_2^-) oxidation, (6) assimilation of nitrate (NO_3^-), (7, 8, 9) denitrification via nitrite, nitric oxide (NO) and nitrous oxide (N_2O), (10) anaerobic ammonia oxidation.

Nitrifying bacteria are found in the upper layer of soils, like the rhizosphere, where organic matter is mineralized, and ammonia and oxygen are present. The slow growth rates and difficulties in recovering pure cultures have hampered cultivation-dependent approaches to investigating the number, community composition, and dynamics of nitrifiers in soil. The number and turnover rate is, therefore, determined by traditional methods like most-probable-number (MPN) technique and activity tests.

During the *Expedition to the Lena Delta* in Summer 2005 and 2007, microbial nitrification was investigated by field experiments. Furthermore, soil and gas samples were taken for further ecological, molecular, and soil analyses.

Investigation Area

The study site is located on Samoylov Island (72°22′N, 126°28′È) in the southern part of the Lena Delta on the north coast of Siberia (Fig. 2).

The climate is true-arctic, continental, and characterized by low annual temperatures (-13,6°C) and low annual precipitation (319 mm) (ROSHYDROMET 2007). The main soil unit of Island Samoylov is covered mainly by the soil-plant-complex consisting of Glacic Aquiturbels and Typic Historthels (Fig. 3b).

The Typic Historthels are Gelisols that have in 30% or more of the pedon more than 40% by volume, organic materials from the surface to depth of 50 cm (Soil Survey Staff 2006). They formed in the depressed centers of low-centered ice wedge polygons characterized by water saturation to the soil surface and organic matter accumulation due to anaerobic condition. The Glacic Aquiturbels formed at the elevated borders of the polygons, are characterized by prolonged inundation, but with less organic matter accumulation and pronounced cryoturbation.

Materials and Methods

The investigations of nitrification were carried out on Samoylov in August 2005 and July 2007. Soil samples were taken from the active layer of two low-centered polygons, at the polygon rim and polygon center, at 3 depths (0–5, 5–15, 15–25 cm) (Fig. 3). Samples were analyzed freshly on-site and after transportation (frozen or unfrozen at about 6°C) lasting for two months to our institute in Hamburg, Germany.

On-site and after transportation, nitrification was determined by enrichment and ammonia oxidizing activity tests. Therefore, ammonia (AOB) and nitrite oxidizing bacteria (NOB) were enriched for further quantification by MPN-technique in media with 1 mM ammonium and 0.3 mM nitrite for three months at about 6°C. The ammonia oxidizing activities were measured at different temperatures (6°C, 12°C, 17°C, 20°C, 28°C, 37°C) and 0.75 mM ammonium sulfate using ISO/DIN 15685:2001 standard tests. The activities were measured by ammonia consumption and nitrite formation up to a period of 6 weeks in the field and eight weeks in the laboratory. Samples for the test were taken twice a week.

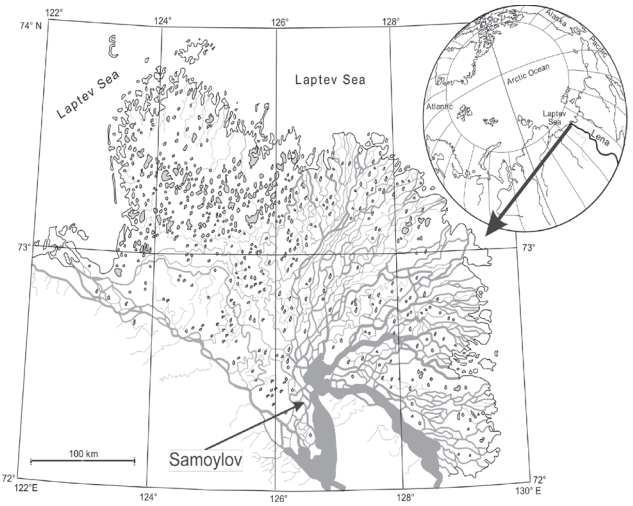

Figure 2. Map of the Lena Delta with location of Samoylov Island.

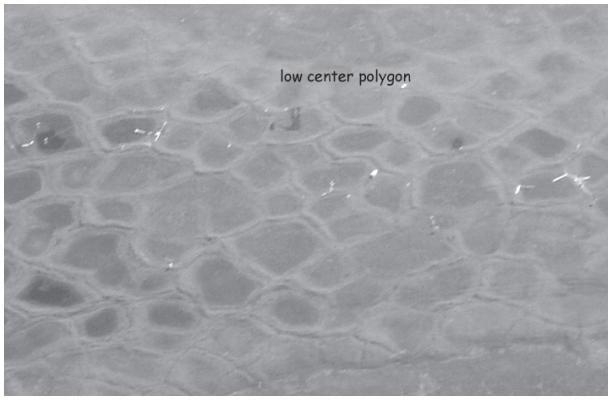

Figure 3a. Low-center polygon landscape on the island Samoylov.

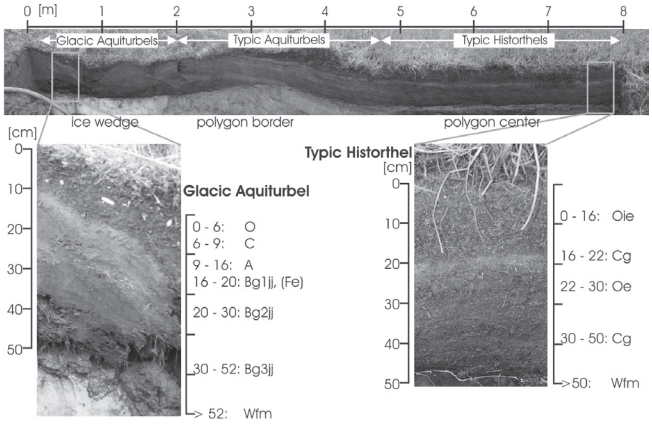

Figure 3b. Soil cross-section of a low-centered polygon and investigated soil-profiles (Classification U.S. Soil Taxonomy).

Chemical characterization of soils was done after transportation. For pH determination, soil suspensions with dest. water were measured after an equilibration of one hour. C/N was analyzed after oven drying (105°C) and grinding by Vario MAX element analysator. For ammonium, nitrite, and nitrate detection, soil samples were extracted with 0.0125 M $CaCl_2$ and were analyzed by spectral photometer tests. Methane was measured in situ by gas chromatography.

Results and Discussion

Chemical parameters

The chemical characterization of the soil samples shows that ammonium accumulates in the moist, anaerobic, and methane-containing Typic Historthel of the polygon center, and only low concentrations of nitrite and nitrate were found (Fig. 4a). In contrast to the moist polygon center, in the Glacic Aquiturbel of the dryer polygon rim, high nitrate concentrations were found in the oxic top soil (Fig. 4b).

Ammonia oxidation

Ammonia oxidation was measured by MPN-counts and ammonia oxidizing activity tests. Highest cell numbers of nitrifiers (AOB and NOB) were found at depths of 5–15 cm in the Glacic Aquiturbel of the polygon rim ($2 \cdot 10^5$ cells/g dw, data not shown).

During the field survey in August 2005 and July 2007, all soil samples were tested for ammonia oxidation activity.

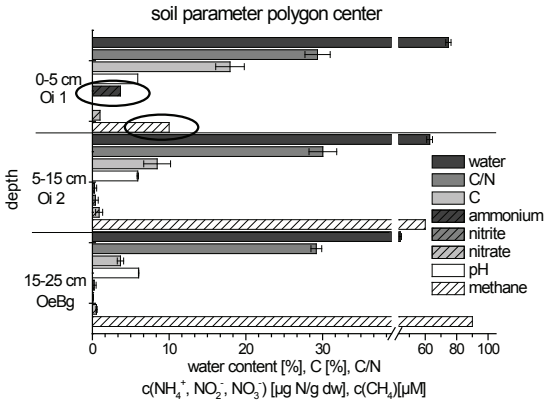

Figure 4a. Chemical soil parameters of the Typic Historthel of the polygon center. Soil samples were taken in August 2005. Error bars represents 4 parallels.

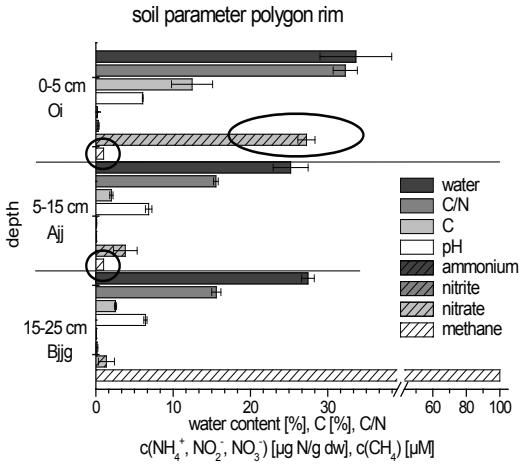

Figure 4b. Chemical soil parameters of the Glacic Aquiturbel of the polygon rim. Soil samples were taken in August 2005. Error bars represents 4 parallels.

Additionally, all soil samples were tested again after two months of transportation.

In the field experiments of 2005 and 2007, ammonia-oxidizing activity was only detected in soil samples in depths 5–15 cm of the Glacic Aquiturbel of the polygon rim. In July 2007, activities of 22,56 ng N-Nitrit per g dry weight and hours were found.

After two months of unfrozen transportation, the same samples were analyzed again. After that time, the activities in the 5–15cm polygon rim sample increased, and few activities were found in the surface sample (0–5 cm) of the polygon center (Fig 5a). In soil samples which were taken one and a half months later (August 2007), ammonia oxidizing activity was also detected in upper layers of the polygon rim and center (Fig. 5b). Higher activities in the upper parts of the center in August might be due to lower water content (July 412 %, August 173%) due to decrease of water level in the polygon center.

The results indicate that small-scale differences in soil hydrology have significant impact on the N-cycle. Better drained, reduced acidity and methane concentration of oxic soil samples of the polygon rim favor nitrification, and therefore, lead to the accumulation of nitrate. Nitrate was possibly not degraded in dry sites, owing to lack of denitrification in these more aerated micro-environments. Instead, in the moist polygon center, nitrification was inhibited by oxygen deficiency, and therefore the ammonium formed by mineralization accumulated. In the moist anoxic environment, nitrate was possibly quickly reduced by denitrification.

Furthermore, the activity of the most active soil sample was analyzed at different temperatures. As shown in Table 1, activities depend on transportation of soil samples and temperature used for activity tests. Generally, higher activities were found in the soil samples after an unfrozen

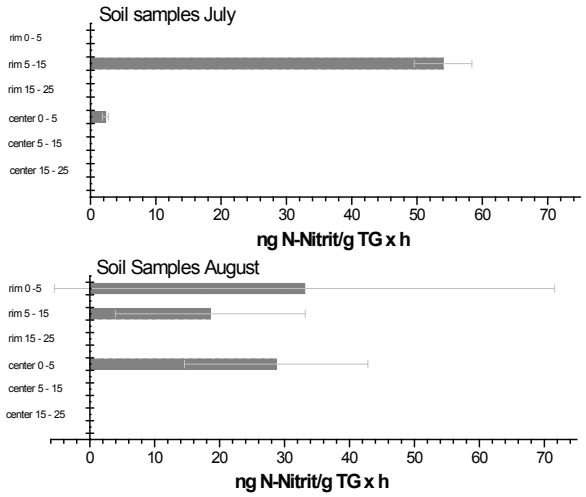

Figure 5. Ammonia-oxidizing activities measured by formation of nitrite in Typic Historthel of the polygon center and Glacic Aquiturbel of the polygon rim. Samples were taken in July (5a) and August (5b) 2007 and activities were measured over a period of 8 weeks at 6 °C. Error bars represent 4 parallels.

Table 1. Activity of the ammonia-oxidizing bacteria at the polygon rim of the depth of 5 to 15 cm at temperatures between 6°C and 37°C. Frozen and unfrozen transported samples were analyzed after two months of transportation.

Temperature [°C]	Ammonia-oxidizing activity [ng N-nitrite/g dw·h]	
	unfrozen	frozen
6	23.4	0.6
12	6.6	1.3
20	60.5	12.0
28	9.1	2.5
37	0.2	0.2

transport of the samples from the field to the laboratory. In frozen transported soil samples, ammonia oxidizing activity is obviously lower. Highest activity was found at tests conducted at 20°C, second highest at 6°C. Therefore, two peaks of activity were found independently of frozen or unfrozen transportation. An explanation for the two peaks could be that two different ammonia-oxidizing communities got different temperature optima.

Summary

The results indicate that small-scale differences in soil hydrology of the polygonal tundra have significant impact on the N-cycle. In the dryer, aerobic Glacic Aquiturbel of the polygon rim, high nitrate and low inhibitory methane concentrations correlated with high cell numbers and activities of ammonia oxidizing bacteria. In contrast, in the moist, anaerobic, methane-containing Typic Historthel polygon center, lower cell numbers and activities of ammonia-oxidizing bacteria were detected. The ammonia-oxidizing activities depended on the temperature. Highest activities were found at 6 and 20°C.

Conclusions

This paper show preliminary results on one special part of the nitrogen cycle. Further investigation will consider unstudied processes and fluxes of the N-cycle like mineralization and denitrification. It should also be clarified which group of ammonia-oxidizing organisms, Proteobacteria or Archaea, take part in the activities in that environment. First results may help to understand how predicted climate changes influence the N-cycle in soils of the polygonal tundra.

Acknowledgments

We thank the Russian–German parties of Expedition Lena 2007 for the pleasant teamwork in the field. Special thanks go to the staff of the Alfred Wegener Institute, Research Unit Potsdam for making the expedition to the Lena Delta possible. Thanks, also, to the University of Hamburg and the Institute of Soil Science for advice in the planning of the work.

References

Adamsen, A.P.S. & King, G.M. 1993. Methane consumption in temperate and subarctic forest soils: rates, vertical zonation, and responses to water and nitrogen. *Appl. Env. Microbiol.* 59: 485-490.

Carini, S.A., Orcutt, B.N. & Joye, S.B. 2003. Interactions between methane oxidation and nitrification in coastal sediments. *Geomicrobiology Journal* 20: 355-374.

Fiencke, C., Spieck, E. & Bock, E. 2005. Nitrifying bacteria. In: D. Werner & W. E. Newton (eds.), *Nitrogen Fixation in Agriculture, Forestry, Ecology, and the Environment.* Springer, The Netherlands, Dordrecht. 12: 255-276.

Gersper, P.L., Alexander, V & Barkley, S.A. 1980. The soils and their nutrients. In: J. Brown, P.C. Miller, L.L. Tieszen, F.L. Bunnell (eds.), *An Arctic Ecosystem. The coastal Tundra at Barrow, Alaska.* Stoudsburg: Dowden, Hutchinson & Ross, 219-254.

Hatzenpichler, R., Lebedeva, E.V., Spieck, E., Stoecker, K., Richter, A., Daims, H. & Wagner, M. 2008. A moderately thermopholic ammonia-oxidizing crenarchaeote from a hot spring. *PNAS* 105(6): 2134-2139.

Könneke, M., Bernhard, A. E., de la Torre, J. R., Walker. C. B., Waterbury, J. B. & Stahl, D. A. 2005. Isolation of an autotrophic ammonia-oxidizing marine archaeon. *Nature 437*: 543-546.

Leiniger, S., Urich, T., Schloter. M., Schwark, L., Qi, J., Nicol, G.W., Prosser, J.I., Schuster, S.C. & Schleper, C. 2006. Archaea predominate among ammonia-oxidizing prokaryotes in soils. *Nature Letters 442: 806- 809.*

Marion, G.M.,& C.H. Black. 1987. The effect of time and temperature on nitrogen mineralization in Arctic tundra soils. *Soil Science Society of America Journal* 51: 1501-1508.

McCown, B.H. 1978. The interactions of organic nutrients, soil nitrogen and soil temperature and plant growth and survival in the arctic. In: L.L. Tieszen (ed.), *Vegetation and production ecology of an Alaskan arctic tundra*. New York: Springer, 435-456.

Nadelhoffer, K.J., Giblin, A.E., Shaver, G.R., and G.R. Laudre. 1991. Effects of temperature and substrate quality on element mineralization in six arctic soils. *Ecology* 72: 242-253.

Nicol, G.W. & Schleper, C. 2006. Ammonia-oxidizing Crenarchaeota: important players in the nitrogen cycle? *Trends in Microbiology 14*: 207-212.

ROSHYDROMET.2007.10.10. Russian Federal Service for Hydrometeorology and Environmental Monitoring. Weather Information for Tiksi. http.//www.worldweather.org/107/c01040.htm.

Schimel, J.P., Kielland, K & Chapin, F.S. 1996. Nutrient availability and uptake by tundra plants. In: J.F. Reynolds & J.D. Tenhunen (eds.), *Landscape function and disturbance in arctic tundra. Ecological Studies 120.* Berlin: Springer, 203-221.

Soil Survey Staff. 2006. Keys to Soil Taxonomy. 10th ed., Washington, D.C.: United States Department of Agriculture 6 Natural Resources Conservation Service, 332pp.

Van Cleve, K., & Alexander, V. 1981. Nitrogen cycling in tundra and boreal ecosystems. In: E.E. Clark, & T. Rosswall (eds.), *Terrestrial nitrogen cycles. Ecol. Bull. Stockholm.* 33: 375-404.

Bending Characteristics of Pipe-in-Pipe Systems

Motohiro Sato
Graduate School of Engineering, Hokkaido University
Kenta Shimazaki
Graduate School of Engineering, Hokkaido University
Shunji Kanie
Graduate School of Engineering, Hokkaido University
Satoshi Akagawa
Graduate School of Engineering, Hokkaido University
Takashi Mikami
Graduate School of Engineering, Hokkaido University

Abstract

Structural pipe-in-pipe cross sections have significant potential for application in oil and gas production systems because of their property that combines insulation performance with structural strength in an integrated way. By making use of such excellent structural properties, however, we consider that this pipe-in-pipe system can be also applicable to pipelines in cold or permafrost regions. In this case, bending characteristics become one of the most important factors for the structural design of the pipelines. The purpose of this research is to investigate the bending characteristics of such pipe-in-pipe systems analytically by considering the Brazier effect. Results are presented to show the variation of the degree of ovalization and the Brazier moment with the relative elastic modulus of the filler and pipe materials, the filler thickness, and the thicknesses of the inner and outer pipes.

Keywords: Brazier effect; pipe-in-pipe; pipeline; pure bending.

Introduction

Structural pipe-in-pipe cross sections have significant potential for application in oil and gas production systems because of their property that combines insulation performance with structural strength in an integrated way. Such cross sections comprise inner and outer thin walled pipes with the annulus between them fully filled by a selectable thick filler material to impart an appropriate combination of properties. The technology of the pipe-in-pipe system has developed in the field of offshore engineering. One of the authors investigated the elastic buckling behaviour of pipe-in-pipe cross sections under external hydrostatic pressure (Sato & Patel 2007). By making use of such excellent structural properties, however, we consider that this pipe-in-pipe system can be also applicable to pipelines in cold or permafrost regions, such as chilled gas pipeline systems installed under ground. In this case, bending rigidity or flexibility near the boundary between permafrost and non-permafrost areas become one of the most important factors for the structural design of the pipelines.

In pure bending, the cross sections of a hollow cylindrical pipe ovalize, and this reduce the flexural stiffness of the pipe as the curvature increases. This is known as *the Brazier effect* (Brazier 1927), and it is quite important to evaluate this effect accurately in order to understand the bending behaviour of the pipe-in-pipe system.

From this point of view, the purpose of this research is to investigate the bending characteristics of such pipe-in-pipe systems analytically by considering the Brazier effect. The *Brazier moment*, which is the maximum moment carrying capacity of the ovalized cross section, can be calculated by introducing the strain energy per unit length of the pipe in terms of the degree of ovalization for outer and inner pipe curvature. The total strain energy of the pipe-in-pipe system is the sum of the strain energy of the outer and inner pipes and the compliant core. It is also clear that the moment of inertia of the cross section is increased by the presence of the core compared with single wall pipes.

Results are presented to show the variation in degree of ovalization and the Brazier moment with the relative elastic modulus of the core and outer/inner pipes materials, the core thickness, and the thicknesses of the inner and outer pipes.

Analytical Model

Figure 1 shows the configuration of a perfectly cylindrical pipe-in-pipe cross section that is analyzed here. The pipe-in-pipe cross sections under consideration have an annulus fully filled with a material that provides continuous structural support to both the thin-walled outer and inner pipes with Young's modulus E_P and Poisson's ratio ν_P. The geometric variables are the thickness of the outer pipe, t_1, that of the inner pipe, t_2, the middle surface of the outer pipe, a_1, and that of the inner pipe, a_2. In the following formulation, the subscripts 1 and 2 correspond to the outer and inner pipes, respectively.

As shown in Figure 2(b), in pure bending the cross sections of a hollow circular cylindrical pipe-in-pipe ovalize and this reduces the flexural stiffness of the pipe as the curvature increases.

Formulation

Strain energy associated with ovalization of the core

The strain energy U_1 per unit length in the ovalized core is expressed as

$$U_1 = \frac{1}{2}\int_0^{2\pi}\int_{a_2}^{a_1}(\sigma_r\varepsilon_r + \sigma_\theta\varepsilon_\theta + \tau_{r\theta}\gamma_{r\theta})rdrd\theta \quad (1)$$

where σ_r, σ_θ, $\tau_{r\theta}$ and ε_r, ε_θ, $\varepsilon_{r\theta}$ are the core stresses and strains in the radial, circumferential, and shear directions, respectively. As shown in Figure 2(b), the radial and tangential displacement, u_i and v_i, respectively, of outer and inner pipes ovalized by ζ_i are (Calladine 1983)

$$u_i = a_i\varsigma_i\cos 2\theta = \delta_i\cos 2\theta \quad (2a)$$

$$v_i = -\frac{1}{2}a_i\varsigma_i\sin 2\theta = -\frac{1}{2}\delta_i\sin 2\theta \quad (2b)$$

The basic equation for the core is expressed by the stress function $\phi(r,\theta)$ in polar coordinates as (see Timoshenko & Goodier 1970)

$$\left(\frac{\partial^2}{\partial r^2}+\frac{1}{r}\frac{\partial}{\partial r}+\frac{1}{r^2}\frac{\partial^2}{\partial\theta^2}\right)^2\phi(r,\theta) = 0 \quad (3)$$

The normal stresses in the radial and circumferential directions σ_r, σ_θ and the shear stress $\tau_{r\theta}$ are determined from

$$\sigma_r = \frac{1}{r}\frac{\partial\phi(r,\theta)}{\partial r}+\frac{1}{r^2}\frac{\partial^2\phi(r,\theta)}{\partial\theta^2} \quad (4a)$$

$$\sigma_\theta = \frac{\partial^2\phi(r,\theta)}{\partial r^2} \quad (4b)$$

$$\tau_{r\theta} = -\frac{\partial}{\partial r}\left(\frac{1}{r}\frac{\partial\phi(r,\theta)}{\partial\theta}\right) \quad (4c)$$

In the problem considered here, the two displacement components for the core, the radial displacement $u(r,\theta)$ and the circumferential displacement $v(r,\theta)$, are assumed to have circumferentially periodic forms written as:

$$u(r,\theta) = u_C(r)\cos 2\theta \quad (5a)$$

$$v(r,\theta) = v_C(r)\sin 2\theta \quad (5b)$$

Therefore, $\phi(r,\theta)$ should be expressed as follows:

$$\phi(r,\theta) = f(r)\cos 2\theta \quad (6)$$

The general solutions of Equation 3 are as follows:

$$f(r) = Ar^{-2} + B + Cr^4 + Dr^2 \quad (7)$$

where A, B, C, D are arbitrary constants. In this case, the corresponding stress components are

$$\sigma_r = -(6Ar^{-4} + 4Br^{-2} + 2D)\cos 2\theta \quad (8a)$$

$$\sigma_\theta = (6Ar^{-4} + 12Cr^2 + 2D)\cos 2\theta \quad (8b)$$

$$\tau_{r\theta} = (-6Ar^{-4} - 2Br^{-2} + 6Cr^2 + 2D)\sin 2\theta \quad (8c)$$

The strain components for the plane strain problem are derived by

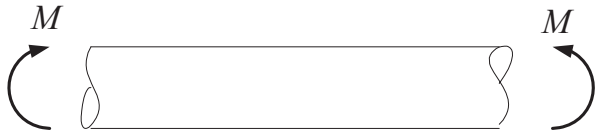

Figure 1. Pipe-in-pipe system in pure bending.

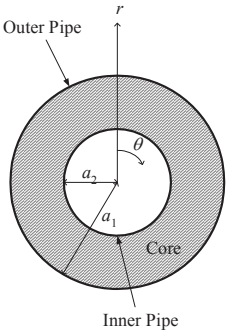

Figure 2. Pipe-in-pipe cross section.

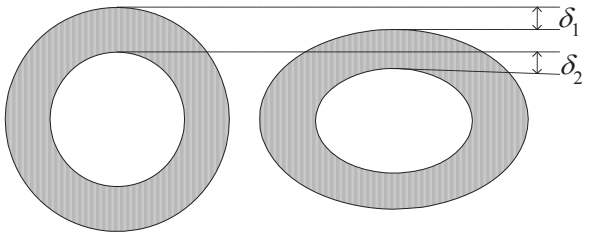

(a)Before bending (b) After bending

Figure 3. Ovalization for pipe-in-pipe cross sections. (The degree of ovalization is $\zeta_i = \delta_i / a_i$ (i = 1, 2).)

$$\begin{Bmatrix}\varepsilon_r\\ \varepsilon_\theta\\ \gamma_{r\theta}\end{Bmatrix} = \frac{1}{E_C}\begin{bmatrix}1-\nu_C^2 & -\nu_C(1+\nu_C) & 0\\ -\nu_C(1+\nu_C) & 1-\nu_C^2 & 0\\ 0 & 0 & 2(1+\nu_C)\end{bmatrix}\begin{Bmatrix}\sigma_r\\ \sigma_\theta\\ \tau_{r\theta}\end{Bmatrix} \quad (9)$$

The corresponding displacements in the radial and circumferential directions $u(r,\theta)$ and $v(r,\theta)$ can be obtained from Equations 8 and 9, and the following displacement-strain relationship is derived:

$$u(r,\theta) = \int\varepsilon_r dr$$
$$= \frac{1+\nu_C}{E_C}\left\{\frac{2A}{r^3}+\frac{4B(1-\nu_C)}{r}-4\nu_C Cr^3 - 2Dr\right\}\cos 2\theta + P \quad (10a)$$

$$v(r,\theta) = \int(r\varepsilon_\theta - u)d\theta$$
$$= \frac{1+\nu_C}{E_C}\left\{\frac{2A}{r^3}+\frac{2B(2\nu_C-1)}{r} + 2C(3-2\nu_C)r^3 + 2Dr\right\}\sin 2\theta + Q \quad (10b)$$

where P and Q are constants of integrations. For the problem considered here, the outer and inner pipes are assumed to be perfectly bonded to the core. The middle surface outer pipe displacements (u_1, v_1) and inner pipe displacements (u_2, v_2) are taken to have circumferentially periodic forms written as:

$$u(a_i,\theta) = u_i \tag{11a}$$

$$v(a_i,\theta) = v_i \tag{11b}$$

From Equations 2, 10, and 11, we can obtain the constants A, B, C, D as functions of δ_1 and δ_2. This fact indicates that the strain energy associated with ovalization of the core (Eq. 1) can be expressed by the displacements of the outer and inner pipes. Substituting the constants in the stresses and strains, we obtain the strain energy which is the function of δ_1 and δ_2.

In addition to this, we find the strain energy of the outer and inner ovalized pipes is (Calladine 1983)

$$U_2 = \sum_{i=1}^{2} \frac{3}{8}\pi E_P \frac{t_i^3}{a_i\sqrt{1-\nu_P^2}}\zeta_i \tag{12}$$

Strain energy associated with bending of the pipe-in-pipe system

The strain energy per unit length to bend a pipe of flexural rigidity $(EI)_{PIP}$ to a curvature C is

$$U_3 = \frac{1}{2}(EI)_{PIP}C^2 \tag{13}$$

where

$$(EI)_{PIP} = E_P(I_1 + I_2) + E_C I_C \tag{14}$$

For a hollow pipe with ovalizaton, the moments of inertia are (Calladine 1983)

$$I_i = \pi a_i^3 t_i\left(1 - \frac{3}{2}\varsigma_i + \frac{5}{8}\varsigma_i^2\right) \tag{15a}$$

$$I_C = \frac{\pi a_1^4}{4}\left(1 - \frac{3}{2}\varsigma_1 + \frac{5}{8}\varsigma_1^2\right) - \frac{\pi a_2^4}{4}\left(1 - \frac{3}{2}\varsigma_2 + \frac{5}{8}\varsigma_2^2\right) \tag{15b}$$

Substituting Equations 14 and 15 into Equation 13 gives

$$\begin{aligned} U_3 = {} & \frac{1}{2}C^2 E_P \pi a_1^3 t_1\left(1 + \frac{E_C a_1}{4E_P t_1}\right)\left(1 - \frac{3}{2}\varsigma_1 + \frac{5}{8}\varsigma_1^2\right) \\ & + \frac{1}{2}C^2 E_P \pi a_2^3 t_2\left(1 - \frac{E_C a_2}{4E_P t_2}\right)\left(1 - \frac{3}{2}\varsigma_2 + \frac{5}{8}\varsigma_2^2\right) \end{aligned} \tag{16}$$

Moreover, the strain energy per unit length associated with Poisson's ratio to maintain the circular cross section due to bending is then (Karam & Gibson 1995)

$$\begin{aligned} U_4 &= \frac{1}{2}\int_{a_2}^{a_1}\int_0^{2\pi} (2\sigma_r\varepsilon_r + \tau_{r\theta}\gamma_{r\theta}) r\,d\theta\,dr \\ &= \frac{\pi}{16}\frac{\nu_C^2(5-2\nu_C)}{(1+\nu_C)(1-2\nu_C)} E_C C^2 (a_1^4 - a_2^4) \end{aligned} \tag{17}$$

Brazier moment

The final result for the strain energy of the pipe-in-pipe system is expressed by the summation as

$$U = U_1 + U_2 + U_3 + U_4 \tag{18}$$

We can find the optimum value of ζ_1 and ζ_2 for a given value of C from the condition $\partial U / \partial \zeta_i = 0$ and then obtain an expression for M from $M = \partial U / \partial C$. Moreover, the Brazier moment and the ovalization at the Brazier moment can be obtained from $\partial U / \partial C = 0$.

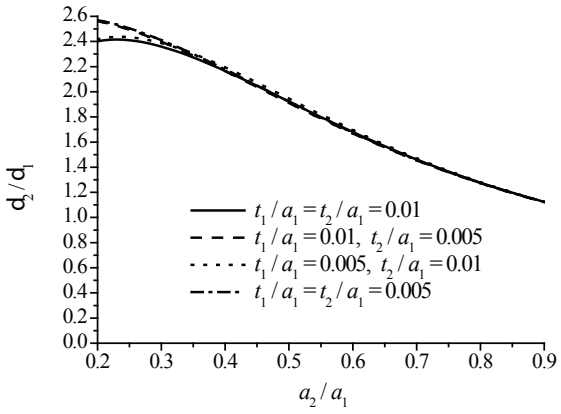

(d) $E_C / E_P = 10^{-2}$

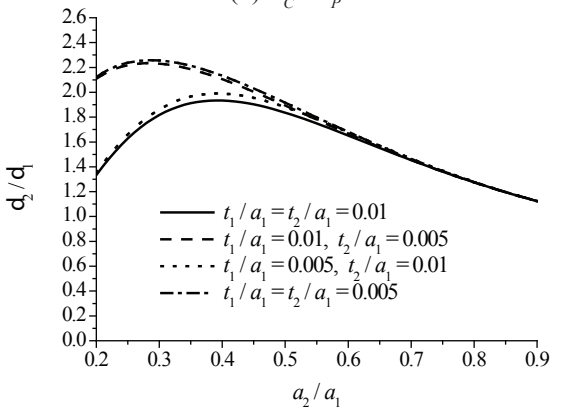

(d) $E_C / E_P = 10^{-3}$

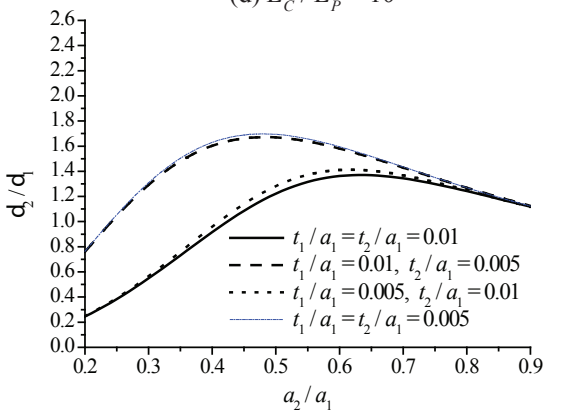

(d) $E_C / E_P = 10^{-4}$

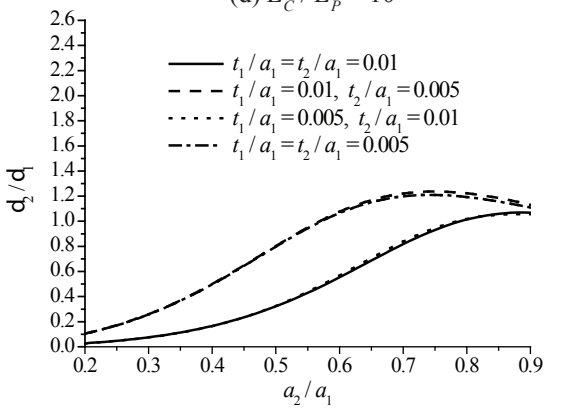

(d) $E_C / E_P = 10^{-5}$

Figure 4. Displacement ratio (Inner to outer pipe, $\nu_P = 0.4$).

Results and Discussion

Ovalization at the Brazier moment

Figures 4a–4d show the plot of the displacement ratio δ_2/δ_1 due to bending against core thickness ratio a_2/a_1 for the various values of outer and inner pipe thicknesses to outer pipe radius ratio and core to pipe stiffness ratio. It is clear from the comparison of these figures that, as the core stiffness increases, the displacement for the inner pipe increases. Moreover, the effect of the change of the outer pipe thickness on the displacement ratio is quite little and this value can be determined by the core thickness and inner pipe thickness ratio.

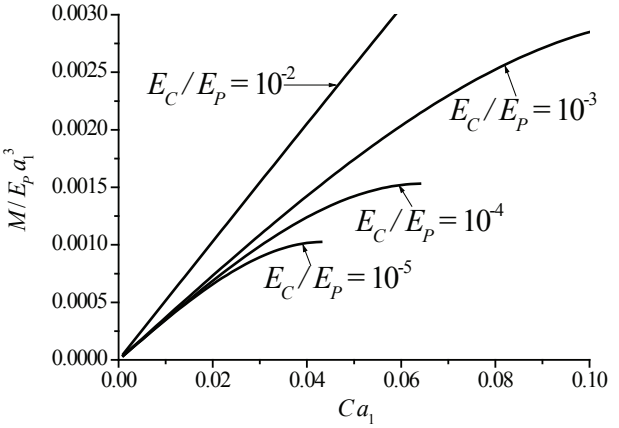

(a) $t_1/a_1 = t_2/a_1 = 0.01,\ a_2/a_1 = 0.5$

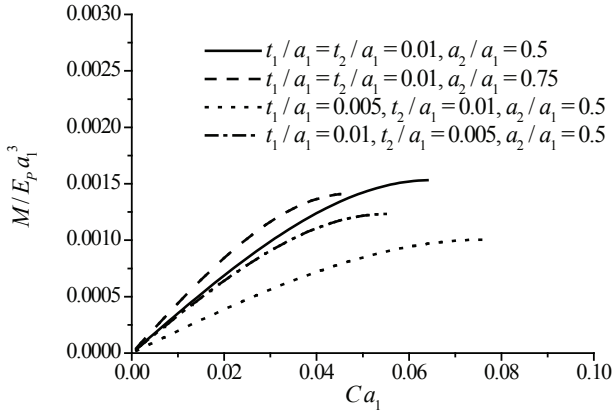

(b) $E_C/E_P = 10^{-4}$

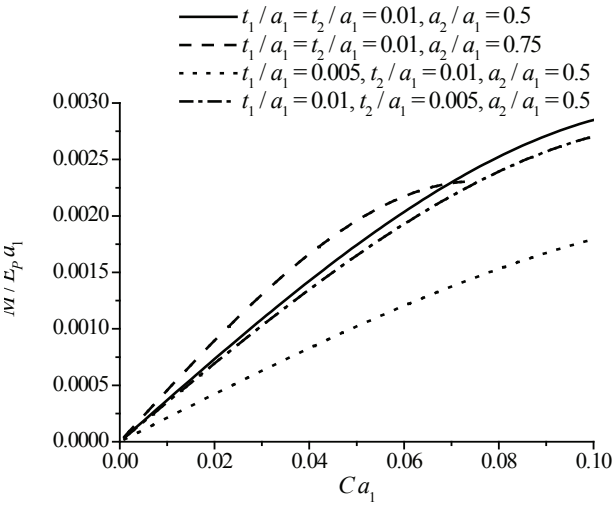

(c) $E_C/E_P = 10^{-3}$

Figure 5. Non-dimensional moment-curvature relationship ($\nu_P = 0.4$).

Moment-curvature relationship and Brazier moment

Figures 5a–5c show the nondimensional bending moment-curvature relationship. In all cases, for small values of Ca_1 we can find that the relationship between bending moment and curvature is almost linear. However, as the curvatures increase, the relation becomes nonlinear and finally the values of M reach maximum, in other words "the Brazier moment." As expected, the Brazier moment increases, with increasing the core thickness. Figures 5b and 5c are the comparison with regard to the different outer/inner pipe thickness and core thickness ratio. The contribution of the outer pipe thickness rather than that for the inner pipe toward bending moment-curvature relationship is significant. In addition, we can find from these figures, that as the core thickness increases, Brazier moment also increases.

Conclusions

This paper presents the bending characteristics of pipe-in-pipe systems analytically by considering the Brazier effect. It should be noted that the outer pipe thickness and the core stiffness, rather than the inner pipe thickness, play an important role in the bending moment-curvature relationship for pipe-in-pipe systems. At the moment, this research is the simplified analytical investigation. However, further studies will address the experimental investigations planned by the authors' research group, and comparisons between analytical and experimental results will be carried out.

Acknowledgment

The support of this work by the Grant-in-Aid for Young Scientists (B) (No. 18760615) of the Ministry of Education, Culture, Sports, Science and Technology (MEXT) in Japan is greatly acknowledged.

References

Brazier, L.G. 1927. On the flexure of thin cylindrical shells and other thin sections. *Proceedings of the Royal Society of London* A116: 104-114.

Calladine, C.R. 1983. *Theory of Shell Structures*. Cambridge: Cambridge University Press.

Karam, G.N. & Gibson, L.J. 1995. Elastic buckling of cylindrical shells with elastic cores – I. Analysis. *International Journal of Solids and Structures* 32: 1259-1283.

Sato, M. & Patel, M.H. 2007. Exact and simplified estimations for elastic buckling pressures of structural pipe-in-pipe cross-sections under external hydrostatic pressure. *Journal of Marine Science and Technology* (in press).

Timoshenko, S.P. & Goodier, J.N. 1970. *Theory of Elasticity*. New York: McGraw-Hill.

Origin and Age of Perennial Ice Within a Block Slope in the Shikaribestu Mountains, Hokkaido, Japan

Yuki Sawada
Institute of Low Temperature Science, Hokkaido University, Sapporo, Japan

Abstract

Borehole drilling and core sampling were conducted at the base of a block slope, where extra-zonal permafrost is preserved by winter air circulation and subsequent formation of the ground ice. A 3.8 m deep borehole displayed a vertical structure of the block slope. The sediment is composed of Sphagnum moss and peat (0–0.1 m depth), boulders (0.1–1.2 m), ice and boulder mixture (1.2–3.2 m), gravelly sand (3.2–3.35 m), and gravelly silt with ice lenses (3.35–3.8 m). Ratios of stable isotopes (δ18O and δD) of the perennial ice show similar linear correlations (gradient 7.5 and intercept 10.5) to the Global Meteoric Water Line, indicating that the ground ice is fed by meteoric water. AMS Radiocarbon datings of the trapped organic materials in the perennial ice indicate that the ground ice started to form between 8411–3728 Cal BP and has accumulated discontinuously throughout the late Holocene. Accumulation of the Sphagnum moss and peat layer on the blocky sediment may contribute to insulation and the gradual growth of the perennial ice.

Keywords: block slope; extra-zonal permafrost; paleoclimate; perennial ice; radiocarbon dating; stable isotope.

Introduction

Permafrost ice has the potential to archive paleo-climatic information within the stable-isotope composition, because most permafrost ice originates from meteoric water. For example, ice-wedge ice in continuous permafrost regions is generally formed by refreezing of snowmelt water. For this reason, stable oxygen isotope signals in the ice wedge have been used as an indicator of paleo-winter temperature (e.g. Mackay 1983, Meyer et al. 2002).

Ground ice in mountain permafrost environments also has a potential for paleoclimate reconstruction (e.g., Steig et al. 1998, Humlum 1999). Humlum (1999) reported that the relict glacier ice within a rock glacier in Greenland exhibits relatively lighter oxygen isotopes, which are indicative of the cooler climate in the little ice age.

Perennial ice bodies are also preserved in block slopes and talus slopes where extra-zonal permafrost is formed by air circulation where mean annual air temperature (MAAT) is positive (Kneisel et al. 2000, Sawada et al. 2003, Sawada 2003, Gude et al. 2003, Delaloye et al. 2003, Gorbunov et al. 2004, Zacharda et al. 2007). Previous studies by the author (Sawada et al. 2003, Sawada 2003) reported that ground ice formed in snowmelt periods and concluded that the ground ice probably originated from refreezing of snowmelt water. If the ground ice is considerably old, ice in the block slope may contain stable isotope signals of past climate changes.

This study presents stratigraphic and stable isotope data from a 3 m long core of ice and boulder mixtures obtained from a block slope in the Shikaribetsu Mountains, Hokkaido Island, Japan. AMS 14C ages of the organic materials in the sediments and ice are measured to determine the age of preserved ice. The oxygen and hydrogen isotope data are used to discuss the origin and formation processes of the perennial ground ice.

Study Area

The study area is located on the summit slope of Mt. Nishi-Nupukaushinupuri (1251 m a.s.l.) in central Hokkaido Island, Japan (Fig.1). This mountain is one of the lava domes which erupted in the last glacial period. MAAT ranged from 0.7°C–1.7°C in 1998–2003. Annual precipitation at the nearest meteorological station (Nukabira, 10 km NW) is 1175.8 mm, an average based on 12 years of data (1979–1990). The drill site is situated on the valley bottom which lies at the base of the block slope (Fig. 1). The lower portion of the block slope is dominated by spruce (Picea glehnii) and dwarf pine (pinus pumila), with ground surface cover of Sphagnum sp. and alpine shrubs (mainly Ledum palustre). Cold air blows during summer and autumn from the hollows opened in the moss mat.

Between 2000 and 2001 the depth of ground ice surface and ground temperatures at the drilling site showed the annual variations of the ground ice and related thermal regime (see for details Sawada et al. 2003, Sawada 2003). In winter the lower block slope was strongly cooled by air circulation driven by the temperature difference between atmosphere and inside of the block slope, while warmer air in the voids of the block slope moved upward and escaped from the top slope. The drained air was compensated by the penetration of colder outside air into the lower and middle part of the block slope (Sawada et al. 2003). Ground ice did not grow in winter, due to the lack of source water. In April, ground ice started to accumulate co-incidentaly with the initiation of the snowmelt (Sawada et al. 2003).

Ice ablation was triggered by heavy rainfall, and it continued until the subsurface was cooled to the freezing point in November 2001 (Sawada 2003). The annual maximum depth of the ground ice (i.e., active layer depth) ranged from -157.8 cm to -143.6 cm between 2001 and 2005 (Sawada unpublished data).

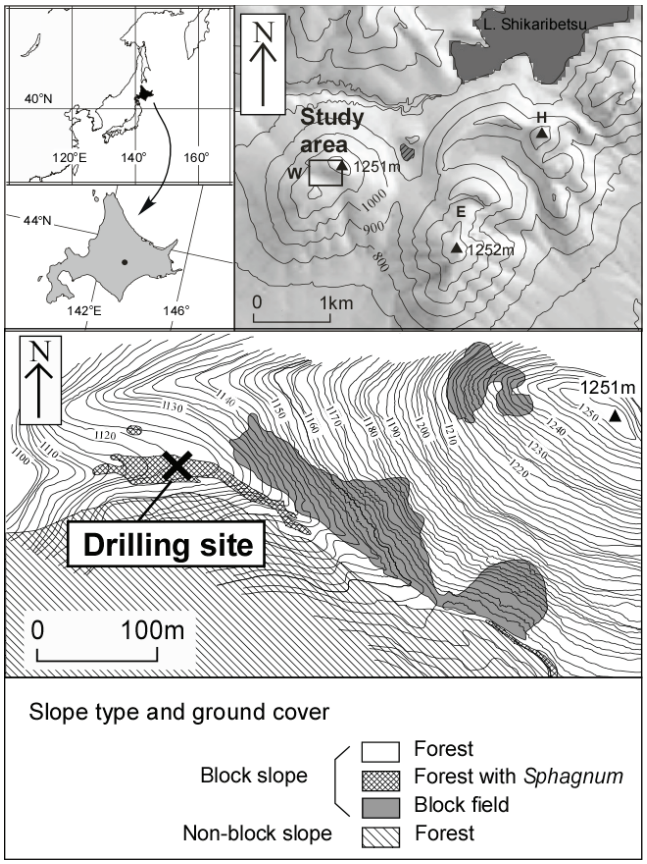

Figure 1. Study area and drilling site.

Methods

Drilling operation

Drilling was conducted on 11 July 2005, when the seasonal ice accumulation reached the annual maximum. The surficial soil and blocks were excavated down to the depth of 1.2 m. Drilling started on the surface of the seasonal ice. A drilling bit with tungsten carbide cutting teeth was used for the ice-predominant part, while a diamond bit with water injection was used for passing through andesite blocks. As a consequence, core samples of the ice and rock mixtures were obtained to the depth of 3.8 m during the 2-day drilling operations.

Sample analysis

The samples were sketched in the cold room at -20°C. Thereafter, these were cut into smaller pieces 2–11 cm in length. The length varied with the material of the samples: shorter length for pure ice, longer samples for ice-boulder mixture. The sample pieces were melted at room temperature. Water and organic materials were separated in the glass vials. AMS 14C datings of organic materials were conducted in Beta Analytic Inc., USA and Paleo Labo Co. Ltd., Japan. The 14C dates were converted into the calendar years with the calibration curve INTCAL04 (Reimer et al. 2004).

Oxygen and hydrogen isotope ratios were measured with the Delta-Plus mass spectrometer and Isoprime-PyrOH mass spectrometer, respectively. Both mass spectrometers are managed at the Institute of Low Temperature Science, Hokkaido University. Stable isotope ratios were given as permil difference to V-SMOW, with errors less than 0.02‰ and 0.5‰ for δ18O and δD, respectively. The results were presented in δ18O-δD diagrams with respect to the Global Meteoric Water Line (GMWL), in which fresh surface water was correlated on a global scale (Craig 1961).

Results

Structure of the core samples

Figure 2 shows sketch and pictures of the sample core. The core is classified into four segments: (A) ice and boulder mixture, (B) boulders, (C) gravelly sand with charcoal fragments, and (D) gravelly silt with ice lenses. Because the maximum thaw depth in the previous year (2004) was -141 cm, the upper 20 cm of ice is interpreted as seasonal ice formed in the spring of 2005.

Segment A contains clear ice and numerous organic materials. The ice displayed a layered structure (Fig. 2) similar to that of the glacier ice. The ice includes organic materials (leaves, branches, and fecal pellets). The fecal pellets piled up on the boundary of the ice layer have rounded shape with a diameter of 2–3 mm. These fecal pellets and plant materials indicate that the voids in the block layer are inhabited by Japanese Pikas (Ochotona hyperborea yesoensis) which commonly live in blocky landforms such as block slopes or moraines. They use the voids as nests or tunnels through which they carry plants (Kawamichi 1969). In addition, Japanese Pikas stock dried plants in the voids to survive in winter (Kawamichi 1969). The presence of the branches, leaves, and fecal pellets within the ice suggests the diets of Japanese Pika in the past.

Segment B does not contain clear ice, and this is probably due to thermal disturbances from drilling with a diamond bit. Because the tungsten bit became unstable at depth, a diamond bit with water injection was used to penetrate this segment. The ice may have melted from the heat of the pouring water.

Segment C consists of gravelly sand. Small particles of charcoal 2–5 mm in diameter are scattered in this layer. Visible ice is absent in this segment.

Segment D is composed of gravelly silt. A number of ice lenses are formed within this layer.

Chronology of the sediments and ground ice

The radiocarbon ages are listed in Table 1. The sediment structure is composed of the upper boulder layer and lower finer materials (sand and silt layers). The charcoal particles within the sand layer (Segment C, Fig. 2) exhibits ages of 8411–8211 Cal BP. There are two possible routes in which the charcoals fall onto the sand layer. One route is direct input to the sand layer. In this case, the accumulation of the boulder layer is considered to occur after the mixing of charcoals with the sand layer. The other is through the voids in the boulder layer. In this case charcoals penetrate into the existing block layer. In both cases the ground ice within the

Table 1. AMS radiocarbon ages of organic remains.

Depth	Host material	Type of organic material	Lab. Number	14C yr BP	Cal. yr BP 2-σ range
−159cm	ground ice	stem	PLD-7814	-65±15	N.A. (1950AD–Present)
−182cm	ground ice	stem	PLD-7815	570±15	633–537
−194cm	ground ice	fecal pellet	PLD-7816	720±15	683–661
−249cm	ground ice	leaf	Beta-213965	3590±40	4065–3728
−324cm	gravelly sand	charcoal	Beta-213966	7530±40	8411–8211

boulder layer is formed after the charcoals are mixed with the sand layer.

Accordingly, the organic materials in the infilling ice (Segment A, Fig. 2) exhibit much younger radiocarbon ages than the charcoals in the sand layer. The oldest age of 4065–3728 Cal BP was obtained from a leaf enclosed within the ice at depth of -249 cm. This leaf was extracted along with fecal pellets from the ice, indicating Japanese Pika stocked leaves in this depth. The age of the leaf also indicates that the ground ice was formed at this depth after the leaf had been transported. Thus, the age of the leaf gives the oldest estimation of the ice that included the leaf.

The ages of the organic materials become younger toward the ground surface. The ages of fecal pellets at -194 cm and stem at -182 cm are 683–661 Cal BP and 633–537 Cal BP, respectively (Fig. 2, Table 1). These two ages indicate that the perennial ice between -194 cm and -182 cm accumulated in 13–15 centuries. The age of stem at -159 cm exhibits a future age, which is apparently affected by recent nuclear testing. Thus, this age of ice shallower than -159 cm is interpreted to be modern (i.e., after 1950 AD).

Stable isotopes

Table 2 shows the isotopic composition of rain, snow, seasonal ground ice, and perennial ground ice samples. These isotope values are also plotted on the δ18O–δD diagram (Fig. 3).

Rain water (N=8) was collected during precipitation events between May and September 2004 at the shore of Lake Shikaribetsu (810 m a.s.l.). The mean isotopic composition of the rainwater was -11.0‰ for δ18O and -78.0‰ for δD. The samples are characterized by the d-excess of 9.7‰ and the slope of 7.4 on the δ18O–δD diagram, which are similar to the GMWL (d-excess of 10 and slope of 8: Craig 1961).

On 17 April 2005, snow cover was sampled at the drilling site (N=5). The snow cover was 2.2 m thick, and the upper 0.2 m started to melt. The isotopic composition of snow differs significantly from that of the rainwater. The mean isotopic composition of snow was -14.7‰ for δ18O and -90.5‰ for δD. The mean d-excess was 27.2‰, and the slope was 7.11. The larger d-excess value of snow indicates non-equilibrium evaporation from the Sea of Japan. In winter, northern Japan suffers westerly prevailing wind which originally blows from Siberia. The cold air causes fast non equilibrium evaporation from the Sea of Japan, where the Tsushima warm current flows from south to north (Waseda & Nakai 1983). Consequently, the winter precipitation has a large

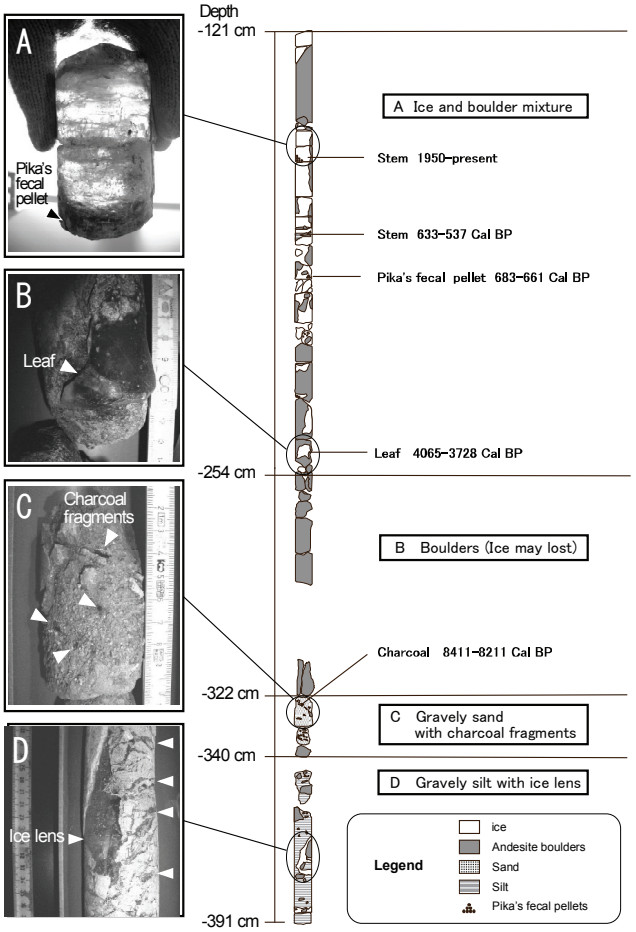

Figure. 2. Stratigraphy of the core samples obtained on the valley bottom.

Figure 2. Stratigraphy of the core samples obtained on the valley bottom.

d-excess value (>20), while the summer precipitation has a small value (<10), because vapor comes from the Pacific Ocean in summer (Waseda & Nakai 1983). Thus, the large d-excess value of snow is thought to originate from vapor from the Sea of Japan in winter.

The mean isotopic composition of seasonal ice formed between April and July 2005 was -12.3‰ for δ18O and -80.5‰ for δD, and mean d-excess was 17.8‰ (Table 2). These values were intermediate between rain and snow water, indicating two possibilities for isotope fluctuations: (1) the recent ground ice was fed by a mixture of rainwater and snowmelt water; (2) the ground ice was fed by snowmelt water, which was isotopically enriched before entering the block slope. Unnikrishna et al. (2002) reported that the initial

Table 2. Minimum, mean and maximum values and standard deviations of stable isotopes (δ18O, δD and d-excess) as well as slopes and intercepts in the δ18O-δD diagram for ground ice and recent precipitation sampled in the study area.

Source	N	slope	Intercept	R^2		$\delta^{18}O$ (‰)	δD(‰)	d-excess(‰)
Perennial ice	19	7.80	13.60	0.98	mean	−11.99	−79.86	16.0
					max.	−11.16	−66.90	18.2
					min.	−14.10	−96.30	14.2
					std. dev.	1.14	9.01	1.2
Seasonal ice formed in 2005 Apr.–Jul.	3	4.99	−19.24	0.99	mean	−12.28	−80.50	17.8
					max.	−10.51	−74.70	20.8
					min.	−13.14	−84.40	14.6
					std. dev.	1.02	5.12	3.1
Rain water in 2004 May–Sep.	8	7.39	3.04	0.98	mean	−10.97	−78.03	9.7
					max.	−4.98	−34.70	17.8
					min.	−18.15	−131.90	0.2
					std. dev.	4.46	33.30	5.4
Snow pack in 2005 Apr.	5	7.11	14.15	0.94	mean	−14.72	−90.52	27.2
					max.	−13.32	−79.80	28.9
					min.	−16.01	−99.70	23.7
					std. dev.	1.09	7.97	2.1

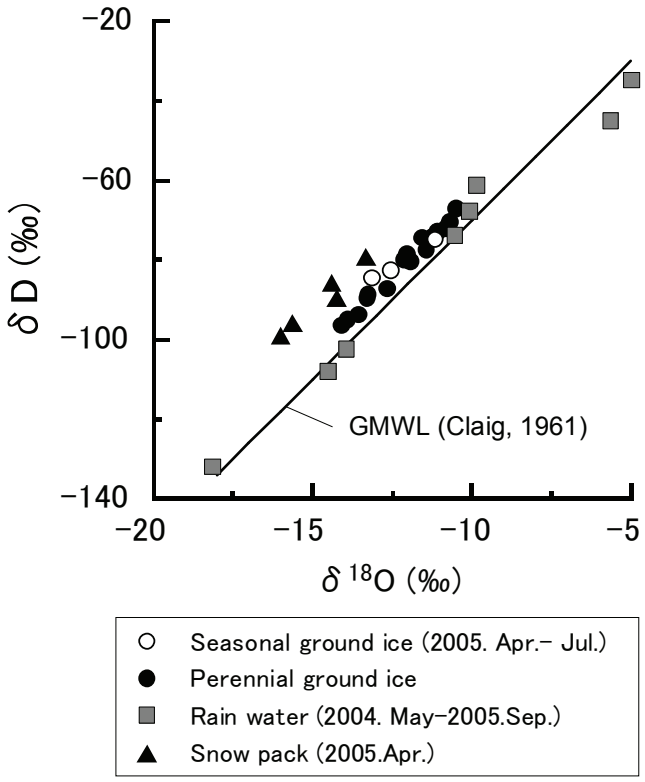

Figure 3. δ18O–δD diagram for rain, snow, seasonal ice, and perennial ice samples. GMWL is the Global Meteoric Water Line.

snowmelt water had higher δ18O than the original snowpack, because it originate from the lower snowpack layers which were isotopically enriched by snowmelt infiltration. This indicates that the rainwater may not be necessary for ground ice, which has a higher (heavier) δ18O than the snowpack.

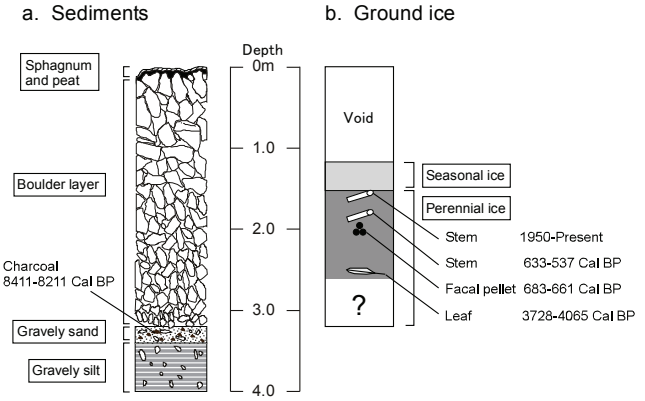

Figure 4. Vertical profiles of (a) sediments and (b) ground ice.

The perennial ground ice also has a smaller range of isotopic composition than rain and snow. The mean isotopic composition of the perennial ice was -11.2‰ for δ18O and -79.9‰ for δD, and mean d-excess was 16.0‰. The ranges were 2.1‰ for δ18O and 23.6 ‰ for δD. These small ranges indicate that the source water of the ground ice is basically unchanged for long periods.

Age and Accumulation Process of the Perennial Ice

The chronology of the sediment and ice of the core samples is shown separately in Figure 4, because the formation ages of these two materials are apparently different. Figure 4a shows the stratigraphy of the sediments. The perennial ice did not formed in the age of the charcoal particle within the sand layer (8411–8211 Cal BP), because the charcoal particles could not

enter the sand layer if the above boulder layer was filled with ice. Thus, initiation of the perennial ice is younger than the charcoal age.

The calibrated age of the leaf trapped in the perennial ice at -249 cm depth (4065–3728 Cal BP: Table 1, Fig. 4b) gives the youngest estimation of the ground ice formation. The leaf had been preserved in good condition in the ice, indicating the leaf did not experience any decomposition. Thus, the real age of the ice formation at -249 cm approaches the age of the leaf. From these assumptions, the onset of the ground ice within the block layer can be assumed to be between 8.4–3.7 ka.

The age of organic materials within the perennial ice decreases toward the top (Fig. 4b), indicating the upward accumulation of the ice. Because the top of the perennial ice is determined by the seasonal thaw depth (active layer thickness), this sequence also suggests upward migration of the permafrost table. In the study site, Sphagnum mat, peat, and tephra layers cover the blocky sediments. These organic and volcanic soils may act as an effective insulator to reduce the heat input and to preserve the perennial ground ice even in the positive MAAT environment.

Conclusions

The drilling operation and subsequent geochemical analysis allowed paleoclimate reconstruction from the perennial ground ice preserved in a block slope. The AMS 14C dating of organic materials revealed that the perennial ground ice is preserved at least 3700 years. The 14C age became younger towards the top of the ice, indicating that the law of superposition is applicable to the ground ice sequence in the block slope.

Comparison of the stable isotope compositions between perennial ice, seasonal ice, rain, and snow suggests that the ground ice originates from purely meteoric water, while the isotope composition is changed from the original source water. The perennial ice has the potential to preserve long-term fluctuation in the isotope composition of the meteoric water.

Acknowledgments

This study was supported by the “Leadership fund” of the Institute of Low Temperature Science, Hokkaido University in 2004, by a research fund from the Tokyo Geographical Society in 2005, and by a research fund by Paleo Labo Co. Ltd. in 2006. The author would like to thank Takeshi Nakatsuka for measuring stable isotopes; Hiroshi Adachi and Nobuyuki Nosaka (Geo act Co. Ltd.) for technical guidance for drilling; Atsushi and Sarasa Ono, Katsuhiko Asahi, Yugo Nakamura, Fumitaka Katamura, and Hiroyori Sugiyama for helping the drilling operation; and Takayuki Shiraiwa and Sumito Matoba for helping with ice-core treatment. The author would like to thank the associate editor and two reviewers for constructive comments and language improvement.

References

Craig, H. 1961. Isotopic variations in meteoric waters. Science 133: 1702-1703.

Delaloye, R., Reynard, E., Lambiel, C. & Marescot, L. 2003. Thermal anomary in a cold scree slope (Creux du Van, Switzerland). Proceedings 8th International Conference on Permafrost, 2003, Zürich, Switzerland, 21–25 July, 2003: 175-180.

Gorbunov, A.P., Marchenko, S.S. & Seversky, E.V. 2004. The thermal environment of blocky materials in the mountains of Central Asia. Permafrost and Periglacial Processes 15: 95-98.

Gude, M., Dietrich, S., Hauck, C., Mäusbacher, R., Molenda, R., Ruzicka, V. & Zacharda, M. 2003. Probable occurrence of sporadic permafrost in non-alpine scree slopes in central-Europe. Proceedings 8th International Conference on Permafrost, 2003, Zürich, Switzerland, 21–25 July, 2003: 331-336.

Humlum, O. 1999. Late-Holocene climate in central West Greenland: meteorological data and rock-glacier isotope evidence. The Holocene 9: 581-594.

Kawamichi, T. 1969. Behavior and daily activities of the Japanese Pika, Ochotona hyperborean yesoensis. Jour. Fac. Sci. Hokkaido Univ. Ser. VI, Zool. 17: 127-151.

Kneisel, C., Hauck, C. & Vonder Mühll, D. 2000. Permafrost below the timberline confirmed and characterized by geoelectrical resistivity measurements, Bever Valley, eastern Swiss Alps. Permafrost and Periglacial Processes 11: 295-304.

Mackay, J.R. 1983. Oxygen Isotope Variations in Permafrost, Tuktoyaktuk Peninsula Area, Northwest Territories. Paper 83-1B, Geological Survey of Canada: 67-74.

Mayer, H., Dereviagin A., Siegert, C., Schirrmeister, L. & Hubberten, H.W. 2002. Palaeoclimate reconstruction on Big Lyakhovsky Island, North Siberia - hydrogen and Oxygen isotopes in ice wedges. Permafrost and Periglacial Processes 13: 91-105.

Unnikrishna, P.V., McDonnell, J.J. & Kendall, C. 2002. Isotope variations in a Sierra Nevada snowpack and their relation to meltwater. Journal of Hydrology 260: 38-57.

Reimer, P.J., Baillie, M.G.L., Bard, E., Bayliss, A., Beck, J.W., Bertrand, C.J.H., Blackwell, P.G., Buck, C.E., Burr, G.S., Cutler, K.B., Damon, P.E., Edwards, R.L., Fairbanks, R.G., Friedrich, M., Guilderson, T.P., Hogg, A.G., Hughen, K.A., Kromer, B., McCormac, F.G., Manning, S.W., Ramsey, C.B., Reimer, R.W., Remmele, S., Southon, J.R., Stuiver, M., Talamo, S., Taylor, F.W., van der Plicht, J. & Weyhenmeyer, C.E. 2004. IntCal04 Terrestrial radiocarbon age calibration, 26–0 ka BP. Radiocarbon 46: 1029-1058.

Sawada, Y. 2003. Monitoring of ground-ice formation in a block slope at Mt. Nishi-Nupukaushinupuri, Hokkaido, Japan. Proceedings 8th International Conference on Permafrost, 2003, Zürich, Switzerland, 21–25 July, 2003: 1001-1005.

Sawada, S., Ishikawa, M. & Ono, Y. 2003. Thermal regime of sporadic permafrost in a block slope on Mt. Nishi-Nupukaushinupuri, Hokkaido Island, Northern Japan. Geomorphology 52: 121-130.

Steig, E.J., Fitzpatrick, J.J., Potter, N., Jr. & Clark, D.H. 1998. The geochemical record in rock glaciers. Geografiska Annaler 80A: 277-286.

Waseda, A. & Nakai, N. 1983. Isotopic composition of metric and surface waters in Central and Northeast Japan. Geochemical Journal 17: 83-89. (In Japanese)

Zacharda, M., Gude, M. & Ruzicka, V. 2007. Thermal regime of three low elevation scree slopes in Central Europe. Permafrost and Periglacial Processes 18: 301-308.

Contribution of Self-Potential (SP) Measurements in the Study of Alpine Periglacial Landforms: Examples from the Southern Swiss Alps

Cristian Scapozza
Institute of Geography, University of Lausanne, Switzerland
Pierre Gex
Institute of Geophysics, University of Lausanne, Switzerland
Christophe Lambiel, Emmanuel Reynard
Institute of Geography, University of Lausanne, Switzerland

Abstract

Measurements of streaming potentials were carried out on rock glaciers and talus slopes in a test site of the southern Swiss Alps. After some theoretical considerations and a brief description of the measurement technique, a method of data treatment in high declivity topography is presented. The results of self-potential prospecting measurements are generally in accordance with the geomorphological observations. In particular, the groundwater runoff is influenced by the occurrence of permafrost, which creates surfaces of water migration partially independent from ground porosity.

Keywords: geophysics; rock glacier; self-potential; streaming potentials; Swiss Alps; talus slope.

Introduction

Self-potential (SP) (or spontaneous potential measurements) in the study of periglacial environments is a recent and not well-developed geophysical method in geomorphology, geocryology, and glaciology. Natural electrical potentials measurements have been carried out to monitor the thawing front movement and to study the active layer and permafrost parameters in arctic periglacial environments (e.g., Gahé et al. 1988, Fortier et al. 1993), for the study of subglacial drainage (e.g., Blake & Clarke 1999, Kulessa et al. 2003) or for the investigation of landslides (e.g., Bogoslowsky & Ogilvy 1977, Gex 1993).

In alpine periglacial environments, no studies on streaming potentials associated with groundwater runoff in rock glaciers and talus slopes have been carried out. Rock glacier hydrology has been studied with water tracing (e.g., Tenthorey 1992, Krainer & Mostler 2002) or thanks to borehole logging (e.g., Haeberli 1985, Vonder Mühll 1992), whereas talus slope hydrology is not well known (e.g., Rist & Phillips 2005).

The present paper presents and discusses results of streaming potentials mapping in the Sceru Valley (Fig. 1), in the Eastern part of the Blenio Valley (Lepontine Alps of the Tessin, southern Switzerland). The objectives are to present the measurement technique and a method of data treatment in high declivity topography.

Theory and Methods

Macroscopic streaming potential mapping was realized from field measurements carried out in 2006 and 2007. The method is completed by geomorphological observations and mapping, frequency-domain electromagnetic lateral mapping and 2D resistivity profiling (Geonics EM-16R and EM-31), direct current (DC) resistivity soundings, and thermal prospecting (miniature ground temperature data loggers and spring temperatures). In this paper, only the field measurement technique and the interpretation of large geomorphological structures (> 1000 m^2) are presented.

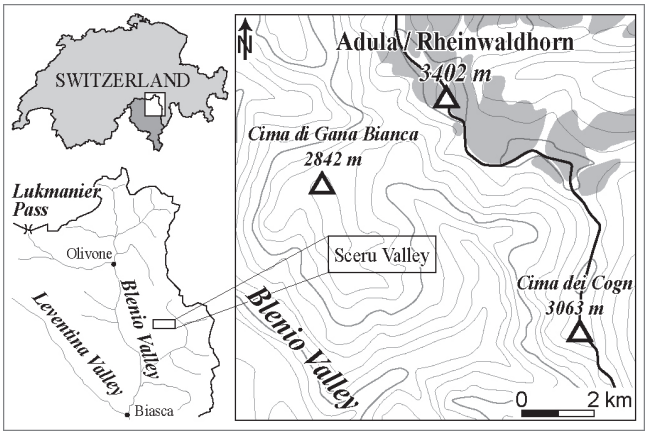

Figure 1. Geographical location of the study area.

The streaming potentials

Streaming potentials, or electrofiltration potentials, are natural electrical potentials produced by water flow through a porous and permeable soil (Reynolds 1997). The streaming potentials are directly proportional to the selective filtration of ions (electrofiltration) at the microscopic scale. Water, acting as an electrolyte, creates at the interface mineral-water a positive load flow between the immobile part of the electrical double layer (composed by the Stern layer—in contact with the mineral and with fixed cations, and the Gouy-Chapman diffuse layer—with a lower cations concentration) and the free neutral electrolyte (Revil et al. 2004). The Helmholtz-Smoluchowski law links up the electrofiltration potential (EF) amplitude with the electrolyte characteristics:

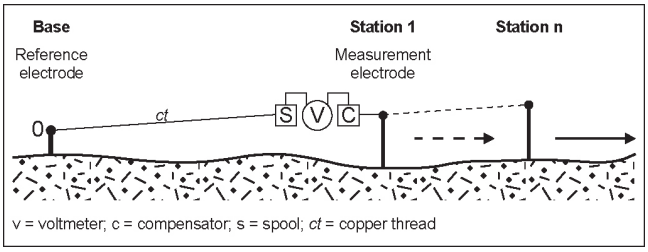

Figure 2. Field acquisition of self-potential data.

$$EF = \frac{\rho \varepsilon \zeta}{4 \pi \eta} \Delta P \quad (1)$$

where ρ is the resistivity, ε the dielectric constant and η the dynamic viscosity of the electrolyte. ζ is the electrical potential of the double layer (zeta potential) and ΔP is the pressure difference between the measurement points of EF.

Ultra-fresh and fresh groundwaters induce the maximum electrofiltration fields (Bogoslowsky & Ogilvy 1973). Indeed, in presence of much conductive water (with a mineral concentration exceeding 5 g/l), the electrolyte short-circuits the spontaneous electrical current.

Self-potential variations are also due to the granulometry and permeability of the soil. In a homogenous and isotropic terrain and where granulometry and permeability are known, the streaming potentials reflect the contours of the water table. In this case, self-potential mapping and inversion can supply information about some characteristics (configuration, direction, and intensity) of seepage flow both in horizontal and vertical planes (Revil et al. 2004).

Measurement of streaming potentials

SP is a passive method. The technique applied in this study is based on the fact that each value of self-potential measured at the ground surface is linked up with one electrode fixed at a base station situated outside of the geomorphological landforms studied. The potential difference (in mV) is measured between the reference electrode and a measurement electrode, which is moved along a traverse (Gex 1993, Reynolds 1997).

The range of the measured potentials is generally comprised between several millivolts (mV) and one volt. Because the sign of the zeta potentials could be positive or negative according to the earth materials, the sign of the difference of voltage measured is an important factor for the interpretation of SP anomalies (Reynolds 1997). For convention, the self-potential value at the reference electrode is zero. SP cartography has been carried out with a distance between every measurement of 3 to 5 m.

The measurement material used in this study was developed at the Institute of Geophysics of the University of Lausanne. The reference electrode of the model non-polarisable with $Cu\text{-}CuSO_4$ was realized in PVC and wood. The measurement electrode is fixed on a stick one meter long; its thin section allows us to drive it into the ground comfortably. It is linked up with the reference electrode by an isolated copper wire. A spool, fixed on the back of the operator, permits us to unwind the copper wire. The measurements are carried out with a high impedance (100 MΩ) digital voltmeter. The scale range of the voltmeter is comprised between -2000 and 2000 mV. A compensator is associated with the voltmeter to settle the SP value to the zero at the reference electrode. Finally, the voltmeter is provided with a filter that permits us to stabilize the measurements when the ground presents perturbations to the natural electrical fields. The field data acquisition is schematized in Figure 2.

Very Low Frequency-Resistivity (VLF-R)

The VLF-R technique (see Hoekstra et al. 1975, Hoekstra 1978, McGrath & Henderson 1985) uses electromagnetic energy radiated by a very low frequency (VLF) transmitter. In this study the Hauderfehn transmitter (23.4 kHz) located in Germany was used. The measurement of the horizontal component of the electric field and of the horizontal magnetic component perpendicular to the azimuth of the transmitting station allows the apparent resistivity of the near surface to be determined using the Cagniard (1953) equation:

$$\rho_a = (0.2/f)(E/H)^2 \quad (2)$$

where ρ_a is the apparent resistivity (Ωm), *f* the frequency (Hz), *E* the electric field (mV/km) and *H* the magnetic field (nT). The ratio between *H* and *E* gives a phase angle that changes according to variations of resistivity with the depth.

The field data acquisition was carried out using a Geonics EM-16R instrument.

Field Site Characteristics and Data Acquisition

The Sceru Valley (46°27'N, 9°01'E) is an east-facing glacial cirque situated between 2000–2787 m a.s.l. The morphology and hydrology of the Sceru Valley were studied by Scapozza (2008). The morphology is characterized by the presence of several rock glaciers with different degree of activity, talus slopes, and Lateglacial moraines (Fig. 3).

Permafrost is present in the Piancabella rock glacier and in the lower part of the Gana Rossa talus slope (Scapozza 2008). The hydrology of the southern part of the Sceru Valley is influenced by the presence of rock glaciers. Because of the high porosity of the blocky surface, no subaerial water runoff can be observed (the spring in the lower part of the Gana Rossa talus slope is situated one meter below the ground surface).

In 2006 and 2007, 17 SP profiles were carried out on the Sceru I rock glacier, 2 on the Piancabella rock glacier, 1 on the Gana Rossa talus slope, and 2 on the Sasso di Luzzone talus slope/rock glacier complex. In total, about 1300 SP measurement points were listed.

In the talus slopes and the active rock glacier, several SP profiles were combined with Geonics EM-16R and/or EM-31 mapping along the same traverse.

Results and Discussion

Data treatment

In high declivity topography like the alpine periglacial

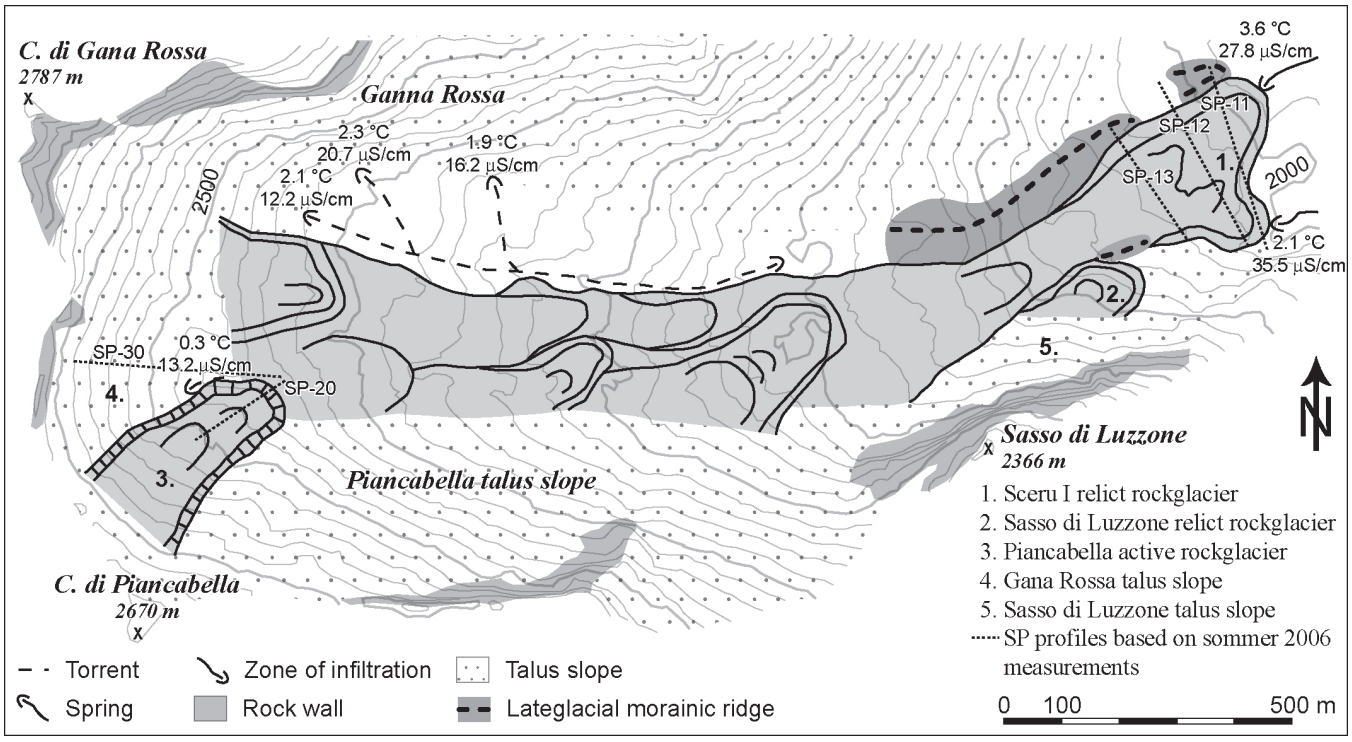

Figure 3. Geomorphological map of the Sceru Valley. For further information, see Scapozza (2008).

environment, the natural streaming potential linked to the slope is important, and its effect on the difference of voltage (in mV) measured by self-potential prospecting is very high. This perturbation, named "Topographic Effect" (TE), has been known to geophysicists for more than 90 years (Ernstson & Scherer 1986). The TE presents, for a constant electric field, an increasing negative potential linked with the elevation in altitude. For these reasons the regional anomaly (due to the TE) has to be subtracted from the measured values, which gives a final residual anomaly. The TE is calculated with a statistical analysis of linear regression between self-potential data and altitude. In practice, the average of the first four values of 11 traverses, measured between 2000–2450 m outside of the body of the Sceru I rock glacier, were used to calculate the TE, with a correlation between SP and altitude of -0.86. The calculated gradient of the TE is -68 mV per 100 m difference in elevation.

SP data were exposed in the form of potential profiles and equipotential maps. For the equipotential maps, a geostatistical interpolation of SP data was made with ordinary kriging. All the SP data (except for profiles SP-20 and SP-30) refer to the reference electrode placed outside the Sceru Valley (Fig. 4). For profiles SP-20 and SP-30, the reference electrode was placed at the Swiss Grid coordinates 720'215/145'660, at 2460 m a.s.l.

Sceru I relict rock glacier

The SP prospecting of this rock glacier shows an almost continuous negative residual anomaly in the northern lobe and another negative residual anomaly in the southern lobe. A zero millivolt residual anomaly is located between the Sceru I rock glacier and the Sasso di Luzzone talus slope/rock glacier complex situated south of it (Fig. 4).

According to the geoelectrical prospecting (2 DC resistivity soundings and one 2D resistivity profile), the bulk resistivity structure of the rock glacier seems to be relatively homogeneous. Indeed, the ground apparent resistivity is comprised between 3–5 kΩm (Scapozza 2008).

The groundwater runoff of two springs with different temperatures and electrical conductivities situated at two different lobes of the rock glacier could be followed by the self-potential prospecting (Figs. 4, 5). The link between the negative anomaly and the groundwater runoff is clearly evidenced in three SP profiles executed in summer 2006 (Fig. 5).

The two continuous anomalies may indicate the presence of two locations of preferential saturated groundwater flow. The two systems are probably independent, as evidenced from the constant difference throughout the year of temperature and conductivity of the two springs situated at the front of the rock glacier. Following this hypothesis, SP measurements would confirm that the two springs are alimented with groundwater of different origin (Fig. 4).

The torrents situated in the northern part of the Sceru Valley possibly feed the northern lobe spring (as pointed out by a warming of water temperatures), whereas the southern lobe spring would be alimented by an important aquifer situated into the Sceru I rock glacier. This water may be stored in the rock glacier for several months. The relatively high water conductivity (compared to the other springs in the valley, see Figure 3) and the constant water temperature (between 2.0°C and 2.2°C) all year long would confirm that the water transfer in this rock glacier is very slow, as it was pointed out by Tenthorey (1992) in a similar environment.

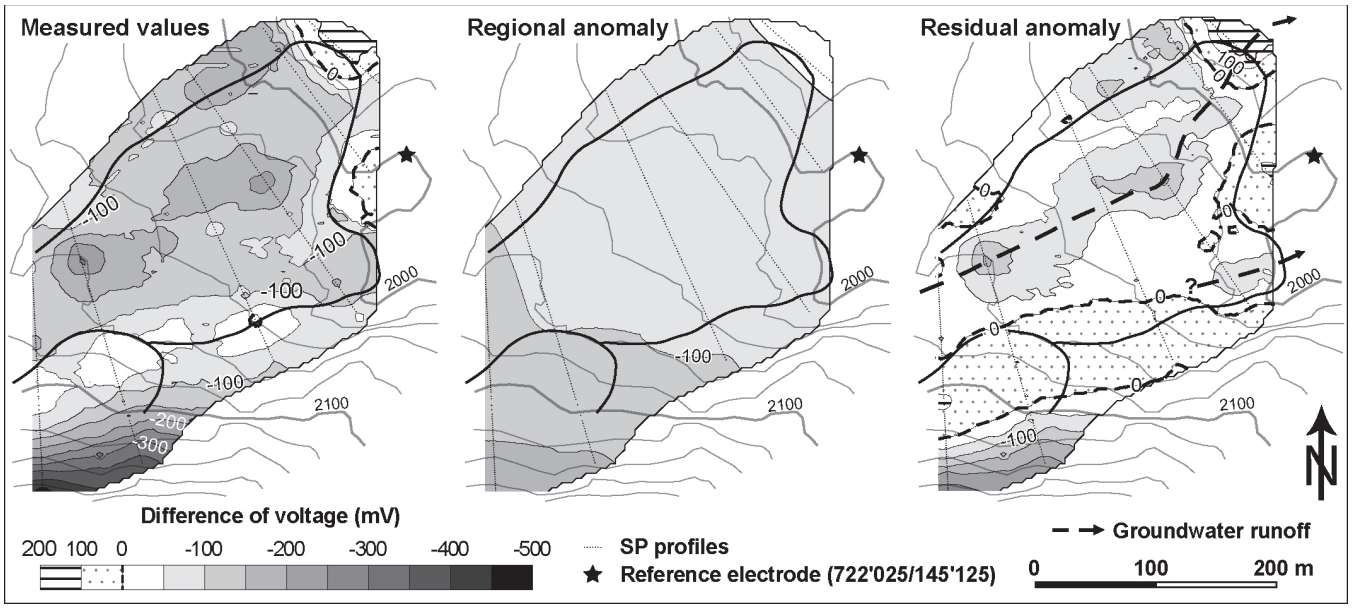

Figure 4. SP equipotential map of the Sceru I rock glacier and the Sasso di Luzzone talus slope/rock glacier complex based on summer 2007 measurements. For topographic names, see Figure 3.

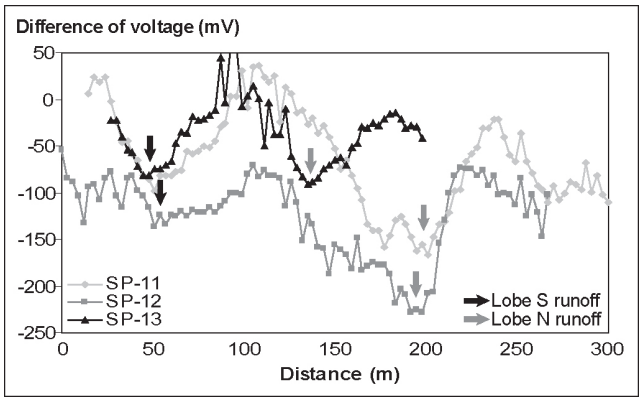

Figure 5. SP profiles executed across the Sceru I rock glacier. The arrows show negative anomalies linked with groundwater runoff. For the location of SP profiles, see the Figure 3.

The cold water temperature of the southern spring may be linked to a process of winter-ascending air circulation (the so-called chimney effect), which facilitates the cooling of the ground in the lower part of a porous sediment deposit (Delaloye & Lambiel 2005).

Piancabella active rock glacier

Prospecting of this landform shows a rise of the SP at the foot of the rock glacier front and a low increase of SP values all along the rock glacier (Fig. 6). Because of the location of the reference electrode (settled to 0) downslope of the rock glacier, the rise of the SP at the front can be interpreted as an important negative residual anomaly of several hundred mV.

A VLF-R tomography performed with the 2LayInv software (Pirttijärvi 2006) allows us to know approximately the active layer depth and the permafrost resistivity. The parameters of the profiling inversion are presented in Figure 6. Maximal VLF-R resistivities are found at the front of the rock glacier, and a decrease of the values toward upslope can be observed. Between 30–70 m, the decrease in the resistivities coincides with a decrease of the active layer depth. At 75 m, an important groundwater runoff has been perceived beneath the surface.

Data from the Piancabella active rock glacier show a connection between changes in SP, changes in active layer properties (particularly, its depth), changes in permafrost structure and/or in bulk resistivity structure (as shown by the VLF-R tomography). Indeed, the correlation between SP and active-layer depth is -0.74, whereas it is -0.85 between SP and permafrost resistivity. The correlation between SP and altitude (in m) is 0.54, which confirms that SP is partially independent from topography.

The permafrost resistivity depends on ground temperature, permafrost ice resistivity and content, and unfrozen water resistivity and content (Haeberli & Vonder Mühll 1996). Thus, it is difficult to separate the effect of change in water conductivity on SP from those on bulk resistivity.

The good connection between SP and permafrost resistivity probably indicates that there is a constant and continuous groundwater flow of constant water electrical conductivity and constant temperature throughout the active layer, and that SP changes are due to changes in the bulk resistivity structure of the rock glacier. This would confirm that the suprapermafrost groundwater runoff is supplied by the melt of annual névés at the root of the rock glacier and by the addition of incidental rainfall (see Tenthorey 1992). It is difficult to know the proportion of ice melt in the active layer and/or at the permafrost table, which is probable for a rock glacier situated at the lower limit of discontinuous permafrost.

Finally, the negative SP residual anomaly at the foot of the rock glacier front evidences an important groundwater runoff. This groundwater runoff is probably linked to suprapermafrost and intra- and subpermafrost water flow, which concentrates at the foot of the rock glacier front (Haeberli 1985).

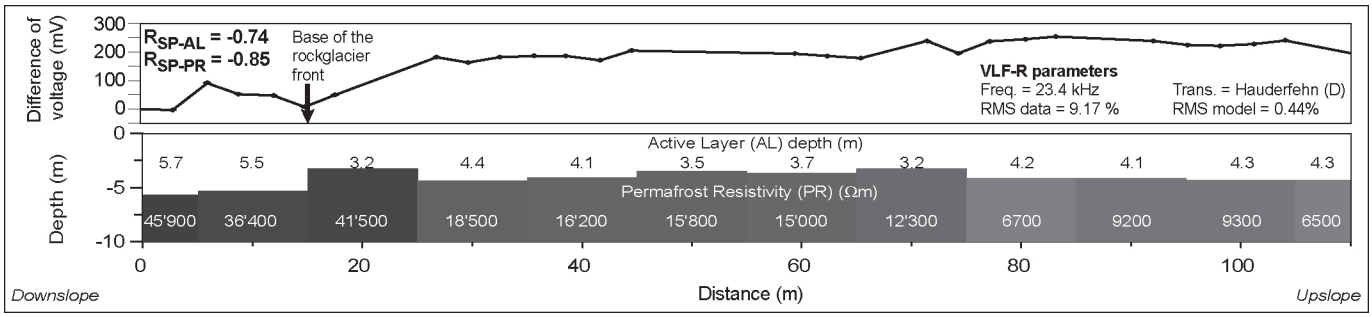

Figure 6. Profile SP-20 (at the top) and VLF-R tomography (below) on the Piancabella rock glacier. The VLF-R profiling inversion was performed with the 2LayInv (©University of Oulu) software (Pirttijärvi 2006).

Gana Rossa talus slope

SP prospecting of the Gana Rossa talus slope (Fig. 7) shows two negative residual anomalies in the lower part of the landform and an important and well-developed positive anomaly between 60–160 m distance. Another positive anomaly is present in the upper part of the talus slope. VLF-R prospecting shows relatively high apparent resistivities (over that 10,000 Ωm) in the lower part and in the middle of the talus slope. According to DC-resistivity, EM-31 and thermal prospecting (Scapozza 2008), permafrost is present only in the lower part of this talus slope (Fig. 7).

The streaming potentials are weakly positively correlated with altitude (R = 0.54), which contrasts with the theory of the TE (see *Data treatment*). Indeed, a test made in the Sasso di Luzzone talus slope (Fig. 3), where permafrost is absent, gives a very high negative correlation between streaming potentials and altitude (R = -0.97). Some results were pointed out by other studies carried out in high declivity slopes (e.g., Jackson & Kauahikana 1988).

Comparison between SP measurements and permafrost distribution shows, for the lower part of the talus slope, a connection between SP residual anomalies and permafrost occurrence. A possible hypothesis to explain this SP positive residual anomaly is the following: the presence of saturated or partially under-saturated permafrost may create a relatively impermeable surface of water runoff, which may modify the direction of the natural streaming potential linked to the slope (which is present between 120–200 m, as pointed out by the negative correlation between streaming potentials and altitude) by the canalization of groundwater flow at the base of the active layer. Following this hypothesis, the negative SP residual anomaly situated at a distance of 25 m may be related to an important water infiltration in the porous sediments, supplied by the melt of annual névés and by the addition of incidental rainfall. Whereas, the negative SP residual anomaly situated at a distance of 50 m may be related to the presence of a talik that would permit an intrapermafrost groundwater flow. The important groundwater runoff in the lower part of the talus is also proved by a spring (Fig. 3). Finally, in the upper part of the talus slope, the SP variations are probably due to the topography of bedrock, which is located only a few meters below the slope surface.

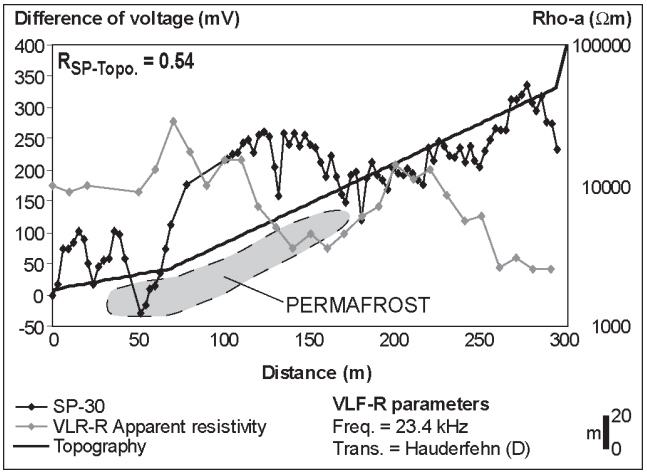

Figure 7. SP profile across the Gana Rossa talus slope.

In conclusion, it is very difficult today to better detail the hydrological and glaciological behavior of this talus slope without short, medium, and long-term thermal and geophysics monitoring at the surface and in boreholes.

Conclusions and Perspectives

The examples discussed show that measurement of streaming potential change on periglacial landforms offers good possibilities for assessing changes in water content and migration. Self-potential measurement could be useful for studying, in accordance with other geophysical methods, the importance of groundwater runoff generated by water infiltration and/or ice melting in permafrost terrains. The repetition of the same SP profile ten months later on a relict and an active rock glacier gave the same results; this confirms that streaming potential monitoring in periglacial landforms is possible. Self-potential monitoring associated with thermal and Electrical Resistivity Tomography (ERT) monitoring could be interesting for quantifying the processes correlated with permafrost degradation in high mountain environments.

Acknowledgments

Special thanks are due to all people who helped in the field, to the Associate Editor and the two anonymous reviewers for their useful feedback, and to Meredith Blake for proofreading the English.

References

Blake, E.W. & Clarke, G.K. 1999. Subglacial electrical phenomena. *Journal of Geophysical Research* 104 (B4): 7481-7495.

Bogoslowky, V.V. & Ogilvy, A.A. 1973. Deformations of natural electric fields near drainage structures. *Geophysical Prospecting* 21: 716-723.

Bogoslowky, V.V. & Ogilvy, A.A. 1977. Geophysical methods for the investigation of landslides. *Geophysics* 42: 562-571.

Cagniard, L. 1953. Basic theory of the magneto-telluric method of geophysical prospecting. *Geophysics* 18: 605-635.

Delaloye, R. & Lambiel, C. 2005. Evidence of winter ascending air circulation throughout talus slopes and rock glaciers situated in the lower belt of alpine discontinuous permafrost (Swiss Alps). *Norsk Geografisk Tidsskrift* 59: 194-203.

Ernston, K. & Scherer, H.U. 1986. Self-potential variations with time and their relation to hydrogeologic and meteorological parameters. *Geophysics* 51: 1967-1977.

Fortier, R., Allard, M. & Seguin, M.-K. 1993. Monitoring thawing front movement by self-potential measurements. *Proceedings of the Sixth International Conference on Permafrost, Beijing, China, July 5–9, 1993*: 182-187.

Gahé, E., Allard, M., Seguin, M.-K. & Fortier, R. 1988. Measurements of active layer and permafrost parameters with electrical resistivity, self potential and induced polarisation. *Proceedings of the Fifth International Conference on Permafrost, Trondheim, Norway, 2–5 August, 1988*: 148-153.

Gex, P. 1993. Mesures d'électrofiltration sur le glissement de la Frasse (Préalpes romandes). *Hydrogéologie BRGM* 3: 239-246.

Haeberli, W. 1985. Creep of mountain permafrost: internal structure and flow of alpine rock glaciers. *Mitteilungen der VAW/ETH Zürich*: 77.

Haeberli, W. & Vonder Mühll, D. 1996. On the characteristics and possible origin of ice in rock glacier permafrost. *Zeitschrift für Geomorphologie N. F.*, Suppl.-Bd. 104: 43-57.

Hoekstra, P. 1978. Electromagnetic methods for mapping shallow permafrost. *Geophysics* 43: 782-787.

Hoekstra, P., Sellmann, P.V. & Delaney, A. 1975. Ground and airborne resistivity surveys of permafrost near Fairbanks, Alaska. *Geophysics* 40: 641-656.

Jackson, D.B. & Kauahikana J. 1988. Regional self-potential anomalies at Kilauea volcano. *Prof. Pap. U.S. Geological Survey* 1350: 947-959.

Krainer, K. & Mostler W. 2002. Hydrology of active rock glaciers: examples from the Austrian Alps. *Arctic, Antarctic, and Alpine Research* 34: 141-149.

Kulessa, B., Hubbard, B. & Brown, G.H. 2003. Cross-coupled flow modeling of coincident streaming and electrochemical potentials and applications to subglacial self-potential data. *Journal of Geophysical Research* 108 (B8): 2381, DOI:10.1029/2001JB001167.

McGrath, P.H. & Henderson, J.B. 1985. *Reconnaissance Ground Magnetic and VLF Profile Data in the Vicinity of the Thelon Front, Artillery Lake Map area, District of Mackenzie.* Paper–Geological Survey of Canada 85-1A: 455-462.

Pirttijärvi, M. 2006. *2LAYINV – Laterally Constrained Two-layer Inversion of VLF-R Measurements*. User's guide, Division of Geophysics, University of Oulu.

Revil, A., Naudet V., Meunier, J.D. 2004. The hydroelectrical problem of porous rocks: inversion of the position of the water table from self-potential data. *Geophysical J. International* 159: 435-444.

Reynolds, J.M. 1997. *An Introduction to Applied and Environmental Geophysics*. Chichester: Wiley, 796 pp.

Rist, A. & Phillips, M. 2005. First results of investigations on hydrothermal processes within the active layer above alpine permafrost in steep terrain. *Norsk Geografisk Tidsskrift* 59 : 157-163.

Scapozza, C. 2008. *Contribution à l'étude géomorphologique et géophysique des environnements périglaciaires des Alpes Tessinoises orientales*. M.S. Thesis. Institute of Geography, University of Lausanne. Published February 28, 2008, on http://doc.rero.ch/

Tenthorey, G. 1992. Perennial nevés and the hydrology of rock glaciers. *Permafrost and Periglacial Processes* 3: 247-252.

Vonder Mühll, D. 1992. Evidence of intrapermafrost groundwater flow beneath an active rock glacier in the Swiss Alps. *Permafrost and Periglacial Processes* 3: 169-173.

Digital Elevation Model of Polygonal Patterned Ground on Samoylov Island, Siberia, Using Small-Format Aerial Photography

M. Scheritz and R. Dietrich
Dresden University of Technology, Institute of Planetary Geodesy, Dresden, Germany
S. Scheller
Dresden University of Technology, Institute of Photogrammetry, Dresden, Germany
W. Schneider and J. Boike
Alfred-Wegener-Institute for Polar- and Marine Research, Potsdam, Germany

Abstract

Accurate land cover, such as meso-scale to high-resolution digital elevation models (DEM), is needed to obtain reliable inputs for modeling the hydrology and the exchange between the surface and atmosphere. Small format aerial photography can be used to acquire high-resolution aerial images using balloons and helicopters. This method presents a low-cost, efficient method to construct a DEM of the polygonal patterned ground on Samoylov Island in the Lena Delta, Northern Siberia (72.2°N, 126.3°E). The DEM should be the foundation for modeling meso-scale hydrological processes on the island and identifying locations of discharge. The whole island could be covered with images taken from heights between 600 m and 800 m. All points of the DEM, with a resolution on the ground of 10 m, have a horizontal and vertical accuracy better than 1.0 m. This accuracy and the resolution depend on the survey height, the resolution of the camera system, the number and the quality of the images, and the algorithms used in the analysis. All listed parameters are explained and discussed in the paper.

Keywords: aerial photography; balloon; digital elevation model; polygonal patterned ground; Samoylov Island.

Introduction

The application of small format aerial photography to acquire high-resolution aerial images is still challenging. Balloons, kites, and helicopters are interesting and valuable tools for aerial photography. Several techniques with their advantages and disadvantages are briefly introduced and discussed in Bigras (1996) and Henry et al. (2002). Boike and Yoshikawa (2003) showed the successful use of balloon aerial photography for mapping snow, ice, and periglacial landforms around Fairbanks and Ny-Alesund, Svalbard. Recently, Vierling et al. (2006) successfully employed a tethered balloon with an altitude up to 2 km to acquire remotely sensed data. Further application fields are briefly explained in Aber and Aber (2002).

The goal of our work was to generate a digital elevation model (DEM, regular or irregular distributed points) of the polygonal patterned ground on Samoylov Island in the Lena Delta, Northern Siberia (72.2°N/126.3°E). The DEM should be the foundation for the modeling of meso-scale hydrological processes on the island for answering questions like: where are polygonal seas, how big are they, and where does the water drain into the Lena?

The landscape of the island is shaped by the micro topography of the wet polygonal tundra. The development of low-centered ice-wedge polygons results in a prominent micro relief with the alternation of depressed polygon centers and elevated polygon rims with elevation differences of up to 0.5 m over a few meters distance. Satellite images with resolutions between 15 m and 30m, such as Landsat (Aber & Aber 2002), do not represent this micro relief sufficiently. Difficulties of using satellite images are discussed in detail by Dare (2005). It is, however, the most important factor for small-scale differences in vegetation type and soil moisture, and is therefore a major variable when considering heat and trace gas fluxes on the meso-scale.

Depending on the general conditions, feasible equipment, cost, and available measurement time, the required horizontal and vertical accuracy of the DEM should be better than 1 m. Since remote-control-aircraft and drones are not permitted in Siberia, we used a tethered helium balloon. In addition it was also possible to take images from a helicopter. The photogrammetric equipment consists of a Nikon D200 with a 14 mm lens, 26 fabric-made targets for ground control points (GCPs), and additional geodetic equipment (tachymeter Elta C30).

This paper presents a low-cost, efficient method to acquire high-resolution aerial images using helium filled balloons. It discusses (1) different steps of obtaining aerial images from a balloon and a helicopter, (2) data analysis, (3) advantages and disadvantages of different assimilation platforms and (4) further improvements to increase the resolution of the DEM and the horizontal and vertical accuracy of the coordinates of each point.

Methods

The motivation mapping of the patterned ground on Samoylov Island was achieved using photogrammetric methods on aerial images with overlapping areas, allowing the determination of 3D coordinates (stereoscopy). There are different methods available ranging from simple stereoscopic methods with two images to a bundle block adjustment (Henry et al. 2002) over all taken images. Here

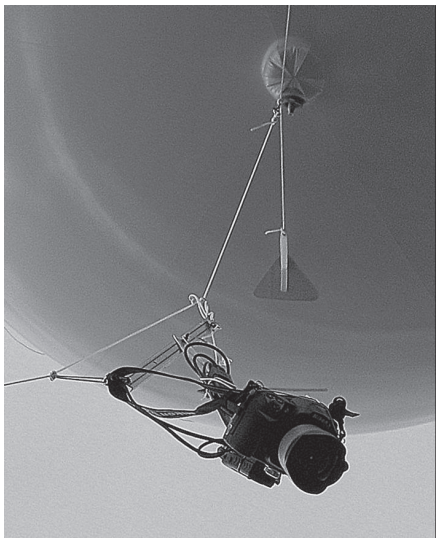

Figure 1. Camera system: Nikon D200, hanging at the tethered helium filled balloon.

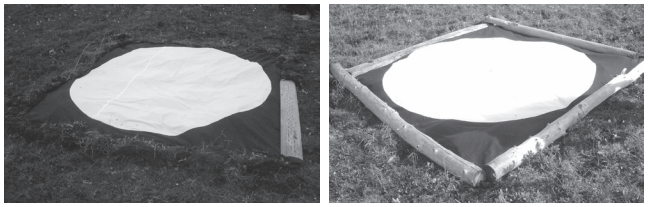

Figure 2. Fabric-made targets used as ground control points with a diameter of 2.5 m.

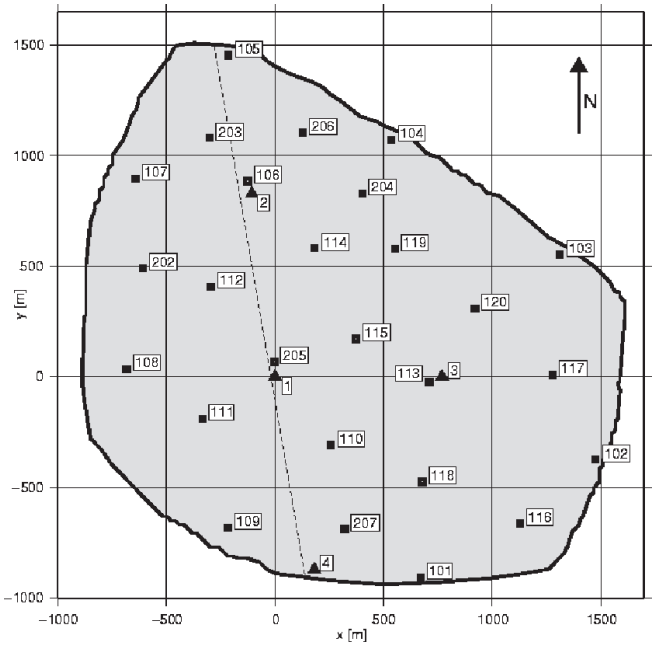

Figure 3. Schematic illustration of Samoylov Island: Network of 26 ground control points (squares); The coordinate (0,0) shows the origin of the local coordinate system with a fixed height of 100 m. The 4 datum points are displayed as triangles. The dashed line separates the flood plain (western part) and the plateau (eastern part).

the former method was used, since the flight path, height, and orientation of the balloon and thus the resulting images were somewhat unpredictable. The data analysis then consisted of two important steps: firstly a separate backward intersection for the calculation of the image orientation and secondly a forward intersection for the calculation of the 3D coordinates of the points of the DEM.

Before the fieldwork was carried out, the optimal camera system and the number of the GCPs was determined. The pre-condition for the DEM was a resolution on the ground better than 10 m with an accuracy in coordinates better than 1 m. Thus prior calculations were done on flight height, the size of the GCPs, the distance between them, and the required number of images covering the whole island. The survey height and the number and size of the GCPs finally were a compromise between the available time for measurement, the investment for the camera system, and the mentioned optimal conditions for resolution and accuracy.

Equipment

The equipment for the aerial photography consists of a Nikon D200 camera with a 14 mm lens (Fig. 1) and 26 fabric-made targets used as GCPs (Fig. 2). The Nikon D200 is a digital mirror reflex camera with a CCD sensor of 10.2 megapixel. With the calculated flight height of 800 m, one pixel maps an area of ~0.12 m² on the ground.

Depending on the flight height, the focal distance of the lens, and the condition that each GCP should represent an area of at least 6 x 6 pixels in the digital images, their diameter had to be greater than 2.0 m (Fig. 2).

To precisely calculate the image orientation, it was necessary to set up enough GCPs on the island to get a minimum of 4 points within each image. Considering the calculated flight height of 800 m, this resulted in at least 20 GCPs (called 101–120) with a spacing of about 500m to get an optimal coverage of Samoylov Island (~5 km²). Six control targets with a diameter of 1.0 m were additionally laid out to condense the point network (point IDs 202–207). The entire network of GCPs is shown in Figure 3.

A local coordinate system on Samoylov Island was fundamental to the photogrammetric fieldwork. Therefore 4 datum points (Fig. 3, point IDs 1–4) were set up, each marked with a 1m iron pipe in the permafrost soil. The distances between these points reached from 800 m to 1200 m. In Figure 3 the coordinate (0, 0) shows the origin of the local coordinate system with a fixed height of 100 m. For setting up the coordinate system we used the tachymeter Elta C30. The repeatability of the coordinates of the datum points was better than +/-2 cm.

Fieldwork

The fieldwork was divided into two parts. Firstly, GCPs were laid out, and their coordinates were surveyed in the local coordinate system. Secondly, aerial photographs were taken using a tethered balloon and a helicopter.

After laying out the GCPs, their registration was conducted

Figure 4. Tethered balloon, filled with helium, diameter 2–3 m.

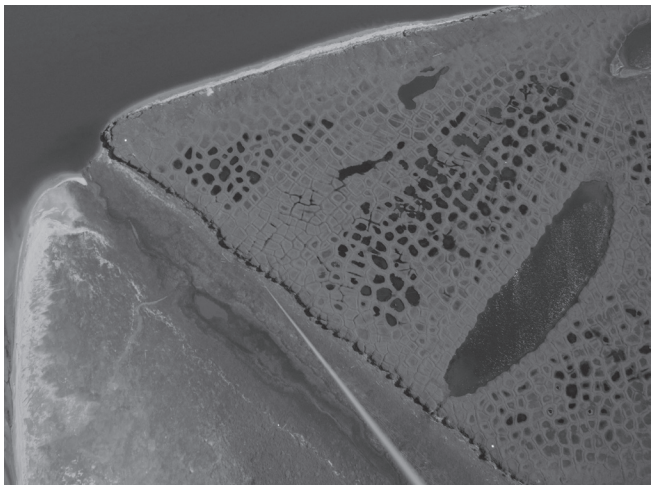

Figure 5. Polygonal patterned ground admitted from a height of ~750 m, in front the rope to the balloon.

in the local coordinate system with help of the tachymeter. The accuracy of the distances between the datum points and the GCPs was better than 1 cm. The coordinates of all GCPs had an absolute accuracy better than +/-5 cm. These accuracies depended on the determination of the center of the GCPs, the accuracy of the angle measurements with the tachymeter, and the distances to the survey points.

The balloon used in mapping the patterned ground on Samoylov Island is depicted in Figure 4, and an example image is given in Figure 5. The interval timer of the camera was adjusted to 1 minute, so the camera could take images for nearly four hours. Using the tethered balloon, one third of the entire island (western part, flood plain, Fig. 3) could be covered from a height of about 800 m.

Additionally, images were captured from a helicopter from altitudes between 600 m and 900 m. Using the helicopter, the middle part of the island could be covered with a flight height of ~600 m, the eastern part with flight heights of nearly 800–900 m.

Table 1. Nikon D200, interior parameters.

Parameter of inner orientation:	
Horizontal size Vertical size	3872 Pixel 2592 Pixel
Pixel size	0.0058mm
Principal point	x_0 = 0.10424mm y_0 = -0.19185mm
Principal distance	c = -13.32284mm
Parameter of distortion dx, dy (without units):	
Radial	a_1 = -0.000495642 a_2 = 1.65615e-006 a_3 = 0.0
Assymetric distortion Tangential distortion	b_1 = 1.72277e-005 b_2 = -1.51355e-005
Affinity Shear	c_1 = 0.000149996 c_2 = 2.72591e-005
r_0 - parameter	r_0 = 8.44

Calibration of the camera system

For the subsequent data analysis it was necessary to determine the parameters of the inner orientation of the camera system (interior parameters: principal distance c, coordinates of the principal point x_0, y_0, parameter of distortion dx, dy). The calibration of the camera system as specified in Luhmann (2000) was conducted before the fieldwork at the Institute of Photogrammetry at the Dresden University of Technology (Table 1).

To verify these camera parameters, a calibration-field was set up on Samoylov Island. Using the Elta C30, the coordinates of these points were measured with a relative accuracy of a few millimeters. The parameters of the inner orientation, that were consecutively determined, were nearly the same as in the laboratory, so the relation between the body of the camera and the objective can be assumed as stable.

Data Analysis

To analyze the collected data, a program was generated based on the algorithms of Luhmann (2000) and Schwidefsky & Ackermann (1976). The program includes the collinearity equations, which correlate the image coordinates (x,y) and the object coordinates (X,Y,Z) for each point:

$$x = x_0 - c \cdot \frac{r_{11}(X - X_0) + r_{21}(Y - Y_0) + r_{31}(Z - Z_0)}{r_{13}(X - X_0) + r_{23}(Y - Y_0) + r_{33}(Z - Z_0)} + dx \qquad (1)$$

$$y = y_0 - c \cdot \frac{r_{12}(X - X_0) + r_{22}(Y - Y_0) + r_{32}(Z - Z_0)}{r_{13}(X - X_0) + r_{23}(Y - Y_0) + r_{33}(Z - Z_0)} + dy \qquad (2)$$

First, a backward intersection was calculated for each single image to determine the outer orientation (perspective center (X_0, Y_0, Z_0) and rotation matrix $\underline{R}$). Approximated

parameters of the outer orientation were necessary and could be calculated applying a special algorithm developed by Schwidefsky and Ackermann (1976). The calculation of the outer orientation was successful for all images, which had minimized 4 GCPs.

Second, approximated coordinates for the points of the DEM were determined with help of a regular raster with a step size of 10 m based on the local coordinate system. The height of each point was set up to the average height of all GCPs. With the known outer orientation of the images a backward intersection could be determined for each preliminary point of the DEM, so the approximated positions could be found in the images. Then a search patch was defined around these locations and a matching-algorithm (with sub pixel accuracy) was implemented to locate precisely the same patch in other images. The matching algorithm was calculated with a cross-correlation:

$$k = \frac{\sum_{x'}\sum_{y'} g_1(x',y') \cdot g_2(x+x',y+y')}{\sum_{x'}\sum_{y'} g_1(x',y')^2 \cdot \sum_{x'}\sum_{y'} g_2(x+x',y+y')^2}$$

$$-1 \le k \le 1$$

At each position (x', y') a correlation coefficient k was determined depending on the gray scale value g of each pixel. The output consisted of a correlation image with all calculated values of k. Then, an algorithm was implemented which fitted an ellipsoidal paraboloid in the correlation image to find the exact position of the correlation maximum. At the end a forward intersection was calculated as a least square adjustment to get the exact 3D-coordinates for the points of the DEM.

The output dataset consists of all calculated coordinates, the standard deviation, and the correlation factor for the matching of one point between different images. If the correlation factor is greater than 0.7, and if the accuracy of the coordinates (horizontal and vertical accuracy) is better than 1 m, the point is stored as a point of the resulting DEM of Samoylov Island.

Results

Figure 6 shows the triangulated DEM. The horizontal and vertical accuracy of the coordinates of each point is better than 1.0 m (1σ, i.e., confidence interval of 68%). Polygonal lakes are easy to distinguish, because the algorithm was not able to match over the uniform water surface. Also, areas with bad data coverage are recognizable, for example in the southeastern part of Figure 6. The main reason for this is that the helicopter height changed very fast during the taking of the subsequent images, resulting in changing scaling factors of these images and smaller correlation factors. Other reasons for degraded correlation are poor illumination conditions and insufficient contours. As a result, only few points were found with a correlation larger than 0.7, whereas for most points the correlation factor was lower than 0.5. The island's center and the western and northern part have the best coverage of points. The helicopter was flying over the center

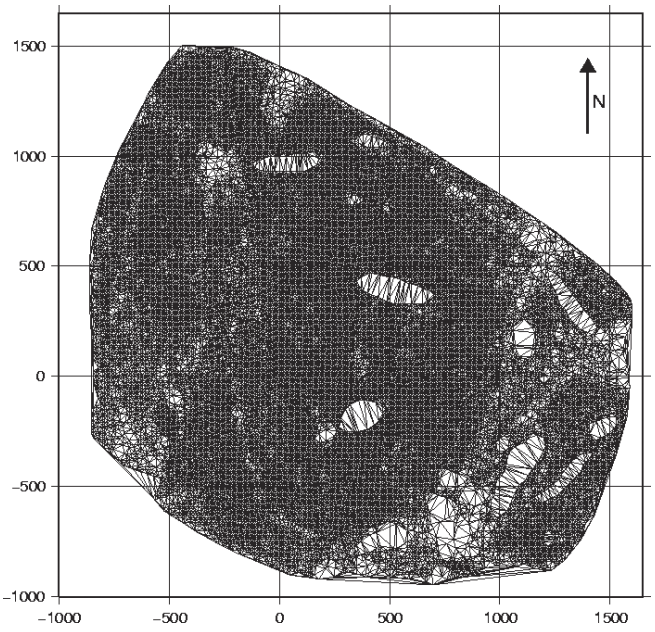

Figure 6. Triangulated irregular DEM with an approximated step size of 10 m of Samoylov Island: *x*- and *y*-coordinates are in a local coordinate-system (scale in m).

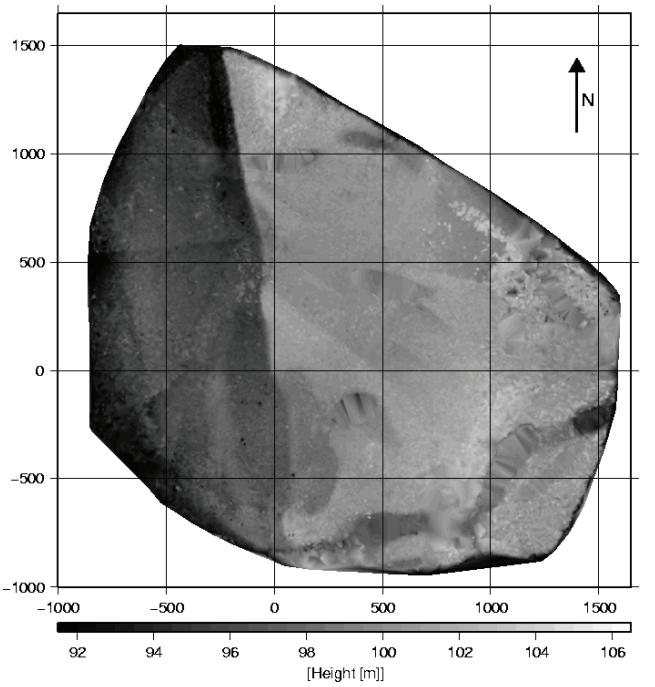

Figure 7. Surface of Samoylov Island: *x*- and *y*-coordinates are in a local coordinate system (scale in m). The heights of the points of the DEM are relative heights with respect to the origin of the local coordinate system (0.0) with a height of 100 m.

at a nearly constant height of 600 m. In addition, the height of the tethered balloon over the flood plain (western part, Fig. 6) was nearly constant, which made the calculations (in particular the matching algorithm) really successful. The estimated points from both datasets could be matched with correlation factors up to 0.99 and with horizontal and vertical accuracies partially better than 0.5 m.

In Figure 7 the triangulated network from Figure 6 is shown as a surface for the whole island. The flood plain is easy to distinguish, as well as the ridge between the flood plain and the plateau and the cliff line with height differences up to 8 m.

Discussion

The goal of this project was to generate a DEM of the whole of Samoylov Island. The short observation period and the cost of and permission for the equipment formed the boundary conditions for the field work, under which a trade-off between the resolution, accuracy, and practicable amount of work for the acquisition and evaluation of photos had to be found. We finally decided to use a tethered, helium-filled balloon and a camera with a high precision lens (Nikon D200 with 14 mm lens). On the ground, 20 fabric-made targets with a diameter of 2.5 m and 6 targets with a diameter of 1.0 m spanned a network of GCPs.

Taking aerial photographs with a balloon is a low-cost and efficient method to acquire high-resolution aerial images. However, to take images with a balloon-borne camera, a calm day with good illumination conditions is required. Especially the wind speeds limit the observation time – during the 3 weeks of the field work on Samoylov Island we had only 2 days with good weather conditions. Taking images from a helicopter is independent from wind conditions and more stable in maintaining the height and the flight path. But this application is very expensive, and it is also dependent on good illumination conditions.

A sensitive step within the data analysis is the matching algorithm, because different illumination conditions like cloud shadows and different scaling factors of the images are a disadvantage. Also the search patch has to be big enough to get sufficient correlations between different images with high correlation factors. To avoid correlations between neighboring points of the DEM (this would degrade the accuracy of coordinates) the step size has to be at least twice the size of the search patch. Depending on the survey height of 800 m and a search patch of 24 x 24 pixel, the resolution on the ground of the DEM was set to 10 m. Therefore, all points of the generated DEM should be independent from each other.

Under these terms each point of the DEM has a horizontal and vertical accuracy better than 1 m. Naturally there are improvement possibilities to retrieve the micro relief of the polygonal wet tundra, such as the use of more and smaller targets for GCPs concomitant with a lower flight height and thus a higher resolution and accuracy. Furthermore the standard deviation of the coordinates of the DEM improve, if the points can be found in more than 2 images. Therefore, a better and regular image-coverage of the whole island from the same survey heights and good stereoscopic bases (relation between survey height and image-spacing) are a requirement for high resolution DEMs.

Conclusions

The method described in this paper is, depending on the measurement time, cost, and equipment, very useful to measure typical permafrost landscapes with the desired resolution and accuracy. Depending on the survey height and conditions described above, the horizontal and vertical accuracy of each point in the generated DEM of Samoylov Island shown in Figures 6 and 7 is better than 1.0 m for nearly 70% of all triangulated points. The obtained resolution of the DEM amounts to 10 m. Additionally, the combination of images from balloon and helicopter was successful if the flight height was approximately equal.

The meso-scale DEM discussed in this paper is now utilized (at the Alfred Wegener Institute for Polar and Marine Research in Potsdam) to determine the channel routing in a spatially distributed hydrologic model for Samoylov Island. Additionally, it is also possible to generate a orthomosaic (Bitelli & Girelli 2004) with the known parameters of the outer orientation of the images. This methodology provides a good basis for quantification of fluctuating coastlines in permafrost landscapes.

Acknowledgments

This work was funded by the Alfred Wegener Institute for Polar and Marine Research in Potsdam, Germany. We are thankful for the logistical and financial support of the Russian-German research station on Samoylov that made this study possible. We also thank Günter Stoof, Moritz Langer, and Maryvonne Landolt for their assistance in the field and for data discussion and analysis.

References

Aber, J.S. & Aber, S.W. 2002. Unmanned small-format aerial photography from kites for acquiring large-scale, high-resolution, multiview-angle imagery. P*ecora 15/Land Satellite Information IV/ISPRS Commission I/FIEOS 2002 Conference Proceedings.*

Bigras, C. 1997. Kite aerial photography of the Axel Heiberg Island fossil forest. *Proceedings of the First North American Symposium on Small Format Aerial Photography.*

Bitelli, G. & Girelli, V.A. 2004. Low-height aerial imagery and digital photogrammetrical processing for archaeological mapping. *International Archives of Photogrammetry, Remote Sensing and Spatial Information Services*: 498-504.

Boike, J. & Yoshikawa, K. 2003. Mapping of periglacial geomorphology using kite/balloon aerial photography. *Permafrost and Periglacial Processes* 14:0 Wiley InterScience, DOI:10.1002/ 437 pp.

Dare, P. 2005. The use of Small Environmental Research Aircraft (SERAs) for environmental remote sensing. *International Journal of Geoinformatics* 1/3: 19-26

Henry, J.-B., Malet, J.-P., Maquaire, O. & Grussenmeyer, P. 2002. The use of small-format and low-altitude aerial photos for the realization of high-resolution DEMs in mountainous areas: Application to the super-sauze earthflow (Alpes-De-Haute-Provence, France). *Earth Surfaces and Landforms* 27: 1339-1350. DOI:10.1002/esp.411.

Luhmann, Th. 2000. *Nahbereichsphotogrammetrie, Grundlagen, Methoden und Anwendungen*. Heidelberg: Herbert Wichmann Verlag, 571 pp.

Schwidefsky, K. & Ackermann, F. 1976. *Photogrammetrie, Grundlagen, Verfahren, Anwendungen.* Stuttgart: B.G. Teubner, 384 pp.

Vierling, L.A., Fersdahl, M., Chen, X., Li, Zh. & Zimmerman, P. 2006. The Short Wave Aerostat-Mounted Imager (SWAMI): A novel platform for acquiring remotely sensed data from a tethered balloon. *Remote Sensing of Environment* 103: 255-264.

The Yedoma Suite of the Northeastern Siberian Shelf Region: Characteristics and Concept of Formation

Lutz Schirrmeister, Hanno Meyer, Sebastian Wetterich, Christine Siegert
Alfred Wegener Institute for Polar and Marine Research, Telegrafenberg A43, D-14473 Potsdam, Germany
Viktor V. Kunitsky
Permafrost Institute RAS-SB Yakutsk, 677010 Yakutsk, ul. Mersoltnaya, Russia
Guido Grosse
University of Alaska Fairbanks, Geophysical Institute, 903 Koyukuk Drive, Fairbanks, AK 99775, USA
Tatyana V. Kuznetsova, Alexander Yu. Derevyagin
Moscow State University, Geological Faculty, 11991 Moscow, Russia

Abstract

The Yedoma Suite is well exposed along coasts and riverbanks in the northeastern Siberian Arctic. The cryotexture of these mostly ice-supersaturated deposits is similar at most sites—ice bands and reticulated ice lenses. The Yedoma Suite is considered a sequence of buried cryosols, formed under predominantly subaerial conditions. It represents an important terrestrial carbon reservoir (TOC 2–5-wt%). The multimodal grain size distribution does not reflect primarily aeolian accumulation, but rather a mixture of various periglacial transport and accumulation processes based on the concept of nival lithogenesis. The Yedoma Suite age lies in the MIS-3 and MIS-2 periods and, in rare cases, already starts during MIS-4. The palaeoecology of the Yedoma Suite can be summarized in the term "Tundra Steppe," combining both tundra and steppe environmental features. The present occurrence of the Yedoma Suite remains is closely related to low mountain ridges surrounding the northern and northeastern Siberian shelves. The concept of nival lithogenesis is presented, explaining the origin of source material and transport medium.

Keywords: cryolithology; late Pleistocene; northeastern Siberia; palaeo-environment; yedoma.

Introduction

The term *yedoma* is often associated with describing possible reactions of permafrost to global warming (Zimov et al. 2006, Walter et al. 2006, Walker 2007). The word *yedoma* probably originated in Kamchatka and described a boggy site or an elevated meadow-like flat plain. It entered science via the expeditions of Vitus Bering in Siberia during the 18th century. Initially, the term *yedoma* was of geomorphologic origin and described the hills separating thermokarst depressions in East-Siberia, especially in the Yana-Indigirka and Kolyma Lowlands (Kolosov 1947, Baranova & Biské 1964, Mursaev 1984, Tomirdiaro 1980). These mounds were considered to be erosional remnants of former accumulation plains. In this sense, yedoma described a special geomorphological relief type in Siberian permafrost regions, directly formed by thermokarst and thermoerosion (Solov'ev 1959, 1989).

The stratigraphical term *Yedoma Suite* was later adopted for middle Pleistocene horizons in the northeastern Siberian Lowlands (Lavrushin 1963, Vas'kovsky 1963). This stratigraphical position was moved to the late Pleistocene based on faunal studies at the Duvanny Yar site in the Kolyma Lowlands (Sher 1971), which became the stratotype for the Yedoma Suite. This categorization was finally confirmed by the decision of the Interdepartmental Commission on Quaternary Stratigraphy of the Soviet Union in Magadan in 1982 (Sher 1987).

Early genetic conceptions of the Yedoma Suite include glacier-dammed basin sediments (Grosswald 1998), alluvial genesis (Rozenbaum 1981), deltaic formation (Nagaoka et al. 1995), proluvial and slope deposits (Slagoda 2004, Gravis 1969), cryogenic-aeolian (Tomirdiaro et al. 1984, Tomirdiaro & Chernenky 1987), and nival deposits (Galabala 1997) as well as polygenetic origins (Sher et al. 1987).

The deposits of the Yedoma Suite represent unique late Pleistocene palaeoenvironmental archives for a large region of the Northern Hemisphere lacking major glacial records. Within the Russian-German project, System Laptev Sea, these deposits were studied with a multidisciplinary approach (cryolithology, sedimentology, palaeontology, palaeobotany, geochronology, mineralogy, isotope geochemistry, GIS, remote sensing) during the last ten years. We here present a first review of some general results on the overarching features of the Yedoma Suite in the Laptev Sea region and a concept of its formation.

Study Region

Since 1998, we have studied the characteristics of the Yedoma Suite at 15 well-exposed sites on the Laptev Sea and the East Siberian Sea coasts, and in the Lena Delta (Fig. 1). These sites are situated in the lowland plains of the continental shelf on both sides of the current seismically active boundary of the Eurasian and the North American continental plates.

Characteristics of the Yedoma Suite

Occurrence and geomorphology

The occurrence of the Yedoma Suite in the study region is closely related to low mountain ridges (ca. 200 to 400 m a.s.l.) surrounding the northern and northeastern Siberian shelves, which are the major sediment sources for the Yedoma Suite. In the western Laptev Sea and the Lena Delta region the occurrence of the Yedoma Suite is strongly connected with the coastal mountains of the Pronchishchev, Chekanovsky, and Kharaulakh Ridges. Heavy mineral studies at various sites have shown that these ridges are a main source of sediment (Siegert et al. 2002, Schwamborn et al. 2002, Schirrmeister et al. 2003). Therefore, foreland accumulation plains were the areas of the formation of the Yedoma Suite. In the eastern part of the study region, the exposed granite and basalt intrusions on Bol'shoy Lyakhovsky Island and Cape Svyatoy Nos as well as the fault ranges on Bel'kovsky, Stolbovoy, and Kotel'ny Islands serve as source areas for sediments of the Yedoma Suite. The distribution of the ice-rich sequences is easily identified by frequent thermokarst depressions or lakes (Grosse et al. 2005, 2006, 2007).

The Yedoma Suite exposes permafrost cliffs in 10- to 40-m-high horseshoe-shaped thaw slumps or thermocirques along sea coasts and riverbanks (Fig. 2).

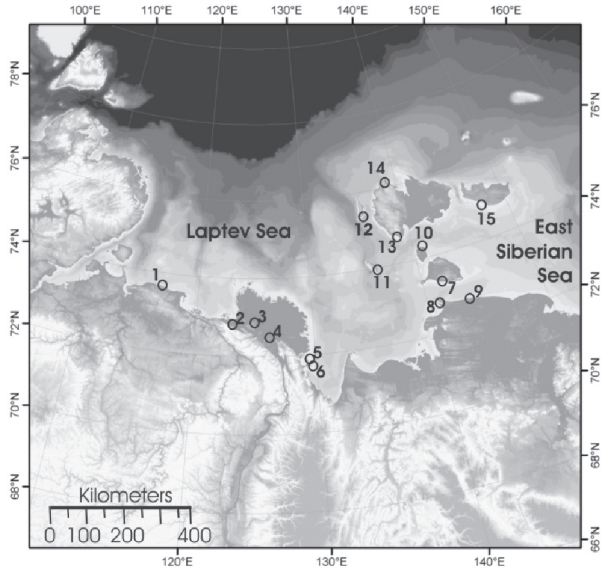

Figure 1. Study sites of the Yedoma Suite between 1998 and 2007. 1: Cape Mamontov Klyk. 2: Ebe Basyn Sise Island. 3: Khardang Island. 4: Kurungnakh Island. 5: Bykovsky Peninsula. 6: Muostakh Island. 7: Bol'shoy Lyakhovsky Island. 8: Syatoy Nos. 9: Oyogos Yar coast. 10: Maly Lyakhovsky Island. 11: Stolbovoy Island. 12: Bel'kovsky Island. 13: Kotel'ny Island. 14: Cape Anisy. 15: Novosibir Island.

Cryolithology

The cliffs are composed of ice wedge bodies and columns of frozen deposits between them, representing vertically or diagonally cut polygonal ice wedge systems. Therefore foliated syngenetic ice wedges of 2–5 m width and 10–40 m height, and separate thermokarst mounds of 2–5 m in diameter and up to 10 m height are the most characteristic features of Yedoma Suite erosion cliffs. Compared to the ice wedges, the intrapolygonal deposits are more resistant to thawing processes because they have a smaller ice content and contain stabilizing peaty paleosol layers alternating with silty-sand layers. These features of continuous permafrost sequences are the result of long-lasting and stable cryogenesis and landscape conditions.

The cryotexture of the Yedoma Suite is quite similar at all of the study sites. The general texture is layered. Ice bands (1–10 cm) alternate with sediment interlayers of variable thickness. These interlayers contain numerous small ice lenses as well as reticulated ice lenses. The frozen sediment sequences are frequently ice-supersaturated, resulting in gravimetric ice contents of 60 to 120% on average (Fig. 3).

Such cryotextures are typical for sediments formed in poorly drained landscapes with a near-surface permafrost table. The formation of these ice bands is a sign of stable surface conditions and stable active-layer depths over a certain time period, resulting in ice aggradation at the top of the permafrost table. The stable isotope signature of ice wedges shows light values for all study sites (site mean

Figure 2. The Yedoma coast at Bol'shoy Lyakhovsky Island. The cliff is about 30 m high (photo: S. Wetterich, July 2007).

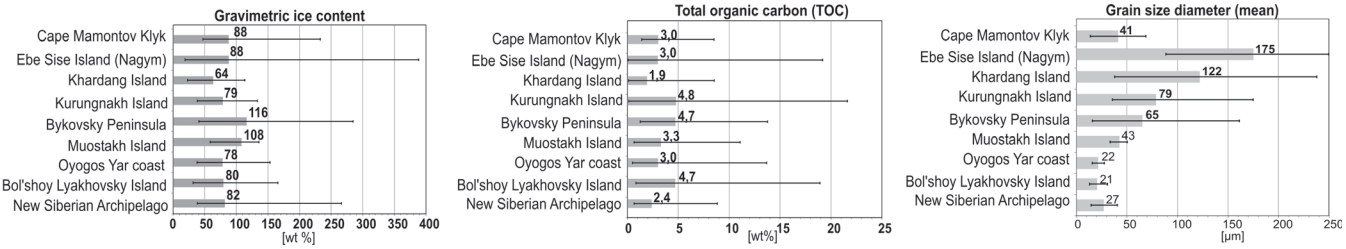

Figure 3. Variation in ice content, TOC content of peat inclusions and sediment, and grain size diameter between various sites of the Yedoma Suite (mean: bar; range: line).

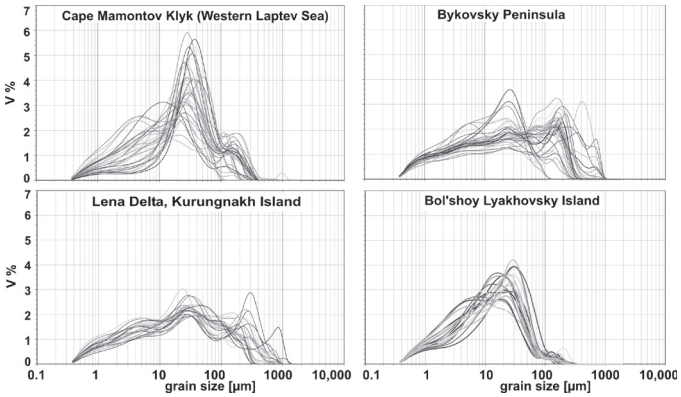

Figure 4. Typical grain-size distribution patterns of the Yedoma Suite at various sites.

values: δD -230 to -260‰, $\delta^{18}O$ -28 to -31‰, d-excess about -6‰) reflecting very cold winter temperatures and moisture sources which are isotopically different from Holocene and modern ones (Meyer et al. 2002a, b).

Organic carbon and grain-size parameters

The Yedoma Suite includes buried cryosols marked by brownish horizons, as well as peat inclusions and/or numerous twigs and leafs. Cryoturbation patterns of 0.5 to 1 m thickness are very common. The organic carbon content is relatively high (1 to > 20 wt%, in average 2 to 5 wt%). Wood fragments and peat are present, with numerous small filamentous rootlets and dispersed organics detritus.

The fine-grained sediments composing the Yedoma Suite are poorly sorted and differ in grain-size parameters from site to site (Fig. 4). Multimodal grain-size distribution patterns reflect a mixture of transport, accumulation, and re-sedimentation processes. Therefore, we conclude that this type of sediment in the Laptev Sea region is not primarily of aeolian origin, a view that is still widely reflected in the scientific literature using the generalizing term "Arctic loess" (e.g., Tomirdiaro 1982, Walker 2007).

Summarizing the special cryolithological and sedimentological characteristics, it is concluded that the frozen deposits of the Yedoma Suite accumulated in a special periglacial facies. The term "Ice Complex" (Soloviev 1959, p. 49) is used for these deposits.

Age determination and stratigraphy

The age of the Yedoma Suite was determined by radiocarbon AMS analyses of about 300 samples and some luminescence datings (Schirrmeister et al. 2002a, 2003, 2008, Grosse et al. 2007, Andreev et al. 2008). The geochronologically determined onset of the Yedoma Suite accumulation varies between about 55 ky BP at the New Siberian Islands and 27 ky BP at the western Laptev Sea coast. The latest deposition is dated between 28 ky BP at the New Siberian Islands and 17 to 13 ky BP in the western Laptev Sea. Unconformities are frequent, up to 20 ky, and probably caused by thermokarst and thermoerosion. The Yedoma Suite predominantly covers the Kargin and Sartan period of the Russian late Pleistocene stratigraphy, which corresponds to the MIS-3 and MIS-2 of the global classification. At Bykovsky Peninsula, the Yedoma Suite is somewhat older, and already started during the Zyryan period (MIS-4) (Meyer et al. 2002a, Schirrmeister et al. 2002b). In general, the lower boundary contrasts sharply with the underlying deposits, which often are fluvial sands with peat layers or loess-like floodplain deposits. These deposits are U/Th and luminescence-dated between 60 and 100 ky). The upper boundary is characterized by separate, locally confined Holocene deposits on top of the Yedoma Suite (Andreev et al. 2004, Krbetschek et al. 2002, Schirrmeister et al. 2003, Grosse et al. 2007).

Table 1. Palaeoenvironmental stages of northeastern Siberian Arctic lowlands during the late Quaternary (inferred from multiproxy analysis of permafrost records, Andreev et al. 2002, 2008).

Allerœd 12 ky	• Tundra with higher bioproductivity • Warming climate • First thermokarst depressions
Sartan 30 - 12 ky	• Sparse grass-sedge tundra • Cold and dry summers, very cold winters • Ice Complex formation
Kargin ca. 50 - 30 ky	• Tundra steppe with high bioproductivity • Relatively warm summers, cold winters • Ice Complex formation
Zyryan ca. 100 - 50 ky	• Sparse grass sedge tundra • Extreme cold and dry climate • Widespread fluvial, lacustrine, and floodplain deposits • Begin of local Ice Complex formation

Palaeoecology (Table 1)

New data for the faunal and floral composition during the formation of the Yedoma Suite in the study region were collected and analyzed within our project "System Laptev Sea" and described in numerous palaeoecological papers (e.g., Andreev et al. 2002, Bobrov et al. 2004, Kienast et al. 2005, Kuznetsova et al. 2003, Sher et al. 2005, Wetterich et al. 2005). The findings are in good agreement with studies; e.g., of Anderson & Lozhkin (2001). The special floral and faunal communities that existed during Yedoma Suite formation disappeared approximately at the Pleistocene-Holocene transition. The palaeo-biosceonosis is called Mammoth Steppe or Tundra Steppe, combining both tundra and steppe features. The climate was more continental in the late Pleistocene Arctic than today, with colder winters and warmer summers and, therefore, stronger seasonal gradients in temperature and precipitation (Meyer et al. 2002a/b, Kienast et al. 2005, Schirrmeister et al. 2002b, 2003, 2008, Wetterich et al. 2008).

Formation of the Yedoma Suite

To explain the formation of the Yedoma Suite, we use the concept of nival lithogenesis proposed by Kunitsky (2007). Several geological processes are important for its formation and can be summarized in four stages (Fig. 6):

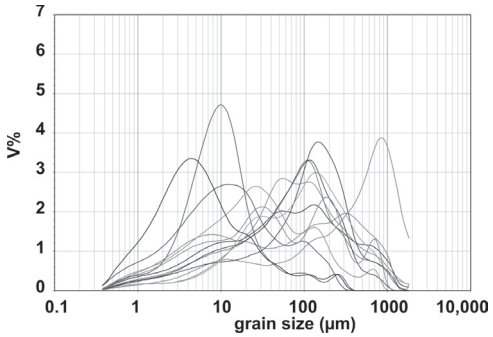

Figure 5. Grain-size distribution curves of clastic remains in various modern snow patches studied around the Laptev Sea.

1. Accumulation of windblown snow together with plant and mineral detritus in numerous perennial snowfields (névés) in topographic features of hills and low mountain ranges (e.g., steep slopes, valleys, cryoplanation terraces, Fig. 6a). Similar processes, but at a smaller scale, are observed today at numerous sites in northeastern Siberia, where nival processes are an essential relief-forming factor (Kunitsky et al. 2002).

2. A concentrated detritus mat forms due to repeated thawing of accumulating snow, transport of detritus by meltwater, and downslope accumulation of plant and mineral debris. Intense freeze-thaw cycles and wet conditions around and below the perennial snowfields support the formation of fine-grained material by frost weathering (Fig. 6b). Such processes are also observed in modern snowfield areas. Grain-size analyses of modern clastic material show similar multimodal patterns as the Yedoma Suite (Fig. 5).

3. Discharge of clastic and organic detritus proceeded by snowfield meltwater runoff. Fine-grained debris was subsequently distributed by alluvial, fluvial, proluvial, and partly also aeolian transport to piedmont plains, cryoplanation terraces or large alluvial fans (Fig. 6c).

4. Ice Complex formation consisted of concurrent processes of sediment accumulation, ground ice segregation, syngenetic ice wedge growth, sediment reworking, peat aggradation, cryosol formation, and cryoturbation (Fig. 6d).

The formation of huge polygonal ice wedge systems and thick continuous sequences of frozen deposits is closely related to the persistence of stable, poorly drained, low-topographic gradient accumulation plains.

Conclusions

The Yedoma Suite is an important paleoenvironmental archive that spans large regional and chronological gaps in the proxy information of the late Pleistocene Arctic. Consistent cryolithological, sedimentological, and palaeo-ecological features (Tab. 2) reflect similar environmental conditions for a wide variety of sites, representing a special periglacial facies.

Concluding, the Yedoma Suite includes a massive carbon and freshwater reservoir susceptible to release by global warming. In order to estimate and calculate the role of these widespread ice- and organic-rich frozen deposits in Siberia in a future warming Arctic, we must improve our knowledge

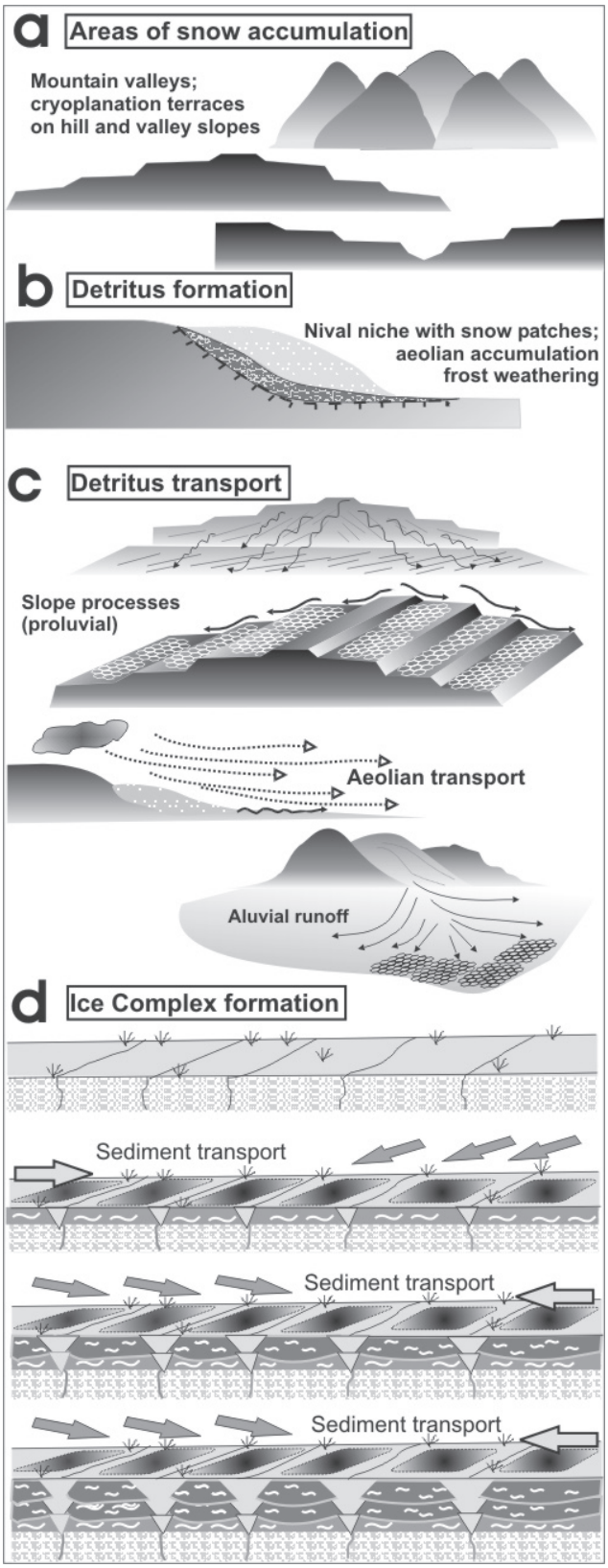

Figure 6. Scheme of Yedoma Suite formation.

of their characteristics and origin. The specific combination of strongly continental climate and the local landscape permitted syngenetic formation of ice wedges and organic-rich, ice-supersaturated sequences, called Ice Complex or the Ice Complexes of the Siberian Arctic.

Table 2. Typical features of the Yedoma Suite in the shelf region of northeastern Siberian.

Cryolithology	Ice-supersaturated, syngenetic ice wedges, segregation ice
Sediment	Poorly sorted, organic-rich silty sand
Formation age	80 to 12 ky BP
Stratigraphy	(MIS-4) to MIS-2
Palaeoecology	Tundra Steppe/Mammoth Steppe
Climate	High continental, arid
Genesis	Nival lithogenesis, alluvial, proluvial, and aeolian accumulation
Landscape	Lowland plains and cryoplanation terraces
Terminology	Ice Complex deposits compose the Yedoma Suite, which is preserved in Yedoma hills

Acknowledgments

This paper is based on the joint Russian-German science cooperation "System Laptev Sea" supported by the German Ministry of Education and Research. The Russian as well as the German Science Foundation promoted these environmental studies with several projects. We thank all Russian and German colleagues who help us during field work and laboratory studies, but especially S. Kuzmina, M. Grigoriev, W. Schneider, V. Tumskoy, A. Sher, V. Rachold, G. Schwamborn, F. Kienast, P. Tarasov, A. Eulenburg, and U. Bastian. In addition, we thank P.P. Overduin for the native speaker correction as well as D. Froese and one anonymous reviewer for their helpful hints.

References

Anderson, P.M. & A.V. Lozhkin 2001. The stage 3 interstadial complex (Karginskii/middle Wisconsinan interval) of Beringia: variations in paleoenvironments and implications for paleoclimatic interpretations. *Quaternary Science Reviews* 20, 93-125.

Andreev, A.A., Schirrmeister, L., Siegert, C., Bobrov, A.A., Demske, D., Seiffert, M. & Hubberten H.-W. 2002. Palaeoenvironmental changes in northeastern Siberia during the Upper Quaternary: Evidence from pollen records of the Bykovsky Peninsula. *Polarforschung,* 70: 13-25.

Andreev, A.A. et al. 2008. Weichselian and Holocene palaeoenvironmental history of the Bol'shoy Lyakhovsky Island, New Siberian Archipelago, Arctic Siberia. *Boreas* (in review).

Baranova, Yu.P. & Biské, S.F. 1964. *North East USSR: History of Relief Formation in Siberia and Far East*. Moscow: Nauka, 290 pp. (in Russian).

Bobrov, A.A., Andreev, A.A., Schirrmeister, L. & Siegert, Ch. 2004. Testate amoebae (Protozoa: Testacea) as bioindicators in the Late Quaternary deposits of the Bykovsky Peninsula, Laptev Sea, Russia. *Palaeogeography Palaeoclimatology Palaeoecology*, 209: 165-181.

Galabala, R.O. 1997. Pereletki and the initiation of glaciation in Siberia. *Quaternary International*, 41/42: 27-32.

Gravis, G.F. 1969. *Slope Deposits in Yakutia*. Moscow: Nauka, 128 pp. (in Russian).

Grosse, G., Schirrmeister, L., Kunitsky, V.V. & Hubberten, H.-W. 2005. The use of CORONA images in remote sensing of periglacial geomorphology: An illustration from the NE Siberian coast. *Permafrost and Periglacial Processes* 16: 163-172.

Grosse, G., Schirrmeister, L. & Malthus, T.J. 2006a. Application of Landsat-7 satellite data and a DEM for the quantification of thermokarst-affected terrain types in the periglacial Lena-Anabar coastal lowland. *Polar Research* 25: 51-67.

Grosse, G., Schirrmeister, L., Siegert, C., Kunitsky, V.V., Slagoda, E.A., Andreev, A.A. & Derevyagyn, A.Y. 2007. Geological and geomorphological evolution of a sedimentary periglacial landscape in Northeast Siberia during the Late Quaternary. *Geomorphology* 86: 25-51.

Grosswald, M.G. 1998. Late-Weichselian ice sheets in Arctic and Pacific Siberia. *Quaternary International,* 45/46: 3-18.

Kienast, F., Schirrmeister, L., Siegert, C. & Tarasov, P. 2005. Palaeobotanical evidence for warm summers in the East Siberian Arctic during the last cold stage. *Quaternary Research* 63: 283-300.

Kolosov, D.M. 1947. *Problems of Former Glaciation of Northeast Siberia*. SevMorPut, 175 pp. (in Russian).

Krbetschek, M.R., Gonser, G. & Schwamborn G. 2002. Luminescence dating results on sediment sequences of the Lena Delta. *Polarforschung* 70: 83-88.

Kunitsky, V.V., Schirrmeister, L., Grosse, G. & Kienast, F. 2002. Snow patches in nival landscapes and their role for the Ice Complex formation in the Laptev Sea lowlands. *Polarforschung* 70: 53-67.

Kunitsky, V.V. 2007. *Nival lithogenesis and Ice Complex on the territory of Yakutia.* Abstract of the state doctoral dissertation. Permafrost Institute Yakutsk, 46 pp. (in Russian).

Kuznetsova, T.V., Sulerzhitsky, L.D., Andreev, A.A., Siegert, C., Schirrmeister, L. & Hubberten, H.-W. 2003. Influence of Late Quaternary paleoenvironmental conditions on the distribution of mammals fauna in the Laptev Sea region. *Occasional Papers in Earth Science*s 5: 58-60.

Lavrushin, Yu.A. 1963. *Lowland Rivers Alluvium of the Subartic Region and Periglacial Area of the Continental Glaciation*. Academy of Science USSR 87, 266 pp. (in Russian).

Meyer, H., Derevyagin, A.Y., Siegert, C. & Hubberten H.-W. 2002a. Paleoclimate studies on Bykovsky Peninsula, North Siberia. Hydrogen and oxygen isotopes in ground ice. *Polarforschung* 70: 37-52.

Meyer, H., Siegert, C., Derevyagin, A.Y., Schirrmeister, L. & Hubberten, H.-W. 2002b. Palaeoclimate reconstruction on Big Lyakhovsky Island, North Siberia: Hydrogen and oxygen isotopes in ice wedges. *Permafrost and Periglacial Processes* 13: 91-103.

Mursaev, E.M. 1984. *Glossary of Local Geographical Terms*. Moscow: Mysl, 653 pp. (in Russian).

Nagaoka, D., Saijo, K. & Fukuda, M. 1995. Sedimental environment of the Edoma in high Arctic eastern Siberia. In: K. Takahashi, A. Osawa, & Y. Kanazawa (eds.), *Proceedings of the Third Symposium on the Joint Siberian Permafrost Studies between Japan and Russia,* 8-13.

Rozenbaum, G.E. 1981. Special features of lithogenesis of the alluvial planes in the Eastern Subarctic as related to the problem of the Ice (Yedoma) Complex. In: *Problems of Cryolithology*, 9. Moscow: MSU Press, 87-100. (in Russian).

Schirrmeister, L., Siegert, C., Kunitsky, V.V., Grootes, P.M. & Erlenkeuser H. 2002a. Late Quaternary ice-rich permafrost sequences as a paleoenvironmental archive for the Laptev Sea Region in northern Siberia. *Int. J. Earth Sci.* 91: 154-167.

Schirrmeister, L. et al. 2002b. Palaeoenvironmental and palaeoclimatic records from permafrost deposits in the Arctic region of Northern Siberia. *Quaternary International* 89: 97-118.

Schirrmeister, L., Kunitsky, V.V., Grosse, G., Schwamborn, G., Andreev, A.A., Meyer, H., Kuznetsova, T., Bobrov, A. & Oezen, D. 2003. Late Quaternary history of the accumulation plain north of the Chekanovsky Ridge (Lena Delta, Russia): A multidisciplinary approach. *Polar Geography* 27: 277-319.

Schirrmeister, L. et al. 2008. Periglacial landscape evolution and environmental changes of Arctic lowland areas during the Late Quaternary (Western Laptev Sea coast, Cape Mamontov Klyk) *Polar Research* (in review).

Schwamborn, G., Rachold, V. & Grigoriev. M.N. 2002. Late Quaternary sedimentation history of the Lena Delta. *Quaternary International* 89: 119-134.

Sher, A.V. 1971. *Mammals and Late Pleistocene Stratigraphy of the Northeast USSR and of North America.* Moscow: Nauka, 312 pp. (in Russian).

Sher, A.V., Kaplina, T.N. & Ovander, M.G. 1987. Unified regional stratigraphic chart for the Quaternary deposits in the Yana-Kolyma Lowland and its mountainous surroundings: Explanatory note. In: *Decisions of Interdepartmental Stratigraphic Conference on the Quaternary of the Eastern USSR*. Magadan, 1982. USSR Academy of Sciences, Far-Eastern Branch, North-Eastern Complex Research Institute, Magadan, USSR, 29-69. (in Russian).

Sher, A.V., Kuzmina, S.A., Kuznetsova, T.V., & Sulerzhitsky, L.D. 2005: New insights into the Weichselian environment and climate of the Eastern-Siberian Artic, derived from fossil insects, plants, and mammals. *Quaternary Science Reviews* 24: 533-569.

Siegert, C., Schirrmeister, L. & Babiy, O. 2002. The sedimentological, mineralogical and geochemical composition of Late Pleistocene deposits from the Ice Complex on the Bykovsky Peninsula, Northern Siberia. *Polarforschung* 70: 3-11.

Slagoda, E.A. 2004. *Cryolithogenic Deposits of the Laptev Sea Coastal Plain: Lithology and Micromorphology*. Tyumen: Publishing and Printing Centre "Express," 119 pp. (in Russian).

Solov'ev, P.A. 1959. *The Cryolithozone in the North Part of the Lena-Amga-Interfluve.* Publ. Academy of Science of the USSR, 144 pp. (in Russian).

Solov'ev, P.A. 1989. Permafrost (Cryolithozone). In: I.A. Matveev et al. (eds.). *Agriculture Atlas of the Yakutian ASSR, 96-97* (in Russian).

Tomirdiaro, S.V. 1982. Evolution of lowland landscapes in northern Asia during Late Quaternary time. In: D.V. Hopkins, J.V. Matthews Jr., Ch.E. Schweger & S.B. Young (eds.), *Paleoecology of Beringia*. New York: Academic Press, 29-37.

Tomirdiaro, S.V., Arslanov, K.A., Chernenkiy, B.I., Tertychnaya, T.V. & Prokhorova, T.N. 1984. New data on formation of loess-ice sequences in Northern Yakutia and ecological conditions of mammoth fauna in the Arctic during the late Pleistocene. *Reports Academy of Sciences USSR* 278, 1446-1449 (in Russian).

Tomirdiaro, S.V. & Chernen'ky, B.I. 1987. Cryogenic deposits of East Arctic and Sub Arctic. AN SSSR Far-East-Science Center, 1-196 (in Russian).

Vas'kovsky, A.P. 1963. Stratigraphic outline of Quaternary deposits in northeastern Asia. In: *Geology of the Koryaksky Mountains.* Moscow: Gostoptekhizdat, 24-53 (in Russian).

Walker, G. 2007. A world melting from the top. *Nature* 446: 718-721.

Walter, K.M., Zimov, S.A., Chanton, J.P., Verbyla, D. & Chapin III, F.S. 2006. Methane bubbling from Siberian thaw lakes as a positive feedback to climate warming. *Nature* 443: 71-75.

Wetterich, S., Schirrmeister, L. & Pietrzeniuk, E. 2005. Freshwater ostracodes in Quaternary permafrost deposits in the Siberian Arctic. *Journal of Paleolimnology* 34: 363-376.

Wetterich, S. et al. 2008. Palaeoenvironmental dynamics inferred from late Quaternary permafrost deposits on Kurungnakh Island (Lena Delta, Northeast Siberia, Russia). *Quaternary Science Review* (in review).

Zimov, S.A., Schuur, E.A.G. & Chapin III, F.S. 2006. Permafrost and the global carbon budget. *Science* 312: 1612-1613.

Mid- to Late-Quaternary Cryogenic Weathering Conditions at Elgygytgyn Crater, Northeastern Russia: Inference from Mineralogical and Microtextural Properties of the Sediment Record

Georg Schwamborn
Alfred Wegener Institut für Polar und Meeresforschung, Potsdam, Germany
Annika Förster
RCOM - DFG Research Center Ocean Margin, Universität Bremen, Bremen, Germany
Bernhard Diekmann
Alfred Wegener Institut für Polar und Meeresforschung, Potsdam, Germany
Lutz Schirrmeister
Alfred Wegener Institut für Polar und Meeresforschung, Potsdam, Germany
Grigory Fedorov
Arctic and Antarctic Research Institute, St. Petersburg, Russia

Abstract

Two sediment-mineralogical properties were tested as proxy data reflecting the intensity of cryogenic weathering. They were applied to lake sediments from Elgygytgyn Crater Lake in Chukotka, Siberia, and to frozen deposits from the catchment that serve as a reference for in situ weathering conditions. (1) The relative amounts of quartz and feldspar in different silt fractions yield the so-called cryogenic weathering index (CWI). High CWI values, as deduced from the samples, are related to the mineralogically selective weathering resulting from freeze-thaw cycles in the upper permafrost. (2) Image analysis of scanning electron micrographs (SEM) of quartz particles allows characterization and semi-quantification of grain morphology and surface features stemming from frost weathering (i.e., flaky surfaces, microcracking). The constant presence of cryogenic weathering signals both in lake sediments and frozen deposits suggests the long-term prevalence of stable permafrost conditions in the area at least since 220 ka.

Keywords: cryogenic weathering; quartz-feldspar ratio; microtextural properties; paleoenvironment reconstruction.

Introduction

Today, the majority of Siberian landmasses are subject to permafrost conditions. This is also the case for most of the Quaternary (Kaplina 1981, Brigham-Grette 2004, Hubberten et al. 2004). Nonetheless, until now no continuous record has been available that could be used to demonstrate variability of permafrost conditions for that time, nor have any suitable proxy data been tested. Such a sediment record could now become available through studies at Elgygytgyn Crater Lake in northeastern Siberia.

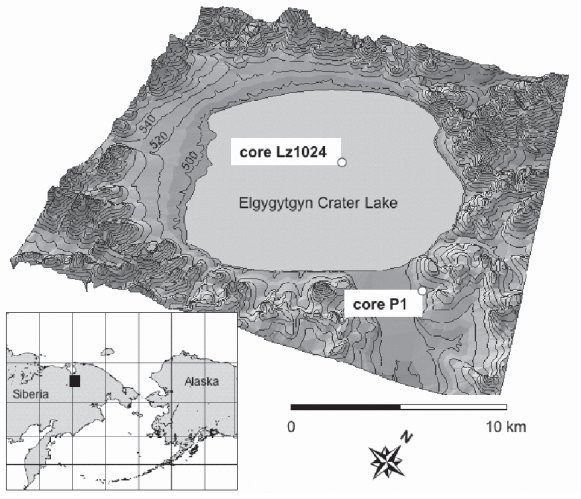

Figure 1. Crater location in NE Siberia (inset) and positions of lake sediment core Lz1024 (67°30.13′N,172°06.46′E) and permafrost core P1. The shoreline is 495 m above sea level.

Frost weathering, slope dynamics, and fluvial outwash are among the main surface processes, and they trigger erosion and detrital sediment transport into the lake basin. Continuous periglacial denudation is assumed for the Quaternary (Glushkova & Smirnov 2007). Tracing signals of cryogenic weathering from the catchment into the lake basin provides a direct land-to-lake linkage within paleoenvironmental reconstruction and will enlighten the permafrost history of non-glaciated NE Siberia. The development of a sediment-mineralogical approach to obtain proxy data for cryogenic weathering is the content of this paper. We use material from former coring into the lake and frozen deposits of the catchment (Melles et al. 2005).

Environmental Setting

Elgygytgyn Crater Lake, 12 km in diameter and 170 m in water depth at maximum (Fig. 1), holds sediments that mirror glacial to interglacial cyclicity and regional environmental change at millennial time resolution (Nowaczyk et al. 2002). The sediments consist of clayey silts and silty clays with occasional sand layers (Asikainen et al. 2007). Based on sedimentological data (physical properties, organic, and

isotope geochemistry), distinct climate-related sediment units have been identified that are primarily controlled by fluctuating carbon, nitrogen, and opal contents and linked to a changing extent of lake ice cover; i.e., "cold + moist," "cold + dry," "warm," and "peak warm" (i.e., Eemian interglacial) (Melles et al. 2007). The sediment units alternate in the last 250 kyr, the time span that is covered by the first recovered sediment cores (Juschus et al. 2007, Nowaczyk et al. 2007). We assume a fairly constant surface denudation processes in the confined catchment of the crater lake, which makes the site a natural laboratory for studying the production of weathering debris in the catchment and its subsequent deposition in the adjacent lake sediment column. Longer core retrieval is planned (Melles et al. 2005), which will yield a climate record more than 3 million years old, since the origin of Elgygytgyn Crater is attributed to a meteoritic impact 3.6 M yr ago (Layer 2000). Thus, there will be the potential to identify the assumed onset of permafrost conditions across the Pliocene/ Pleistocene boundary. The altitude of the lake is 495 m above sea level (a.s.l.), and the highest peaks forming the crater walls are about 900 m a.s.l. Local basement rocks are of volcanic origin and are part of the Late Cretaceous Okhotsk-Chukotka volcanic belt (Belyi 1998, Layer 2000, Ispolatov et al. 2004). The rocks consist largely of andesitic to rhyolitic tuffs and ignimbrites of primarily acidic composition. Some subalkaline basaltic andesites have been identified framing the crater lake to the southwest.

Methods

Indicator data for paleo frost weathering: (I) mineral composition

In terms of sedimentology, the destruction of quartz grains is a basic process during the formation of cryogenic debris. As established in experiments, cryogenic disintegration promotes a relative accumulation of quartz grains in the silt fraction (10–50 microns); whereas fresh feldspars and heavy minerals accumulate in the sand fraction (50–100 microns) (Konishchev 1982). This mineralogically selective weathering is active under water-saturated freezing-thawing cycles (Minervin 1982). Expressed in a so-called *Cryogenic Weathering Index* (CWI), the role of cryogenic weathering in frozen soil formation can be estimated (Konishchev 1998):

$$CWI = (Q_1 / F_1) / (Q_2 / F_2) \quad (1)$$

where Q_1 is quartz content (%) in the fine fraction; F_1 is feldspar content (%) in the fine fraction; Q_2 is quartz content (%) in the coarse fraction; and F_2 is feldspar content (%) in the coarse fraction.

CWI values greater than 1.0 argue for cryogenic weathering that influences the grain-size dependent mineral composition. Comparison of measurements from regionally distributed sediment samples of Arctic Siberia show that warm-climate sediments clearly can be discriminated from cold-climate samples (Konishchev & Rogov 1993). According to that study, Palaeogene-aged samples have CWI values ranging clearly below 1. Towards the Late Neogene and the Early Quaternary, the CWI values reach 1.7. In the lower and middle Pleistocene, values become as high as 3.3. The Eemian has falling values down to 1.7, before values rise again to a maximum of 3 at Weichselian time. Holocene CWI values range from 1.6 to 2.1. Indication of cryogenic weathering according to the CWI has already been implemented into permafrost modeling spanning the last 400 kyr (Romanovskii & Hubberten 2001). In our study, relative quartz and feldspar contents have been determined using standard x-ray diffractometry methods (Ehrmann et al. 1992, Vogt 1997) on a Philips PW 1820 goniometer that used a CoKα radiation (40 kV, 40 mA).

Indicator data for paleo frost weathering: (II) grain morphology and grain surfaces

Grain shapes and grain surface microtextures of mostly quartz and feldspar are well-established means to characterize sedimentary deposits and infer the environmental history from single grain morphology (Krinsley & Doornkamp 1973, Diekmann 1990, Mahaney 2002). Whereas single grain features are well-defined in the case of aeolian, glacial, and fluvial sediments, comparable features associated with mechanical encroachment in frozen ground is only sparsely documented, but appears distinctive (Konishchev & Rogov 1993, Van Hoesen & Orndorff 2004). Angular outlines and micromorphology such as high relief, sharp edges, and articulate steps are most frequent. They have been found in Holocene samples of Elgygytgyn Crater slope deposits (Schwamborn et al. 2006). Here, considerable amounts of grains are characterized by weathered surfaces; flakiness and microcracks were common features when inspected on SEM imagery. The grain surface features are particularly diagnostic for frozen ground sediments, since their production can be directly linked to the destructive effect of thaw-freeze alternation.

Sedimentary material

Lake sediments from core Lz1024 (Fig. 1) down to 12.2 m sediment depth were first measured for grain size distributions of 43 non-turbidite samples using a laser particle analyser (LS200, Beckman Coulter, Inc.). The studied interval spans the last 220 kyr according to the age model of Juschus et al. (2007). In contrast to Konishchev & Rogov (1993), CWI measurements are based on fractions 2–20 microns and 20–63 microns, since first grain size measurements revealed that lake sediments have a major mode at about 20 microns (Fig. 2). Grain shape and grain surface features have been characterized on at least 20 randomly selected quartz grains in each of 28 lake sediment samples. Chemical treatment of the samples followed standard techniques that are outlined elsewhere (Schwamborn et al. 2006). Hereafter, CWI calculations and SEM analysis have been applied.

Frozen deposits were recovered down to 5 m depth in a slope at the crater margin (P1 in Fig. 1). The dated core material shows a correct age-to-depth relation back into the Late Pleistocene (Schwamborn et al. 2006). For CWI

calculation, seven samples have been selected that extend over the Holocene. They serve as a reference of in situ cryogenic weathering of the periglacial landscape.

Results and Discussion

Mineral composition

The clayey silts and silty clays from lake sediment core Lz1024 yielded a mean CWI value of 1.6, whereby the minimum value is 1.0 (11.7 m depth), and the maximum value is 3.5 (11.2 m depth) (Fig. 3). The silty sands and sandy silts from permafrost core P1 have a mean CWI value of 1.1, whereby the minimum value is 0.9 (0.7 m depth), and the maximum value is 1.4 (3.7 m depth) (Fig. 3).

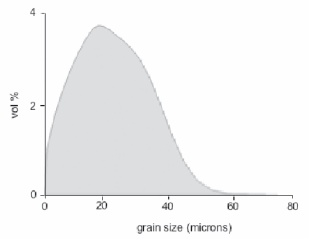

Figure 2. A typical grain size curve of lake sediments displaying the mode at 20 microns (sample from 10.64 m core depth).

All lake sediment CWI values are higher than 1.0 and thus fit well into the range of sediments from the glacial cycles. This argues for the presence of cryogenic conditions throughout the studied time interval. The variability around the mean is independent from sediment units and glacial to interglacial modes (Fig. 3). Several aspects are considered, which influence grain break-up and mixture of cryogenic detritus in the basin. (1) Warm periods are associated with higher temperature gradients in the active layer, thus increasing thermal stress to the grains and subsequent mechanical break-up. (2) Increasing moisture promotes the frequency of microcracking, when water migrates into fissures and subsequently disrupts the grains when crystallizing to ice. Both aspects (1 and 2) are also taking place in soil layers with fluctuating negative temperatures, but to an unknown degree. (3) Varying microclimates at rock surfaces, varying salt concentrations, and biotic encroachment (i.e., lichen growth) contribute to rock fragmentation to an unknown degree (Miotke 1988, Hall & André 2003, Guglielmin et al. 2005). (4) The particle size of source material may vary through time. (5) Soil weathering products that have been eroded and transported into the lake basin are reworked in the

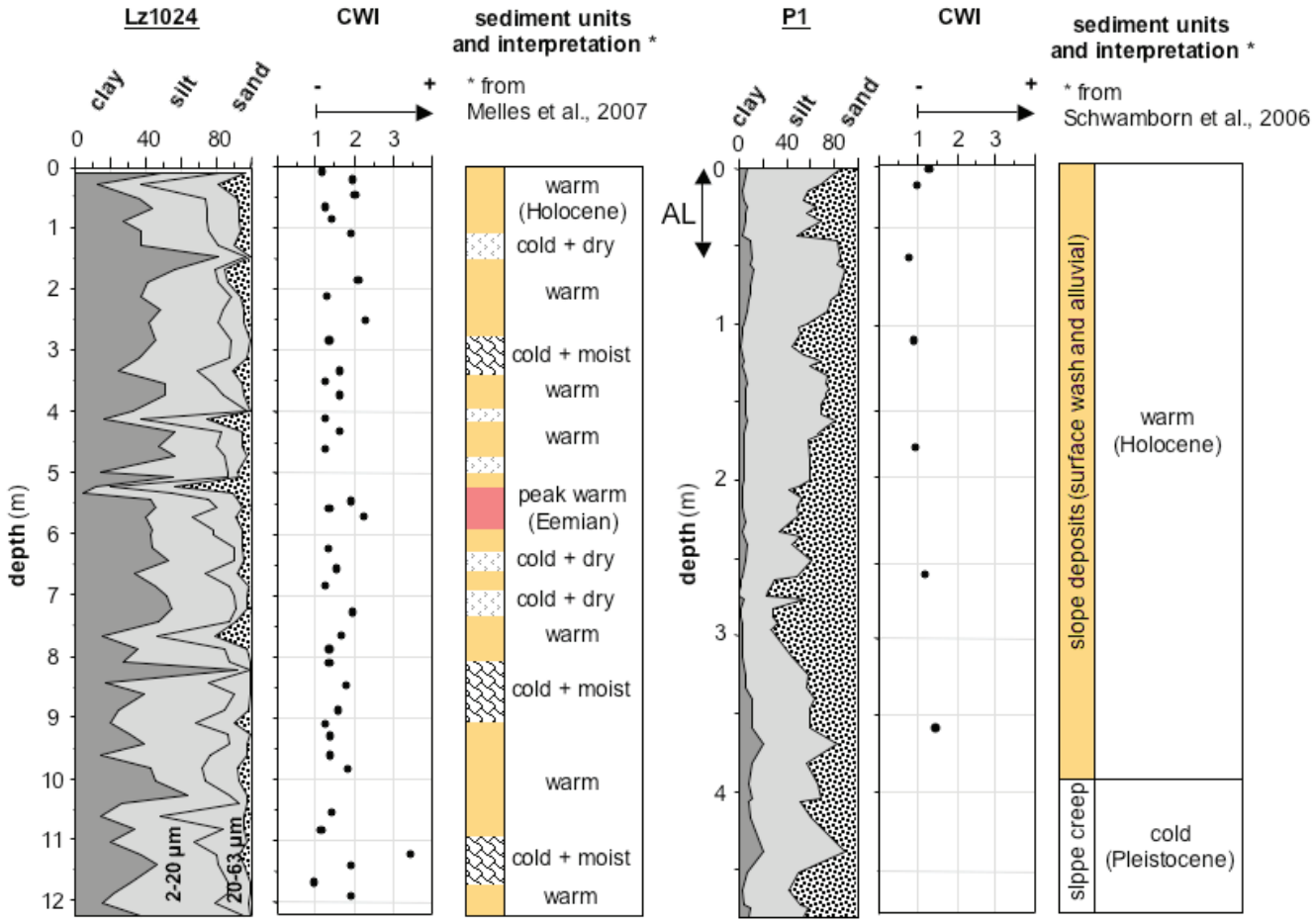

Figure 3. Values of the cryogenic weathering index (CWI) calculated for lake sediment core Lz1024 and permafrost core P1. Basic sediment interpretation schemes are added (see references). AL = Active layer.

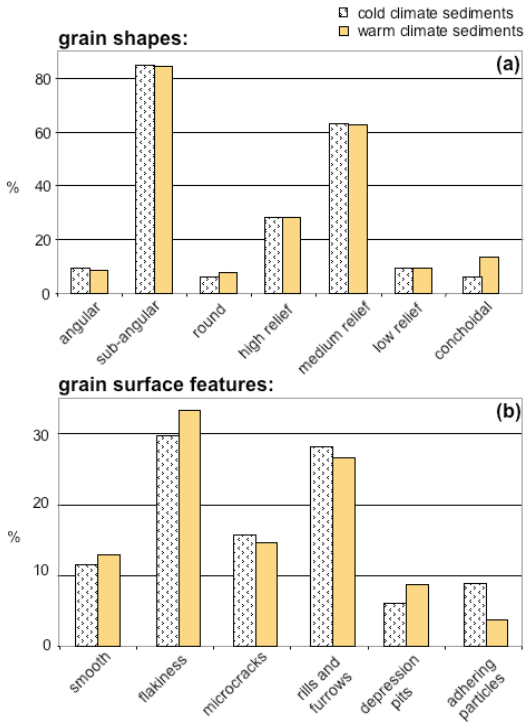

Figure 4. Grain shapes (a) and surface features (b) counted with quartz grains (63–125 microns) from lake sediment core Lz1024 (n=560).

shoals when strong winds from NW or SE lead to a thorough turbulence of the uppermost water column during the open water season. This leads to sediment mixing in the marginal shoals that also may add to blur the original CWI signal. (6) Changing lake levels contribute to sediment mixing, since the exposed and subsequently eroded areas around the lake have changed through time (Glushkova & Smirnov 2007, Schwamborn et al. 2007).

The near-surface permafrost around the lake produces low CWI values under Holocene warm-climate conditions (~1.0). Minor sediment mixing due to transport and reworking processes are associated with the environmental setting of P1 deposits (e.g., hill creep, slope wash, alluvial deposition), since the weathering debris is accumulated in a piedmont setting (Schwamborn et al. 2006).

Grain morphology and grain surfaces

Subangular grains are most common, but angular and round grains can also be found at all lake sediment core depths (Figs. 4, 5). Grains with conchoidal fractures, with smooth surfaces, brittle surfaces, and microcracks occur throughout the lake sediments, but to a lesser extent. Irregular, angular shapes (Fig. 5-1) argue for a short-distance transport, whereas conchoidal features (Fig. 5-4) suggest that pressure occurs either during in situ rock fragmentation or hill creep. Rounded grains (Fig. 5-3) represent the eolian portion that is drifted and deposited in the lake basin. However, estimates of the modern eolian input into the lake sediments yield a portion smaller than 5% (Fedorov pers. com.). V-shaped depression pits occur occasionally and point to grain-to-grain percussion during aquatic transport.

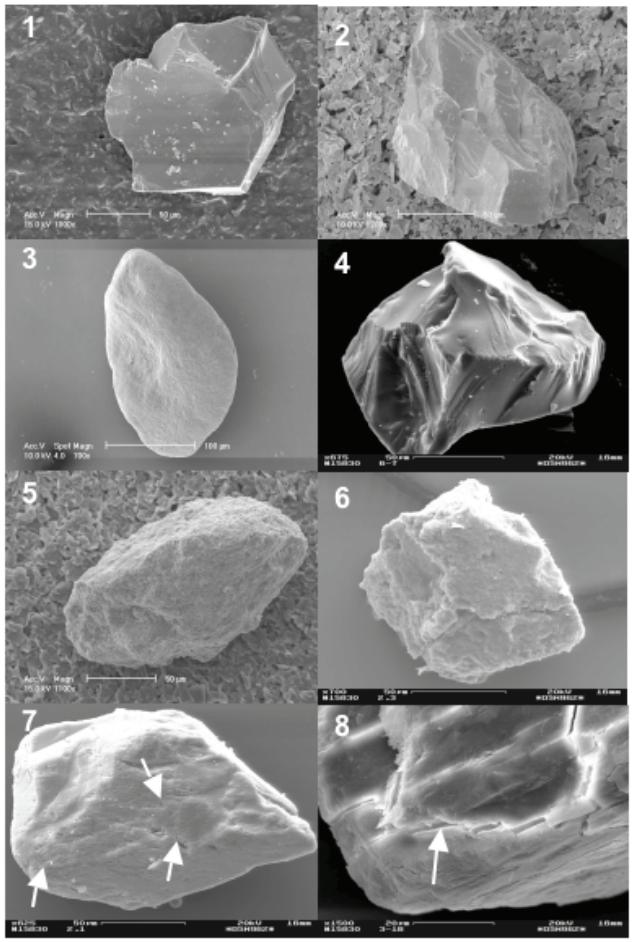

Figure 5. Examples of SEM micrographs from lake sediment quartz grains (63–125 microns); grain shapes: angular (1), subangular (2), rounded (3), conchoidal (4); grain surface features: brittle and flaky surfaces (5 + 6), cryogenic microcracking (7 + 8, see arrows).

Quartz grains exhibit abraded and softened areas, which can act as source areas for silt particles (Figs. 5-5, 5-6). Likewise, microcracks promote separation of silt-sized fragments and conspicuously display the destructive effect of cryogenic widening in the microscale to a varying degree (Figs. 5-7, 5-8). Descriptions of brittle grain surfaces along with microcracks are associated with cryogenic destruction within the thaw-freeze cycles in the uppermost permafrost (Konishchev. & Rogov 1993), or they have been described as crushing features (Van Hoesen & Orndorff 2004). They are present in Elgygtygyn lake sediments, and when medium- to high-relief grains become fragmented due to cryogenic cracking, the connection between SEM and CWI analysis is most obvious.

The discrimination between cold-climate and warm-climate sediments (Fig. 4) does not exhibit prominent quantitative differences between the two. All characteristics can be identified to varying degrees at all sediment depths. Frost weathering features like brittle surfaces and microcracking demonstrate that traces of cryogenic destruction inherited from permafrost processes are well-preserved within the lake sediment column.

For frozen deposits from the catchment, grain micromorphology assessments are already available (Schwamborn et al. 2006). Angular outlines and microfeatures such as high relief, sharp edges, and articulate steps were most common and were consistently observed for all samples. This was linked to short transport distances from their source rocks. Many grains were characterized by rough and weathered surfaces. Flakiness and microcracks were common features. The grain surface textures appear particularly diagnostic for frozen ground sediments, since their production can be directly linked to the destructive effect of thaw–freeze alternation. Frost weathered surfaces and cryogenic cracking point to the sandy grains as the source areas of silt particles. This highlights in situ disintegration, especially of quartz grains, after they were subject to thaw–freeze dynamics (Konishchev and Rogov, 1993).

Conclusions

Despite some blurring effects (e.g., mixing of detritus resulting from weathering and from depositional processes, and sediment reworking in the lake margins due to lake level changes) CWI and SEM analysis can link lake sediments and frozen slope deposits for paleoenvironment interpretation. The studied sediment properties suggest that cryogenic weathering was persistent around Elgygytgyn Crater Lake for at least the last 220 kyr.

An unknown temporal offset between the creation of cryogenic features in the catchment and the material deposition in the lake has to be taken into account when interpreting the timescale within the paleoenvironmental archives.

The combination of grain size, CWI, and SEM results is considered a helpful technique to identify on- and off-set of permafrost conditions in the area when inspecting future drill cores that go beyond 3 M yr back in time.

Acknowledgments

Martin Melles and Olaf Juschus, Cologne University, provided access to the lake sediment samples, Helga Kemnitz, GFZ Potsdam, helped with the SEM facilities. Their assistance is greatly appreciated. Financial support has been granted by the BMBF (German Ministry of Science and Education). The reviewers' comments helped to improve the paper.

References

Asikainen, C.A., Francus, P. & Brigham-Grette, J. 2007. Sedimentology, clay mineralogy and grain size as indicators of 65 ka of climate change from El´gygytgyn Crater Lake, Northeastern Siberia. *Journal of Paleolimnology* 37: 105-122.

Belyi, V.F. 1998. Impactogenesis and volcanism of the El'gygytgyn depression. *Petrology* 6(1): 86-99.

Brigham-Grette, J. 2004. Response to Grosswald and Hughes (2004)–Letter to the Editor, *Quaternary Research* 62: 227-232.

Diekmann, B. 1990. Granulometrie und Sandkornmorphoskopie alpiner Glazialsedimente. *Zbl. Geol. Paläont*. Teil 1, 1989 (9/10): 1407-1421.

Ehrmann, W., Melles, M., Kuhn, G. & Grobe, H. 1992. Significance of clay mineral assemblages in the Antarctic Ocean. *Marine Geology* 107: 249-273.

Glushkova, O.Yu. & Smirnov, V.N. 2007. Pliocene to Holocene geomorphic evolution and paleogeography of the El´gygytgyn Lake region, NE Russia. *Journal of Paleolimnology* 37: 37-47.

Guglielmin, M., Cannone, N., Strini, A. & Lewkowicz, A.G. 2005. Biotic and abiotic processes on granite weathering landforms in a cryotic environment, Northern Victoria Land, Antarctica. *Permafrost and Periglacial Processes* 16: 69-85.

Hall, K. & André, M.-F. 2003. Rock thermal data at the grain scale: applicability to granular disintegration in cold environments. *Earth Surface Processes and Landforms* 28: 823-836.

Hubberten, H.W., Andreev, A., Astakhov, V., Demidov, I., Dowdeswell, J.A., Henriksen, M., Hjort, C., Houmark-Nielsen, M., Jakobsson, M., Kuzmina, S., Larsen, E., Lunkka, J.P., Lysa, A., Mangerud, J., Möller, P., Saarnisto, M., Schirrmeister, L., Sher, A.V., Siegert, C., Siegert, M.J. & Svendsen, J.I. 2004. The periglacial climate and environment in northern Eurasia during the last glaciation. *Quaternary Science Reviews* 23(11-13): 1333-1357.

Ispolatov, V.O., Tikhomirov, P.L., Heizler, M. & Cherepanova, I.Yu. 2004. New 40Ar/39Ar ages of Cretaceous continental volcanics from Central Chukotka: implications for initiation and duration of volcanism within the northern part of the Okhotsk Chukotka volcanic belt (Northeastern Eurasia). *The Journal of Geology* 112: 369-377.

Juschus, O., Preusser, F., Melles, M. & Radtke, U. 2007. Applying SAR-IRSL methodology for dating fine-grained sediments from Lake El´gygytgyn, northeastern Siberia. *Quaternary Geochronology* 2: 187-194.

Kaplina, T.N., Kartashova, G.G., Nikitin, V.P. & Shilova, G.N. 1983. New data about sand sequence in the Tuostakh depression. *Bulletin of the Comission of Quaternary Studies* 52: 107-122 (in Russian).

Konishchev, V.N. 1982. Characteristics of cryogenic weathering in the permafrost zone of the European USSR. *Arctic and Alpine Research* 14(3): 261-265.

Konishchev, V.N. 1987. Origin of loess-like silt in Northern Siberia. *GeoJournal* 15(2): 135-139.

Konishchev, V.N. 1998. Relationship between the lithology of active layer materials and mean annual ground temperature in the former USSR. *Proceedings 7th International. Conference Permafrost, June 23-27, Yellowknife, Canada,1988*: 591-594.

Konishchev, V.N. & Rogov, V.V. 1993. Investigations of cryogenic weathering in Europe and Northern Asia. *Permafrost and Periglacial Processes* 4: 49-64.

Krinsley, D.H. & Doornkamp, J.C. 1973. *Atlas of quartz sand surface textures*. Cambridge: Cambridge University Press; 91 pp.

Layer, P. 2000. Argon-40/Argon-39 age of the El'gygytgyn impact event, Chukotka, Russia, *Meteoritics & Planetary Science* 35: 591-599.

Mahaney, W.C. 2002. *Atlas of sand grain surface textures and applications*. Oxford: Oxford University Press, 237 pp.

Melles, M., Minyuk, P., Brigham-Grette, J. & Juschus, O. (eds.) 2005. *The Expedition El'gygytgyn Lake 2003 (Siberian Arctic)*. Bremerhaven: Reports on Polar and Marine Research 509, 139 pp.

Melles, M., Brigham-Grette, J., Glushkova, O.Yu., Minyuk, P.S., Nowaczyk, N.R. & Hubberten, H.W. 2007. Sedimentary geochemistry of core PG1351 from Lake El´gygytgyn–a sensitive record of climate variability in the East Siberian Arctic during the past three glacial-interglacial cycles. *Journal of Paleolimnology* 37: 89-104.

Minervin, A.V. 1982. In: Konishchev, V.N. & Rogov, V.V. 1993. Investigations of cryogenic weathering in Europe and Northern Asia. *Permafrost and Periglacial Processes* 4: 49-64.

Miotke, F.D. 1988. Microclimate, weathering processes and salt within ice-free continental Antarctica. *Polarforschung* 58(2/3): 201-209.

Nolan, M. & Brigham-Grette, J. 2007. Basic hydrology, limnology, and meteorology of modern Lake El´gygytgyn, Siberia. *Journal of Paleolimnology* 37: 17-35.

Nowaczyk, N.R., Minyuk, P., Melles, M., Brigham-Grette, J., Glushkova, O., Nolan, M., Lozkhin, A.V., Stetsenko, T.V., Anderson, P.M. & Forman, S.L. 2002. Magnetostratigraphic results from impact crater Lake El´gygytgyn, northeastern Siberia: a 300 kyr long high-resolution terrestrial paleoclimatic record from the Arctic. *Geophysical Journal International* 150: 109-126.

Nowaczyk, N.R. & Melles, M. 2007. A revised age model for core PG1351 from Lake El´gygytgyn, Chukotka, based on magnetic susceptibility variations tuned to northern hemisphere insolation variations. *Journal of Paleolimnology* 37: 65-76.

Romanovskii, N.N. & Hubberten, H.W. 2001. Results of permafrost modeling of the lowlands and shelf on the Laptev Sea region, Russia. *Permafrost and Periglacial Processes* 12: 191-202.

Schwamborn, G., Meyer, H., Fedorov, G., Schirrmeister, L. & Hubberten, H.W. 2006. Ground ice and slope sediments archiving Late Quaternary paleoclimate and paleoenvironment signals at the margins of Lake El'gygytgyn impact crater, NE Siberia. *Quaternary Research* 66: 259-272.

Schwamborn, G., Fedorov, G., Schirrmeister, L., Meyer, H. & Hubberten, H.-W. 2007. Periglacial sediment variations controlled by lake level rise and Late Quaternary climate at El'gygytgyn Crater Lake, Arctic Siberia. *Boreas*. DOI: 10.1111/ j.1502-3885.2007.00011.x.

Van Hoesen, J.G. & Orndorff, R.L. 2004. A comparative SEM study on the micromorphology of glacial and nonglacial clasts with varying age and lithology. *Canadian Journal of Earth Sciences* 41: 1123-1139.

Vogt, C. 1997. *Regional and temporal variations of mineral assemblages in Arctic Ocean sediments as climatic indicator during glacial/interglacial changes*. Bremerhaven: Reports on Polar Research 251(30-42), 309 pp.(in German).

Investigation and Monitoring of Tailing Dams in Northeast Russia Using Geoelectrical Methods

Boris M. Sedov
North-Eastern Scientific Research Institute, Far East Branch, Russian Academy of Science, Magadan, Russia
Alexander V. Muslimov
JSC "Ecogeophysics"
Pavel E. Tikhmenev
Omolon Gold Mining Company, Kubaka Mine

Abstract

Geoelectrical methods are recommended for identification and location of seepage zones in permafrost areas. These include vertical electric sounding, and profiling of apparent electric resistances and self-potential. Methods are based on significant specific electric resistance difference between frozen and thawed soils, and self-potential is generated by filtrating flows. Changing the distance between points of vertical electric sounding allows us to build 3D fields of electric resistance $\rho_a(x_i, y_i, z_i)$. Filtration zones appear with low ρ_a values and low (negative) self-potential. Comparison of ρ_a fields measured in different periods allows use to monitor the temperature changes and state of the frozen material, and to forecast and prevent possible seepage with minimum financial effort. Use of the described techniques demonstrate their high efficiency during technical condition determination of water reservoirs dams, technical water retention dams at gold and silver mining enterprises, and at diamond mines.

Keywords: control; dam; filtration; geoelectrical methods; monitoring; permafrost.

Introduction

Northeastern Russia is part of the cryolithozone, with its permafrost base stretching from tens to hundreds of meters in depth. Despite this, the upper soil layer has fluctuating temperatures, often above the melting point. This balanced natural process causes no negative environmental changes. Under technogenic influence, geochemical and thermal changes are much greater then natural factors. In northeast Russia, such negative technogenic effects on soils are caused by hydrotechnical facilities such as tailings and water reservoirs.

Use of cyanide process for gold and silver extraction in Northeast Russia brings up the problem of massive toxic waste storage in permafrost zones. Besides tailings facilities, there are varieties of clean and technical water reservoirs, reservoirs for thermal and hydro-electrical plants, tailings facilities of diamond mines, and more. All these hydrotechnical structures are formed with dams, and are mostly situated in river valleys. Depending on the object's use, dams could be permeable or water retaining. Large volumes of water affect the temperature of the frozen material up to its thaw. Lowering the melting point of frozen material in contact with highly mineralized technical solution can also lead to solution seepage. Investigation of such seepage zones, the determination of their location, and monitoring of technical status of hydro technical structures is successfully performed with use of geoelectrical methods.

Geotechnical Characteristics of Dams and Underlying Base Rock in Permafrost Zones of Northeast Russia

Most rivers at Northeast Russia follow tectonic fault zones. Besides tectonic fracture, vertical cracking as a result of cryogenic deformation appears even in solid bedrock. For example, at Kupol Mine (Central Chukotka), such cracks in basalt are 50–70 m deep and can be traced for hundreds of meters on the surface. Similar cracking in a different rock type were observed in Saha (Yakutia), when tailings facilities for diamond mines were in construction. Granites in the area of the Kolyma River Hydroelectrical Plant have very similar block type form. The absence of tectonic mirrors on joint surfaces within fault zones testifies to the cryogenic genesis of these fractures, as does the absence of tectonic displacement. Such cracks, as a rule, are not filled with ice, but just "capped" with delluvial material 1–2 m at the top. Mostly, such cracks were found during removal of the upper delluvial layer. Filling these cracks at road crossings was not successful, nor was filling with concrete as large amounts were simply draining in.

Basic Technical Peculiarities of Dam Structure in the Russian Northeast

Currently in Northeastern Russia (Yakutia, Chukotka and Magadan Regions), there are number of operating and abandoned tailings facilities and reservoirs. Places in Magadan Region, where geoelectrical investigations were performed, are shown on Figure 1.

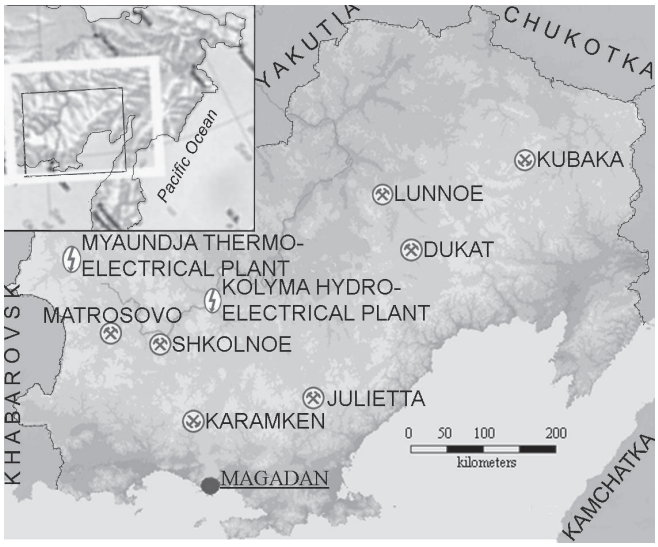

Figure 1. Location of sites where geoelectrical methods were applied to investigate the dam status.

Regardless of design, dams in Russian Northeast are constructed of local materials. Depending on the dam's purpose, there are two different types: permeable (filtering) and watertight (water retaining) (Biyanov 1983) Permeable (filtering) dykes are designed to separate technical solutions and solid parts from sludgy tailings. Sometimes, additional filtering dykes are built on the surface of the tailings for the same reason. Below the filtering core, reclaimed technical water is taken back into the process.

What follows is a general overview of tailings facilities structural peculiarities at various mining enterprises. As a good example, we will describe Kubaka gold mine, the first joint-stock gold mining enterprise with a foreign investor in Magadan Region. During operation from 1997 to 2006, over 90 tons of gold were mined and extracted using the cyanide process. During exploitation, dams were raised to increase the tailings facility capacity. It was situated on the valley side, so no upper dam was needed (Fig. 2). Cleared water was draining through the filtering dyke into a reclaimed water pond, where it was taken into the process again. The water retention dam had a frozen core, formed by over 100 thermo siphons inserted through the dam into bedrock. These were installed in 1998, when geoelectrical sounding showed that dam's core and underlying bedrock had melted zones and technical solution was seeping through. Pipes were filled with carbon dioxide. Foreign engineering companies were developing most sufficient variants of Kubaka deposit mining and foreign investors were implementing them. Kubaka's tailings facilities are example of good handling of a variety of technical challenges. Tailings facilities were inspected with geoelectrical methods several times during operation.

The Kubaka mine was performing a closure procedure during 2007; tailings were caped with 1.5 m of waste rock, 0.5 m of silty shale and 0.3 m of top soil for vegetation. Since waste rock was placed during winter time on frozen tailings, it remained frozen during summer and heavy mining equipment was hauling material on top of capped tailings without sinking. This is a unique example of full reclamation of a tailing facility in Northeast Russia.

Karamken Gold Mine (operated from 1978 to 1995) is situated 100 kilometers north of Magadan. Karamken Mine Tailings facility is situated in the mid-flow of Tumanniy creek. There was a need to prevent inflow of upper creek water into the tailings facility. An impermeable upper dam was guiding into a diversion channel.

In order to maintain impermeability of the upper dam, a row of holes with pipe casing was emplaced. A refrigerator was pumping the cooling agent ($CaCl_2$). Freezing the dam's core created an impermeable barrier. The diversion channel was originally made of concrete U-shaped sections which deformed quickly, and steel lining was placed inside to maintain the level needed for water flow. Its abandoned tailings facility used a different approach for separation of water from the slurry then used at the Kubaka mine. The technical solution was settling and seeping through the dykes and tails and was accumulating at the sump, which was dug at the deepest point of the wooden tunnel and down to the bedrock below the dam.

Currently, despite shut down of the Karamken mine, liquid waste from the Kolyma Refinery is frequently discharged in the Karamken tailings facility.

Tailings facilities at other Magadan region gold and silver mines which use the cyanide process were constructed later then the Karamken and Kubaka facilities. Mostly, they have polymer lining. Tailings facilities of the Vetrenskoe mine was very similar to Kubaka, with reclaimed water sump in the old bed of the diverted creek.

Tailings facilities of Saha (Yakutia) diamond mines have only one watertight dam, the frozen core providing its impermeability. The core is kept frozen by pipes filled with kerosene. Reclaimed water was accumulating in the pond next to the dam.

There are many more plains in Saha (Yakutia) then in the Magadan region, so the areas occupied by diamond mines in Saha (Yakutia) are greater, and dams are lower but longer then tailings facilities in Magadan region mines.

Besides mining enterprises, there are a variety of hydrotechnical structures in the region such as reservoirs for domestic use near towns, and technical water reservoirs for hydro and thermoelectrical plants. The largest volume of water is held by a major dam 150 m high at the Kolyma River Hydroelectrical Plant. The dam is constructed in highly fractured granite, where the fractures have different genesis.

Miaundja Thermo Electrical Plant, built in the early 1950s, has a technical water reservoir. It has a frozen core, which is cooled with air circulating through a wooden tunnel throughout the dam's center during the winter period. The dam is constructed on highly fractured shales.

Dams have a shape of trapezium in cross-section, with the lower face terraced with benches.

Another peculiarity of the Russian Northeast that affects

hydrotechnical structures besides permafrost is the high seismicity of some areas in the region.

Tailings facilities, water reservoirs and other hydrotechnical structures bring a local influence to a surrounding frozen material. This includes heat brought with highly thermo conductive water or technical solutions. To protect a dam from melting, extra material is placed from its influenced upper face. This material protects frozen material from heat exchange with water. In addition, heat exchange tailings facilities are influenced by mineralized solution which lowers the ice melting point.

These would be two main reasons for infiltration appearance; through the dam's core as well as through fractured bedrock. A variety of technical accidents on hydrotechnical facilities in Chukotka emphasizes the seriousness of such infiltrations. Roughly every reservoir was loosing water because of infiltrations (Demchenko et al. 2005).

Localizing infiltration zones using non-geophysical methods like drilling is slow and costly, and introduces additional heat to dam's material.

Geoelectrical Methods of Controlling and Monitoring Dams in Northeast Russia

Geoelectrical methods of determining filtration zones is widely used in permafrost free regions; e.g., for mudslides sounding (Bogoslovsky & Ogilvy 1970). Their localization is determined by self-potentials survey, their minimums show the object.

Physical Basis of Geoelectrical Methods for Detection of Seepage and Melting Zones

In permafrost regions, the first applications of geoelectrical methods for determining melted zones in dams and bedrock where performed after several accidents involving water reservoirs (Kadykchan town, Miaundja Thermo Electrical Plant) occurred in permafrost areas of Northeast Russia. Geoelectrical methods from geophysics were used for localization of melting areas and filtration zones. Water flow in a filtration zone creates a field of self-potentials; the magnitude increases with an increase of mineralization level and flow speed. During methods development, the fact of low self-potentials in fresh water filtrations was discovered. Soil resistivity in permafrost studies showed that melting soils increases their conductivity by three orders of magnitude (Frolov 1998, Yakupov 2000). In the case of mineralized solution, resistivity of melted soils is near zero Ω-m. Later, during investigation of seepage zones at the Northeastern (permafrost zone) mining enterprises' tailings facilities, highly mineralized solutions were stated as significant sources of self-potentials as well.

Complex of Geoelectrical Methods for Detection of Dams' Melting and Seepage Zones

Geoelectrical methods from geophysics are used by our team for determination of filtration zones through dams and bedrock, during technical control and monitoring at Northeast Russia (Saha (Yakutia) and Magadan Regions) (Muslimov & Sedov 2006). They include vertical electric sounding (VES), electrical profiling of CD (Schlumberger array), very low frequency (VLF) and self-potential (SP) profiling; all performed on standard equipment. VES uses a symmetrical Schlumberger array (C_1O = 1,5; 2,0; 3,0; 4,5; 6; 9; 12; 16; 20; 30; 40; 80; 110; 150; 200 and 300 m, P_1P_2 = 2; 10 m, C_2 - ∞). Lateral profiling used a half Schlumberger array P_1P = 2.0 m. In winter, we have electrode contact problems and then VES and electric profiling are replaced by alternate current (AC) methods. Time domain electromagnetic survey (TDEM) is search conductor mineralized filtrate. Configuration uses central loop mode and transmitting loop of 20x20 m. The seepage zone has very low resistance. TDEM is faster and cheaper, and can be used all year round since grounding is not needed. Electrical profiling is typically performed on two feeder distances or two different frequencies. This gives the apparent resistances typical for two different depths.

VES, electrical profiling, VLF and TDEM with measuring stations on the dam's crest, benches and lower face is performed as an initial step. Stations interval is 20 m. Electrical profiling of the perimeter may be done as well, if needed. VES measurements are done on dam's crest and benches, as well as at locations which showed low resistances on initial electrical profiling.

Depending on the approach used, geoelectrical sounding results are presented as graphs with resistivity profiles - $\rho_a(x_i)$, pseudo depth plot - $\rho_a(x_i, z_i)$, apparent resistivity contours - $\rho_a(x_i, y_i)$, profile and contours in mV SP, VES curves - $\rho_a(z_i)$ and its interpretation. For technical monitoring of dams, VES provides the most interesting data. It is presented as three dimension (3D) coordinates ρ_a (x_i, y_i, z_i). The developed software allows one to use any "slice" of the collected data for determination of the filtration zones. Mostly, apparent resistance profiles ρ_a (x_i, z_i) and ρ_a (y_i, z_i) along and across the dam body are used. Lateral sections ($z_к$) ρ_a for different depths ρ_a (x, y, z_n) can be done. Quantitative interpretation (determination of true specific resistance ρ_n) at a certain point with (x_i, y_{ii}, z_i) coordinates is very difficult. This statement is based on the fact that a dam's structure, even if it would be made out of material with invariable resistance, is very complex and does not correspond to conditions required for quantitative interpretation of VES, developed for horizontal stratum of infinite stretch (Hallof 1981). This limitation of VES is valid for any other geological task. The accuracy of the quantitative interpretation is determined by intersecting VESs. Coinciding resistance curves testify that the stratum is horizontal and infinite. Despite quantitative interpretation of VES is not possible, the technical monitoring task was fulfilled successfully, as experimental works results show. Let us describe this statement with the following example. Despite any misrepresentations caused by a complex dam profile, apparent resistances along or across dam's axis will be similar if there are no filtration zones. Only along the dam's flanks, where interfacing environments have some influence, will variations be seen. Abnormally low resistances in the

cross section will appear in the filtration (melting) zones, despite their scale, and are very well distinguished on the apparent resistance minimum cross sections. The coordinates of the filtration zone is determined by tracing this zone of low resistances in the row of profiles for the dam's body, or in the bedrock beneath. Besides VES, self-potential profiling

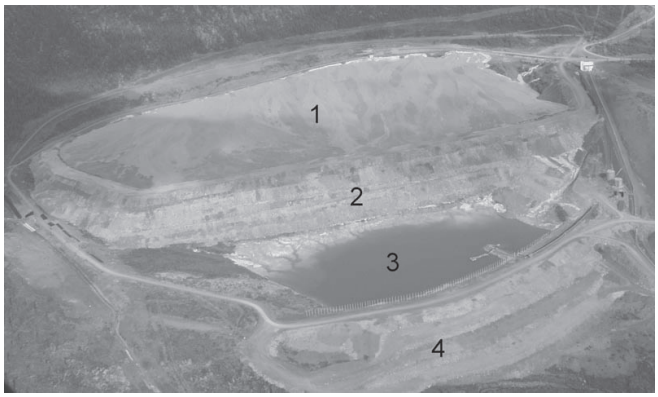

Figure 2. Kubaka Mine tailings facility (Omolon Gold Mining Company, KINROSS GOLD).

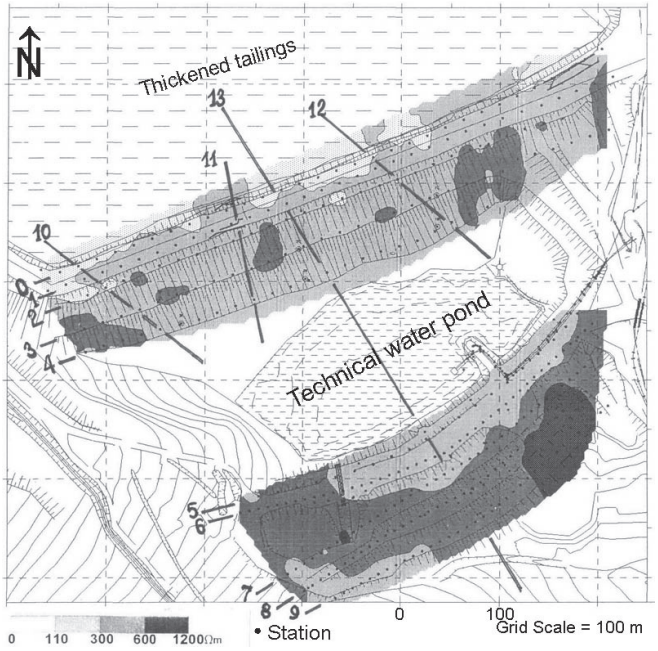

Figure 3. Apparent resistivity contours (Ω-m) for upper (filtering) dyke and lower (water retention) dam, Kubaka Mine (Schlumberger array AO = 2 m).

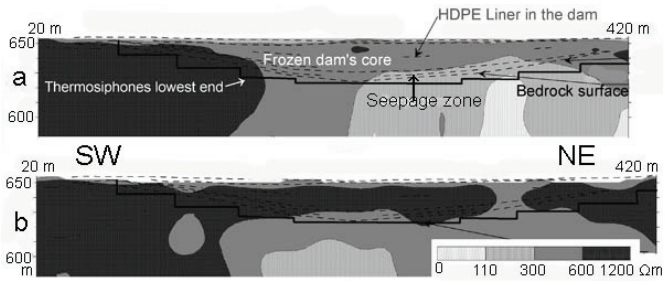

Figure 4. (a) – profile of resistivity in year 1998; (b) – year 2003 (profile position is shown on Fig. 3).

along the dam's axis is performed during summer and early autumn. Filtration zones are seen as negatives anomalies. This anomalies SP depend on flow velocity and increases with higher flow velocity.

Examples of Determining Location of Filtration and Melting Zones by Geoelectrical Methods for Controlling and Monitoring Dams in Permafrost Regions of Northeast Russia

Using geoelectrical methods described above to locate melting and seepage zones, we will discuss results on specific hydrotechnical structures of different genesis and use. As a very positive example, we will discuss results of monitoring at Kubaka Mine tailings facility (Fig. 2).

It includes thickened tailings (1), filtering dyke (2), reclaimed water pond (3) and water retention dam (4), which holds highly mineralized technical solution.

During seven years, the filtering dyke was built up several times to increase projected capacity. The first year of water retention dam surveying indicated dam instability, and signs of minor seepage of technical solution into the creek below. After geoelectrical control in 1998 was performed on both structures, seepage zones were identified. For seepage zones

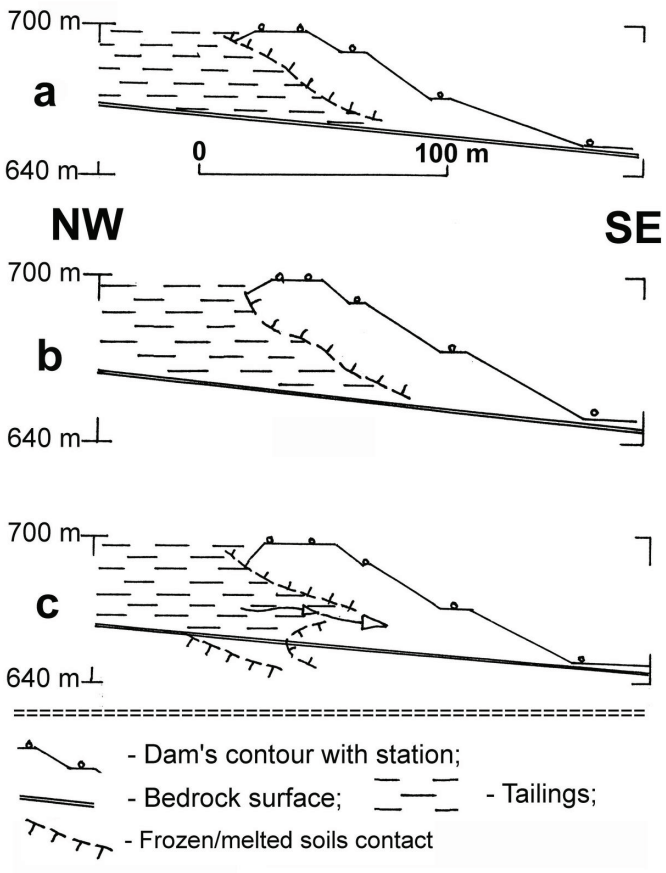

Figure 5. Seepage locations in the upper (filtering) dyke, according to the cross section resistances profiling. Geoelectrical control performed in year 2003.

determination, longitudinal VES profiling was performed (Fig. 3).

Seepage zones were marked with self-potential minimums on the profile, which was compared with VES stations. Later, melted and seepage zone distribution in the dam was confirmed during drilling work to install thermosiphons. The distance between thermosiphons pipes was around 2.0 meters, and they were nailed through the dam into the bedrock. Their bottom line is shown as a step-looking straight line. Figure 4a shows the location of melting and seepage zones four months after the thermosiphons were installed in 1998. Technical solution seepage was stopped after melted zones froze. Soil freezing increased ρ_a (x_i, z_i) and showed clearly during VES. Bedrock resistivity changed insignificantly (Figure 4b). Ceased seepage was marked by negative anomalies of SP disappearance. Geoelectrical methods (VES, SP TDME) were used for melting zones and filtration location in the filtering dyke, as well. Geoelectrical data complex interpretation allowed us to determine the location of filtration zones, pointing out areas blocked with compacted pulp (Fig 5a and 5b). Filtration zones were marked not only with low resistivity ρ_a, but with significantly low SP (Fig. 5c).

On the pseudo plot, melting and seepage zones were shown as areas with minimum apparent resistances.

A 3D apparent resistivity model indicates the distribution of dyke and dam melting zones. Upper face material is influenced with technical solution, and has zones with temperatures above the melting point. This zone is shown as an area with low electric resistance (Fig. 6). The melting and seepage zones pseudo plots for longitudinal profile across Kubaka Mine tailings facility is shown in Figure 7.

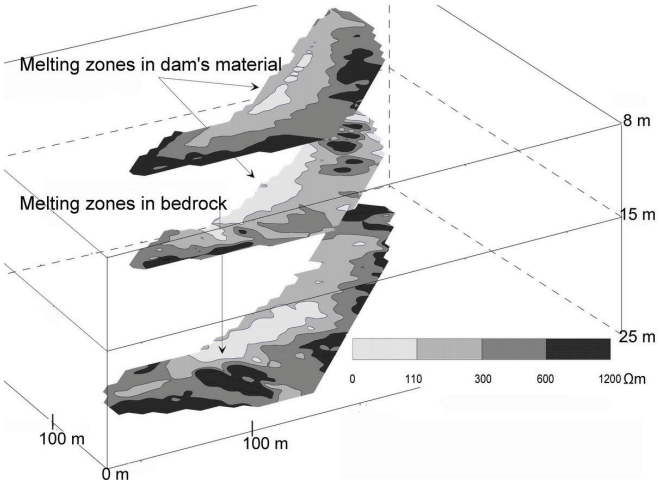

Figure 6. 3D model of showing low resistivity of melted material zones in the dam and bedrock.

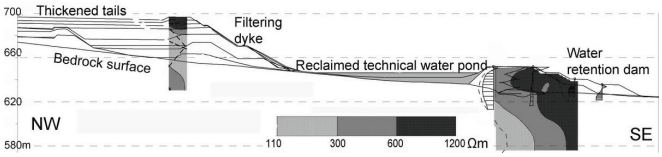

Figure 7. Pseudo plot for longitudinal profile of apparent resistivity across Kubaka Mine tailings facilities.

Geoelectrical methods of investigation used at others dams in the Magadan Region allowed us to determine seepage zones and to perform adequate measures for their elimination.

Yakutia diamond mine tailings facilities hold low mineralized technical water. A frozen core is usually created with thermosiphons filled with kerosene, and seepage zones appear either in fracture zones of bedrock, or where thermosiphons are not functioning. Seepage of fresh water there is indicated the same way as seepage of technical solution described above; these places demonstrate low electric resistivity (Fig. 8).

A complex of geophysical approaches consisting of VES, apparent resistivity and self-potential profiling were used for seepage determination at Marha' tailings dam ALROSSA. Seepage elimination was achieved with kerosene filled

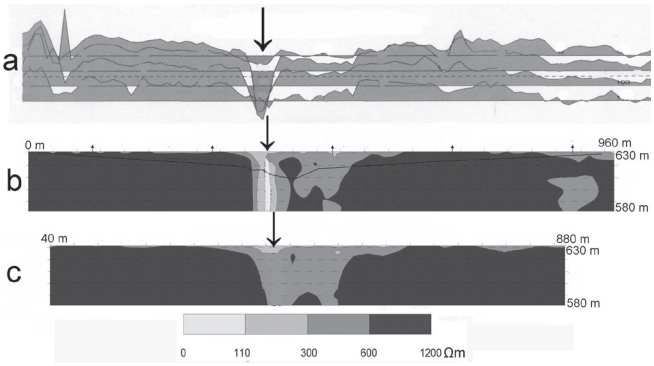

Figure 8. Seepage zone determination with VLF profiling along the crest (Marha Dimond Mine, Saha (Yakutia), ALROSSA). VLF resistivity profiles (a), pseudo plot with melted zone, June 2003 (b), pseudo plot after melted zone congealing, July 2003 (c). Arrows show seepage zone location.

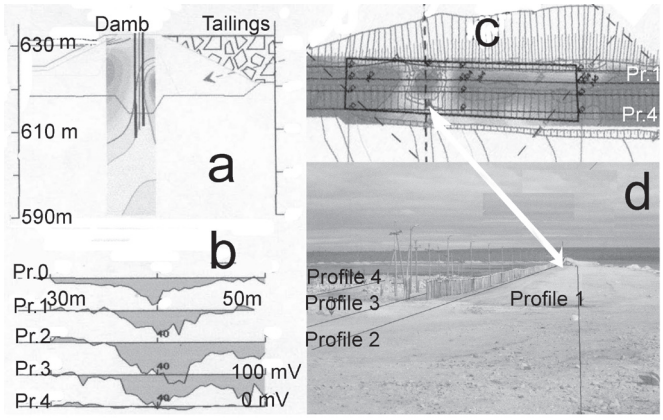

Figure 9. Seepage zone determination with geoelectrical methods (Complex VES, SP and resistivity profiling). Apparent resistivity distribution with depth (a) and on the dam's surface (c) indicates that melted material zone with electric conductivity formed around non-operating thermo needle. Since the dam was constructed with coarse material, seepage occurred in a melted zone, which was distinctly indicated with negative SP anomalies (b). SP and electric resistivity profiles were along the dam's crest (d). Profiles were done using 10 m spacing.

thermo needles and graphical interpretation of achieved results (Fig. 9).

In order to eliminate seepage determined with geoelectrical methods, a new thermo needle was installed and the location refroze. Graphs show self-potential minimums above the seepage zone. The pictures show the dam crest with thermo needles and seepage location with formed depression across.

Conclusions

Experience obtained during several years of using geoelectrical methods for monitoring and controlling the technical status of hydrotechnical structures in the permafrost zone shows high efficiency compared to other methods. They are fast and productive. High resolution mapping allows us to detect melted material zones with volumes as small as 0.1 m^3, in the dam or bedrock beneath it. Measurement can be performed on solid surfaces as well as on the water. Geoelectrical methods of control are remote and do not influence sampled material by introducing heat or highly mineralized technical solutions. This fact is very important for rock material containing ice, when contacting the solution can significantly change the melting point. With all benefits, the described methods are much cheaper then any other.

Acknowledgments

We express our gratitude to JSC "Ecogeophysics" director Alexander Sadikov for fruitful discussions on theories, methods, implementation, and sharing results obtained during geophysical control of structures in permafrost zones of Magadan Region, Chukotka and Saha (Yakutia).

References

Biyanov, G.F. 1983. *Dams in Permafrost Regions*. Moscow: Energoatomizdat, 174 pp.

Bogoslovskiy, V.A. & Ogilvy, A.A. 1970. Natural potential anomalies as a quantitative index of the water seepage from reservoirs. *Geophys. Prosp*. 18: 261-268.

Demchenko, T.V., Krivonogova, N.F., Krivozshekov, V.S. et al. 2005. Hydrotechnikal structures of Chukotka: geocriological and ingineering conditions. *Proceedings of Chikchi Branch of NEISRI FAB RAS, Magadan:* 68 pp.

Frolov, A.D. 1998. *Electrical and Elastic Properties of Frozen Earth Materials*. Pushino, 515 pp.

Hallof, P.G. 1981. *Practical Geophysics for Exploration Geologist.* Compiled by V. Blaricom, Spokane, Northwest Mining Association, 39-154.

Muslimov, A.V. & Sedov, B.M. 2006. Geophysical control and monitoring of technical status of hydrotechnical structures in permafrost region. *Proceedings of International Conference "Modern climatic and ecosystem processes in naturally vulnerable zones (Arctic, aired and mountain zones), Rostov-on-Don:* 233-235.

Muslimov, A.V. & Sedov, B.M. 2006, Geophysical Technique Applied to Control Technical Status of Dams in Permafrost. Geology, Geografy and Biologic Diversity of Northeast Russia. *Proceedings of the Far East Regional Conference Dedicate to the Memory of A.P. Vaskovsky and his 95th Anniversary, Magadan, November 28–30, 2006.* NESC FEB RAS, 252-255

Sharma, P.V. 2002. *Environmental and Engineering Geophysics*. Cambridge University Press, 475 pp.

Yakupov, V.S. 2000. *Investigation of Permafrost by Geophysical Technique.* Yakut Branch of Siberian Branch of RAS, Yakutsk, 335 pp.

Geochemical Analysis of Groundwater Dynamics in Permafrost Regions

Sarah J. Seelen
Water and Environmental Center, University of Alaska Fairbanks, Fairbanks, AK, USA
Kenji Yoshikawa
Water and Environmental Center, University of Alaska Fairbanks, Fairbanks, AK, USA
Tom Trainor
Department of Chemistry & Biochemistry, University of Alaska Fairbanks, Fairbanks, AK, USA
Larry Hinzman
International Arctic Research Center, University of Alaska Fairbanks, Fairbanks, AK, USA

Abstract

The presence or absence of permafrost plays a significant role in balancing the infiltration process between surface water and groundwater. These interactions between surface water and groundwater are poorly understood, yet will have a significant affect on the winter base flow discharge of most Arctic rivers as permafrost degrades. To better understand the base flow variability within the Arctic freshwater system, it is important to document and analyze the geochemical characteristics of groundwater. Spring water from 16 aufeis sites in the foothills of the Alaskan Brooks Range was collected during the summer of 2006. Results indicate that three distinct aquifer systems or hydrologic pathways exist in this region. Major ion chemistry of the waters is dominated by Ca^{2+} and HCO_3^-. Geothermal waters are dominated by SO_4^{2-}. Increased knowledge of geochemical characteristics of base flow will provide more insight into the long-term changes of the hydrologic cycle on the Arctic North Slope of Alaska.

Keywords: Brooks Range; geochemistry; groundwater interactions; PCA; infiltration.

Introduction

The hydrology in the Arctic is responding to an already changing climate. One of the major changes is the degradation of permafrost. As permafrost degrades, surface water and precipitation will infiltrate into the deeper sub-permafrost aquifer for the first time in recent geologic history (Clark et al. 2001). These interactions between the surface water and groundwater are poorly understood and will affect the amount and type of winter base flow reaching the Arctic Ocean. These interactions will also introduce new irregularity into an already sensitive hydrologic cycle. In an effort to better understand the base flow variability within the Arctic freshwater system, it is important to document and analyze the geochemical characteristics of groundwater in the dynamic hydrologic system of the Brooks Range.

Water balance studies are integral to quantifying the amount of water entering the Arctic Ocean from runoff, aufeis fields, and springs of the northern Brooks Range. Traditional thought surrounding water balance studies is that water enters the system from topographic highs and exits at topographic lows. The presence of faults, fractures, and permafrost in this study region introduces complexity to the water balance studies being performed. One of several working hypotheses for this research project is that water enters the watershed from the southern slope of the Brooks Range and then travels through the complex fracture system to emerge on the northern slope as spring water and aufeis fields. Geochemical characteristics, as well as dating, of the water will lead to knowledge of flow paths as these characteristics are indicative of specific water-rock interactions (Gomez et al. 2006).

The spatial expanse and remoteness of the eastern Brooks Range has resulted in a limited number of detailed geological studies, whereas much work has been done on the western and central Brooks Range as a result of the development of Red Dog Mine and National Petroleum Reserve – Alaska (NPRA) (Dumoulin et al. 2004, Kelly et al. 2004, Morelli et al. 2004, Slack et al. 2004). At this time, extrapolation of the subsurface stratigraphy from the drill logs in the west and central Brooks Range has been used in conjunction with limited subsurface evidence from the eastern Brooks Range to conceptualize the subsurface pathways and corresponding water-rock interactions in the study area.

One objective of the project is to collect spring water emerging from known aufeis sites in the foothills of the eastern Brooks Range. Aufeis sites are evidence for subterranean water channels that remain open due to the combination of adequate flow rates and warmer water temperatures. Spring water samples collected during the summer of 2006 were analyzed for major chemical characteristics. The data obtained will later be compared to previous chemical data of similar spring sites in an effort to distinguish whether changes have occurred in the hydrologic system of the Brooks Range. However, this paper will address interpretation of results from only those waters collected during 2006 and their geochemical properties, as well as those of several surface precipitate phases collected at the surface exposures. It is believed that these precipitates will lead to a better understanding of the subsurface water-rock interactions, as they are an indicator of the fluid chemistry (e.g., mineral saturation indices) immediately upon exposure at the surface.

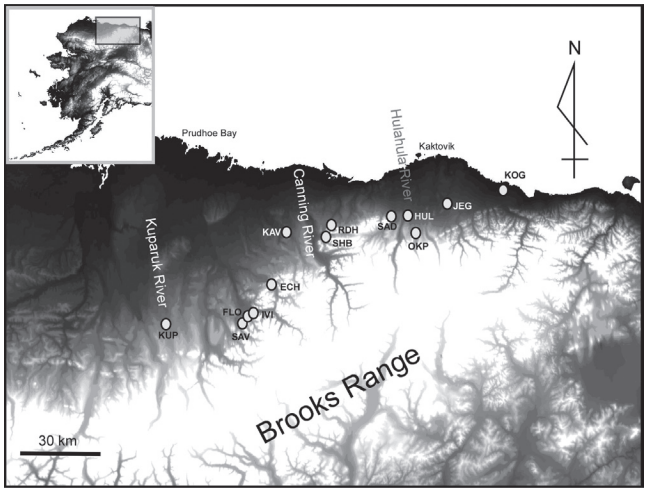

Figure 1. Location map with spring water sites and identifying features.

Methodology

Spring water samples were collected in July of 2006 (Fig. 1). Measurements of pH were conducted in situ with a hand-held meter calibrated at ambient temperatures with pH 4 and pH 7 buffers before and after the sampling trip. Spring water temperature was collected using the same meter. Several liters of water were collected in 1-L HDPE Nalgene bottles. One liter was reserved for alkalinity tests, while the remaining sample volume was then brought back to the lab, filtered through a 0.45um filter, and acidified, if necessary, for further analyses. Alkalinity was determined using HACH method 8203 WAH. Dissolved major cations (Ca^{2+}, Mg^{2+}, Na^{+}, and K^{+}) were analyzed with a Perkin Elmer AAnalyst 300 Atomic Absorption Spectrophotometer; Sr^{2+} was analyzed with an Aglient 7500 CE Inductively Coupled Plasma-Mass Spectrometer. Major anions (Cl^{-}, F^{-}, B^{-}, and SO_4^{2-}) were analyzed with a Dionex LC20 Ion Chromotograph. Hydrothermal precipitates were collected as grab samples in the summer of 2006 at 2 of the 12 spring water sites. The major element compositions of the hydrothermal precipitates were analyzed using a PANAlytical Axios wavelength dispersive x-ray fluorescence (XRF).

Results

Geochemical results indicate that spring waters in the eastern Brooks Range are characterized by varied and distinct water-rock interactions (Table 1). Emerging water temperatures varied by nearly 50°C and pH ranged by a factor of 3. Waters were found to be dominated by either Ca-HCO_3 or SO_4 signature, indicative of the predominant type of water-rock interactions.

Identifying potential flow paths

Principal component analysis (PCA) was used to investigate the underlying relationships among samples. This multivariate statistical analysis reduces the number of variables of a complex system to a lower dimension

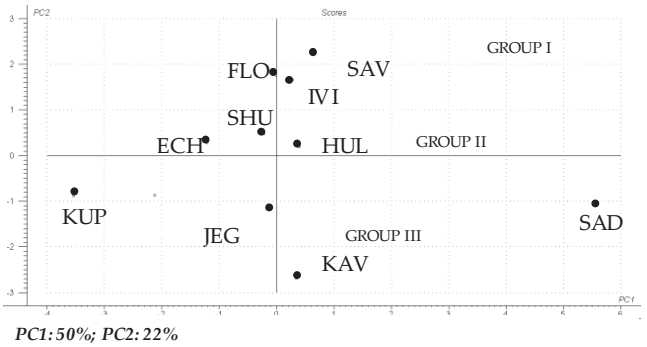

Figure 2. PCA score plot indicating grouped sites.

(from 12 variables to 2 in this case) (Güler et al. 2002). Unscrambler® software was used in calculating principal components (PCs). An initial PCA was created using all sites listing in Table 1. Due to the significant separation between the geothermal springs, OK, RDH1 and RHD2, and the decreased resolution for the remaining spring water sites, it was decided to exclude the geothermal springs to increase the resolution of the remaining spring water sites. The inputs were all those data listed in Table 1, excluding temperature and pH. Figure 2 is the score plot based on these inputs. Principal component one (PC1) explains 50% of the variance and PC2 explains 22% of the variance. PC1 is interpreted to represent flow path interactions. Those samples in the extreme (+) x-direction are subjected to more interactions with material surrounding the flow path while those in the extreme (-) x-direction has little interaction with surrounding material. Those sites lining up on the x-axis indicate site with moderate to limited interactions with surrounding material. The relative distance between sample site SAD and all other sites indicate water at this site interacts with a different type of material or an additional layer than the other sites. SAD water samples have high concentrations of Mg^{2+}, Sr^{2+}, and SO_4^{2-} relative to the others included in this computation.

PC2 is interpreted as segregating the spring sites into groups. Group I sites (IVI, FC, and SAV) not only have similar geochemical characteristics but also spatial proximity (refer to Fig. 1). The same is true for Group II sites (ECH, SHU, and HUL). Sample sites identified to be Group III sites (KUP, JEG, and KAV) are those with a shorter flow distance and, therefore, decreased interactions with more individual, site-specific characteristics.

Precipitates

Several spring water sites had physical evidence of fracture flow through a limestone bedrock formation. Upon surface exposure, the fluids are concentrated during ice-formation, leading to formation of an amorphous precipitate. Spring water site KAV was the most prominent with several mounds of 30 cm in diameter and height. Spring water sites RDH and HUL also had water with a milky-white appearance at the sample site. XRF analysis indicated precipitates at KAV and RDH to be composed principally of CaO (63.76%; 58.24 %), SiO2 (18.6%; 14.9%), and S (17.51%; 26.56%), respectively. The CaO fraction is most likely derived from

Table 1. Geochemistry data of spring waters (mg/L).

Sample ID	pH	T (°C)	Na^+	K^+	Sr^{2+}	Mg^{2+}	Ca^{2+}	Cl^-	F^-	Br^-	SO_4^{2-}	Alkalinity as HCO_3^-
IVI	8.02	7.30	2.38	0.132	5.589	8.77	33.8	0.66	0.60	nd†	14.41	97.8
SAV	7.78	7.81	2.12	0.101	8.271	9.83	45.44	0.49	0.66	nd	10.79	110.0
ECH	8.24	0.60	1.85	0.117	2.709	6.38	31.88	0.51	0.27	nd	11.38	80.5
FLO	8.13	6.06	2.23	0.12	6.912	8.52	29.8	0.40	0.61	nd	14.46	96.7
SAD	8.34	13.1	7.3	0.928	15.67	16.57	39.52	1.70	0.73	nd	76.34	108.3
SHU	8.14	5.27	1.68	0.184	11.08	7.64	26.36	0.30	0.42	nd	49.56	90.1
HUL	8.38	3.94	3.11	0.303	1.888	10.33	46.72	0.30	0.39	nd	69.58	85.5
JEG	8.11	8.26	1.6	0.284	3.12	6.4	50.68	0.62	0.00	nd	83.09	124.4
KAV	7.62	0.46	3.42	0.404	1.544	11.17	18.89	0.30	0.00	nd	119.76	147.3
KUP	6.38	1.69	2.13	0.106	0.2725	1.21	4.37	0.20	0.00	nd	2.83	23.3
OKP	8.79	48.1	102.72	5.356	3.079	0.1	1.543	18.00	15.81	nd	196.04	45.6
RDH1§	7.80	3.96	89.92	6.153	13.59	25.68	55.8	83.00	1.01	0.48	75.97	268.3
RDH2	7.54	27.7	96.8	6.585	18.24	22.12	49.12	87.00	1.05	0.55	26.43	248.7

Sites are listed from west to east; †below detection limits; §duplicate samples were collected for this site; ‡additional precipitate grab samples collected.

one of the several limestone lithologies. The emerging temperatures and geochemical characteristics at the spring water sites suggest S and SiO_2 portions are preferentially removed from the flow path as the water reaches the surface. Without more specific subsurface lithologies, it is difficult to determine how similar the flow paths are for the KAV and RDH. Preliminary results based on interpolated subsurface information and multivariate statistical analysis, indicate the two sites do not share flow paths.

The oxide percentages, dominated by CaO, seem to be further evidence of water-rock interaction with carbonate rocks. As the projected infiltration region of the Brooks Range is composed of carbonate rock, it is of little surprise to see a large percentage of the hydrothermal precipitates as CaO. Also of little surprise are the remaining two dominant components, SiO_2 and S. The assumed geothermal properties in the subsurface suggested by well log data, as well as concentrations of Si and S in the spring waters, imply a definite heat source and interaction with sulfide minerals (likely pyrite). Elemental concentrations of Zn, Pb, Zr, Sr, and Ba suggest further comparisons with stratigraphy connections with the region surrounding the Red Dog Mine in the western Brooks Range (Dumoulin et al. 2004, Kelly et al. 2004, Morelli et al. 2004, Slack et al. 2004).

Conclusion

All 12 spring water sites sampled exhibited unique geochemical markers as a result of specific water-rock interactions as the water reached the surface. Using a multivariate statistical technique, PCA, spring water samples were differentiated into groups based on these unique geochemical markers. Precipitate data suggest the type of water-rock interactions that dominate on the path to the surface. Further work is needed to identify potential correlation between spring water sites and fractures as well as subsurface lithologies among those spring water sites grouped according to PCA score plot results.

Acknowledgments

The authors are very grateful to Tevis Underwood and Richard Voss (US Fish and Wildlife Service; ANWR) for providing permit to access Arctic National Wildlife Refuge. Special thanks to the U.S. National Science Foundation (OPP-0229705) for providing funding. Special thanks to Jason Addison, Vanessa Ritchie, and Shane Billings for assistance in sample analysis.

References

Clark, I.D., Lauriol, B., Harwood, L. & Marschner, M. 2001. Groundwater contributions to discharge in a permafrost setting, Big Fish River, NWT, Canada. *Arctic, Antarctic, and Alpine Research* 33: 62-69.

Dumoulin, J.A., Harris, A.G., Blome, C.D., Young, L.E., Johnson, C.A., Kelley, K.D., Leach, D.L. & Anonymous. 2004. Depositional Settings, Correlation, and Age of Carboniferous Rocks in the Western Brooks Range, Alaska: Stable isotopic evidence that barite deposits in the western Brooks Range, Alaska, mark the sites of Mississippian methane seeps. *Geological Society of America, 2003 Annual Meeting in Boulder, CO,* 99: 1355-1384.

Gómez, P., Turrero, M.J., Garralón, A., Peña, J., Buil, B., de la Cruz, B., Sánchez, M., Sánchez, D.M, Quejido, A., Bajos, C. & Sánchez, L. 2006. Hydrogeochemical characteristics of deep groundwaters of the Hesperian Massif (Spain). *Journal of Iberian Geology* 32: 113-131.

Güler, C., Thyne, G.D., McCray, J.E. & Turner, A.M. 2002. Evaluation of graphical and multivariate statistical methods for classification of water chemistry data. *Hydrogeology Journal* 10: 455-474.

Kelley, K.D., Leach, D.L., Johnson, C.A., Clark, J.L., Fayek, M., Slack, J.F., Anderson, V.M., Ayuso, R.A. & Ridley, W.I. 2004. Textural, compositional, and

sulfur isotope variations of sulfide minerals in the Red Dog Zn-Pb-Ag deposits, Brooks Range, Alaska: Implications for ore formation. *Economic Geology*, 99: 1509-1532.

Morelli, R.M., Creaser, R.A., Selby, D., Kelley, K.D., Leach, D.L. & King, A.R. 2004. Re-Os sulfide geochronology of the Red Dog sediment-hosted Zn-Pb-Ag deposit, Brooks Range, Alaska. *Economic Geology* 99: 1569-1576.

Slack, J.F., Kelley, K.D., Anderson, V.M.; Clark, J.L. & Ayuso, R.A. 2004. Multistage hydrothermal silicification and Fe-Tl-As-Sb-Ge-REE enrichment in the Red Dog Zn-Pb-Ag district, northern Alaska: Geochemistry, origin, and exploration applications. *Economic Geology* 99: 1481-1506.

Interactions Between Human Disturbance, Demographics of *Betula fruticosa* Pall., and Permafrost in the Vitimskoye Upland, East Siberia

I.R. Sekulich
Institute of General and Experimental Biology SB RAS, Ulan-Ude, Russia

Abstract

The demographic structure of coenopopulations of *Betula fruticosa* Pall. in birch-shrublands is described in relation to off-road vehicle and agricultural disturbance and changes in terrain at the southern limit of continuous permafrost. It was determined that the degree of change in the demographic structure of the shrub affects the dynamics and processes of the permafrost condition. Heavy use of vehicles and ploughing lead to loss of shrubs and to grassy pasture. These changes contribute to major changes in soil temperature, moisture, and drainage conditions, followed by thermokarsting and solifluction. In the case of slight anthropogenic impact, such as the single passage of a tracked vehicle, the birch populations recover and the soil and terrain environment returns to the original condition.

Keywords: anthropogenic disturbances; *Betula fruticosa*; coenopopulations; demography.

Introduction

The major ecostabilizing element in a permafrost ecosystem is vegetative cover. However, the influence of human activity becomes more and more noticeable, and this, first of all, has an effect on vegetation. In this connection, research on the structure of vegetative cover, its stability in relation to anthropogenic disturbances, and its ability to self-recover has become most important.

The study of plant species coenopopulations gives the possibility to reveal the actual reaction of plants to various ecological factors on two levels: the individual level and the populations level.

According to Harper's studies in England (Harper & White 1974, Harper 1977, Harper 1992, etc.) and Rabotnov's, and Uranov's in Russia (Rabotnov 1950, 1964, 1969, 1975, 1978, 1985; Uranov 1960, 1975, 1977) the coenopopulation approach is widely developed, particularly in Russia.

The demographic structure of a plant's coenopopulations is one of the basic criteria of estimation of the modern state of species in coenosis, the level of vital condition of its coenopopulations, the degree of their stability and prospects of development.

Study Area

Our research was performed on the central part of the Vitimskoye upland, which is located in Eastern Siberia in the depths of the Eurasian continent to the east of Lake Baikal (Fig. 1). It is a large isolated area situated at the southern limit of continuous permafrost. The permafrost is the major ecological factor which determines the character and distribution of vegetation here.

Larch forests (from *Larix gmelinii* [Rupr.] Rupr.) and communities formed of low birches or birch-shrublands (in Russia termed *yernik)* are the most widespread here.

The capacity of permafrost in the research area is from 50 m to 250 m with temperatures from 0°C to -3°C, and depth bedding of permafrost in birch-shrublands and lighted larch

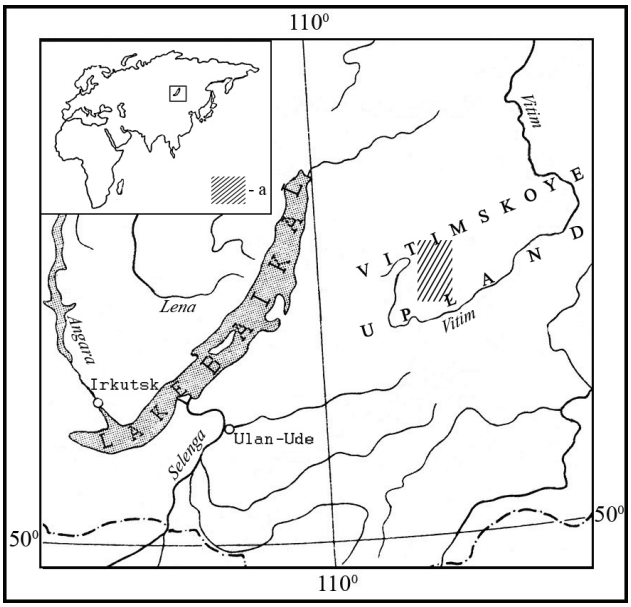

Figure 1. Map of location of research area.

forests in August-September is about 1.0–1.6 m (Vtorushin & Pigareva 1996).

The character of anthropogenic impact on birch-shrublands is developed in the following directions: their total destruction at strip-mining of minerals and ploughing up the earth, influence of track-type transport, and pasturing.

Material and Methods

The object of our research is *Betula fruticosa* Pall. subsp. *montana* M. Schemberg, the basic dominant of birch-shrublands, which occupy hollow inclined slopes, above the floodplain terraces, high parts of valley bottoms; that is, just those sites which are widely used by humans on the Vitimskoye upland.

Research was carried out, spent on model area in 100 square meters on which continuously calculated individuals on age groups.

Table 1. Age stages and age groups of the plants.

The age stages	The age groups	The letter code
latent	seed	sm
pre-generative	germ	pl
	juvenile	j
	immature	im
	virginile	v
generative	young generative	g_1
	mature generative	g_2
	old generative	g_3
post-generative	subsenile	ss
	senile	s

Table 2. Age groups of plants, coefficient of age (m_i) and efficiency of plants (e_i).

Age groups	The coefficient of age (m_i)	The efficiency of plants (e_i)
pl	0.0067	0.0266
j	0.018	0.0707
im	0.0474	0.1807
v	0.1192	0.42
g_1	0.2689	0.7864
g_2	0.5	1
g_3	0.7311	0.7864
ss	0.8808	0.42
s	0.9820	0.1807

The whole life cycle of plants can be divided into the age stages and age groups (Rabotnov 1950) submitted in Table 1. The letter code of each age group has been offered by Uranov (1960).

Determination of age groups is based on a number of complex signs, such as seed or root nutrition of plants, presence of juvenile or adult structures and their quantitative parities at the individuals, seed or vegetative reproduction, a parity and intensity of these processes, a parity of processes of new growth and dying, and degree of basic signs of biomorph generated at the individual.

The age level of the coenopopulations is estimated by the index of age (Δ) proposed by Uranov (1975) and by the index of effectiveness of the populations (ω) proposed by Zhivotovsky (2001). Values of Δ and ω were calculated by the following formulas:

$$\Delta = \sum n_i m_i \Big/ \sum n_i \quad (1)$$

$$\omega = \sum n_i e_i \Big/ \sum n_i \quad (2)$$

where n_i is the number of individuals of each age group; m_i is the coefficient of the age group, calculated by Uranov (1975); and e_i is the efficiency of plants of each age group, calculated by Zhivotovsky (2001). Values of m_i and e_i are submitted in Table 2.

Indexes Δ and ω vary from 0 to 1, and the highest value characterized the elder coenopopulation (Uranov 1975, Zhivotovsky 2001).

Results and Discussion

We studied the changes of demographic structure of the coenopopulations of *Betula fruticosa* on sites with partial destruction of vegetative cover as a result of the influence of track transport and pasturing. In estimating the degree of anthropogenic influence on the demographic spectrum of disturbed coenopopulations, it is necessary to compare them with a base spectrum, which, as considered Smirnova (1987), is the modal characteristic of dynamic balance of a coenopopulation. The base spectrum coenopopulations *B. fruticosa* on the Vitimskoye upland is full-constituent, has one peak, with absolute maximum on old generative individuals.

Two variants of modification of the demographic structure were marked.

One of them shows in increase of the quantity of pregenerative individuals at remaining big amount of generative individuals. An age spectrum of such coenopopulations has two peaks, the first maximum on immature individuals and the second maximum on old generative individuals. As an example, the age spectrum coenopopulation in a community of Multiherboso–Betuletum fruticosae is shown (Fig. 2). The community is situated near settlement along a highway and often exposed to influence of track-type vehicle.

At unitary passage of the cross-country vehicle according to mechanical influence, integrity of vegetative cover is broken, shrubbery and herbs are damaged, the moss and lichen cover are destroyed. As a result of these disturbances gaps formed, which are the microecotope for renewal *B fruticosa.* There is a rejuvenation of the coenopopulation at the expense of the big number of young individuals (Table 3). Short-term influence of transport does not effect adult individuals of *B. fruticosa* essentially. After termination of anthropogenic impact, individuals can quickly restore their habitus to former level. It is connected with formation of new suckers from sleeping buds which are on underground xylopodium parts. The growth of these suckers can reach 30–50 centimeters in the first year. At multiple or constant impact of track-type transports, the adult individuals finally perish, which leads to growth of grassy plants (cereals and sedges).

Replacement of birch-shrublands on grassy communities of meadow type leads to change of hydrothermal condition of soil. In space between ruts under the grassy vegetation, the depth of seasonal melting of permafrost is increased, raised soil temperatures, the moisture of soil is decreased. In ruts the temperature is decreased, which is connected with superfluous moisture of a surface (Moskalenko 1999).

Another variant of anthropogenic change occurs with pasturing. There are regressive changes in age structure. As a result of trampling and pasturing the young individuals of

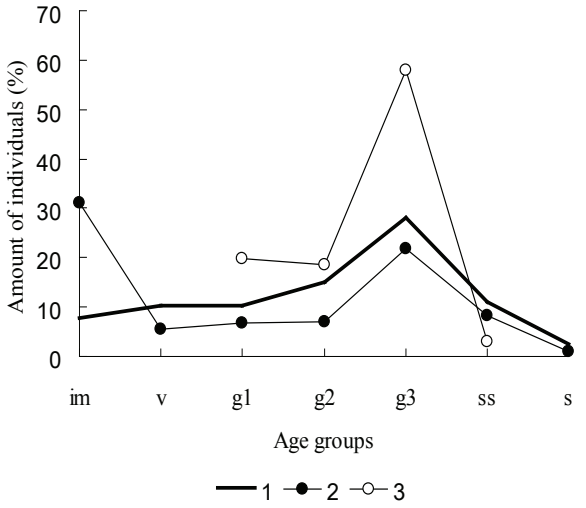

Figure 2. The age spectrums coenopopulations of *Betula fruticosa*. 1 – base spectrum; 2 – community of Multiherboso–Betuletum fruticosae; 3 – community of Kobresio filiformis– Betuletum fruticosae. Characteristic of age groups was explained above.

B. fruticosa disappear from structure of community together with grassy plants. The coenopopulation is presented by old-age plants. A community of Kobresio filiformis–Betuletum fruticosae located on an abrupt slope can be an example of such kind of coenopopulation. The age spectrum here has one peak, but differs from base spectrum. This age spectrum is not full-constituent and presented by old individuals (Fig. 2). This spectrum completely correlated with the regressive coenopopulations type of the spectrum, described by T.A. Rabotnov (1950). The quantity of individuals of *B. fruticosa* in this coenopopulation is small (Table 3). Gradual aging of coenopopulation without young individuals can lead to disappearing. The hydrothermal conditions of soil are changed on the bared sites, therefore cryogenic processes, such as erosion and solifluction, can develop.

The low index of age and index of effectiveness of coenopopulation of *B. fruticosa* occurred in community of Multiherboso–Betuletum fruticosae shows the invasive character of coenopopulation. The high index of age and index of effectiveness in community of Kobresio filiformis–Betuletum fruticosae show, that this coenopopulation mostly consists of old individuals and testifies decreasing of dominant role of species in coenosis (Table 3).

The coenopopulation in community of Multiherboso–Betuletum fruticosae it is considered as young, and the coenopopulation in community of Kobresio filiformis–Betuletum fruticosae – as becoming old according to "delta-omega" classification (Zhivotovsky 2001).

Thus, human-induced disturbances on the demographic structure of coenopopulation *B. fruticosa* in birch-shrublands on the Vitimskoye upland promote development of various geocryological processes, such as bogging, thermokarst, erosion, and solifluction. When the disturbances of demographic structure are slight, fast restoration of coenopopulation and ecological conditions occurs.

Table 3. The quantity, index of age (Δ), and index of effectiveness (ω) of anthropogenic disturbed coenopopulations of *Betula fruticosa*.

Community	Multiherboso-Betuletum fruticosae	Kobresio filiformis-Betuletum fruticosae
The general quantity, pcs. / 100м^2	482,3 ± 17,2	23,3 ± 3,2
The quantity on age groups, pcs. / 100м^2:		
j	89,4 ± 9,6	-
im	149,4±11,7	-
v	25,9±4,1	-
g_1	32,9±4,3	4,6 ±0,6
g_2	34,1±4,3	4,3 ± 0,5
g_3	105,9±6,4	13,7±2,4
ss	40,0 ±3,9	0,7 ±0,1
S	4,7 ±0,6	-
Δ	0,32	0,65
ω	0,43	0,81

Acknowledgments

The author is grateful to Dr. D.V. Sandanov (Institute of General and Experimental Biology, Siberian Divisions, Russian Academy of Sciences, Ulan-Ude) for valuable advice and for help during preparation of this paper.

References

Harper, J.L. & White, J. 1974. The Demography of Plants. *Annu. Rev. Ecology Syst.* 5: 419-463.

Harper, J.L. 1977. *Population Biology of Plants*. New York: Acad. Press, 892 pp.

Harper, J.L. 1992. *Population of Plants.* Oxford: The Alden Press, 892 pp.

Moskalenko, N.G. 1999. *Antropogennaya dynamika rastitel'nosty ravnin kryolytozony Rossii* [*Anthropogenic Dynamics of Vegetation of Flat Lands of Cryolithozone of Russia*]. Novosibirsk: Nauka. The Siberian publishing house of the RAS, 280 pp. (in Russian).

Rabotnov, T.A. 1950. Voprosy izuchenja sostava populjacyi dlja celei fytocenologii [Questions of studying of structure of populations for the purposes of phytocenology]. In: *Problemy botaniki* [*Problems of Botany*]. Moscow: Publishing house of AS SSSR, 465-483 (in Russian).

Rabotnov, T.A. 1964. Opredelenie vozrastnogo sostava populjacyi vidov v soobshestve [Determination of age composition of species populations in a plant community]. In: E.M. Lavrenko & A.A. Korchagin (ed.) *Polevaja geobotanika* [*The Field of Geobotany*]. Moscow- Leningrad: Nauka, 132-145 (in Russian).

Rabotnov, T.A. 1969. Nekotorye voprosy izucheniya cenoticheskih populyacyi [Some problems of study of coenotic populations]. *Bulleten' Moskovskogo obshestva ispytatelei pryrody, otdel biologicheskyi* [*Bulletin of Moscow Society of Naturalists, Biological Series*] 3: 141-149 (in Russian).

Rabotnov, T.A. 1975. Izuchenie cenoticheskih populacyi v celyah vyyasneniya strategyy jyzny [The study of coenotic populations for the purpose of find out of life's strategies]. *Bulleten' Moskovskogo obshestva ispytatelei pryrody, otdel biologicheskyi* [*Bulletin of Moscow Society of Naturalists, Biological Series*] 80(2): 5-17 (in Russian).

Rabotnov, T.A. 1978. On coenopopulations of plants reproducing by seeds. In: *Structure and Functioning of Plant Populations*. Amsterdam, 1-26.

Rabotnov, T.A. 1985. Dynamics of plant coenotic populations. In: J. White (ed.), *The Population Structure of Vegetation*. Dordrecht; Boston; Lancaster, 121-142.

Smirnova, O.V. 1987. *Struktura travjanogo pokrova shirokolistnyh lesov* [*The Grass Layers Structure of Broad-leaved Forests*]. Moscow: Nauka, 207 pp. (in Russian).

Uranov, A.A. 1960. Jyznennoe sostoyanye vyda v rastytel'nom soobshestve [The life state of species in a plant community]. *Bulleten' Moskovskogo obshestva ispytatelei pryrody, otdel biologicheskyi* [*Bulletin of Moscow Society of Naturalists, Biological Series*] 67(3): 77-92 (in Russian)

Uranov, A.A. 1975. Vozrastnoi spektr fytocenopopuljacyi kak funkcija vremeny I energetycheskih volnovyh processov [The age spectrum of phytocoenopopulation as a function of time and power wave of processes]. *Biologycheskye nauki* [*Biological Sciences*] 2: 7-34 (in Russian).

Uranov, A.A. 1977. Voprosy izucheniya structury fytocenozov y vydovyh cenopopulacyi [The questions study of phytocenosis and species coenopopulations]. In: *Cenopopulacyy rasteny.: Razvytye y vzaymootnoshenyya* [C*oenopopulations of Plants. The Development* and interrelations]. Moscow: Nauka, 8-20 (in Russian).

Vtorushin, V.A. & Pigareva, N.N. 1996. *Kryomorfnye pochvy: perspektivy ich effektivnogo ispol'zovaniya* [*Criomorphic Soils: Prospects of their Effective Utilization*]. Ulan-Ude: BSC SB RAS, 295 pp. (in Russian).

Zhivotovsky, L.A. 2001. Ontogeneticheskie sostojanija, effectivnaja plotnost' i klassifikacija populjacyi rastenyi [Ontogenetic states, effective density, and classification of plant populations]. *Ecologija* [*Russian Journal of Ecology*] 1: 3-7 (in Russian).

Permafrost in the South Shetland Islands (Maritime Antarctica): Spatial Distribution Pattern

E. Serrano
Dpt. Geografía, Universidad de Valladolid. Spain
J. López-Martínez
Dpt. Geología y Geoquímica, Universidad Autónoma de Madrid. Spain
J.A. Cuchí
Escuela Politécnica Superior de Huesca, Universidad de Zaragoza. Spain
J.J. Durán
Instituto Geológico y Minero de España. Madrid. Spain
S. Mink
Dpt. Geología y Geoquímica, Universidad Autónoma de Madrid. Spain
A. Navas
Estación Experimental de Aula Dei, CSIC, Zaragoza. Spain

Abstract

Maritime conditions in the South Shetland Islands allow the presence of ice-cemented permafrost and an active layer from 25 cm to more than 1 m thick. In this work permafrost distribution has been studied from detailed geomorphological maps in 14 areas. Periglacial maps derived from the general ones allowed us to differentiate areas where permafrost-related landforms and processes occur and to compile permafrost distribution maps. Field observations and other methods have been used to check mapping interpretations. The spatial location of permafrost-related landforms allowed us to differentiate the following permafrost spatial-distribution pattern: (1) non-existing or sporadic permafrost at altitudes below 20 m a.s.l., (2) mainly discontinuous permafrost between 20 and 40 m a.s.l., and (3) mainly continuous permafrost at more than 70% of ice-free surfaces above 40 m a.s.l. Field observations pointed out important spatial and seasonal local variability in the presence of permafrost.

Keywords: ANTPAS project; geomorphology; Maritime Antarctica; periglacial landforms; permafrost distribution; South Shetland Islands.

Introduction

The South Shetland Islands are located in the Maritime Antarctica, between the Drake Passage and the Bransfield Sea, at 61°59′S/63°20′S, and 57°40′W/62°45′W (Fig. 1). The archipelago occupies about 4700 km^2 and only 10% are ice-free areas. The region has a cold maritime climate with annual mean surface air temperature at the coast line about -2°C, and daily summer temperatures above 0°C. Annual precipitation is between 400 mm/yr and 800 mm/yr and rain occurs in summer.

Studies on permafrost have been carried out on different places in the South Shetland Islands. There are works on Deception Island (López-Martínez et al. 1996, 2000, 2002), Media Luna Island (Corte & Somoza 1954, Serrano & López-Martínez 1997a), Robert Island (Serrano & López-Martínez 1997b, 1998), Nelson Island (Araya & Hervé 1972a, 1972b), King George Island (Simonov 1977, Barsch et al. 1985, Quinsong 1989, Zhu et al. 1996, Serrano & López-Martínez 2004) and Livingston Island (Thom 1978, López-Martínez et al. 1996, Serrano et al. 1996, Bergamín et al. 1997, Ramos 1998, Ramos et al. 2002, Ramos & Vieira 2003, Hauck et al. 2007). These studies provide information about the presence of permafrost and the active layer at different locations and altitudes in different islands. The aim of this work is to show an overview of the permafrost presence and distribution on ice-free areas of the South Shetland Islands from gepomorphological mapping and field observations. It is a contribution to the ANTPAS projects for compiling a map of permafrost in Antarctica. Bockheim (1995) pointed out the necessity to better know the extent of permafrost linked to the soils evolution and the recent global change.

Methods

This work is mainly based on the use of periglacial landforms as indicators of permafrost existence and distribution. Periglacial landforms and processes have been used as indicators of permafrost environments on Arctic and mountain environments with useful results (Black 1976, Washburn 1979, Harris 1982, Karte 1983, Clark 1988, Bockheim 1995, Barsch 1996). On the active layer a widespread group of landforms and processes are developed and relations between landforms, processes, existence, and extension of permafrost have been established (Harris 1982, French 1996). Rock glaciers, patterned ground, protalus lobes, frost mounds, frost creep, and gelifluction features point out the existence of mophodynamic and environmental conditions

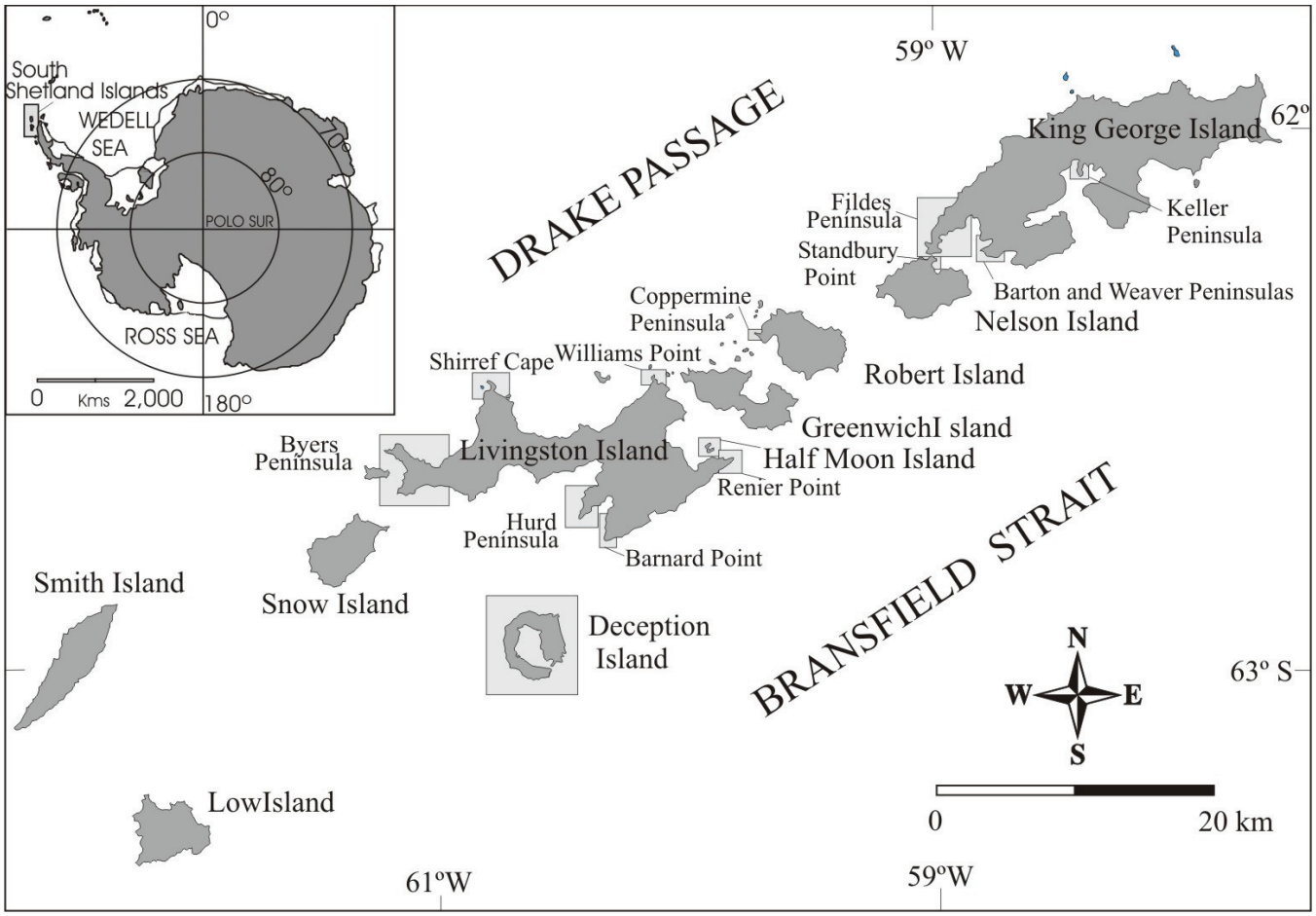

Figure 1. Location map of South Shetland Islands and places where geomorphological maps have been made by our group. Elephant Island not included in the map.

linked to permafrost (Black 1976, Barsch 1978, 1996, Harris 1982, Karte 1983, Haeberli 1985, Clark 1988, Huizjer & Isarín 1997). Differences between permafrost-related periglacial landforms and those periglacial landforms not related to permafrost occurrence have been used in this work to study the distribution and nature of permafrost in the South Shetland Islands. In addition and in order to check the validity of the interpretations in several places other techniques such as BTS measurements, vertical electric sounding, slope transects, mechanical sounding, active layer measurements, and water and permafrost analysis have been used.

Our group has compiled fourteen geomorphological maps between 1:25,000 and 1:10,000 scales (Table 1).

From the geomorphological maps simplified periglacial maps, showing such type of information only, have been made. Landforms valid as indicators of permafrost existence have been selected to deduce permafrost occurrence. The location and altitudinal distribution of permafrost-related landforms have been quantified to produce synthetic simplified maps of permafrost distribution.

Results: Permafrost Distribution

In the study region there is ice-cemented permafrost and the active layer is in general from 25 cm up to more than 1 m thick. Buried or ground ice has been recognized in several places at different altitudes.

Twelve types of landforms related to permafrost have been inventoried in the study areas in the South Shetland Islands and used for permafrost mapping (Table 2). Landforms related to frost heave and frost creep are the most common periglacial landforms in the archipelago. Patterned ground occurs in a wide altitudinal range, mainly between 10–100 m a.s.l. and being the dominant landforms above 25 m a.s.l. Stone fields are located mainly between 10–118 m a.s.l. The permafrost-related landforms and processes comprise 80% of the surface occupied by periglacial shapes on ice-free areas of the South Shetland Islands. Rock glaciers and protalus lobes are indicators of continuous or discontinuous permafrost, and are spread in several peninsulas and other places of the archipelago. Eight active rock glaciers have been identified in the South Shetland Islands but protalus lobes located between sea level and 300 m a.s.l. are more common features (Birkenmajer 1981, 1997, Barsch et al. 1985, Serrano & López-Martínez 2000). The rock glacier fronts have as a mean altitude 13 m a.s.l. and the upper ends 67 m a.s.l. and they are mainly developed below 70 m a.s.l. (Serrano & López-Martínez 2000). The mean altitude of rock glacier upper ends and protalus lobes point out the existence of continuous permafrost, although the fronts are located in

Table 1. Geomorphological maps of the South Shetland Islands compiled by our group.

Place	Island	Scale	Publication
Fildes Peninsula	King George	1:15,000	Not published
Barton and Weaver Pen.	King George	1:10,000	*1
Keller Peninsula	King George	1: 10,000	Not published
Byers Peninsula	Livingston	1:25,000	*2
Hurd Peninsula	Livingston	1:10,000	Not published
Williams Point	Livingston	1:10,000	Not published
Renier Point	Livingston	1:10,000	Not published
Barnard Point	Livingston	1:10,000	Not published
Cape Shirref	Livingston	1:10,000	Not published
Coppermine Pen.	Robert	1:10,000	*3
Deception Island	Deception	1:25,000	*4
Half Moon Island	Half Moon	1:10,000	*5
Standbury Point	Nelson	1:15,000	Not published
Stinker Point	Elephant	1:10,000	Not published

*1, López-Martínez et al. 2002. *2, López-Martínez et al. 1996. *3, Serrano & López-Martínez 1997b. *4, López-Martínez et al. 2000. *5, Serrano & López-Martínez 1997a.

areas without permafrost-related landforms.

The altitudinal analysis point out that at very low altitudes (between 0–20 m a.s.l.) patterned ground exists only occasionally. Three rock glacier fronts reach the sea or lowest beaches, permafrost occur at 2.5 m a.s.l. in Deception Island and at 7 m a.s.l. in Livingston Island (López-Martínez et al. 1996, Bergamín et al. 1997). Below 10 m a.s.l. the permafrost indicator features occupy only 12% of the surface with periglacial landforms, insufficient to be considered as discontinuous permafrost. From these data and the mentioned periglacial maps it is possible to deduce that on the lowest beach levels permafrost is sporadic or non-existing. Above 20 m a.s.l. landforms and processes related to permafrost are dominant (72% of periglacial landforms are permafrost-related) and point out a mainly discontinuous permafrost environment. Above 40 m a.s.l. debris lobes, protalus lobes, patterned ground and frost creep processes are dominant and the mean altitude of rock glacier upper ends and the location of all the protalus lobes point out a mainly continuous permafrost environment from 40–300 m a.s.l.

The distribution of the mentioned features allows to differentiate the following altidudinal distribution of permafrost:

• Between 0–20 m a.s.l. Non-existing or sporadic permafrost environments are dominant.

• Between 20–40 m a.s.l., mainly discontinuous permafrost environments are developed.

• Above 40 m a.s.l. mainly continuous permafrost environments are common, being at those altitudes more than 70% of ice free areas surface occupied by permafrost-related landforms and processes.

Field observations pointed out the important spatial and temporary variability in the presence of permafrost. Altitude plays an important role but also topography, soil characteristics, and orientation. Variations in meteorological conditions and snow coverage may change the active layer thickness in different years.

Table 2. Processes and landforms related to permafrost inventoried in the South Shetland Islands.

PROCESSES	LANDFORMS	LANDFORMS ELEVATION
Frost creep Gelifluction	- Protalus lobe - Rock glaciers - Block streams - Ploughing blocks - Gelifluction sheets - Gelifluction lobes - Debris lobes	40-100 m 0-300 m 30-100 m 10-90 m 0->100 m 10-300 m 0-100
Frost heaving Cryoturbation Sorting	- Stone stripes: Coarse stone stripes Fine stone stripes - Stone fields - Patterned ground: Stone circles Earth circles Stone polygons Earth polygons - Frost mounds	45-90 m 10-90 m 10-300 m 45-50 m
Thermokarst	- Melting hollows	40-100 m

Conclusions

The analysis of permafrost related landforms and processes allowed us to establish the wide distribution of permafrost in the South Shetland Islands but also to assert that not all ice free areas in the archipelago have permafrost environments. The altitudinal analysis of the periglacial landforms denotes a distribution of permafrost environments in three areas with different morphodynamic systems:

• A sporadic permafrost environment (from 2.5–20 m a.s.l.), where less than 15% of the surface is occupied by permafrost related landforms.

• A mainly discontinuous permafrost environment (between 20–40 m a.s.l.)

• A mainly continuous permafrost environment (above 40 m a.s.l.) where more than 70% of periglacial landforms are related to permafrost.

From geomorphological maps it is possible to point out an altitudinal distribution of periglacial landforms and processes characterized by the lack of intense periglacial processes near the sea level, and the domain of permafrost related landforms on higher heights, dominated by the presence of patterned ground.

Acknowledgments

This work has been supported by the Spanish Polar Program (project CGL2005-03256) and it is a contribution to the project Antarctic Permafrost and Soils (ANTPAS) included in the program of the International Polar Year 2007–2008.

References

Araya, R. & Hervé, F. 1972a. Periglacial phenomena in the South Shetland Islands. In: R.J. Adie (ed.), *Antarctic Geology and Geophysics*. Oslo: International Union of Geological Science Series B 1: 105-109.

Araya, R. & Hervé, F. 1972b. Patterned gravel beaches in South Shetlands. In: R.J. Adie (ed.), *Antarctic Geology and Geophysics*. Oslo: International Union of Geological Science, Series B 1: 111-114.

Barsch, D. 1996. *Rock Glaciers. Indicators for the Present and Former Geoecology in High Mountain Environment*. Heidelberg: Springer Verlag.

Barsch, D. 1978. Active rock glaciers as indicators for discontinuous alpine permafrost. An example from the Swiss Alps. *Proceeding of Third International Conference on Permafrost, Edmonton* 1: 349-352.

Barsch. D., Blümel, W.D., Flügel, W.A., Mäusbacher, R., Stäblein, G. & Zick, W. 1985. *Untersuchungen zum Periglazial auf der König-Georg-Insel üdshetland-insel/Antarktika.* Deutsche Physiogeographische Forschungen in der Antarktis. Bericht über die Kampagne 1983/84. Bremenhaven: Reports on Polar Research, nº24. Alfred Wegener Institute, 75 pp.

Bergamín, J.F., Durán, J.J., González-Casado, M. & López-Martínez, J. 1997. Morfología y estructura del basamento pre-Cuaternario de la Caleta Española, Península Hurd, Isla Livingston. *Boletín Real Sociedad Española de Historia Natural (Secc. Geol*.) 93: 189-196.

Birkenmajer, K. 1981. Lichenometric dating of raised marine beaches at Admiralty Bay, King George Island South Shetland Islands, West Antarctica. *Bulletin Academy Polish Science* 29 :119–127.

Birkenmajer, K. 1997. Map of Quaternary geology at Artowsky Station, King George Island, South Shetland Islands (West Antarctica), 1:25,000. *Studia Geológica Polonica* 110: map.

Black, R.F. 1976. Periglacial features indicative of permafrost: ice and soil wedges. *Quaternary Research* 6: 3-26.

Bockheim, J.G. 1995. Permafrost distribution in the southern circumpolar region and its relation to the environment: a review and recommendations for further research. *Permafrost and Periglacial Processes* 6: 27-45.

Clarck, M.J. 1988. *Advances en periglacial geomorphology*. Chichester: Wiley & Son.

Corte, A.E. & Somoza, A.L. 1954. *Algunas observaciones geológicas y criopedológicas en la Antártida*. Buenos Aires: Instituto Antártico Argentino.

French, H.M. 1996. *The Periglacial Environments*. Essex: Longmann.

Haeberli, W. 1985. *Creep of Mountain Permafrost: Internal Structure and Flow of Alpine Rock Glaciers*. Zurich: Mitt. Versuchsants Wasserbau Hydrologie und Glaziologie, ETH nº 77.

Harris, S.A. 1982. Identification of permafrost zone using selected permafrost landforms. *Proceeding Fourth Canadian Permafrost Conference*, *Calgary, Alberta, March 2-6, 1981*, 49-57.

Hauck, C., Vieira, G., Gruber, S., Blanco, J. & Ramos, M. 2007. Geophysical identification of permafrost in Livingston Island, maritime Antarctica, *Journal of Geophysical Research* 112: F02S19, doi:10.1029/2006JF000544.

Huizer, A.S. & Isarin, R.F.B. 1997. The reconstruction of past climates using multiproxy evidence: an example of the weichselian Pleniglacial in northwest and central Europe. *Quaternary Science Review* 16: 513-533.

Karte, J. 1983. Periglacial phenomena and their significance as climatic and edaphic indicators. *GeoJournal* 74: 329-340.

López-Martínez, J. & Serrano, E. 2002. Geomorphology. In: J. López-Martínez, J.L. Smellie, J.W. Thomson & M.R.A. Thomson (eds.), *Geology and Geomorphology of Deception Island.* BAS GEOMAP Series, Sheets 6-A and 6-B, 1:25.000, with supplementary text. Cambridge: British Antarctic Survey, 31-39.

López-Martínez, J., Serrano, E., Rey, J. & Smellie, J.L. 2000. *Geomorphological Map of Deception Island* E. 1:25,000. BAS Geomap series, 7B. Cambridge. British Antarctic Survey.

López-Martínez, J., Serrano, E. & Lee, J.I. 2002. Geomorphological map of Barton and Weaver Penisnulas. King George Island, Antarctica (1:10,000). Seoul. Polar Science Laboratory, Korean Ocean Research and Development Institute KARP.

López-Martínez, J., Ramos, M., Criado, C., Serrano, E. & Nicolás, P. 1996. Anomalías geotérmicas y permafrost en la Isla Decepción, Antártida. *Pro-ceeding of V Simposio de Estudios Antárticos*, *C.I.C.Y.T, Madrid*: 223-234

López-Martínez, J., Thomson, J.W. & Thomson, M.R.A. (eds.). 1996. *Geomorphology of Byers Península, Livingston Island.* BAS GEOMAP Series, Sheet 5-A, 1:25,000, with supplementary text. Cambridge: British Antarctic Survey.

Qingsong, Z. 1989. A comparison of periglacial landforms between the Vestfold Hills, East Antarctica and the Fildes Península of King George Island, west Antarctica. *Proceedings of International Symposium on Antarctic Research*. Beijing: Chinese Committee on Antarctic Research, 74-81.

Ramos, M., Vieira, G., Crespo, F. & Bretón, L. 2002. Seguimiento de la evolución temporal del gradiente térmico de capa activa en las proximidades de la B.A.E Juan Carlos I. In: E. Serrano & García (eds.), *Periglaciarismo en montaña y altas latitudes*. Valladolid: Universidad de Valladolid, 257-276.

Ramos, M. & Vieira, G. 2003. Active layer and permafrost monitoring in Livingston Island, Antarctic. First results from 2000 and 2001. *Proceedings of the Eighth International Conference on Permafrost, Zurich*, *Switzerland*: 929-933.

Ramos, M. & Vieira, G. 2004. Variabilidad térmica de la capa activa y evaluación de la energía perdida por el suelo, durante el proceso de congelación en la isla Livingston (Antártida). Inviernos 2000, 2001, 2002. *Boletín Real Sociedad Española de Historia Natural (Secc. Geol.)* 99: 83-92.

Serrano, E., Martínez de Pisón, E. & López-Martínez, J. 1996. Periglacial and nival landforms and deposits. In: J. López-Martínez, J.W. Thomson & M.R.A. Thomson (eds.), *Geomorphological map of Byers Península, Livingston Island.* BAS GEOMAP Series, Sheet 5-A, 1:25,000, with supplementary text. Cambridge: British Antarctic Survey, 28-34.

Serrano, E. & López-Martínez, J. 1997a. Evolución de las formas de relieve y los depósitos superficiales cuaternarios en la Isla Media Luna. Islas Shetland del Sur. *Boletín Real Sociedad Española de Historia Natural (Secc. Geol.)* 93: 207-218.

Serrano, E. & López-Martínez, J. 1997b. Geomorfología de la Península Coppermine, Isla Robert, Islas Shetland del Sur, Antártida. *Serie Cientifica INACH* 47: 19-29.

Serrano, E. & López-Martínez, J. 1998. Caracterización y distribución de las formas y los procesos periglaciares en las Islas Shetland del Sur (Antár-tida). In: A. Gómez, F. Salvador, L. Schulte & A. García (eds.), *Procesos biofísicos actuales en medios fríos. Estudios recientes*. Barcelona: Universitat de Barcelona, 181-204.

Serrano, E. & López-Martínez, J. 2000. Rock glaciers in the South Shetland Island, Western Antarctica. *Geomorphology* 35: 145-162.

Serrano, E. & López-Martínez, J. 2004. Morfogénesis periglaciar y deglaciación en las penínsulas Barton y Weaver (Islas Shetland del Sur, Antártida). *Boletín Real Sociedad Española de Historia Natural (Secc. Geol.)* 99(1-4): 131-140.

Simonov, I.M. 1977. Physical-geographic description of the Fildes Peninsula (South Shetland Islands). *Polar Geography* 1: 223-242.

Thom, G. 1978. Disruption of bedrock by the growth and collapse of ice lenses. *Journal of Glaciology* 20: 571-575.

Washburn, A.L. 1979. *Geocryology. A Survey of Periglacial Processes and Environments.* London: Edward Arnold.

Zhu, C., Cui, Z. & Zhang, J. 1996. Relationship between the distribution of periglacial landforms and glaciation history, Fildes Península, King George Island, Antarctica. *Permafrost and Periglacial Processes* 7: 95-100.

Effects of Vegetation and Grazing on Soil Temperature, Soil Moisture, and the Active Layer in the Hovsgol Mountain Forest Steppe Zone, Mongolia

Anarmaa Sharkhuu
University of North Dakota, Grand Forks, North Dakota, USA
Natsagdorj Sharkhuu
Institute of Geo-Ecology, Mongolian Academy of Sciences, Mongolia
Bernd Etzelmuller
Department of Geosciences, University of Oslo, Norway
Eva S. Flo Heggem
Department of Geosciences, University of Oslo, Norway
Clyde E. Goulden
Institute of Mongolian Biodiversity and Ecological Studies, Academy of Natural Sciences, Philadelphia, Pennsylvania, USA

Abstract

In this paper we present initial results from observations of the effects of a series of natural vegetation covers and several experimental plots manipulated to mimic local grazing practices on soil temperatures, moisture content, and active-layer thickness in the Dalbay ILTER (International Long Term Ecological Research) study site in the Hovsgol Mountain forest steppe zone, northern Mongolia. We set up experimental plots with three types of treatments—control plot and plots that mimicked light and heavy grazing by clipping vegetation cover. The results show that both live and dead plants (especially moss, shrubs, forest, and dense grass) produce considerable insulation effects, maintaining low permafrost temperatures and protecting soil moisture from high evaporation. Therefore, both natural vegetation cover characteristics and grazing practices are important factors in preventing permafrost degradation in arid mountain environments.

Keywords: active layer; Hovsgol; soil moisture; soil-surface temperatures; soil temperatures; vegetation cover.

Introduction

The mountain forest steppe zone along the eastern shore of Lake Hovsgol Mongolia is characterized by mountains with altitudes of 1700 to 2200 m a.s.l. It is located in the southern fringe of the Siberian continuous permafrost and taiga forest zones. The forest is predominantly Siberian larch (*Larix sibirica*), distributed on crests and north-facing slopes. South-facing slopes and valley bottoms are generally dominated by *Poa* and *Carex* species. Shrubs, lichens, and thick grasses with abundant dead plant materials are widespread on gentle north-facing slopes and along river channels. There are 2–15 cm thick moss layers in the forest and 5–30 cm thick layers of peat in some valley bottoms (Goulden et al. 2006). Discontinuous permafrost is characteristic of the region near the lake. Active-layer depths are highly variable, ranging from 1 to 5 m depending on the topographic setting and vegetation cover. Permafrost thickness is between 5 to 20 m in the valley bottoms and thicker on the forested north-facing slopes. Permafrost is absent on south-facing slopes without forest (Etzelmuller et al. 2006, Heggem et al. 2006).

Permafrost degradation under the influence of climate warming in the Hovsgol region has been more intense during the last 15 years (1991–2006) than the previous 20 years (Sharkhuu et al. 2007). Mean annual air temperature at the Hatgal weather station, located on the most southern shore of the Lake Hovsgol, has increased by 1.86°C during the last 40 years (Nandintsetseg et al. 2006). Within the framework of the International Hovsgol Project supported by the Global Environmental Facility and implemented by World Bank (GEF/WB) in 2002–2006, Norwegian and Mongolian permafrost researchers studied the distribution and thermal conditions of permafrost in the region characterizing topography, snow and vegetation cover, soil texture, and soil moisture. The rate of increase in mean annual permafrost temperature varies from 0.02 to 0.04°Ca^{-1} per year, depending on landscape and ground conditions (Sharkhuu et al. 2007). In addition, human activities such as livestock grazing, anthropogenic forest fires, and some engineering works have led to local intensive degradation of permafrost. In some valleys of the study area especially,, livestock grazing has had negative effects not only on the permafrost but also on the ecosystem. The objective of this study was to estimate these anthropogenic effects, focused on grazing and forest fires. Hence studies on vegetation cover, soil-surface temperature, and active layer thickness were conducted in the Dalbay and Borsog Valleys between 2004 and 2007.

Study Area

The study area includes six valleys (Borsog, Dalbay, Sevsuul, Noyon, Shagnuul, Turag) on the eastern shore of Lake Hovsgol (Fig. 1).

Parts of the eastern shore area have been extensively used for grazing by nomadic families. Grazing is most intense

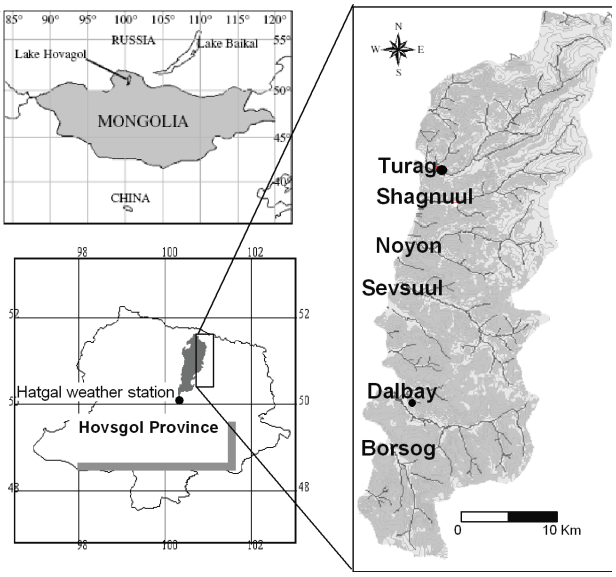

Figure 1. Location of the study sites along the eastern shore of Lake Hovsgol, Mongolia.

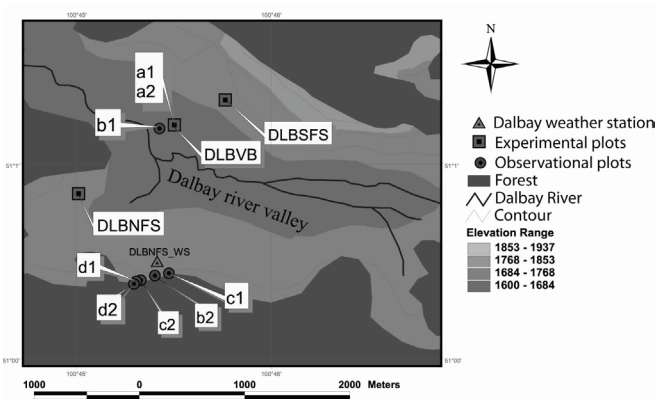

Figure 2. Topographic map of Dalbay Valley showing the locations of the eight plots used to study the effects of natural land-cover types. Points indicate locations of dataloggers used for SST measurements. Several points are overlaid on this map due to the short distance between them (e.g., *a1* and *a2*). Plots used for experimental study were shown as rectangular, labeled DLBSFS (plots on south-facing slope), DLBVB (plots in valley bottom), and DLBNFS (plots on north-facing slopes). Weather station location is illustrated with a triangle, labeled DLBNFS_WS.

in the northern valleys, especially in Turag and Shagnuul Valleys. Sevsuul and Noyon Valleys are only moderately grazed; whereas, Dalbay and Borsog Valleys have little or no pastoral use. Compared with Turag Valley, the present shallow active layer and low permafrost temperatures in Dalbay Valley are apparently insulated from thaw by the thicker vegetation cover (Table 1)

Methods

Natural land-cover plots

In order to estimate the thermal insulative effect of a range of naturally occurring vegetation cover year-round (October 2004–October 2005), soil-surface temperature (SST) recordings at eight observation plots in the Dalbay Valley (Fig. 2) were made. All soil-surface temperature recordings were made at 2–5 cm depth under soil-surface in order to prevent temperature recordings affected by direct sun radiance. These plots represent the range of vegetation available within the valley.

Table 1. Vegetation cover and land-use characteristics in the study valleys.

Valley	Borsog	Dalbay	Shagnuul	Turag
Livestock numbers (sheep units)	51	530	3001	3330
Dry plant biomass, gm^{-2}	660	585	48	116
Active-layer thickness, m	2.1	1.4	4.3	4.8
Mean annual permafrost temperature, °C	-0.91	-1.25	-0.56	-0.42
Estimated permafrost thickness, m	35	45	25	20

In addition, some observations on the effects of forest fire on soil-surface temperature were made on north-facing slopes with larch forest in Shagnuul Valley Soil-surface temperatures at 2–5 cm depth and ground temperatures at 1 m depth were recorded by UTL-1 datalogger year-round.

Experimental plots

In order to explore effects of grazing on soil temperature, moisture and active layer, three 2×6 m^2 experimental grids were established along a topographic transect (south-facing lower slope, valley bottom, north-facing lower slope) in Dalbay and Borsog Valleys (Fig. 2). Within each grid six 2×2 m^2 plots were established with three different treatments: (*CO*) dead plant material and vegetation cover were both left intact, as control plots; (*CL*) vegetation cover was clipped but dead plant material was not removed (hereafter referred to as clipped plots); and (*CR*) vegetation cover was clipped and dead plant material was removed (hereafter referred to as cleared plots).

Soils within the active layer in valley bottoms and on north-facing gentle slopes consisted of gravelly silt and sands, covered by a 10–20 cm layer of humus. In summer, supra-permafrost waters are usually formed with a thickness of 10 to 30 cm, depending upon the amount of precipitation. Gravelly sands are characteristic of the south-facing slope.

Soil-surface temperature observations at 2–5 cm at each of the experimental plots began in October 2005. Unfortunately, these stopped in late March 2007 after 1½ years of observations, due to low battery power in the loggers. However, during each field season, measurements of soil temperatures and active layer thickness were made in the experimental plots.

UTL-1 dataloggers (interval 1.5 h, accuracy ±0.25°C) were used to record soil surface and soil temperatures for both natural and experimental plots. In addition, the MMT-4 thermistors and probes (accuracy ±0.1°C) were used. Mean winter temperature was calculated from mean December, January, and February temperatures, while mean summer temperature was calculated using June, July, and August means.

Live and dead plant biomass in each experimental plot was sampled from a 0.5×0.5 m² area in late June and early September–October of 2006. Biomass was determined after drying the sampled plants at room temperature for more than 48 hours. Dry plant biomass at each Dalbay plot is shown in Table 2. Clipped and cleared (CL and CR, respectively) plots were manually clipped monthly during the summer months of 2006.

Soil moisture in each experimental plot was determined by weight method monthly during summer. Soil samples were taken at each 50 cm depth from surface 0.1 m depth to a depth of 2 m. In addition, we determined soil density by core method to use for a model estimation. Soil samples were obtained using a hand drill (augur) and weighed using a digital balance with an accuracy of 0.1 g. Active layer thickness was measured using a 1.85 m long steel probe and several thaw tubes placed in some of the boreholes in early September and October, 2005–2006.

Table 2. Dry plant biomass (gm^{-2}) at each experimental plot in the Dalbay Valley

Vegetation cover at each site	CO	CL	CR	
			CR_{bj}	CR_{aj}
Grass, forb dry steppe on south-facing slope	340	135	96	118
Forb, grass meadow in valley bottom	625	375	135	160
Grass, forb wet steppe on north-facing slope	560	485	62	36

CO-unclipped control plot; CL-clipped plot with litter left in place; CR-cleared plot (vegetation cover was clipped and litter was removed): CR_{bj}-before July; CR_{aj}-after July.

Results and Discussion

Effect of natural vegetation on soil-surface temperatures

Initial results of quantifying the thermal insulation effect of different vegetation covers on soil-surface temperature are presented in Table 3. In particular, 10 cm thick (*Rhytidium rugosum*) moss cover decreased soil-surface mean summer temperature by 6.4°C as compared to plot without moss cover. Dense 1.8 m (*Salix* sp.) shrubs decreased soil-surface summer temperature by 1.4°C as compared to 0.5 m shrubs, and young dense larch forest decreased soil-surface mean summer temperature by 1.1°C as compared to sparse larch forest. Dense grass decreased soil-surface summer temperature by 2.2°C as compared to mown grass plot. In general, all types of vegetation cover decreased soil-surface summer temperatures by 5–9°C as compared with mown grass plot. Summer temperature differences (R_s) between different types of vegetation cover and mown grass plot are shown in Table 4. The temperatures under sparse forest, 50 cm high shrubs, and dense grass are reduced by 2–4°C. However, mean winter temperatures under dense vegetation cover were increased considerably, due to the accumulation of relatively loose and thick snow. Values of the mean annual temperature and the annual temperature amplitude under

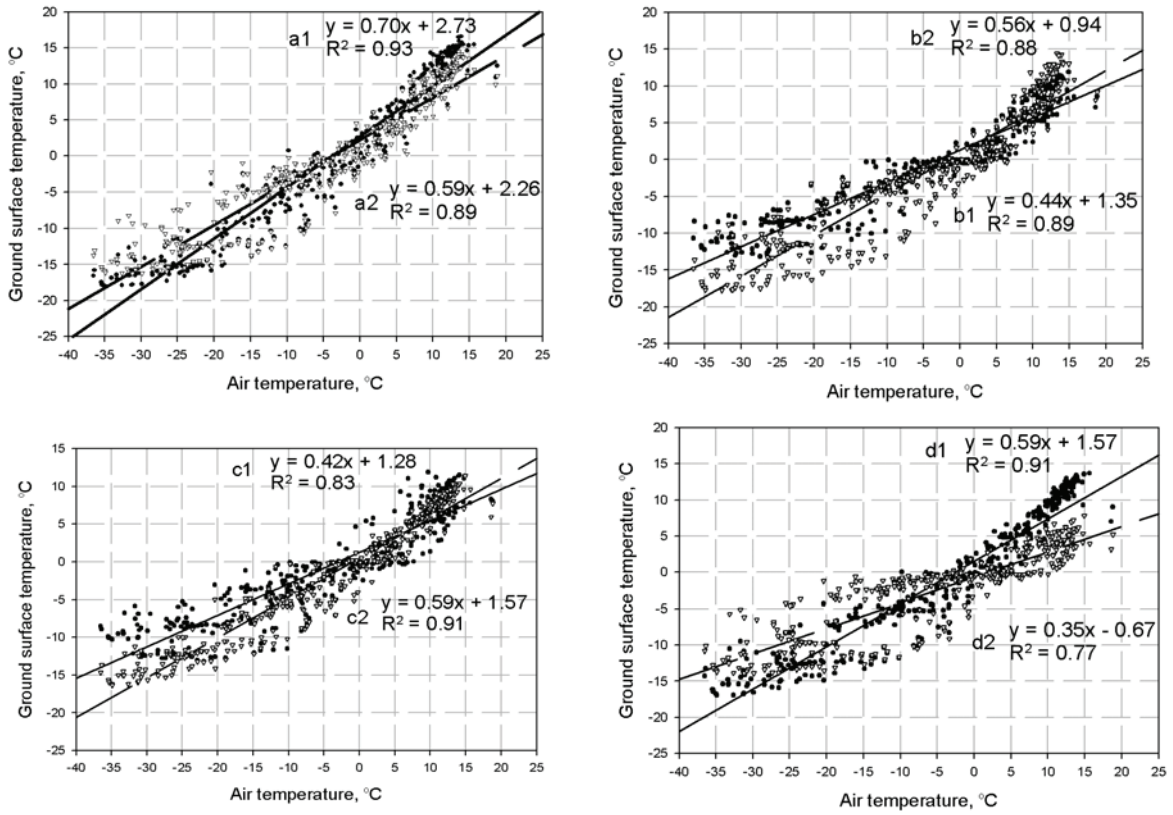

Figure 3. Linear least-squares regressions between daily air temperatures and soil-surface temperatures under different land-cover types at the experimental plots.

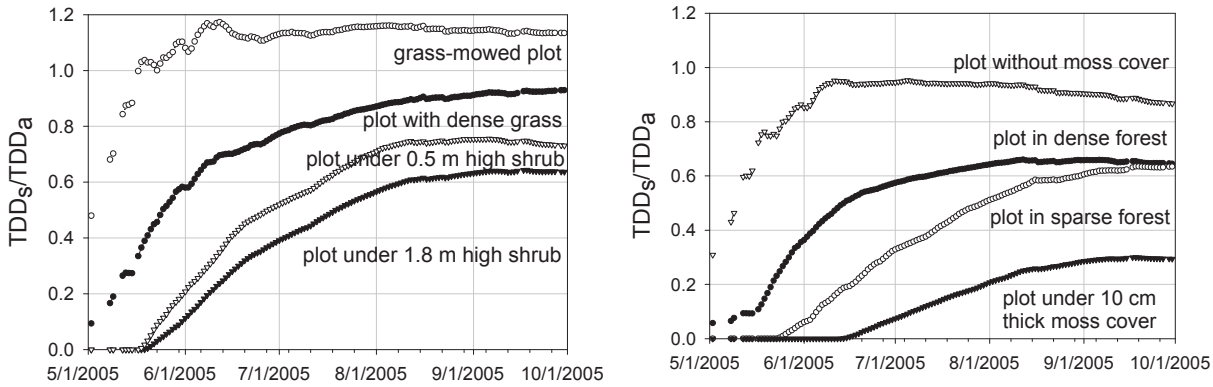

Figure 4. Daily n-factors (ratio of soil-surface to air temperatures) over the course of summer 2005 at each of the eight study plots.

Table 3. Mean soil-surface temperatures, temperature amplitude, summer temperature reduction (Rs) and summer n-factor in plots of different natural land cover in the Dalbay Valley (Oct. 2005 to Oct. 2006).

Plots	Land cover	Mean temperatures, °C			Temperature amplitude	R_s	Summer n-factor
		winter	summer	annual			
d2	10 cm thick moss	-8.6	3.4	0.29	6.8	9.0	0.29
b1	1.8 m high dense shrub	-7.4	7.4	0.63	7.8	5.0	0.63
c2	Dense forest	-11.7	7.5	0.64	10.5	4.9	0.64
c1	Sparse forest	-14.8	8.6	0.72	13.0	3.8	0.72
b2	50 cm high dense shrub	-11.4	8.8	0.73	11.3	3.6	0.73
d1	On moss surface	-11.5	9.8	0.86	11.9	2.6	0.86
a2	Dense grass	-11.1	10.2	0.93	11.9	2.2	0.93
a1	Grass mowed	-13.7	12.4	1.13	14.7	0.0	1.13
Air temperature at Dalbay		-23.9	10.8	-5.3	18.8	-	-

different land-cover types differ by 0.5 to 2.0°C and 3.0 to 7.0°C, respectively.

Linear least-squares regressions between daily air temperatures from the Dalbay automatic weather station and soil-surface temperatures under different land-cover types at the experimental plots were fitted. The linear regression analysis shows that the presence of thick moss is a major factor in insulating the ground from the heat. While slope value of linear regression between daily air temperature and soil-surface temperature under moss cover is 0.35, slope value of regression between air temperature and soil-surface temperature in mown grass plot is 0.70 (Fig. 3). *P* values for r^2 and slopes of all regression analyses were significant ($P<0.0001$).

Seasonal n-factors (Lunardini 1978), the ratio between thawing degree-days at the soil-surface (TDD_s) and in the air (TDD_a), were calculated for each day at plots of different land covers in Dalbay Valley and are shown in Figure 4. Usually n-factors are calculated using seasonal degree-day sums (Smith & Riseborough 1996). Here, n-factor was calculated using running sum of thawing degree-days at the soil surface and the air to show the seasonal progression.

These observations, though based on just one season of data, clearly demonstrate the importance of vegetation cover on ground thermal regime. In addition, in Shagnuul forest the mean annual surface temperatures were -3.1°C and -3.9°C in burned and unburned forest, respectively.

Effect of vegetation cover manipulation on soil temperatures

The initial results from the experimental plots are presented in Table 5. Compared to the control plots CO, the mean monthly summer soil-surface temperatures in the CR plots (clipped and litter removed) were higher by 0.7–1.7°C on the north-facing slope, by 2.3–2.7°C on the south-facing slope, and by 3.2–5.6°C in the valley bottom, depending upon plant biomass and surface wetness. Meanwhile, the undisturbed presence of dead plant matter (litter) in the valley bottom decreased the temperatures by 0.7–2.0°C. As compared to control plot CO, mean winter soil temperature at a depth of 1.2 m in the CR plot of the valley bottom was higher by 0.3°C, due to accumulation of summer heat into soil. However, the temperature at depth of 0.1 m was lower by 4.3°C due to relatively thin and dense snow accumulation in the clipped and cleared plot. Differences in near-surface soil temperatures between CO and CR plots were higher in summer than in autumn. The difference also decreased gradually with depth. In general, mean annual active layer temperatures in CR plots were significantly warmer than in CO plots.

Effect of vegetation cover manipulation on soil moisture

Not only live vegetation but also dead vegetation reduces near-surface soil moisture evaporation. Soil analysis shows that soil moisture content in CO and CL plots were always

Table 4. Soil temperatures (°C) at the grazing experimental plots in the Dalbay Valley at depths from the surface to 1.2 m.

Topographic position		South-facing		Valley bottom			North-facing	
Plot		CO	CR	CO	CL	CR	CO	CR
Mean soil-surface temperatures for 2006								
June		11.2	13.5	5.7	9.4	10.1	7.2	7.9
July		13.8	16.5	9.2	12.8	14.8	9.9	11.6
August		12.3	14.8	9.2	11.6	12.4	9.9	10.7
Mean winter soil temperatures								
Oct 2006–Mar 2007	0.1 m	-	-	-3.9	-5.5	-8.2	-	-
	0.6 m	-	-	-2.4	-	-2.4	-	-
	1.2 m	-	-	-0.7	-0.8	-0.4	-	-
Soil temperatures								
June 18, 2006	0.1 m	12.5	14.7	3.3	6.0	7.7	2.1	4.5
	0.5 m	7.1	7.4	0.8	1.5	3.5	-	-
Oct 7, 2006	0.1 m	2.3	2.3	0.8	0.9	1.1	-	-
	0.5 m	5.0	5.3	1.7	2.0	2.4	-	-
	1.0 m	5.8	6.0	1.0	1.2	1.4	-	-
Sep 7, 2007	0.1 m	13.0	13.2	9.2	10.1	11.9	8.1	8.8
	0.5 m	9.4	9.8	5.9	6.2	7.0	5.5	5.7

Note: CO – control plot; CL – plot, vegetation cover clipped and dead material left; CR – vegetation cover clipped and dead plant material removed plot

Table 5. Changes in soil moisture content (%),in the experimental plots in the Dalbay Valley.

Date	Depth m	Valley bottom			South-facing	
		CO	CL	CR	CO	CR
Oct 5, 2005	0.1	54.6	-	42.1	-	-
	0.5	45.0	-	36.8	4.7	-
June 18, 2006	0.1	40.9	35.4	32.0	14.1	12.3
	0.5	41.7	33.7	30.1	9.6	8.7
Oct 7, 2006	0.1	61.5	55.1	40.2	20.3	17.8
	0.5	50.2	43.0	35.1	13.8	12.1
	1.0	30.3	27.9	26.2	8.7	8.4
Sep 7, 2007	0.1	42.7	34.4	19.7	4.6	6.1
	0.5	30.5	23.3	18.1	4.6	4.4

Table 6. Changes in active-layer thickness (cm) in the experimental plots in the Dalbay Valley.

Date	Valley bottom			North-facing slope		
	CO	CL	CR	CO	CL	CR
Oct 5, 2005	123	-	158	103	-	-
June 2006	35	49	61	13	20	29
Oct 7, 2006	125	138	177	102	113	143
Sep 7, 2007	123	140	185	101	116	147

higher than in CR plots (Table 5). Due to plant biomass, hydrology, and soil characteristics, the differences in soil moisture content between CO and CR plots ranged from 5% to 20% in the valley bottom and did not exceed 2%–3% on south-facing slope. The difference decreased with depth.

Effect of vegetation cover manipulation on active layer thickness

In 2006 and 2007, the second and third years of the experiment, the thickness of the active layer in the CR plots in the valley bottom and the north-facing slope increased by 40–60 cm due to increased soil-surface temperatures and amplitudes, and decrease in soil moisture content. Each year, active layer thickness increased, though the rate of change decreased after the second year. Active layer thickness in CL plots also increased by about 15 cm (Table 6).

Conclusion

Vegetation cover acts as a cooling factor and reduces mean annual soil-surface temperatures. As compared to the mown grass site, mean summer soil-surface temperatures decreased by about 2.2°C under dense grass, 3.6°C under sparse forest and dense shrubs, 4.9°C under dense forest and bushes, and by 6.4°C under 10 cm thick moss at the Dalbay observation sites. As compared to Turag Valley where livestock grazing removes vegetation, the low grazing pressure maintains shallower active layer and lower permafrost temperatures in Dalbay Valley. Moss cover, dense grass, and forest are natural insulators, protecting soil moisture from high evaporation and maintaining low soil temperatures. The shallower active layer and low permafrost temperature found in the control (CO) and clipped (CL) plots, in contrast to the cleared plots are caused by live and dead vegetation cover. Thus, the main approach for preserving permafrost and ecosystems, especially in the Hovsgol forest steppe zone, must be based primarily on protecting vegetation cover.

Acknowledgments

These observations were conducted within the framework of the International Hovsgol Project, supported by a grant from the Global Environmental Facility and implemented by the World Bank to the Geo-Ecology Institute, Mongolian Academy of Sciences.

Two anonymous reviewers provided stimulating and helpful comments and suggestions on the draft manuscript. We want to thank all the mentioned persons and institutions.

References

Etzelmuller, B., Heggem, E.S.F., Sharkhuu, N., Frauenfelder, R., Kaab, A. & Goulden C.E. 2006. Mountain permafrost distribution modelling and validation using a multi-criteria approach and DC resistivity tomography in continental Central Asian mountains-example from Hovsgol Area, Northern Mongolia. *Permafrost and Periglacial Processes* 17: 91-104.

Goulden, C.E., Tumurtogoo, O., Karabanov, E. & Mongontsetseg, A. 2006. The geological history and geography of Lake Hovsgol, Mongolia. In: C.E. Goulden et al. (eds.), *The Geology, Biodiversity and Ecology of Lake Hovsgol (Mongolia)*. Leiden, The Netherlands: Backhuys Publisher, 1-20.

Heggem, E.S.F., Etzelmuller, B., Anarmaa, Sh., Sharkhuu, N., Goulden, C.E. & Nandintsetseg, B. 2006. Spatial modeling of ground surface temperatures in the Hövsgöl area, Northern Mongolia. *Permafrost and Periglacial Processes* 17: 375-369.

Lunardini, V.J. 1978. Theory of N-factors. *Proceedings of the Third International Conference on Permafrost, Edmonton, Canada*: 41-46.

Nandintsetseg, B., Greene, J.S. & Goulden, C.E.. 2007. Trends in extreme daily precipitation and temperature in the Lake Hövsgöl basin area, Mongolia. *Int. J. Climatology* 27: 341-347.

Sharkhuu, A., Sharkhuu, N., Etzelmuller, B., Heggem, E.S.F., Nelson, F.E., Shiklomanov, N.I., Goulden, C.E. & Brown, J. 2007. Permafrost monitoring in the Hovsgol mountain region, Mongolia. *J. Geophys. Res.* 112: F02506, doi:10.1029/2006JF000543.

Smith, M.V. & Riseborough, D.W. 1996. Permafrost monitoring and detection of climate change. *Permafrost and Periglacial Processes* 7: 301-309.

Thermal State of Permafrost in Mongolia

Natsagdorj Sharkhuu
Institute of Geo-Ecology, Mongolian Academy of Sciences, Mongolia
Anarmaa Sharkhuu
University of North Dakota, Grand Forks, North Dakota, USA
Vlad E. Romanovsky
Geophysical Institute, University of Alaska Fairbanks, USA
Kenji Yoshikawa
Geophysical Institute, University of Alaska Fairbanks, USA
Frederick E. Nelson
Department of Geography, University of Delaware, USA
Nikolay I. Shiklomanov
Department of Geography, University of Delaware, USA

Abstract

The thermal state of permafrost (TSP) in Mongolia is studied within the framework of mapping and monitoring of permafrost. Main parameters for estimating TSP are mean annual surface temperature (MAST), mean annual ground temperature (MAGT), or mean annual permafrost temperature (MAPT), and permafrost temperature gradient obtained during borehole temperature measurements by movable thermistors and data loggers. In this paper we will analyze and summarize initial data on estimating (1) changes in MAST and MAGT, depending on different natural factors, and (2) trends of increase in MAPT, based on data from 38 GTN-P and CALM borehole measurements in Mongolia. According to the results, the average rate of increase in MAPT in the Hentei and Hangai regions is 0.01°C–0.02°C a year, and in the Hovsgol region it reaches 0.02°C–0.03°C a year. Permafrost degradation under influence of climate warming was more intense during the last 15–20 years than during the previous 15–20 years (1970–1980s).

Keywords: boreholes; ground temperature; Mongolia; permafrost monitoring; soil surface temperature.

Introduction

Mapping and monitoring of permafrost is based mainly on the study of the thermal state of permafrost (TSP) (Kudrayvtsev et al. 1974). Main parameters for estimating TSP are mean annual surface temperature (MAST), mean annual ground temperature (MAGT), or mean annual permafrost temperature (MAPT), and permafrost temperature gradient (PTG). Values of MAGT are estimated by yearly average temperatures at depths of permafrost table or zero amplitude temperatures. They have a close relationship through thermal offset in active layers. For the last 40 years, Sharkhuu (2000) has measured ground temperatures in hundreds of shallow to deep boreholes in Mongolia. The data of borehole temperature measurements are useful for modeling and mapping distribution and thickness of permafrost in Central Asia. During the last 12 years Sharkhuu (2003 and 2005) also conducted permafrost monitoring in Mongolia within the international framework of GTN-P and CALM program (Burgess et al. 2000, Nelson et al. 2004). Initial results on CALM and GTN-P programs in Mongolia are presented in a number of publications (Brown et al. 2000, Sharkhuu 2003, Sharkhuu & Anarmaa 2005, Anarmaa et al. 2007). In addition, the Mongolian Expression of Intent #1129, main components of CALM and GTN-P programs in Mongolia, are part of the Thermal State of Permafrost IPY Project 50. According to the Expression, in 2007–2008 we are to extend boreholes and observations, improve quality of borehole temperature measurements, and generate new permafrost researchers. In this paper we analyze and summarize initial data obtained for mapping and monitoring of permafrost in Mongolia.

Permafrost zones occupy almost two-thirds of Mongolia, predominantly in the Hentei, Hovsgol, Hangai, and Altai Mountains and surrounding areas (Gravis et al. 1974). The territory is characterized by mountainous arid-land permafrost, sporadic to continuous in its extent, and it occupies the southern fringe of the Siberian permafrost zones (Fig. 1). In the continuous and discontinuous permafrost areas, taliks are found on steep south-facing slopes, under large river channels and deep lake bottoms, and along tectonic fractures with hydrothermal activity. In sporadic and isolated permafrost areas, frozen ground is found only on north-facing slopes and in fine-grained and moist deposits. The lower limit of continuous permafrost on south-facing slopes ranges from 1400 to 2000 m in the Hovsgol and Hentei Mountains, and from 2200 to 3200 m in the Altai and Hangai Mountains. The lowest limit of sporadic permafrost is found between 600 and 700 m a.s.l. Most of the permafrost is at a temperature close to 0°C, and thus, thermally unstable. However, average thickness and mean annual temperature of continuous permafrost is 50–100 m and -1°C to -2°C in valleys and depressions, and 100–250 m and -1°C to -3°C on mountains, respectively.

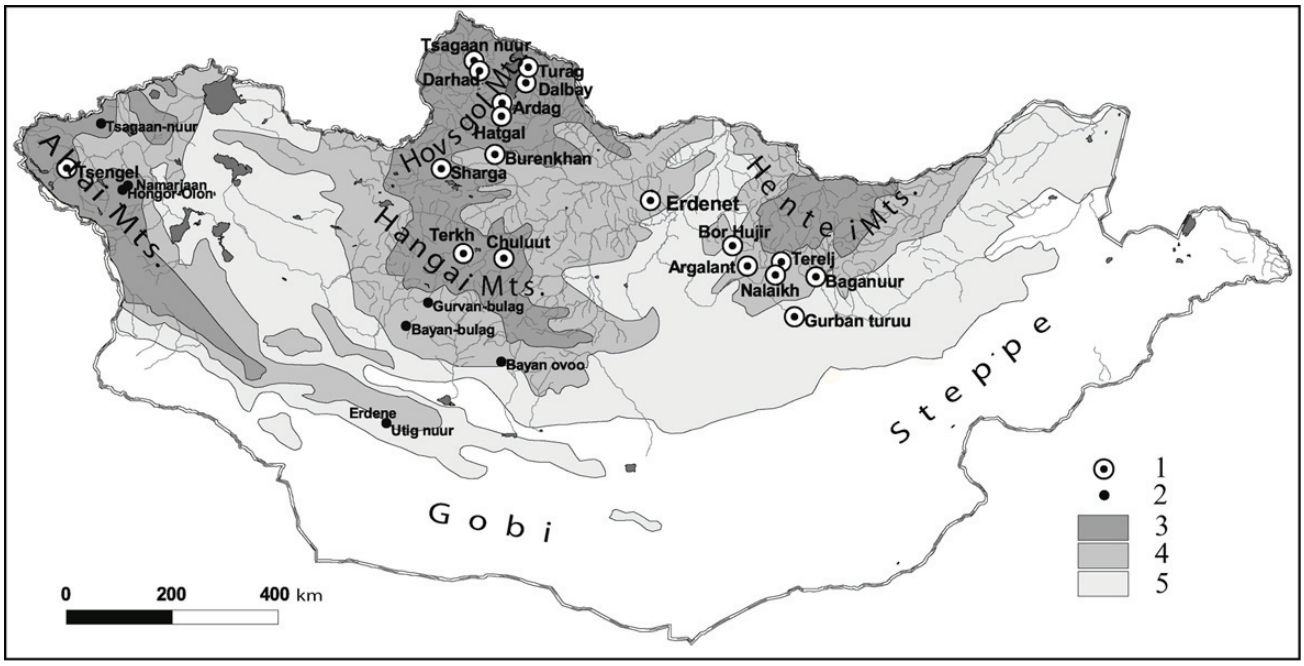

Figure 1. Location of permafrost monitoring boreholes in Mongolia 1 – Permafrost monitoring sites with GTN-P; 2 – Boreholes, planned to drill for permafrost monitoring; 3 – Continuous permafrost and discontinuous permafrost; 4 – Isolated permafrost; 5 – Sporadic permafrost.

Permafrost in Mongolia is characterized mainly by low and moderate ice content in unconsolidated sediments. Ice-rich permafrost is characteristic of lacustrine and alluvial sediments (Gravis et al. 1974, Sharkhuu 2003).

Permafrost in Mongolia is degrading under the influence of climate warming. According to the climate change studies (Natsagdorj et al. 2000), the mean annual air temperature has increased by 1.56°C during the last 60 years. Winter temperature has increased by 3.61°C. and spring-autumn temperature by 1.4°C–1.5°C. However, the summer temperature has decreased by 0.3°C. In the period from 1940–1990, mean annual air temperatures have increased by 1.8°C in northern and western Mongolia, 1.4°C in central Mongolia, and 0.3°C in southern and eastern Mongolia. For example, during the last 40 years mean annual air temperature at Hatgal weather station has increased by 1.86°C. Meanwhile, the air temperature trend was 0.61°C in the period from 1963–1989, and it reached 0.84°C in the period from 1990–2003 (Nandintsetseg & Goulden 2005).

Borehole Temperature Measurements

Methods

Ground temperatures in research boreholes have been measured by using movable thermistor strings and a digital multimeter of the MB-400 type. Temperature accuracy of thermistors of the MMT-4 type was 0.05°C. Temperature measurements in the permafrost monitoring boreholes are made using the same thermistors at the corresponding depths, and carried out on the same dates of any year. In addition, Stow-Away and HOBO, U-12 data loggers have been installed in most of the monitoring boreholes. UTL-1 and TR-52 data loggers have been used for measuring soil surface temperatures. Temperature accuracy of all the loggers is 0.25°C. Terrain and ground characteristics in most of the monitoring and research boreholes are determined in detail. Values of MAGT are estimated at depth of 10 m, although MAGT at depth of zero amplitude temperatures usually ranges from 10 m in fine-grained sediments with high moisture content to 20 m in bedrock and sandy sediments with course fragmental rock. A depth of MAGT also depends on yearly amplitude of soil surface temperatures. Mean winter temperature (MWT) is obtained by average value of air temperatures for December, January, and February. Mean summer temperature (MST) is estimated by the average value of air temperatures for June, July, and August. The frost number (FN) is calculated by a relation of values between thawing degree-days (TDD) and freezing degree-days (FDD) (Nelson & Outcalt 1987). A value of FN > 0.5 indicates more FDD than TDD, and is an indication of permafrost presence. This is, however, dependent on ground conditions, notably the thermal offset to the top of permafrost and therefore is not an absolute confirmation of permafrost existence (Heggem et al. 2006). Values of ground temperature gradient are estimated in the boreholes deeper than 30–50 m. Analysis of surface and ground temperature regime, or changes in MAST and MAGT depending on different natural factors, is made based on scientific methodology, developed at the Geocryology Department of Moscow State University (Kudrayvtsev et al. 1974).

Key study area

There are eight (Baganuur, Nalaikh, Argalant, Erdenet, Burenkhan, Hatgal, Ardag and Dalbay) key study areas with hundreds of geological and geocryological boreholes, where we measured and analyzed changes in MAGT depending on

different natural factors. In addition, during the last 40 years ground temperatures have been measured in more than 100 geocryological and engineering-geological boreholes with permafrost in different areas of Mongolia.

Monitoring sites

Monitoring of permafrost in Mongolia, based on studies of TSP within the framework of GTN-P and CALM programs, has been conducted since 1996 and extended from year to year. At present, there are 17 monitoring sites, including 38 GTN-P and CALM boreholes in Mongolia. For the last 5–10 years, some boreholes with an average depth of 10–15 m were drilled in the locations with the temperature measurements which were made 15–40 years ago in old boreholes. We also plan to extend boreholes, especially in the Altai region (Fig. 1). All the monitoring boreholes are situated in natural conditions without thermal disturbance. Most of the monitoring boreholes are instrumented in order to decrease air temperature convection and to protect them from human damage. All the redrilled boreholes are cased by parallel steel and plastic pipes of 3–5 cm diameter with the mouth of the pipe at a depth of about 15–20 cm and covered by soil. The empty space outside of casing pipes is filled with fine sands.

Results and Discussion

Surface temperature regime

Soil surface temperatures in mountainous regions depend on mountain altitudes, slope aspect and steepness, and snow and vegetation covers. Selected data from soil surface temperature recordings on Tsengel (Altai), Solongot (Hangai), and Bogd (Hentei) mountain slopes are presented in Table 1.

Table 1. Year-round recordings of surface temperatures (°C), depending on topography and elevation (H).

Mts	Aspect/ Angle	H, m (a.s.l)	MWT	MST	MAT	A	FN
Altai	flat watershed	3370	-21.5	5.4	-7.48	14.6	0.71
	north/8°	2675	-17.1	10.9	-3.77	12.7	0.59
	north/6°	2400	-20.7	16.4	-1.46	21.3	0.53
	south/10°	2400	-14.0	16.2	1.32	14.7	0.47
	valley bottom	2150	-16.7	16.1	0.11	16.2	0.50
Hangai	flat watershed	2900	-19.7	7.2	-5.77	14.8	0.66
	north/20°	2625	-16.6	8.4	-3.79	13.6	0.61
	north/25°	2230	-17.1	12.3	-1.30	16.5	0.53
	south/25°	2230	-14.6	15.6	1.59	16.5	0.47
	valley bottom	2050	-22.0	15.6	-1.56	20.3	0.53
Hentei	flat watershed	2200	-8.9	10.8	0.02	11.2	0.50
	north/25°	1950	-8.9	7.3	-1.66	8.8	0.57
	south/25°	1920	-13.9	13.5	0.37	15.0	0.49
	north/25°	1600	-17.2	17.5	-0.28	19.3	0.51
	valley bottom	1300	-19.3				

Notes: Mean winter (MWT), summer (MST) and annual (MAT) surface temperatures; FN–frost number; A–amplitude temperature.

There are observed winter air temperature (MWT) inversions in some valleys and depressions which are located at altitudes of 1200 to 1800 m a.s.l in the Hentei Mountain region. A MWT inversion is not characteristic of the Altai high mountains. MST, MAT, and A in all the mountains are decreased in different gradients with mountain surface height. FN is increased with altitude. A south-facing slope, depending on its steepness, is warmer by about 0.5°C–2.0°C than a north-facing slope.

Thermal insulation of snow in severe climate conditions with high soil surface amplitude temperatures is essential (intensive), although average thickness of snow in Mongolia is about 5–20 cm. Experimental observations for studying the thermal insulation effect of snow cover on soil surface temperatures from November to March have been conducted in the Hustai and Terelj areas near Ulaanbaatar and at the Dalbay study site (See Table 2). Thick snow cover of 10–20 cm can warm mean winter surface temperatures by about 3°C–5°C. However, the thermal insulation effect of snow is gradually decreased with an increase in snow density and thickness which is more than 20–40 cm. It should be noted that the warming effect of snow on soil surface in the forest and with thick vegetation cover was more intensive than at open and bare sites.

Experimental observations for studying thermal insulation of different vegetation cover on soil surface temperatures have been conducted at the Dalbay and Hustai study sites (Heggem et al. 2006, Anarmaa et al. 2007). Data from Table 3 show that moss cover, dense grass, and forest are natural insulators, maintaining low soil temperatures. In particular, as compared with the grass mowed site, MSTs under different vegetation cover are decreased by 2°C–9°C. However, MWTs are increased 1°C–5°C, due to accumulation of relatively loose and thick snow in plants. Meanwhile, MSTs under dense

Table 2. Mean winter surface temperatures (T_s) under snow cover with different thickness and density at the Dalbay experimental site.

Data loggers No	M31	M32	M33	M34	M35	M36
Thickness (cm)	40.0	32.9	25.8	18.7	11.6	0
Density (g/cm^3)	0.20	0.17	0.14	0.12	0.10	0
T_s (°C)	-8.5	-8.9	-9.5	-10.9	-12.7	-16.3

Table 3. Mean surface temperatures in single plots with different vegetation cover at Dalbay observation site.

Data loggers under	Mean surface temperatures, °C			
	winter	summer	annual	A
10 cm thick moss	-8.6	3.4	0.29	6.8
1.8 m high dense shrub	-7.4	7.4	0.63	7.8
Dense forest	-11.7	7.5	0.64	10.5
Sparse forest	-14.8	8.6	0.72	13
50 cm high dense shrub	-11.4	8.8	0.73	11.3
On moss surface	-11.5	9.8	0.86	11.9
Dense grass	-11.1	10.2	0.93	11.9
Grass mowed	-13.7	12.4	1.13	14.7
Air temperature	-29.3	10.8	-5.3	18.8

grass, forest, and 10 cm thick moss cover, are colder by 2.2°C, 4.2°C and 6.4°C, respectively. Therefore, the main factor in preserving permafrost and ecosystem in the Hovsgol and Hentei taiga zone must be based, first of all, on protection of vegetation cover (Sharkhuu & Anarmaa 2005).

Ground Temperature Regime

According to general regularities in TSP formation, MAGTs at depths of 10 m are decreased by about 0.4°C–0.6°C for each 100 m rise in mountain altitudes, and increased by 0.8°C–1.0°C for each 100 km moved from north to south. Ground temperature gradient varies from 0.01°C–0.02°C/m on mountain slopes and watersheds to 0.02°C–0.03°C/m in valleys and depressions. Meanwhile, the temperature gradient in unconsolidated sediments is more than in bedrock (Sharkhuu 2000). Changes in MAGTs, depending on different natural factors, are determined as follows:

Data from Table 4 show that forest cover can reduce MAGTs by about 0.5°C–1.2°C. Besides, as compared with south-facing slopes, MAGTs on gentle and steep north-facing slopes are colder by about 0.3°C–0.7°C and 0.8°C–1.5°C, respectively. Thus, north-facing slope and forest cover serve as favorable natural factors for TSP or permafrost existence.

Cold winter air temperatures are able to accumulate in rockfall and talus, which are widespread in the Altai, Hentei and Hovsgol Mountains. As compared with meadow, MAGTs at a depth of 2 m in talus and rockfall were colder by more than 1.7°C and 2.9°C, respectively. Value of low MAGTs in the course fragmental rocks such as rockfall and talus depends on porosity or the empty space in them (Table 5).

The thermal effect of underground waters on MAGT depends on river size, water stream, and water-bearing sediments. Data from Table 6 show that underground water streams along big and medium river valleys in continuous and discontinuous permafrost zones lead to taliks, due to an increase in MAGT. For example, as compared with large rivers, MAGT at a depth of 10 m in water-bearing sediments along medium and small river valleys and near brooks are colder by more than 2°C, 5°C, and 7°C, respectively.

Thermal offset enables permafrost to form and survive even when MASTs are positive (Osterkamp & Romanovsky 1999). Small patches and islands of permafrost in sporadic and isolated permafrost zones of Mongolia are formed as a result of thermal offset caused by differences of ground moisture content and thermal conductivity in the active layer (Sharkhuu 2000, Ishikawa et al. 2005). Observed values of MAGT for the thermal offset at Argalant borehole sites were typically 0.5°C to 1.5°C (Table 7).

Permafrost Temperature Monitoring

Main results on permafrost temperature monitoring in Mongolia are as follows: Permafrost in Mongolia is degrading at various rates, depending on climate and natural factors. In general, permafrost under influence of climate warming was degrading more intensely during the last 15–20 years than during previous 15–20 years (1970–1990). Permafrost degradation in bedrock is more intense than in unconsolidated sediments. For example, a rate of increase in MAPT in the Nalaih borehole with unconsolidated sediments does not exceed 0.02°C/year, but in the Burenkhan borehole with bedrock, it reaches 0.04°C/year (Fig. 2).

Moreover, the increasing permafrost temperature gradients with depth can be addressed as an indicator of recent and former degradation of permafrost (Harris & Haeberli 2003).

Table 4. MAGT depending on vegetation, slope aspect and steepness in Erdenet mountain area.

Slope aspect	Slope angle	Elevation, m	Vegetation	Ground	MAGT at 10 m, °C	Difference
South-facing	10°	1430	grass	bedrock	2.6	0.9
South-facing	10°	1430	forest	bedrock	1.7	
South-facing	15°	1420	forest	bedrock	1.7	0.7
North-facing	15°	1420	forest	bedrock	1	
South-facing	5°	1300	grass	sand	1.8	0.5
North-facing	5°	1300	grass	sand	1.3	

Table 5. Amplitude temperature (A) and MAGT at various depths of meadow, talus, and rockfall in Bogd Mountain.

Depth, m	Meadow		Talus		Rockfall	
	A	MAGT	A	MAGT	A	MAGT
0.5	22	1.08	32	-2.32	42	-2.07
1.0	17	1.19	26	-2.28	39	-2.94
1.5	13	0.62	21	-2.62	37	-3.67
2.0	10	1.17	16	-2.91	36	-4.09

Table 6. MAGT in the boreholes, located in different river valleys near Erdenet area.

Name and size of river	Predominant ground	Water stream	MAGT at 10 m, °C	h, m
Orhon large river	Gravel and pebbles	high	6.5	1.7
Burgaltai medium river	Sandy gravel	medium	4.5	2.3
Chingeltei small river	Gravely sand	low	1.2	2.7
Zunigol brook	Silt and clay	no	-0.4	3.4

Note: h – depth of seasonal freezing of ground.

Table 7. Thermal offset caused by differences of ground moisture content in Argalant boreholes.

Borehole No	Predominant ground	Average moisture, %	MAGT, at 10 m, °C	Thermal offset, °C
26	Sandy loam	12	0.4	0.6
126	Sandy loam	20	-0.2	
58	Loam	11	1.0	1.0
3	Loam	21	0.0	
15	Silt	10	1.2	1.3
18	Silt	23	-0.1	

Figure 3 demonstrates that Darhad site would represent a warming trend during the early 1980s, while the Burenkhan site would respond to warming trends during the early 1960s. Both warming episodes are recorded according to climate data from the Muren, Hatgal, and Rinchinlhumbe weather stations (Anarmaa et al. 2007).

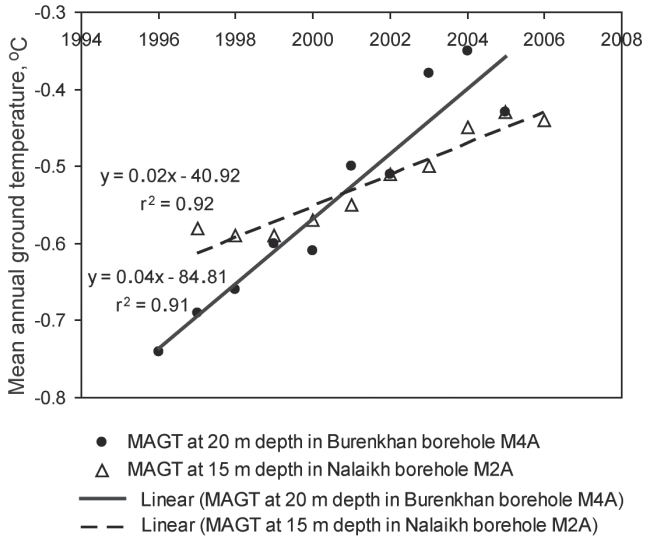

Figure 2. Trend of mean annual permafrost temperatures.

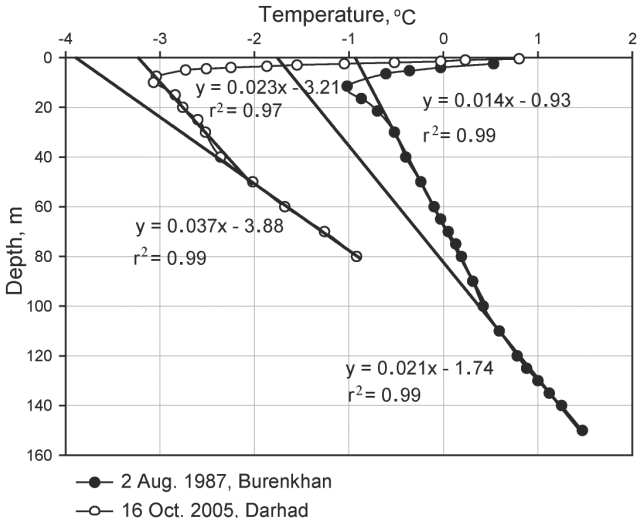

Figure 3. Change in permafrost temperature gradients with depth.

The average rate of increase in MAPT at 10 m depth in the Hovsgol Mountain region reaches 0.02°C–0.03°C/year, but in the Hangai and Hentei Mountain regions it does not exceed 0.01°C–0.02°C/year (Table 8). As compared with central Asia and European mountain territories, average trends of recent degradation of permafrost in Mongolia have almost similar values (Harris & Haeberli 2003, Marchenko 2007). However, as compared with eastern Siberia and Alaska, the average trends have smaller values (Osterkamp & Romanovsky 1999, Gavrilova 2003, Pavlov & Perlshtein 2006).

Conclusions

Main natural factors for determining thermal state and distribution of permafrost in the Altai, Hangai, Hovsgol, and Hentei Mountain regions are altitudes, slope aspect, and sometimes forest cover. The factors in arid land region surrounding the mountains are fine sediments with high moisture content and sometimes course fragmental deposits in mountains. Values of MAST and MAGT under influence of warming (5–20 cm thick snow cover and ground water stream) and cooling (forest and moss covers, fine-grained sediments with high moisture content and course fragmental deposits) factors are reduced within 0.5°C–2.5°C in every factor.

In general, permafrost under influence of climate warming in Mongolia is degrading at different rates. The permafrost in the Hovsgol Mountain region is degrading more intensely than in the Hangai and Hentei Mountain regions. Meanwhile, permafrost degradation under influence of climate warming was more intense during the last 15–20 years than during previous 15–20 years (1970–1980). Studies of TSP are of both scientific and practical significance for mapping and monitoring permafrost.

Acknowledgments

The University of Delaware and the University of Alaska Fairbanks, USA, have provided us with a number of loggers and financial support for conducting CALM and GTN-P programs in Mongolia. We also thank Jerry Brown, IPA president, for coordinating the Mongolian TSP/ INPO for IPY activities.

Table 8. Changes in the mean annual permafrost temperature at 10 m depth in the Hentei, Hangai, and Hovsgol Mountain regions.

Mts region	Hentei				Hangai				Hovsgol			
Borehole No	Baganuur		Argalant		Terkh		Chuluut		Sharga		Tsagaan nuur	
Elevation, m asl	1350		1385		2075		1870		1864		1547	
Land form	Plain of depression		Small valley bottom		High flood plain		Top of the pingo		Wide valley bottom		Lake depression	
Ground	Sandstone		Loam		Gravelly sand		Ice and clay		Gravelly sand		Silt and clay	
Ice content	Low		Medium		Medium		High		Medium		High	
Measured years	1976	2006	1988	2006	1969	2006	1969	2006	1968	2006	1989	2006
MAPT at 10 m	-0.50	-0.09	-0.40	-0.24	-1.96	-1.49	-1.12	-0.80	-2.35	-1.63	-3.91	-3.37
Trend of MAPT,	0.013	0.013	0.009	0.009	0.015	0.015	0.011	0.011	0.019	0.019	0.032	0.032
°C/year	0.01-0.02								0.02-0.03			

References

Anarmaa, Sh., Sharkhuu, N., Etzelmuller, B., Heggem, E.S.F., Nelson, F.E., Shiklomanov, N.I., Goulden, C.E. & Brown, J. 2007. Permafrost monitoring in the Hovsgol mountain region, Mongolia. *J. Geophys. Res.* 112:F02506, doi:10. 1029/2006JF000543.

Brown. J., Hinkel, K.M. & Nelson, F.E. 2000. The Circumpolar Active Layer Monitoring (CALM) Program: Research Designs and Initial Results, *J. Polar Geography* 24(3):258.

Burgess, M., Smith, S.L., Brown, J., Romanovsky, V.E. & Hinkel, K. 2000. Global Terrestrial Network for Permafrost (GTN-P): Permafrost monitoring contributing to global climate observations. *Geol. Surv. Can. Current Res. 2000-E14, 8 pp*.

Gavrilova, M.K. 2003. Recent climatic change in Asia along Yakutia-Mongolia transect. *Papers in Meteorology and Hydrology 25/4. Ulaanbaatar,* 11-17.

Gravis. G.F, Zabolotnik, S.I, Sukhodrovsky, V.L.,.Gavrilova, M.K. & Lisun, A.M. 1974. *Geocryological Conditions in the People's Republic of Mongolia*. Moscow: Nauka Publishing, 200 pp. (in Russian).

Harris, C. & Haeberli, W. 2003. Warming permafrost in Europe. *World Meteorological Organization Bulletin* 52: 252-257.

Heggem, E.S.F., Etzelmuller, B., Anarmaa,S., Sharkhuu, N., Goulden, C.E. & Nandintsetseg, B. 2006. Spatial distribution of ground surface temperatures and active layer depths in the Hovsgol area, Northern Mongolia. *Permafrost and Periglacial Processes* 17: 357-369.

Ishikawa, M., Sharkhuu, N., Zhang, Y., Kadota, T. & Ohata, T. 2005. Ground thermal and moisture conditions at the southern boundary of discontinuous permafrost, Mongolia. *Short Communication in Permafrost and Periglac. Process*. 16: 209-216.

Kudrayvtsev, V.A., Gragula, L.S., Kondratyeva, K.A. & Melamed, V.G. 1974. *Fundamentals of Frost Forecasting in Geological Engineering Investigations*. Moscow: Moscovskogo University, 431 pp. (in Russian).

Marchenko, S.S., Gorbunov, A.P. & Romanovsky, V.E. 2007. Permafrost warming in the Tien Shan mountains, Central Asia. *Global and Planetary Change* 56: 311-327 (available online at www.sciencedirect.com).

Nandintsetseg, B. & Goulden,.C.E. 2005. Recent change in the Northern Mongolia and its impact on ecosystem. *Proceedings of the International Symposium on Terrestrial and Climate Change in Mongolia*, *Ulaanbaatar, July 26-28, 2005:* 19-21.

Natsagdorj, L., Dagvadorj, D., Batima, P. & Tumurbaatar, D. 2000. Climate change and its impacts in Mongolia. *JEMR Publishing*, 226 pp.

Nelson, F.E, & Outcalt, S.I. 1987. A computational method for prediction and regionalization of permafrost. *Arctic and Alpine Research 19:* 279-288.

Nelson, F.E., Shiklomanov, K.M., Hinkel, K, & Christiansen, H.H. 2004. The Circumpolar Active Layer Monitoring (CALM) Workshop and the CALM 2 Program. *Polar Geogr.* 28: 253-266.

Osterkamp, T.E. & Romanovsky, V.E. 1999. Evidence for warming and thawing of discontinuous permafrost in Alaska. *Permafrost and Periglac. Process.* 10:17-37.

Pavlov, A.V. & Perlshtein, G.Z. 2006. Monitoring and modeling the permafrost dynamics under climate changes. *Abstracts of Asia Conference on Permafrost. Lanzhou, China*, 160-161.

Sharkhuu, N. 2000. Regularities of permafrost distribution in Mongolia. *Transactions of Institute of Geo-Ecology, MAS:,* 217-232 (in Mongolian).

Sharkhuu, N. 2003. Recent changes in the permafrost of Mongolia. *Proceedings of the Eighth International Conference on Permafrost, Zurich, Switzerland:* 1029-1034.

Sharkhuu, N. & Anarmaa, Sh. 2005. Recent degradation of permafrost in Mongolia. *Proceedings of the International Symposium on Terrestrial and Climate Change in Mongolia*, *Ulaanbaatar, Mongolia, July 26-28, 2005*: 99-101.

Thaw Settlement Behavior of Permafrost Along an Oil Pipeline to be Constructed in Northeastern China

Yu Sheng, Zhi Wen, Guoyu Li
State Key Laboratory of Frozen Soil Engineering, CAREERI, CAS, P.R. China
Jiaqian Hao, Wei Wu
Oil Engineering limited, Daqing Oil Field Company, Daqing, P.R. China

Abstract

An oil pipeline is to be constructed in northeastern China, which will transport oil from Russia to Daqing, China. Along the pipeline which runs from north to south, there exists continuous permafrost, discontinuous permafrost, sporadic permafrost, and seasonally frozen soil. A large number of undisturbed permafrost samples were collected to carry out thaw settlement tests in order to predict the potential deformation from thawing of permafrost. Test results include both thaw settlement parameters and the coefficients of compressibility dependent on total water content of samples. Regressive envelopes of the test results are suggested to analyze the relationships between the two parameters and water content for predicting the thaw settlement of permafrost for both fine- and coarse-grained soils. A comparison of thaw settlement parameters obtained using the proposed method and those estimated from specifications was carried out to clarify the thaw settlement behavior of permafrost along the pipeline.

Keywords: coefficient of compressibility; permafrost; pipeline; thaw settlement parameter.

Introduction

A pipeline is to be constructed in northeastern China to transport crude oil from Russia to China, in nearly a straight line in a north-to-south direction within a latitude range from 53°28′N to 46°30′N. The 960 km long, 914 mm diameter pipeline has been designed to be buried at a depth of 1.8 m (from ground surface to top of pipe) along most of the route. The pipeline has to traverse about 450 km of continuous permafrost, discontinuous permafrost, and sporadic permafrost zone from the most north to the south. The oil temperature at the inlet of the pipeline is estimated to be changing between -6°C to +10°C during the year. There will be no temperature control of the oil along the route. According to a preliminary estimate, the underlying permafrost would thaw to a depth of 1.5–4 m in the coming 30 years of service time, depending on the ice content of the permafrost.

Thaw settlement is one of the most critical design issues for a pipeline buried in permafrost. Uneven deformation of the pipe due to thaw settlement of permafrost may induce pipe breakage, especially in a large diameter pipeline. For many existing pipelines in permafrost regions attention was given to engineering permafrost problems in order to optimize design and maintain a good permafrost environment (Greenslade & Nixon 2000, Burgess 1988, Hanna & McRoberts 1988, Hanna et al. 1983, Nixon & Maclnnes 1996). Thaw settlement behavior of permafrost is an essential property for estimating the deformation of pipeline due to permafrost thawing. Some engineering specifications involving permafrost suggest values of thaw settlement based on the ice content of permafrost. However, measured results from tests are not always consistent with the estimated values suggested by the specifications because of the variety of soil type. Also, the compressibility after thaw of the permafrost is generally not considered in any specifications.

In the geological survey for the pipeline, many permafrost samples from boreholes were collected to study the thaw settlement behavior of permafrost. This paper documents the results of thaw settlement tests, which are proposed to be a reference in estimating the thaw settlement of permafrost along the pipeline.

Samples and Testing

Undisturbed frozen samples collected from boreholes were transported to a laboratory for testing. All thaw settlement tests were conducted in a confined condition using a cylinder of 79.8 mm ID and 40 mm height. Samples were carefully trimmed to fit to the test cell. Additional parts of the samples were used to measure their physical properties.

Samples were generally divided into two groups; these were fine-grained silty clay and coarse-grained soils including sand, sand with gravel and strongly weathered sandstone. Soil samples of both groups had a wide range of ice content and bulk density. The average plastic limit and liquid limit of the fine-grained soil were about 12.5% and 31.5%, respectively.

The total thaw settlement strain of a frozen sample generally consists of two components expressed as follows (Tsytovich 1975, McRoberts et al. 1978):

$$\alpha = A_0 + a_0 p \tag{1}$$

where

α is the total thaw settlement ratio, %;
A_0 is the thaw settlement parameter, %;
a_0 is the average coefficient of compressibility, 1/MPa;
p is the pressure applied to the permafrost sample, MPa;
A_0 and a_0 are determined using the thaw settlement test.

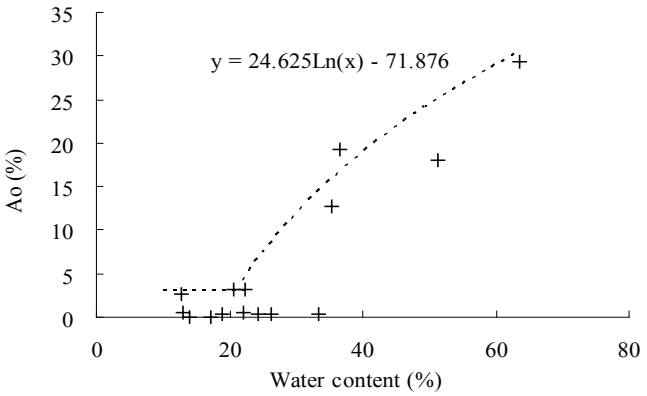

Figure 1. Thaw settlement parameter vs. water content for the fine-grained silty clay.

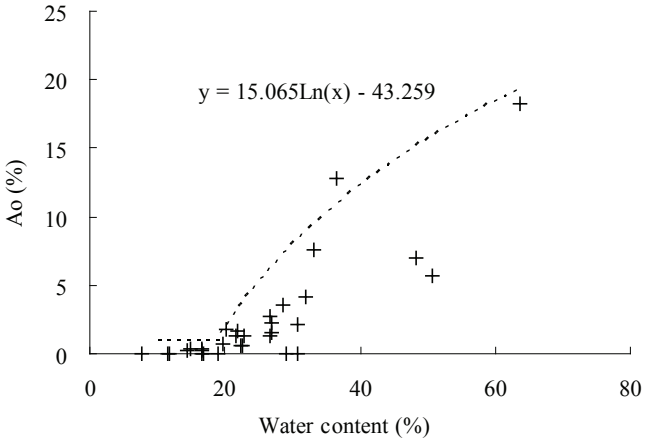

Figure 2. Thaw settlement parameter vs. water content for the coarse-grained soils.

After putting the sample into the test cell, the sample is allowed to thaw under uncontrolled conditions. For the thaw settlement parameter a pressure of about 1 kPa is maintained to overcome the friction between the sample and the cell wall. After the deformation stabilizes, subsequent increments of pressure are applied to determine the coefficient of compressibility. Three pressure stages, 50 kPa, 100 kPa, and 150 kPa are used in the tests. The coefficient of compressibility is determined as the average at the three pressure levels.

Test Results

Thaw settlement parameter A_0

The values of thaw settlement parameter are plotted against the initial water (ice) content of the samples as shown in Figure 1 for the fine-grained silty clay and Figure 2 for the coarse-grained soils. For both groups of soil, the relationship between A_0 and water content shows a two-stage phenomenon. There is a low and comparatively stable value when the water content is less than a certain value (defined as initial water content of thaw settlement for the soil type along the oil pipeline). Once the water content is greater than initial water content of thaw settlement, A_0 starts to increase considerably with the increase in water content. To be safe, it is not thought appropriate to fit a formula to all the test data. A regressive envelope of the data is, therefore proposed to predict A_0 for samples with high water contents. A logarithmic relationship was found to be a good choice (see dotted line in Figs. 1 and 2). The thaw settlement parameters for both soils can be predicted by the following relationships:

For fine-grained silty clay:

$$A_0 = \begin{cases} 3 & w \le 21\% \\ 24.625\ln w - 71.876 & w > 21\% \end{cases} \quad (2)$$

For coarse-grained soil:

$$A_0 = \begin{cases} 1 & w \le 19\% \\ 15.065\ln w - 43.259 & w > 19\% \end{cases} \quad (3)$$

where w refers to the initial water content of the samples.

Table 1. A_0 suggested in Specification GB50324-2001.

A_0 (%)	Total water content, w (%)	
	Silty clay	Coarse soil
< 3	$w < w_p+4$	$w < 15$
3~10	$w_p+4 \le w < w_p+15$	$15 \le w < 25$
10~25	$w_p+15 \le w < w_p+35$	$25 \le w$

Note: w_p is the plastic limit water content.

When the thaw settlement parameter is less than 3%, thaw settlement is generally considered to be negligible. In Equations (2) and (3), the first constant term corresponds to a water content range of less than the initial water content of thaw settlement. The initial water contents of thaw settlement are 21% and 19% for the fine-grained silty clay and coarse-grained soil, respectively.

Comparing Figure 1 with Figure 2, it is found that the value of A_0 for the fine-grained silty clay is greater than that for the coarse-grained soil at the same water content. This means that engineers should pay particular attention to silty clay permafrost soils with high ice content.

Comparison with specifications

In some specifications in China, thaw settlement parameters are suggested for different types of soil. Table 1 lists a typical summary of A_0 according to Specification for Survey of Frozen Soil Engineering Geology (GB50324-2001).

In terms of the classification of A_0 in the specification, water content ranges from test results can be calculated from the proposed predicting formulae. Table 2 lists the results.

It was found that the test results for the fine-grained silty clay roughly agreed with the suggestion in the specification, especially for the permafrost with high water-ice content. For the coarse-grained soils, test results indicated that the water content ranges generally had higher values than those suggested in the specification. In other words, the thaw settlement of coarse-grained permafrost soil would be much lower than that estimated in the specification.

Table 2. Water content ranges from test results in terms of the classification of A_0 in specification.

A_0 (%)	Total water content, w (%)			
	Silty clay		Coarse soil	
	Specification	Test	Specification	Test
< 3	<16.5	< 21	< 15	< 21.5
3~10	16.5~27.5	21~28	15~ 25	21.5~35
10~25	27.5~47.5	28~51	≥ 25	≥ 35

Coefficient of compressibility a_0

Results of the coefficients of the compressibility test are shown in Figures 3 and 4 for the fine-grained silty clay and the coarse-grained soil, respectively. It can be seen that there is a scatter in the test results. Although linear relationships can be used to approximate the test results (solid line in Figures), we suggest that the regressive envelopes of the data provide a reasonable and safe prediction. Logarithmic relationships are found to be quite appropriate for both fine-grained silty clay and coarse-grained soil (shown in dotted line in Figs. 3, 4). Therefore, the coefficient of compressibility for both soils can be predicted according to the following formulae:

For the fine-grained silty clay:

$$a_0 = 0.8514 \ln w - 1.5224 \quad (4)$$

For coarse-grained soil:

$$a_0 = 1.25 \ln w - 2.3146 \quad (5)$$

Although the thaw settlement parameter of the fine-grained silty clay is higher than that of the coarse-grained soil, the coefficient of compressibility of the coarse-grained soil appears to increase faster with increasing water content. This means that the frozen coarse-grained soil has more potential to deform than the fine-grained silty clay when loaded. The total thaw strain of permafrost depends on both A_0 and a_0 for different pressures. Based on the proposed estimate, the total thaw strain can be plotted as shown in Figure 5. It can be seen that if the pressure is less than 100 kPa, the silty clay deforms more than the coarse soil. For pressures greater than 100 kPa, the coarse soil deforms more than the silty clay.

The pipeline is designed to be buried at a depth of about 1.8 m; the depth at the bottom of the pipeline is about 2.7 m. Within the range of 4.0 m below the pipeline, where underlying permafrost may thaw, the soil pressure applied on permafrost is about in the range from 50–150 kPa, which falls within the pressure range of the tests. If an insulation layer is packed around the pipeline to reduce the depth of permafrost thaw, the thaw settlement should be comparatively low. In this case more attention should be paid to the deformation of the frozen silty clay. If there exists a frozen coarse layer with high water content at a deeper location below the pipeline (e.g., 3–4 m below the bottom of the pipeline), the possible deformation from permafrost thawing may be greater than that of the frozen silty clay at the same ice content. Engineers should consider the difference in the thaw settlement behavior with comprehensive permafrost geological data to optimize the design, so as to choose a reasonable treatment to the permafrost section.

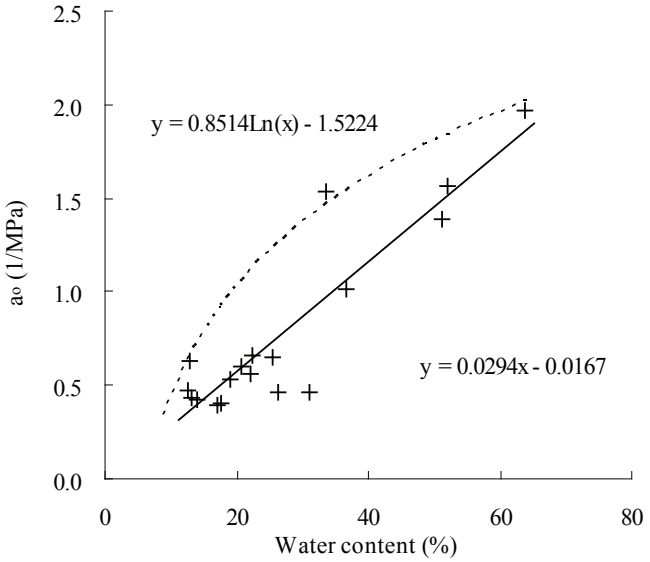

Figure 3. Coefficient of compressibility vs. water content for the fine-grained silty clay.

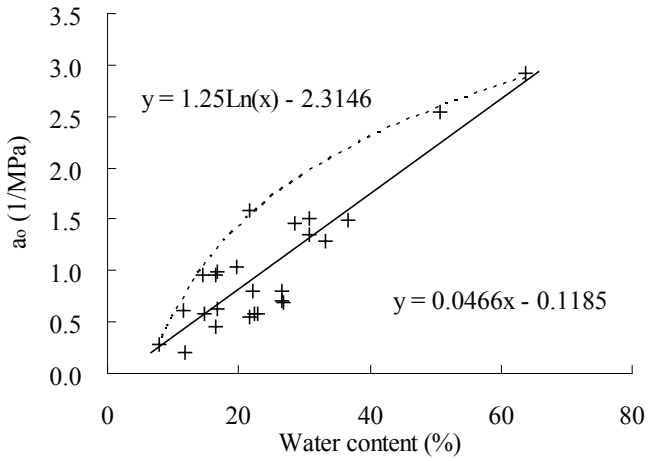

Figure 4. Coefficient of compressibility vs. water content for the coarse-grained soil.

Conclusions

Based on test results, thaw settlement behavior was analyzed for both fine-grained silty clay and coarse-grained soil. Water content appeared to be a dominant factor in the test results. The following suggestions are proposed to provide a guide for the design of the pipeline.

(1) The thaw settlement parameter of the fine-grained silty clay has a high value, which is roughly in agreement with the suggestion in specifications. The thaw settlement parameter of the coarse-grained soil is, however, lower than the value suggested in specifications.

(2) When the water content of the frozen sample is greater than the initial water content of thaw settlement, it was suggested that the thaw settlement parameters of both

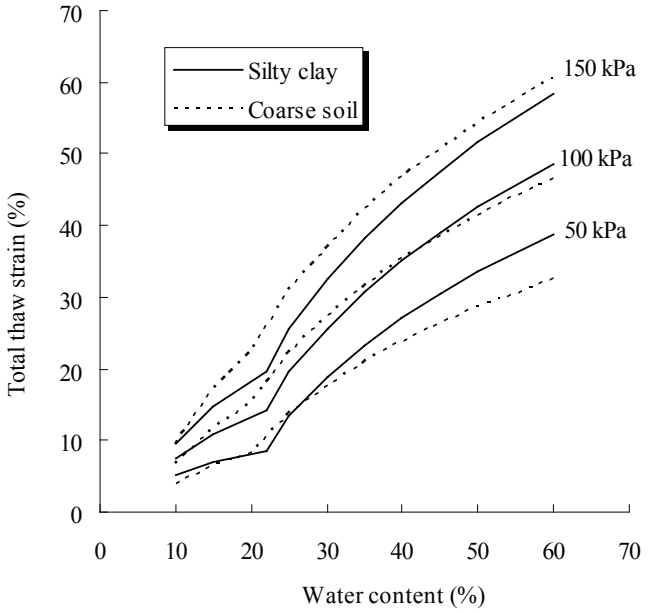

Figure 5. Total strain of the thawed permafrost vs. water content under different pressure.

fine-grained silty clay and coarse-grained soil be predicted using their envelopes of the test results, instead of all data. A logarithmic relationship is proposed to describe the relationship.

(3) The coarse-grained soil has more potential to deform under comparatively high pressures. Its coefficient of compressibility was higher than that of the fine-grained silty clay with increasing water content. Logarithmic envelopes of test results are also useful for predicting the coefficients of compressibility.

Acknowledgments

This work was carried out under the auspices of the Key Directional Project of the CAS Knowledge Innovation Program "Mechanisms and mitigation of frost heaving and thaw settlement of pipeline foundation soils in permafrost regions" (Grant No. KZCX2-YW-311), and Permafrost Research Projects of PetroChina Daqing Oilfield Engineering Company "Assessment and forecast of permafrost conditions along the China-Russia crude oil pipeline route, Thermal/strain analyses on pipeline-soil interactions in permafrost regions."

References

Burgess, M. 1988. Permafrost and terrain preliminary monitoring results, Norman Wells pipeline, Canada. *Proceedings of the 5th International Conference on Permafrost* Vol. 1: 916-921.

Greenslade, J.G & Nixon, D. 2000. New design concepts for pipelines buried in permafrost. *2000 International Pipeline Conference* Vol. 1: 135-143.

Hanna, A.J. & McRoberts, E.C. 1988. Permafrost slope design for a buried oil pipeline. *Proceedings of the 5th International Conference on Permafrost* Vol. 1: 1247-1252.

Hanna, A.J., Saunders, R.J., Lem, G.N. & Carlson, L.E. 1983. Alaska Highway Gas pipeline project (Yukon) section thaw settlement design approach. *Proceedings of the 4th International Conference on Permafrost* Vol. 1: 439-444.

McRoberts, E.C., Law, T.C. & Moniz, E. 1978. Thaw settlement studies in the discontinuously pemafrost zone. *Proceedings of the 3rd International Conference on Permafrost* Vol. 1: 700-706.

Nixon, D. & Maclnnes, K.L. 1996. Application of pipe temperature simulator for Norman Wells oil pipeline. *Canadian Geotechnical Journal* 33: 140149.

Tsytovich, N.A. 1975. *The Mechanics of Frozen Soil.* New York: McGraw-Hill Book Company.

Impact of Surface Air Temperature and Snow Cover Depth on the Upper Soil Temperature Variations in Russia

Artem B. Sherstyukov
All-Russian Research Institute of Hydrometeorological Information - World Data Centre (RIHMI-WDC), Obninsk, Russian Federation

Boris G. Sherstyukov
All-Russian Research Institute of Hydrometeorological Information - World Data Centre (RIHMI-WDC), Obninsk, Russian Federation

Pavel Ya. Groisman
UCAR Project Scientist at National Climatic Data Center, Asheville, North Carolina

Abstract

From 1965–2004, data from all Russian meteorological stations with long-term soil temperature observations at depths 80, 160, and 320 cm were compiled and analyzed. It was found that the prevailing influence on soil temperature variations in the European part of Russia was surface air temperature and in the Asian part of Russia was snow cover depth. By preserving the heat accumulated in the warm season, an observed increase of the winter snow depth in the permafrost zone promotes annual soil temperature increase and therefore may foster the further permafrost degradation associated with on-going regional warming.

Keywords: Eurasia; permafrost; snow depth; soil temperature; warming.

Introduction

According to Izrael et al. (2002), beginning in the mid-1960s, northern Russia experienced climate warming. For the whole of northern Russia, the air temperature rise trend was 0.47ºC/decade. As the sampling stations in Izrael et al. (2006) show, this was accompanied by the soil temperature rise at 80 and 160 cm depths. However, the agreement between air temperature and soil temperature trends has not occurred everywhere. At some stations, soil temperature trends are higher than air temperature trends. The causes of this behavior are to be identified. This work aims at deriving quantitative estimates of the influence of the two major factors of changing climate: air temperature and snow depth, on the soil temperature. The problem is addressed by using data from the network of Russian stations, where soil temperatures have been recorded at depths to 320 cm since 1965.

Temperature rise in the permafrost zone can lead to frozen ground degradation and can change the characteristics of soil toughness. Therefore, the problem of frozen ground degradation is of major practical importance. The Russian permafrost zone contains more than 30% of the developed oil reserves available in Russia; about 60% of natural gas, hard-coal and peat deposits; a significant portion of hydropower resources; deposits of non-ferrous metals, gold and diamond and vast reserves of timber and fresh water. Expensive and vulnerable infrastructure was created here, i.e., petroleum field facilities; main oil and gas pipelines extending thousands of kilometers; mines and pits; and hydroelectric plants. Additionally, settlements and towns, highways and railways, aerodromes, and ports were built in this region (Pavlov et al. 2000). The foundations and base plates of all the structures are supported by pilings frozen in the ground. Melting of frozen ground violates the stability and operational capability of all these engineering facilities (Demchenko et al. 2001).

Analysis and Results

Soil temperature data at depths 80, 160, and 320 cm, as well as air temperature and snow depth data, were analyzed for all Russian meteorological stations for 40 years (for the 1965-2004 period). The monthly data for 150 stations (shown by stars in Fig. 1) were retrieved from the National Roshydromet archive. Thereafter, we conducted multiple correlation analyses searching the factors that control the soil temperature seasonal variations across the Russian Federation.

Correlations, R, between summer soil temperatures at the 160 cm depth and summer air temperatures (mean temperature for June to August) are presented in Figure 1. From the western border of the Russian Federation to 75°E, the Figure shows significant positive R-values (> 0.6). East of 75°E, across West Siberia, southeast Siberia, and at the Far East stations of Sakhalin and Primorie Krai, correlation coefficients (being of the order of 0.4 to 0.5) are still statistically significant at the 0.05 level. The highest positive correlation coefficients (R>0.60) between summer air temperatures and soil temperatures at all depths (with appropriate shifts depending upon the depth, e.g., for 160 cm this shift is around 2 months) are primarily observed outside the permafrost zone. In the vast central part of the permafrost zone, the correlation is close to zero (Fig. 1).

In winter (December to February), the correlations between soil temperatures and air temperatures are weaker

and the *R*-values above 0.6 are absent across the entire nation (Fig. 2). Statistically significant correlation coefficients (0.4 to 0.6) between winter air temperatures and soil temperatures at depths of 80 and 160 cm are observed only over Russia west of the Ural Mountains. Only here in the southernmost part, the impacts of winter air temperature are observed as deep as 320 cm. In winter in the permafrost zone, the impact of long-term surface air temperature changes on soil temperatures is practically unnoticeable at all depths.

The analysis of correlations between winter soil temperatures at different depths and February snow depth shows that significant positive correlation coefficients (0.4 to 0.6) prevail at soil depths of 80 and 160 cm over most of Russia east of the sub-Urals (50°E, with exceptions of the North Siberia Plain, Kamchatka, and southeast Siberia). At the 320 cm soil depth, a significant positive correlation is observed only in small isolated areas in southwest Siberia, Central Yakutia, and Primorie. No significant correlations were found between the February snow depth and winter soil temperatures at all depths over European Russia. The warming influence of snow at each soil depth is recorded over most of Asian Russia, but it becomes weaker as the soil depth increases and is not observed at all in European Russia.

Mean annual soil temperature in different regions is formed in different ways. In European Russia, it is controlled by air temperature changes rather than by snow depth. The warming effect of snow here is practically absent. In Asian Russia, on the contrary, changes in mean annual soil temperature are controlled by snow depth changes rather than by air temperature changes.

The contribution of the mean annual air temperature and the snow depth to the change in mean annual soil temperature was estimated in percent of the total variance of the soil temperature. The analysis of this quantity shows that in European Russia, the main contribution to the total variance is made by the air temperature (23% to 46% of the contribution to the total variance) and the contribution of snow here is minimal (from 0.4% to 8.0%). The impact of snow on the soil temperature in this region is so small that even with negative snow depth trends in northwestern Russia (e.g., in Karelia and Arkhangelsk district; cf. Fig. 3), soil temperature trends are positive and significant.

Tendencies for the increase in mean winter snow depth are observed over most of the Russian territory (mainly in Siberia). But northern regions of European Russia, show a tendency for decreasing snow depth (Bulygina et al. 2007).

Across Asian Russia and in the Urals Region, the values of soil temperature trends are higher than the air temperature trends. Positive soil temperature trends are observed even at the stations with negative air temperature trends (Nizhni Tagil 57.9°N, 60.1°E; Kupino 54.4°N, 77.3°E; Pudino 54.4°N, 79.2°E, and Bokhan 53.2°N, 103.8°E). At the last station (Fig. 4), the contribution of the mean annual air

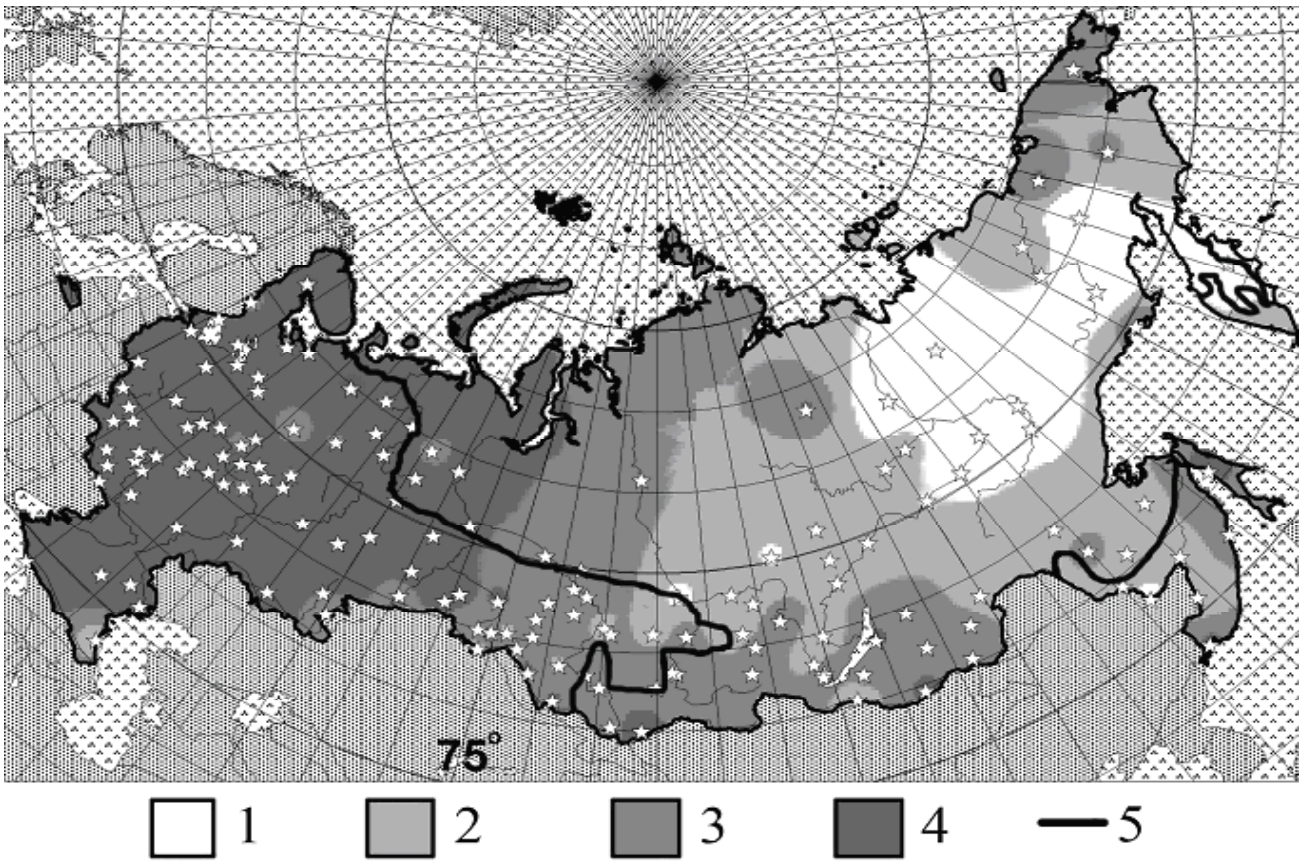

Figure 1. Correlation coefficient (R) between air temperatures and soil temperatures at the 160 cm depth in summer.
1 – $0.1 \le k < 0.2$, 2 – $0.2 \le R < 0.4$, 3 – $0.4 \le R < 0.6$, 4 – $0.6 \le R < 0.8$, 5 – southern border of the permafrost zone.

temperature to the total variance of soil temperatures at 160 cm is only 4.7%, while the contribution of the snow depth is 30%.

A geographical distribution of the contributions of the two factors to the total variance of mean annual soil temperatures at 160 cm is shown as diagrams on the map (Fig. 5). Nearly everywhere in European Russia, the long-term changes in mean annual soil temperature are greatly controlled by air temperature changes (light columns in diagrams, 20% to 50%).

The snow changes here determine no more than 10% of the variance (dark columns in diagrams). In Central Volga, the Urals, and over most of Asian Russia, the long-term changes in mean annual soil temperature are primarily controlled by snow depth changes (10% to 50% of the variance) and air temperature is responsible for less than 10% of soil temperature variability.

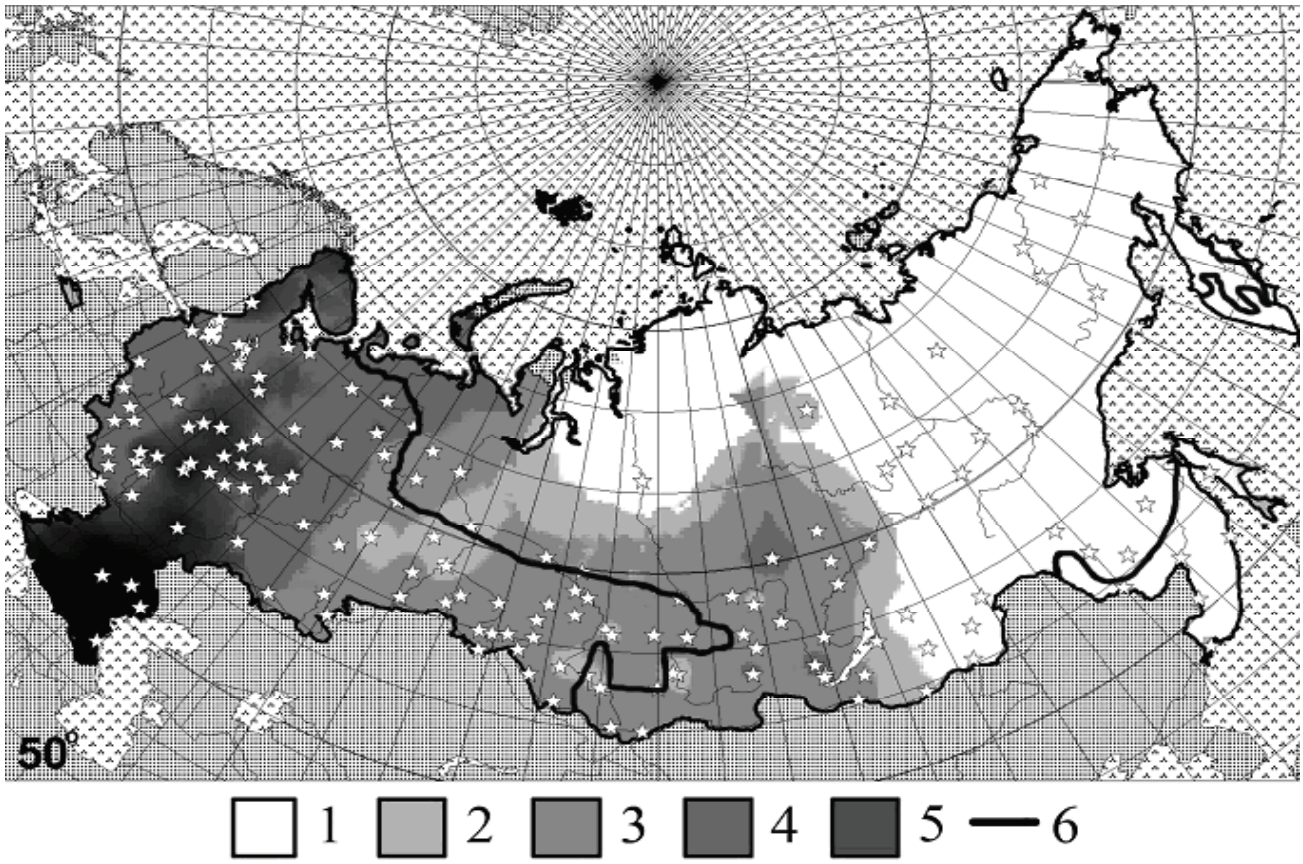

Figure 2. Correlation coefficient (R) between air temperatures and soil temperatures at the 160 cm depth in winter.
1 – 0.1≤R<0.2, 2 – 0.2≤R<0.3, 3 – 0.3≤R<0.4, 4 – 0.4≤R<0.5, 5 – 0.5≤R<0.6, 6 – southern border of permafrost.

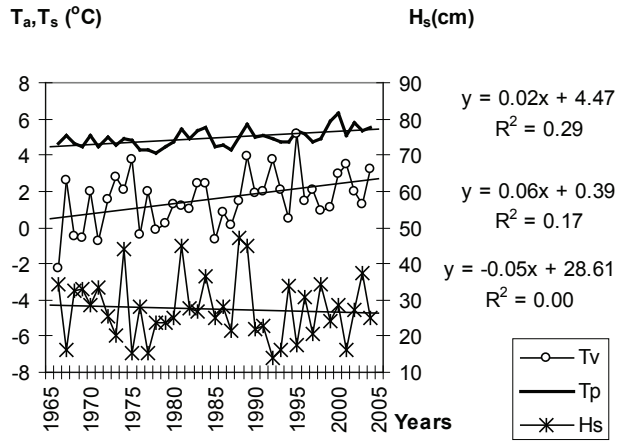

Figure 3. Long-term trends of mean annual air temperatures (T_a), soil temperatures at 160 cm depth (T_p), and snow depth (H_s) at Onega station (63.9°N, 38.1°E, Arkhangelsk district).

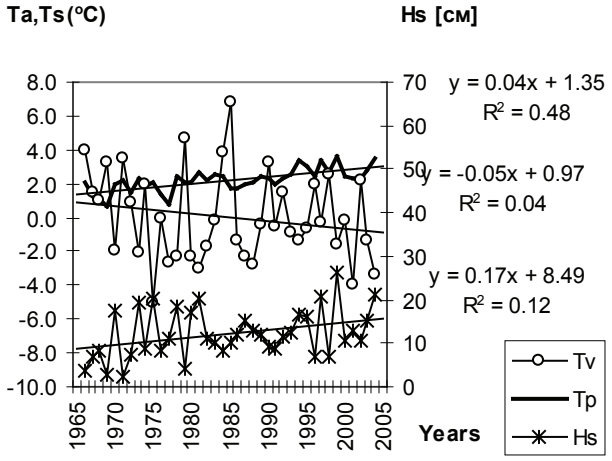

Figure 4. Long-term trends of mean annual air temperatures (T_a), soil temperatures at 160-cm depth (T_p) and snow depth (H_s) at Bokhan station (53°08′N, 103°46′E, elevation 446 m).

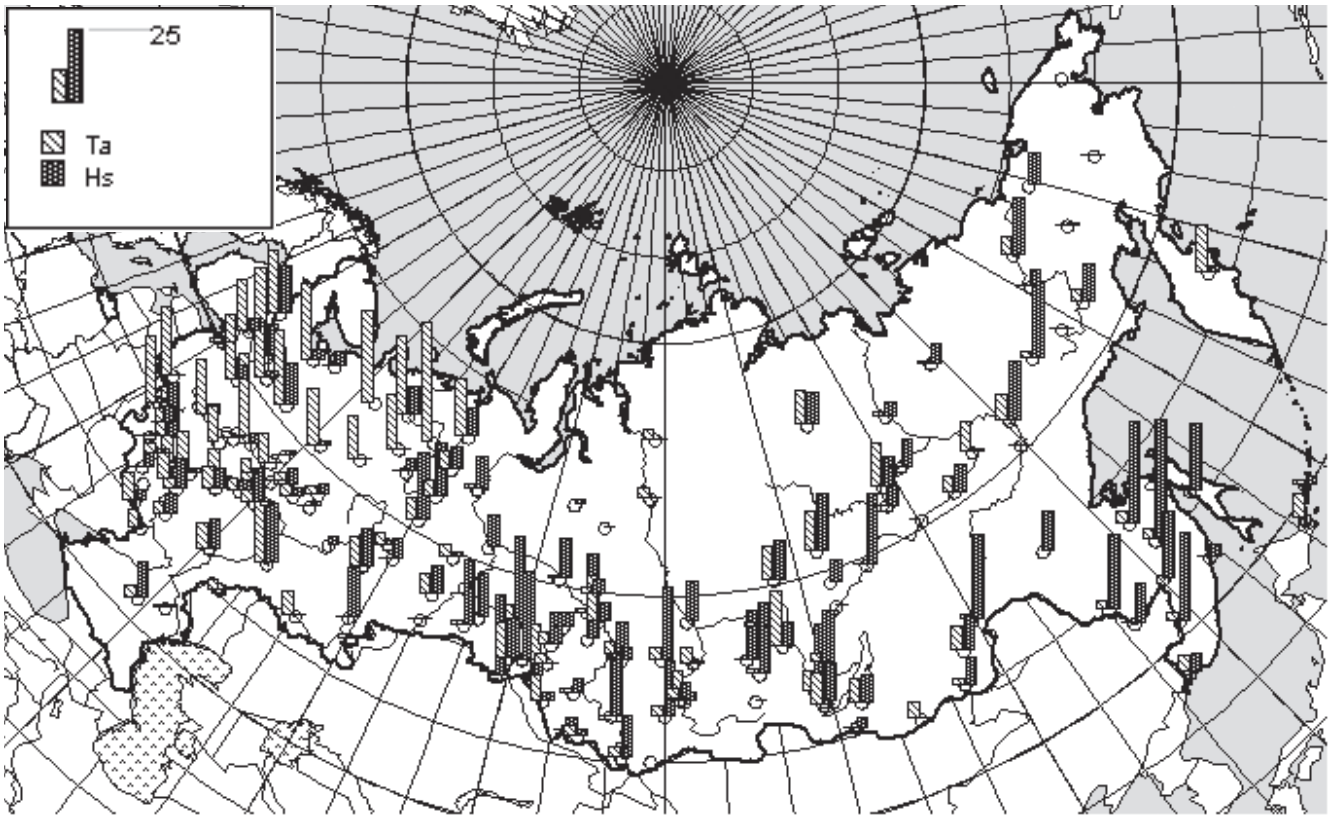

Figure 5. Contribution (in percent of variance) of mean annual air temperature (T_a) and snow depth (H_s) to long-term changes in mean annual soil temperature at 160 cm depth.

At the 320 cm depth, the effect of surface meteorological conditions is very weak and uneven over the Russian territory and is probably controlled by local micrometeorological and soil conditions. The increasing snow accumulation in Siberia results in an additional increase in mean annual soil temperatures and their relatively more rapid increase compared with the lower atmosphere. This fact is of particular importance in the permafrost zone since the increasing snow accumulation here strengthens one of the components likely to contribute to the permafrost degradation.warming.

The impact of long-term changes in air temperatures on soil temperatures in the central regions of the permafrost zone is weak both in summer and in winter. However, in regions with intermittent permafrost, the impact is substantial. The impact of snow depth on soil temperatures is observed throughout the entire permafrost zone of Russia.

Acknowledgments

This research was conducted with the support of the Russian Hydrometeorological Service (Roshydromet) and in the framework of the Northern Eurasia Earth Science Partnership Initiative (NEESPI).

References

Bulygina, O.N., Korshunova, N.N. & Razuvaev, V.N. 2007. Variations in snow characteristics over the Russian territory in the recent decades. *Proc. RIHMI-WDC*, 173: 41-46.

Demchenko, P.F., Velichko, A.A., Golitsin, G.S., Eliseev, A.V. & Nechaev, V.P. 2001. The permafrost fate: seeing the future from the experience of the past. *Prirod* 11: 43.

Izrael, Yu.A., Anokhin, Yu.A., Myach, L.T. & Sherstyukov, B.G. 2006. Analyzing the trends in the change of climate elements under global climate warming in permafrost regions based on meteorological observations. *Meteorology and Hydrology* 5: 27-38.

Izrael, Yu.A., Pavlov, A.V. & Anokhin, Yu.A. 2002. Evolution of the permafrost zone under current global climate change. *Meteorology and Hydrology* 1: 22-32.

Pavlov, A.V. &. Gravis, G.F. 2000. The permafrost and the current climate. *Priroda* 4: 10-18.

The Circumpolar Active Layer Monitoring (CALM) Program: Data Collection, Management, and Dissemination Strategies

N.I. Shiklomanov, F.E. Nelson, D.A. Streletskiy
Department of Geography, University of Delaware, Newark, DE 19716, USA
K.M. Hinkel
Department of Geography, University of Cincinnati, Cincinnati, OH 45221, USA
J. Brown
International Permafrost Association, Woods Hole, MA 02543, USA

Abstract

The Circumpolar Active Layer Monitoring (CALM) program, established in the early 1990s, was designed to observe temporal and spatial variability of the active layer and near-surface permafrost parameters, and their response to changes and variations in climatic conditions. CALM is the world's primary source of information about the active layer. Auxiliary information includes air temperature, soil moisture, soil temperature at different depths, snow cover, soil composition, and landscape characterization and frost heave and thaw subsidence. Metadata include detailed descriptions and photographs for each site. Several groups of sites have been used to create regional maps of active layer thickness. CALM data are distributed through the program's website (www.udel.edu/Geography/calm) and are also archived in and distributed through the Frozen Ground Data Center at the University of Colorado. This paper provides details about the nature, availability, and uses of data from the CALM network.

Keywords: active layer; data analysis; data archive; permafrost; polar regions; sampling design.

Introduction

The Circumpolar Active Layer Monitoring (CALM) program is a network of sites at which data about active layer thickness (ALT) and dynamics are collected. CALM was established in the 1990s to observe and detect the long-term response of the active layer and near-surface permafrost to changes in climate. CALM is among the international permafrost community's first large-scale efforts to construct a coordinated monitoring program capable of producing data sets suitable for evaluating the effects of climate change. Together with the IPA's Thermal State of Permafrost program, CALM comprises GTN-P, the Global Terrestrial Network for Permafrost. The CALM network's history and organizational structure are reported in Brown et al. (2000) and Nelson et al. (2004).

CALM is currently administered through the University of Delaware (UDel) Department of Geography. Analysis, archiving, and distribution of CALM's long-term observations are integral components of the project. Collected measurements are provided by participants to the CALM office at UDel, where they are subsequently incorporated into several databases. The data are distributed through the program's website, and through data products produced by the Frozen Ground Data Center at the University of Colorado. This paper provides details about the nature, availability, and uses of data from the CALM network. Scientific results are presented regularly at national and international meetings and have been published widely in international scientific journals and symposia proceedings. Several edited volumes focused on the CALM program have been published to date (Brown et al. 2000, Nelson ed. 2004a, 2004b). Several papers focused on CALM appear elsewhere in these proceedings.

Distribution of Sites

The distribution of CALM observational sites in the Northern Hemisphere is shown in Figure 1. The CALM network incorporates sites in arctic, subarctic, antarctic, and mountainous regions. Several sites constitute longitudinal and latitudinal transects across northwestern North America, Europe, and the Nordic region, and northeastern and northwestern Russia. Sites in Europe, China, Mongolia, and Kazakhstan provide high-elevation locations. About 70% of the sites are located in arctic and subarctic lowlands underlain by continuous permafrost. Discontinuous and mountainous permafrost areas contain respectively 20% and 11% of sites. The distribution of sites is not uniform, a circumstance attributable to historical circumstances and logistical constraints. The sites were established in regions of extensive economic activity and/or in areas of long-term climatic, permafrost, and ecosystem research. This logistically driven approach to site selection was adopted to insure regularity and periodicity of measurements. Assessment of the representativeness of the CALM network with respect to climatic and environmental conditions is currently in progress, and initial results were reported by Anisimov et al. (2007).

Monitoring Procedures

Three methods are used to determine the thickness of the active layer: (1) Mechanical probing using a graduated metal rod; (2) temperature measurements; (3) frost/thaw tubes.

The method-specific measurement procedure adopted by the CALM program is described in detail at the CALM web site (www.udel.edu/Geography/calm) and by Brown et

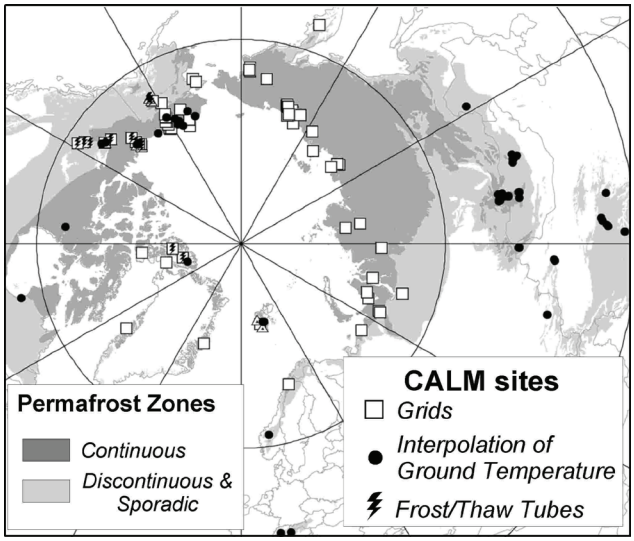

Figure 1. Permafrost distribution and location of CALM sites in the Northern Hemisphere. Sites are grouped according to active layer monitoring methods.

al. (2000). At 86 of the sites the active layer is measured by mechanical probing on regular grids of sampling points ranging from 10×10 m to 1000×1000 m. The time of probing varies from mid-August to the end of September; i.e., when thaw depth is at or near the maximum. More frequent measurements are made at some sites and in some years. The gridded sampling design allows for analysis of intra- and inter-site spatial variability and yields information useful for examining interrelations between physical and biological parameters. Grids are established at undisturbed locations characteristic of dominant environmental conditions. Their size varies depending on site geometry and the level of natural variability of surface and subsurface conditions. In general, 10×10 m to 100×100m size grids are established within relatively homogeneous landscape units. Several sites contain a number of grids representing various landscape units within the area. The 100×100 m to 1000× 1000 m grids usually encompass several characteristic landscapes within the area. CALM adopts a systematic sampling scheme for thaw depth measurements on most grids. The effectiveness of this sampling strategy has been investigated extensively and compared with alternative designs (Nelson et al. 1999). The systematic sampling design involves annual replicate measurement at regularly spaced grid nodes. With a few exceptions, each 10, 100, and 1000 m side grid contains 121 nodes distributed evenly at 1, 10, and 100 m spacing respectively. At some grid nodes thaw depth measurements are not possible due to deep water, roads, or gravel pads. These missing data points are not reported.

At 87 of the sites active layer thickness is determined exclusively by interpretation of ground temperature measurements, obtained by an array of thermistors distributed vertically from the ground surface downward into the permafrost (Romanovsky & Osterkamp 1997, Romanovsky et al. 2003). This method is primarily used in mountain regions and areas with deep (>1.5 m) annual thaw propagation, where spatially oriented measurements by probing are impossible. The depth and spacing of thermistor installation depends on local conditions and the needs of individual research projects.

Liquid- or sand-filled thaw tubes (Nixon & Taylor 1998, Nixon 2000) are employed in 11 Canadian and 3 Alaskan sites. When read periodically, frost tubes provide information about seasonal progression of thaw and maximum seasonal thaw. However, as with temperature measurements, thaw tubes do not provide the information on local variability. Individual thaw tube measurements are highly dependent on location of installation. To address this deficiency, thaw tube measurements are complemented by grid sampling of the active layer.

Data Availability

One of CALM's primary objectives is to develop coherent, quality-controlled datasets of long-term observations on the active layer and upper permafrost, suitable for assessing changes in polar terrestrial ecosystems. At present, the CALM database consists of annual submissions from 168 sites, and includes ALT, soil temperature and moisture (where available), and heave/subsidence data (where available). The majority of available data are distributed through the CALM website maintained by the University of Delaware's Department of Geography. (www.udel.edu/Geography/calm). The web-based summary table contains average ALT at all stations for all years and is linked to metadata and individual data sets. The following subsections provide a brief inventory of available data for specific geographic regions.

Alaska

At 30 out of 41 CALM-designated sites in Alaska periodic active layer observations are conducted on regular grids ranging from 10 m to 1000 m on a side. Geographically, grids are arranged in three north-south transects: (1) Fairbanks to the Beaufort Sea, along the Trans-Alaska Pipeline; (2) Ivotuk to Barrow (Chukchi Sea), and (3) Council and Kougarok, across the Seward Peninsula. These latitudinal transects, positioned from the Bering Sea eastward, encompass areas of steadily increasing continentality from west to east. For 25 of the grids, 10 or more years of consecutive active layer data are available. These include seven sites with 1 km^2 grids (Hinkel & Nelson 2003, Streletskiy et al. 2008), 15 1 ha grids, and three transects with thaw tubes. Two 1 km^2 grids in the Seward Peninsula (Council and Kougarok) and one near Ivotuk have data records dating to 1999. The 1 ha grid at Farmers Loop north of Fairbanks was added to the network in 2005. Pre-1990 data are available for a series of 20 10×10 m Cold Region Research and Engineering Laboratory (CRREL) plots near Barrow (1962–1970, and 1991–2007) and two sites in interior Alaska (Perl Creek, 1969–2007, and Wickersham Dome, 1975–2007).

All grids have data loggers for monitoring air and soil temperatures at various depths. Several sites have installations for continuous monitoring of soil moisture. Detailed spatial

characterization of topography and surface and subsurface conditions are available for each spatially heterogeneous 1 km^2 grid. These include DEMs, vegetation, soil, and landform characterization, and organic layer thickness. Annual spatial snow surveys have been conducted at the Barrow 1 km^2 grid, beginning in 1995. In 2000, spatially oriented monitoring of frost heave and thaw subsidence using the Differential Global Positioning System (DGPS) was initiated at three sites representing broad landscape units characteristic of the North Slope of Alaska (Little et al. 2003).

An additional eleven U.S. Geological Survey sites have been established near deep boreholes. At these sites active layer thickness is determined by interpolation of ground temperature measurements. Data from these sites are currently being processed.

Canada

Of the 21 active CALM-designated sites in Canada, 15 are located along the latitudinal transect situated in the Mackenzie River Valley and operated by federal government agencies: Geological Survey of Canada (Nixon et al. 2003) and Agriculture and Agri-Food Canada (Tarnocai 1995, Tarnocai et al. 2004). Several additional long-term, active layer monitoring programs include CALM sites on the Arctic Islands (four sites), and two sites in the Hudson Bay region (Allard et al. 1995, Smith et al. 2001). The spatial active layer observations on grids are conducted at twelve 1 ha and one 1 km^2 grids. The most comprehensive data sets are available for eight 1 ha grids in the Mackenzie River Valley. The data include 10 or more years of active layer observations on grids and thaw tubes, spatial characterization of subsurface conditions (organic layer thickness, organic composition, mineral strata), and several annual snow surveys.

Nordic region

The seven Nordic CALM sites are located in several areas surrounding the North Atlantic: two 1 ha grids in northeast Greenland at Zackenberg; one 1 ha grid in west Greenland on Disko Island (Christiansen 2004); 1 ha grid on the west coast of Svalbard at Kapp Linne (Akerman 1980); four transects constitute two sites at Calypostranda, Svalbard (Repelewska-Pekalowa & Pekalowa 2004); and an alpine-subarctic 1 ha grid in the vicinity of Abisko, northern Sweden. With the exception of Disko and one of the Calypostranda sites, the active layer record for the Nordic region grids is available for 10 or more years. The record for the Abisko site extends back to 1972 and includes thickness of active layer in different landscapes, mean monthly air temperature, and degree days of thawing. The Zackenberg database includes weekly active layer observations for the 1996–2006 thawing periods and snow thickness surveys for selected years.

Russia

Of the 41 CALM sites in Russia, 31 have continuous periodic active layer monitoring. The remaining 10 were either discontinued or are visited only sporadically. All Russian sites have grids ranging from 100 m^2 to 1 km^2. Several sites have supplemental transects that pre-date the establishment of CALM. The Russian CALM network extends from the European tundra of the Pechora and Vorkuta regions to West Siberia and the Lena Delta, eastward to the lower Kolyma River, and to Chukotka and Kamchatka. Most of these sites are within the continuous permafrost zone.

European North: Three 1 ha grids are located in the discontinuous permafrost region of the European tundra: Ayach-Yakha and Talnik near Vorkuta, and Bolvansky in the Pechora lowlands (Mazhitova et al. 2004). Each site has 7 to 11 years of continuous active layer record. The auxiliary data include detailed soil and vegetation characterization, soil temperature, and soil moisture records. Since 1999 periodic, spatially oriented frost heave and ground subsidence measurements using optical leveling are conducted at the Ayach-Yakha site.

West Siberia: Eight active CALM sites are located in West Siberia. The core of the data sets consists of observations from two 1 ha grids at Mare Sale and Vaskiny Dachi in the continuous permafrost zone and 1km^2 Nadym grid in the discontinuous zone (Vasiliev et al. 2008). The active layer observations for Mare Sale are available since 1978 and for Nadym since 1972. The active layer record at the Vaskiny Dachi site dates to 1991. Pre-CALM (1993) observations were performed at the environmentally homogeneous 10 × 10 m plots, and along several transects incorporating the dominant landscape units. Each site has continuous soil temperature records of variable length and detailed spatial landscape, soil, and vegetation characterizations. An additional 1 ha site was established in the continuous permafrost zone in 2005 (Zepalov et al. 2008). During the summer of 2007 four grids were established in the discontinuous permafrost zone in landscapes inadequately represented by the Nadym grid. At present these sites are in the process of being characterized and instrumented.

Central Siberia: In association with the GEWEX Asian Monsoon Experiment (GAME) program in the Siberian Arctic, a 1 km^2 CALM grid was established in 1997 near Tiksi, on the Lena River (Watanabe et al. 2003). The site-specific data base is available in the GAME Siberia website (http://www.hyarc.nagoya-u.ac.jp/game/siberia/index.html). Thaw depth measurements are also available for two 1 ha grids representing different landscapes of the Lena delta since 2004.

Lower Kolyma River: Beginning in 1996, a series of fifteen 1 ha grids spanning a distance of approximately 300 km was established to represent characteristic climatic and environmental conditions in the Kolyma-Indigirka lowlands on the northeast Eurasian tundra (Fyodorov-Davydov et al. 2004). At present, 11 sites are reporting data. Annual active layer and soil temperature observations are carried out at the five most accessible sites situated in close proximity to the North-East Scientific Station in Cherskyi in the transitional zone between taiga and tundra. Logistical problems led to some interruptions in observations at the remaining six sites. All sites have detailed descriptions of surface and subsurface conditions.

Chukotka and Kamchatka Peninsulas: Beginning in 1996, a Mt. Dionisy site was established on the Chukotka Peninsula. A new site was initiated at Lavrentia along the Chukchi Sea coast in 2000 (Zamalodchikov et al. 2004). Both sites consist of 1 ha grids. Annual soil moisture observations and detailed soil characterizations are available for the Lavrentia site. Active layer records are also available for two 1 ha grids on Kamchatka since 2003.

Mongolia

The Mongolian network consists of a series of instrumented boreholes located in the arid land permafrost at the southern fringe of the Siberian permafrost zones. An original network of 12 sites (Sharkuu 2003) was expanded to 37 sites during the last 2–5 years. The majority of the new sites are located in the Hovsgol region. Seventeen boreholes were drilled with depths ranging from 5 to 80 m, and two deep boreholes from the mid-1980s were instrumented for permafrost and active layer monitoring. An additional eight sites were instrumented for shallow ground temperature monitoring (Sharkhuu et. al. 2007). All sites report ground temperature and active layer thickness determined by interpolation of ground temperature profiles obtained in late September and early October.

Mountain permafrost regions

Permafrost occurs in all mountainous regions of the high latitudes and is widespread at higher elevations in mid latitude mountain ranges including the Qinghai-Tibet Plateau. The mountain permafrost is represented in the CALM data base by one site in Norway, one site in Svalbard (Isaksen et al. 2007), two sites in Switzerland (Harris et al. 2001), two sites in Kazakhstan (Marchenko et al. 2007), and six sites on the Qinghai-Tibet Plateau, China (King et al. 2006). All sites consist of boreholes of variable depth. With the exception of Kazakhstan sites, only interpolated active layer values are reported annually.

Southern Hemisphere

The Antarctic Permafrost and Soils (ANTPAS) program (Parsons et al. 2008) incorporates several sites known collectively as CALM-South (CALM-S). Periodic ground temperature monitoring at depths to 2.4 m is conducted at three sites in South Victoria Land, Antarctica and at two others on Livingston Island/South Shetland Islands (Hauck et al. 2007). Data are reported as interpolated maximum annual thaw depth. Detailed site descriptions are available at the ANTPAS website (http://erth.waikato.ac.nz/antpas/). Plans to expand ANTPAS /CALM-S by developing 12 to 15 sites distributed across environmental gradients from the Andes to the subantarctic islands and through the Antarctic Peninsula and Transantarctic Mountains to the McMurdo Dry Valleys are currently under development (Bockheim 2005).

Regional Active Layer Characterization

Several regions with large assemblages of sites and representative of high-latitude climatic/landscape gradients are suitable for spatial data integration. Examples are the North West Siberia region (Yamal-Gydan Peninsulas), the Lower Kolyma River, northcentral Alaska, and the Mackenzie River region (Canada). Each of these regions has been the subject of extensive geocryological research and contains information sufficient to facilitate regional-scale mapping.

At present the CALM database contains two regional (broad-scale) active layer maps compiled from data sampled from multiple sites. The first is a 14-year series of maps (1 km^2 resolution) depicting annual active layer thickness and the probability of the active layer exceeding certain thresholds for the 27,000 km^2 Kuparuk Region in northcentral Alaska (Shiklomanov & Nelson 2002, Anisimov et al. 2002). The second regional compilation is a detailed digital landscape and active layer map of northern West Siberia. The map was compiled in cooperation with the Earth Cryosphere Institute (Russia) and depicts a hierarchy of landscapes units, organic layer thickness, lithology, and the landscape-specific characteristic values of active layer thickness. At present the map is being refined and extended.

Several other regional maps are under construction, including an active layer map for the Kolyma-Indigirka lowlands of Russia, a map of the North Atlantic region, and a map of the Barrow Peninsula on Alaska's North Slope.

Data Use for Models

Active layer observations and auxiliary information from the CALM network provide an extensive circumpolar database which has been used extensively to validate process-based geocryological (e.g., Oelke & Zhang 2003, Shiklomanov et al. 2007) and hydrological (Rawlins et al. 2003) models. Obviously, data obtained from individual observational CALM sites should be used with caution for evaluating model-produced gridded fields, owing to possible discrepancies between the size of observation plots and those of model grid cells. It is well known that active layer thickness and other near-surface permafrost parameters can be highly variable in time and space (e.g., Nelson et al. 1998, Shiklomanov & Nelson 2002). Observational locations may not represent generalized conditions prescribed for the model's grid cells. The use of individual CALM grids or groups of grids representing the diversity of environmental conditions in particular regions can compensate somewhat for such deficiencies. The development/implementation of regional scaling approaches addresses the problem of discordance in resolution between empirical and simulation studies further, and facilitates development of procedures for assimilating geocryological data and modeling results. Shiklomanov et al. (2007) provided an example of a hierarchical approach for evaluating spatial permafrost models. The methodology incorporates empirical data from point locations and observational plots provided through the CALM observational networks, provides regional characterization of permafrost conditions, and can be extended with continental- and circumpolar-scale models.

Conclusions

CALM is the oldest and most comprehensive permafrost-oriented international global-change monitoring program, and has achieved considerable success in this role. Although the CALM network continues to grow in terms of the number of participating sites and the quantity and quality of observations, two outstanding data issues remain to be resolved: (1) Continuation of periodic measurements; this problem relates to difficulties associated with unattended operation of scientific equipment at remote locations and periodic accessibility of sites. For example, approximately one-fourth of Russian sites were discontinued during the last five years due to substantial increases in logistical costs. A large number of sites have suffered from equipment malfunction and vandalism; (2) The methodology of simple sharing of basic data, adopted by CALM in the late 1990s, does not entirely satisfy the growing needs of the increasingly international and interdisciplinary scientific community and general public. Newly developed web-based database and mapping applications provide more advanced, user-friendly vehicles for presenting and sharing geographically referenced information. The first step toward enhancing CALM's archival and dissemination strategies will be to prepare data for the upcoming Circumpolar Active layer Permafrost System (CAPS) Version 3 database compilation developed by the Frozen Ground Data Center and Standing Committee for Data Information and Communication within the IPA (Parsons et al. 2008).

Acknowledgments

The components of the CALM program operating in Alaska, Russia, Mongolia, and Kazakhstan have been supported though the U.S. National Science Foundation's Office of Polar Programs under grants OPP-9732051 to the University of Cincinnati and OPP-0352958 to the University of Delaware. Opinions, findings, conclusions, and recommendations expressed in this paper are those of the authors and other CALM investigators and do not necessarily reflect the views of the National Science Foundation. Transitional (one year) support between USA/NSF grants was provided by the University of Delaware's Center for International Studies. Financial support for CALM activities in other locations has been provided by governmental agencies in the countries of the various CALM investigators. CALM is a collaborative global-change monitoring program and could not exist without good will, generosity, and a spirit of cooperation from scientists from many nations and scientific disciplines.

References

Akerman, J. 1980. *Studies on Periglacial Geomorphology in West Spitsbergen*. Meddelanden Fran Lunds Universitets Geografiska Institution Avhandlingar, 89: 1-297.

Anisimov, O.A., Lobanov, V.A., Reneva, S.A., Shiklomanov, N.I., Zhang, T. & Nelson F.E. 2007, Uncertainties in gridded air temperature fields and effects on predictive active layer modeling. *Journal of Geophysical Research* 112: F02S14, doi:10.1029/2006JF000593.

Anisimov, O.A., Shiklomanov, N.I. & Nelson, F.E. 2002. Variability of seasonal thaw depth in permafrost regions: a stochastic modeling approach. *Ecological Modeling* 153: 217-227.

Bockheim, J. 2005. *International Workshop on Antarctic Permafrost and Soils: Final Report*. November 14-18, 2004, University of Wisconsin, Madison, WI (http://erth.waikato.ac.nz/antpas/pdf/FIN_REP_Ant_Wk3.pdf) , 84 pp.

Brown, J., Hinkel, K.M. & Nelson, F.E. 2000. The circumpolar active layer monitoring (CALM) program: Research designs and initial results. *Polar Geography* 24(3): 165–258.

Christiansen, H.H. 2004. Meteorological control on interannual spatial and temporal variations in snow cover and ground thawing in two northeast Greenlandic Circumpolar-Active layer-Monitoring (CALM) sites. *Permafrost and Periglacial Processes* 15(2): 155-169.

Fyodorov-Davydov, D.G., Sorokovikov, V.A., Ostroumov, V.E., Kholodov, A.L., Mitroshin, N.S., Mergelov, I.A., Davydov, S.P., Zimov, S.A. & Davydova, A.I. 2004. Spatial and temporal observations of seasonal thaw in the Northern Kolyma Lowland. *Polar Geography* 28(4): 308-325.

Harris, C., Haeberli, W., Vonder Muehll, D. & King, L., 2001. Permafrost monitoring in the high mountains of Europe: The PACE Project in its global context. *Permafrost and Periglacial Processes* 12: 3-11.

Hauck, C., Vieira, G., Gruber, S., Blanco, J. & Ramos, M. 2007. Geophysical identification of permafrost in Livingston Island, maritime Antarctica. *Journal of Geophysical Research* 112: F02S19, doi:10.1029/2006JF000544.

Hinkel, K.M. & Nelson, F.E. 2003. Spatial and temporal patterns of active layer thickness at Circumpolar Active Layer Monitoring (CALM) sites in northern Alaska, 1995-2000. *Journal of Geophysical Research* 1089(D2): 8168.

Isaksen, K., Sollid, J.L., Holmlund, P. & Harris C. 2007. Recent warming of mountain permafrost in Svalbard and Scandinavia. *Journal of Geophysical Research* 112: F02S04, doi:10.1029/2006JF000522.

King, L., Herz, T., Hartmann, H., Hof, R., Jiang, T., Ke, C., Wei, Z., Liu, J. & Yi, C. 2006. The PACE monitoring strategy: A concept for permafrost research in Qinghai-Tibet. *Quaternary International* 154: 149-157.

Klene, A.E. 2005. *Climate and Urbanization in Barrow, Alaska*. Ph.D. Dissertation. Department of Geography. Newark, DE: University of Delaware.

Little, J., Sandall, H., Walegur, M. & Nelson, F.E. 2003. Application of differential GPS to monitor frost heave and thaw settlement in tundra environments. *Permafrost and Periglacial Processes* 14(4): 349-357.

Marchenko, S.S., Gorbunov, A.P. & Romanovsky, V.E. 2007. Permafrost warming in the Tien Shan Mountains, Central Asia. *Global and Planetary Change* (3-4): 311-327.

Mazhitova, G., Malkova, G., Chestnykh, O. & Zamolodchikov, D. 2004. Active layer spatial and temporal variability at European Russian circumpolar-active-layer-monitoring (CALM) sites. *Permafrost and Periglacial Processes* 15(2): 123-139.

Nelson, F.E., Shiklomanov, N.I., Christiansen, H.H. & Hinkel, K.M. 2004a. The circumpolar-active-layer-monitoring (CALM) Workshop: Introduction. *Permafrost and Periglacial Processes* 15: 99-101.

Nelson, F.E., Shiklomanov, N.I., Hinkel, K.M & Christiansen, H.H. 2004b. The Circumpolar Active Layer Monitoring (CALM) Workshop and the CALM II Program: Introduction. *Polar Geography* 28(4): 253-266.

Nelson, F.E., Shiklomanov, N.I. & Mueller, G.R. 1999. Variability of active-layer thickness at multiple spatial scales, North-Central Alaska, U.S.A. *Arctic, Antarctic, and Alpine Research* 31(2): 179-186.

Nixon, F.M. 2000. Thaw-depth monitoring. The Physical Environment of the Mackenzie Valley, Northwest Territories: a Base Line for the Assessment of Environmental Change. *Geological Survey of Canada Bulletin* 547, 119-126.

Nixon, F.M. & Taylor, A.E. 1998. Regional active layer monitoring across the sporadic, discontinuous and continuous permafrost zones, Mackenzie Valley, northwestern Canada. In: Lewkowicz, A. G. and Allard, M. (eds.), *Proceedings of the Seventh International Conference on Permafrost.* Quebec: Centre d'Etudes nordiques, Universite Laval, 815-820.

Oelke, C. & Zhang, T. 2003. Comparing thaw depths measured at CALM field sites with estimates from a medium-resolution hemispheric heat conduction model. *8th International Conference on Permafrost: Extended Abstracts on Current Research and Newly Available Information.* Zurich, Switzerland: Department of Geography, University of Zurich, 117-118.

Rawlins, M.A., Vorosmarty, C.J., Lammers, R.B., Frolking, S. & Fekete, B.M. 2003. Simulating pan-Arctic runoff with a macro-scale terrestrial water balance model. *Hydrological Processes* 17(13): 2521-2539.

Repelewska-Pêkalowa, J. & Pêkala, K. 2004. Active-Layer Dynamics at the Calypsostranda CALM Site, Recherche Fiord Region, Spitsbergen. *Polar Geography* 28(4): 326-340

Romanovsky, V.E. & Osterkamp, T.E. 1997. Thawing of the active layer on the coastal plain of the Alaskan Arctic. *Permafrost and Periglacial Processes* 8:1-22.

Romanovsky, V.E., Sergueev, D.O. & Osterkamp, T.E. 2003. Temporal variations in the active layer and near-surface permafrost temperatures at the long-term observatories in northern Alaska. *Proceedings of the Eighth International Conference on* Permafrost, vol. 2. Lisse, A.A. Balkema, 989-994.

Sharkhuu A., Sharkhuu, N., Etzelmüller, B., Heggem, E.S.F., Nelson, F.E., Shiklomanov, N.I., Goulden, C.E. & Brown J. 2007. Permafrost monitoring in the Hovsgol mountain region, Mongolia, *Journal of Geophysical Research* 112: F02S06, doi:10.1029/2006JF000543.

Sharkhuu, N. 2003. Recent changes in the permafrost of Mongolia. *Proceedings of the Eighth International Conference on Permafrost*, 2. Lisse: A.A. Balkema, 1029-1034.

Shiklomanov N.I., Anisimov, O.A., Zhang, T., Marchenko, S.S, Nelson, F.E. & Oelke C. 2007, Comparison of model-produced active layer fields: Results for northern Alaska. *Journal of Geophysical Research* 112, F02S10, doi:10.1029/2006JF000571.

Shiklomanov, N.I. & Nelson, F.E. 2002. Active-layer mapping at regional scales: a 13–year spatial time series for the Kuparuk Region, north-central Alaska. *Permafrost and Periglacial Processes* 13: 219-230.

Streletskiy, D.A., Shiklomanov, N.I., Nelson, F.E. & Klene, A.E. 2008. Long-term active and ground surface temperature trends: 13 years of observations at Alaskan CALM sites. *Proceedings of the Ninth International Conference on Permafrost, Fairbanks, Alaska, June 29–July 3, 2008* (this proceedings).

Vasiliev, A.A., Leibman, M.O. & Moskalenko, N.G. 2008. Active layer monitoring in West Siberia under the CALM II program. *Proceedings of the Ninth International Conference on Permafrost, Fairbanks, Alaska, June 29–July 3, 2008* (this proceedings)

Watanabe, K, Kiyosawa, H., Fukumura, K., Ezaki, T. & Mizoguchi, M. 2003. Spatial and temporal variation in thaw depth in Siberian tundra near Tiksi. *Proceedings of the Eighth International Conference on Permafrost*, 2. Lisse: A.A. Balkema, 1211-1216.

Zamolodchikov, D.G., Kotov, A.N., Karelin, D.V. & Razzhivin, V.Y. 2004. Active-Layer Monitoring in Northeast Russia: Spatial, Seasonal, and Interannual Variability. *Polar Geography* 28(4): 286-307

Zepalov, F.N., Grebenets, V.I., Streletskiy, D.A. & Shiklomanov, N.I. 2008. Active-layer Monitoring at a New CALM Site, Taimyr Peninsula, Russia. *Proceedings of the Ninth International Conference on Permafrost, Fairbanks, Alaska, June 29–July 3, 2008* (this proceedings).

Evaluation of Recent Changes in the Ground Thermal State, Central Yakutia

P.N. Skryabin
Melnikov Permafrost Institute, SB RAS, Yakutsk, Russia
S.P. Varlamov
Melnikov Permafrost Institute, SB RAS, Yakutsk, Russia
Yu.B. Skachkov
Melnikov Permafrost Institute, SB RAS, Yakutsk, Russia

Abstract

Developing an understanding of permafrost evolution in relation to observed climatic warming requires evaluation of changes in the thermal state of near-surface layers. This paper is based on the results of 25 years of geothermal monitoring at 60 sites. The study is focused on the upper permafrost within the depth of annual temperature variation (10–15 m). The integrated research program involves landscape, microclimatic, thermophysical, and hydrothermal methods. Systematization and mapping generalization of permafrost landscapes have been made with indication of the complexity of geocryological conditions. During the last 30 years, the study area has experienced the highest increasing trend in mean annual air temperature in northern Russia. A database has been compiled that includes parameters needed for geocryological predictions. Proposals for cooperation in implementing IPY projects and establishing a single observational network for geocryological monitoring in cold regions of Russia are presented. Experimental research made it possible to quantitatively evaluate the interannual and perennial variability of the active layer thickness and thermal state of the ground within the depth of annual temperature variations.

Keywords: climate; monitoring; permafrost landscapes; temperature regime.

Introduction

Research on the impact of climate warming on permafrost involves a wide variety of issues, including the thermal evolution of upper permafrost. The ground thermal regime is controlled by energy exchange between the ground and atmosphere and is characterized by spatial and temporal variability. Anthropogenic impacts of varying type and magnitude (clear-cutting, fires, removal of surface vegetation and organic mat, etc.) disturb the natural ground thermal state, trigger adverse cryogenic processes and change the ecology of environmental complexes.

In recent years, the development of research on predicted climate warming in many countries has led to an increasing interest in the response of permafrost to projected warming. It may be said without exaggeration that this problem has become one of the most important issues in geocryological research, both in scientific and practical terms.

Most of the research on this problem has been conducted in northern regions of Russia, Canada, Alaska, and Europe (Pavlov 1994, Varlamov et al. 1990, Burgess & Lawrence 1997, Osterkamp et al. 1994, Harris et al. 2000).

Central Yakutia is a region characterized by complicated geocryological conditions, such as continuous permafrost and the presence of water-bearing taliks and polygonal wedge ice. Continuous monitoring of the thermal regime of the ground, which has been implemented by the authors since 1981, illustrates the dynamics of its thermal state in natural and disturbed landscapes. The research project statement and the results of the first stages of its implementation were set out in the authors' early publications (Skryabin et al. 1998, 2001, Varlamov et al. 2002). This report presents a summary of the results obtained during the entire period of observations.

Objectives and Methods of Research

Investigations are conducted on the west and east sides of the Lena River at the latitude of Yakutsk which are characterized by complicated permafrost conditions. Evaluation of changes in thermal state of near-surface layers of permafrost within the frameworks of climatic warming and man-caused impacts (fires, deforestation, embankment), was effected based on integrated data, acquired from regular observations in Chabyda and Yakutsk stations, sites in Tuymaada Valley, and in the northern section of the prospective Tommot-Yakutsk railroad (Fig. 1).

The basis for this research is the variation in temperatures for shallow soils (upper 10–15 m). The main thermal parameters which can indicate an evolution of near-surface layers of permafrost are: seasonally thawed layer thickness (X) and mean annual temperature at corresponding depth (T_x) and at the depth of zero annual amplitude (T_o). It is known that interannual changes in these parameters depend on peculiarities of climatic features (air and surface temperature, precipitation amount, snow depth and density) and terrain conditions (vegetation and ground cover, soils composition, ground water, etc.). The research area shows X variations from 0.5 to 4 meters, and T_0 variations from 0.5 to -6.0°C, depending on terrain conditions.

Experimental observations of varied duration have been carried out since 1981 at 200 localities covering 6 physiographic regions, 9 landscape types, and more than 100 stows. The research involves a variety of integrated

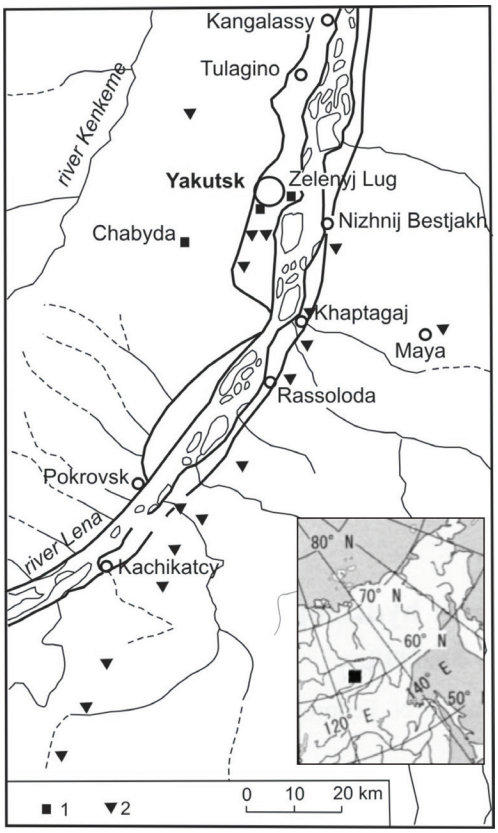

Figure 1. Map of the study area: 1 – stations, 2 – monitoring sites.

techniques and tools used in studying landscape, climate, thermal physics, as well as hydrothermal studies. The project implementation included remote and ground-based sensing of the landscapes, their classification, and mapping summary. The following terrain types were identified in the area covered: flood plain, low-terrace, sand ridge, inter-ridge depression, alas, inter-alas, small valley, upland, and slope.

Long-term records from the nearest weather stations are employed during the study. Snow surveys are carried out in representative permafrost landscapes. The texture and properties of the active layer were determined in test pits. Information on the composition and structure of permafrost soils was obtained from boreholes. Active layer depths are determined by pit measurements, probing with a steel rod, and from soil temperature profiles. To measure temperatures at the snow surface, at the surface and base of the surface vegetation, and in the ground, thermistor and thermocouple sets and cables were used. After installing the cables, the holes were backfilled. Ground temperatures were taken with an accuracy of ± 0.1°C.

Investigations at the Chabyda station included measurements of climatic parameters (air temperature, wind speed, precipitation, evaporation, and snow depth and density) and ground hydrothermal parameters (snow and ground surface temperatures, ground temperature, heat flows, thermal properties of surface covers and ground, and freeze-thaw depths). During the intensive observation period, measurements were made 7 times daily in the warm seasons of 1981 and 1982 and 4 times a day in the cold season of 1982–1983. In the following years, observations were taken once every pentad at 4 standard times and then 1 to 3 times monthly. Since November 1987, measurement frequencies have been reduced at the Chabyda, Yakutsk, and Tyumaada stations, and measurements are now taken on the 15th day of each month. On the east side of the Lena River, observations are made once or twice in the warm and cold seasons. The total number of monitoring locations on the east side of the Lena River is 60.

Results

Central Yakutia is among the areas in Russia that have experienced the highest increasing trends in mean annual air temperature over the last 30 years (up to 0.07°C/yr). Warming of the climate, which was slight in the 1960–1970s became significant in the 1980s. The last decade (1998–2007) has been the warmest in the instrumental record for the region. At Yakutsk, mean annual air temperature increased at a rate of 0.06°C/yr between 1982 and 2007. Mean annual air temperatures were below the normal of -10°C (USSR Hydrometeorological Service 1989) only in four of the last 25 years. All other years were consistently warmer (Fig. 2a).

The rise of the mean annual air temperature is primarily associated with the increasing number of anomalously warm winters which in turn is due to changes in atmospheric circulation. In the period 1982–2007, there were 19 winters with a freezing index higher than the long-term mean. The increase of summer air temperatures was less significant.

In this study, anomalous climatic seasons are defined as those with the average values of climate elements ($\Sigma(-T_{air})$, $\Sigma(+T_{air})$ and h_c^{max}) beyond the average standard deviation σ. If the value is within σ, but it is larger than ½ σ, the season is referred to as warm or cold, and low-snow or snowy. By average winter air temperature, there were 6 normal, 2 warm, 16 anomalously warm winters, and only 1 anomalously cold winter during the observation period. By snow depth, there were 11 normal, 5 anomalously snowy, 4 snowy, 3 low-snow, and 2 anomalously snowy winters.

Variations in X, T_x, and T_o have been studied over 25 years in the Chabyda station, west of the Lena River, where experimental sites were set on the bottom of a small valley (3a, 8a, and borehole 1), gentle slope (5), interfluve (7b), bottom of a drainage depression (8), watershed area (9), moderate north-facing slope (10), and moderate south-facing slope (11).

Active layer depth depends on weather conditions, vegetation, surface cover, soil type, and soil moisture. Interannual variability of active layer thickness is thought to be primarily controlled by the air thawing index and summer precipitation. However, investigations in northern Russia have found no clear correlation between the long-term variations in thaw depth and the air thawing index (Pavlov et al. 2004). Ground conditions, especially soil moisture variations, appear to have significant effects on thaw depth. Data from the Chabyda station indicate that the most

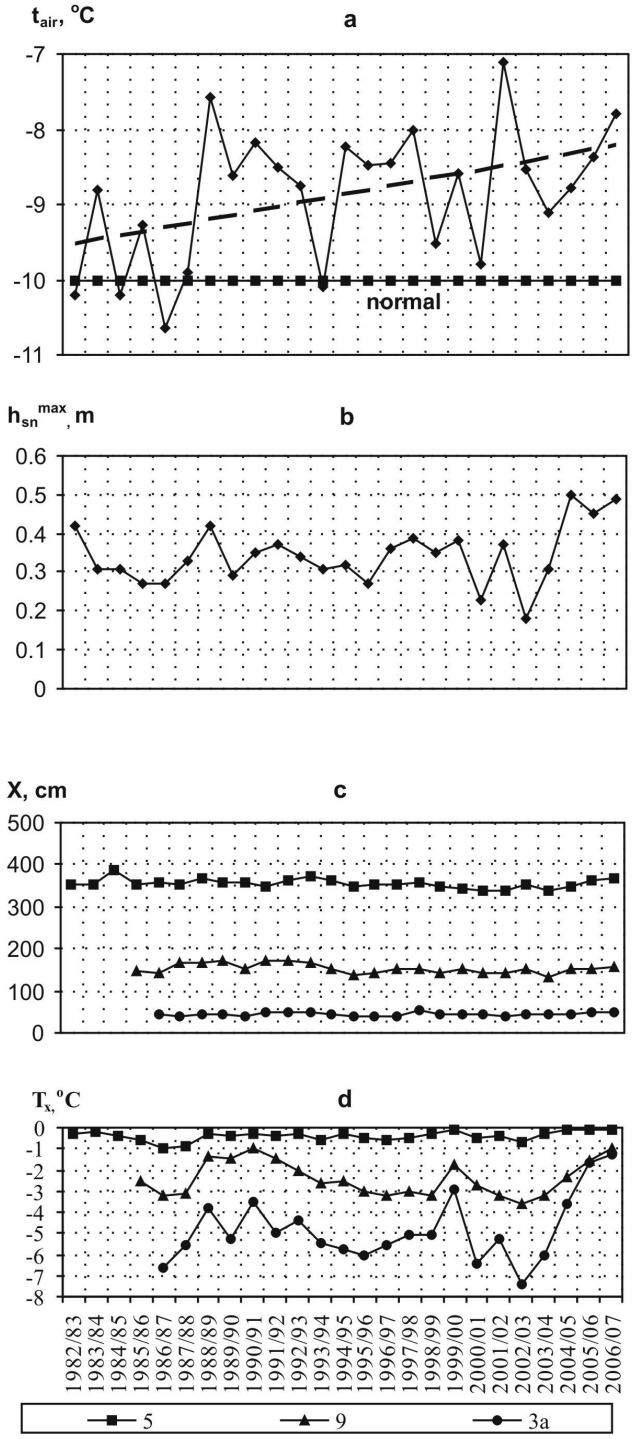

Figure 2. Long-term variations of mean annual air temperature at Yakutsk (a), maximum snow cover depth (b), active layer thickness (c), and mean annual ground temperature (d) in the small valley (3a – bottom of stream valley) and slope (5 – gentle slope, 9 – watershed area) terrain types at the Chabyda station.

significant interannual variations in X (up to 73 cm) occur in small valleys with organic soils. Slope sites on sandy soils show thaw depth variations of 30 to 58 cm. No statistically significant increasing trend in thaw depth has been observed for any of the sites. To the contrary, three sites (5, 6b, and 9) in the slope terrain type show a decreasing trend. The three longest series are given in Figure 2c to illustrate the interannual variations in active layer depth.

Table 1. Variations in mean annual ground temperature (T_x) and its trends in 1986-2007 at the Chabyda station.

Experimen. sites	Soil texture	Mean °C	Max °C	Min °C	Trend T_x, °C/10 yr
Slope terrain type					
5	Sand, sandy silt	-0.4	-0.1	-1.0	0.20
7b	Sandy silt, sand	-1.2	-0.4	-2.2	0.25
9	Sandy silt, clayey silt	-2.4	-1.0	-3.6	-0.10
10	Sandy silt, sand	-1.8	-0.7	-2.8	0.15
11	Sandy silt, sand	-1.0	-0.2	-2.2	-0.10
Small valley terrain type					
Bor. 1	Peat, sand	-2.7	-0.6	-5.1	0.10
3a	Peat, sand	-4.9	-1.3	-7.4	0.80
8	Sand	-3.7	-1.3	-5.5	0.45
8a	Peat, sand	-3.6	-0.1	-6.5	0.65

Depending on terrain and soil conditions, ground temperature is controlled by the same factors as is X. The interannual variation of ground temperature is predominantly related to winter weather factors, such as the air freezing index and snow cover. Table 1 illustrates the complete set of variations in T_x for the warmest and coldest terrain types.

Ground temperature is a better indicator of the long-term changes in the thermal state of near-surface permafrost compared to active layer thickness. The temperature variation was largest in the small-valley areas, as was the thaw depth fluctuation (Fig. 2d). This variation was mainly due to the effect of two winter factors: snow cover conditions and air freezing index. In the continental climate of central Yakutia the first factor appears to be more important. The lowest mean annual permafrost surface temperatures were observed in the winter of 2002–2003 which had an anomalously thin snow cover (see Fig. 2d). In subsequent snowy years (2004–2007) which had the largest snow depths in the last 25 years (0.45 to 0.50 m), the ground temperatures were warmest. Variation in T_x due to anomalous winter conditions can be as high as 1.2–3.5°C. One warm, low-snow winter will cool ground temperatures more than a cold, snowy winter. The effect of one anomalously cold winter will be stronger than that of a few successive anomalously warm winters. However, statistically significant trends in mean annual ground temperature have been observed only for four sites. A positive trend in T_x of 0.2°C per decade was found at site 5, and a negative trend of 0.1°C per decade at site 9. At a depth of 10 m, warming of 0.2°C per decade occurred at site 7b and cooling of 0.1°C per decade at site 9 and 0.1°C per decade at site 11.

On the east side of the Lena River, monitoring of the ground temperature regime has been conducted in 8 terrain

types during the last 20 years. The observations have identified the landscapes that are most sensitive to changes of climatic factors. The terrain units have been classified into three sensitivity categories, high, moderate and low, in the following order: small valley → inter-alas, inter-ridge depression, floodplain, slope → low terrace, sand ridge, alas, interfluve. Respective ranges of interannual T_o variations for these categories are 1.0–2.3°C; 0.2–1.2°C and 0.1–0.9°C.

Observational data from 1987 to 2006 show that the trend of mean annual temperatures at the depth of zero annual amplitude varies from negative to positive in different terrain types (Table 2). Negative trends are detected in low terrace, sand ridge, and inter-ridge depression terrain types (up to -0.02°C/yr), while positive trends occur in floodplain and small valley terrain (0.02–0.04°C/yr). Monitoring observations suggest that there is no uniform pattern in t_o variation, and lowering of ground temperature in some landscape units indicates their stability. In the Yakutsk area, snow depth, especially in the early winter, had been decreasing over 20 years until 2004, with a corresponding decrease in its warming effect. This factor, although not alone, has probably been decisive for the ground temperature evolution in the last 20 years. However, during the last three winters of 2005–2007, which had anomalously deep snow and warm air temperatures, there was a notable increase in ground temperature. For northern Alaska, Romanovsky et al. (2003) report increasing trends in air temperature and active layer thickness over the period of 1987 to 2001. Mean annual ground temperatures at several sites increased by 1–2°C over the 15-year period.

Experimental investigations were carried out in order to quantitatively evaluate the anthropogenic impact (ground cover disturbance and stripping, deforestation, fires, etc.) on the thermal regime of the ground in 40 stows within five terrain types.

At an alas site, snow and dwarf-birch/sedge tussock covers were removed in March 1989. This disturbance increased the active layer thickness by 0.4 m and the ground temperature at 10 m depth by 0.4°C (Br. 68 and 186 compared to the undisturbed site. Seven years later, the depth of seasonal thaw was 0.5 m deeper, and T_x was 2.7°C warmer than at the undisturbed site. At an inter-ridge depression site, a moss-lichen layer was stripped in July 1990. The mean annual ground temperature increased by 0.8°C in the second year and by 1.8°C in the third year after disturbance. The depth of seasonal thaw increased by 0.5 by the end of the first summer and by about 1 m, or 2.8 times, by the end of the second summer (Br. 205). At inter-alas sites supporting larch stands, the removal of a *Vaccinium vitis-idea*/moss cover resulted in an increase in upper permafrost temperature of 1 to 0.2°C. Thaw depths increased by less than 0.5 m (Br. 1601). Similar observations conducted from 1984 to 2000 along the Norman Wells oil pipeline in northern Canada indicate that thaw depths increased most rapidly in the first 7 years after disturbance and continued to increase slowly thereafter, reaching depths of 3 to 5 m in fine-grained and organic units and 5 to 7 m in coarse mineral soils (Burgess & Smith, 2003).

Table 2. Variations in mean annual ground temperature (T_0) and its trends in 1987–2006 in landscapes at the right-bank area of the Lena River.

Terrain type	Soil texture	Mean, °C	Max °C	Min °C	Trend T_0, °C/10 yr
Floodplain	Sand, sandy silt	-1.6	-0.8	-2.3	0.2
Low-terrace	Sand, sandy silt	-1.2	-0.1	-2.4	-0.2
Slope	Sand, sandy silt	-1.4	-0.3	-2.4	~0.0
Small valley	Peat, sandy silt	-5.2	-3.6	-6.9	0.4
Sand ridge	Sand	-0.9	0.7	-2.5	0.0…-0.2
Inter-ridge depression	Peat, sand	-2.4	-0.6	-4.1	-0.1…-0.2
Inter-alas	Sandy silt, Clayey silt	-1.4	-0.7	-2.2	~0.0
Alas	Peat, clayey silt	-0.4	-0.1	-0.8	~0.0

In sand-ridge terrain, clear-cutting of pine stands increased thaw depths by 1.8 m and ground temperatures by 1.0°C. In inter-alas terrain, clear-cutting of larch trees resulted in 1°C warming of ground temperatures after 3 years (Br. 12/93).

Removal of pine trees and lichen cover in warm soils (T_o = -0.1…-0.3°C) of well-drained sand ridges resulted in a dry talik (Br. 1324). Clearing of a pine/lichen/ *Arctostaphylos* stand in low-terrace terrain type caused an increase in T_o by 0.3°C and in X by 1 m (Br. 177).

At a sand-ridge site in pine forest burned by a fire in 1987, ground temperatures increased by 0.7–1.5°C during the first two years. From the fourth year after the fire, ground temperatures on the burn began to stabilize with vegetation regrowth. (Br. 13). In low-terrace terrain, the larch stand burned by a fire in 1986 was removed (Br. 166). A considerable increase in T_o, by 0.3–0.5°C, occurred in the first 5 years after the fire. The recovery of vegetation in 6-8 years stabilized the ground thermal state. In an inter-ridge depression, selective tree cutting, surface cover disturbance in 1988, and fire in 1993 (Br. 30) increased T_o by 0.3–1.0°C over 9 years. Gradual cutting of a burned larch stand in inter-alas terrain type resulted in a 1–1.5°C increase in T_o and a 0.7 m increase in thaw depth during 15 years (Br. 56). Selective tree cutting with surface cover disturbance after a 1986 fire in inter-alas terrain (Br. 209) resulted in warming of T_o in the first years. Vegetation recovery lowered ground temperatures (Fig. 3). The T_o difference over the 18-year period was 1.3°C.

Maximum impact on the thermal state of ground results from ground cover stripping and post-fire deforestation in inter-alas type terrain. In inter-alas where wedge ice occurs close to surface, a more intensive thermokarst activity is indicated. The dynamics of the ground thermal state at sites of anthropogenic activity demonstrate dependence on types of impact, their duration, and stages of revegetation during post-anthropogenic period. On the whole, the ground thermal

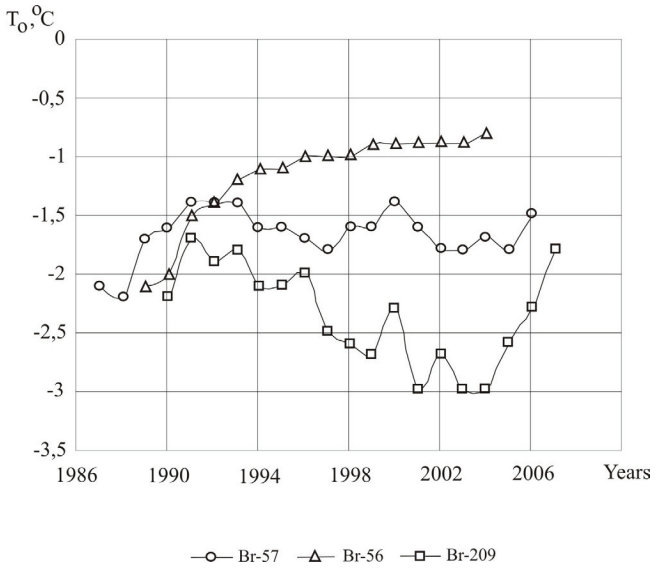

Figure 3. Variations of mean annual ground temperature in the inter-alas terrain unit: larch forest site (Br-57), site of gradual tree removal (Br-56) and burned site with recovering vegetation (Br-209).

state recovery after man-caused damage in sand ridge terrain type is mainly reversible, while in inter-alas type it is either reversible or not.

The database of facts, accumulated during a long period of time is comprised of the following: climatic features, natural and anthropogenic landscapes, content and structure of permafrost, ground cover temperature, temperature, water content ratio, and thermophysical characteristics of ground, seasonal thawing, temperature of water, and bottom sediments in lakes.

Further enhancement of the geothermal monitoring network utilizing automatic loggers is thought to have a great potential. This essential project's feasibility depends on joint Russian and international investigations, pooling human and material resources.

Conclusions

1. Change trends were identified for climate, active layer thickness, and temperatures of natural and anthropogenic landscapes.

2. Small valley and inter-alas terrain types are the most sensitive to man-triggered damage and climatic changes.

3. Long-term dynamics of the ground thermal state illustrate relatively high resistance to climate warming, due to a tendency towards a thinner snow cover during the first half of winter season and, as a result, a lower warming effect.

4. A database was created containing information on landscapes, frozen soils, climate parameters, and ground thermal state.

The results of this study are used in the design and construction of the northern section of the Tommot-Yakutsk railroad. Information obtained is also used in numerical modeling of ground temperature variations and in the Yakutian Permafrost GIS Project.

References

Burgess, M.M. & Lawrence, D.E. 1997. Thaw settlement in permafrost soils: 12 years of observations on the Norman Wells pipeline right of-way. *Proceedings of the Canadian Geotechnical Society Conference*, *Ottawa*: 77-84.

Burgess, M.M. & Smith, S.L. 2003. 17 years of thaw penetration and surface settlement observation in permafrost terrain along the Norman Wells pipeline, Northwest Territories, Canada. *Proceedings of the Eighth International Conference on Permafrost*, *Zurich*: 107-112.

Harris, C., Vonder Mohll, D. & Isaksen, K. 2000. The European pace project transect of instrumented permafrost boreholes: preliminary results of permafrost monitoring. *Abstracts Rhythms of Natural Processes in the Earth Cryosphere*, Pushcnino: 256.

Osterkamp, T.E., Zhang, T. & Romanovsky, V.E. 1994. Evidence for a cyclic variation of permafrost temperatures in Northern Alaska. *Permafrost and Periglacial Processes* 5: 137-144.

Pavlov, A.V. 1994. Current changes of climate and permafrost in the Artic and Sub-Artic of Russia. *Permafrost and Periglacial Processes* 5: 101-110.

Pavlov, A.V., Skachkov, Yu.B. & Kakunov, N.B. 2004. Interaction between long-term changes in seasonal thaw depth and meteorological factors. *Earth Cryosphere* VIII(4): 3-11.

Romanovsky, V.E., Sergueev, D.O. & Osterkamp, T.E. 2003. Temporal variations in the active layer and near-surface permafrost temperatures at the long-term observatories in Northern Alaska. *Proceedings of the Eighth International Conference on Permafrost, Zurich*: 989-994.

Skryabin, P.N., Skachkov, Yu.B. & Varlamov, S.P. 2001. Monitoring of thermal state of soils in Central Yakutia. *Proceedings of the Fifth International Study Conference on GEWEX in Asia and GAME (volume 1), Aich Trade Center, Nagoya, Japan*: 170-174.

Skryabin, P.N., Varlamov, S.P. & Skachkov, Yu.B. 1998. *Annual Variability of Ground Thermal Regime in Yakutsk Area.* Novosibirsk: SB RAS Press, 144 pp.

USSR Hydrometeorological Service. 1989. *Handbook on the USSR Climate, Vol. 24, Yakut ASSR, part 1*. Leningrad: Gidrometeoizdat, 608 pp.

Varlamov, S.P., Skachkov, Yu.B. & Skryabin, P.N. 1990. Interannual variability of ground thermal parameters at Chabyda station, Central Yakutia. In: *Permafrost Changes and Economic Development*. Yakutsk: Permafrost Institute Press, 68-75.

Varlamov, S.P., Skachkov, Yu.B. & Skryabin, P.N. 2002. *Ground Temperature Regime in Permafrost Landscapes, Central Yakutia.* Yakutsk: Permafrost Institute SB RAS Press, 216 pp.

Micromorphological Analyses of Main Genetic Permafrost Types in West Siberia

E.A. Slagoda
Earth's Cryosphere Institute, RAS, Russia
A.N. Kurchatova
Tyumen State Oil & Gas University, Russia

Abstract

The formation of the geomorphological structure on the northern West Siberian plain and the main genetic types of sediments were caused by Arctic Sea regressions during the Pleistocene-Holocene period. Postcryogenic features in the upper part of all terraces testify of climatic cooling in the Latest Pleistocene. During this stage, syngenetic freezing on sites of accumulation and epigenetic freezing of the earlier melted deposits had occurred. Syngenetic sediments are characterized by the postcryogenic voids associated with sedimentary lamination and complex morphology. Walls of voids are coated by clayish particles and iron hydroxides, and filled by oriented mineral grains. The research of epigenetic sediments has shown the deformed sublayers in the form of tongues and displacements of ground blocks. Micromorphological analyses for correlation of cryogenic events in the upper part of Cenozoic sediments sections should be based on the regional database of microtexture of different genetic permafrost types in West Siberia.

Keywords: micromorphological analyses; postcryogenic microtexture; syngenetic and epigenetic permafrost.

Introduction

The present two-layer permafrost on the northern West-Siberian Plain formed during the Late Pleistocene-Holocene. After Arctic Sea regressions, the marine clayish sediments drained and froze as epigenetic permafrost. They were partially transformed to an active layer in subaerial conditions and deeply thawed during the periods of climate warming or sea transgressions (Dubikov 2002). It is possible to distinguish the sequence of cryogenic events using micromorphological features of syngenetic and epigenetic sediments. Results of micromorphological analyses of the main genetic types of permafrost are presented in the report. Samples were taken from sediment sections of exposures and borehole cores (up to 30 m depth) located at the main geomorphological levels within the territory between Nadym and Pur Rivers and on Yamal Peninsula (Fig. 1). Fifty thin soil sections were studied in all.

Study Region

The terrain of the Nadym-Pur watershed is a plain gently inclined to the north and divided by several geomorphological levels consisting of marine and lacustrine-alluvial facies (Baulin et al. 1996, Dubikov 2002).

A flat, slightly wavy plain is located at an elevation of 65–90 m above see level and consists of the loamy Middle Pleistocene Salekhard Suite made of marine and glacial-marine genesis (m,gmQ_{II}^{2-4}). Sediments are characterized by non-clear lamination, lumpy structure, regular distribution, and inclusion of coarse-sized mineral grains, gravels, pebbles as well as sublayers and lenses of sand (Fig. 2, I). Frozen grounds have layered cryostructure. The thickness of ice layers changes from 0.2–4 cm. Thick layered kinds of cryostructure up to 5–6 cm thick have been observed at 4–10 m below the surface and deeper. Total water content in

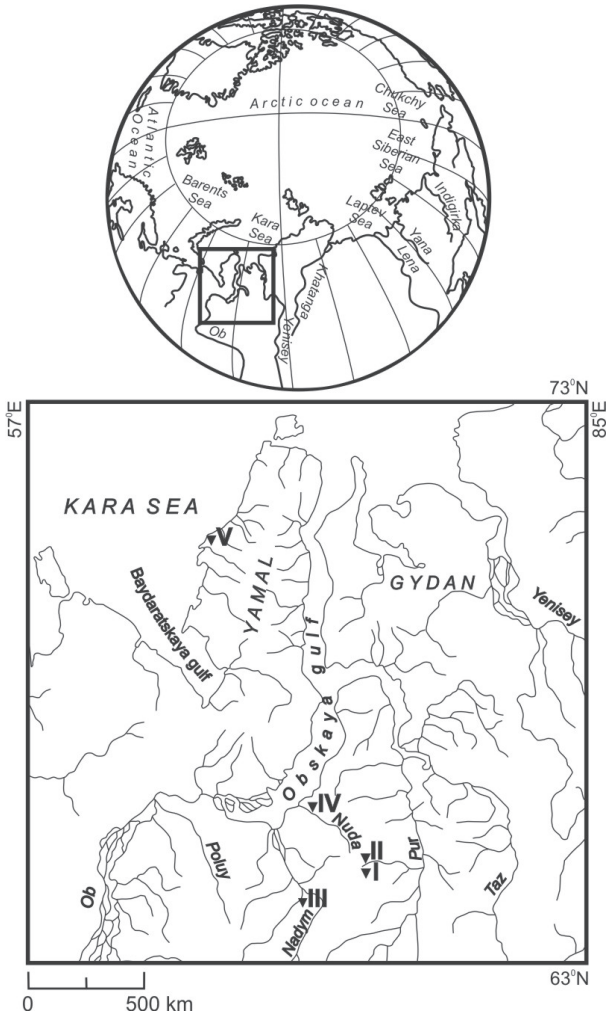

Figure 1. Location of the working sites (I-V) within research area.

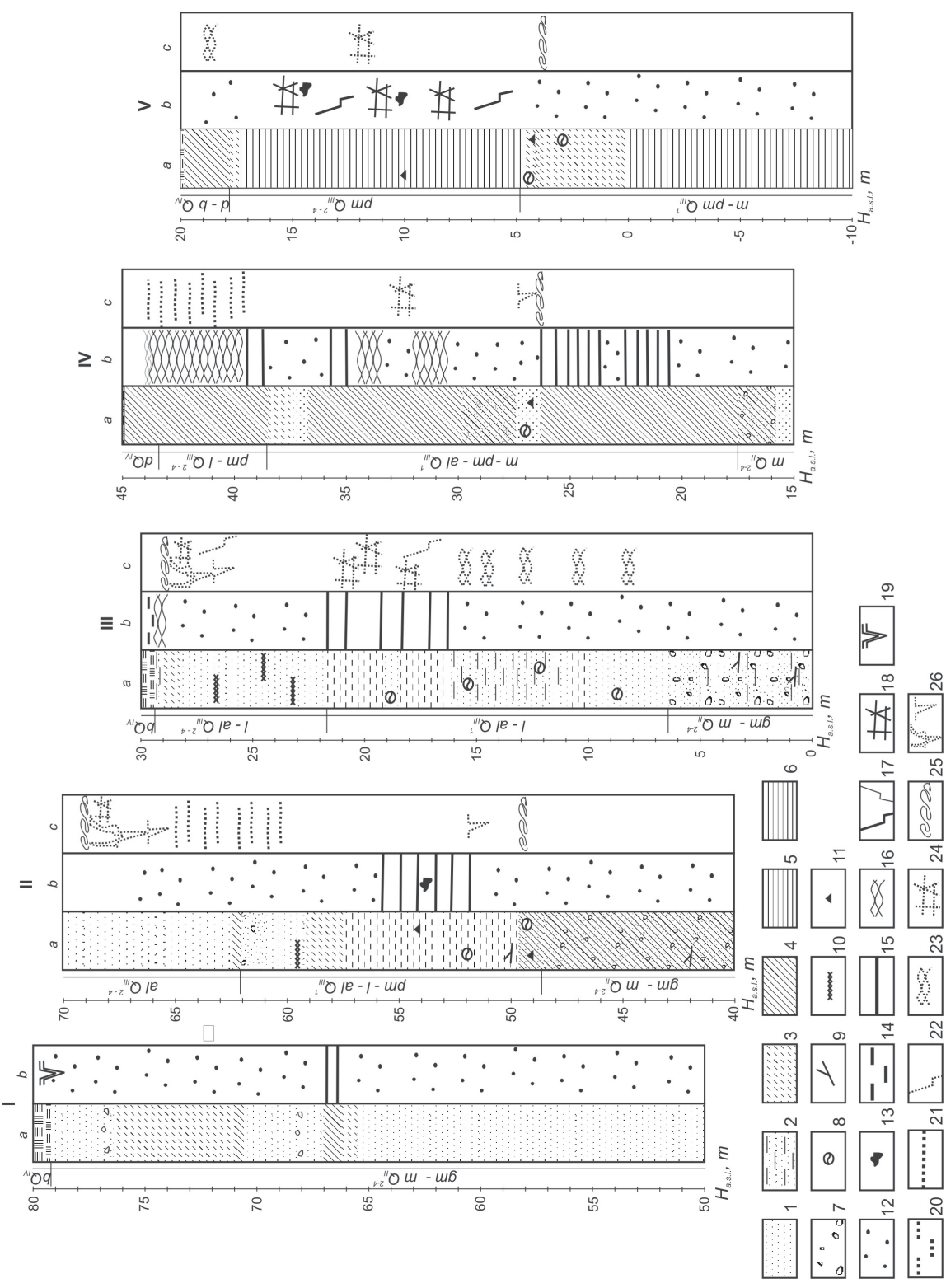

Figure 2. Lithology (a), cryostructure (b), and postcryogenic elements (c) of the main genetic types of permafrost in northern West Siberia. I – the 5th marine terrace; II–III – the 4th and 3rd lacustrine-alluvial terraces; IV – the 3rd marine terrace; V – the 2nd marine terrace. *Lithology: 1 – sand; 2 – silty sand; 3 – sandy-loam; 4 – loam; 5 – silt; 6 – clay; 7 – pebbles; 8 – clayish fragments; 9 – wooden remnants; 10 – allochtonous peat; 11 – carbonized organic debris. Cryostructure: 12 – massive; 13 – massive-agglomerate; 14 – lens-type; 15 – layered; 16 – reticulate-blocky; 17 – vertical veins; 18 – ice wedge. Postcryogenic elements: 20 – lens-type structure; 21 – layered structure; 22 – vertical veins; 23 – reticulate-blocky structure; 24 – reticulate structure; 25 – involution; 26 – ice wedge cast.*

these horizons changes from 30–50%. A massive cryogenic structure with ice-cement is typical for frozen grounds of the drained sites (total water content is 15–25%). On the marsh sites of the flat plain, the Salekhard Suite is overlain by the Holocene palsas.

A flat plain located at an elevation of 55–65 m above sea level (up to 70 m in the southern part) surrounds as a rather narrow strip the highest terrain, and consists of regressive marine series of the Late Pleistocene Kazantsevsky Suite (Q_{III}^{1}). The bottom of the sediment section is presented by light gray homogeneous loams accumulated under shallow sea conditions. Towards the top, they are replaced by sandy loams and silts of lacustrine-alluvial genesis (*lal*), and sometimes form an alternation with layered alluvial sands that are characterized by the presence of thin sublayers and lenses of allochthonous peat and plant detritus. Kazantsevsky sediments have a thickness 15–20 m and are covered by a indurate silty-loamy layer. Frozen loam has layered and reticulate-layered cryogenic structures. Sands have basically a massive cryostructure. Thin-layered cryostructures are widespread (Fig. 2, II). The thickness of ice layers is 0.2–0.7 cm with distance between them of 2–4 cm. Total water content changes from 25–35%, sometimes increasing up to 40%.

3. The third geomorphological level of the West Siberian Plain is located at an elevation of 35–55 m and formed during the Latest Pleistocene (Q_{III}^{2-4}), the Kargian-Sartanian stage of the regional stratigraphy. On the north of the territory, the marine terrace consists of estuary and delta sediments (Fig. 2. IV). On the southern part of the plain, the sediments are presented by an alternation of sands, sandy-loams and loams of the lacustrine-alluvial genesis with a total thickness 10–20 m (Fig. 2, III). Usually, light–grey, slanting layered sands have been observed at the bottom of the section. Small lenses of slightly decomposed fibrous allochthonous peat are distinguished in sands. The layered cryostructure is typical for loam and massive structure for sands. Horizontal and wavy ice layers occurred at the distance 2–3 cm from each other. Their thickness is 0.1–0.2 cm. Total water content is 20–25%.

Permafrost thickness changes south to north from 220–430 km and has a two-layer structure. The thickness of the upper sediment complex is 30–50 m; the second layer was revealed at the depth 70–75 m. The frozen layers are divided by a horizon of thawed and often water-saturated sediments with thickness up to 10–15 m and more. Average annual ground temperature varies from 0.0 to -3.0°C (Baulin et al. 1996).

Complex post-sedimentary deformation structures, extending to depths of 3–4 m below the surface have been observed in many localities within lacustrine-alluvial terraces. The deformations include ice wedge casts, involuted beddings, and sediment-filled kettle-like depressions.

The other working area is located on the territory of the gas-condensate field Kharasavey (West Yamal Peninsula) in a continuous permafrost area with an average annual ground temperature of -4 to -6°C (Vasilchuk et al. 2006).

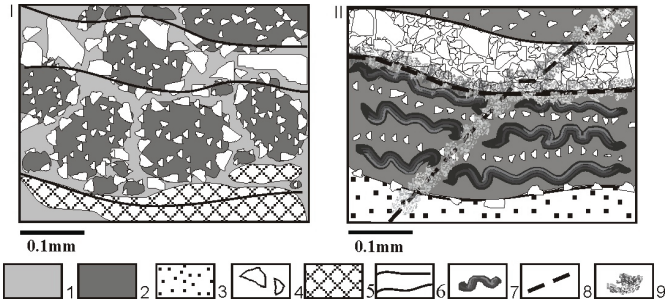

Figure 3. Microstructural scheme of the syngenetic (I) and epigenetic (II) sediments. I – the voids divided the complex aggregates, rock fragments and grains form circular pattern. II – shallow involutions, closed postcryogenic fissures coated by iron.
1 – voids; 2 – fine material; 3 – silt; 4 – debris; 5 – plant remnants; 6 – sediment lamination; 7 – involution; 8 – closed postcryogenic fissures; 9 – ferruginate zone

The thickness of the upper part of cryolithozone within the high terraces is 140–170 m; the lower part is presented by a cryotic saline ground up to the depth of 300 m. Within the gas field, the permafrost thickness and the bottom boundary of cryotic ground are distorted by the thermal influence of gas cupola and a high salinity of marine sediments.

The formation of the terraces on Yamal Peninsula was also associated with Late Pleistocene regressions of the Arctic Sea. The discrete fragments of the first marine terrace (mQ_{III-IV}), located at an elevation of 8–12 m above see level, are extended along the shoreline. The highest third terrace (mQ_{III}^{2-3}) is located at an elevation of 25–35 m a.s.l. and has been observed only in the northeastern part of the territory (Fig. 2, V). The second marine terrace (mQ_{III}^{3-4}), located at an elevation of 12–25 m, consists of loam and clay of the shallow sea with inclusions of a large amount of plant remnants, carbonized organic fragments, and layered sands of lagoon-littoral genesis. Epigenetic permafrost is characterized by massive, massive-agglomerate, and layered cryostructure. The thickness of horizontal, vertical, and broken layers is 0.5–1.5 cm.

Method

As was established and tested on the permafrost objects in the different Arctic regions, the sediments remain postcryogenic textures corresponding to distribution and form of melted-ice inclusions (Slagoda 2005, Konischev et al. 2006, Kurchatova & Slagoda 2006).

Subaerial facies of syngenetic sediments are characterized by microscale fissures which resulted from repeated thermal contraction-expansion in an active layer (Fig. 3, I):

1. mineral grains and debris which have cracked in situ;
2. sediment fragments and blocks which have moved concerning the former texture orientation;
3. complex aggregates of the fine material and debris, and associated with sediment lamination;
4. voids and postcryogenic textures corresponding to aggregates.

Change of structural-textural features of the epigenetic

sediments is observed locally near the contact zone of the ice lenses and is characterized by Figure 3, II:

1. ferruginate borders and concentration or dispersion of the fine material observed along the contact zone of the postcryogenic voids, and
2. block-moving of sediment fragments, microfaults of layers without the deep structural unconformity.

The study of macro- and microscale features of sediment structure in the borehole sections was used to determine a type of freezing with complex of facies-genetic analysis.

Results

Salekhard Suite (m, gmQ_{II}^{2-4}) was revealed by boreholes only within Nadym-Pur terrain. Sediments are presented by non-sorted sandy loams with gravel inclusions of 1–2 cm size. Toward the top of the terraces, loams are overlain by small- and fine-grained sands usually with inclined alternation. In the loam layers the microtexture is presented by non-homogeneous material with rare coarse-sized grains included in the silty-clayish fabric. Sandy fraction consists mainly of rounded to subangular quartz grains. Some coarse grains are covered by a clayish coating. Finer material has a chaotic texture. There are fragments of mussels.

Sediments of the *Kazantsevsky Suite* (*la, pmQ_{III}^{1}*) of the third and second terraces are distinguished by finer material of the marine facies to compare with the lacustrine-alluvial ones. However, the common feature of them is a layered structure of sediment and an increase in the sandy fraction towards the top of the section right up to the formation of sandy layers within the lacustrine-alluvial facies.

Silty loam lying at the bottom of lacustrine-alluvial terraces is characterized by banded fabric. Coarse-sized particles often form lenses and sublayers. Particles are mainly presented by rounded quartz grains with hydromica coating. Sediments include a large amount of plant remnants of different decomposition and also fragments of marine fauna. Silts in the middle part of the terrace section have a clear layered structure presented by alternation of mineral sublayers and organic matter. Silts have a reticulate-blocky network cryostructure, and mineral layers have a massive postcryogenic microtexture. In several layers, there are traces of thawing and repeated freezing of sediments. They are presented by deformation of the lamination, tongue-like features of the overlying deposits along the melted ice veins, ferruginate spots, and layers enriched by iron.

The finer material of the second marine terrace on Yamal Peninsula is characterized by a reticulated postcryogenic microtexture that changes into lens-layered ones due to an increase in the quantity of coarse-sized grains. The distinctive feature of Kazantsevsky sediments is a large amount of undestroyed green hydromica particles and clayish rounded debris. There are also sublayers of ferrous diffusion that did not associate with the lamination of clayish plasma. The amount of carbonized organic debris and big plant remnants with good cellular structure (moss?) increases in the loamy-sandy horizon. Similar to lacustrine deposits the

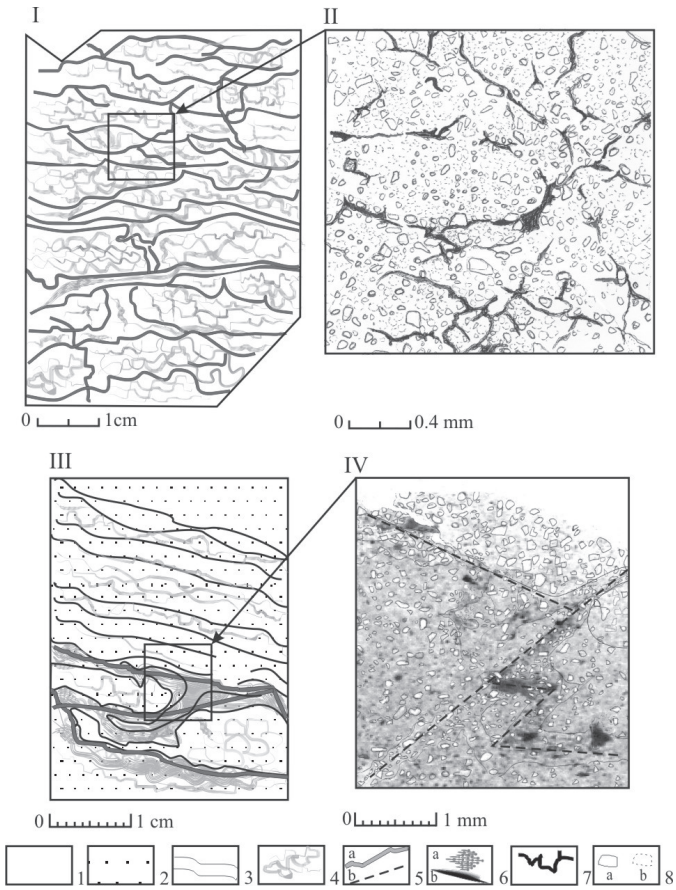

Figure 4. Scheme of macrostructure (I, III) and microstructure (II–IV); I–II – syngenetic sediments of the 3rd terrace, 42 m a.s.l; III–IV – epigenetic sediments of the 2nd terrace, 4 m a.s.l. *1 – silt; 2 – silty-sand; 3 – sediment lamination; 4 – unclear clotted pattern of the fine material underlined by ferruginate; 4 – postcryogenic fissures: a) closed, b) opened; 5 – ferruginate: a) monolith, b) thin soil section; 6 – voids; 8 – debris and coarse-size particles (a) and microaggregates (b).*

shallow-water estuary deposits of the second marine terrace are characterized by layers with sedimentary deformation (involutions).

Karginian-Sartanian sediments (*la, pmQ_{III}^{2-4}*) of the research area are presented by sandy to sandy-loam composition with inclusions of allochthonous peat. Sands of marine and lacustrine-alluvial facies consist of quartz grains with sublayers and lens of the plant detritus. Micromorphological analyses of the shallow-water deposits in the upper part of the third lake-alluvial terrace have shown horizons with clear evidence of syngenetic permafrost. Fine material is characterized by conglomeric fabric with discrete fragments and rounded grains, a circular pattern of coarse-sized grains (orbiculic fabric), lens-type, and layered and reticulate postcryogenic microtexture formed by processes of ground freezing and thawing in a wet active layer.

Sediments in the upper part of the second marine terrace are presented by loam with ferrous spots and a large amount of plant remnants. The micromorphology is characterized by

a conglomeric fabric of the complex discrete rounded units consisting of clayish particles and mineral grains. Plant remnants mark sedimentary lamination. An increase in the amount of green hydromica has been observed in the sandy-loamy and loamy layers. Hydromica particles are presented by fresh grains and also by chemically decomposed ones. Plates are split and became colorless around. Iron hydroxides that are the indicators of subaerial oxidation occur in sediments of the upper part of the terraces. Horizons with postcryogenic microtexture of the repeated freezing in the form of downward-penetrating sediment tongues and deformed wedges enriched by finer material along cracks and by oriented mineral grains filling the voids have been observed there.

Conclusions

All marine and lacustrine-alluvial terraces within the research area are overlain by regressive formation with cryogenic and postcryogenic features that testify of climatic cooling in the Late Pleistocene. During this stage the syngenetic freezing on sites of accumulation and epigenetic refreezing of the earlier melted deposits had occurred.

Research of continental and shallow-water marine sediments in northern West Siberia has shown that equally, with direct indicators of syngenetic and epigenetic freezing, the distinct soil micromorphology is formed (Fig. 4):

- Syngenetic permafrost of the different genesis is characterized by postcryogenic voids associated with sedimentary lamination and cryogenic fabric, complex discrete fragments of fine material enclosed by a circular to ellipsoidal pattern of the mineral grains, and coarse-size particles. The walls of the postcryogenic voids are coated by clayish particles and iron hydroxides; the voids are filled by oriented mineral grains.
- Micromorphological analyses of epigenetic permafrost have revealed postcryogenic microtexture in the form of involutions, deformations of sedimentary lamination associated with broken vertical and reticulate-blocky cryostructure.

Permafrost micromorpology can be used for reconstruction of the cryological history of northern West Siberia. The method allows the distinguishing of syngenetic and epigenetic sediments in the section, and therefore, the determination of subaerial conditions of syngenetic stratum accumulation and subaqueous conditions of the cryogenic transformation of the marine facies of epigenetic permafrost.

Results of the micromorphological research for correlation of cryogenic events in sections of upper Cenozoic sediments should be based on the regional database of microtexture of the different genetic permafrost types in West Siberia.

Acknowledgments

This work was supported by the Integration Research Programs (N16; 7.14) of the Russian Academy of Science in the frame of the International Polar Year. Tyumen State Oil and Gas University provided logistical support and drilling. We are also grateful to anonymous reviewers for the constructive comments and assistance in editing this paper.

References

Baulin, V.V., Aksenov, V.I., Dubikov, G.I. et al. 1996. *Engineering-Geological Monitoring of the Gas Fields on Yamal,* Vol. I, II. Tyumen (in Russian).

Dubikov, G.I. 2002. *Composition and Cryogenic Structure of the Permafrost in West Siberia*. Moscow: GEOS (in Russian).

Konischev, V.N., Lebedeva-Verba, M.P., Rogov, V.V. & Stalina, E.E. 2005. *Cryogenesis of the Present-Day and Latest Pleistocene Sediments of Altay and Periglacial Areas in Europe*. Moscow: GEOS (in Russian).

Kurchatova, A.N. & Slagoda, E.A. 2006. Reconstruction of paleocryogenic strata through micromorphological indications. *Proceedings of Asian Conference on Permafrost, Lanzhou, China, August 7–9, 2006:* 115.

Slagoda, E.A. 2004. *Cryogenic sediments of the coastal plain of Laptev Sea: lithology and micromorphology*. Tyumen (in Russian).

Vasilchuk, Y.K., Krylov, G.V., Podborny, E.S. et al. 2006. *Cryosphere of the Oil and Gas Condensate Fields of Yamal Peninsula,* Vol. I. St-Petersburg: Nedra (in Russian).

Ground Temperature and Thaw Settlement in Frozen Peatlands Along the Norman Wells Pipeline Corridor, NWT Canada: 22 Years of Monitoring

Sharon L. Smith, Margo M. Burgess, and Daniel W. Riseborough
Geological Survey of Canada, Natural Resources Canada, Ottawa, Canada

Abstract

A monitoring program along the Norman Wells pipeline corridor has generated 22 years of observations of ground temperature and thaw settlement in frozen peatlands south of Fort Simpson NWT. Thawing beneath the right-of-way (ROW) and associated thaw settlement in response to vegetation clearing, surface disturbance, pipeline construction and operation is still continuing. Where alteration of the ground thermal regime was greater, significant settlement (>2 m) and collapse of peat across the ROW has been observed especially near the edge of a peat plateau. Complete degradation of thin permafrost has been observed in undisturbed terrain adjacent to the ROW which may be a result of the natural evolution of peatlands and recent warming. Thaw depths off-ROW have increased by up to 0.9 m following fires that burned extensive areas of peatlands in 2004.

Keywords: active layer; peatland; permafrost; thaw settlement; thermal regime.

Introduction

Permafrost in the southern portion of the discontinuous zone in western Canada is largely confined to organic terrain. Much of this permafrost likely formed during the Little Ice Age (e.g., Halsey et al. 1995) and has been preserved under subsequent warmer climatic conditions by a thick layer of insulating peat. These frozen peatlands may be particularly sensitive to small changes in the ground thermal regime that may result from construction and operation of infrastructure, forest fires, or climate change. Thawing of ice-rich organic terrain may have implications for infrastructure integrity, hydrological processes, and ecosystems, and it may result in alterations to carbon sources and sinks (ACIA 2005).

The Norman Wells oil pipeline (in operation since 1985), 869 km in length, crosses the discontinuous permafrost zone (Fig. 1) of the Mackenzie Valley, Northwest Territories and northern Alberta. Organic and morainic terrain units dominate the southern portion of the route. Since the mid-1980s the Canadian government and the pipeline company, Enbridge Pipelines (NW) Inc., have collaborated in a permafrost, terrain, and geotechnical research and monitoring program which includes a network of long-term instrumented sites located along the pipeline corridor in organic terrain south of Fort Simpson NWT. This network has generated over 20 years of data on the ground thermal regime and ground movements and provides the opportunity to investigate the response of frozen peatlands to both environmental disturbance and climate change and variability.

This paper focuses on environmental changes at 5 frozen peatland sites, associated with pipeline construction and operation and with natural changes such as fire and climate change and variability. An updated documentation is presented (updates Burgess & Tarnocai 1997) of the evolution of the ground thermal regime both beneath the pipeline right-of-way (ROW) and the adjacent undisturbed terrain over a 22-year period. Changes in thaw depth and settlement of the ground surface are also documented.

Background

Peatlands in the corridor

Peatlands are organic wetlands that have 40 cm or more of peat. They cover over 60% of the terrain along the pipeline corridor south of Fort Simpson (Burgess & Lawrence 2000). The two major classes in the Mackenzie valley are bog and fen, and each has distinctive vegetation assemblages, morphologies, water regimes, and thermal conditions (Aylsworth & Kettles 2000).

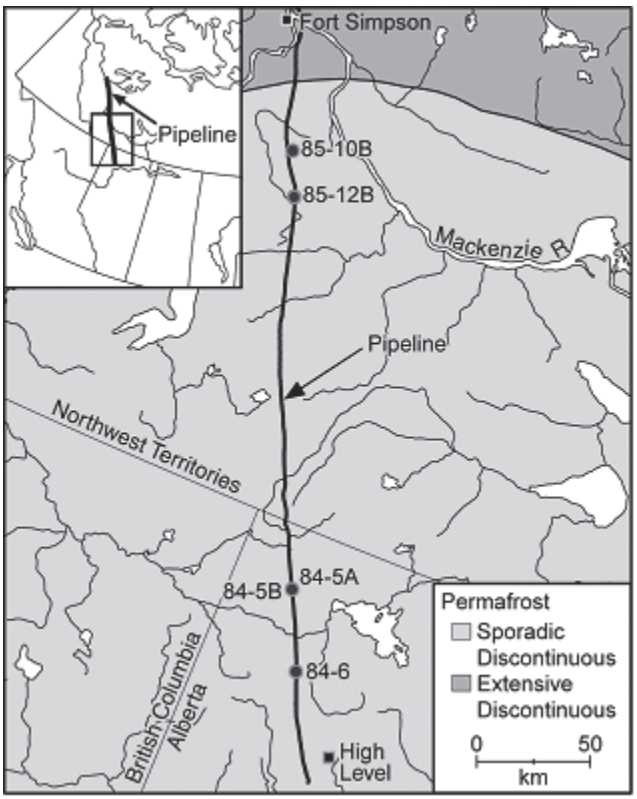

Figure 1. Location of the Norman Wells pipeline and permafrost distribution in the Mackenzie Valley.

Bogs are flat or very gently inclined plains either raised about 1 m above surrounding fens or peat filling slight depressions. Along the pipeline route, the common bog types include peat plateaus, palsa bogs, and collapse scar bogs. Fens and collapse scar bogs are generally unfrozen, while all other bog types are associated with permafrost.

Dominant peat materials of bogs are undecomposed *Sphagnum* and moderately decomposed woody moss peat underlain, in places by moderately- to well-decomposed sedge peat. Heath shrubs are also common. Trees, if present, tend to be low and stunted, forming open canopy forests. Fens are flat to very gently inclined plains which tend to be featureless although some have a reticulate network of low ridges. Dominant peat materials in fens are shallow to deep well- to moderately-decomposed sedge or woody sedge peat. Fens may or may not be vegetated with trees or shrubs (Burgess & Tarnocai 1997).

Bogs commonly developed from fens which in turn formed as organic materials accumulated in lakes or poorly drained depressions. Collapse scars in degrading peat plateaus may develop into fens (Aylsworth & Kettles 2000).

Climate

The Norman Wells pipeline corridor experiences a cold and relatively dry continental climate. Mean annual air temperature, based on 1971–2000 climate normals, is -3.2°C at Fort Simpson and -1.3°C at High Level. Normal annual precipitation is 369 mm at Fort Simpson and 394 mm at High Level with 40–45% falling as snow.

There has been a general increase in air temperature since the mid 1980s (Fig. 2) with the largest changes tending to occur during the winter. A number years with extreme temperatures (>1 standard deviation from normal) have also occurred over the last three decades including extreme warm and dry summers (for example in 1994, 1995, and 2004) that were also associated with forest fires.

Pipeline construction and operation

Pre-construction activities consisted of clearing a ROW up to 25 m wide during the winter mainly between January and March 1983 with the remainder completed by early 1984. Construction occurred over two winters (1983–84 or 1984–85) and involved blading and scraping of the peat surface to provide a stable work platform along the ditchline and travel side of the ROW. A trench about 1 m wide and 1 to 1.2 m deep was excavated for pipe installation. Excavated material (native spoil) was generally mounded over the trench following pipe installation. In peatlands, the native spoil was often blocky frozen peat that was not easily compacted. Although revegetation for erosion control occurred through seeding and fertilizing mineral soils, no revegetation was conducted where peat was greater than 1 to 1.2 m thick (present below the trench bottom).

Oil is chilled as it enters the line at Norman Wells, approximating the temperature of the surrounding permafrost. Although the pipeline operates as an ambient line, the oil warms by 1.5 to 3°C as it passes through the pump station compressors and the temperature remains elevated for more than 20 km downstream. Mean annual pipe temperatures in the southern section of the route have been above 2°C since the second year of operation. A pump station is located just south of Fort Simpson at KP 585, and downstream mean annual pipe temperatures have reached values greater than 6°C (Burgess 1992). During operation, winter pipe temperatures have generally never been below 0°C in the southern peatlands.

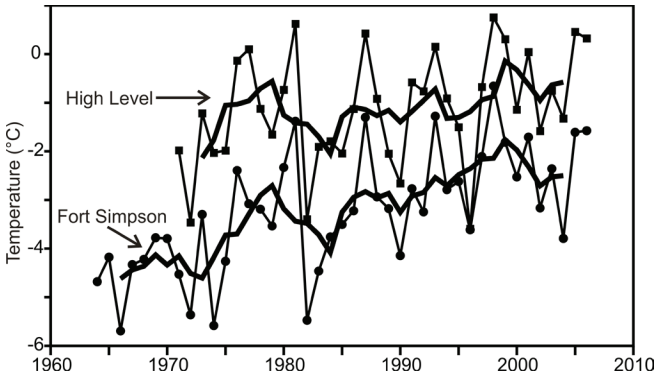

Figure 2. Mean annual air temperature record for the Environment Canada weather station at Fort Simpson, NWT (61°45′N 121°14′W) and High Level Alberta (58°37′N 117°09′W). The 5- year running mean is also shown.

Study sites and instrumentation

A description of the 5 peatland study sites is presented in Table 1. Generally 4 boreholes 5 to 20 m deep were drilled in 1984 or 1985 at each site. Three of these were located on the cleared right-of-way (on-ROW) at varying distances from the pipe and a fourth was located in the adjacent undisturbed terrain (off-ROW), 10–15 m from the edge of the ROW. Temperature cables placed in PVC casing, in each borehole, measure ground temperatures. The accuracy of the temperature sensors is ±0.1K, while the measurement system allows for a resolution of ±0.01K. Details on the site establishment and initial instrumentation are provided in Pilon et al. (1989). Manual measurements of ground temperature were made at monthly to quarterly intervals until 1996. Since 1996, dataloggers have been used at some sites and at least one complete site visit has occurred each fall close to the time of maximum active layer development. Thaw depths based on the maximum annual depth of the 0°C isotherm were determined by interpolation of the ground temperature profile between sensors. At some off-ROW sites a ground temperature sensor has been placed at 2–5 cm depth.

Thaw settlement across the ROW has been determined through level surveys initiated at site establishment and repeated at intervals of 2 to 5 years. The accuracy of these surveys ranges from less than 1 cm for compacted soil surfaces to about 15 cm for softer wet and compressible soils (Burgess & Lawrence 1997).

Observations and Discussion

Initial observations at undisturbed off-ROW sites (Fig. 3) indicate that mean annual ground temperatures in frozen peatlands are close to 0°C (above -0.3°C). Temperature gradients are small or near isothermal within the permafrost although steeper gradients are found below small bodies of permafrost surrounded by unfrozen terrain (e.g., 85-12B, KP608). Permafrost thickness (Table 1) varies from a few metres to greater than 10 m. Thaw depths were initially less than 1 m. The ground thermal regime responds to changes at the ground surface, such as clearing of vegetation related to ROW preparation and pipeline construction. Climate change and variability and natural factors such as fire may also lead to alterations in the ground thermal regime. These factors are discussed below.

Effects related to pipeline construction and operation

Changes in the ground temperature on and off the ROW over the monitoring period observed at a peat plateau near Fort Simpson and one in northern Alberta are shown in Figure 3. Initial observations off-ROW indicate that ground temperatures were colder and permafrost was thicker (10–11 m) at 84-5B (KP783) than at 85-12B (4–7 m). The warmer conditions at 85-12B are due to its lower elevation and also its proximity to the unfrozen fen as the monitoring site is located near the edge of the 2 m high peat plateau.

Over time, temperatures beneath the ROW increased above those in the surrounding undisturbed terrain in response to clearing of the vegetation and other disturbance to the ground thermal regime. This warming of the ground has led to increases in thaw depth (Table 1). At 85-5B, the increase in thaw depth beneath the ROW was about 3 m. At 85-12B, where the disturbance to the ground thermal regime has been greater, the thin permafrost completely degraded beneath the ROW.

The greater amount of warming and thawing beneath the ROW at 85-12B is due to both natural effects and those

Table 1. Characteristics of study sites discussed in this paper (updated from Burgess and Tarnocai 1997). ON and OFF refer to on-ROW and off-ROW, KP refers to kilometre post. The range in thaw depths observed at the site is given. Where the thaw depth is given as less than or greater than a given value, this indicates the depth of thaw is above the shallowest sensor or below the deepest sensor.

Site	KP	Elev m asl	Location	Peat Thickness (m)		Initial Permafrost Base (m)		Initial Thaw Depth (cm)		2006 Thaw depth (cm)	
				ON	OFF	ON	OFF	ON	OFF	ON	OFF
85-10B	588	244	61.3°N 120.9°W	2.4-2.6	2.3	1.8-2.6	2.3	Unfrozen or <100	50-100	Thawed	Thawed
85-12B	608	300	61.2 °N 120.7°W	2.9-3.2	4.8	6.7-7.0	4.5-6.1	50-100	50-100	Thawed	140
84-5A	783	552	59.7°N 119.5°W	3.2-3.7	3.8	14.7	14	<100-200	<100	>500	390 (300 in 2003)
84-5B	783	552	59.7°N 119.5°W	6.6-7.0	6.9	10.7	11.3	<50-200	<100	~400	260 (200 in 2003)
84-6	819	575	59.5°N 119.2°W	4.6-5.5	5.6	6.5-9.8	8.8	50-100	<100	Thawed	Thawed

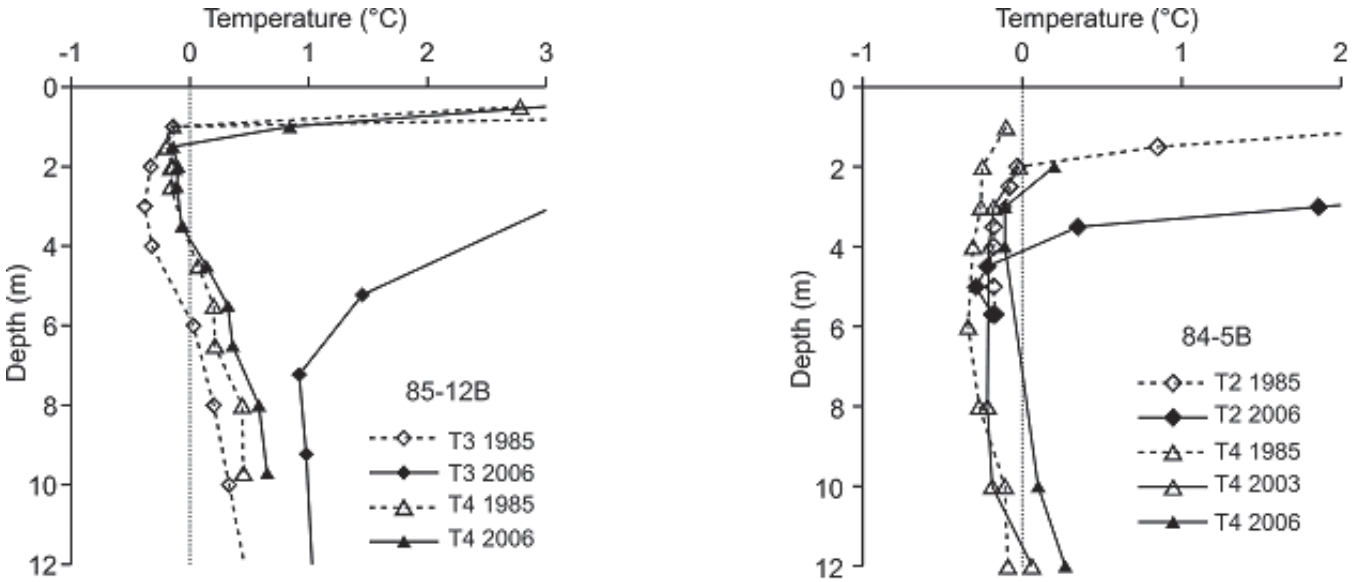

Figure 3. September ground temperatures at 85-12B (KP608) and 84-5B (KP783) on-ROW (T2, T3) and off-ROW (T4). Profiles before (2003) and after (2006) the fire are shown for T4 at 84-5B.

related to environmental disturbance. Since the site is near the collapsing edge of the peat plateau, effects related to the natural evolution of peatlands such as thermal and hydrological erosion will be important (Burgess & Tarnocai 1997). Disturbance due to blading was greater than at 84-5B. In addition, the site is located about 25 km downstream from the pump station, and the ground will be subject to warmer pipe temperatures than at 84-5B which is located much farther south. At 85-10B (KP588), located just a few kilometres south of the pump station, degradation of thin permafrost has also occurred.

Thawing of ice-rich soil can result in thaw settlement. Peat is particularly ice-rich and thaw strains of 30% or more have been determined for the pipeline sites in organic terrain (Burgess & Smith 2003). Surface settlement data obtained through periodic level surveys are presented for three sites in Figure 4. They show the ground surface movements that have occurred across the ROW between 1985 and 2006 (except for 84-6, KP819, where the most recent survey was 2001). At all sites settlement that has occurred on-ROW exceeds that occurring off-ROW due to the greater disturbance and increases in thaw depth that have occurred beneath the ROW.

During the first few years following clearing and construction, the greatest settlement generally occurred near the ditchline. This is partially due to the trenching and settlement of native backfill in the trench. Additional thawing and settlement occurred around the warm pipeline and as the thaw bulb grew, collapse of peat into the trench occurred (Burgess & Tarnocai 1997). Farther from the pipe, settlement was generally less and is mostly associated with thawing of the ground in response to clearance of vegetation. Over time, rates of settlement generally decreased as the thaw progression slowed. However, thaw settlement is still continuing on the ROW 22 years after the initial clearing. The amount of settlement on the ROW has been up to 2 m at the ditchline and up to 0.5 m toward the edge of the ROW.

The greater amount of disturbance related to ROW preparation, trench excavation and warm pipe temperatures has led to greater subsidence and collapse of peat at 85-12B than at 84-5B and 84-6. The higher ice content of the underlying material and higher associated thaw strains at 85-12B are also factors. Proximity to the edge of the peat plateau and the thermal and hydrological erosion along the subsided ditchline at 85-12B has resulted in accelerated collapse of peat into the ditch (Burgess & Tarnocai 1997) and considerable ponding on-ROW which contributed to further thermal disturbance beneath the ROW. Collapse of peat has continued and the area of ponding has enlarged over the 22-year period. By 2006 the area of collapse was found to extend to the edge of the ROW (Fig. 4a), and the trench had widened from an original width of about 1 m to about 16 m. In fact, this area of collapse has extended to the temperature cable (T3) that is near the edge of the cleared ROW and complete degradation of permafrost has occurred (Fig. 3). Although ponding has made it difficult to determine the total amount of settlement that has occurred in the trench area at 85-12B, it is at least 2 m. Toward the ROW edge (right side

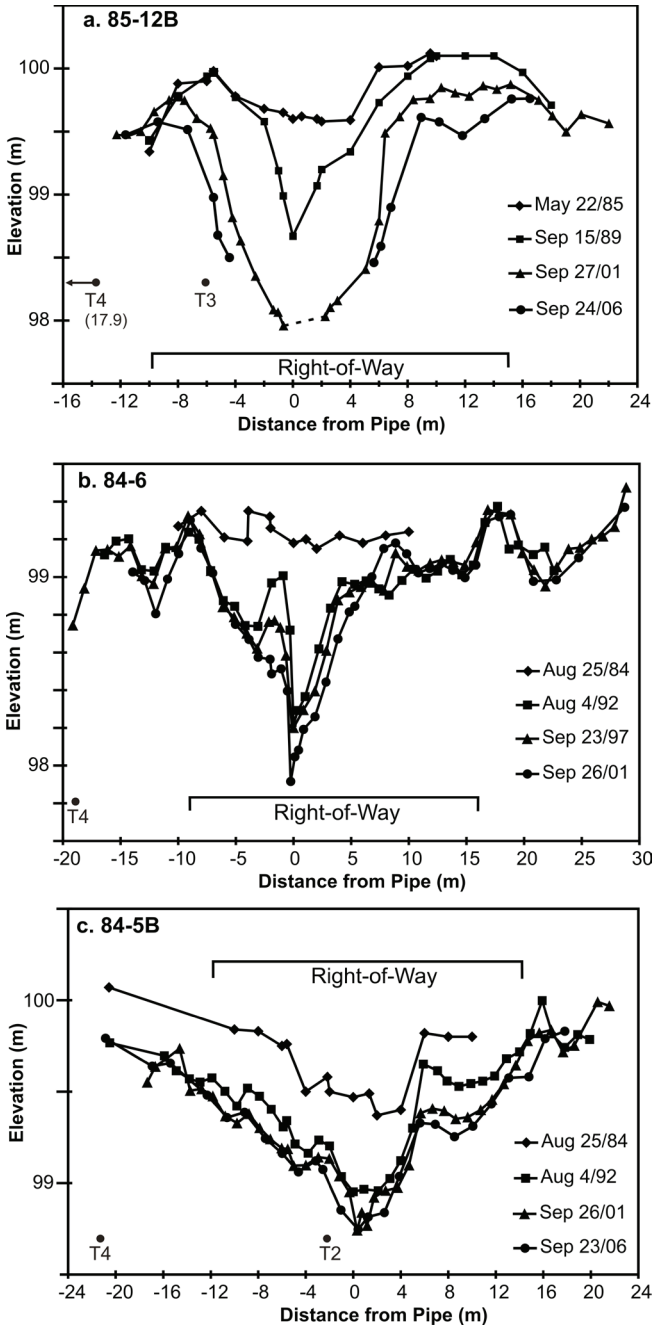

Figure 4. Ground surface elevation (relative to local datum) for peat plateau sites located at (a) KP608, (b) KP819 and (c) KP783.

Fig. 4a) up to 0.6 m of settlement has been observed.

Settlement and collapse of peat is observed to a lesser extent at 84-5B and 84-6. At the most southerly site (84-6), settlement of up to 1.3 m occurred in the trench area between 1984 and 2001. Collapse of peat is also observed and this has occurred over a distance of up to 10 m from the pipe and has extended to the edge of the ROW on one side (Fig. 4b). Farther from the trench, settlement ranges from 0.2 to 0.3 m (right side Fig. 4b). Proximity of this site to the edge of a collapse scar bog is probably also a factor in addition to the disturbance related to the trench excavation, ROW clearing and warming around the pipe.

At 84-5B where permafrost was initially colder and thicker and where effects related to the pipe temperature are less than that at 85-12B, settlement and collapse of peat has been less. Total settlement between 1984 and 2006 within the trench has been about 1m (Fig. 4c) with less collapse, which is limited to about 4 to 5 m from the pipe. Toward the edge of the ROW, settlement up to 0.5 m is observed.

Other effects

The record of ground temperatures at the off-ROW sites provides an indication of the baseline conditions and also the potential effect of climate warming on frozen peatlands. Increases in shallow permafrost temperatures at all off-ROW sites along the pipeline route have been observed over the monitoring period (Smith et al. 2005). The rate of change, however, has varied with smaller changes, or no obvious trend (<0.01°C per year) where permafrost temperatures are close to 0°C, likely due to the latent heat required to thaw the ice-rich soil. In the ice-rich organic terrain south of Fort Simpson, particularly sites with thicker permafrost, the change in ground temperatures at off-ROW sites has been small, but thaw depth has increased at some sites (Table 1). Part of this increase in thaw depth (especially in the first few years following site establishment) is likely due to surface disturbance related to borehole drilling. The general increase in thaw depth, however, is consistent with the increasing air temperature over the monitoring period (Fig. 2) and also the increase in thaw depth observed at other active layer monitoring sites in the Mackenzie Valley in the 1990s (Nixon et al. 2003).

Where permafrost was initially thin, complete degradation of permafrost off-ROW has been observed. At 85-10B, located near the edge of a degrading peatland near Fort Simpson, very warm permafrost less than 3 m thick was present in 1985 (Fig. 5). Ground temperatures then increased, with most warming occurring in the 1990s. The rate of warming was initially slow due to the energy required for phase change. By 2001, ground temperatures were greater than 1°C and permafrost was no longer present (Fig. 5). This warming (and subsequent degradation of permafrost) may be partly due to proximity of the site to the edge of the frozen peatland. Perennially frozen peatlands go through a natural cycle of early (when permafrost development begins), mature (stable), and overmature stages (Burgess & Tarnocai 1997). Thermal degradation results in thawing of ground ice and collapse of peatland surfaces during the later stage. The progression to the latter stages of the natural cycle may therefore be a factor in permafrost degradation at 85-10B.

The loss of permafrost at 85-10B may also be related to extreme warming during the summer of 1998 followed by warm winters over the next three years. Less cooling of the ground during the winter following a period of high heat input may have limited the cooling and freezing of the active layer and resulted in a general warming of the ground (Fig. 5). Both long-term trends in climate and shorter-term variations may be important, therefore, in the maintenance of these marginally frozen peatlands.

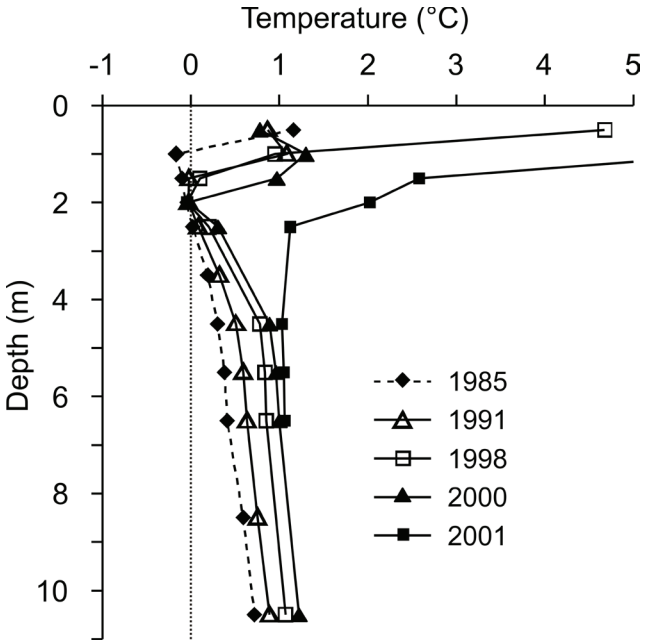

Figure 5. September ground temperature profiles off-ROW at 85-10B (KP588).

Other natural factors are also important in the evolution of the ground thermal regime. Wild fires may have an important influence on permafrost conditions. Burning of vegetation and the organic layer reduces the buffer layer and the surface albedo leading to overall increases in ground surface temperature, which over time propagate to the ground below (e.g., Viereck 1982). In summer 2004 for example, extensive areas of the southern portion of the pipeline corridor were burned. While the ROW acted as a firebreak and was generally not affected by the fire, areas adjacent to the ROW were burned including sites 84-5A and 84-5B. Figure 3 shows the increase in ground temperature and thaw depth (see also Table 1) that occurred in the two years following the fire. Thaw depths increased about 0.5 – 0.9 m over the 2 years following the fire. Analysis of data obtained from the temperature sensor placed at 2 to 5 cm depth at 84-5B indicates that mean annual near-surface ground temperature was about 1°C higher following the fire (2004–2006) than during the 3 years prior to the fire. The level survey data for 84-5B (Fig. 4c) indicates that some settlement did occur off-ROW between 2001 and 2006, but this appears to be limited to within a few metres of the edge of the ROW. Some of this settlement may be related to the burning and subsequent thawing of ground ice. However, a few more years of monitoring will be required to fully assess the impact of the fire in terms of thawing of the frozen peatland and related settlement and collapse of the peat.

These examples of permafrost degradation off-ROW associated with natural causes or climate warming show that during some periods, there may be larger changes in permafrost conditions off-ROW than on-ROW. In addition, some of the changes to permafrost off-ROW may eventually impact the ROW as surface settlement and collapse of peat progresses to the ROW edge in response to thawing.

Summary

Observations from the monitoring program in the Norman Wells pipeline corridor have provided information on the long-term evolution of the thermal regime and ground movements associated with thawing of peatlands in response to environmental disturbance related to pipeline construction and operation and natural factors. Ongoing warming at peatland sites has been observed, with the greater amount of warming occurring beneath the ROW and near the pipe. This warming and thawing of permafrost has led to settlement, particularly within the trench area. At sites where permafrost was initially warm and thin, and also adjacent to the edge of the peat plateau, disturbance to the thermal regime related to both a warm pipe and vegetation clearing has resulted in settlement of up to 2 m. Collapse of peat into the trench is also observed at these sites, in one case extending to the edge of the ROW. The possibility of permafrost thaw, settlement, and collapse of peat extending into the area adjacent to the ROW is also illustrated by these results and indicates that impacts related to infrastructure development may not be confined to the cleared ROW.

Other factors such as climate change and variability and the natural evolution of peatlands are also important. The complete degradation of thin permafrost off-ROW is observed to occur at sites near the edge of the peat plateau (and adjacent to unfrozen terrain). Warmer climate conditions over the last decade have also likely been a factor in thawing of thin permafrost. Forest fires have also resulted in changes to the ground thermal regime, especially in the off-ROW areas, resulting in permafrost thaw and settlement. The effect of fire indicates that changes off- ROW may over time affect ROW conditions should settlement and collapse of peat continue to occur.

The results generated from the monitoring program provide information to improve our understanding of the response of frozen peatlands to environmental disturbance and for planning and design of future infrastructure in similar environments.

Acknowledgments

This project has been supported over the years by: the federal departments of Natural Resources Canada and Indian and Northern Affairs Canada, federal programs of PERD (Panel on Energy Research and Development), NOGAP (Northern Oil and Gas Action Plan) and Northern Energy Development Memorandum to Cabinet, and Enbridge Pipeline (NW) Inc. Numerous colleagues have contributed to data collection and analysis over the life of the monitoring program.

References

ACIA 2005. *Arctic Climate Impact Assessment.* Cambridge University Press, 1042 pp.

Aylsworth, J.M. & Kettles, I.M. 2000. Distribution of peatlands. In: The Physical Environment of the Mackenzie Valley, Northwest Territories: A Base line for the Assessment of Environmental Change *Geological Survey of Canada Bulletin 547*: 49-55.

Burgess, M.M. 1992. Analysis of the pipe and ditch thermal regime, Norman Wells Pipeline. *Proceedings of the 11th International Conference on Offshore Mechanics and Arctic Engineering*. American Society of Mechanical Engineers V: 575-584.

Burgess, M.M. & Lawrence, D.E. 2000. Permafrost and subsurface materials along a north-south transect in the Mackenzie Valley: Observations from the Norman Wells pipeline. In: The Physical Environment of the Mackenzie Valley, Northwest Territories: A Baseline for the Assessment of Environmental Change. *Geological Survey of Canada Bulletin 547*: 127-141.

Burgess, M.M. & Lawrence, D.E. 1997. Thaw settlement in permafrost soils: 12 years of observations on the Norman Wells pipeline right-of-way. *Proceedings of the 50th Canadian Geotechnical Society Conference*, *Ottawa*: 77-84.

Burgess, M.M. & Smith, S.L. 2003. 17 years of thaw penetration and surface settlement observations in permafrost terrain along the Norman Wells pipeline, Northwest Territories, Canada. *Proceedings of Eighth International Conference on Permafrost*, July 2003, Zurich, Switzerland: 107-112.

Burgess, M.M. & Tarnocai, C. 1997. Peatlands in the discontinuous permafrost zone along the Norman Wells Pipeline, Canada. *Proceedings of the International Symposium on Physics chemistry, and Ecology of Seasonally Frozen Soils,* Fairbanks Alaska. US Army Cold Regions and Engineering Laboratory, CRREL Special Report 97-10: 417-424

Halsey, L.A., Vitt, D.H. & Zoltai, S.C. 1995. Disequilibrium response of permafrost in Boreal Continental Western Canada to climate change. *Climate Change* 30: 57-73.

Nixon, M., Tarnocai, C. & Kutny, L. 2003. Long-term active layer monitoring: Mackenzie Valley, northwest Canada. *Proceedings of Eighth International Conference on Permafrost,* July 2003, Zurich, Switzerland: 821-826.

Pilon, J.A., Burgess, M.M., Judge, A.S., Allen, V.S., MacInnes, K.L., Harry, D.G., Tarnocai, C. & Baker, H. 1989. Norman Wells to Zama pipeline permafrost and terrain research and monitoring program: site establishment report. *Geological Survey of Canada, Open File* 2044, 332 pp.

Smith, S.L., Burgess, M.M., Riseborough, D. & Nixon, F.M. 2005. Recent trends from Canadian permafrost thermal monitoring network sites. *Permafrost and Periglacial Processes* 16: 19-30.

Viereck, L.A. 1982. Effects of fire and firelines on active layer thickness and soil temperatures in interior Alaska. *Proceedings of Fourth Canadian Permafrost Conference.* National Research Council, Ottawa, Canada: 123-135.

Systematization of Underground Ice

V.I. Solomatin, N.G. Belova
Moscow State University, Department of Geography, Moscow, Russia

Abstract

This paper examines the history and problems of classification of underground ice. A new approach to genetic classification of ground ice in the permafrost area, taking into account cryolithological, geological, and geographical aspects, is suggested. The general picture of the role of different ice types in permafrost regions is shown.

Keywords: genesis; ice structure; recrystallization; systematization of underground ice; underground ice.

Introduction

Ice with its specific properties has a special place and plays a special role in cold areas of the Earth. These properties reveal themselves in global and micro processes and in events in formation of the Earth's cryosphere.

The basic principles of general systematization of natural ice have been substantiated by Dobrowolsky (1923), Veinberg (1940), Shumskii (1955, 1959) and others. Later, as new facts and theoretical ideas were accumulated, the problem of systematization and structural-genetic conceptions were elaborated (Grave 1951, Pihlainen & Johnston 1963, Katasonov 1965, Popov 1967, Vtiurina & Vtiurin 1970, Mackay 1972, Solomatin 1986, Murton 1999, French 2007 and others).

Ground ice classifications proposed by different authors were based on origin, type, and age of ice formation, relationship between ice formation and formation of the deposit containing ice, source and properties of the water used for ice crystallization, a morphology of ice body, an origin of host deposits, and other characteristics. The classification by Mackay (1972) takes into account the source of water and processes of its movement.

Shumskii (1964) considers ice as a variety of rock. It is necessary to recognize that ice is an unusual rock, the place of which in classifications of rock is hard to describe.

In this paper, the history and problems related to classification of ground ice are examined, and a new approach to genetic classification of ground ice in the permafrost, which takes into account cryolithological, geological, and geographical features, is suggested.

Classification of Ground Ice by Shumskii

The first step in systematization of ground ice is a recognition of its place among the other objects similar in nature and in methodology of study. We already mentioned above that ground ice obviously belongs to rocks, but not what place it occupies among rocks and what class of rocks to which it can be referred. It is clear that ground ice is widespread in absolutely certain geographical space—in the permafrost zone. It is a light mineral and rock, and due to this feature, it lies mainly in the uppermost layers of the lithosphere, at depths of first tens of meters (rarely hundreds) from the surface. Formation of ground ice depends on environmental (facial) and thermal conditions. As with other rocks, ice occupies its own inherent place in the lithosphere, forms unique geological bodies due to specific mechanisms and factors of ice formation, and is characterized by individual features of structure.

Shumskii (1955, 1959, 1964), on the basis of his own studies and analysis of works by Dobrowolski (1923), Veinberg (1940), Tolstikhin (1936) and other founders of glaciology, came to the conclusion that the crystal structure of ice and its formation from a liquid phase during crystallization provides the basis for attributing it to magmatic rock. Also, some types of ice (e.g., glacier ice) have similarities with metamorphic rocks, affected by deep recrystallization and metamorphic transformation of their primary structure. At the same time, the direct analogy of natural ice with magmatic or metamorphic rocks is not completely correct, even though some types of ice are formed by crystallization of the liquid phase and others undergo deep forms of dynamic metamorphism. Ice differs sufficiently from all other rocks in its physical properties and, first of all, in density and thermal properties. Understanding the tentative character of his classification, Shumskii after Veinberg suggested the definition of ice, which is formed from a liquid phase, as *congelation ice*. Shumskii considered glacier ice as metamorphic rock, while snow cover he attributed to sedimentary rocks. The scheme of natural ice classification (including ground ice) suggested by Shumskii, appears to be the least contradictory in the general system of rocks, considering the unique nature of ice-formation processes. Usage of concepts of magmatic and metamorphic rock formation in glaciology establishes important principles and methods of structural-petrographic study, helps to comprehend physical and genetic processes of natural ice formation, and at the same time, allows the use of direct terminological analogies.

Subdivisions of Underground Ice

Applying Shumskii's approach, we can distinguish the following types of ground ice (Table 1):

1. Congelation ice – the analogue of magmatic rocks, the structure of which is determined mainly by processes of crystallization of a liquid phase, with subsequent structural

Table 1. The schematic classification of underground ice.

Group of ice rock	Ice rocks		Physical processes and conditions of formation	Structure
Deposit like ice (buried ice)	All types of primarily surface ice in permafrost		Burial of primarily surface ice in permafrost	The reduced structures of corresponding surface formed ice
Metamorfic ice	Wedge ice	Syngenetic	Dynamic metamorphism of congelation ice of yearly ice veins in thermal crack	Laminated schistose structures
		Epigenetic		
	Regelation-segregation (regelation-migration) ice		Regelation and migration of ice in weakened zones of dislocated frozen soil	Catablastic structures
Congelation ice	Segregated ice		Migration and crystallization of a interfacial water	Hypidiomorphic-granular, less often allotriomorphic-granular structure fabric
	Ice-cement		Crystallization of the free and interfacial water *in situ*	Anisomerous allotriomorphic-granular
	Injection ice		Slow crystallization of free pressurized water in closed and partly closed volumes of a freezing ground	Massive coarse-grained ice fabric of slow not orthotropic crystallization
	Cave ice	Thermokarst-cave ice	Volumetric crystallization of free water in cavities of a ground	Laminated prismatic-granular structures of orthotropic growth
		Incrusted ice	Layer-by-layer crystallization of free water	Laminated fine-grained ice fabric
		Sublimation (hoar) ice	Ice crystal growth from water vapor on cave wall	Conglomerate of crystals
	Crack ice		Crystallization of water in cracks of rock	Prismatic-granular structures of orthotropic growth with axial junction of ice crystal proceeding growth from opposite crack wall

transformations insignificant. Ice of cracks and injective and thermokarst-cave ice can be attributed to this type.

2. Metamorphic ice – first of all wedge ice, the development of which is not limited by formation of elementary vein structure, but includes also the determining role of the subsequent dynamic metamorphism.

3. Buried ice – which remains a still poorly-studied group of underground ice. It is possible to consider this ice as an analogue of sediment.

Of course there are some terminological uncertainties in this interpretation, but not more than in other cases of terminology of ice formation as a geological body. The petrography of buried ice is the result of its formation on the surface and slight changes in ice structure during sediment accumulation. On the other hand, a development of syngenetic wedge ice is also in very close connection with the accumulation of containing deposits. Therefore, the syngenetic ice wedges of Pleistocene sediments, which widely occur in northern Siberia and are up to 30 m tall, should be placed in the classification system between metamorphic (as all ice wedges) and sedimentary ice rocks. The term *sedimentary ice*, however, is used usually for products of snow accumulation (Shumskii 1955, 1964). Therefore, in this classification, we offer the term *deposit like ice* for buried ice and partly for any syngenetic ice.

Modification of Ice Structure with Time

The classification scheme (Table 1) reflects existing uncertainty and terminological inconsistency, which is impossible to avoid if we consider ice (including ground ice) as a type of rock. Shumskii (1955) uses widely the concept of natural ice metamorphism. Thermodynamic conditions, even in the most severe areas of the Earth during parts of the year, are close to a point of phase change of water which determines the unstable condition of ice and its transformation by recrystallization and change in its initial structure.

Ice is always subjected to transformations of any scale due to internal or external stock of free energy. This transformation reveals itself in recrystallization and in different scale changes of primary structures. Especially deep changes of primary ice structure occur during and after dynamic metamorphism, associated with movements of ice masses by external forces. Shumskii (1955) showed that thermometamorphism of ice reaches sufficient results only at temperatures close to a melting point of ice and for ice crystals of smallest size. Rogov (1981) compared size of ice grains in ice veins of ice wedges of Pleistocene and Holocene age and found that size of crystals of Pleistocene ice wedges are greater than in Holocene ice wedges, which shows that the size of ice crystals has increased with time. However, dynamic metamorphism has a more significant influence. The degree of dynamic metamorphism is determined by the origin of ice. For example it has an obvious effect in ice wedges but not in segregation ice, even in layers close to soil surface where tension is maximal.

Every rock undergoes the certain processes of diagenesis, but that does not mean that a structure of the natural ice,

which is subjected to deep transformations, has completely lost its primary features with the origin of rock having become unrecognizable. On the contrary, ice as well as other metamorphic rocks, retains features of primary structure, even after intensive metamorphism. For example the sea origin of gneisses is out of doubt, despite intensive thermo and dynamic metamorphic processes through which the rock has passed after sedimentation. So we may say that ice recrystallization is a part of its petrogenesis, and in a certain sense, is an attribute and distinctive feature of its origin. Despite recrystallization, ice masses of different origin, which have formed at the same time and experienced since then identical thermodynamic conditions, preserve features of structure developed during their formation.

Spatial Patterns of Underground Ice-Formation

Because formation of ground ice is determined by thermodynamic conditions of adjacent rocks, patterns and genetic types of ice rocks vary with change in these conditions. In other words, the origin of ice is a function of physiographic conditions and depth of ice-forming horizon. Natural geographical changes and depth of frozen ground in earlier-described sediments should be reflected in permafrost structure (Solomatin 1982, 1996). However, patterns of ground ice predetermined by zonal factors are also affected by azonal lithogenic factors. This should be taken into consideration while studying the formation of ice at spatial boundaries of areas with different genetic types of ground ice.

Conclusions

Underground ice is a special natural mineral and rock. It is the main product and factor of permafrost forming, and is distinct as frozen ground from all other rocks.

The authors try to develop a classification of underground ice, which could help in understanding the general mechanism and spatiotemporal distribution and development of ice-rich permafrost. The classification offered in this paper takes into account the existing ideas, and also is based on initial structural features of different types of underground ice. The general picture of the role of different ice types in permafrost regions has been shown.

References

Dobrowolski, A.B. 1923. Historia naturalna lodu. Warszawa. 191 pp. (in Polish).

French, H.M. 2007. *The Periglacial Environment*. 3rd Ed. Chichester: Wiley.

Grave, N.A. 1951. Geographical distribution of large masses of underground ice in permafrost region. *Proceedings of the Conference on Ice and Snow Investigations*. Moscow: USSR Academy of Sciences Publishing House, 151-218 (in Russian).

Katasonov, E.M. 1965. Cryofacial studies of permafrost and problems of the Quaternary research in Siberia. In: *The Main Problems of Quaternary Studies*. Moscow: Nauka, 286-294 (in Russian).

Mackay, J.R. 1972. The world of underground ice. *Annals of the American Association of Geographers* 62(1): 1-22.

Murton, J.B. 1999. Permafrost: a case study in cryostratigraphy, Mackenzie Delta area, Western Canadian Arctic. In: A.P. Jones, M.E. Tucker & J.K. Hart (eds.), *The Description and Analysis of Quaternary Stratigraphic Field Sections*. Technical Guide 7. Quaternary Research Association, London, 249-266.

Pihlainen, J.A. & Johnston, G.H. 1963. *Guide to a Field Description of Permafrost*. National Research Council, Associate Committee on Soil and Snow Mechanics, Technical Memorandum 79, Ottawa.

Popov, A.I. 1967. *Geocryological Phenomena in the Earth's Crust (Cryolithology)*. Moscow State University, Moscow, 303 pp. (in Russian).

Rogov, V.V. 1981. Structures of wedge ice as an indicator of age of ice. *Problems of Cryolithology,* Issue 9. MSU Publishing, 57-69 (in Russian).

Shumskii, P.A. 1955. *Principles of Structural Glaciology*. Moscow: USSR Academy of Sciences Publishing House, 492 pp. (in Russian).

Shumskii, P.A. 1959. Ground ice. In: *Principles of Geocryology*, Vol. 1. Moscow: USSR Academy of Sciences Publishing House, 274-327 (in Russian).

Shumskii, P.A. 1964. *Principles of Structural Glaciology*. New York: Dover Publications, Inc., 497 pp.

Solomatin, V.I. 1983. Problems of underground ice systematization. *Problems of Cryolithology,* Issue 11. Moscow State University, Moscow, 38-56 (in Russian).

Solomatin, V.I. 1986. Petrogenesis of the underground ices. Novosibirsk: Sciense, 215 pp. (in Russian).

Tolstikhin, N.I. 1936. On classification of ice and ice bearing soils. VI(7): 628-636 (in Russian).

Veinberg, B.P. 1940. *Ice*. Moscow-Leningrad: Gostechizdat: 524 pp. (in Russian).

Vtiurin, B.I. & Vtiurina, E.A. 1969. Genetic classification of ground ice. *Permafrost Research Issue* 9. Moscow: Moscow State University, 165-167 (in Russian).

Nearshore Ground Temperatures, Seasonal Ice Bonding, and Permafrost Formation Within the Bottom-Fast Ice Zone, Mackenzie Delta, NWT

Steven M. Solomon
Natural Resources Canada, Dartmouth, Nova Scotia, Canada
Alan E. Taylor
Alan E. Taylor Geophysics, Sidney, British Columbia, Canada
Christopher W. Stevens
University of Calgary, Calgary, Alberta, Canada

Abstract

The Beaufort Shelf offshore the Mackenzie Delta is characterized by shallow nearshore slopes that result in extensive regions where seasonal bottom-fast ice (BFI) can develop with attendant ground freezing and aggradation of permafrost. Ground temperatures in four 10-m deep boreholes were measured for 2 years along an ~18 km transect from a distributary channel across a nearshore shoal. Maximum BFI thickness in March was 1.05 m with the coldest ground temperatures occurring where BFI was thinnest. Field observations constrained a two-dimensional geothermal model for the study area. The observations and model show the sensitivity of permafrost and ice bonding to subtle changes in bathymetry and to the residency period of BFI. The permafrost table rises beneath shallow water where annual residency of BFI is the greatest, and a subsurface talik develops beneath deeper water where residency is minimal.

Keywords: bathymetry; bottom-fast ice; ground temperature; ice-bonding; nearshore; permafrost.

Introduction

The Mackenzie Delta, located in the western Canadian Arctic (Fig. 1), is under intensive exploration for natural gas, and a proposed gas pipeline may pave the way for production of known reserves in the nearshore off the delta front. Environmentally-sound development of hydrocarbon resources in this region will require an understanding of the processes that govern coastal stability, nearshore morphology, and sediment properties in the extensive, very shallow coastal zone. In water depths <2m during the winter months, sea ice forms and thickens until it contacts the seabed (i.e., becomes "bottom-fast"). Once the ice is bottom-fast, heat is rapidly removed from sediments by conduction via the strong temperature gradient induced by the very cold air temperatures at the ice surface. This facilitates the formation of seasonal frost, and creates conditions conducive to permafrost aggradation into sediments which were formerly unfrozen. This paper reports on recent ground temperatures measured beneath zones of BFI, and on efforts to develop a thermal model for the shallow seabed along a borehole transect.

Study area

Our study transect lies at the northwest edge of the Holocene ("modern") Mackenzie Delta (Fig. 1). The shoreline of the Holocene delta is characterized by lobe-shaped vegetated islands separated by funnel-shaped bays (Hill et al. 2001). The erosional nature of the delta front, drowned morphology, and other features indicate that the Mackenzie Delta is undergoing transgression resulting in limited water depths for sediment accumulation (Hill et al. 2001). However, bar accretion still occurs within large embayments and at the mouths of most distributary channels. In general, the nearshore, seaward of the Holocene delta, is very shallow. Water depths are less than 2 m (relative to chart datum) at distances in excess of 15 km from the shore. Mean tides are 0.3 m and large tides range up to 0.5 m, whereas winds may raise water levels up to 2.4 m (Hill et al. 2001) or lower them by up to 1 m (Henry 1975).

The Mackenzie River is the largest of North American rivers supplying water and sediment to the Arctic Ocean. The abundant supply of freshwater is maintained throughout the year as a surface plume in the summer and as an under-ice freshwater "lake" during the winter (MacDonald & Carmack 1991). Thus the "sea" ice that forms in the winter is primarily formed from Mackenzie River water. Similarly, nearshore sediments deposited beneath the plume have been found to exhibit low pore water salinities (unpublished data).

The Holocene delta is underlain by permafrost to depths of 40–90 m (Judge et al. 1987). Offshore the Holocene delta, the depth to the top of permafrost is variable or absent (e.g., Judge et al. 1987, Pullan et al. 1987). Several drilling transects undertaken in the region have illustrated the nature of the onshore-offshore transition for a range of coastal morphological conditions (Dallimore et al. 1988). As described by Dyke (1991), the thermal state of sediment in the nearshore region depends on the period of time during which the sea ice is bottom-fast. In bottom-fast ice (BFI) zones, permafrost can be aggrading (in shallower water where ice becomes bottom-fast early in the winter) or degrading (where water depths are greater and ice does not become bottom-fast or does so later in the winter). Subtle changes in water depth may play an important role in determining whether or not BFI is present, and therefore can make a significant difference in the thermal state of the nearshore

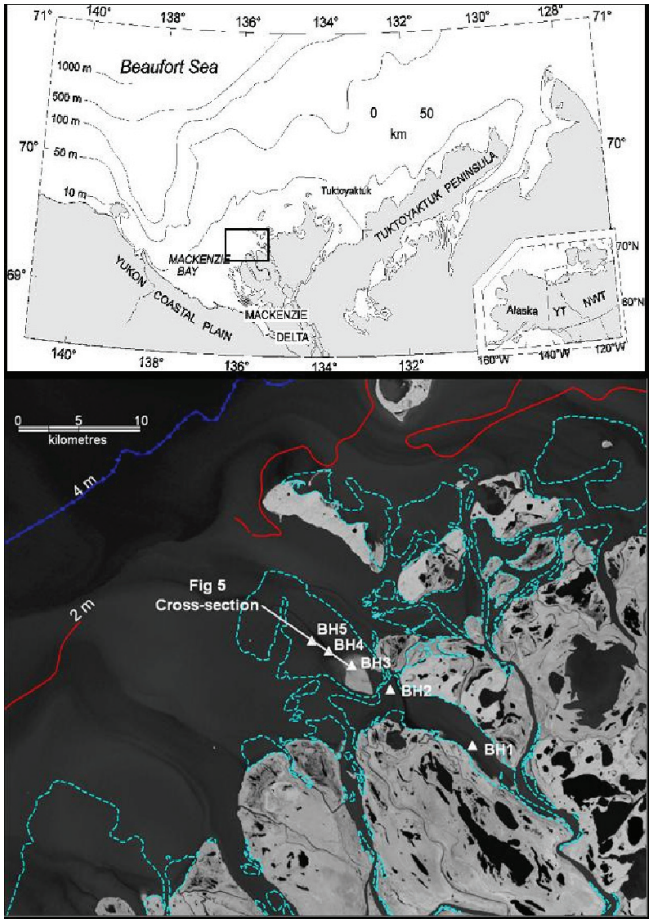

Figure 1 General and detailed location of the study area and boreholes. The Landsat image (lower, composite of summer scenes in 2000-2003) depicts the 2 and 4 m bathymetric contours, the distribution of bottomfast ice (in light blue; as mapped using synthetic aperture radar – Solomon et al. 2005), and the borehole locations (triangles). The 2 m contour is discontinuous due to a lack of data.

sediments since that will determine to what extent (if any) the seabed is coupled through BFI to very cold winter air temperatures (Dyke 1991).

Once the sea ice has become bottom-fast, the active layer above permafrost (or the zone of seasonal freezing) begins to refreeze (e.g., Osterkamp et al. 1989, Dyke 1991, Wolfe et al. 1998). This zone is also characterized by large horizontal spatial variability in temperature and seasonally reversing vertical temperature (Hunter 1988).

Methods

Ground temperature

Ground temperatures were measured in four boreholes drilled to 10 m using a seismic shothole rig. A fifth borehole was drilled in deeper water but not instrumented because of hole problems. Boreholes were located along a transect extending from a partially infilled distributary channel across a large nearshore shoal (Fig. 1). Borehole locations with varying thicknesses of BFI were chosen (Table 1). The boreholes were cased with 2" PVC pipe coupled to 4" pipe

Table 1. Borehole characteristics and thermal parameters derived from ground temperature data (2005–06).

			"Depth"	"MAGT$_0$"	"MaxT$_0$"	"MinT$_0$"	"MAGT$_{AL}$"
	Mean BFI thickness 2005-07	Base of ice-bonding (driller)	upper sensor depth	mean annual seabed temperature	maximum annual seabed temperature	minimum annual seabed temperature	mean annual ground temperature at AL depth
	(m)		(m)	(°C)	(°C)	(°C)	(°C)
BH1	0.3	frozen	0.67	0.52	14.83	-17.83	-2.34
BH2	1.0	~5 m	0.60	2.03	14.35	-9.94	-0.28
BH3	0.1	frozen	0.82	-4.24	12.04	-25.55	-3.74
BH4	0.5	frozen	0.86	-1.24	12.41	-15.64	-2.42
	"MaxT$_{AL}$"	"MinT$_{AL}$"	"Z$_{zero-ampl}$"	"T$_{Gzero-ampl}$"	"Z$_{AL}$""	"MaxT$_{AL}$"	"MinT$_{AL}$"
	maximum annual ground temperature at AL depth	minimum annual ground temperature at AL depth	depth of seasonal "zero" temperature amplitude	temperature at depth of seaspnal "zero" temperature	depth of active layer (permafrost below)	maximum annual ground temperature at AL depth	minimum annual ground temperature at AL depth
	(°C)	(°C)	(m)	(°C)	(m)	(°C)	(°C)
BH1	0.00	-12.68	deep	deep	1.80	0.00	-12.68
BH2	0.00	-0.62	3.76	-0.31	2.99	0.00	-0.62
BH3	0.00	-12.74	deep	deep	1.95	0.00	-12.74
BH4	0.00	-11.44	deep	deep	2.13	0.00	-11.44

for the upper metre. The larger diameter pipe was required to house the 8-channel RBR™ data logger. One borehole (BH3) was completely filled with silicone oil while the remaining boreholes were filled to 7 m (from the bottom). The temperature cable consisted of eight YSI™ thermistors spaced at varying intervals (0.5 m, 0.5 m, 0.5 m, 1 m, 2 m, 2.5 m, 2.5 m) with the uppermost thermistor located approximately 0.5–1.0 m below the riverbed or seabed surface from which all depths are measured; we use the term "seabed" for all boreholes.. An independent temperature logging unit (Vemco™ Minilog) was mounted inside the casing at the seabed surface. Seabed surface temperatures were logged every 3 hours and subseabed temperatures were logged every 8 hours. The YSI thermistors have an accuracy of ±0.1°C and the measurement system can resolve changes in temperature of 0.1°C (S. Smith, pers. com. 2007). The Vemco™ surface temperature loggers are specified to have a resolution of ±0.3°C and an accuracy of ±0.5°C.

Borehole positions were surveyed using a geodetic quality global positioning system. The positions were then used to relocate the borehole sites during the recovery of the data loggers.

Finite element geothermal model

Ground thermal modeling was undertaken to investigate the spatial variations in ground thermal conditions that attend BFI, such as the initiation of seasonal seabed freezing and the possibility of the growth of permafrost. The modeling was performed using the software TEMP/W™ (Geo-Slope International Ltd. 2004). This two-dimensional finite-element program combines the physics of heat transfer and phase change in porous media and realistic geologic and temporal boundary conditions to model transient thermal conditions. The model has been verified extensively against analytic solutions and is used widely by the permafrost community.

Boundary conditions, both spatial and temporal, are critical to match observations and for model predictions. The seabed temperatures along the modeled transect throughout the 2005–06 year are crucial "forcing functions" for the numerical model. They were estimated from two sources: (1) the temperature time series from a logger placed at the seabed inside each borehole collar (referred to as $BC_{measured}$), and (2)

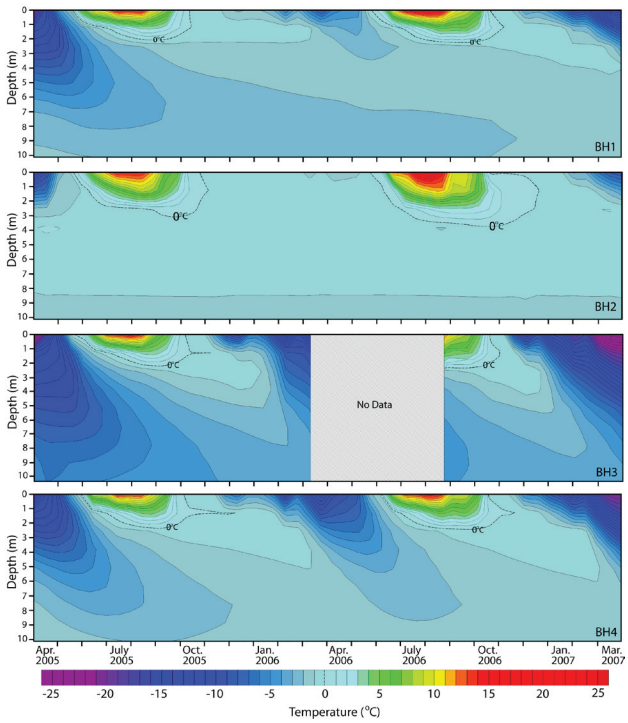

Figure 2 Two years of ground temperature variations for the 4 boreholes are illustrated as depth versus time plots. BH2 (thickest BFI) exhibits the warmest temperatures; BH3 (sub-aerial shoal), the coldest. Part of the data from BH3 is missing due to a malfunctioning data logger.

a temperature time series developed from Tuktoyaktuk air temperatures, ice thickness growth rates (Menard & Duguay 2006), and near-shore distributary water temperatures (Dyke, pers. com. 2006; $BC_{estimated}$). The first, $BC_{measured}$, is a borehole-specific measurement of temperatures over the periods during which water or BFI covers the seabed along our borehole transect. $BC_{estimated}$ is a regional estimate of seabed conditions based on independent, external data. The latter were used to interpolate conditions between boreholes.

Results

Ground temperatures

The annual ground temperature cycle over the two years of record (2005–2007) is illustrated by Figure 2. Annual ground temperature envelopes ("trumpet curves") calculated from the 2005–06 data were used to calculate a range of parameters pertinent to geothermal interpretations (Table 1, after definitions in Brown & Kupsch 1974).

The general trends in temperature show cooling of the ground in the winter and warming in the spring and summer with illustrated inter-annualinterannual variability. All of the boreholes terminate above the depth of zero annual amplitude and therefore experience changes in ground temperatures that relate to fluctuations in air temperature. The most obvious difference between the four temperature records is the warm and nearly isothermal ground temperatures below 3 m at BH2 (beneath ~1m of BFI) in contrast to colder temperatures at the other three boreholes.

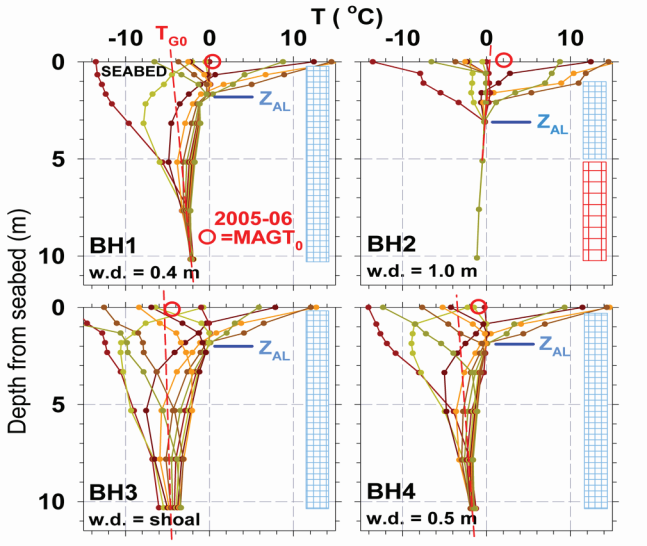

Figure 3 Monthly temperature envelopes for year Mar. 2005 – Mar. 2006 showing diverse character of borehole thermal conditions. Z_{AL}, $MAGT_0$ and T_{G0} are indicated (Table 2). Depth 0 m is at seabed. Hachured, state during drilling: blue = frozen, red=thawed.

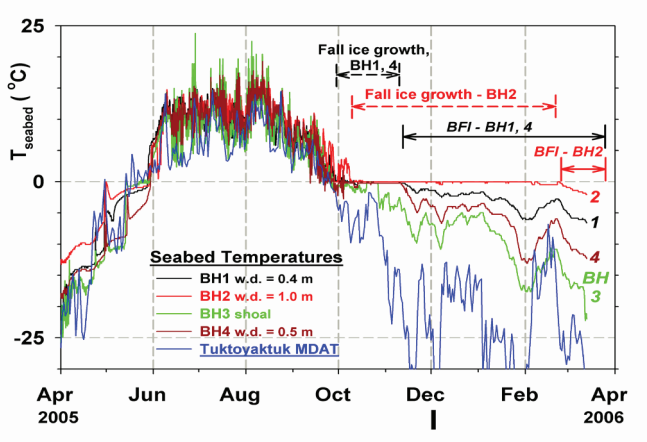

Figure 4 Tuktoyaktuk mean daily air temperatures and seabed temperatures measured at the borehole collars. Onset of fall sea ice freezing (floating), and onset of BFI (grounded) are shown. w.d. = water depth.

Figure 3 shows plots of mean monthly ground temperatures for 2005–2006 versus depth ("trumpet curves") below the seabed. Permafrost (annual temperatures <0°C, (Brown & Kupsch 1974) underlies an active layer (Z_{AL}) of ~2 m at three of the boreholes (~3 m at BH2, Table 1). Ground temperatures that are below freezing combined with observations made during drilling (March 2005) indicate that the sediments below Z_{AL} in BH1, 3, and 4 are partially or fully frozen throughout the year. Mean annual seabed temperatures ($MAGT_0$) range from ~-4°C on the intertidal shoal (BH3), to >0°C at BH1 and BH2 within the river distributary, and to <0°C offshore at BH4 (Table 1, Fig. 2).

The seabed along the transect experiences a wide range in temperatures, from 14.8°C to -26°C throughout the year,

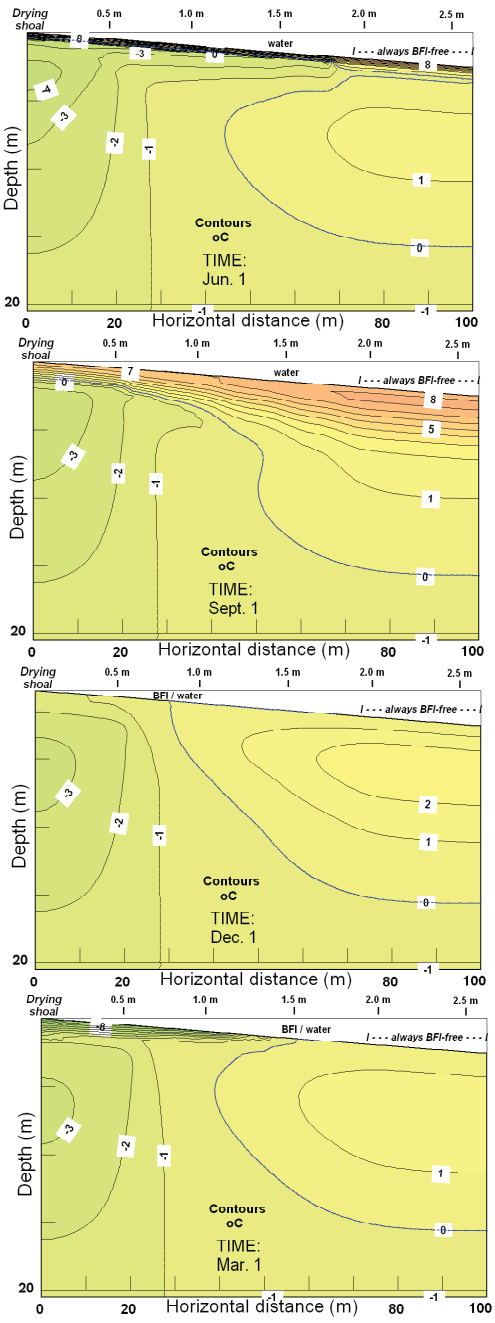

Figure 5 Temperature contours at times indicated for the hypothetical model (using $BC_{measured}$) of linearly increasing water depth (upper scale). The interpreted maximum offshore extent of the seasonal boundary between BFI and a water-covered seabed is shown.

with the greatest annual variation occurring at BH3 where BFI is thinnest (Fig. 4). The rate of change at the seabed is most rapid in the spring coincident with river breakup. As river discharge increases in late May, water overflows onto the surface of bottom-fast ice and under the ice and causes warming of the sea bed. During the open water of summer, the river and seawater are the dominant control on the seabed and riverbed temperatures. During fall and winter, seabed or riverbed cooling occurs more slowly and differs more markedly between boreholes than spring warming. Water cools first to the freezing point, where it remains for several weeks as ice forms. In shallow water, ice becomes bottom-fast relatively early in the winter, allowing low air temperature to penetrate the ice column and freeze the seabed (BH1 and BH4). In deeper water, ice does not become bottom-fast, and therefore, the seabed remains within a narrow range around the freezing point throughout the winter. At intermediate water depths, the onset of BFI is delayed resulting in a shorter duration of BFI than in the shallow water case with proportionally less freezing of the seabed. In the case of BH2, bottom-fast ice conditions were not achieved until mid- February during the winter of 2005–06 (Fig. 4). The late winter ice contact is reflected in the near-isothermal temperatures below 3 m in depth at BH2. Subsequently, freezeback of the active layer also occurs in late winter which results in minimal heat exchange at depth. The following year BFI conditions at BH2 occurred two months earlier (late December), resulting in more rapid freezeback of the active layer and colder shallow ground temperatures (Fig. 2). BH1 and BH4 were bottom-fast early in both the 2005–06 and 2006–07 freeze-up seasons (mid-October to mid-November; Fig. 4). In general, temperatures at the base of BFI correlate with air temperatures but are attenuated to about -2°C to -10°C (Fig. 4).

Numerical modeling

Figure 5 shows the thermal impact of BFI for a modeled scenario in which water depth increases linearly from a shoal to depths beyond maximum seasonal ice thickness. Using a seabed temperature boundary condition based on Figure 4 ($BC_{measured}$) as forcing function, we model the thermal impact on subsurface temperatures throughout the year. An unfrozen seabed is pervasive in summer, with seabed cooling in the fall and nearshore BFI forming in November (compare to Fig. 4). Note how the BFI/seawater boundary moves gradually further offshore during the winter, reaching its maximum extent in late April when sea ice thickness is maximum. In the process, seasonal freezing of the seabed due to BFI develops to ~2 m nearshore and becomes less deep further offshore at the maximum extent of BFI. In May, the spring freshet of warm water floods the ice and detaches it from the seabed, initiating summer open water conditions and thaw of the seasonally-frozen seabed. The effect of BFI is to support offshore permafrost, as indicated by the 0°C isotherms in Figure 5, at shallower sub-seabed depths than in open water areas.

Four zones may be identified in Figure 5: (1) the shoal that is intertidal and over-washed irregularly to create thin BFI, and

where frozen sediments occur from the ground surface to >10 m during winter (cf. BH3, Fig. 3), (2) water depths <1/2 of the maximum ice thickness of BFI, where residency of BFI is the longest, and beneath which the permafrost table lies (in this example) at 1 to ~5 m (cf. BH1 and BH4), (3) a transitional zone landward of the BFI-water margin where water depth is somewhat less than the maximum seasonal ice thickness, and (4) water depths > maximum ice thickness where BFI never occurs and beneath which the permafrost table lies deeper (here ~15 m). Note that for a water depth of ~1 m (Zone 3), the model predicts seabed temperatures to be nearly isothermal around -1°C from ~4 to 10 m depth, with a seasonal variation from -8 to +8°C in the upper 4 m. Temperatures at BH2 (Fig. 3) also exhibit an isothermal section <-1°C below 3 m, with a seasonal variation from -14 to +14°C in the upper 3 m.

Discussion

The borehole data presented in this study illustrate the inter-annual variability in ground temperatures and permafrost conditions within the shallow nearshore environment (Fig. 2) resulting from subtle changes in water depth (Fig. 3). Permafrost *sensu strictu* (<0°C) exists at all boreholes; however, differences in the extent of ice-bonding were found to occur. Drilling data indicates that the sites located beneath the shallowest water (BH1, BH3, and BH4) host ice-bonded permafrost to the maximum drilled depth (10 m), while a deeper water site (BH2) with temperatures marginally below 0°C hosts unfrozen to marginally ice-bonded sediment at depth. Seabed temperatures were found to track variations in air temperature closely with some thermal offset (Fig. 4).

Unique, continuously recorded temperature data collected throughout the fall and winter seasons reveal differences between rates of cooling and warming that are indicative of the processes occurring at those times of year (Fig. 4). Rapid warming at all of the water depths in spring is a response to overflow of warm river water originating at southern latitudes onto the ice surface and eventually melting or floating BFI off the seabed. The relatively slower cooling in the fall is a consequence of ice thickening and the gradual increase in the seaward extent of the zone of bottom-fast ice.

While the borehole temperatures quantify the impact of BFI on the seabed, other unmeasured parameters (sediment type and water content, thermal properties, sediment scour and deposition, snow cover, tidal range, storm surges, etc.) complicate the detailed interpretation of ground temperatures. Numerical modeling of a simplified case provided additional insight into the impact of BFI versus water depth. As described above, the two-dimensional model of a linear increase of water depth in the offshore direction clearly demonstrates the spatial variability of the subsurface thermal and permafrost regime across the complete range of water depths as opposed to the discrete measurements at the boreholes (Fig. 5). Clearly, the impact of residence times of BFI and summer water temperatures on the seabed are primarily a function of water depth. The "end members" are the shoal (thin intertidal BFI) and water deeper than maximum seasonal ice thickness (no BFI and perpetually submarine).

Other investigators have observed similar phenomena. For instance, previous work in the Prudhoe Bay area (e.g., Osterkamp et al. 1989 Osterkamp & Harrison 1982) examined the properties of nearshore permafrost in a narrow bottom-fast ice zone exposed to saline marine waters. They found that development of brines through salt exclusion had a significant effect on the properties of shallow materials. However, as observed in our study, they also noted the presence of an active layer where water depth or ice thickness is about 1.2–1.3 m. Temperature measurements in sediment beneath BFI were made to depths of 2 to 22m in the spring (late May–early June) and fall (November) over the course of one year. These discrete measurements have some similarities to those shown here but lack sufficient temporal detail for in-depth comparisons. The Prudhoe Bay site also differs from our study area in that Prudhoe Bay is far from any major rivers and is in an area of active coastal erosion, where thick onshore permafrost is being transformed into subsea permafrost by erosion and subsequent submergence. In contrast, the Mackenzie Delta study site is likely recording the initiation and evolution of permafrost in an aggradational setting of a freshwater-dominated delta-front of a major river.

A geotechnical investigation undertaken approximately 50 km northeast of the present study site (Hunter & Pullan 1986, Kurfurst & Dallimore 1991) examined ground temperatures across a wide sand flat adjacent to and north of the Mackenzie Delta. A series of 10 temperature cables were installed out to 800 m from the tundra shoreline and were all within the zone of bottom-fast ice. Temperatures recorded in September 1985 and April 1986 show very similar patterns to our data presented above, with a wide range of temperatures at the surface where BFI thickness was relatively thin and a much narrower range where ice was thicker (similar to BH2). Most of their boreholes were drilled to 30 m depth and all were ice-bonded throughout with little annual fluctuation below 12–16 m. Their study differed from ours in that the sand flats are interpreted to overlie older and likely previously frozen material. We believe that our sites are characterized by deposition over unfrozen seabed (based on unpublished drilling results obtained in March 2007).

Conclusions

1. Observations and model results show the importance of the duration of BFI in controlling the temperature regime at the seabed surface.
2. There is a strong seasonality to the influence of BFI with rapid and nearly simultaneous removal of BFI at all four boreholes in spring, and slower, more depth-dependent onset of BFI conditions in the fall.
3. Small changes in water depth causing ongoing natural deposition and erosion or resulting from human intervention (e.g., dredging or trenching) are likely to have dramatic effects on subsea ground temperatures and therefore ice-bonding and permafrost.

Acknowledgments

Funding was provided by Natural Resources Canada, Office of Energy Research and Development, and the Northern Energy Development Project. Logistic support was provided by Aurora Research Institute, Polar Continental Shelf Project, Chevron Canada, and Shell Canada. Field assistance was provided by Dustin Whalen and J.C. Lavergne. Caroline Duschesne and two anonymous reviewers provided comments that improved the paper substantially.

References

Are, F.A. 1988. Thermal abrasion of sea coasts (Parts I and II). *Polar Geography and Geology* 12: 1-157

Brown, R.J.E. & Kupsch, W.O. 1974. *Permafrost Terminology.* Technical Memorandum No. 111. Associate Committee on Geotechnical Research, National Research Council of Canada 14274, 61 pp.

Dallimore, S.R., Kurfurst, P.J. & Hunter, J.A.M. 1988. Geotechnical and geothermal conditions of nearshore sediment, southerm Beaufort Sea, Northwest Territories, Canada. *Proceedings of the Fifth International Conference on Permafrost, Trondheim*, *Norway, Aug. 2–5, 1988*: 127-131.

Dallimore, S.R. & Matthews, J.V. (eds.), 1997. *The Mackenzie Delta Borehole Project.* Environmental Studies Revolving Funds Report No. 135, Calgary, Canada. CD-ROM.

Dyke, L.D. 1991. Temperature changes and thaw of permafrost adjacent to Richards Island, Mackenzie Delta, N.W.T. *Canadian Journal of Earth Sciences* 28: 1834-1842.

Dyke, L.D., 2005. Shoreline permafrost along the Mackenzie River; In: L.D. Dyke & G.R. Brooks (eds.), *The physical environment of the Mackenzie Valley, Northwest Territories: a base line for the assessment of environmental change*. Geological Survey of Canada, Bulletin 547, 143-151.

Dyke, L.D. & Wolfe, S. 1993. Ground temperatures and recent coastal change at the north end of Richards Island, Mackenzie Delta, Northwest Territories. In: *Current Research, Part E.* Geological Survey of Canada Paper 93-1E, 83-91.

GeoSlope International Ltd. 2004. *TEMP/W, Software for finite element geothermal analysis, Version 6*. Calgary, AB: Geo-Slope International Ltd.

Henry, R.F. 1975. *Storm Surges.* Environment Canada, Beaufort Sea Project. Technical Report 19, 41 pp.

Hill, P.R., Lewis, C.P., Desmarais, S., Kauppaymuthoo, V. & Rais, H. 2001. The Mackenzie Delta: sedimentary processes and facies of a high-latitude, fine-grained delta. *Sedimentology* 48: 1047-1078.

Hunter, J.A.M. 1988. Permafrost aggradation and degradation on Arctic coasts of North America. *Proceedings of the Fifth International Conference on Permafrost, Trondheim, Norway, Aug. 2–5, 1988.* Trondheim: Tapir Publishers, 27-34, 127-131.

Hunter J.A.M., Judge, J.A., MacAulay, H.A., Good, R.L., Gagne, R.M. & Burns, R.A. 1976. *Permafrost and frozen sub-seabottom materials in the southern Beaufort Sea.* Beaufort Sea Technical Report 22, 174 pp.

Hunter, J.A.M. & Pullan, S. 1986. Sub-seabottom temperature measurements. In: P.J. Kurfurst (ed.), *Geotechnical investigations of the near-shore zone, North Head, Richards Island, N.W.T.* Geological Survey of Canada Open File Report 1376, 36-52.

Judge, A.S., Pelletier, B.R. & Norquay, I. 1987. Permafrost base and distribution of gas hydrates. In: B.R. Pelletier (ed.), *Marine Science Atlas of the Beaufort Sea: Geology and Geophysics.* Geological Survey of Canada, Miscellaneous Report 40. Map 39.

Kurfurst, P.J. & Dallimore, S.R. 1991. Engineering geology of nearshore areas off Richards Island, N.W.T.: A comparison of stable and actively eroding coastlines. *Canadian Geotechnical Journal* 28(2): 179-188.

Macdonald, R. & Carmack, E. 1991. The role of large-scale under-ice topography in separating estuary and ocean on an Arctic shelf. *Atmosphere-Ocean* 29:37-53.

Mackay, J.R. 1972. Offshore permafrost and ground ice, southern Beaufort Sea, Canada. *Canadian Journal of Earth Sciences* 9: 1550-1561.

Ménard, P. & Duguay, C.R., 2005. *Thermal modeling of ice growth in support of GSC Mackenzie Delta research*. Contract report submitted to Geological Survey of Canada Atlantic.

Osterkamp, T.E.; Baker, G.C., Harrison, W.D., & Matava, T. 1989. Characteristics of the active layer and shallow subsea permafrost. *Journal of Geophysical Research* 94(C11): 16227-16236.

Osterkamp, T.E. & Harrison, W.D. 1982. Temperature measurements in subsea permafrost off the coast of Alaska. In: H.M. French (ed.), *Proceedings of the Fourth Canadian Permafrost Conference*, *Calgary, Alberta, March 2–6, 1982:* 238-248.

Pullan, S., MacAulay, H.A., Hunter, J.A.M., Good, R.L., Gagne, R.M. & Burns, R.A., 1987. Permafrost distribution determined from seismic refraction. In: B.R. Pelletier (ed.), *Marine science atlas of the Beaufort Sea: geology and geophysics.* Geological Survey of Canada, Miscellaneous Report 40. Map 37.

Solomon, S.M., Fraser, P. & Manson, G. 2005. Nearshore morphology derived from Synthetic Aperture Radar in the Mackenzie Delta region of the Beaufort Sea. *Proceedings of the 12th Canadian Coastal Conference*, *November 6–9, 2005, Dartmouth, Nova Scotia.*

Taylor, A.E., Dallimore, S.R. & Outcalt, S.I. 1996. Late Quaternary history of the Mackenzie-Beaufort region, arctic Canada, from modelling of permafrost temperatures: 1. The onshore–offshore transition. *Canadian Journal of Earth Sciences* 33(1): 52-71.

Wolfe, S.A, Dallimore, S.R. & Solomon, S.M. 1998. Coastal permafrost investigations along a rapidly eroding shoreline, Tuktoyaktuk, N.W.T. *Proceeedings of the Seventh International Conference on Permafrost, June 23–27, Yellowknife, Canada*: 1125-1131.

New Data on the Ice Complex of the Lena-Amga Rivers Plain (Central Yakutia)

Vladimir B. Spektor
Melnikov Permafrost Institute SB RAS
Valentin V. Spektor
Melnikov Permafrost Institute SB RAS
Nadezhda T. Bakulina
State Unitary Enterprise of the Republic Sakha, Central Geologic and Analytic Laboratory

Abstract

Some new forms of buried ice and firn were recovered in the section of the Late Pleistocene deposits by drilling in several near-watershed sites (220–250 m a.s.l.) on the Lena-Amga Rivers Plain (Russia, Central Yakutia). The recovered section consists of three separate horizons of ice and firn formations occurring between 2.5, 5.0, 12.0, 17.0, 33.6, and 39.0 m from the ground surface. The ice and firn horizons are divided by strata of epigenetically frozen sandy silts and silts.

Keywords: Central Yakutia; cryolithology; ground ice.

Introduction

During several cryostratigraphical expeditions to Central Yakutia undertaken by the authors in recent years, two boreholes were drilled in autumn 2004 and spring 2005 to the depths of 50 m on the near-watershed areas (220–250 m a.s.l.) of the Lena-Amga Rivers interfluve. The boreholes located, correspondently, 82 km (62°08'N, 131°18'E) and 94 km (62°04'N, 131°33'E) east of Yakutsk (Fig. 1) recovered strata of wedge ice and horizontally layered ice and buried firn divided by silt and sandy silt horizons.

The investigated area is located on the high Lena-Amga plain (200–300 m a.s.l.) which is restricted to the group of plains separating the Central Siberian Plateau and Prilenskoe Plateau. It is situated within the continuous permafrost zone with ground temperatures at the depth of zero annual variations as low as -3°C to -6°C (Ivanov 1984).

In winter the Siberian anticyclone extends over the whole region resulting in falling of winter temperatures down to -50°C–60°C. The mean annual air temperature in Yakutsk is -10.3°C; mean annual precipitation amounts to 250–300

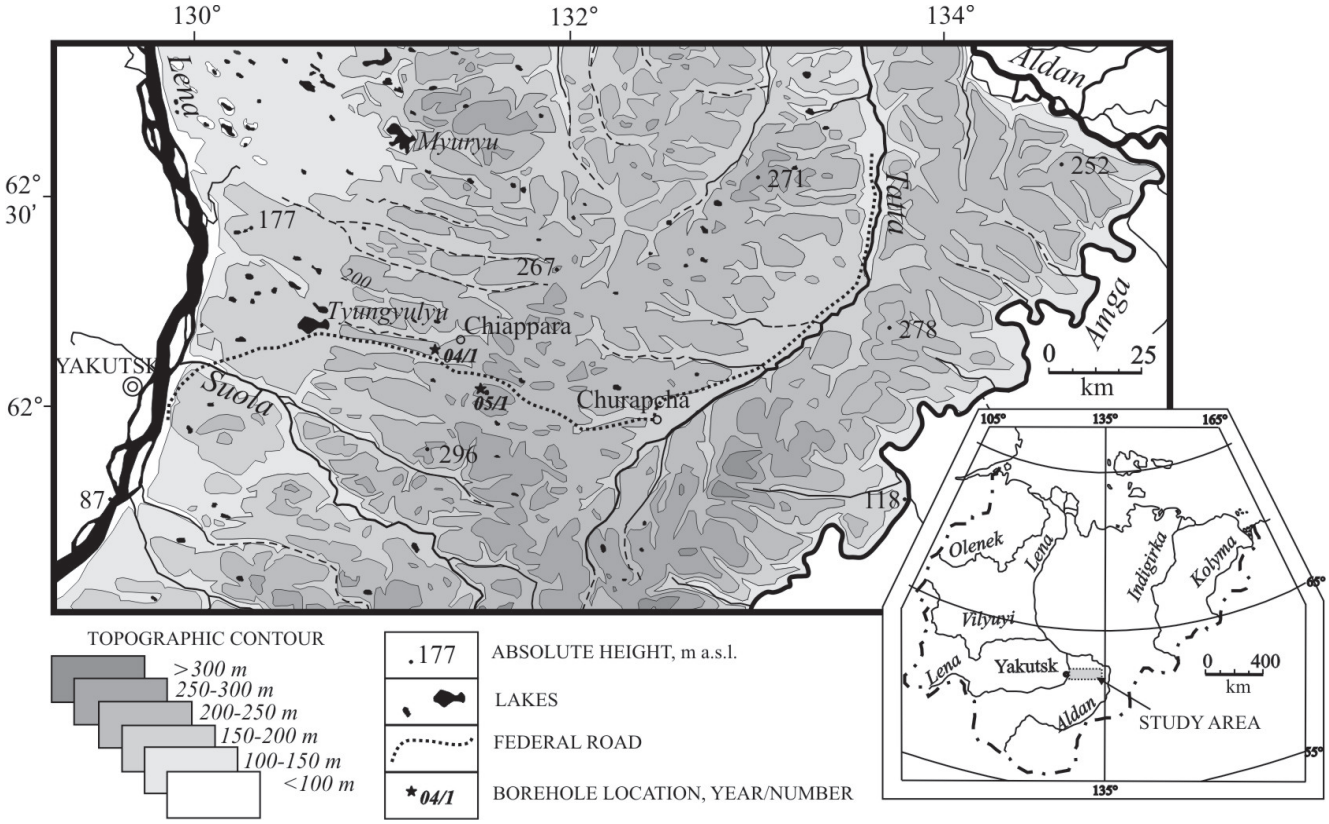

Figure 1. A map view of the study area with the borehole locations within the Lena-Amga Rivers Plain (Central Yakutia).

mm, and the height of snowpack varies between 5–30 cm (Fundamentals 1998). The permafrost thickness may be as much as about 300 m (Ivanov 1984). The upper 150 m of the geological section is loose Quaternary deposits.

According to previous investigations (Solov'ev 1959, Structure 1979, Katasonov 1975, Péwé and Journaux 1983, Ivanov 1984, Spektor & Spektor 2004), a unified stratum of ice complex containing ice wedges and structure ice is widespread on the areal surface. By different accounts the depths of ice complex with syncryogenic ice wedges vary between 10–30 m (Fundamentals 1998) to 50–60 m (Ivanov 1984).

In the course of studies made in 2004–2005, we observed new, not earlier noted, horizontally layered "sedimentary" types of ice, as well as poorly metamorphized buried firn and delineated a rhythmical texture of the upper permafrost section. Probably, similar formations were indicated by P.A. Solov'ev (1959) on the watershed of the Tatta and Amga Rivers (Central Yakutia), which he referred to the category of segregation ice. Later, the same ice forms encountered by P.A. Solov'ev were classified as buried icings (Shpolyanskaya & Streletskaya 2004).

Observation

A most complete and deep section including various forms of buried ice was observed in the borehole drilled in 2004, 82 km east of Yakutsk. The drilling was conducted, successively, by core barrels with reamer bits 147 mm, 127 mm, 108 mm, 89 mm, and 76 mm in diameter. Using air blowing, the core recovery from coring tubes was easy, and the preservation of thin cryostructures inside the core was good. The crushed ground portions up to 20 cm in thickness, caught during tripping process between well-preserved cores, were in a melted state and clearly differed from the rest of the core.

The studied section comprises three irregular intervals of ice and firn formations: upper (2.5–5.0 m from the ground surface), middle (12.0–17.0 m), and lower (33.6–39.0 m) divided by horizons of epigenetically frozen silts and sandy silts. The description of this section is given below. The second borehole drilled in 2005, 94 km east of Yakutsk, recovered buried firn and ice at a depth of 2.8–8.2 from the surface. By its stratigraphic position and cryolithological peculiarities, this horizon can be correlated to the interval 33.6–39.0 m of the 2004 borehole.

The upper ice horizon (2.5–5.0 m) is represented by ice wedge ice. The cored ice wedge had width of not less than 30 cm, and thickness of not less than 2.5 m. The wedge ice is semitransparent and yellowish. It exhibits a vertically layered structure with bands containing different amounts of mineral and organic matter and gas bubbles. The widths of the vertical bands are 1–2 cm.

The middle ice horizon (12.0–17.0 m) is represented by thin, horizontally layered, fine-crystalline and, rarer, coarse-crystalline ice (Fig. 2A). The formation of this type of ice is associated with recrystallization of snow.

The ice has a complex multi-ordered layering. It consists of several packs of layers including: 1_{M*}) packs of clean micro-layered firn, 3–5 cm in thickness, 2_M) packs of thin-layered mineralized firn, 1–2 cm in thickness, and 3_M) packs

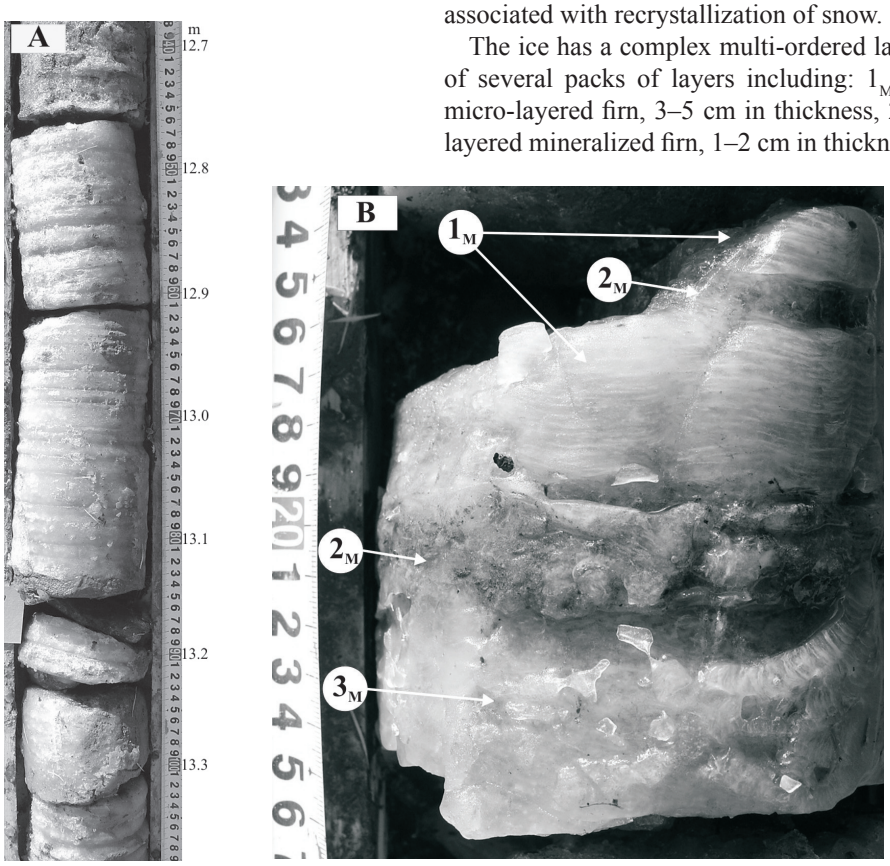

Figure 2. A – The ice core from the middle horizon represented by the horizontally-layered ice (firn) in the interval 12.7–13.4 m from the day surface. B – The multi-ordered layering of ice in the interval of 13.75–13.85 m from the day surface. Index explanation is given in the text.

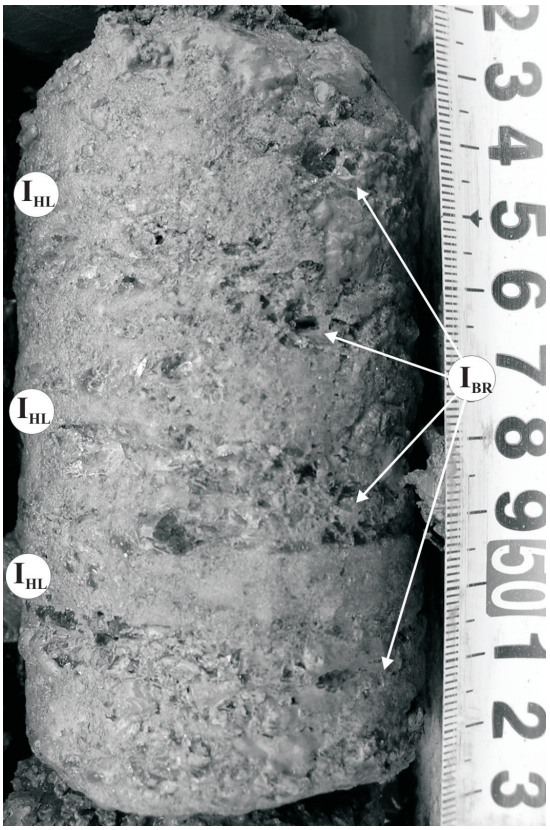

Figure 3. The alternation of ice breccia (I_{BR}) and horizontally-layered ice (I_{HL}) from the lower ice horizon in the interval of 34.02–34.13 m from the day surface.

of brecciated and coarse-crystalline firn, 1–4 cm in thickness ($*_M$ – index of layers, see Fig. 2B).

Separate interlayers of the brecciated and coarse-crystalline firn are 1–3 cm. They consist of partially-melted and rounded crystals of ice of round- or right-angled form up to 5 mm in diameter. Also, sectors with vertically orientated ice crystals, as well as hollows 1 cm in height and several cm in width are marked here.

The lower ice horizon(33.6–39.0 m) consists of big layers with different cryostructures. The upper part of the interval is divided into the layers of 1) horizontally-layered milky fine-crystalline ice (33.60–33.75 m), and 2) the alternation of ice breccia (Fig. 3, index I_{BR}) and horizontally-layered ice (33.75–34.50 m) (Fig. 3, index I_{HL}).

The ice breccia, mineralized in more or less extent, consists of pieces of fine-crystalline ice from the first to 15 mm in size. The pieces are acute-angled, rarer elongated and partly melted. The breccia cement represents milky, semitransparent, coarse-crystalline ice containing mineral particles. The cryostructure of the breccia interlayers is likely massive-agglomerate. The thickness of separate interlayers is 1–3 cm, up to 5 cm in the upper part.

The alteration of horizontally layered mineralized ice bodies and icy silts (ice-ground) is developed down the section (33.5–35.5 m). The layers are often lens-shaped, having first cm in thickness.

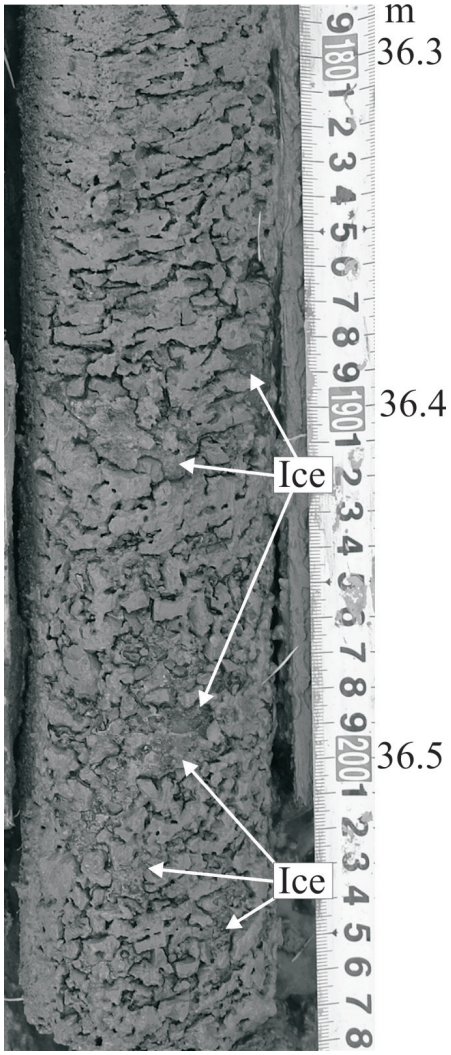

Figure 4. Ice-ground in the interval 36.30–36.58 m from the day surface. Ice, partially melted from the surface, forms the lens-braided structure in the enclosing bluish-grey silts.

Ice-ground with lens-braided cryostructure predominates in the lower part of the interval (35.5–39.0 m) (Fig. 4). This type of ice likely formed due to syncryogenic freezing of unconsolidated silty sediments from a downward direction (Fundamentals 1996).

The uppermost ice horizon is overlain by a stratum of homogeneous yellowish silts, which is developed under a thin soil cover to the depth of 2.5 m. The intervals of 5.0–12.0 m and 17.0–33.6 m are represented by strata of epigenetically frozen silts and sandy silts. A coarse, latticed cryostructure with a predominance of vertical lens ice is characteristic for them. Ice lenses are thicker (up to 3 cm), more frequent, and longer in the layers bedding directly above the ice horizons. The density and thickness of ice lenses decline upward along the section, which becomes almost iceless in the upper parts of these strata. A thin horizontal lens cryostructure appears at the upper contacts with the overlying ice horizons.

Conclusions

In our opinion, the horizontally layered ice strata of the middle and lower ice horizons had formed on the ground surface and present, probably, buried snow fields in contrast to "buried icings." This is supported by their high position on the Lena-Tatta Rivers watershed. The modern icings of the region are, as a rule, restricted to valley bottoms or watershed slopes foot. Besides, these formations are not remnants of modern perennial snowbanks because they are buried under thick (more than 10 m) ground strata. The overlying strata have spore and pollen complexes characteristic of the Late Pleistocene deposits of the region. The presence of various buried firn, ice, and ice-ground formations in the upper portion of the Lena-Amga Rivers plain loose cover points to a more complex, than it was supposed earlier, history of the cryolithozone evolution in the study area.

Acknowledgments

The investigation was made under the support of the Russian Fund of Fundamental Investigations, No. 06-05-65039-a; the Integration program SB RAS No. 71; and the Russian Science Support Foundation.

References

Fundamentals of Geocryology. 1996. E.D. Ershov (ed.), Vol. II. Lithogenous geocryology. Moscow State University. 399 pp. (in Russian).

Fundamentals of Geocryology. 1998. E.D. Ershov (ed.), Vol. III. Regional and historical geocryology of the world. Moscow State University. 575 pp. (in Russian).

Ivanov, M.S. 1984. *Cryogenic Structure of Quaternary Deposits of the Lena-Aldan Depression.* Novosibirsk: Nauka, 126 pp. (in Russian).

Katasonov, E.M. 1975. Frozen-ground and facial analysis of Pleistocene deposits and paleogeogrpaphy of Central Yakutia. In: *Paleogeography and Pleistocene Periglacial Phenomena.* Moscow: Nauka, 16-22 (in Russian).

Péwé, T.L. & Journaux, A. 1983. *Origin and Character of Loesslike Silt in Unglaciated South-Central Yakutia, Siberia, USSR*. Geological Survey Professional Paper 1262: 1-46.

Shpolyanskaya, N.A. & Streletskaya, I.D. 2004. Genetic types of massive ground ices and peculiarities of their distribution in Russian Subarctic. *Earth Cryosphere* 8(4): 56-71 (in Russian).

Solov'ev, P.A. 1959. *Permafrost zones of the northern part of the Lena-Amga Watershed.* Moscow, AN SSSR, 144 pp. (in Russian).

Spektor, V.B. & Spektor, V.V. 2002. On genesis of high Lena-Amga Rivers periglacial plain. *Earth Cryosphere* 6(4): 3-12 (in Russian).

Structure and Absolute Geochronology of the Alas Deposits of Central Yakutia. 1979. E.M. Katasonov (ed.) Novosibirsk: Nauka, 96 pp. (in Russian).

—Plenary Paper—

Recent Advances in Permafrost Geotechnics

S.M. Springman
Institute for Geotechnical Engineering, ETH Zurich, Switzerland
L.U. Arenson
BGC Engineering Inc., Vancouver, Canada

Abstract

Tribute is paid to progress in Permafrost Science and Engineering, from a geotechnical point of view, since the Millennium. Advances and concerns will be presented, embellished with thoughts about geotechnical aspects of the Ultimate and Serviceability Limit State requirements for cold regions infrastructure "Soil Structure Interaction," to be able to answer the challenges posed by climate change on a warming planet. Improvements and new developments have been described, briefly, for laboratory testing, physical and coupled numerical modeling. However, recent research progress in geotechnical aspects has not always permeated into practice, and a fundamental need remains to develop, calibrate and validate fully coupled thermo-hydro-mechanical models. This short review paper does not claim to cover all research and developments and will attempt to summarise topical findings in cold regions geotechnics.

Keywords: field Investigation; laboratory testing; modeling, permafrost engineering; review.

Introduction

This paper was commissioned to focus on geotechnical advances in Permafrost Science and Engineering, which can not be decoupled from the effects of global climate change. This has dominated recent work, as researchers seek ways of identifying the hazards to infrastructure in cold regions (ACIA 2005, IPCC 2007, U.S.A. RCPTF 2003), to establish distinct uncertainties through a risk based consideration of sensitivity and consequences and thereby mitigate the risk of permafrost degradation (e.g., Hayley & Horne 2006).

Reliable climate modeling on a regional scale for 30 to 100 years in the future is essential, as geotechnical engineering should also play an important role in integrated strategies. Designers of new infrastructure or rehabilitation measures wish to guarantee that both Ultimate (failure: ULS) and Serviceability (deformation: SLS) Limit States will be achieved throughout the life cycle of their project. Allowable deformations will be dependent upon the structure concerned. Allowable movements are more restrictive for a machinery hall than for a "flexible" pipeline that can sustain greater average and differential settlements.

Hayley & Horne (2006) condemn broad generalisations, which they comment are misleading. The same is true with geotechnical aspects. Each project must be treated on its own merits, to the level of detail required. Some progress has been made on long term solutions to practical issues relating to "Soil-Structure-Environment Interaction." This paper argues that significant fundamental work still remains to be done on geotechnical issues, and outlines contributions required over the next quadrennial. Examples are cited from mainly northern hemisphere polar and mountain permafrost: from America, Canada, Russia, China and Europe.

The authors recognise early literature on topics discussed herein, and have elected to concentrate on recent progress. References of earlier works are in the publications cited.

The Influence of Climate Modeling

When designing structures, engineers are challenged with forecasting future trends in soil properties over the entire expected lifetime. Since the deformation behaviour and strength of foundations in frozen soils depend on soil temperature (e.g., Arenson et al. 2007a), some predictions are required of combinations of permafrost temperatures, active layer thicknesses, freeze thaw cycles or frost penetration. Ultimately, all these parameters, of which further technical detail can be found elsewhere in this conference volume, depend on the climate and hence geotechnical engineers have to understand the strengths and limitations of climate models. Climate trends predicted by such models not only influence the design method, but also form the basis for site investigations and/or monitoring that has to be performed.

In addition to air temperatures, precipitation strongly influences the ground temperatures, and this has increased in toto over the past century, at a rate of about 1% per decade (ACIA 2005, Instanes 2006). Trends in precipitation are hard to assess because precise measurement is difficult in the cold arctic environment. Snow cover extent around the periphery of the Arctic also appears to have decreased.

The latest IPCC report (IPCC 2007) summarises past permafrost and snow conditions, with temperature increasing at the top of the permafrost layer in the Arctic by ≤ 3°C since the 1980s. The permafrost base has been thawing at a rate ranging up to 0.04 m/yr in Alaska since 1992 and 0.02 m/yr on the Tibetan Plateau since the 1960s. Permafrost degradation is also causing changes in land surface characteristics and drainage systems. Furthermore, snow cover has decreased in most regions, especially in spring and summer. Where snow cover or snowpack decreased, temperature often dominated; where snow increased, precipitation almost always dominated, reflecting the feedback between snow and temperature. Decline in snow cover area in the mountains of western North America and in the Swiss Alps has been greatest at lower elevations.

Even with physical evidence of ground property changes, predicting the future is challenging. Global climate models (GCMs) do not represent permafrost dynamics and potential critical feedbacks on climate. Nicolsky et al. (2007) and Alexeev et al. (2007) evaluate the land surface scheme Community Land Model (CLM3), against observations, and identify potential modifications to improve fidelity of permafrost and soil temperature simulations. Soil thickness should be > 30 m, to compute annual temperature dynamics cycle for cold permafrost. Decadal-to-century time scales require significantly deeper soil layers, e.g., > 100 m.

Vegetation changes and thermal disturbances in lowland permafrost environments due to forest fire activities, lead to increased active layer depth through reduction of the insulating quality of the surface and potentially greater likelihood of instabilities (Anisimov & Reneva 2006, Dyke 2004). This further complicates prediction of future ground temperature trends and hence the effect on frozen soil properties (Yoshikawa et al. 2003).

Site Investigation and Monitoring

The basis of any geotechnical input is an effective mixture of site investigation and monitoring of response to environmental conditions, especially of deformations in conjunction with thermal details. More progress has been made in the latter area than the former recently, although there remains significant potential for in situ tests in fine grained permafrost, in more advanced forms, or as combinations of pressuremeter, cone penetration (e.g., Buteau et al. 2005, with seismic measurement LeBlanc et al. 2004, 2006) or dilatometer testing in order to determine selected soil parameters such as shear strength, small and large strain stiffness for subsequent modeling. Obtaining basic classification data from disturbed samples, without mineralogical or strength testing, is currently the industry standard (e.g., Couture et al. 2000), with thermal properties estimated empirically from earlier consulting reports.

Sometimes, insitu permeability tests may be helpful if drainage conditions in degrading permafrost are relevant. Using probes to determine associated thermal properties is also advantageous (Overduin et al. 2006). However, thermal disturbances due to drilling, or through variations in thermal contact resistance between sensor and soil, make insitu determination of these properties challenging.

Samples must be extracted with minimal disturbance in terms of melting of the frozen phase and rearrangement of soil grains, and protected during transport for storage and subsequent testing in the laboratory for obtaining accurate soil parameters for constitutive modeling (e.g., Arenson & Springman 2005b). While this does not necessarily pose significant difficulties in polar permafrost, inevitably, this is further complicated by altitude and the blocky nature of the soils encountered when dealing with mountain permafrost. Despite additional expense during drilling, further studies are required on natural soil samples under permafrost conditions to investigate responses under selected stress-strain paths, suitable for a slowly warming environment from below to above zero °C (see laboratory testing).

Geophysical approaches are now common for spatial determination of frozen/unfrozen zones (Hauck et al. 2007, Kneisel & Kääb 2007, Maurer & Hauck 2007, Wu et al. 2005, Musil et al. 2002). Tomographic inversion techniques are adopted to reveal ground structure and for monitoring thaw in the seasonal active layer (Hauck et al. 2003, Ribolini & Fabre 2007). The challenge is to determine geotechnical parameters. This is possible through seismic approaches, although the small strain stiffness obtained can not represent stiffness over the entire strain range to failure and particularly less so in a creeping soil. Consequently, adopting geophysical approaches to determine a ground model and associated parameters is not the sole solution.

In parallel with site investigations, it is essential to plan monitoring experiments to deliver optimal data for design decisions, considering geotechnical aspects in conjunction with predictions of the conditions pertaining over the lifecycle. Monitoring should be used for design of a structure and as a part of ongoing observation that regulates future maintenace requirements. A conservative prognosis should be made of lifetime deformations, including surface deformation fields (e.g., Kääb et al. 2007, Kääb et al. 2005) as well as the deformation fields and structure (e.g., Arenson et al. 2003, Hausmann et al. 2007). GTN-P, CALM, PERMOS 2000-4 provide data of standard temperature measurements with depth, and will not be discussed here.

Inclinometers are effective only when they are able to move with the surrounding soil and when a measuring probe is able to pass through the deflecting tubing (Arenson et al. 2003). Shearing of the tube may occur eventually in slopes demonstrating considerable creep. Recent advances have been made by using TDR cables in a rock glacier to locate a concentrated creep zone, but the data are inconclusive, and the magnitude of strains can not be measured. Novel techniques for fibre optic strain measurements in boreholes, are becoming available and might be valuable in the future.

Laboratory Testing

Some recent papers report the mechanical properties of alpine permafrost both in a natural state (undisturbed) or reconstituted from soil particles extracted by “undisturbed” sampling in boreholes (Vonder Mühll et al. 2003, Arenson et al. 2004, Arenson & Springman 2005a). Issues remain about selecting an appropriate laboratory test to represent stress history and path, as well as to allow for sample heterogeneity and size effects. Interface tests have also been carried out on ice filled joints and between active layer and underlying permafrost (Günzel 2008, Rist 2007, Arnold et al. 2005). Additionally, thermal properties are required to be able to carry out integrated “thermo-hydraulic-mechanical” (THM) modeling, although their determination is well established and will not be discussed further in this paper.

Triaxial testing

Triaxial constant strain rate and constant stress tests have been performed on artificially frozen soil specimens as well

as samples won from, for example, rock glaciers (Arenson et al. 2004, Arenson & Springman 2005a). Mainly two types of tests were carried out: constant strain rate (CSR) and constant stress, creep (CSC) tests, to study the effect of the volumetric ice-solid-air fractions, temperature, strain rate and also confining stress on the mobilised shear strength.

Peak shear strengths of artificial samples increased with lower volumetric ice content and faster strain rates. Loading conditions influenced modes of deformation and eventual mechanical failure. The existence of significant percentages of air within the frozen matrix changed mobilised stiffness, strength and volumetric response from ongoing dilatancy, interlocking particles, higher stiffness and strength, in conjunction with increasing volume and rubblisation (see Yasufuku et al. 2003, Da Re et al. 2003 for artificial samples with no air) to lower stiffnesses and strength, with ductile contraction (Arenson & Springman 2005a).

Hydrate bearing soils are important because they contain natural gas (energy resource), and function as a source or sink for atmospheric methane, which may influence global warming (Brouchkov & Fukuda 2002). They are suspected to be a potential factor in the initiation and propagation of submarine slope failures (Anuruddhika & Grozic 2007, Nixon & Grozic 2007). Determining geotechnical properties of such "gassy" deposits may prove to be much more important in future. Tomographic imaging techniques (e.g., Calmels & Allard 2004 determined gas content) offer potential for integration into geotechnical laboratory studies on frozen soils. Other recent advances focus on improved methods of examining cylindrical sample response through the entire stress strain range in triaxial compression, under confining pressures as great as 20 MPa, by including small strain measurement (Da Re et al. 2003) or with radial laser measurements (e.g., Messerklinger & Springman 2007).

Interface testing

Arnold et al. (2005) conducted direct shear tests on active layer material from a 38° rock glacier slope (Pontresina-Schafberg), in support of Rist (2007). Significant dilation under low normal stresses was obtained for elongated rough particles excavated within the active zone, mobilising maximum angles of friction > 60°, and confirming that the active layer was stable for insitu conditions. Replacing the bottom half of the shear box with smooth clean ice reduced the interface friction to just over 30°. It is unlikely that such a smooth surface will form during annual freezing and thawing processes at the base of the active layer. Reliable interface friction values will lie between these two limits.

Rist (2007) created an inclinable sled model filled with active layer material to slide on a permafrost surface to investigate the shear resistance and hence to determine an interface friction angle. Grain size and volumetric water content of an artificial active layer and the degree of ice saturation of the permafrost were varied, with the latter proving to be the most important influencing factor. Soil grains embedded in an ice matrix at the permafrost surface increased the mobilised friction angle by 8° compared to a dry permafrost block, without ice. This implies a probable long term decrease of the active layer slope stability in alpine permafrost terrain under warming conditions.

Günzel (2008) carried out direct shear tests on analogue models of ice filled rock joints to determine the temperature dependent strength. She confirmed earlier findings by Davies et al. (2003) that the strength is lowest for temperatures fractionally below 0°C.

Physical Modeling

Physical modeling offers good opportunities to expose mechanisms of deformation and failure in frozen soil and in interaction with structures. Harris et al. (2003) summarise scaled, centrifuge modeling experiments in fine sandy silt, designed to simulate multi cycle thaw-related gelifluction. They concluded, from considerations of scaling laws, that flow was elastoplastic in nature with a "flow" law based on the "Cam Clay" constitutive model for soils, in which frictional shear strength is dependent on effective stress. Response was not time dependent and viscosity controlled.

Stability of model ice filled jointed rocks has been studied in a geotechnical centrifuge by Davies et al. (2003). Warming rock joints through permafrost degradation can lead to increased instabilities and rock fall events in high mountain permafrost areas. This trend was also noted by Gruber et al. (2004) and Gruber & Haeberli, (2007), who studied Alpine rock walls, and Schwab et al. (2003) for rock avalanches in West Central British Columbia, Canada.

A further series of centrifuge tests (Günzel & Davies 2006) was performed with an ice filled joint within a model rock slope, reinforced by rock bolts, and allowed to thaw. The slope was instrumented with thermocouples, displacement transducers and load cells for observation of stress development and movement during the experiment.

The combination of centrifuge experiments and direct shear tests confirmed that warming of ice inside a joint critical to the stability of a slope could lead to slope failure, even if the slope had an initial safety margin of over 200%, when the joint was filled with "cold" ice or was dry. Reinforcing a slope with pre-stressed bolts should be effective, although the bolts would need to be tested regularly in practice in case of loss of tension during joint closure. The findings from these experiments may offer a valuable means of mitigating the consequences of slope failure in high mountain areas, if the thickness of permafrost ice inside a joint can be assessed and measurements of temperature, displacement, and bolt tension are carried out regularly. Validation of these results with instrumented field tests would be most valuable.

Coupled Modeling

Constitutive and numerical modeling

Existing geotechnical models have become increasingly complex as demands to represent specific aspects of soil response become essential when designing to ULS and SLS. Mohr Coulomb approaches based on one value of cohesion and angle of friction are too simplified to account for the

effects of temperature, strain magnitude and rate, relative density and opposing effects of dilatancy and crushing.

Various forms of elastoplasticity offer a modeling basis for coupled thermo-hydro-mechanical (THM) response of soils and rocks. Significant improvements are due to long term investment from the unsaturated soil community (e.g., Sánchez et al. 2002, Khalili et al. 2000). Hydromechanical (HM) aspects are well reproduced by critical state concepts of plasticity. Models for surface cracking at low stresses have also been presented in the literature.

Thermal aspects have mainly been related to temperatures > 0°C, e.g., for radioactive waste disposal. Phase change around 0°C is not covered, although applications such as ground freezing offer interesting perspectives. The representation of thawing and freezing under variable groundwater flow regimes is well modelled (e.g., Pimentel et al. 2007). However links to volume change, ice lensing and the related mechanical behaviour are not yet established.

Recent creep modeling (e.g., Haeberli et al. 2006, Arenson & Springman 2005a) is able to represent time dependent deformations, however, imposing a valid failure criterion remains somewhat empirical. Since large strains have a significant influence on the mobilised strength of frozen geomaterials, establishing insitu strain states is necessary when analysing stability of frozen slopes.

While TH modeling has advanced from one up to three dimensions (Liu et al. 2006), more advanced approaches, (e.g., Zhang et al. 2007a, who couple water flow and heat transfer in soil with water phase change) may still only be available in 1D to date. This can be problematical when the prototype "structure" investigated is multidimensional.

Despite new findings from laboratory and field investigations, no novel constitutive relationships have been presented in recent years for frozen soils. Often only one or two dimensional solutions are adopted, when reality is three dimensional. It is no surprise then that limited progress has been made in developing new numerical models. To the authors' knowledge, none exist for practical engineers to couple thermo-hydro-mechanical processes fully. Mostly, only two elements are modelled and used as an input in the third. Future research efforts should therefore focus on such coupling. Realistic risk assessments in permafrost environments due to changing climatic conditions can benefit significantly from simulation of transient conditions under varying boundary conditions that continuously alter thermal, hydrological and mechanical soil properties. It is important to remember that a true risk analysis incorporates the variability in the predictions, which is extremely challenging for cold region climates.

Challenges for continuum analysis methods lie in the inability to model penetration installation effects or to deal with tension cracking and discontinuities. Future advances are expected in discrete element modeling, in conjunction with validation from physical modeling or field monitoring.

GIS-based modeling

GIS technologies are increasingly powerful and have recently been used for risk assessments or as visualisation tools (Giardino et al. 2004, Heggem et al. 2006, Kneisel et al. 2007, Romanovsky et al. 2006). However, they are only as powerful as the constitutive relationships and the risk determination behind the GIS model when they are used for more than visualisation or database purposes. Insufficient information on the complex interaction between the atmosphere and the ground currently limits the area of applications, which would be a helpful instrument for stakeholders and decision makers.

Phenomena

Frost heave

Frost heave presents severe challenges to owners of infrastructure threatened by temperature and groundwater dependent volume change. Segregation potential or the discrete ice lens theory are still used in practice to estimate frost heave. However, ongoing developments in the laboratory are generating opportunities to achieve greater certainty about soil parameters derived (e.g., Konrad 2005).

Côté & Konrad (2007) demonstrate the use of a heat balance model at the freezing front to compute the frost depth and the frost heave as a routine tool for moderately cold regions pavement designs based on the concept of segregation potential. Studies on the influence of fines on the frost susceptibility of base-course crushed aggregates showed that for a given kaolinite fraction, the segregation potential increases linearly with fines content, until the fines create a matrix in which the coarser particles are embedded (Konrad & Lemieux 2005). Uthus et al. (2006) present frost heave data showing sensitivity, with significantly different heave rates for almost equally graded materials. The occurrence of temperature induced vapour flow in a non-frost-susceptible granular material of pavement base layer was studied by Guthrie et al. (2006). Their laboratory tests demonstrated increased water contents, which may lead to frost heave and thaw weakening behaviour typical of that associated with water ingress through capillary action.

Based on freezing tests on small physical clay models tested under 1g as well as in a centrifuge, Han & Goodings (2006) confirm that low permeability clays experience closed freezing conditions that limit the frost heave.

Improvements in measuring techniques led to detailed observations of ice lens formation and driving mechanisms behind frost heave. Water migrated through the frozen fringe from the unfrozen soil towards the warmest ice lens, while colder ice lenses continued to grow without access to the unfrozen zone, because water was sucked from soil beds between ice lenses (Arenson et al. 2006, 2007b).

Application to road pavements has confirmed again from case histories that frost heave contributes to thermal cracking and unstable permafrost (Dunn & Gross 2006, Mills et al. 2006, Doré et al. 2006). The number of freeze thaw cycles combined with precipitation, particularly on low volume roads in seasonal frost areas, plays a role in the vulnerability of this type of lifeline (Kestler 2003).

Impurities within frozen soils may change thermo-mechanical behaviour completely. Hydrocarbons affect soil

properties, such as the unfrozen water content (Siciliano et al. 2007), or the permeability of the permafrost and how contaminants spread (Fourie et al. 2007). They change not only contaminant transport but also the frost heave behaviour of a soil, because chemicals may alter the availability of unfrozen water to migrate towards the freezing front. Laboratory investigations and theoretical considerations have demonstrated the relevance of pore water chemistry on frost heave potential and ice formation (e.g., Beier et al. 2007, Vidstrand 2007, Arenson & Sego 2006b, Arenson et al. 2006, Torrance & Schellekens 2006).

Slope stability

Local physiographic landforms will experience different modes of failure in slopes, despite the same temperature change signatures. Thickening of the active layer and subsequent detachment failures, formation of taliks, debris flows, bi-modal flows, retrogressive slumps, deep seated rotational slides are some of the failure modes reported recently by authors in China, Canada and Russia (Chenji et al. 2006, Wei et al. 2006, Lyle et al. 2004, Dyke 2004, Mazhitova et al. 2004). The presence and exposure of massive ice that released moisture into the slope was found to be critical during permafrost degradation.

Wei et al. (2006) also investigated thaw induced gelifluction in cut slopes along the Qinghai Tibet railway. Thaw slump and retrogressive debris flows developed after only one year, causing unexpected damage to the lifelines. Local erosion due to floods, waves or sea ice (e.g., at lake margins or undercutting coastal tundra blocks; Forbes 2004) or the influence of clay and mineralogy should also be accounted for. Dyke (2004) discussed the loss of both thickness and cohesive strength in an ice bonded surface layer that cracked in tension, due to thaw settlement initiating bending in the ice slab.

Such events are episodic and of a spatially discontinuous nature. Future global climatic conditions will influence site-level slope stability and require transcendence of multiple levels of uncertainty and complexity (Huscroft et al. 2004).

As in any unfrozen geotechnical system, pore water is also the critical element in frozen soil mechanics. An understanding of the pore water pressure response in thawing permafrost is key to ensuring the slopes along linear structures such as roads, railways and pipelines, remain stable. Analysis of over 20 years of pore water pressure data from the Norman Wells pipeline suggests that the sites monitored encountered lower excess pore water pressures than expected and that many slopes experienced long-term drainage as the permafrost degraded (Oswell et al. 2007). Likewise, pore pressure changes induced by sea level rise in coastal regions will cause reduced effective stresses and hence lower stiffness and strength.

But also in other permafrost environments, large slope failures, mainly active layer detachments (e.g., Lewkowicz 2007), are observed that may jeopardise engineered structures. In addition, thermal regime changes can cause slope instability to develop so that mitigation measures must be implemented (e.g., Niu et al. 2005). Field studies on solifluction processes, currently ongoing in Svalbard, highlight the correlation between thaw consolidation, reduced effective stress and pore pressures in the active layer (Harris et al. 2007). These data confirm earlier field measurements by Kinnard & Lewkowicz (2005).

Simple decoupled analyses can be carried out using a combination of conduction and convective heat flow caused by water flow in the active layer. Limit equilibrium slope stability analyses can then be used to examine the effect of degrading permafrost and different water regimes on a traditional global factor of safety. However, neither these nor coupled finite element analyses can represent large strain problems close to the ULS and caution is required in the analysis of the results. Back analysis and verification with field mesurements are crucial in the interpretation of such numerical simulations.

Natural convection

Some progress has been made in numerical TH modeling of natural convection in granular soils in cold regions to demonstrate the cooling generated in embankments or heaps of coarse stones (e.g., Cheng et al. 2007, Lebeau & Konrad 2007, Sun et al. 2007, Arenson & Sego 2006). Ventilation properties (He et al. 2007), wind direction (Zhang et al. 2006, Pham et al. 2008) and embankment surface permeability, geometry of slopes, layers and revetments (Klassen et al. 2007, Sun et al. 2007, 2005, Lai et al. 2004) influence the convection potential, and conditions should be optimised to promote cell formation.

Winter convection effects benefit from embankment surface air permeability, and largely eliminate the 0°C horizon within the subsoil, even after a few summer seasons, apart from at the embankment toe. Davies et al. (2003) have already pointed out that temperatures even marginally below 0°C can still be critical. So, geotechnical implications are that stiffness and strength are raised through reduction of the underlying thaw bulb. Settlements and possibility of failure decrease and the embankment system will be more sustainable, with reduced maintenance costs over the lifetime of the structure. However, load transfer inside embankments brings greater loads onto the toes through arching (e.g., Ellis & Springman 2001), coinciding with zones marginally softened by partial thawing. This must be allowed for in predictions of relative settlement (SLS).

Sun et al. (2005) recognise that reality differs from numerical assumptions made, although many simulations are supported by laboratory and field investigations (e.g., Zhang et al. 2006, 2007a, b, Yu et al. 2006, Goering 2003). Indeed, there is some danger in performing numerical experiments without due consideration of geotechnical effects such as abrasion and long term, often cyclic, mechanical and clastic effects in dense, coarse grained fill (e.g., McDowell 2003). For example, compaction is essential during construction to densify the fill and minimise subsequent settlement. This will cause dilatancy on shearing as well as abrasion and crushing of the coarse stone layers and possible cyclic shakedown

(settlements) in long term (Festag 2002). This will lead to fouling, whereby smaller particles will trickle down through the voids creating anisotropy, particularly in respect of water and air permeability in the fill, and will block development of the convection cells over the lifetime of the structure. In addition, layers of low air permeability that form during construction change the formation of convective cells, hence the cooling effect of the embankment/pile. Even though innovative solutions might be derived from numerical modeling with adjacent layers of coarse and fine grained material, the fundamental basics of soil mechanics must not be forgotten, such as maintaining filter relationships to prevent internal erosion.

Soil Structure Interaction – SLS & ULS

Soil Structure Interaction (SSI) represents the inter-dependent reaction between ground and structure, in which both ULS and SLS must be assured. Foundations for typical infrastructure, including linear structures such as pipelines, road pavements, railway beds, communication cables, electrical power lines, or more two dimensional loading problems typical in oil tanks, buildings, airports, embankments, dams, mines, encapsulated landfill sites, are all susceptible to thaw and creep settlement (SLS) and reduced bearing capacity (ULS), under warming planetary conditions, as well as mobility of groundwater (and any related soluble or immiscible contaminants) (e.g., Mills et al. 2006, Mazhitova et al. 2004, Hayley et al. 2004, Cole 2002, Couture et al. 2000). Furthermore, relative or interactive seasonal effects (such as thermal cracking and frost heave, Tighe et al. 2006, frost heave and upheaval of pipelines buried in cold regions, Kanie et al. 2006, Palmer & Williams 2003, or creep of pylons founded on creeping permafrost, Phillips et al. 2007) may threaten the integrity of structures and exacerbate damage.

Mazhitova et al. (2004) call for long term investments in adequate infrastructure in Russia, with consideration of lifetime effects, for oil and gas pipelines, given the potential for serious environmental disasters. Adaptability must also be well thought out, so that design can be enhanced for most vulnerable infrastructure, as geotechnical risk is minimised within an integrated risk approach that considers the entire lifecycle (e.g., Auld et al. 2006).

Solutions that promote improved SSI performance can be described as either active or passive by ensuring the ground remains frozen (e.g., assisted by thermosyphons or thermopiles) or by avoiding, changing or modifying the SSI conditions. Innovative thermosyphon technology that will be operational to 100 m depth, was investigated within a large scale field experiment by Noël & Hockley (2004) and offers tremendous opportunities for future active measures. Managing the effects of thaw in a controlled fashion, or by adding berms to prevent thaw softening developing under the toe of embankments by natural convective air flow are other examples. Numerical modeling confirmed that thermal insulation (e.g., using expanded polystyrene at different embedment depths combined with construction in the cold season, Wang & Dou 2007) can contribute to active measures, although the long term performance at SLS must be guaranteed as well.

Innovative long term solutions are required:

- to place constraints on perennially frozen ground by maintaining a frozen state (Bjella 2006), or
- for structural measures by developing devices to permit superstructures to be realigned on foundations to fulfill SLS requirements (Phillips et al. 2007), or by adopting stabilising measures such as rock bolts and anchors.

Conclusions

Contemporary advances in frozen soil mechanics and geotechnical engineering in cold regions have been described for application to natural permafrost and infrastructure built on or within permafrost. Recent work on field studies, laboratory investigations, physical modeling and coupled simulations are reviewed, in connection with warming planetary conditions, under which permafrost has been recognised as an indicator for climate change. Some phenomena related to frost heave during cyclic freezing and thawing, slope and active layer stability, and convection cooling in coarse granular fill, are discussed within this framework as well.

Urgent need has been identified for ongoing basic geotechnical research in permafrost engineering and science. Investment must be made in site investigations for high risk projects, supported by effective monitoring regimes and advanced laboratory testing to determine key parameters. Challenges were also pinpointed relating to understanding the thermo-hydro-mechanical behaviour of frozen soils and implementing new constitutive relationships into numerical models to represent this behaviour. Physical models, especially those exposed to the correct stresses and environmental conditions, were accepted as providing excellent opportunities for validating and calibrating such codes.

Acknowledgements

The authors thank the conference organisers for their invitation to publish this overview and the anonymous reviewer for his/her helpful comments.

References

ACIA 2005. *Arctic Climate Impact Assessment 2005.* Cambridge, U.K. and New York: Cambridge University Press.

Alexeev, V.A., Nicolsky, D.J., Romanovsky, V.E. & Lawrence, D.M. 2007. An evaluation of deep soil configurations in the CLM3 for improved representation of permafrost. *Geophysical Research Letters* 34: L09502.

Anisimov, O. & Reneva, S. 2006. Permafrost and changing climate: The Russian perspective. *Ambio.* Royal Swedish Academy of Sciences 35(4): 169-175.

Anuruddhika, G.J & Grozic, J.L.H. 2007. An experimental investigation of temperature induced dissociation of

methane hydrate in porous soil media. *Proceedings, 60th Canadian Geotechnical Conference,* Ottawa, ON, Canada, October 21-24, 2007: 2062-2067.

Arenson, L., Hoelzle, M. & Springman, S.M. 2003. Borehole deformation measurements and internal structure of some rock glaciers in Switzerland. *Permafrost and Periglacial Processes* 13(2): 117-135.

Arenson, L., Johansen, M.M. & Springman, S.M. 2004. Effects of volumetric ice content and strain rate on shear strength under triaxial conditions for frozen soil samples. *Permafrost and Periglacial Processes* 15(3): 261-271.

Arenson, L.U. & Springman, S.M. 2005a. Triaxial constant stress and constant strain rate tests on ice-rich permafrost samples. *Canadian Geotechnical Journal* 42(2): 412-430.

Arenson, L.U. & Springman, S.M. 2005b. Mathematical description for the behaviour of ice-rich frozen soils at temperatures close to zero centigrade. *Canadian Geotechnical Journal* 42(2): 431-440.

Arenson, L.U. & Sego, D.C. 2006a. Considering convective air fluxes in the design of engineered structures in cold regions. *Proceedings, 59th Canadian Geotechnical Conference,* October 1-4 2006, Vancouver, BC, Canada: 1033-1040.

Arenson, L.U. & Sego, D.C. 2006b. The effect of salinity on the freezing of coarse grained sands. *Canadian Geotechnical Journal* 43(3): 325-337.

Arenson, L.U., Xia, D., Sego, D.C. & Biggar, K.W. 2006. Change in ice lens formation for saline and non-saline Devon silt as a function of temperature and pressure. *Proceedings, 13th International Conference on Cold Regions Engineering,* July 23-26, 2006, Orono, Maine, USA. CD-Rom.

Arenson, L.U., Springman, S.M. & Sego, D.C. 2007a. The Rheology of Frozen Soils. *Applied Rheology* 17(1): 12147-1 - 12147-14.

Arenson, L.U., Take, W.A. & Sego, D.C. 2007b. Measurement of ice lens growth and soil consolidation during frost penetration using particle image velocimetry (PIV). *Proceedings, 60th Canadian Geotechnical Conference,* October 21-24, 2007, Ottawa, ON, Canada. 2046-2053.

Arnold, A., Thielen, A. & Springman, S.M. 2005. On the stability of active layers in alpine permafrost. *Proceedings, 11th International Conference and Field Trip on Landslides* (ICFL), Trondheim, Norway, 1.-10.9.2005: 19-25, Taylor & Francis, Netherlands.

Auld, H., MacIver, D. & Klassen, J. 2006. Adaptation options for infrastructure under changing climate conditions. *Proceedings, Climate Change Technology Conference 2006,* Ottawa, ON, Canada, May 10-12, 2006: CD-Rom.

Beier N., Sego D., Donahue, R. & Biggar, K. 2007. Laboratory investigation on freeze separation of saline mine waste water. *Cold Regions Science and Technology* 48(3): 239-247.

Bjella, K. 2006. Engineering studies for degrading permafrost. *Proceedings, 13th International Conference on Cold Regions Engineering,* July 23-26, 2006, Orono, Maine, USA. CD-Rom.

Brouchkov, A. & Fukuda, M. 2002. Preliminary measurements on methane content in permafrost, central Yakutia, and some experimental data. *Permafrost and Periglacial Processes* 13: 187-197.

Buteau, S, Fortier, R. & Allard, M. 2005. Rate-controlled cone penetration tests in permafrost. *Canadian Geotechnical Journal* 42(1): 184-197(14).

Calmels, F. & Allard, M. 2004. Ice segregation and gas distribution in permafrost using tomodensitometric analysis. *Permafrost and Periglacial Processes* 15: 367–378.

Cheng, G.D., Lai, Y.M., San, Z.Z. & Jiang, F. 2007. The 'thermal semi-conductor' effect of crushed rocks. *Permafrost and Periglacial Processes* 18(2): 151-160.

Chenji, Huzeyong, Doushun & Qianzeyu. 2006. Yin-Yang Slope problem along Qinghai-Tibetan Lines and its radiation mechanism. *Cold Regions Science and Technology* 44(3): 217-224.

Cole, D.M. 2002. Permafrost degradation: problem statement, knowledge gaps and related research activities. Hanover, NH: Cold Regions Research and Engineering Laboratory. ERDC/CRREL LR-02-71.

Côté, J. & Konrad, J.M. 2007. Practical pavement frost heave assessment considering regional specific ground heat flux. *Proceedings, 60th Canadian Geotechnical Conference,* Ottawa, ON, Canada, October 21-24, 2007: 2092-2098.

Couture, R., Robinson, S.D. & Burgess, M.M. 2000. Climate change, permafrost degradation, and infrastructure adaptation: preliminary results from a pilot community case study in the Mackenzie valley. Geol. Survey of Canada. Current research 2000-B2.

Da Re, G., Germaine, J.T. & Ladd, C.C. 2003. Triaxial testing of frozen sand: equipment and example results. *Journal of Cold Regions Engineering* 17(3): 90-118.

Davies, M.C.R., Hamza, O. & Harris, C. 2003. Physical modelling of permafrost warming in rock slopes. *Proceedings, 8th International Conference on Permafrost,* Zurich, Switzerland: 169-174.

Doré, G., Beaulac, I. & Van Gassen, W. 2006 Performance of the Beaver Creek section of the Alaska Highway. *Proceedings, 13th International Conference on Cold Regions Engineering,* July 23-26, 2006, Orono, Maine, USA. CD-Rom.

Dunn, P. & Gross, K. 2006. Standard methods used to mitigate seasonal frost in highway projects. *Proceedings, 13th International Conference on Cold Regions Engineering,* July 23-26, 2006, Orono, Maine: CD-Rom.

Dyke, L. 2004. Stability of frozen and thawing slopes in the MacKenzie valley, NW Territories. Géo-Québec, 57th Canadian Geotechnical Conference, 1G: 31-38.

Ellis, E.A. & Springman, S.M. 2001. Modelling of soil-structure interaction for a piled bridge abutment in plane strain FEM analyses. *Computers and Geotechnics* 28(2): 79-98.

Festag, G. 2002. Experimental investigations on sand under cyclic loading. Constitutive and Centrifuge Modelling: two extremes, Monté Verità. Ed. S.M. Springman. Balkema, Lisse, 269-275.

Forbes, D.L. 2004. Climate-change impacts in the coastal zone: implications for engineering practice. Géo-Québec, 57th Canadian Geotech. Conf., 7A: 10-17.

Fourie, W., Barnes, D.L. & Adhikari, H. 2007. Influence of pore ice on the movement of petroleum and contaminated water through coarse media. *Proceedings, Conference on Assessment and Remediation of Contaminated Sites in Arctic and Cold Climates.* Edmonton AB, Canada, May 6-8, 2007: 99-103.

Giardino, M., Giordan, D. & Ambrogio, S. 2004. GIS technologies for data collection, management and visualization of large slope instabilities: two applications in the Western Italian Alps. *Natural Hazards and Earth System Sciences* 4(2): 197-211.

Goering, D.J. 2003. Passively cooled railway embankments for use in permafrost areas. *Journal of Cold Regions Engineering* 17(3): 119-133.

Gruber, S., Hoelzle, M. & Haeberli, W. 2004. Permafrost thaw and destabilization of Alpine rockwalls in the hot summer of 2003. *Geophysical Research Letters* 31: L13504.

Gruber, S. & Haeberli, W. 2007. Permafrost in steep bedrock slopes and its temperature-related destabilization following climate change. *Journal of Geophysical Research-Earth Surface* 112(F2).

Günzel, F.K. & Davies, M.C.R. 2006. Influence of warming permafrost on the stability of ice filled rock joints. *Proceedings, 6th International Conference on Physical Modelling in Geotechnics,* 343-348.

Günzel, F.K. 2008. Shear Strength of Ice Filled Joints. *Proceedings, Ninth International Conference on Permafrost,* June 29-July 3, 2008, Fairbanks, Alaska, USA (this proceedings).

Guthrie, W.S., Hermansson, Å. & Woffinden, K.H. 2006. Saturation of granular base material due to water vapor flow during freezing: Laboratory experimentation and numerical modeling. *Proceedings, 13th International Conference on Cold Regions Engineering.* July 23-26, 2006, Orono, Maine: CD-Rom.

Haeberli, W., Hallet, B., Arenson, L., Elconin, R.O., Humlum, O., Kääb, A., Kaufmann, V., Ladanyi, B., Matsuoka, N., Springman, S.M. & Vonder Mühll, D. 2006. Permafrost Creep and Rock Glacier Dynamics. Final Report of the IPA/ICSI Task Force. *Permafrost and Periglacial Processes* 17(3): 189-214.

Han, S.J. & Goodings, D.J. 2006. Practical model of frost heave in clay. *Journal of Geotechnical and Geoenvironmental Engineering* 132(1): 92-101.

Harris, C., Luetschg, M., Davies, M.C.R., Smith, F., Christiansen, H.H. & Isaksen, K. 2007. Field instrumentation for real-time monitoring of periglacial solifluction. *Permafrost and Periglacial Processes* 18(1): 105-114.

Harris, C., Davies, M.C.R. & Rea, B.R. 2003. Gelifluction: viscous flow or plastic creep? *Earth Surface Processes and Landforms* 28(12): 1289-1301.

Hauck, C., Vieira, G., Gruber, S., Blanco, J. & Ramos, M. 2007. Geophysical identification of permafrost in Livingston Island, maritime Antarctica. *Journal of Geophysical Research-Earth Surface* 112(F2).

Hauck, C., Vonder Mühll, D. & Maurer, H. 2003. Using DC resistivity tomography to detect and characterize mountain permafrost. *Geophysical Prospecting* 51(4): 273-284.

Hausmann, H., Krainer, K., Bruckl, E. & Mostler, W. 2007. Internal structure and ice content of reichenkar rock glacier (Stubai Alps, Austria) assessed by geophysical investigations. *Permafrost and Periglacial Processes* 18(4): 351-367.

Hayley, D. & Horne, B. 2006. Rationalizing climate change for design of new structures on permafrost. *Proceedings, Climate Change Technology Conference 2006*, Ottawa, ON, Canada, May 10-12, 2006: CD-Rom.

Hayley, D.W., Seto J.T.C., Gräpel, C.K., Cathro, D.C. & Valeriote, M.A. 2004. Performance of two rockfill dams with thermosyphons on permafrost foundations, Ekati Diamond Mine, NT. *Proceedings, 57th Canadian Geotechnical Conference,* Quebec, QC: 5F 32-39.

He, P., Zhang, Z., Cheng, G.D. & Bing, H. 2007. Ventilation properties of blocky stones embankments. *Cold Regions Science and Technology* 47(3): 271-275.

Heggem, E.S.E., Etzelmüller, B., Anarmaa, S. Sharkhuu, N., Goulden, C.E. & Nandinsetseg, B. 2006. Spatial distribution of ground surface temperatures and active layer depths in the Hovsgol area, northern Mongolia. *Permafrost and Periglacial Processes* 17(4): 357-369.

Huscroft, C.A., Lipovsky, P. & Bond, J.D. 2004. Permafrost and landslide activity: Case studies from southwestern Yukon Territory. In: *Yukon Exploration and Geology 2003.* Yukon Geological Survey, 107-119.

Instanes, A. 2006. Impacts of a changing climate on Infrastructure: Buildings, Support Systems, and Industrial Facilities. *Proceedings of the Climate Change Technology Conference 2006,* Ottawa, ON, Canada, May 10-12, 2006: CD-Rom.

IPCC 2007. *Climate Change 2007: The Physical Science Basis Contribution of Working Group I to the Fourth Assessment Report of the IPCC.* Cambridge, U.K. and New York: Cambridge University Press.

Kanie, S., Akagawa, S., Kim, K. & Mikami, T. 2006. Estimation method of frost heaving for chilled gas pipeline buried in frost susceptible soil. *Proceedings, 13th International Conference on Cold Regions Engineering.* July 23-26, 2006, Orono, Maine: CD-Rom.

Kääb, A., Frauenfelder, R. & Roer, I. 2007. On the response of rockglacier creep to surface temperature increase. *Global and Planetary Change* 56(1-2): 172-187.

Kääb, A., Lefauconnier, B. & Melvold, K. 2005. Flow field of Kronebreen, Svalbard, using repeated Landsat 7 and ASTER data. *Annals of Glaciology* 42: 7-13.

Kestler, M.A. 2003. Techniques for extending the life of low volume roads in seasonal frost areas, Transportation Research Board, Washington, D.C.

Khalili, N., Valliappan, S. & Geiser, F. 2000. A fully coupled thermo-hydro-mechanical model for double porous media. European Congress on Computational Methods in App. Sciences Engineering. ECCOMAS.

Kinnard, C. & Lewkowicz, A.G. 2005. Movement, moisture and thermal conditions at a turf-banked solifluction lobe, Kluane Range, Yukon territory, Canada. *Permafrost and Periglacial Processes* 16(3): 261-275.

Klassen, R., Arenson, L.U., Sego, D.C. & Biggar, K.W. 2007. Heat convection modeling in waste rock piles. *Proceedings, 5th Biennial Workshop on Assessment and Remediation of Contaminated Sites in Arctic and Cold Climates* (ARCSACC), May 6-8, 2007, Edmonton, AB, Canada.

Kneisel, C. & Kääb, A. 2007. Mountain permafrost dynamics within a recently exposed glacier forefield inferred by a combined geomorphological, geophysical and photogrammetrical approach. *Earth Surface Processes and Landforms* 32: 1797-1810.

Kneisel, C., Rothenbuhler, C., Keller, F. & Haeberli, W. 2007. Hazard assessment of potential periglacial debris flows based on GIS-based spatial modelling and geophysical field surveys: A case study in the Swiss Alps. *Permafrost and Periglacial Processes* 18: 259-268.

Konrad, J.M. 2005. Estimation of the segregation potential of fine-grained soils using the frost heave response of two reference soils. *Canadian Geotechnical Journal* 42(1): 38-50.

Konrad, J.M. & Lemieux, N. 2005. Influence of fines on frost heave characteristics of a well-graded base-course material. *Canadian Geotechnical Journal* 42(2): 515-527.

Lebeau, M. & Konrad, J.M. 2007. The effects and significance of natural convection in rockfill dams under cold climate conditions. *Proceedings, 60th Canadian Geotechnical Conference,* Ottawa, ON, Canada, October 21-24, 2007: 2084-2091.

LeBlanc, A.M., Fortier, R., Allard M., Cosma, C. & Buteau, S. 2004. Seismic cone penetration test and seismic tomography in permafrost. *Canadian Geotechnical Journal* 41(5): 796-813.

LeBlanc, A.M., Fortier, R., Cosma, C. & Allard, M. 2006. Tomographic imaging of permafrost using three-component seismic cone-penetration test. *Geophysics* 71(5): H55-H65.

Lewkowicz, A.G. 2007. Dynamics of active-layer detachment failures, Fosheim Peninsula, Ellesmere Island, Nunavut, Canada. *Permafrost and Periglacial Processes* 18(1): 89-103.

Lai, Y.M., Zhang, S.J., Zhang, L.X. & Xiao, J.Z. 2004. Adjusting temperature distribution under the south and north slopes of embankment in permafrost regions by the ripped-rock revetment. *Cold Regions Science and Technology* 39(1): 67-79.

Liu Z.Q., Lai, Y.M. & Yu, W.B. 2006. Three-dimensional numerical analysis for temperature characteristic of ventilated embankment with insulated door. *Proceedings, 13th International Conference on Cold Regions Engineering,* July 23-26, 2006, Orono, Maine: CD-Rom.

Lyle, R.R., Hutchinson, D.J. & Preston, Y. 2004. Landslide processes in discontinuous permafrost, Little Salmon Lake (NTS 105L/1 and 2), south-central Yukon. In: *Yukon Exploration and Geology.* Yukon Geological Survey: 193-204.

Maurer, H. & Hauck, C. 2007. Instruments and methods: Geophysical imaging of alpine rock glaciers. *Journal of Glaciology* 53(180): 110-120.

Mazhitova, G., Karstkarel, N., Oberman, N., Romanovsky, V. & Kuhry, P. 2004. Ambio 33(6), Royal Swedish Academy of Sciences: 289-294.

McDowell, G. R. 2003. Micromechanics of creep of granular materials. *Géotechnique* 53(10): 915-916.

Messerklinger, S. & Springman, S.M. 2007. Local radial displacement measurements of soil specimens in a triaxial test apparatus using laser transducers. *Geotechnical Testing Journal* 30(6): GTJ100735.

Mills, B., Tighe, S., Andrey, S., Huen, K. & Parm, S. 2006. Climate change and the performance of pavement infrastructure in southern Canada: Context and case study. *Proceedings, Climate Change Technology Conference 2006,* Ottawa, ON, Canada, May 10-12, 2006: CD-Rom.

Musil, M., Maurer, H., Green, A., Horstmeyer, H., Nitsche, F.O., Vonder Mühll, D. & Springman, S.M. 2002. Case history: Shallow seismic surveying of an Alpine rock glacier. *Geophysics* 67(6): 1701-1710.

Nicolsky, D.J., Romanovsky, V.E., Alexeev, V.A. & Lawrence, D.M. 2007. Improved modeling of permafrost dynamics in a GCM land-surface scheme. *Geophysical Research Letters* 34: L08501.

Niu, F.J., Cheng, G.D., Ni, W.K. & Jin, D.W. 2005. Engineering-related slope failure in permafrost regions of the Qinghai-Tibet Plateau. *Cold Regions Science and Technology* 42(3): 215-225.

Nixon, M.F. & Grozic, J.L.H. 2007. Submarine slope failure due to gas hydrate dissociation: a preliminary quantification. *Canadian Geotechnical Journal* 44(3): 314-325.

Oswell, J., Skibinsky, D. & Radmard, S. 2007. Pore water pressure response to thawing permafrost. *Proceedings, 60th Canadian Geotechnical Conference,* Ottawa, ON, Canada, October 21-24, 2007: 2068-2075.

Overduin, P.P., Kane, D.L. & VanLoon, W.K.P. 2006. Measuring thermal conductivity in freezing and thawing soil using the soil temperature response to heating. *Cold Regions Science and Technology* 45(1): 8-22.

Palmer, A.C. & Williams, P.J. 2003. Frost heave and pipeline upheaval buckling. *Canadian Geotechnical Journal* 40(5): 1033-1038.

Pham, H.N., Arenson, L.U. & Sego, D.C. 2008. Numerical analysis of forced and natural convection in waste-rock piles in permafrost environments. Proceedings, Ninth International Conference on Permafrost, June 29-July 3, 2008, Fairbanks, Alaska, USA (this proceedings).

Phillips, M., Ladner, F., Müller, M., Sambeth, U., Sorg, J. & Teysseire, P. 2007. Monitoring and reconstruction of a chairlift midway station in creeping permafrost terrain, Grächen, Swiss Alps. *Cold Regions Science and Technology* 47(1-2): 32-42.

Pimentel, E., Sres, A. & Anagnostou, G. 2007. Modelling of ground freezing in tunnelling. ITA-AITES World Tunnel Congress "Underground Space: the 4th Dimension of Metropolises," Prague.

Ribolini, A. & Fabre, D. 2007. Shallow active layer temperature and DC resistivity of a rock glacier in the Argentera Massif, Maritime Alps, Italy. *Zeitschrift für Geomorphologie* 51: 55-77.

Romanovsky, V., Marchenko, S., Duguay, C., Zheleznyak, M. & Sergeev, D. 2006. Monitoring and modeling of the Northern Eurasia permafrost dynamics. *Arctic Science Conference Abstracts* 58.

Rist, A. 2007. Hydrothermal processes within the active layer above alpine permafrost in steep scree slopes and their influence on slope stability. Ph.D. thesis. Swiss Federal Institute for Snow and Avalanche Research and University of Zurich, 168 pp.

Sánchez, M., Gens, A. & Olivella, S. 2002. A coupled double structure formulation for THM analysis. Environmental Geomechanics. Monté Verità, eds Vulliet, Laloui, Schrefler, EPFL Press 315-320.

Schwab, J.W., Geertsema, M. & Evans, S.G. 2003. Catastrophic rock avalanches, West-Central British Columbia. *Proceedings, 3rd Canadian Conference on Géotechnique and Natural Hazards,* Edmonton, AB, Canada: 252-259.

Siciliano, S., Schafer, A. & Snape, I. 2007. Liquid water content increases in frozen Antarctic soils that are contaminated with hydrocarbons. *Proceedings, Conference on Assessment and Remediation of Contaminated Sites in Arctic and Cold Climates*. Edmonton AB, Canada, May 6-8, 2007: 92-98.

Sun, B.X., Yang, L.J. & Xu, X.Z. 2007. Onset and evaluation on winter-time natural convection cooling effectiveness of crushed-rock highway embankment. *Cold Regions Science and Technology* 48(3): 218-231.

Sun, B.X., Xu, X.Z. Lai, Y.M. & Fang, M.X. 2005. Evaluation of fractured rock layer heights in ballast railway embankment based on cooling effect of natural convection in cold regions. *Cold Regions Science and Technology* 42: 120-144.

Tighe, S.L., Cowe Falls, L., Haas, R. & MacLeod, D. 2006. Climate impacts and adaptations on roads in Northern Canada. TRB 85th Annual Meeting: CD-Rom.

Torrance, J.K. & Schellekens, F.J. 2006. Chemical factors in soil freezing and frost heave. *Polar Record* 42(220): 33-42.

U.S. Arctic Research Commission Permafrost Task Force. 2003. Climate Change, Permafrost, and Impacts on Civil Infrastructure. Special Report 01-03, U.S. Arctic Research Commission, Arlington VA, USA.

Uthus, L., Hermansson, Å., Horvli, I. & Hoff, I. 2006. A study on the influence of water and fines on the deformation properties and frost heave of unbound aggregates. *Proceedings, 13th International Conference on Cold Regions Engineering,* July 23-26, 2006, Orono, Maine: CD-Rom.

Vidstrand, P. 2007. Density-driven flow beneath a continuous permafrost layer: generic simulations of hydrodynamic effects due to salt rejection. *Proceedings 60th Canadian Geotechnical Conference,* Ottawa, ON, Canada, October 21-24, 2007: 341-346.

Vonder Mühll, D.S., Arenson, L.U. & Springman, S.M. 2003. Temperature conditions in two Alpine rock glaciers. *Proceedings, 8th International Conference on Permafrost,* Zurich, 21-25.7.2003, (2): 1195-1200, Rotterdam: Balkema.

Wei, M., Fujun, N., Satoshi, A. & Dewu, J. 2006. Slope instability phenomena in permafrost regions of Qinghai-Tibet Plateau, China. *Landslides* 3: 260-264.

Wu, T.H., Li, S.X., Cheng, G.D. & Nan, Z.T. 2005. Using ground-penetrating radar to detect permafrost degradation in the northern limit of permafrost on the Tibetan Plateau. *Cold Regions Science and Technology* 41(3): 211-219.

Yasufuku, N., Springman, S.M., Arenson, L.U. & Ramholt, T. 2003. Stress-dilatancy behaviour of frozen sand in direct shear. *Proceedings, 8th International Conference on Permafrost*, Zurich, 21.-25.7.2003, (2): 1253-1258, Rotterdam: Balkema.

Yoshikawa, K., Bolton, W.R., Romanovsky, V.E., Fukuda M. & Hinzman, L.D. 2003. Impacts of wildfire on the permafrost in the boreal forests of interior Alaska. *Journal Geophysical Research* 108 (D1): 8148.

Yu, W.B., Lai, Y.M., Sun, Z.Z., Jin, H.J. & Zhang, X.F. 2006. Experimental studies on the ripped-rock revetment embankment in permafrost regions of the Qinghai-Tibet railroad. *Cold Regions Science and Technology* 45(1): 1-7.

Zhang, X., Sun, S.F. & Xue, Y.K. 2007a. Development and testing of a frozen soil parameterization for cold region studies. *Journal of Hydrometeorology* 8(4): 690-701.

Zhang, M.Y., Lai, Y.M., Yu, W.B. & Huang, Z. 2007b. Experimental study on influence of particle size on cooling effect of crushed-rock layer under closed and open tops. *Cold Regions Science and Technology* 48(3): 232-238.

Zhang, M.Y., Lai, Y.M., Li, S.Y. & Zhang, S.J. 2006. Laboratory investigation on cooling effect of sloped crushed-rock revetment in permafrost regions. *Cold Regions Science and Technology* 46(1): 27-35.

Thermal State of Permafrost in Northern Transbaykalia, Eastern Siberia

Julia Stanilovskaya
Institute of Environmental Geoscience, Russian Academy of Sciences, Moscow, Russia
Julia Ukhova
Institute of Environmental Geoscience, Russian Academy of Sciences, Moscow, Russia
Dmitry Sergeev
Institute of Environmental Geoscience, Russian Academy of Sciences, Moscow, Russia
Irina Utkina
Environmental Analytical Center, "Gazprom" company, Moscow, Russia

Abstract

Temperature monitoring is important for studying the modern permafrost dynamics in mountains of Northern Transbaykalia. The authors combined the permafrost observation with the microclimatic study. The criteria were proposed to estimate the representativeness of each observing site. Middle-scale hypsometric and vegetation maps with other kinds of descriptive information were used. In choosing each monitoring site, it is necessary to take into account the site accessibility, the state of the borehole, and the extent of characterized landscape (limits of homogenous conditions of relief, vegetation, and permafrost). The measurements have shown a 0.5ºC final increase in permafrost temperatures at the 20 m depth from 1987 to 2007.

Keywords: site selection; temperature measurement; temperature observation sites; TSP program.

Introduction

In view of the International Polar Year, the Permafrost Laboratory of the Institute of Environmental Geoscience RAS was involved in the Thermal State of Permafrost (TSP) program with regard to permafrost temperature observations. The permafrost of Northern Transbaykalia is well studied; consequently there was an interest in repeating the measurement characteristics of permafrost. Notice was taken of the boreholes 20 m deep that are located in undisturbed conditions. More than 200 of such boreholes were constructed especially for temperature observations in 1970–80.

The work on logger installation in Northern Transbaykalia started in 2005. While working on logger installation, the question arose, "What principle should we use to choose boreholes and to place loggers in them?" For the rationalized work, it is necessary to zone territory and to allocate sites that are better than the others reflected by geographical conditions. For this purpose, a multifaceted approach has been chosen. Our observation points are considered to be the representative sites.

Basic Assumptions and Research Objective

The aim of the research is substantiation of representative temperature observations under the TSP program. Our purpose is the following:

1. To collect 200 boreholes from different sources constructed especially for temperature observations for 1970–80.
2. To chart the vegetation and hypsometric maps.
3. To give consideration of the borehole construction conditions and the site accessibility.

Research Area

The region of research is located south of the Siberian platform and includes the Kodar Ridge, the Udokan Ridge, and the intermountain of the Chara Depression (Fig. 1).

The coordinates of the Chara settlement are 56.9ºN and 118.4ºW. The Chara Depression extends 120 km southwest to northeast, and its width is 30–35 km. The northwest side of the Chara Depression is formed by the abrupt, almost rectilinear slopes of the Kodar Ridge; the southeast border is formed by foothills slopes of the Udokan Ridge that are smoothly de-

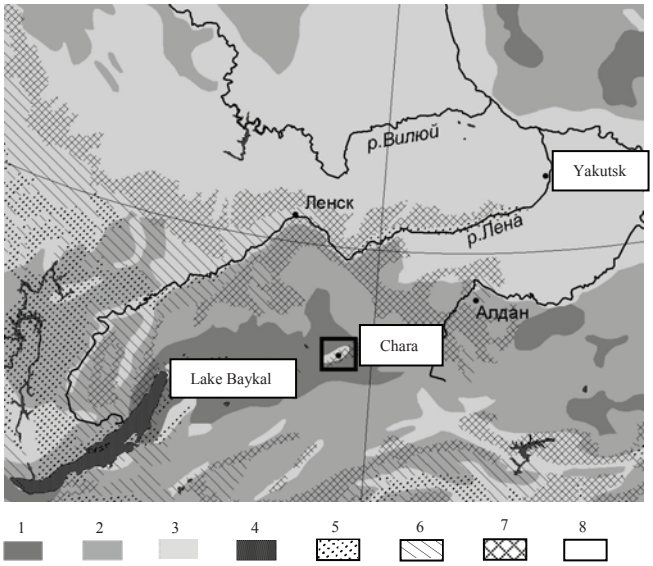

Figure 1. The location of investigation area (shown as a square). 1–3 – Relief types (1, high mountains with glaciers; 2, middle mountains; 3, plaines), 4 – Lakes; 5–8 – Permafrost extent (5, isolated patches; 6, sporadic; 7, discontinuous; 8, continuous). A circumpolar permafrost map was used (Brown et al. 2003).

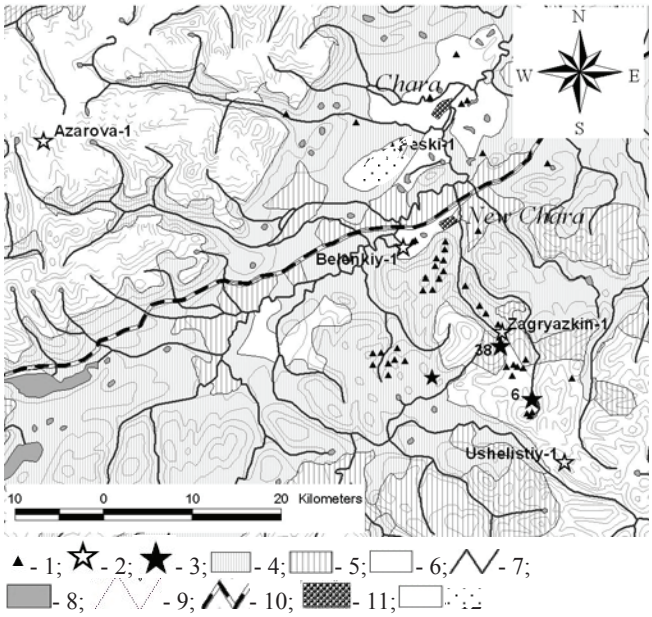

Figure 2. Scheme of investigation region with the location of the original and selected boreholes
1 – original boreholes and wells clusters; 2 – soil temperature observation sites; 3 – actual temperature boreholes. Vegetation: 4 – larch forest; 5 – open woodland; 6 – no forest vegetation (alpine tundra or bogs); 7 – rivers; 8 – lakes; 9 – relief isolines; 10 – railroads; 11 – town; 12 – the Chara Sandy Desert.

scending towards the bottom of the Chara Depression. There are 3 macro levels on investigated territory: the Kodar Ridge with alpine relief and with absolute heights of 3073 a.s.l. (the Peak of the BAM), the Udokan Ridge with golets (smooth mountains) and absolute heights up to 2515 a.s.l. and the Chara Depression with average heights of 600–800 a.s.l. The climate of the territory in question is characterized by extreme continentality with air temperature inversion. The monthly average air temperature in January is -23.9ºC, and in July is +12.5ºC. Average annual precipitation is 700 mm.

Method

The authors used six criteria choosing representative sites: distribution of available boreholes, relief, vegetation, permafrost, state of borehole, and site accessibility.

1. *The distribution of available boreholes*. The mountain permafrost is the science-intensive and engineering-important object of investigation. The intensive permafrost survey was conducted in the Northern Transbaykalia region by the Permafrost Institute in 1960s and by the Chitageologia, the ZabTISIZ, the Chita Institute of Natural Resources and the Moscow State University in the 1970s (Chastkevich 1966, Klimovsky 1966, Nekrasov & Chastkevich 1966, Leibman 1979, Romanovskii et al. 1989, Shesterniov & Yadrishensky 1990).

Regular observations were interrupted in the middle of the 1990s. Figure 2 presents the map showing the location of the original 200 boreholes with the 7 boreholes and monitoring sites selected.

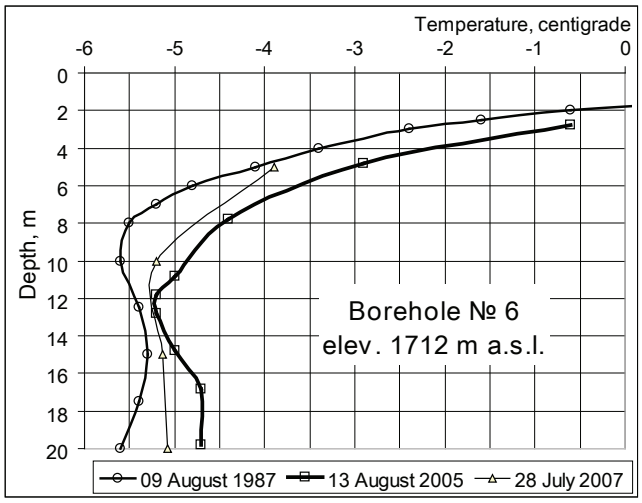

Figure 3. Temperature observation results in the borehole #6 for 1987–2007.

The boreholes are mainly located in the Udokan Ridge, where engineering projects were carried out in the 1970s. Three temperature monitoring sites have been chosen, therefore, including 20 m deep boreholes for 2005–2007. These boreholes are called #6, #38, and Peski-1. The temperature results from #6 and #38 boreholes have been obtained for 2006–2007. The measurements have shown an increase in permafrost temperatures at the scale of 0.5ºC on the 20 m depth for 1987–2006 (Fig. 3).

Figure 4 shows the invasion course of a seasonal wave of temperature fluctuations in coarse debris. The seasonal fluctuations are observed to be 20 meters deep along of low moisture content of rocks and high heat conductivity of quartzitic sandstone.

The Peski-1 borehole is located in the Chara Depression on isolated sandy desert where permafrost is absent. Thus, we have obtained temperatures concerning the Chara Sandy Desert.

There are four active layer observing points with air temperature measurements (kurum's pit – Zagryazkin-1, #5301; Ushelistiy-1; Belenkiy-1; Azarova-1) that were chosen by the authors for 2005–2007. Table 1, which summarizes the characteristics of the chosen boreholes and active layer observing points, is presented at the end of the paper.

The kurum's pit – Zagryazkin-1 (#5301) was produced by scientific and production forces in the 1980s. The authors obtained the temperature data in 2006 (Fig. 5). That allowed for typical block slope detailed information about temperature regime in the active layer where the intensive air convection and water condensation processes are usual.

The kurum's deposits occupy at least 50% of the slope area in the upper belt of The Udokan Ridge and result in a freezing effect on the underlying rocks (Romanovskii et al. 1991, Harris & Pedersen 1998, Gorbunov et al. 2004).

In 2007 three representative sites (Ushelistiy-1; Belenkiy-1; Azarova-1) were established. The active layer observing points have been chosen to proceed from the

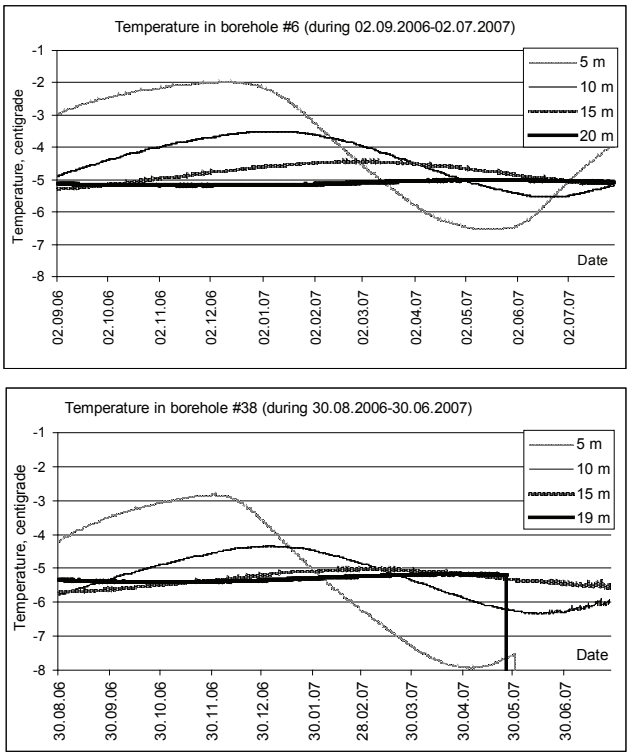

Figure 4. Temperature observations results in the borehole #6 and #38 for 2006–2007 (two channels, 5m and 19m. failed after April 2007).

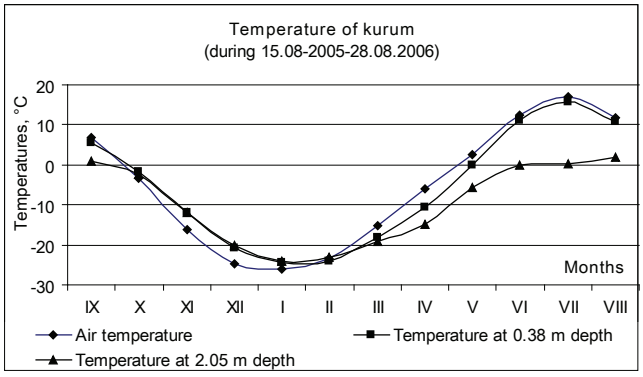

Figure 5. The mean monthly temperature data of kurum's pit in 2006.

premise that the point "Ushelistiy-1" represented the relict ice wedge polygons in the high mountain zone. The point "Belenkiy-1" took advantage of an active layer and relict ice wedge polygons in the Chara Depression. The point "Azarova-1" represented an active layer in moraine near the tongue of the Azarova Glacier in the Kodar Ridge.

The air, soil surface, and active layer temperatures were measured every 3 hours.

2. *The relief*. Whereas we study the alpine region, we take into account the geomorphology of different parts of the region. The orography is the product of tectonical and climate evolution and has a great impact on formation of natural territory conditions. That is why this territory has altitudinal landscape zonality.

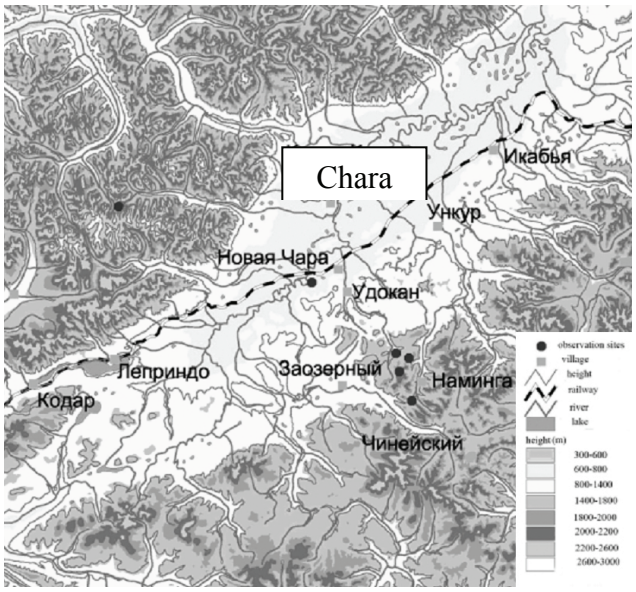

Figure 6. The hypsometric map of investigation territory.

In Figure 6, the hypsometric map is presented. The authors equipped the boreholes and active layer observing points by loggers at dominant heights.

The permafrost observations are based in a range of the heights from 730 m to 2200 m a.s.l. (see Table 1). Viz: Belenkiy-1 on 720 m a.s.l., Peski-1 on 767 m a.s.l., kurum's pit – Zagryazkin-1 (#5301) on 1155 m a.s.l., #6 on 1712 m a.s.l., #38 on 1464 m a.s.l., Ushelistiy-1 on 1651 m a.s.l., and Azarova-1 on 2036 m a.s.l. The height of temperature observation sites are shown in Figure 7.

The monitoring sites are accordingly located in the mountain altitudinal belt, in the upper part of mountain-taiga belt and at the bottom of the Chara Depression.

3. *The landscapes*. All the observing sites represent the nondisturbed landscapes. There are three dominated vegetations—such as "larch forest," "open woodland," and "alpine tundra"—that are presented in Figure 2. Our observing points are located in almost all types of vegetation. For example, the point "Belenkiy-1" is in a bog with larch; the kurum's pit (Zagryazkin-1, #5301) and #38 are in open woodland; the point "Azarova," #6 and Ushelistiy-1 are in alpine tundra. The borehole "Peski-1" is located in the unique Chara Sandy Desert. Knowledge of the cryological conditions is also possible through studying the external physionomical shape of a landscape.

4. *The permafrost*. Northern Transbaykalia is situated in a continuous permafrost zone. Cryological conditions are characterized by high heterogeneity. A local distribution of permafrost varies from sporadic to continuous thickness—from several meters up to 1200 m—and temperature from 0ºC up to -12ºC.

The permafrost conditions are different in depressions and mountains. A maximal thickness of permafrost is found at the foothills of northern expositions and at the bottoms of deep valleys in a depression. Permafrost thickness increases toward watersheds. On watersheds with the dominating

Table 1. The data of the temperature monitoring sites.

Site number/ characteristics	6	38	Peski-1	Zagryazkin-1 (kurum's pit #5301)	Ushelistiy-1	Belenkiy-1	Azarova-1
Latitude and longitude	N56º 36.329' E118º25.591'	N56º 40.017' E118º 21.648'	N56º 50'33.30' E118º 09'15.93'	N56º 40.567' E118º 21.621'	N56º 40.017' E118º 21.648'	N56º 45'39.63' E118º 11'24.53'	N56º 54' 23.33' E117º 34'41.64'
Borehole depth or pit depth (m)	20	19	15.33	2.05	0.33	1.3	1
Elevation (above sea level , m)	1712	1464	767	1155	1651	720	2036
Site slope (angle - degrees, aspect)	15 East-North-East	Flat	Flat	11 South-West	Flat	Flat	Flat
Site topography and local relief	Slope (Top of hill or ridge)	Top of hill or ridge	Plain	Slope	Valley	Valley	Valley
Landform or geo-morphologic description and history of site (age)	Left slope of the the Nirungnacan River – the surface has formed in middle time of Pleistocene. The block slope deposit (kurums)	Left divide surface of the Klyukvenniy River – the surface has formed in middle time of Pleistocene. The stone circles at coarse eluvium's deposits	Sand massif	Low part of the slope; the upper part of the Klyukvenniy River – the glacial valley that has formed in middle time of Pleistocene. The kurum's deposits have originated from a moraine.	Dividing saddle is located between the Ushelistiy Sike and the Ingamakit River of the Udokan Ridge. Pleistocen	First terrace of the Chara River. Pleistocene.	Moraine near the tongue of the Azarova Glacier (the Kodar Ridge)
Geology (brief description of bedrock, sediments)	From the top: 0.0-5.5 m – coarse debris; 5.5-20.0 m – quartzite sandstone of Early Proterozoic Age	From the top: 0.0-3.5 m – coarse debris eluvium with sand; 3.5-19.0 m – quartzite sandstone of Early Proterozoic Age	Sands	From the top: 0.0-2.2 m – active layer in kurum (debris slope) with large blocks (0.2-1.0 m); 2.2-8.0 m – moraine deposits with ice; 8.0-20.0 m – quartzite sandstone of Early Proterozoic Age.	From the top: 0.0-0.38 m – dark-brown peat; 0.38-0.45 m – peat; 0.45-… m ice wedge	From the top: 0.00-0.10 green moss; 0.10-0.20 brown peat; 0.20-1.30 dark-brown clay sand with ice wedges	From the top: 0.0-1.00 m – coarse debris with sand
Dominant site vegetation	Mountain tundra with crustose lichens	Upper limit of mountain taiga – larch tundra-forest with cedar elfin wood shrubs	Sand desert	Large kurum-clearing with crustose lichens (within mountain taiga – larch tundra-forest with "cedar elfin wood" shrubs)	Upper limit of mountain tundra - forest with cedar elfin wood shrubs	Taiga with fire-damaged forest	Alpine tundra
Permafrost presence	Permafrost	Permafrost	No permafrost	Permafrost	Permafrost	Permafrost	Permafrost

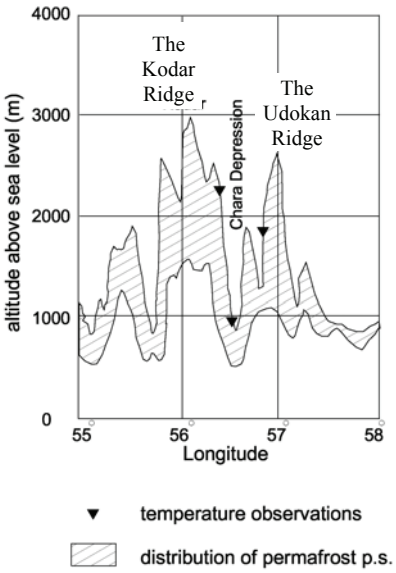

Figure 7. The temperature observation sites on the schematic geocryological profile (cryohydrological conditions, 1984).

heights of 2000–2200 m a.s.l., the thickness of permafrost is 800–900 m, and temperatures are -6 ºC to -8ºC. The point "Azarova-1" was equipped by loggers here. Under peaks with the heights of 2300–2700 m a.s.l., permafrost temperatures are -10ºC … -12ºC, and thickness is 1000–1200 m (Nekrasov & Klimovsky 1978). The Chara Depression is characterized by a most severe environment that promotes continuous development of permafrost at the bottom of the depression with the thicknesses of 100–500 m, with temperatures being -1.5ºC … -6.0ºC (Nekrasov & Klimovsky 1978). In marginal parts of a depression, the thickness of permafrost does not exceed 100–200 m, and an annual average temperature of rocks in most cases is -3ºC. The taliks are distributed within the limits of the Chara Sandy Desert on the left bank of the Chara River and under the riverbeds of large rivers (rivers Chara, Verkhniy and Sredniy Sakukan, etc.). Not far from the Chara Sandy Desert the authors measured temperature in the borehole "Peski-1."

The altitudinal zonality markedly affects the formation of landscape and cryological conditions. The cryological conditions become more severe, the area of taliks decreases, and massive-island distribution of permafrost is replaced by continuous permafrost at the height over 1000 a.s.l. with the altitude increasing.

5. *The state of borehole*. Obviously the good condition of original (old) observation boreholes decreases the expenses of monitoring installation. The boreholes need the special thermal insulation collar to decrease the influence of high thermal conductivity of the steel conductor. If the collar tube is not hermetic, it is possible that ice plugging will form. All sites of actual observation are in good shape.

6. *Accessibility* (mode of transportation: helicopter, road, off-road vehicle, river, etc.). All the temperature observation sites are not far from roads. The real obstacle for the work is the coordinate data absence of the original (old) boreholes. It is difficult to find a small collar in a bush. The active layer observing points have a GPS-affixment.

Conclusions

At the first stage of the TSP program realization in Northern Transbaykalia, the authors obtained a set of observation sites that are almost all located at high-altitude levels, in all landscapes and in all permafrost conditions. This set is unique in Russia, representing the highest altitudinal level of mountain.

Besides the temperature logger installation, the authors have gathered available data on the region (maps, rows of previous monitoring data, descriptions of landscape and natural processes, etc.). This information is important in allocating representative sites on which loggers have already been placed, in estimating the priority of site installation, and in helping to correctly analyze the results of actual permafrost observation. The authors can allocate the most valuable and prime boreholes for temperature measurements analyzing the whole set of boreholes (200 boreholes).

The use of remote sensing materials has been found to be rational at all stages of cryological research and helps to map permafrost and general natural conditions of the territory in tight deadlines and with economic consideration of material resources. It will allow the saving of time and money for expeditions and will improve the accuracy and informativeness of temperature regime monitoring for Northern Transbaykalia.

The results of temperature monitoring will be published on the Internet for practical and educational purposes.

Acknowledgments

This work is supported by grants of Russian Fund of Basic Research (06-05-64959a, 05-05-64390a, 05-05-64215a), National Science Foundation (Polar Earth Science Program, Office of Polar Programs – ARC-0632400, ARC-0520578), NASA THP Discovery Investigation "Current climate changes over Eastern Siberia and their impact on permafrost landscapes, ecosystem dynamics, and hydrological regime," and INTAS 06-1000013-8593 "Evaluating the Recent and Future Climate Change and Glacier Dynamics in the Mountains of Southern Siberia."

Special thanks to Vladislav Podgorbunsky who provided the sustainable fieldwork in the Chara settlement and to all Soviet geologists who conducted the permafrost observation in 1970s and 1980s.

References

Brown, J., Ferrians, O.J., Heginbottom, J.A. & Melnikov, E.S. 2003. Circum-Arctic Map of Permafrost and Ground-Ice Conditions. International Permafrost Association Standing Committee on Data Information and Communication (comp.). *Circumpolar Active-Layer Permafrost System, Version 2.0.* Edited by M. Parsons and T. Zhang. Boulder, CO: National Snow and Ice Data Center/World Data Center for Glaciology. CD-ROM.

Gorbunov, A.P., Marchenko, S.S. & Seversky E.V. 2004. The thermal environment of blocky materials in the mountains of Central Asia. *Permafrost and Periglacial Processes* 15: 95-98.

Klimovsky, I.V. 1966. Geocryological characteristic of the massif of blowing sands in the Chara Depression. Geocryological Condition of Transbaykalian North, Novosibirsk, Nauka, 181-186 (in Russian).

Leibman, M.O. 1979. Vertical geotemperature zonality in the mountain regions adjacent to BAM railroad. Engineering survey in construction, Collected abstracts, Issue 1, PNIIIS, Moscow: 114 (in Russian).

Nekrasov, I.A. & Klimovsky I.V. 1978. Permafrost of BAM. Novosibirsk, Nauka, 119 pp. (in Russian).

Nekrasov, I.A. & Shastkevich, J.G. 1966. Some data about permafrost in Kodar Ridge. Geocryological Condition of Transbaykalian North, Novosibirsk, Nauka, 100-106 (in Russian).

Romanovsky, N.N., Tyrin, A.I. & Sergeev, D.O. 1989. Kurums in the bald mountains. Novosibirsk, Nauka, 150 pp. (in Russian).

Shastkevich, J.G. 1966. Permafrost of high mountain part of Udokan Ridge and conditions of this temperature regime formation. Geocryological Condition of Transbaykalian North, Novosibirsk, Nauka, 24-43 (in Russian).

Shepelev, V.V., Tolstichin, O.N. & Piguzova, V.M. 1984. Cryo-hydrological conditions of Eastern Siberia, Novosibirsk, Nauka, 191 pp. (in Russian).

Shesternyov, D.M. & Yadrichensky, G.E. 1990. Structure and peculiarities of rocks in Udokan's cryolithozone. Novosibirsk, Nauka, 126 pp. (in Russian).

Dry Climate Conditions in Northeast Siberia During the MIS2

Georg Stauch
Department of Geography, RWTH Aachen University, Templergraben 55, D-52056 Aachen, Germany
Frank Lehmkuhl
Department of Geography, RWTH Aachen University, Templergraben 55, D-52056 Aachen, Germany

Abstract

Late Quaternary glaciations in the Verkhoyansk Mountains (NE Siberia) indicate extremely dry conditions during the global Last Glacial Maximum (MIS2). According to geomorphological investigations and IRSL dating results, the last major glaciation in the mountain system occurred before 50 ka. No glaciers were present in the area during the global Last Glacial Maximum. In the early part of the Last Glacial Maximum, precipitation was sufficient for the growth of large mountain glaciers. Precipitation during the stadial is strongly dependent on the size of the western sector of the Eurasian Ice Sheet.

Keywords: glacier; palaeoclimate; Siberia; Verkhoyansk Mountains.

Introduction

The Verkhoyansk Mountains in northeastern Siberia are the easternmost mountain system on the Eurasian continent which receives precipitation mainly from the Atlantic. Therefore the area is quite sensitive to changes on the northern part of the Eurasian continent. However, paleoclimatic studies in the area are very rare and mainly limited to palynological studies (e.g. Andreev et al. 1997, Anderson & Lozhkin 2001, 2002, Anderson et al. 2002, Kienast et al. 2005). Despite that, many new results emerged from the surrounding areas like western Siberia (Svendsen et al. 2004, Hubberten et al. 2004), the Laptev Sea coast (Bauch et al. 1999, Schirrmeister et al. 2002a, b, Grosse et al. 2007) and the Russian Far East (Gualtieri et al. 2000, 2003, 2005, Brigham-Grette 2001, 2003). In this last region Lake El'gygytgyn is located and it revealed a wealth of new information about the palaeoclimate of the area east of the Verkhoyansk Mountains (e.g. Brigham-Grette et al. 2007, Melles et al. 2007).

Quaternary glaciations are good indicators of the paleoclimatic environment as they are sensitive to temperature and moisture changes on a broader timescale. Up to now there have been only a few studies available dealing with Quaternary glaciations in the Verkhoyansk Mountains (Kind 1975, Kolpakov 1979, Kolpakov & Belova 1980). Research in the area was carried out in the 60th and 70th with only poor constraints on absolute dating. A summary of these works has been presented by Zamoruyev (2004). According to these authors the area was shaped by three major glaciations during the last glacial. The last glaciations occurred during the Marine Isotope Stage 2 (MIS2) of the global Last Glacial Maximum (gLGM). Another major ice advance happened during the MIS3 around 32 ka and one in the early part of the last glacial. Every one of the glacial advances in the last glacial was smaller than the previous one. However, new absolute dating results indicate that the morainic deposits in the area are older than previously assumed (Stauch et al. 2007).

Study Area

The Verkhoyansk Mountains (Fig. 1) are located in northeastern Siberia in the zone of continuous permafrost. The mountain range stretches for about 1200 km from the Laptev Sea at 72°N to Central Yakutia at 59°N. To the west, the Verkhoyansk Mountains are bordered by the Lena and Aldan Rivers and to the east by the Jana Highlands. While in the northernmost part, in the Kharaulakh area, maximum elevation is about 1400 m a.s.l., most summits in the south reach elevations of about 2000 to 2400 m a.s.l. The highest summit (2959 m a.s.l.) is reached in the Suntar Chajata, a southern branch of the mountain system. To the west, extended lowlands with elevations between 50 and 400 m a.s.l. stretch along the Verkhoyansk Range.

The climate in the area is extremely continental. Mean monthly air temperature varies between -40°C in January and +20°C in July. Annual precipitation ranges between 220 mm in the lowlands around Yakutsk and up to 700 mm on the western flank of the Verkhoyansk Mountains; on the eastern side of the mountain range the annual precipitation is only up to 200 mm (Lydolph 1977, Shagadenova et al. 2002). In the Verkhoyansk Mountains there are only a few small glaciers, mostly in the area of the Suntar Chajata. The recent snowline is between 2200 and 2400 m a.s.l. (Koreischa 1991, Murzin 2003, Ananicheva & Krenke 2005).

The study area was located in the central Verkhoyansk Mountains between 63°10′N and 66°40′N. The area consists of four large catchment areas on the western side and several smaller ones on the eastern flank of the mountains (Fig. 1) which sum up to an overall area of 150,000 km². The Tumara and Djaunshka valleys were chosen for the field work.

Methods

For the reconstruction of former glaciations, glacial-geomorphological landforms in the central part of the Verkhoyansk Mountains were mapped. Due to the remoteness of the area, without roads and settlements, remote sensing

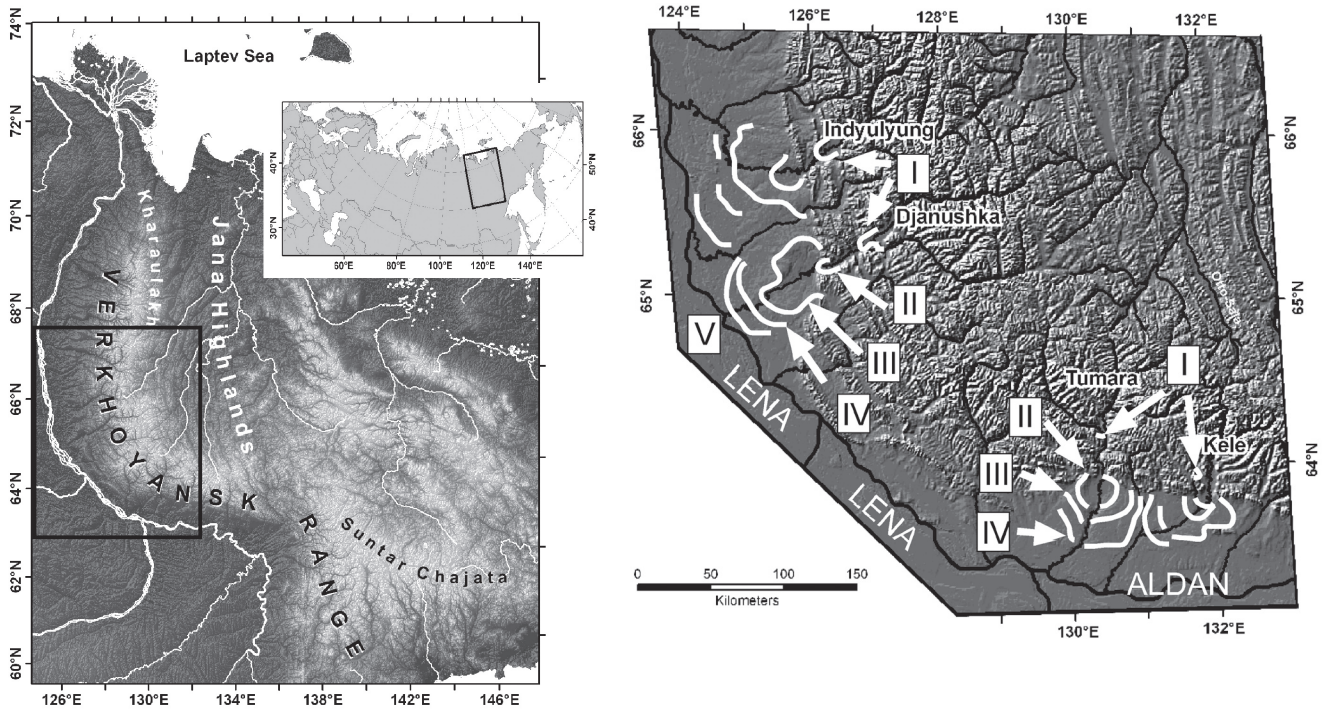

Figure 1. Study area, the Verkhoyansk Mountains (right side) and the central Verkhoyansk Mountains with the selected terminal moraines (left side).

data was utilized for the overall mapping of the region. The results of the image interpretation were in the second stage checked during two field seasons on the western side of the mountains, at which time samples for sedimentological analysis as well as for absolute dating were also taken. We used mainly aeolian cover sediments for IRSL (InfraRed Stimulated Luminescence), however at some points we also dated glacial-fluvial deposits. All samples were processed at the GGA Institute in Hannover, Germany. For a detailed description of the method and the complete table of the IRSL results see Stauch et al. (2007).

For the remote sensing analysis we used Landsat7 Data with a resolution of 30 m and 15 m respectively. A visual image interpretation approach was used for this study (Stauch 2006). This method was useful for identifying terminal moraines inside of the mountains as well as in the southern and western foreland. Besides the field work, crosschecking of the results was done with high resolution Corona images with a resolution of up to 2 m. Both methods showed that Landsat Data was sufficient for mapping of the glacial landforms in the area.

Moraines in the different catchment areas were grouped according to geomorphological criteria and relative position. The geomorphological criteria included degree of weathering and slope wash as well as the number and size of kettle lakes on the surface. Older moraines with a position most distant to the center of glaciation have a smoothed surface with low slope angles, while on younger moraines features of ice decay and moraines of small secondary re-advances are still visible. Kettle lakes are larger on older moraines than on younger ones. This is caused by longer lasting permafrost processes, which often resemble the former ice margins. Besides morphological criteria these older moraines show distinctive differences in the mineralogical composition of the sediments (Popp et al. 2006, 2007).

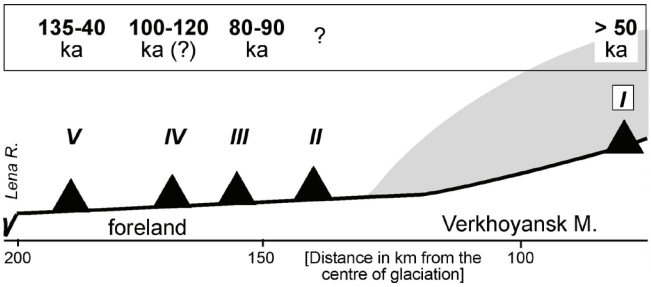

Figure 2. Schematic cross section of the western foreland and the Verkhoyansk Mountains with the ages of the terminal moraines (Stauch et al. 2007).

Results

Geomorphological mapping revealed four to five sets of terminal moraines on the western and southern side of the Verkhoyansk Mountains. The uppermost moraines (named I, Fig. 1) are located inside of the mountains system about 50 to 80 km away from the supposed center of glaciations, while the other moraines (II to V) have been deposited either at the mountain front or in the foreland (Fig. 2). These later moraines are generally much larger in size than the ones further upstream. On the eastern site the terminal moraines

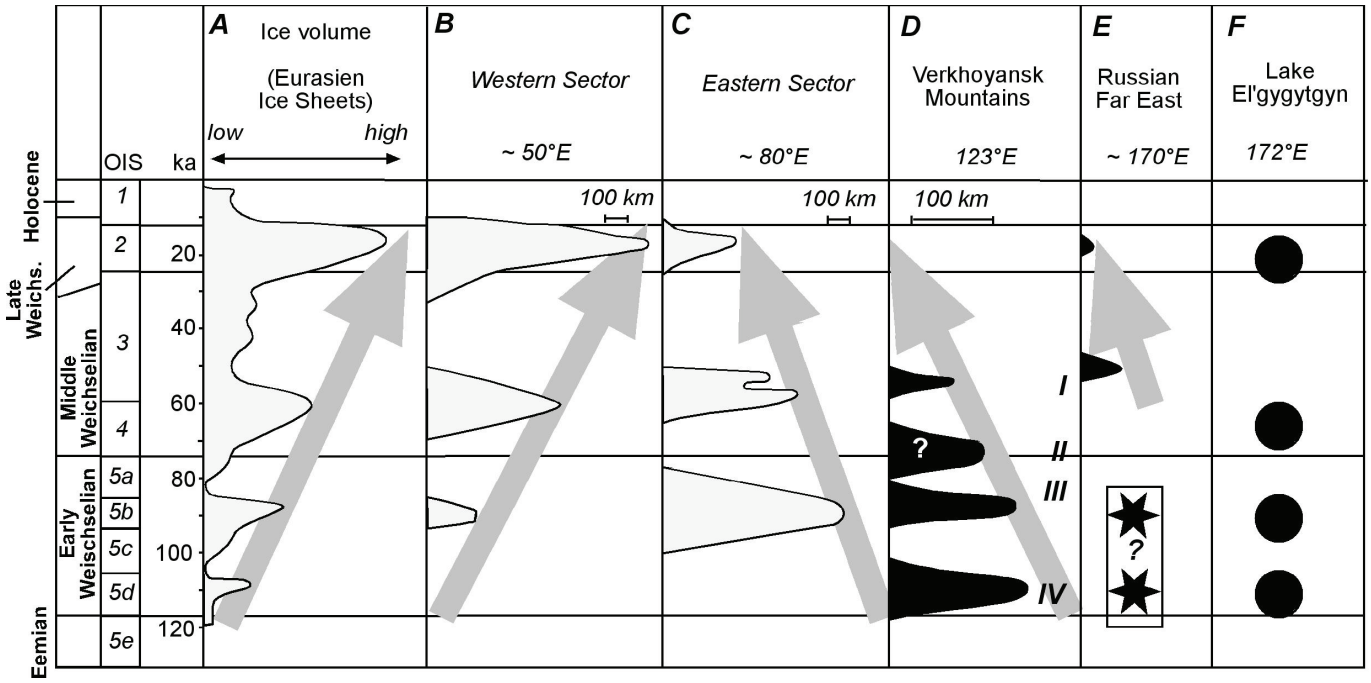

Figure 3. Time distance diagram of glaciations in the northern Asia (A-C: Svendsen et al. 2004, D: Stauch et al. 2007; E: Stauch & Gualtieri *subbm.*, Stars: Brigham-Grette 2001) and cold phases (F: dots) according to Brigham-Grette et al. (2007).

are much smaller and strongly eroded. Therefore, correlation of moraines on the eastern and western side is complicated and mainly based on the relative location of the sediments to the supposed center of glaciations.

However, dating of the moraines revealed that they are much older than previously assumed. Moraine I is older than 50 ka (Fig. 2). Aeolian cover sediments on a glacio-fluvial fan directly upstream of Moraine I in the Tumara catchment has an IRSL age estimate of 52.8 ± 4.1 ka (V09, Stauch et al. 2007). In the Djanushka catchment aeolian sands have been deposited above lacustrine sediments about six kilometers downstream of moraine I. These lacustrine sediments were formed sometime after the retreat of the glacier. The aeolian sediments on the top gave an IRSL age estimate of 39.7 ± 3.1 ka (Dj01). As no terminal moraines could be identified upstream of moraine I in any of the landforms in the northernmost, we suggest that the last studied catchment areas, except some small dubious glacial advance in the Verkhoyansk Mountains occurred before 50 ka. None of our results indicate a glaciation during the global Last Glacial Maximum during the MIS2.

Up to now no absolute ages for the second moraine are available. Aeolian sediments on top of the moraine point to a formation before 46.8 ± 3.1 ka (V17). However, this moraine is older than moraine I according to its stratigraphic position.

The formation of Moraine III presumably finished around 80 to 90 ka. This age estimation is based on two samples. In the Tumara catchment, glacio-fluvial sand in between the till gave an age of 86.9 ± 6.8 ka (V25). At the Djanushka River sand above Moraine III was dated to 92.3 ± 6.5 ka (Dj22).

Four IRSL samples have been dated at Moraine IV in the Tumara catchment. Glacio-fluvial sand at the top of the morainic sediments gave an IRSL age estimate of 97.6 ± 6.8 ka (V29). However, aeolian silt covering these sediments yielded IRSL ages of 123 ± 10 ka (V28) and 107 ± 10 ka (V27). Fluvial sediments on top of glacio-fluvial gravel in front of the moraine resulted in an IRSL age of 107 ± 10 ka. Despite the somewhat dubious due age in one of the profiles, we suppose that the formation of the moraines was completed between 100 and 120 ka.

For the outermost Moraine V two samples from glacial deformed sand between two thin layers of till resulted in IRSL ages of 135 ± 9 ka (DJ30) and 141 ± 10 ka (Dj31).

Discussion

Throughout the late Quaternary, glaciations in the Verkhoyansk Mountains became smaller indicating a reduction in precipitation during the different glacial phases. Comparing the results from the Verkhoyansk Mountains with neighboring regions indicates some continental trends in northern Asia (Fig. 3). Svendsen et al. (2004) compared the development of the western (Finland and western Russia) and the eastern (Arctic Russia, Siberia) sectors with the overall ice volume of the Eurasian Ice Sheets (British Scandinavian and Barents-Kara Ice sheets) throughout the last glacial. Taking all Ice Sheets together there is an overall trend in a growing ice volume during the pace of the last glacial. This trend is also reflected in the waxing of the Ice Sheet in the western sector, where the largest ice extent was reached in the later phase of the glacial during the MIS2.

The eastern sector of the Eurasian Ice Sheet developed the other way round, a large glaciation in the early part of

the last glacial and a considerably smaller one during the MIS2. A similar trend can be observed in the Verkhoyansk Mountains. However, while there are multiple glaciations in the early part of the glacial, no glaciation occurred during the last 50 ka. East of the Verkhoyansk Mountains only a few absolute datings are available (Stauch & Gualtieri subbm.). Studies of e.g. the Pekulney Mountains (Brigham-Grette et al. 2003) or the Koryak Mountains (Gualtirie et al. 2000) point to progressively smaller glaciations during the last glacial. The last glaciations occurred during the MIS2. Glacial advances in the early phase of the last glacial are still in debate (Brigham Grette 2001). Similar to the glacial advances in Eastern Siberia, several cold phases have been recognized in a core of Lake El'gygytgyn (Brigham-Grette et al. 2007).

The main factor controlling glaciations in Eastern Siberia was the amount of available precipitation, as much of the continent up to the Verkhoyansk Mountains depends (and depended) on the moisture-bearing winds from the west. During the glaciations this moisture was blocked depending on the size of the western sector of the Eurasian Ice sheet. In the early part of the last glacial, the western part of the Ice Sheet was relatively small leading to major glaciations in western Siberia (eastern sector of the Eurasian Ice Sheet) and to mountain glaciations in the Verkhoyansk Mountains. During the MIS2 the western part of the Eurasian Ice Sheet reached its maximum extent of the last glacial blocking most of the moisture. Therefore, the eastern sector of the Eurasian sector was comparable small, while no glacier developed in the Verkhoyansk Mountains despite very low temperatures. Models of western Siberia show similar results (e.g., Siegert & Marsiat 2001, Siegert & Dowdeswell 2004).

East of the Verkhoyansk Mountains in eastern Russia, the Pacific was at least an additional moisture source which, in turn, led to several mountain glaciations. In Western Siberia and the far east of the Asian continent at least little moisture was available. The environment in Eastern Siberia was cold and very dry during the MIS2.

Acknowledgments

The authors would like to thank the Deutsche Forschungsgemeinschaft (DFG; Le 730/10-1,2) for funding the project. Thanks also to Manfred Frechen for the IRSL dating, and all the Russian and German colleges we worked with in the Verkhoyansk Mountains.

References

Ananicheva, M.D. & Krenke, A.N. 2005. Evolution of climatic snow line and equilibrium line altitudes in the North-Eastern Siberian Mountains (20th Century). *Ice and Climate News* 6: 3-6.

Anderson, P.A. & Lozhkin, A.V. 2001. The stage 3 interstadial complex (Karginskii/ middle Wisconsinan interval) of Beringia: variations in paleoenvironments and implications for paleoclimatic interpretations. *Quaternary Science Reviews* 20: 93-125.

Anderson, P.A. & Lozhkin, A.V. 2002. Palynological and radiocarbon data from late Quaternary deposits of northeastern Siberia. In: P.A. Anderson & A.V. Lozhkin (eds.), *Late Quaternary Vegetation and Climate of Siberia and the Russian Far East (Palynological and Radiocarbon Database)*. Magadan: NESC FEB RAS, 27-34.

Anderson, P.A., Lozhkin, A.V. & Brubaker, L.B. 2002. Implications of a 24,000 yr palynological record for a Younger Dryas cooling and for boreal forest development in Northeastern Siberia. *Quaternary Research* 57: 325-333.

Andreev, A.A, Klimanov, V.A. & Sulerzhitsky, L.D. 1997. Younger Dryas pollen records from Central and Southern Yakutia. *Quaternary International* 41/42: 111-117.

Bauch, H.A., Kassens, H., Erlenkeuser, H., Grootes, P.M. & Thiede, J. 1999. Depositional environment of the Laptev Sea (Arctic Siberia) during the Holocene. *Boreas* 28: 194-204.

Brigham-Grette, J. 2001. New perspectives on Beringian Quaternary paleogeography, stratigraphy, and glacial history. *Quaternary Science Reviews* 20: 15 - 24.

Brigham-Grette, J., Gualtierie, L.M., Yu Glushkova, O., Hamilton, T.D., Mostoller, D. & Kotov, A. 2003. Chlorine-36 and 14C chronology support a limited last glacial maximum across central Chukotka, northeastern Siberia, and no Beringian ice sheet. *Quaternary Research* 59: 386-398.

Brigham-Grette, J., Melles, M, Minyuk, P. & Scientific Party 2007. Overview and significance of a 250 ka paleoclimate record from El'gygytgyn Crater Lake, NE Russia. *Journal of Paleolimnology* 37: 1-16.

Grosse, G., Schirrmeister, L., Siegert, C., Kunitsky, V.V., Slagoda, E.A., Andreev, A.A. & Dereviagyn, A.Y. 2007. Geological and geomorphological evolution of a sedimentary periglacial landscape in Northeast Siberia during the Late Quaternary. *Geomorphology* 86: 25 - 51.

Gualtieri, L., Glushkova, O. & Brigham-Grette, J. 2000. Evidence for restricted ice extent during the last glacial maximum in the Koryak Moutains of Chukotka, far eastern Russia. *Geological Society of America, Bulletin* 112: 1106-1118.

The Fate of Greenland's Permafrost: Results from High-Resolution Transient Climate Simulations

Martin Stendel, Jens Hesselbjerg Christensen, Guðfinna Aðalgeirsdóttir
Danish Meteorological Institute, Copenhagen, Denmark
Ronnie Daanen, Sergey Marchenko, Vladimir Romanovsky
University of Alaska, Fairbanks, Alaska, USA

Abstract

Simulations with global circulation models (GCMs) clearly indicate that major climate changes for Greenland can be expected during the 21st century. Due to their coarse resolution, contemporary global climate models (GCMs) have so far been unable to give a realistic representation of the dynamics of the Greenland ice sheet as well as the permafrost underlying the ice-free regions. Even relatively high-resolution regional climate models (RCMs) may fail in this respect. To improve climate projections, we have therefore conducted a transient simulation for the period 1950–2080 for the whole of Greenland with very high resolution. Based on these simulations, we present modeled changes in permafrost in an unprecedented high resolution.

Keywords: climate change; Greenland; permafrost; regional climate model.

Introduction

There is ample observational evidence for recent warming in high latitudes. Observed changes include air (Moritz et al. 2002) and soil temperature (Majorowicz & Skinner 1997, Osterkamp & Romanovsky 1999, Romanovsky et al. 2002, Osterkamp 2003), vegetation cover (Sturm et al. 2001), sea ice (Bjorgo et al. 1997), glacier mass balance (Arendt et al. 2002) and ice sheets (Rignot & Kanagaratnam 2006). Many of these changes affect the permafrost body (perennially frozen ground) and the seasonally thawed layer between it and the surface, the active layer. Climate change scenarios (e.g., IPCC 2007) indicate that warming due to anthropogenic activities will be greatest in polar regions. Changes involving permafrost may affect infrastructure and regional ecosystems due to thawing of the ground and development of thermokarst depressions (Romanovskii et al. 2000), or they may contribute to the release of large amounts of greenhouse gases.

Model studies with comprehensive coupled ocean-atmosphere general circulation models (AOGCMs) show that the area of the Northern Hemisphere underlain by permafrost could be reduced substantially in a warmer climate (Smith & Burgess 1999, Anisimov et al. 2001, Nelson et al. 2001, Stendel & Christensen 2002). However, thawing of permafrost, in particular if it is ice rich, is subject to a time lag due to the large latent heat of fusion of ice, which implies that permafrost in relict form can persist in deep layers for centuries or even millennia as in western Siberia. State-of-the-art AOGCMs are unable to adequately model these processes for three reasons: even the most advanced subsurface schemes rarely treat depths below 5 m explicitly; soil thawing and freezing processes cannot be dealt with directly due to the coarse resolution of present AOGCMs; and the required simulations covering millennia cannot be conducted due to computer power limitations.

It is important to note that any attempt to model subsurface processes needs information about soil properties, vegetation, and snow cover; but these are hardly realistic on a typical GCM grid. Furthermore, simulated GCM precipitation is often underestimated, and the proportion of rain and snow is incorrect (e.g., Christensen & Kuhry 2000). One possibility to overcome resolution-related problems is to use regional climate models (RCMs). Such an RCM, HIRHAM4 (Christensen et al. 1996), has until now been the only one used for the entire circumpolar domain (ACIA 2005), and it has also been used in this study. No specific treatment of soil freezing and thawing is done in HIRHAM, so the same limitations as for the GCM apply, and so far only studies based on frost indices have been conducted. As for coarser-scale models, these simulations also lack sufficient information about soil properties.

Instead of calculating a degree-day-based frost index from RCM data, we use the regional model to create boundary conditions for an advanced permafrost model. This approach, described in Stendel et al. (2007) in a proof-of-concept study, is novel in two aspects. Firstly, the RCM (and therefore the permafrost model) runs on an unprecedented horizontal resolution of 25 km for the entire region covering Greenland and the surrounding seas. Secondly, while most comparable studies have used "time-slices" due to computer limitations, we here present a fully transient simulation covering the period 1950–2080.

Model Hierarchy and Downscaling Procedure

The models used in this study are briefly described below. The driving AOGCM is the state-of-the-art, coupled ocean-atmosphere model ECHAM5/MPI-OM1 (Roeckner et al. 2003, Marsland et al. 2003, Jungclaus et al. 2006). All the forcing data for the Greenland simulation have been taken from a transient simulation with this model (May 2007) at T63 resolution (~1.8° by 1.8°). ECHAM5 no longer requires a flux correction, as opposed to previous versions

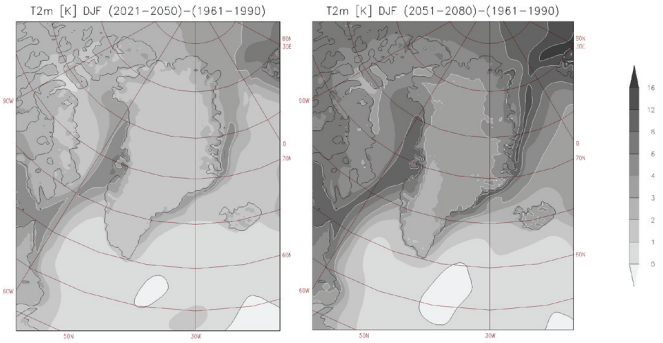

Figure 1. Simulated mean near surface (2 m) air temperature change [K] in HIRHAM4 in winter (December–February). Left panel: 2021–2050 minus 1961–1990, right panel: 2051–2080 minus 1961–1990. Isolines every 4 K.

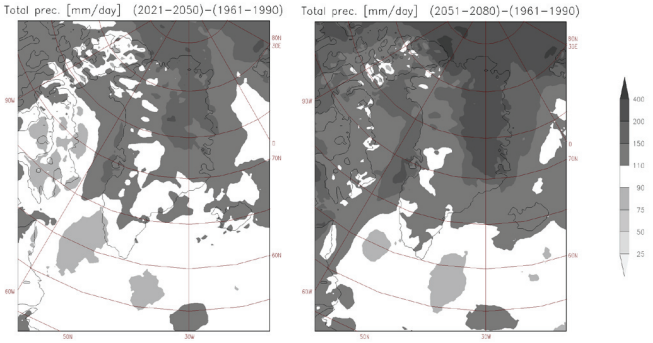

Figure 2. Change in annual precipitation expressed in percent of present-day (1961–1990) precipitation for 2021–2050 (left panel) and 2051–2080 (right panel).

of this model. Walsh et al. (2008) found in a comparison study between 14 of the CMIP3 participating models, that ECHAM5 is a top ranking model with respect to simulating present day conditions in the Arctic, including seasonal sea ice distributions.

The regional model is HIRHAM4 (Christensen et al. 1996), which is based on the adiabatic part of the HIRLAM (High-Resolution Limited Area Model) short-range weather forecast model (Källén 1996). For climate modeling purposes, the standard physical parameterisation of HIRLAM was replaced by that of the global climate model ECHAM4 (the predecessor of ECHAM5), so that HIRHAM4 can be thought of as a high resolution limited area version of ECHAM4. The boundary forcing from the global model (see previous paragraph) is updated every six hours in a region 10 grid points wide with a simple relaxation of all prognostic variables. It has been shown that HIRHAM4 is able to realistically simulate present-day climate (e.g., Christensen et al. 1998).

Varying concentrations of well-mixed greenhouse gases (CO_2, CH_4, N_2O, CFC-11, and CFC-12) as well as ozone (O_3), and sulphate aerosols (SO_4) have been prescribed from observations over the period 1861–2000 and according to the SRES A1B scenario (Nakićenović et al. 2000) thereafter. In this scenario the CO_2 concentration in 2100 is near 700 ppm, and the globally averaged warming with respect to present-day climate is 3.5°C.

To model regional permafrost, we have used the GIPL 1.1 model (Geophysical Institute Permafrost Lab) of the University of Alaska Fairbanks (Sergeev et al. 2003), which is a one-dimensional, spatially distributed, physically based multi processor numerical model for the solution of the non-linear heat transfer equation. The model solves for ground temperatures and active layer thickness. The input data for GIPL 1.1 are air temperature, snow depth and density, soil composition, water content and thermal properties, as well as characteristics of vegetation cover, geomorphologic features, and the geothermal flux as a bottom boundary.

Future Climate Evolution

As discussed above, the driving model for the 25 km HIRHAM simulation is a coupled atmosphere-ocean model; that is, the atmosphere is forced by modeled SSTs and sea ice concentrations rather than by observed ones. This implies that in order to assess variability and change, the considered periods need to be long enough; that is, cover several decades. From the transient simulation covering the complete period 1950–2080, we compare two thirty-year averages for periods in the 21st century (2021–2050 and 2051–2080) to modeled present-day conditions (1961–1990).

Temperature

Figure 1 shows seasonal changes in 2 m air temperature over Greenland for the two periods with respect to present-day conditions. For 2021–2050 a general temperature increase of 3°C in winter and 2°C in summer (not shown) is found. In winter locally larger values up to 6°C along the west coast and 4°C along the east coast and further northeast to Svalbard are simulated, which are related to regions covered with sea ice under present-day conditions but not in future climate. For the second period (2051–2080), warming accelerates considerably, with an increase of 7–8°C along the west and 12°C along the east coast in winter and a maximum increase of more than 18°C in winter at Svalbard's northeast coast, a region which has also been prone to large, recently-observed temperature anomalies.

The predicted temperature changes along the coast of Greenland are larger than in available GCM simulations (including ECHAM5, which provided the driving data for this simulation). We note that sea ice is not a prognostic variable in HIRHAM but is rather interpolated from the driving model. In ECHAM and HIRHAM any sea ice in a grid box is thawed first before near-surface temperatures can increase further. When sea ice retreats, there will be grid cells in HIRHAM free of ice earlier than in ECHAM, just because of the grid size (which is roughly 50 times larger in the GCM). These changes in sea ice cover and the projected increase in the positive phase of the North Atlantic Oscillation (Stendel et al. 2007, Stendel et al. 2008) lead to an increase in wind speed and changes in heat transport from the ocean, compared to the driving model, in particular along the east coast.

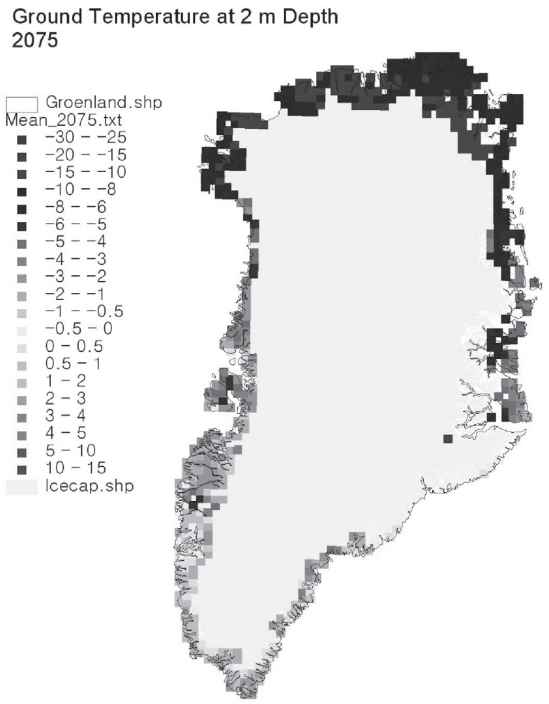

Figure 3. Ground temperatures (°C) at 2 m depth obtained with GIPL for exposed bedrock forced with HIRHAM4. Snapshot for 2075.

As a result, late summer sea ice disappears around 2060 in our simulation (not shown). Winter sea ice generally retreats northward by 100–200 km until 2050 and further (300–400 km) by 2080. Around Svalbard, sea ice totally disappears (even in winter) after 2070.

Precipitation

In Figure 2 precipitation changes are shown. In agreement with ACIA (2005) and Christensen et al. (2007), an increase in precipitation is projected for most of Greenland. With respect to present-day conditions, 15% more precipitation over western and 40% over interior and eastern Greenland are predicted for 2021–2050, while there is an increase of 30%–40% over western and interior and about 60% over eastern Greenland for 2051–2080. A distinct decrease in both snowfall amount and frequency is projected along the coasts except in the north, whereas more snow is projected on the lower parts of the ice sheet, in particular along the east coast (not shown). No information about changes on the ice sheet can be modeled, since it is treated as passive even in the contemporary models. That means that snow is allowed to accumulate on the ice sheet until a predefined maximum snow cover is reached, and no thawing or ablation is taken into account so that in practice the ice sheet is covered by a layer of snow of constant thickness throughout the year.

Permafrost

Rising temperatures, increasing precipitation, and a decrease in the number of snow days all contribute to conditions favorable for permafrost retreat; a decrease in snow depth and duration has the opposite effect. How fast

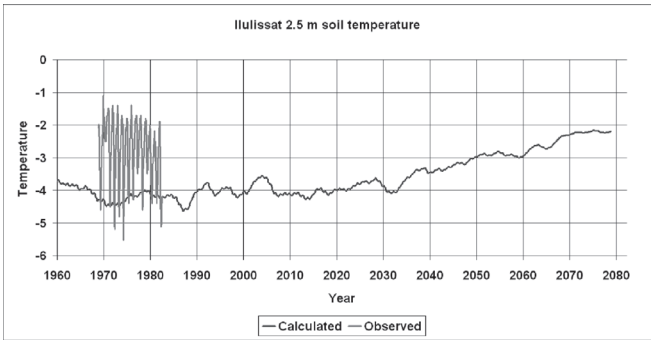

Figure 4. Soil temperature at a depth of 2.5 m in Ilulissat. Blue curve: GIPL 1.1 forced with HIRHAM4. Red curve: observations (van Tatenhove & Olesen 1994).

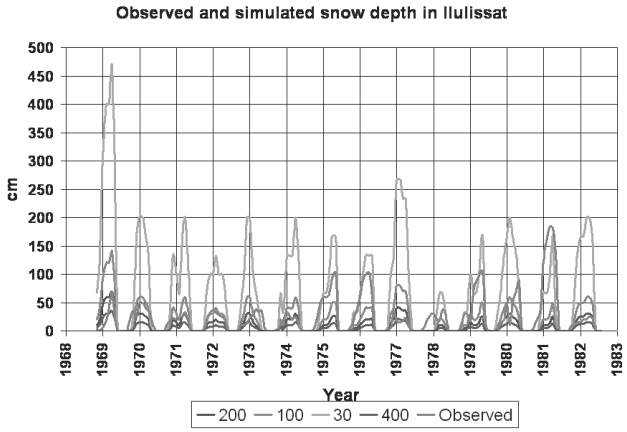

Figure 5. Observed and simulated snow depth (cm) in Ilulissat for mass densities of 30, 100, 200, and 400 kg m^{-3}.

changes in permafrost will take place furthermore depends on soil and vegetation properties, which are not known well on the spatial scale of interest for large parts of Greenland. We have run GIPL 1.1 using variations in snow thermal conductivity and organic layer thickness (Daanen et al. poster, this meeting). As an example, Figure 3 shows a snapshot of the temperature at 2 m depth for 2075.

Figure 4 shows the simulated and observed temperature evolution at 2.5 m depth for Ilulissat, taken from observations during the period 1968 to 1981 (van Tatenhove & Olesen 1994). A cold bias in the model data is obvious. As a consequence, the active layer in the model is too thin, and the permafrost table is too close to the surface, resulting also in a damping of temperature variability compared to the observations.

The model grid point representing Ilulissat is situated on the ice sheet, so an adjacent grid point, 25 km west, was chosen for comparison. This demonstrates that a horizontal resolution of 25 km is not sufficient to successfully model permafrost processes. Despite the strong warming signal in the atmosphere, the warming at the permafrost level is quite moderate. By the end of the period, temperatures at 2 m depth are above or just below freezing south of Maniitsoq and Tasiilaq, respectively, but remain below 0°C further north. This result points out the importance of a realistic simulation

of snow depth. The model slightly underestimates the snow cover compared to observations (Fig. 5). However, modeled snow cover is given in water equivalent and thus crucially depends on the mass density. Referring to Raab and Vedin (1995), a density on the order of 100 kg m^{-3} (newly fallen snow) gives reasonable results most of the time. There are, however, indications for winters with much smaller density on the order of 30–50 kg m^{-3}, the cold winters of 1975 and 1981 for example. High values up to 300–400 kg m^{-3} apply at the end of the winter. Of course, warm atmospheric conditions and a decrease in snow cover will eventually lead to permafrost degradation and thawing. However, since Greenland is comparably cold also in summer (when compared to Alaska), and due to the large thermal inertia of the frozen ground, only a part of this warming will be realized within the next decades.

Conclusions

Most state-of-the art GCMs project warming on the order of 2°C–3°C in the southern and larger warming (around 7°C) for the northern part of Greenland. A transient climate simulation at an (for Greenland) unprecedented horizontal resolution of 25 km has been conducted, which was forced by a GCM with a rather high resolution (T63; i.e., roughly 1.8° in latitude and longitude). Our regional model shows considerably stronger temperature increase in regions where sea ice retreats than the driving global model, with largest differences and largest changes along the east coast. Most of Greenland, especially the northeast, is projected to receive more precipitation. In particular at lower elevations, an increasing percentage of this precipitation can be expected to fall as rain rather than snow under present-day conditions. According to the model, present-day permafrost is rather cold in the Ilulissat region, which we have chosen as an example. With ongoing warming, the increase in rainfall events and decrease in snow fall, depth, and duration will lead to a warming of permafrost. Given the existence of marine permafrost along the west coast of Greenland, permafrost degradation can be expected to start at the end of this century.

Acknowledgments

This research was partly funded by the Polar Earth Science Program, Office of Polar Programs, National Science Foundation (ARC-0612533) and by the Danish Environment Agency (Miljøstyrelsen) under grant no. M127/001-0237.

References

ACIA. 2005. *Arctic Climate Impact Assessment.* Cambridge University Press, 1042 pp.

Anisimov, O., et al. 2001. Polar Regions (Arctic and Antarctic). C*limate Change: Impacts, Adaptation and Vulnerability Panel on Climate Change, Contribution of Working Group II of the Intergovernmental, Third Assessment Review.* Cambridge: Cambridge University Press, 801-841.

Arendt, A.A., Echelmeyer, K.A., Harrison, W.D., Lingle, C.S. & Valentine, V.B. 2002. Rapid wastage of Alaska glaciers and their contribution to rising sea level. *Science* 297: 382-386.

Bjorgo, E., Johannessen, O.M. & Miles, M.W. 1997. Analysis of merged SMMR/SSMI time series of Arctic and Antarctic sea ice parameters 1978–1995. *Geophys. Res. Lett.* 24: 413-416.

Christensen, J.H. & Kuhry, P. 2000. High-resolution regional climate model validation and permafrost simulation for the East European Russian Arctic. *J. Geophys. Res.* 105: 29647-29658.

Christensen, J.H., Christensen, O.B., Lopez, P., van Meijgaard, E. & Botzet, M. 1996. *The HIRLAM4 Regional Atmospheric Climate Model.* Danish Met. Inst. Sci. Rep. 96–4.

Christensen, J.H., et al. 2007. Regional climate projections. In: S. Solomon, D. Qin, M. Manning, Z. Chen, M. Marquis, K.B. Averyt, M. Tignor & H.L. Miller (eds.), *Climate Change 2007: The Physical Science Basis.* Cambridge University Press.

Christensen, O.B., Christensen, J.H., Machenhauer, B. & Botzet, M. 1998. Very high-resolution regional climate simulations over Scandinavia–present climate. *J. Climate* 11: 3204-3229.

IPCC. 2007. *Climate Change 2007: The Physical Science Basis.* S. Solomon, D. Qin, M. Manning, Z. Chen, M. Marquis, K.B. Averyt, M. Tignor & H.L. Miller (eds.), Cambridge, United Kingdom and New York, NY, USA: Cambridge University Press, 996 pp.

Jungclaus, J.H., Keenlyside, N., Botzet, M., Haak, H., Luo, J.-J., Latif, M., Marotzke, J., Mikolajewicz, U. & Roeckner, E. 2006. Ocean circulation and tropical variability in the AOGCM ECHAM5/MPI-OM. *J. Climate* 19: 3952-3972.

Källén, E. (ed.) 1996. *HIRLAM Documentation Manual, System 2.5.* Norrköping: Swed. Meteorol. and Hydrol. Inst., 126 pp.

Majorowicz, J.A. & Skinner,W.R. 1997. Potential causes of differences between ground and surface air temperature warming across different ecozones in Alberta, Canada. *Glob. Plan. Change* 15: 79-91.

Marsland, S.J., Haak, H., Jungclaus, J.H., Latif, M. & Roeske, F. 2003. The Max Planck Institute global ocean/sea ice model with orthogonal curvilinear coordinates. *Ocean Modelling* 5: 91-127.

May, W. 2007. Climatic changes associated with a global "2ºC-stabilization" scenario simulated by the ECHAM5/MPI-OM coupled climate model. *Clim. Dyn.* (submitted).

Nakicenovic, N. et al. 2000. *IPCC Special Report on Emissions Scenarios*. Cambridge, UK: Cambridge University Press 599 pp.

Osterkamp, T.E. 2003. A thermal history of permafrost in Alaska. In: M. Phillips, S.M. Springman & L.U. Arenson (eds.), *Proceedings of the 8th Int. Conf. on Permafrost, July 21–25, 2003, Zurich, Switzerland.* Lisse, The Netherlands: A.A. Balkema, 863-868.

Osterkamp, T.E. & Romanovsky, V.E. 1999. Evidence for warming and thawing of discontinuous permafrost in Alaska. *Permafr. Periglac. Proc.* 10: 17-37.

Raab, B. & Vedin, H. 1995. *Climate, Lakes and Rivers: National Atlas for Sweden*. SNA Publishing, 176 pp. +198 plates.

Rignot, E. & Kanagaratnam, P. 2006. Changes in the velocity structure of the Greenland ice sheet. *Science* 311: 986-990.

Roeckner, E. et al. 2003. *The Atmospheric General Circulation Model ECHAM 5. PART I: Model Description.* Max Planck Institute for Meteorology Report 349, 127 pp.

Romanovskii, N.N., Hubberten, H.-W., Gavrilov, A.V., Tumskoy, V.E., Tipenko, G.S. & Grigoriev, M.N. 2000. Thermokarst and land-ocean interactions, Laptev Sea region, Russia. *Permafr. Periglac. Proc.* 11: 137–152.

Romanovsky, V.E., Burgess, M., Smith, S., Yoshikawa, K. & Brown, J. 2002. Permafrost temperature records: indicator of climate change. *Eos* 83: 593-594.

Sergeev, D.O., Tipenko, G.S. & Romanovsky. V.E. 2003. Mountain permafrost thickness evolution under influence of long-term climate fluctuations (results of numerical simulations). In: Phillips, Springman, & Arenson (eds.), *8th International Conference on Permafrost*. Balkema, Zurich, 1017-1021.

Smith, S.L. & Burgess, M.M. 1999. Mapping the sensitivity of Canadian permafrost to climate warming. *Proc. IUGG 99 Symp. HS2, vol. 256*. IAHS Publications, 71-80.

Stendel, M. & Christensen, J.H. 2002. Impact of global warming on permafrost conditions in a coupled GCM. *Geophys. Res. Lett.* 29, 10.1029/2001GL014345.

Stendel, M., Romanovsky, V.E., Christensen, J.H. & Sazonova, T. 2007. Global warming and permafrost: Closing the gap between climate model simulations and local permafrost dynamics *Glob. Plan. Change* 56: 203-214.

Stendel, M., Christensen, J.H. & Petersen, D. 2008. Arctic climate and climate change with a focus on Greenland. In: H. Meltofte, T.R. Christensen, B. Elberling, M.C. Forchhammer & M. Rasch (eds.), *The dynamics of a High Arctic ecosystem in relation to climatic variability and change - Ten years of monitoring and research at Zackenberg Research Station, Northeast Greenland*. Adv. in Ecol. Res., Elsevier. (in press).

Sturm, M., Racine, C. & Tape, K. 2001. Climate change: increasing shrub abundance in the Arctic. *Nature* 411: 546–547.

van Tatenhove, F.G.M. & Olesen, O.B. 1994. Ground temperature and related permafrost characteristics in West Greenland. *Permafr. Perigl. Proc.* 5: 199-215.

Walsh, J.E., Chapman, W.L., Romanovsky, V., Christensen, J.H. & Stendel, M. 2008. Global climate model performance over Alaska and Greenland. *J. Clim.* (In revision).

Detection of Frozen and Unfrozen Interfaces with Ground Penetrating Radar in the Nearshore Zone of the Mackenzie Delta, Canada

Christopher W. Stevens
University of Calgary, Calgary, Alberta, Canada
Brian J. Moorman
University of Calgary, Calgary, Alberta, Canada
Steven M. Solomon
Natural Resources Canada, Dartmouth, Nova Scotia, Canada

Abstract

Multi-frequency Ground Penetrating Radar (GPR) surveys were conducted within the nearshore zone of the Mackenzie Delta to determine the spatial distribution of frozen and unfrozen sediment. Late winter GPR surveys over zones of bottom-fast and floating ice indicate that significant spatial variations in the thermal state of sediments exist. Where ice was bottom-fast, two laterally-continuous high amplitude reflections were verified to represent a transition in thermal state of sediment. These thermally-related interfaces closely correlate with changes in ground temperatures from above freezing to below -0.5°C. At locations where bottom-fast ice thickness was less than 1 m complete freezeback of the active layer occurred. Where bottom-fast ice thickness was greater than 1 m thaw exceeded freezeback of the active layer and a near-surface talik was identified. The depth of seasonal frost decreased towards zones of floating ice, beneath which no near-surface thermal interfaces were resolved.

Keywords: bottom-fast ice; ground penetrating radar; nearshore zone; seasonal frost; thermal interfaces.

Introduction

In the nearshore zone of the Mackenzie Delta (Fig. 1), the occurrence of seasonal frost and the sustainability of permafrost are closely related to the presences of bottom-fast ice (Dyke 1991, Kurfurst & Dallimore 1991, Wolfe et al. 1998). At locations where seasonal landfast ice comes in contact with the sediment bed (bottom-fast ice), heat is readily conducted from the underlying sediment. Several factors control the onset of bottom-fast ice and therefore the extent of heat exchange and ground freezing. Of particular importance are water bathymetry and those influences affecting ice growth (e.g., snowpack thickness). The ice contact time, in part, controls freezeback of the active layer and permafrost cooling (Stevens 2007). The outer delta, seaward of the delta front, is characterized by a shallow-water platform of gentle slope and subtle changes in water depth. As a result, complex thermal structures occur beneath seemingly similar regions of bottom-fast ice.

Under such nearshore conditions, subsurface characterization of the distribution of frozen and unfrozen sediment becomes difficult when solely relying on point-specific measurements such as drill and ground-temperature data. These datasets, although important, can lead to inaccurate correlation between data points and the oversimplification of the current subsurface conditions where rapid changes occur.

The thermal state of ground in this region is important to oil and gas development, as the stability of infrastructure in permafrost environments is greatly dependent on engineering designs that are specific to the existing and naturally changing thermal conditions.

In order to improve the subsurface understanding of ground conditions in the coastal zone, we used Ground Penetrating Radar (GPR) to detect thermal interfaces. Similar GPR surveys conducted over ice-covered rivers (Delaney et al. 1990, Arcone et al. 1992, Arcone et al. 1998) and lakes (Arcone et al. 2006) have identified sub-ice reflections that relate to frozen-unfrozen boundaries.

In this paper we discuss the sources of thermal interfaces detected with GPR in sediments, and characterize the spatial complexity of frozen and unfrozen transitions located beneath bottom-fast ice within the Mackenzie Delta coastal zone.

Detection of frozen and unfrozen sediment

Among the electrical, electromagnetic, and reflection-based geophysical methods utilized for the study of frozen ground, GPR in particular is considered to be a reliable and effective method for identifying thermal interfaces that indicate a change in thermal state (Moorman et al. 2003). In general, two aspects of frozen ground contribute to the wide use and success of GPR in cold regions: the decreased signal attenuation (losses) related to reduced ionic conduction as the phase change of pore water to ice takes place, and the large dielectric contrast that exists between frozen and unfrozen materials (Table 1), which typically causes a highly reflective interface.

The dielectric constant (k) of a material is a function of its ice and liquid water content. As interstitial ice begins to form in the pores of freezing sediments, both the liquid water content and the dielectric constant decreases (Table 1). This results in a large reflection coefficient (-0.34) between

Table 1. Typical dielectric properties of frozen and unfrozen materials. The volumetric unfrozen water content (θuf) for clay is given at various temperatures. (Sources: Patterson & Smith 1981, Davis & Annan 1989).

Material	Dielectric constant	Attenuation dB/m
liquid water	80	0.1
pure ice	3-4	0.01
unfrozen sand	20-30	0.03-0.3
(-1.5°C) frozen sand	4	2
(-0.5°C) clay (θ uf =40%)	27	65
(-1 °C) clay (θ uf =25%)	12	60
(-2 °C) clay (θ uf =17%)	8	47

frozen (*k = 6)* and unfrozen (*k = 25*) sediment (Stevens 2007). As such, the dielectric gradient is mainly controlled by the temperature gradient, textural characteristics of the sediment, and pore-water chemistry.

Study Area

The Mackenzie Delta is located within the western Canadian Arctic (Fig. 1a). Permafrost beneath the upland Pleistocene delta can be in excess of 500 m thick; however, beneath the modern delta plain, permafrost is generally less than 100 m thick (Taylor et al. 1996) with the exception of where channels and lakes restrict cooling of the ground (Smith 1976). Seaward of the delta plain, a shallow-water platform of water depths less than 2 m extends for approximately 17 km. Winter ice growth in this region is commonly in excess of 1 m, and therefore seasonal ice freezes to the sediment bed (bottom-fast ice) over extensive nearshore areas. The thermal regime beneath shallow water in this area has been shown to be regulated by bottom-fast ice, as heat is readily conducted from the ground during the period of ice contact (Dyke 1991).

GPR surveys were conducted from an ice surface over a distributary bar at the mouth of Middle Channel in late March. The area surveyed extended from within Middle Channel to a nearshore location adjacent to Garry Island (Fig. 1b). Fresh water (<0.2 mS/m) and ice dominate this site due to its close proximity to the outflow from Middle Channel. Similarly, pore-water salinity analyzed from sediment cores indicates values below 4 ppt (5 mS/m) within the upper 5 m of sediment. Sediment cores also indicate an overall coarsening upwards sequence of sediment, ranging from silty clay to sandy silt. The low electrical conductivity of ice and water promotes subsurface propagation of EM energy at this site. However, similar application of GPR would be hindered in coastal environments dominated by seawater.

Data Acquisition

A total of 154 line km of GPR data was collected in March of 2005, 2006, and 2007. The GPR surveys were conducted using a PulseEKKO 100 with 100 MHz antennas and a Noggin Plus system with both 500 MHz and 250 MHz antennas. Data from each system were recorded on individual data loggers. The radar systems and corresponding antennas were configured in an array so that simultaneous acquisition of the data could take place by towing the systems at a constant rate of 5 km/hr (Fig. 2). In order to acquire a high density of GPR traces (5 cm/trace) at the towing speed of 5 km/h, low stacking and short time window settings were used. Spatial positioning of each trace was recorded with either a Wide Area Augmentation Service (WAAS) corrected or real-time kinematic GPS unit. The processing of the GPR data included enhancement of weaker reflections using an Automatic Gain Control (AGC).

The subsurface transition in material properties from ice to water and frozen and unfrozen sediment corresponds to significant changes in the propagation velocity of radar waves. This study uses an average velocity of 0.16 m/ns for ice, 0.03 m/ns for water, 0.15 m/ns for frozen sediment, and 0.10 m/ns for unfrozen sediment, based on CMP

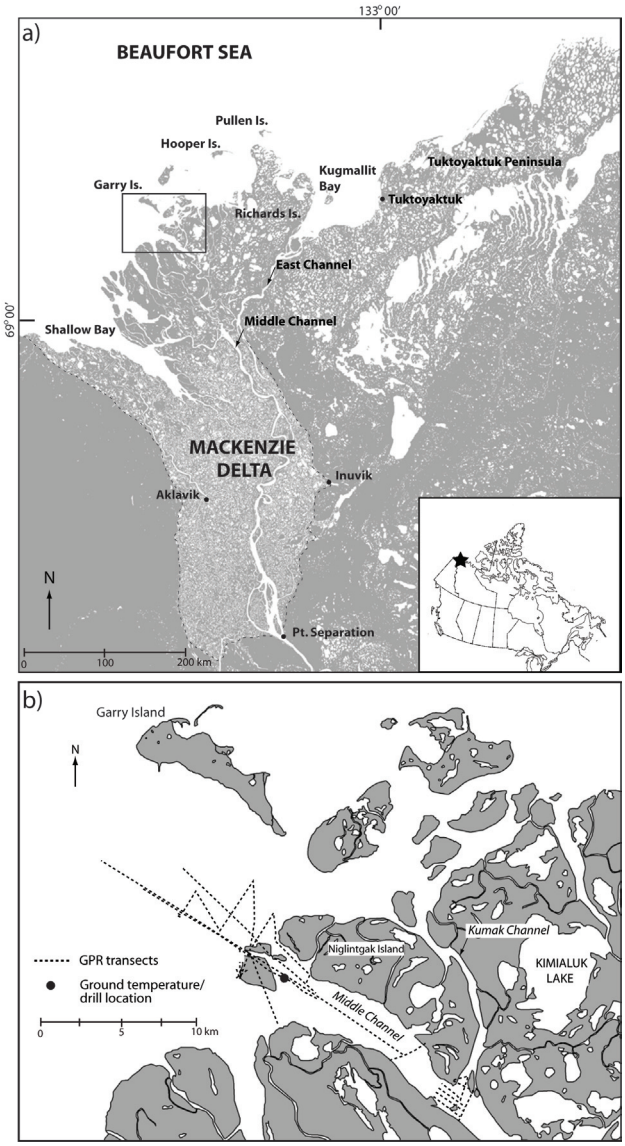

Figure 1. Study area map: a) regional view of the Mackenzie Delta located in the western Canadian Arctic and b) site map showing the orientation of GPR transects surveyed over the distributary bar at the mouth of Middle Channel.

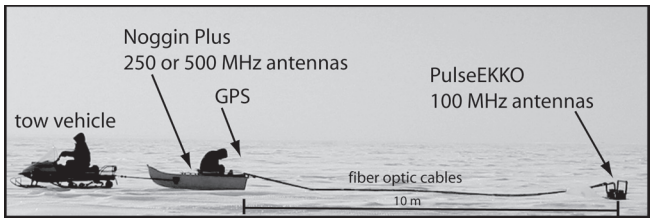

Figure 2. Multi-frequency GPR setup towed behind a snowmachine. GPR systems include a PulseEKKO 100 with 100 MHz antennas and a Noggin Plus systems with 250 and 500 MHz antennas. Positional data was acquired with GPS for each radar trace.

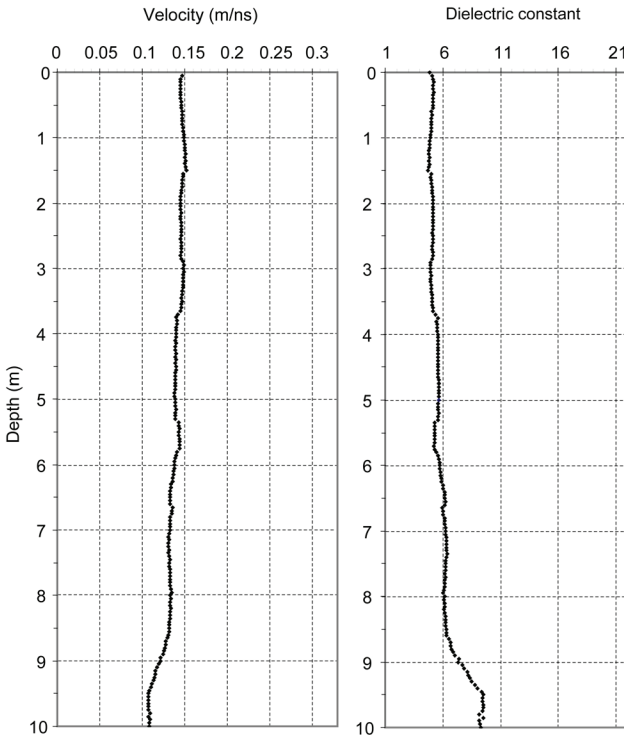

Figure 3. Calculated wave velocities and dielectric constants in frozen sediment obtained from cross-borehole measurements. The average wave velocity in the upper 5 m of sediment was 0.15 m/ns.

measurements, direct drill verification, and cross-borehole radar measurements conducted within the area. The GPR propagation velocities calculated from cross-borehole surveys were relatively consistent within the upper 5 m of sub-bottom sediment and therefore reflect the values used for depth conversions (Fig. 3).

Ground temperature measurements used for this study were recorded up to 10 m beneath zones of bottom-fast ice. Measurements were made every eight hours with RBR™ data loggers and YSI thermistors. The thermistors are accurate to $\pm 0.1^{o}$C. Information gained from two years of ground temperature data collected within the study site supports the GPR findings and aids in further radar interpretation where such subsurface verification was not present.

Results and Discussion

Figure 4 shows the GPR trace response to changes in ground temperatures and the thermal state of sediment beneath bottom-fast ice. At this locality, borehole (GSC 2007-301-063) indicates two thermal interfaces 3 m and 5.5 m in depth. Unfrozen saturated sediment in this depth range corresponds to ground temperatures between -0.06°C and -0.48°C. Although these sediments are cryotic, the complete lack of ice bonding observed in core suggests a freezing-point depression.

The radar trace response indicates relatively high amplitude reflection events that correspond to the upper and lower thermal interfaces (Fig. 4). These interfaces exhibit opposing wavelet phase under constant antenna directivity. In this study, antennas were orientated to produce a + - + wavelet phase from the base of the ice. This allowed for a + - + reflection wavelet when transitioning from frozen to unfrozen sediment and - + - phase from unfrozen to frozen sediment. In theory, different reflection polarity occurs when wave impedance is caused by the transition from materials of high-to-low versus low-to-high dielectric constant (Arcone et al. 2006).

In Figure 4, the depth of signal penetration achieved with 250 MHz is limited to the first frozen-unfrozen interface, as a result of high signal attenuation in the unfrozen sediment. The signal attenuation exhibited in fine-grained saturated sediment results from the interaction between the polar water molecules and the charged sediment surfaces. However, greater penetration depths were obtained with lower antenna frequencies (e.g., 100 MHz) which allowed for multiple frozen–to-unfrozen transitions to be imaged up to 10 m in depth.

The upper thermal interface was identified in a cross-sectional profile as a laterally continuous reflection (Fig. 5). Internal reflections resolved from within the zone of frozen sediment represent sedimentary structure. The upper thermal interface was verified to represent the depth of seasonal frost with temperature data. Beneath zones of bottom-fast ice, seasonal frost develops as a result of seasonal cooling in the ground that is prompted by ice contact with the sediment bed (Dyke 1991). Seasonal frost typically extended less than 3 m below the ice surface.

At greater depths, an additional frozen-unfrozen interface (lower thermal interface) was detected using 100 MHz antennas (Fig. 6). This lower thermal interface represents the approximate position of the permafrost table. At locations where the permafrost table remains detectable by late winter, seasonal thaw exceeds freezeback of the active layer and a talik is present.

Similarly, more isolated zones of unfrozen sediment relating to the presence of taliks result from bathymetric depressions in the sediment bed (Fig. 7). At this location, the talik zone corresponds to an area where ice thickness is in excess of 40 cm. The deeper water limits the ice contact time with the sediment bed, as the duration of winter ice growth is extended. Subsequently, seasonal cooling of the ground is less, and thaw exceeds freeze back. These sites demonstrate the relationship that exists between ice thickness and the spatial complexity of frozen-unfrozen zones beneath bottom-fast ice.

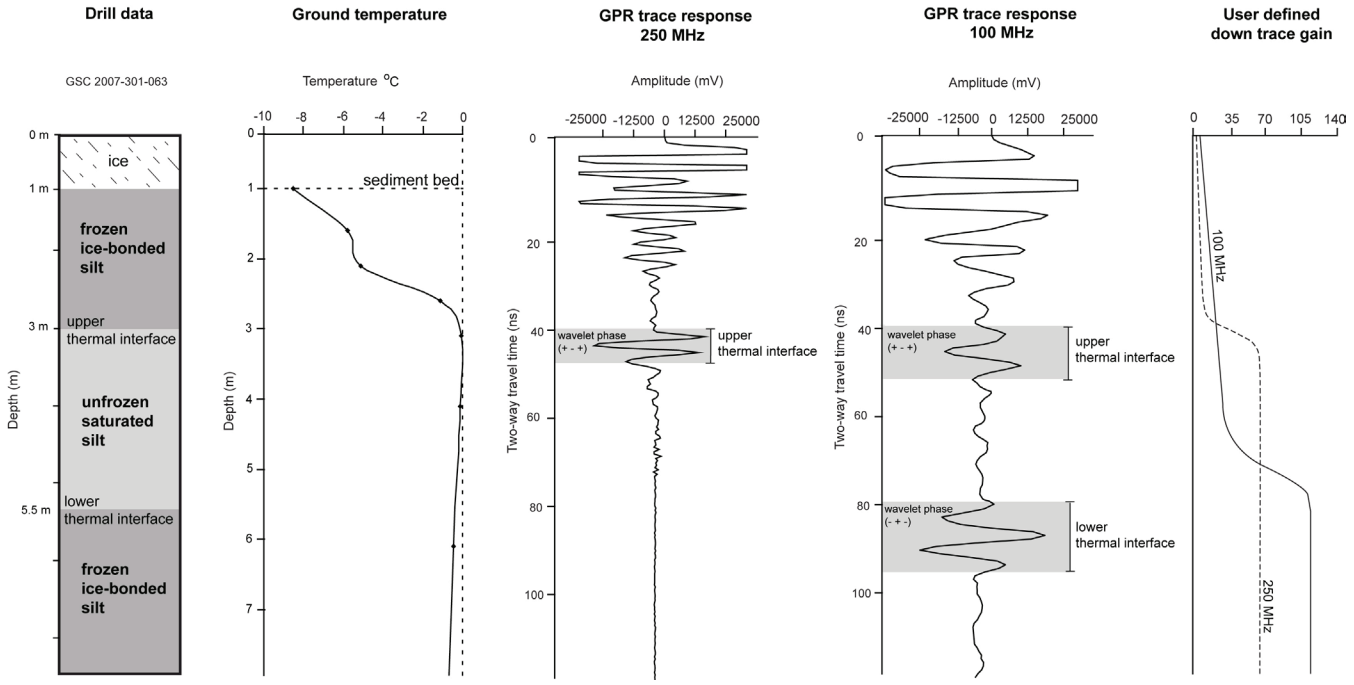

Figure 4. Comparison between drill data, ground temperatures and GPR trace response for 250 and 100 MHz antennas. Drill data at GSC 2007-301-063 indicates a frozen-to-unfrozen interface at 3 m and an unfrozen-to-frozen interface at 5.5 m. The zone of unfrozen sediment corresponds to ground temperatures between -0.06 and -0.48°C. The GPR trace response to these conditions shows two reflective events; an upper thermal interface resolved at 40 ns with 250 MHz, and a lower thermal interface identified at 80 ns with 100 MHz antennas.

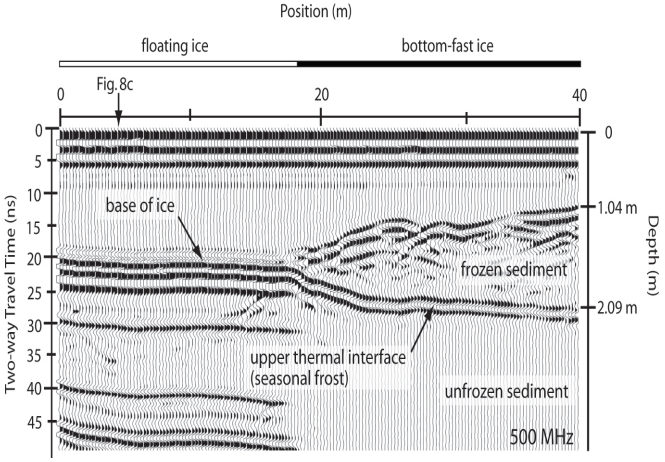

Figure 5. A 500 MHz GPR profile across zones of bottom-fast and floating ice. Beneath the bottom-fast ice an upper thermal interface representing the depth of seasonal frost was detected at 2 m below the ice surface. Ice-bottom multiples are present from 40-50 ns beneath the zone of floating ice.

Interpretations of GPR profiles collected over zones of bottom-fast and floating ice indicate a complex cryostratigraphy with multiple near-surface transitions from frozen to unfrozen sediment occurring over short distances (e.g. <10 m) by late winter. Typically, where bottom-fast ice thickness was less than 1 m, complete active layer freezeback has occurred (Fig. 8a); whereas beneath bottom-fast ice greater than 1 m thick, a talik existed between seasonal frost and the permafrost table (Fig. 8b).

This reflects conditions where seasonal thaw exceeds freezeback of the active layer over one year or a number of years. At locations occupied by floating ice, near-surface sediments were unfrozen to the depth of penetration of the GPR (Fig. 8c). The depth of seasonal frost also decreased towards zones of floating ice, as lateral heat flow restricts the surrounding sediments from freezing.

In general, a strong relationship between bottom-fast ice thickness and nearshore cryostratigraphy exists. As previously noted, the increased duration of ice growth in areas of deeper water restricts the extent of seasonal frost in the ground. This relationship between ice thickness the development of seasonal frost are demonstrated in Figures 6 and 7. The thermal region of the permafrost body is also affected where thaw exceeds complete freezeback of the active layer, as seasonal cooling of the permafrost body is minimal (Stevens 2007). Using this information, the interpretation of GPR profiles also allows the identification of sites where permafrost is potentially degrading.

The variability that exists in the near-surface distribution of frozen and unfrozen sediment may also be influenced by seasonal changes in the rate of ice growth and localized sediment erosion and accretion, which alter the previous water depth.

The GPR reflections from thermal interfaces relate to change in state of pore water, as verified with both drill and ground temperature data (Fig. 4). Therefore, the ability to coherently resolve these two interfaces may be limited where marginally bonded sediments and gradual changes in the dielectric contrast occur over a depth range greater than the transmitted wavelength. Similarly, only under thermal conditions where ice nucleation occurs near 0°C, will GPR reflections correlate with the zero degree isotherm.

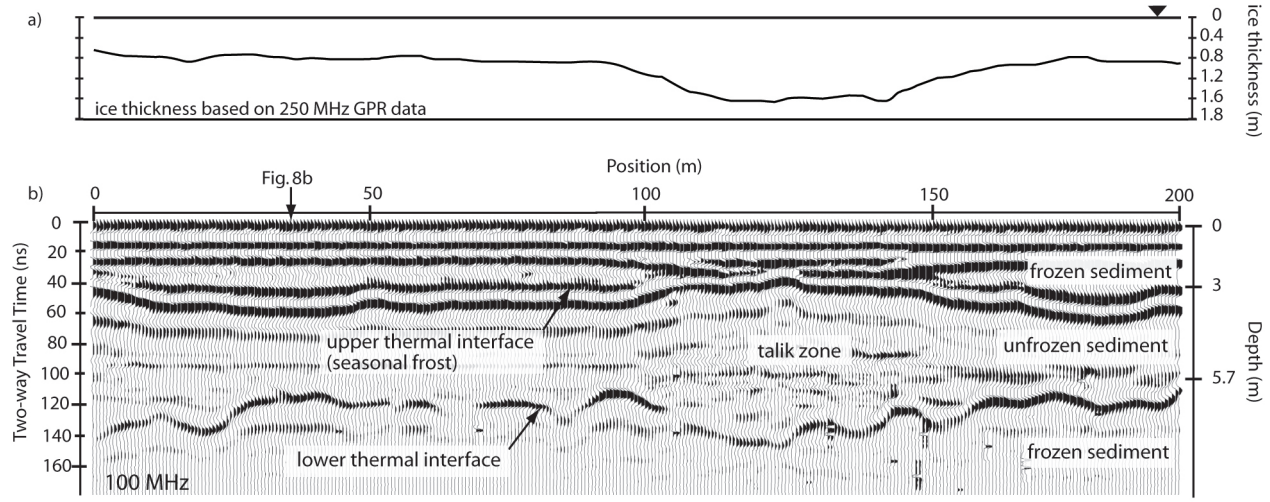

Figure 6. a) Profile of ice thickness obtained across a 200 m section of bottom-fast ice and b) corresponding 100 MHz GPR profile showing both an upper and lower thermal interface which defines a talik zone between ~3 m and 5.7 m.

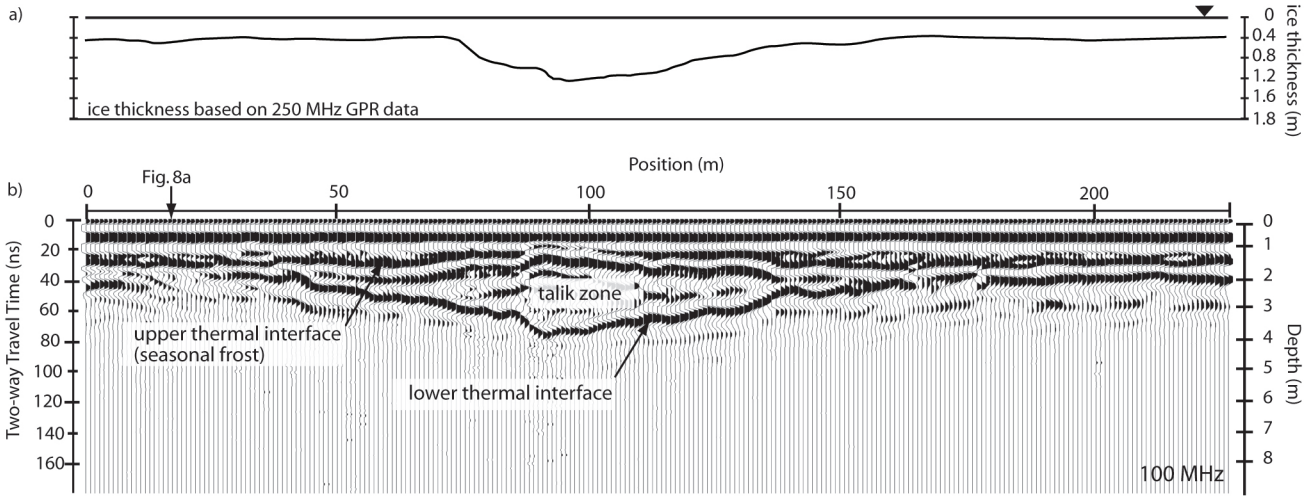

Figure 7. a) Profile of ice thickness obtained across a 225 m section of bottom-fast ice and b) corresponding 100 MHz GPR profile showing the location of an isolated talik. At this location, the talik zone corresponds to ice thickness greater than 40 cm.

Thus, the width of the freezing fringe that is determined by the temperature gradient becomes important to reflection characteristics.

Based on the ground temperature profile presented in Figure 4, a large temperature gradient exists at the upper thermal interface (i.e., the transition from the seasonally frozen to underlying unfrozen sediment). This results in a narrow freezing fringe and a sharp interface between frozen and unfrozen material. This is in contrast to the permafrost table, which exhibited a lower temperature gradient over an equivalent subsurface distance. Therefore, the lower temperature gradient has the potential to cause some misinterpretation of the permafrost table due to more subtle changes in the dielectric properties over the wavelength. In addition, a freezing-point depression would offset the ice nucleation temperature and the recorded position of the permafrost table. As GPR can only resolve changes in the thermal state of pore water and cannot directly detect ground temperatures, the latter information can only be inferred.

Conclusions

Ground penetrating radar surveys conducted within the nearshore zone of the Mackenzie Delta were effective in resolving thermal interfaces up to 6 m beneath zones of bottom-fast ice. With 250 MHz antennas, the depth of penetration was limited to an upper thermal interface which corresponds to the extent of seasonal frost. In contrast, an upper and lower thermal interface delineating talik zones were resolved with 100 MHz antennas. Thermal interfaces closely correlate with frozen-unfrozen transitions of sediment and changes in ground temperatures from above freezing to below -0.5°C.

Complete freezeback of the active layer was exhibited beneath bottom-fast ice less than 1 m thick in contrast to locations where ice was greater than 1 m thick, beneath which talik zones were identified. Sediments were unfrozen at the sediment-water interface where ice remained floating.

The multiple thermal interfaces detected beneath bottom-

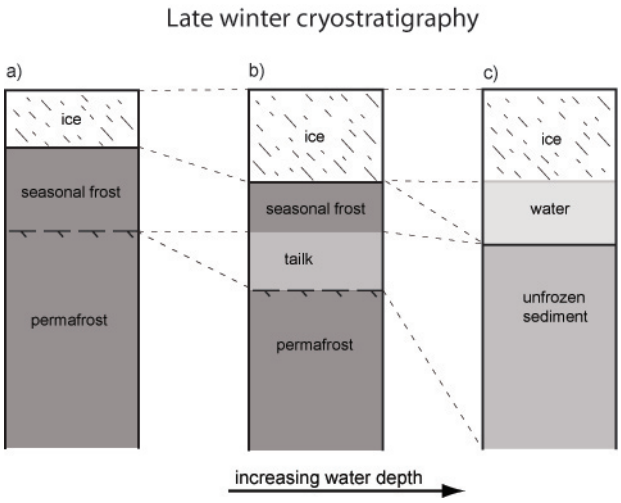

Figure 8. Schematic illustration of late winter cryostratigraphy interpreted from GPR data: a) bottom-fast ice less than 1 m thick characterized by complete freezeback of active layer; b) bottom-fast ice greater than 1 m thick characterized by a talik where thaw exceeds freezeback of the active layer; and c) floating ice where sediments are perennially unfrozen within the upper 3 m of the sediment bed.

fast ice suggest a complex thermal regime that exists at scales not easily characterized by point-source drill and ground-temperature datasets. However, multi-frequency GPR surveys provide high resolution reflection-based data which can detect vertical and spatial variations in the thermal state over large coastal regions. Such subsurface datasets become critical to further understanding permafrost conditions and freeze-thaw processes in the coastal zone.

Acknowledgments

This research was financially supported by the Natural Resources Canada and NSERC. Logistical support was provided by Shell Canada, Chevron Canada, Devon Energy, and the Aurora Research Institute. We also acknowledge Dustin Whalen, J.C. Lavergne, and Jen Bode for assisting with data collection.

References

Arcone, S.A., Chacho Jr., E.F. & Delaney, A.J. 1992. Short-pulse radar detection of ground water in the Sagavanirktok River flood plain in early spring. *Water Resources Research* 28: 2925–2936.

Arcone, S.A., Chacho, E.F. & Delaney, A.J. 1998. Seasonal structure of taliks beneath arctic streams determined with ground-penetrating radar. *Proceedings of the Seventh International Conference on Permafrost, Yellowknife, Canada, June 23-27, 1998*: 19-24.

Arcone, S.A., Finnegan, D.C. & Lanbo, L. 2006. Target interaction with stratigraphy beneath shallow, frozen lakes: Quarter-wave resonances within GPR profiles. *Geophysics* 71: k119-k131.

Davis, J.L. & Annan, P. 1989. Ground-penetrating radar for high-resolution mapping of soil and rock stratigraphy. *Geophysical Prospecting* 27: 531-551.

Delaney, A.J., Arcone, S.A. & Chacho, E.F. 1990. Winter short-pulse radar studies on the Tanana River, Alaska. *Arctic* 43: 244-250.

Dyke, L.D. 1991. Temperature changes and thaw of permafrost adjacent to Richards Island, Mackenzie Delta, N.W.T. *Canadian Journal of Earth Sciences* 28: 1834-1842.

Kurfurst, P.J. & Dallimore, S.R. 1991. Engineering geology of nearshore areas off Richards Island, N.W.T., a comparison of stable and actively eroding coastlines. *Canadian Geotechnical Journal* 28: 179-188.

Moorman, B. J., Robinson, S. D. & Burgess, M.M. 2003. Imaging periglacial conditions with ground-penetrating radar. *Permafrost and Periglacial Process* 14: 319-329.

Patterson, D.E. & Smith, M.W. 1981. The measurement of unfrozen water content by time domain reflectomerty: results from laboratory tests. *Canadian Geotechnical Journal* 18: 131-144.

Smith, M.W. 1976. Permafrost in the Mackenzie Delta. *Geological Survey of Canada*, Paper 75-28: 31.

Stevens, C.W. 2007. Subsurface investigation of shallow-water permafrost. *Unpublished M.Sc thesis* Department of Geography, University of Calgary, Calgary, Alberta 127.

Taylor, A.E., Dallimore, S.R. & Judge, A.S, 1996. Late Quaternary history of the Mackenzie-Beaufort region, Arctic Canada, from modelling of permafrost temperatures. 2. The Mackenzie Delta- Tuktoyaktuk coastlands. *Canadian Journal of Earth Sciences* 33:62-71.

Wolfe, S. Dallimore, S. & Solomon, S.M. 1998. Coastal permafrost investigations along a rapidly eroding shoreline, Tuktoyaktuk, N.W.T. *Proceedings of the Seventh International Conference on Permafrost, Yellowknife, Canada, June 23-27, 1998*: 1125-1131.

Atlas of Northern Circumpolar Soil

Vladimir Stolbovoy
European Commission Joint Research Centre, Institute for Environment and Sustainability, Ispra, Italy
Arwyn Jones
European Commission Joint Research Centre, Institute for Environment and Sustainability, Ispra, Italy
Charles Tarnocai
Agriculture and Agri-Food Canada, Ottawa, Canada
Gabriele Broll
ISPA, Vechta University, Vechta, Germany
Luca Montanarella
European Commission Joint Research Centre, Institute for Environment and Sustainability, Ispra, Italy

Abstract

Cooperation between soil scientists from Canada, European Union, Russia, and the USA has resulted in an Atlas of Northern Circumpolar Soil which brings together soil data for all northern countries to better understand soil resources in these regions. The Atlas aims to raise public awareness of the value of soil in the north and support further research in this area (for example, the European Union's Thematic Strategy for Soil Protection). The Atlas contains a richness of information on soil diversity, the mapping and classification of permafrost-affected soil, the role of soil in the global carbon cycle, and atmospheric concentrations of biospheric greenhouse gases in the past and the future. The publication has fostered cooperation between several countries and bridges the gap between soil science, the permafrost community, policy makers, educators, and the general public. The Atlas is a contribution of the European Union to the International Polar Year 2008.

Keywords: atlas; climate change; cryosols; permafrost; soil.

Introduction

The Arctic plays a key role in the global environment. The region accumulates a huge mass of ice which controls sea level, heat exchange in the atmosphere, and the cold oceanic currents driving atmospheric and oceanic processes. NASA observation shows that perennial Arctic sea ice, which normally survives the summer melt season, has shrunk by 14% between 2004 and 2005. The melting of the ice cap indicates a warming of the marine environments. On the continental land, such a climatic warming will lead to a degradation of the permafrost, which affects the behavior of terrestrial ecosystems including humans (e.g., sinking houses, weakening roads, runways, and pipelines).

While there is considerable research interest in the Arctic region on socioeconomic and broad environmental issues, there is a growing awareness of the importance of soil in the northern circumpolar region. Soil is a surface layer which has resulted from the interaction of climate, relief, parent material, vegetation, and time. As a natural body, soil supports basic physical, chemical, and biological processes in ecosystems and provides principle ecological services for humans. Being sensitive to environmental changes, soil in northern regions is projected to undergo the greatest impact from climate warming. The consequences of changes to the principle soil-forming processes regulating biogeochemical cycles and ecosystems functioning are uncertain at present. In order to draw a reliable picture on the future changes, soil scientists have over the last decades focused efforts to improve the basic and applied knowledge of the circumpolar soil.

One of the specific features of the north circumpolar region is that it is occupied by developed countries (USA, Canada, EU, and Russia) with strong national traditions in soil classifications, survey, and mapping. The diversity of national traditions results in a mosaic of soil inventories, which make joint analysis of soil resources difficult. This situation is a serious constraint for the communication and implementation of agreed environmental policies in the region. Soil scientists have attempted to overcome this gap by focusing on the development of a common circumpolar soil database. All national soil terms and data in this area were combined, correlated, and presented in a common harmonized GIS-compatible database (Tarnocai et al. 2001, Cryosol Working Group 2004). The database has enabled the first estimate of the carbon stock in cryosols (Tarnocai & Broll 2008, Tarnocai et al. 2007, Tarnocai et al. 2006, Tarnocai et al. 2003). It was found that soil in the circumpolar region accumulates about 30% of the world's soil organic carbon. The release of the database stimulated a fundamental review of the knowledge on the permafrost-effected soil. This basic revision has been outlined in Kimble et al. (2004).

However, the soil database, its analysis and related scientific publications address professionals and are too specific for the general public. To bring available information to the latter, a group of scientists from Canada, European Union, Russia, and the USA have collaborated to produce a high quality Atlas on soil in the northern circumpolar

regions that is easily readable and graphically stimulating. This publication intends to raise public awareness of the value of soil in northern latitudes supporting further research in this area - for example, Soil Thematic Strategy for Soil Protection in Europe (COM (2006)231, COM(2006)232).

The compilation of the Atlas is a contribution to the Polar Year (IPY) 2007-2008 collaborative science program. This work is included in the IPY CAPP Project #373. It contributes to multidisciplinary approach, incorporating physical and biological sciences, social sciences, and a large education component.

The objective of the paper is to introduce the Atlas of Northern Circumpolar Soil with special emphasis on:

1. Methods and data used;
2. Content of the Atlas;
3. Demonstrate major findings and conclusions.

Methods and Materials

The Atlas is a compilation of different data originating from published and unpublished sources. A substantial portion of the data, including maps, texts, photos, and graphs, is new and was produced specifically for the Atlas. The cartographic coverage originates from a variety of sources: 1) for the North America, Greenland, Mongolia, and part of Kazakhstan: the Northern and Mid Latitude Soil Database (Cryosol Working Group 2004); 2) for Northern Eurasia and Iceland: the Soil Geographical Database of Eurasia (Van Liedekerke et. al. 2004); 3) for China and part of Kazakhstan: Digital Soil Map of the World (FAO 1990). All these databases have been combined to create a single database that covers a circle with the North Pole in the center and limited by 50°N latitude to the south. The database has been translated into the international World Reference Base correlation system (IUSS 2006).

In addition to maps, the Atlas contains explanatory texts illustrated by photographs and graphics that are specially written to address those who are interested in learning more about northern soil characteristics and environments.

Technically, the Atlas is a book of 144 A3 pages illustrated by a mix of text, colored maps, pictures, diagrams, and photographs.

Results

The Atlas (Fig. 1) consists of the following main sections:

1. Introduction
2. The Northern Environment
3. Soil in Northern Latitudes
4. Soil Classification
5. Soil Maps
6. Northern Soils and Global Change
7. Conclusions and Future Perspectives
8. Additional Information

Figure 1. Cover page showing the extent of the northern circumpolar area addressed by the Atlas.

Introduction

This section contains the list of authors, includes acknowledgements, outlines the scope of the Atlas, and presents an overview of EU policy for soil protection within the context of the International Polar Year.

The northern environment

This section is intended to provide the reader with a range of general information on the circumpolar region through a series of documented thematic maps (i.e., sea ice extent, mean annual temperature, mean annual precipitation, permafrost extent, soil temperature, relief, parent material, land cover, population density, permafrost, and patterned ground). Data for this section come from well-distinguished sources. For example, the soil temperature map originates from the US Department of Agriculture; the vegetation patterns were extracted from the Global Land Cover 2000 database; while information on permafrost is provided by the International Permafrost Association.

Soil in northern latitudes

The scope of this section is to provide a basic understanding of what is soil and, in particular, soil in northern regions. The section outlines the main soil functions, especially those related to the principle soil-forming processes in northern latitudes with specific attention being given to cryogenic processes associated with freeze-thaw cycle, cryoturbation, polygonal cracking, and stone sorting. The section also describes soil biodiversity in cold climates.

Soil classification

This section introduces the most widely-used national soil classification systems in the circumpolar region (e.g., Canadian, USA, and Russian). Special attention is paid

to the latest version of the World Reference Base for soil classification (IUSS 2006). All classification systems are illustrated by examples of their main concepts, taxonomic systems, and description of the principle soil types. One page of the Atlas is devoted to the correlation and comparison of different classification systems. Examples demonstrate that soil inventories based on the varying concepts used in different soil classifications result in a markedly different outputs (e.g., Cryozems in Russian soil classification are exclusively restricted to highly cryoturbated soils that cover only a part of the Gelisols Order in the USDA Soil Taxonomy, Cryosols in Canadian system and WRB).

The different number of the highest level taxonomic classes is another example of the conceptual differences between national soil classifications: Soil Taxonomy (USDA) uses twelve Orders; the Canadian soil classification system exploits ten soil Orders; the Russian soil classification contains fifteen soil Divisions while the WRB system assigns all soil types to thirty two Reference Soil Groups.

As the conceptual inconsistency is difficult to overcome, many scientists suggest comparing national soil classifications on the basis of physically measured soil parameters (e.g., pH, organic carbon content, base saturation, etc.). Unfortunately this approach has some limitations as soil characteristics are measured differently in different countries. This inconsistency is because of the national traditions, the availability of equipment, economic reasons, etc. For example, the determination of soil organic carbon (SOC) according to the methodology proposed by Walkley–Black (Canada) or Turin (Russia) is based on "wet combustion" (carbon oxidation is performed by dichromate solution). This method recovers about 70%-80% of the total SOC content. Other countries use a dry combustion method, where the soil is heated to 950°C in an oven. In this method the recovery of SOC is 100%. Similar differences can be found in many other analytical methods, such as the detection of soil texture, soil pH, cation exchange capacity, etc. Therefore, an understanding of the methodologies used to measure soil characteristics is crucial for the correlation of national soil classifications.

Other variations in soil characteristics arise from differences in ecological and land-cover interpretations in different countries. For example, the thickness of the peat layer is one of the criteria used to distinguish forest from bog in land cover mapping. In Canada, this threshold is 40 cm, while being 30 cm in Russia. As a result, maps of peat areas using the two approaches look substantially different.

In spite of the differences in national classification schemes and the lack of full coincidence between soil terms, the occurrence of the soil in the same natural zone could be a good basis to correlate soil classifications. For example, Mollisols (the USDA Soil Taxonomy), Chernozems (in Canadian and WRB systems) and Humic-accumulative soils (Russia) are formed under steppe and the prairies vegetation. Therefore, these differently termed soils have many common characteristics and could be regarded as being very close.

The section also contains a description of the Reference Soil Groups of the WRB, illustrated by maps showing the broad distribution patterns of each reference group together with high-quality photographs of characteristic soil profiles and associated landscapes. The section is concluded by examples of soil surveys in the Arctic.

Soil maps

The heart of the Atlas contains 30 plates of soil maps at a scale of 1:3,000,000. The map legend is based on the second level units of the WRB (IUSS 2006). This is the first application of the revised WRB system for this territory. It is important to emphasize that the maps were harmonized at the border between some countries (e.g., USA (Alaska) and Canada, Russia and Finland, Russia and China). All maps contain short explanatory texts aiming to draw the attention to the specific features of this particular circumpolar area.

A short section is devoted to other regions for the world where cold soil can be found, and includes some information on the soil types of Antarctica. The section concludes with an overview of the circumpolar soil database and introduces the basic principles of Geographic Information Systems (GIS) and its use in the Atlas.

Northern soils and global change

This section provides information on the relationship between soil and global change, in particular, climate change. A brief overview of glacial periods is used to introduce the concept of palaeosols that illustrate the ability of soil to preserve indications of past climate change.

The section progresses to consider the role of the circumpolar region in the global carbon cycle, which is highly debated at present. Besides general information, this section demonstrates the special role of the organic and mineral soil types in the north for the sequestration of organic carbon. Through cryoturbation and other pedogenic processes, organic carbon can be moved deep in the soil and preserved from decay by the permafrost for very long periods of time (Fig. 2).

Figure 2. Organic matter translocation by cryoturbation. East European tundra near Vorkuta, Russia. Cryoturbation in permafrost-affected soils removes peat, litter, wood debris, and other kinds of organic matter (fragments of H horizon – the darker parts in the above profile) from the surface deeper into the soil leading to preservation of organic matter in deeper, colder, and less biologically active layers (photo by M. Drewnik).

Such special mechanisms make cryosols and organic-rich soil a unique instrument to mitigate greenhouse gas concentration in the atmosphere. The Atlas explains the processes for the decomposition of vegetation residues and the associated emissions of carbon dioxide and methane, and pays special attention to the potential evolution of organic and mineral soil under present and future climate warming scenarios.

The variation in the characteristics of soil in the northern circumpolar region is striking. The Atlas illustrates this richness through a series of plates devoted to the soil types of Scandinavia, Iceland, Greenland, Canada, Alaska, and Central Siberia.

Conclusions and future perspectives

The last section considers future perspectives for soil in northern areas, raising attention to the need for soil conservation in the area. One page is devoted to the high value of the Atlas as an educational resource. This is supplemented by a glossary of terms, contact information for soil scientists in northern countries, and references for those who wish to know more about the unique world of northern circumpolar soils.

Summary

The Atlas of Northern Circumpolar Soil is the first document of its kind to bring together soil data for all the northern countries in a style designed to better explain and protect soil resources in these areas. The Atlas has fostered cooperation between several countries and bridges the gap between soil science, the permafrost community, policy makers, educators, and the general public.

Core support for the project has been provided by the European Commission's Joint Research Centre (JRC).

References

Cryosol Working Group. 2004. *Northern and Mid-Latitude Soil Database, Version 1*. Data set. Available on-line http://www.daac.ornl.gov] from Oak Ridge National Laboratory Distributed Active Archive Center, Oak Ridge, Tennessee, USA.

EC. 2006. Communication of 22 September 2006 from the Commission to the Council, the European Parliament, the Economic and Social Committee and the Committee of the Regions: Thematic Strategy for Soil Protection (COM [2006] 231 final).

EC. 2006. Proposal for a Directive of the European Parliament and of the Council establishing a framework for the protection of soil and amending Directive 2004/35/EC [COM (2006) 232 final].

FAO. 1990. *Digital Soil Map of the World.* Distributed by UN FAO, http://www.fao.org/

IUSS Working Group WRB. 2006. *World Reference Base for Soils Resources 2006.* World Soil Resources report No. 103. Rome: FAO.

Kimble, J. (ed.). 2004. *Cryosols, Permafrost-Affected Soils*. Berlin Heidelberg : Springer-Verlag, 726 pp.

Van Liedekerke, M., Panagos, P., Darossin, J., Jones, R., Jones, A. & Montanarella, L. (eds.), 2004. *The European Soil Database. Version 2.0*. Ispra, Italy: the EU JRC. CD-ROM.

Tarnocai, C. & Broll, G. 2008. Soil Organic Carbon Stocks in the Northern Permafrost Region and Their Role in Climate Change. *Proceedings of the Ninth International Conference on Permafrost, Fairbanks, Alaska, June 29-July 3, 2008* (this proceedings).

Tarnocai, C., Swanson, D., Kimble, J. & Broll, G. 2007. *Northern Circumpolar Soil Carbon Database.* Research Branch, Agriculture and Agri-Food Canada, Ottawa, Canada.

Tarnocai, C., Lacelle, B., Broll, G., Mazhitova, G., Pfeiffer, E.-M., Stolbovoi, V., Ping, C.L. & Kimble, J.M. 2006. Organic carbon in northern circumpolar soils. *Presented at the World Congress of Soil Science Philadelphia, Pennsylvania, USA, July 9-14, 2006.*

Tarnocai, C., Kimble, J., Swanson, D., Goryachkin, S., Naumov Ye.M., Stolbovoi, V., Jakobsen, B., Broll, G., Montanarella, L., Arnoldussen, A., Orozco-Chavez, F. & Yli-Halla, M. 2001. Soils of Northern and Mid Latitudes. Research Branch, Agriculture and Agri-food Canada, Ottawa, Canada (1:15,000,000 scale map).

Tarnocai, C., Kimble, J. & Broll, G. 2003. Determining carbon stocks in cryosols using the Northern and Mid Latitudes Soil Database. *Proceedings of the Eighth International Conference on Permafrost, 21-25 July 2003, Zurich, Switzerland.* In: M. Phillips, S. Springman, & L. Arenson (eds.), *Permafrost,* volume 2, Lisse/Abingdon/Exton (PA)/Tokyo: A.A. Balkema Publishers, 1129-1134.

Freezing of Marine Sediments and Formation of Continental Permafrost at the Coasts of Yenisey Gulf

Irina D. Streletskaya
Moscow State University, Moscow, Russia
Alexander A. Vasiliev
Earth Cryosphere Institute SB RAS, Tyumen, Russia
Mikhail Z. Kanevskiy
University of Alaska Fairbanks, USA

Abstract

The Quaternary geology of the coasts of Yenisey Gulf is characterized by the prevalence of marine saline sediments. As a rule, the upper parts of coastal sections are of continental origin. Active denudation processes take place in locations with ice-rich sediments, especially where tabular ground ice and ice wedges are present. Massive ground ice bodies with 2–15 m of visible thickness were found in late Pleistocene marine sediments at the Taimyr coasts of Yenisey Gulf. Ice-rich sediments are widespread; they form the "Ice Complex" at the top part of the Quaternary section of west Taimyr. The "Ice Complex" sediments form a geomorphic surface with a height of about 12–15 m a.s.l. These sediments were formed during late Pleistocene sea regression, at a time when the mouth of the Yenisey River was about 300 km to the north from its present location. Ice-rich syngenetic Holocene sediments accumulated mostly at slopes and bottoms of thaw-lake basins and other depressions associated with thawing of Pleistocene ice wedges and tabular massive ice bodies.

Keywords: grain size; heavy minerals; ice wedges; ion composition; quaternary sediments; tabular massive ice.

Introduction

Ground ice studies help to obtain significant paleo-geographical information. Huge syngenetic ice wedges, forming specific "Ice Complex" (or "Yedoma") sediments, and tabular massive ice with thicknesses up to 50 m, are unique natural formations. According to most recent publications, "Ice complex" silty sediments of late Pleistocene are polygenetic; they were formed due to aeolian, fluvial, slope-wash, nival, and solifluction processes.

"Ice Complex" sediments have been studied mainly in central and northern Yakutia; similar sediments were observed also in Chukotka, West Siberia, Taimyr, Alaska, and Canada (Péwé 1975, Katasonov 1978, Popov et al. 1985, Carter 1988, Romanovskii 1993, Shur et al. 2004). Many publications are also based on studies of tabular massive ice bodies, but numerous hypotheses on their origin are still controversial (Streletskaya et al. 2003). Sections where both tabular and syngenetic ice-wedge bodies can be observed have a special value (Danilov 1969, Trofimov & Vasilchuk 1983, Vasilchuk 2006, Kunitskiy 2007).

Coastal bluffs of the Yenisey Gulf are formed mostly by Quaternary marine and littoral sediments with tabular massive ice bodies (Danilov 1969, Soloviev 1974, Danilov 1978). The upper part of the section is formed by continental sediments with huge ice wedges (Karpov 1986).

Beginning in 2004, we studied permafrost at the coasts of the Yenisey River and Yenisey Gulf between Dudinka and Dikson. This area is located within the continuous permafrost zone (Fig. 1). Our work was aimed at solving the problem of the history of permafrost development during the Pleistocene and Holocene. The purpose of our research included the study of cryogenic structure, chemical and mineralogical composition; estimation of ice content, salinity, grain size, organic carbon content, and age of the Quaternary sediments.

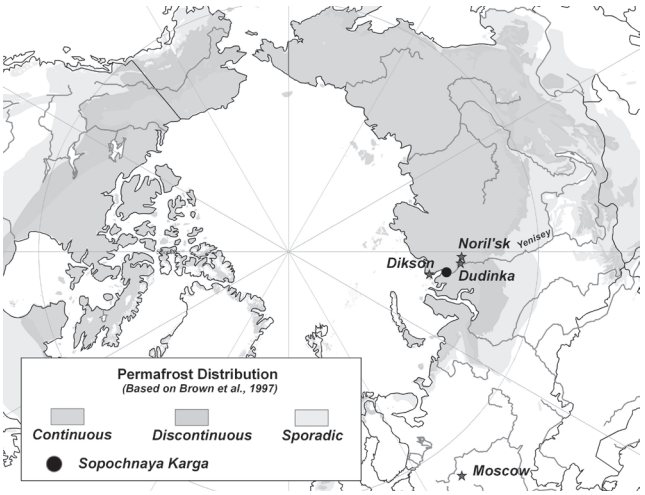

Figure 1. Location of the study area.

During field work, several sections of Quaternary sediments with different types of massive ice were studied (Streletskaya et al. 2005, Streletskaya et al. 2007, Shpolyanskaya et al. 2007). Our research of ground ice and sediments included field investigations and laboratory analyses (chemical, faunistic, micro-pollen and spores, oxygen-isotope, grain size and mineralogical, radiocarbon dating).

Results

One of the most interesting sections was studied in the 30–35 m high coastal bluff located near the "Sopochnaya Karga" Polar Station (71°57′N, 82°41′E), where the tabular massive ice body with a visible thickness of 10–12 m was observed (Fig. 2). This body is overlain by taberal (thawed and refrozen) clayey silts 8–10 m thick. The upper part of section is formed mostly by ice-rich syngenetically frozen silt with a belt-like cryostructure; the cryostructure between ice belts varies from reticulate and ataxitic (suspended) to micro-lenticular. The gravimetric moisture content reaches 80% and more. This layer includes ice wedges that vary from 0.4 m to 3.0 m in width.

The isotope composition (^{18}O) of the intrasedimental ice lenses reaches -17.50‰ to -17.73‰, while the composition of wedge ice varies from -19.04‰ to -20.92 ‰. Wedge ice mineralization reaches 22.04 mg/l, while the silts, including ice wedge, are fresh.

The horizon with ice wedges is underlain by dark-brown peat 1.0–1.5 m thick. The peat transforms with depth into brown organics-rich clayey silt with lenticular-braided, ataxitic (suspended), and micro-lenticular cryostructures (Fig. 2B). Radiocarbon dating of peat samples showed the age 7320 ±130 yr BP (GIN 13056) and 8050 ±60 yr BP (GIN 13055). Thus, radiocarbon dating indicates a Holocene age for the ice wedges.

Peat and peaty silt horizons are underlain by dark-grey silty clay with numerous inclusions of pebbles and boulders. This horizon, which is 10–15 m thick, overlies the body of tabular massive ground ice. Silty clays are characterized by

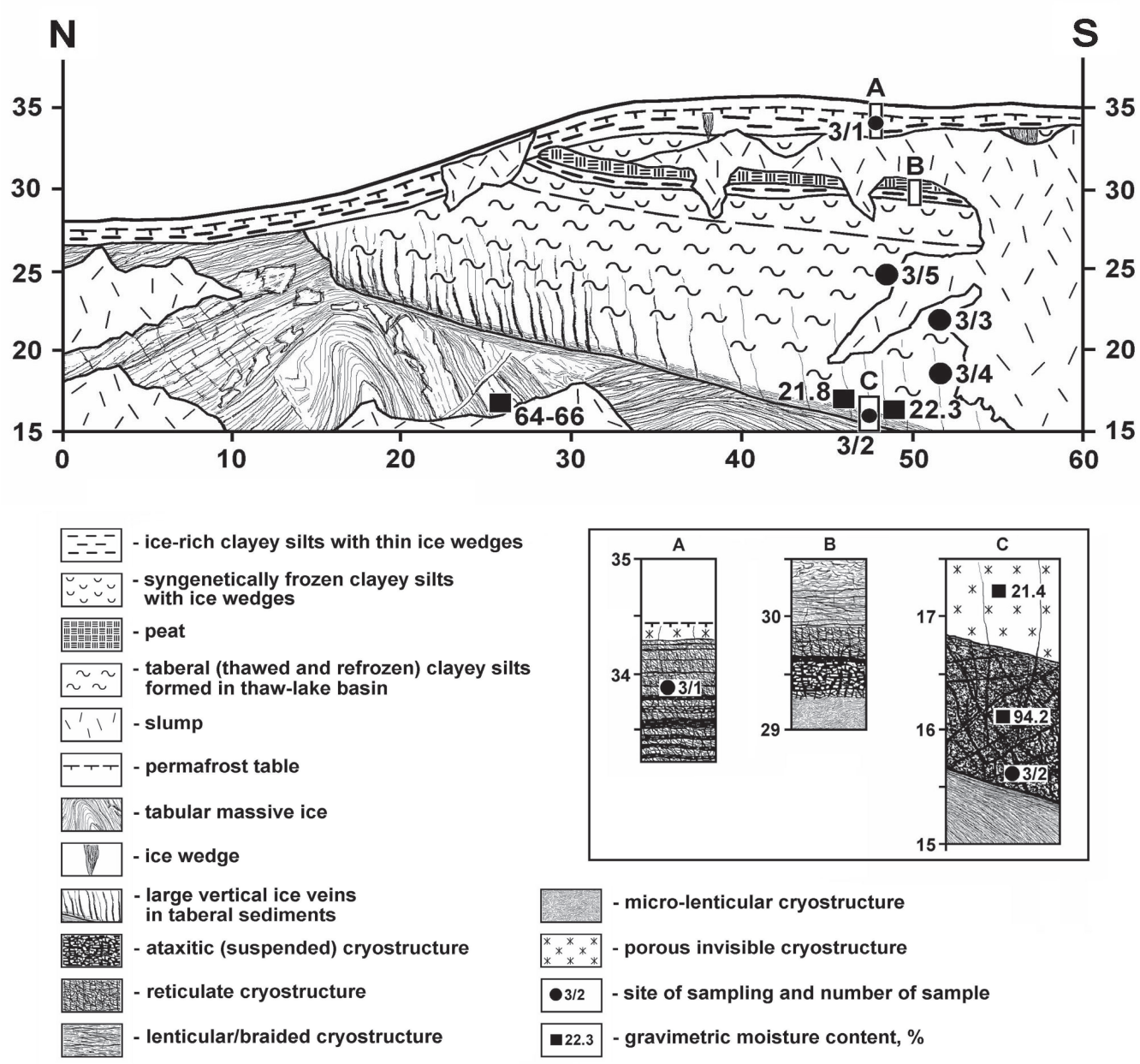

Figure 2. Cryostratigraphic section #3 in the area of "Sopochnaya Karga" Polar Station. Horizontal and vertical scales in meters. A, B, C – details of cryogenic structure.

porous cryostructure; their average gravimetric moisture content is about 22%. At the bottom part of this horizon, above the boundary with the massive ice, thick ice veins, wedging out upwards, were observed. Close to the boundary incline (parallel to the boundary), an ice-rich horizon with the thickness up to 1.2 m was observed. This horizon is characterized by ataxitic (suspended) cryostructure; its gravimetric moisture content reaches 94%.

Silty clays are fresh in general, but their ion composition changes with depth (Fig. 2, samples 3/5, 3/3, 3/4). Bicarbonate-ions and sulfate-ions amounts increase from 0.46 up to 1.92 mg-eqv/l and from 0.18 up to 1.82 mg-eqv/l, respectively. Chlorine-ion content increases from 0.30 up to 0.98 mg-eqv/l. At the boundary with the massive ice body (Fig. 2C, sample 3/2), silty clays contain more soluble salts (salinity is about 0.14%), and contents of bicarbonates and sodium exceeds the contents of all other ions.

A tabular massive ice body is characterized by frequent alternation of folded layers of pure ice and relatively ice-rich soil, with a cryostructure that varies from micro-ataxitic (micro-suspended) to micro-porphyritic (porous visible) with a gravimetric moisture content of 64–66%.

Mineralization of pure ice varies from 46.74 mg/l to 247.87 mg/l. Ion composition shows the prevalence of bicarbonate-ions, which reaches 92% near the upper boundary of the massive ice body and 81.8% at its base. Among cations, sodium-ions prevail, their content increasing towards the center of the massive ice body; ice mineralization and amount of soil inclusions decrease in the same direction. The isotope composition (^{18}O) of the massive ice reaches -22.84‰ to -23.15‰; these values are similar to the composition of wedge ice.

In the section of the other coastal bluff (Fig. 3), also located in the area of "Sopochnaya Karga" Polar Station, three horizons of Quaternary sediments with a total thickness of about 12 m were observed.

The upper part of the section to a depth of 6.2 m is formed by syngenetically frozen silts of alluvial-lacustrine genesis (Fig. 3A). The silts include ice wedges up to 2 m wide. The isotope composition (^{18}O) of the wedge ice varies from -24.46‰ up to -24.84‰. The silts are underlain by ice-poor fine sands and coarse gravelly laminated sands (Fig. 3). At the boundaries of the wedges, strong upward tilting of sands was observed (Fig. 3B). Gravimetric moisture content of

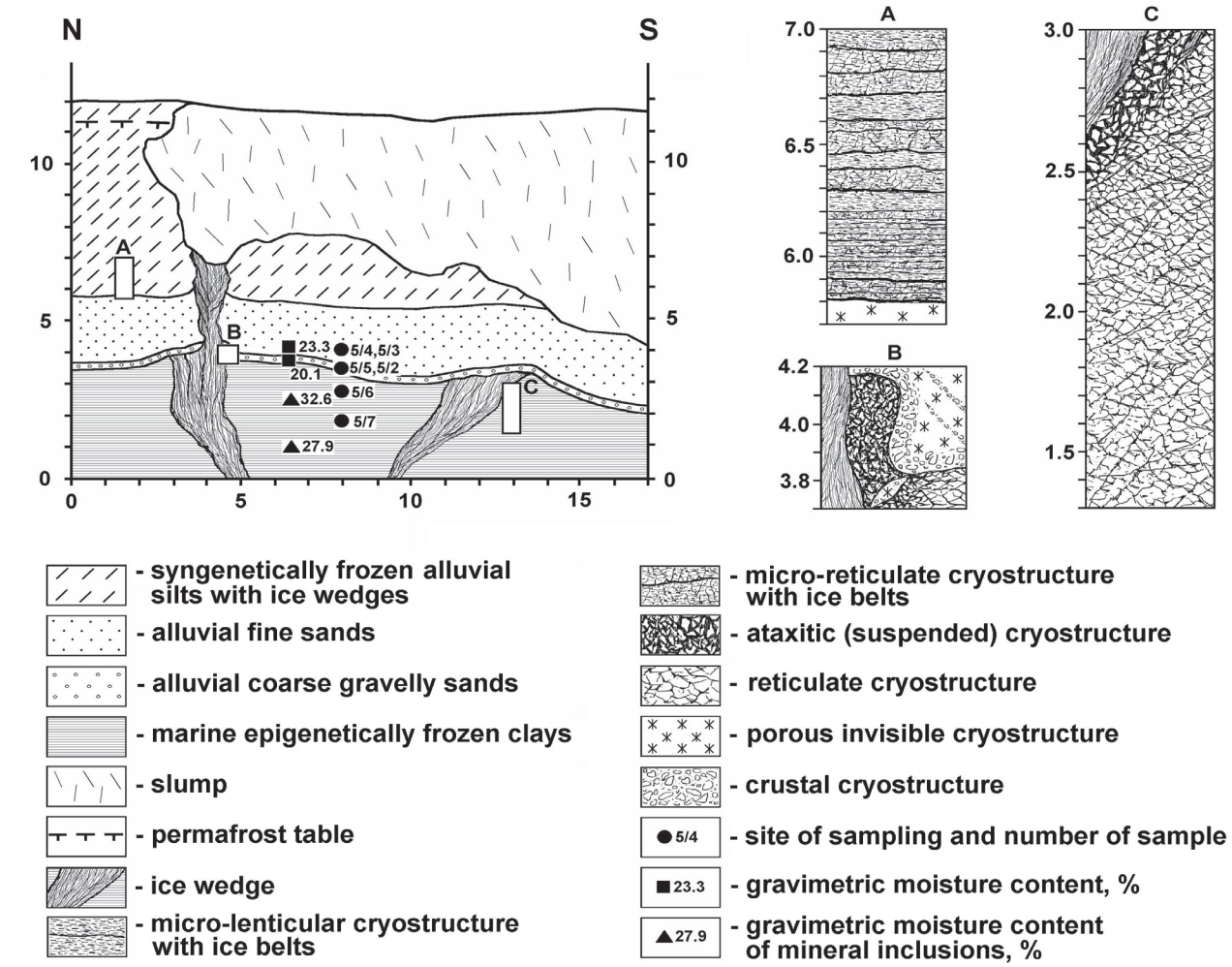

Figure 3. Cryostratigraphic section #5 in the area of "Sopochnaya Karga" Polar Station. Horizontal and vertical scales in meters. A, B, C – details of cryogenic structure.

sands reaches 20–23%. Both silts and sands are fresh. Ion composition shows the prevalence of bicarbonate-ions and sodium-ions.

From a depth of 8.5 m and downward to sea level, dark-gray clays were observed. The clays include ice wedges up to 2 m wide. Sufficient increase in the ice content was observed near the boundaries of the ice wedges (Fig. 3B, C). The clays are saline (salinity is about 0.5%), and the composition of soluble salts is characteristic for marine conditions (chlorine-ion content is 70–85 mg-eqv%, sodium-ion content is 97 mg-eqv%).

Discussion

Analysis of obtained data allows for reconstruction of the freezing conditions of studied strata. In both sections we can see evidence of transformation from marine to continental conditions, which resulted in freezing of Late Pleistocene marine sediments, formation of tabular massive ice, and deposition of syngenetically frozen "Ice Complex" sediments.

We believe that the tabular massive ice body, studied at section #3, could be formed due to an injection of water-soil slurry into epigenetically frozen strata of marine clay. The alternative hypothesis of possible massive ice origin is glacial; it is based on similarity of the studied ice body with the basal ice of modern glaciers (Kanevskiy et al. 2006).

In general, mineralization of the tabular massive ice body is typical for closed taliks: freezing from different directions results in the increase of mineralization near the margins of freezing body. The ion composition is also similar to ion composition of sub-lake taliks. In the studied section, Na/Cl ratio is 3.0–3.7. For example, in sub-lake taliks in Yakutia, this ratio varies from 3.2 to 7.5 (Anisimova 1981).

Development of the thermokarst process resulted in partial thawing of the tabular massive ice body, formation of a thaw bulb beneath the lake, and accumulation of taberal sediments. These sediments formed as a result of thawing and refreezing of epigenetically frozen marine clay. Taberal origin of silty clays can be proved by the absence of lamination, typical for lacustrine sediments, and increase of soluble salts content with depth. Such distribution of soluble salts indicates the process of salts migration towards the freezing front. Originally these sediments were formed at the littoral; marine-type composition of salts transformed to continental as a result of thawing of sediments.

Marine origin of these sediments was also confirmed by complex mineralogy and grain size analysis (Surkov 1993, Surkov 2000). According to this method, the origin of sediments can be distinguished by the patterns of distribution of heavy minerals relating to size and shape of grains (for example, grains of marine sands are better rounded and have a flat shape). Standard patterns for different types of sediments were developed (Surkov 2000); comparison with these patterns allows definition of the origin of sediments and condition of sedimentation.

A study of heavy minerals from the silty clay layer (section #3) shows that this horizon originally was formed in littoral conditions with alongshore currents and big wave activity. Minerals from the tabular massive ice body are well-sorted; the stable assemblage of heavy minerals (magnetite, ilmenite, garnet) indicates a constant source of denudation during the sedimentation process.

Micro-faunistic analysis shows that the foraminifer complex is typical for the low-salinity Arctic basin, which existed presumably in the end of Eemian and after the Eemian stage of the late Pleistocene (Streletskaya et al. 2007). Therefore, the sediments overlaying massive ice and the soil inclusions in the ice itself have the same marine origin and differ sufficiently from the upper horizon with ice wedges.

We believe that talik freezing, triggered by elimination or migration of the lake, started from the surface. An ice-rich layer parallel to the boundary with tabular massive ice (Fig. 2C) was formed due to freezing from below of water-saturated soils at the base of the talik. Simultaneously with the freezing of the talik, the formation of syngenetically frozen soils with micro-lenticular cryostructure started at the surface. The complex mineralogy and grain size analysis of heavy minerals shows that sorting of such minerals as magnetite, ilmenite, garnet, and pyroxene is typical for continental conditions of floodplains with numerous peaty ponds. The prevalence of flat quartz grains with a specific wing-like shape reflects the role of aeolian transportation in sedimentation process (Surkov 1993, Surkov 2000).

Peat accumulation at the bottom of the thaw lake basin during the climatic optimum of the Holocene resulted in the active layer reduction and formation of an ice-rich intermediate layer (Shur 1988) about 0.6 m thick (Fig. 2B). The peat layer was buried beneath syngenetically frozen slope sediments. Termination of slope sedimentation resulted in the formation of the contemporary intermediate layer with thin ice wedges (Fig. 2A).

The formation of silt with syngenetic ice wedges (section #5) started during marine regression at the end of the late Pleistocene, when the mouth of the Yenisey River moved northward more than 300 km in comparison with its contemporary position (Stein 2002). At this period, ice wedge growth occurred in west Siberia, at the west and east coasts of Yamal Peninsula (Forman 2002, Kanevskiy et al. 2005, Vasilchuk 2006), in central parts of Yamal Peninsula, and at Gydan Peninsula (Bolikhovskiy 1987), in different parts of Taimyr at Cape Sabler (*Anthropogen* 1982, Derevyagin et al. 1999) and Labaz Lake (Siegert et al. 1999).

Before syngenetic permafrost formation, the epigenetic freezing of marine clays started, accompanied by frost cracking. In section #5, the transition from sub-aquatic to sub-aerial condition is marked by strong oxidation of the top part of the marine clays sequence; the thickness of the oxidized layer is about 1 m. Clays have a reticulate cryostructure; the size of mineral blocks increases with depth, while their moisture content decreases. It indicates slowing of the freezing rate with depth.

The formation of clays in this section occurred in conditions

of marine sedimentation below the level of wave sorting. Properties and composition of the clays show similarity with the silty clays from the previous exposure (Streletskaya et al. 2007).

A break in sedimentation, during which relatively large epigenetic ice wedges formed in the marine clay, was followed by a period of erosion activity. Erosion processes led to truncation of the upper part of clay strata. We could observe several evidences of very cold climate at this period: absence of significant thermokarst features at the surface of truncated ice wedges; light isotope composition of the wedges. The patterns of heavy minerals distribution in overlying sands are shown at the Figure 4. Study of the gravelly sands patterns reveals far transportation of grains by high-energy river flow. Heavy minerals composition and distribution are similar to contemporary alluvial sediments of the Yenisey River in the area of Dudinka city; they differ from contemporary beach deposits of Yenisey Gulf (Streletskaya et al. 2005).

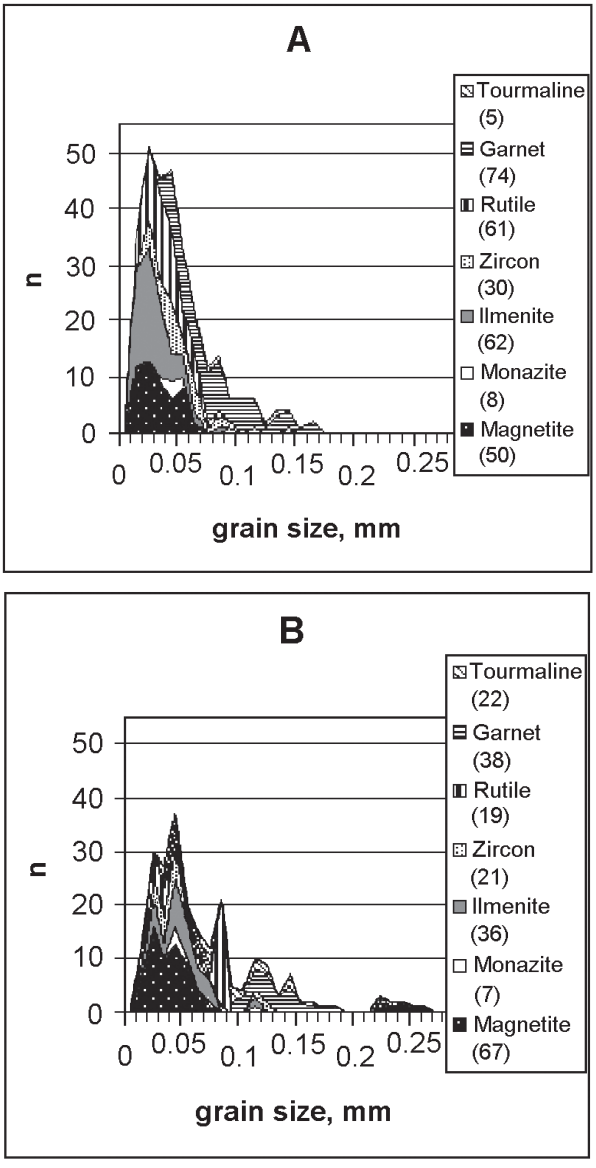

Figure 4. Patterns of heavy minerals distribution vs. thickness of grains (C-axis), Sopochnaya Karga, section #5. Amount of grains is shown in parentheses. A – fine sands; B – coarse gravelly sands.

During the period of alluvial sands accumulation, the growth of part of the ice wedges was terminated (right wedge, Fig. 3). A high sedimentation rate and relatively coarse composition of soils resulted in low ice content and an abrupt decrease in the width of ice wedges still continuing their growth.

We believe that syngenetically frozen silts at the top part of this section have an alluvial-lacustrine genesis. The pattern of heavy minerals distribution showed that they were formed at the floodplain of the big river. The main evidences of a syngenetic type of freezing are the rhythmic cryogenic structure (Fig. 3A); a prevalence of micro-lenticular and micro-reticulate cryostructures; and the occurrence of undecomposed rootlets.

Conclusions

At the coasts of Yenisey Gulf, tabular massive ice bodies are included in littoral clayey sediments of the late Pleistocene, while large syngenetic ice wedges are typical for Late Pleistocene–Holocene continental deposits. Ice-rich sediments are widespread; they form the "Ice Complex" at the top part of the Quaternary section of west Taimyr. The wedges, up to 12 m high, started their development at the end of the late Pleistocene as epigenetic wedges, and continued their growth at the period of syngenetic permafrost formation. They have the same age as thin till deposits of the last glaciation. It confirms the relatively small scale of the last glaciation in Taimyr (Svendsen 2004). Ice-rich syngenetic Holocene sediments accumulated mostly at slopes and bottoms of thaw-lake basins and other depressions associated with thawing of Pleistocene ice wedges and tabular massive ice bodies.

Acknowledgments

We are particularly grateful to Dr. Evgeny Gusev and Dr. Fedor Romanenko for their field assistance, Dr. Boris Vanshtein and Dr. Alexandr Surkov for lab analysis of soil samples, and Dr. Hanno Meyer for lab analysis of isotope composition of ice samples. The work was supported by the "Leading scientific schools of Russia" project 500.2008.5 and by Tyumen Regional Academy.

References

Anisimova, N.P. 1981. *Hydrogeochemical features of the permafrost zone.* Novosibirsk: Nauka, 153 pp. (in Russian).

Anthropogen of Taimyr Peninsula. 1982. Moscow: Nauka, 184 pp. (in Russian).

Bolikhovskiy, V.F. 1987. Yedoma sediments of Western Siberia. In: *New data on Quaternary chronology, XII INQUA Congress (Canada, 1987)*. Moscow: Nauka, 128-135 (in Russian).

Carter, L.D. 1988. Loess and deep thermokarst basins in Arctic Alaska. *Proceedings of the Fifth International Conference on Permafrost.* Tapir publishers, Trondheim, Norway: 706-711.

Danilov, I.D. 1978. *Pleistocene of marine subarctic plains*. Moscow: Moscow University Press, 198 pp. (in Russian).

Danilov, I.D. 1969. Cryofacial structure of Pleistocene sediments of dividing ridges in the lower course of Yenisey River. In: *Problems of Cryolithology 1*, Moscow University Press: 93-105 (in Russian).

Derevyagin, A.Yu., Chizhov, A.B., Brezgunov, V.S., Hubberten, H.-W. & Siegert, C. 1999. Isotope composition of ice wedges at Cape Sabler (Taimyr Lake). *Kriosfera Zemli (Earth Cryosphere)* III (3): 41-49 (in Russian).

Forman, S.L., Ingolfsson O., Gataullin, V., Manley, W.F. & Lokrantz, H. 2002. Late Quaternary stratigraphy, glacial limits and paleoenvironments of Maresale area, Western Yamal Peninsula, Russia, *Quaternary Research* 21: 1-12.

Kanevskiy, M.Z**,** Streletskaya, I.D. & Vasiliev, A.A. 2005. Formation of cryogenic structure of Quaternary sediments in Western Yamal. *Kriosfera Zemli (Earth Cryosphere)* X (2): 16-27 (in Russian).

Kanevskiy, M., Tumskoy, V., Fortier, D., Jorgenson, T. & Shur, Y. 2006. Structure and properties of basal ice and subglacial till. *Abstracts of Arctic Science Conference "State of the Arctic: Current State of the Arctic – Observations of Arctic Change," Fairbanks, Alaska, 2-4 October 2006*: 37-38.

Katasonov, E.M. 1978. Permafrost-facies analysis as the main method of cryolithology. *Proceedings of the Second International Conference on Permafrost*, *July 13-28, 1973*. *USSR Contribution*. Washington: National Academy of Sciences, 171-176.

Karpov, E.G. 1986. *Ground ice of Yenisey North*. Novosibirsk: Nauka, 133 pp. (in Russian).

Kunitskiy, V.V. 2007. *Nival lithogenesis and Ice Complex in Yakutia.* Author's summary of Dr.S. Thesis. Yakutsk: Permafrost Institute Press, 46 pp. (in Russian).

Péwé, T.L. 1975. *Quaternary geology of Alaska. Geological survey professional paper 835*. Washington: United States Government Printing Office, 145 pp.

Popov, A.I., Rozenbaum, G.E. & Tumel, N.V. 1985. *Cryolithology*. Moscow: Moscow University Press, 239 pp. (in Russian).

Romanovskii, N.N. 1993. *Basics of cryogenesis of lithosphere*. Moscow: Moscow University Press, 336 pp. (in Russian).

Shpolyanskaya, N.A., Streletskaya, I.D. & Surkov, A.V. 2007. Comparative genetic analysis of tabular massive ice and adjacent Pleistocene sediments of the northern part of West Siberia. *Geoecology. Engineering Geology. Hydrogeology. Geocryology* 3: 212-224 (in Russian).

Shur Y.L. 1988. *Upper horizon of the permafrost soils and thermokarst.* Nauka, Siberian Branch, Novosibirsk: 210 pp. (in Russian).

Shur, Y., French, H.M., Bray, M.T. & Anderson, D.A. 2004. Syngenetic permafrost growth: cryostratigraphic observations from the CRREL Tunnel near Fairbanks, Alaska. *Permafrost and Periglacial Processes* 15(4): 339-347.

Siegert, C., Derevyagin, A.Y., Shilova, G.N., Hermichen, W.-D. & Hiller, A. 1999. Paleoclimate indicators from permafrost sequences in the Eastern Taymyr Lowland. In: H.Kassens, H.A.Bauch, I.A.Dmitrenko, H.Eicken, H.-W.Hubberten, M.Melles, J.Thiede, L.A.Timokhov (eds.), *Land-Ocean Systems in the Siberian Arctic. Dynamic and History. Berlin*. Heidelberg: Springer-Verlag, 477-499.

Soloviev, V.A. 1974. Experience of study of the ground ice of Yenisey North aimed on paleo-geographical and neotectonic reconstructions. In: *Natural conditions of West Siberia 4*. Moscow: Moscow University Press, 34-48 (in Russian).

Stein, R. et al. 2002. Siberian river run-off and late Quaternary glaciation in the southern Kara Sea, Arctic ocean: Preliminary results. *Polar Research* 21(2): 315-322.

Streletskaya, I.D. et al. 2007. New results of Quaternary sediment Studies of Western Taimyr. *Kriosfera Zemli (Earth Cryosphere)* XI (3): 14-28 (in Russian).

Streletskaya, I.D., Surkov, A.V. & Semenov, S.V. 2005. Studies of Quaternary sediments of Russian North with the method of complex mineralogy and grain size analysis (Yamal Peninsula, Yenisey River estuary). *Quarter-2005. IV All-Russia Conference on Quaternary researches: Proceedings (Syktyvkar, August 23-26, 2005). Institute of Geology of Komi SC UB RAS*, Syktyvkar, Geoprint: 405-407 (in Russian).

Streletskaya, I.D., Ukraintseva, N.G. & Drozdov, I.D. 2003. A digital database on tabular ground ice in the Arctic. *Proceedings of the Eighth International Conference on Permafrost, 21-25 July 2003, Zurich, Switzerland.* A.A. Balkema Publishers 1: 1107-1110.

Surkov, A.V. 1993. Method of complex mineralogy and grain size analysis and its application for study of sediments. *Geology and Reconnaissance* 3: 36-43 (in Russian).

Surkov, A.V. 2000. *New methods of study of sand-silt component of placers and sedimentary rocks*. Moscow: E. Razumova, 286 pp. (in Russian).

Svendsen, J.I., Alexanderson, H., Astakhov, V. et al. 2004. Late Quaternary ice sheet history of northern Eurasia. *Quaternary Science Reviews* 23: 1229-1271.

Trofimov, V.T. & Vasilchuk, Yu.K. 1983. Syngenetic ice wedges and tabular massive ice in Pleistocene sediments of the northern part of West Siberia. *Bulletin of the Moscow Society of Natural Scientists, Geology Department* 58 (4): 113-121 (in Russian).

Vasilchuk, Yu.K. 2006. *Ice wedges: Heterocyclicity, Heterogeneity, Heterochrony.* Moscow: Moscow University Press, 404 pp. (in Russian).

Thirteen Years of Observations at Alaskan CALM Sites: Long-Term Active Layer and Ground Surface Temperature Trends

Dmitry A. Streletskiy, Nikolay I. Shiklomanov, and Frederick E. Nelson
Department of Geography, University of Delaware, Newark, USA
Anna E. Klene
Department of Geography, University of Montana, Missoula, USA

Abstract

Active layer monitoring is an important component of efforts to assess the affects of global change in permafrost environments. In this study we used data from 13 (1995–2007) years of spatially oriented field observations at a series of 16 representative Circumpolar Active Layer Monitoring (CALM) sites in northern Alaska to examine temporal and spatial trends in active layer thickness and its relation to climatic, surface, and subsurface conditions. The observation strategy consisted of measuring active layer thickness on regular 1-ha and 1-km^2 grids representative of environmental conditions on Alaska's North Slope. The measurement program also involves continuous air and soil temperature monitoring, periodic frost heave and thaw subsidence using Differential Global Position System (DGPS) as well as landscape, vegetation, and soil characterization. This paper showcases CALM observation procedures and analysis designed to monitor processes and detect changes not anticipated in the original CALM protocol of the early 1990s.

Keywords: active layer; Alaska; CALM; Circumpolar Active Layer Monitoring; surface temperature; thaw subsidence.

Introduction

The active layer is the most dynamic part of the permafrost system and undergoes many changes in its properties during each annual cycle. These fluctuations involve variations of ice/water content, thermal conductivity, density, mechanical properties, and solute redistribution (Ershov 2002), all of which are of critical importance for many natural phenomena and processes in permafrost and periglacial environments (French 2007). Most biological and hydrological activities in arctic soils are confined to the layer of seasonal thaw (Hinzman 1991). Active layer monitoring is an important component of efforts to assess the effects of global climate change in arctic environments. The Circumpolar Active Layer Monitoring (CALM) program is a network of sites at which data about active layer thickness (ALT) and related climatic, vegetation, and soil parameters are collected. The CALM network involves more than 160 sites underlain by permafrost in polar regions and selected mountainous environments (Brown et al. 2000, Nelson et al. 2004).

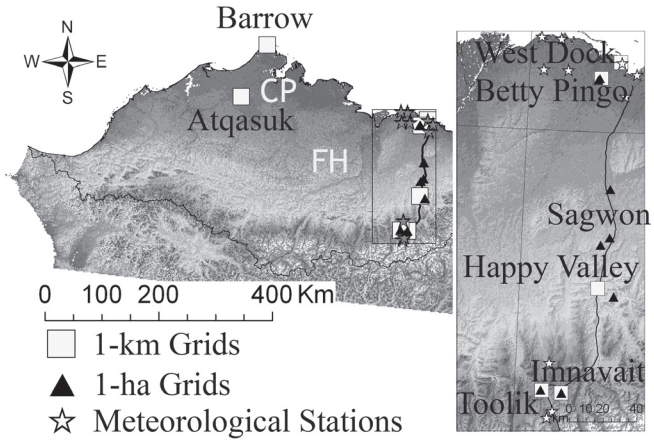

Figure 1. Geographic distribution of Alaskan CALM observational sites used in the present study. Gray tones represent elevation, with brighter shades indicating higher elevations. Physiographic provinces are indicated by white lettering: CP – Coastal Plain, FH – Foothills. Black font is used for name specific sites mentioned in the text.

In this study we used data from 13 years (1995–2007) of extensive, spatially oriented field observations at a series of 16 CALM sites on the North Slope of Alaska to examine landscape-specific temporal trends in active layer thickness and air and soil temperature. CALM strategies are evolving constantly, and this paper showcases CALM observation procedures and analysis designed to monitor processes and detect changes not anticipated in the original CALM protocol of the early 1990s. Details of the analyses and results will be presented in a series of manuscripts currently in preparation.

Study Area

Of the 41 CALM-designated sites in Alaska, 29 are located on the North Slope (Shiklomanov et al. 2008). In this paper we report observed long-term trends of air and ground surface temperature and active layer thickness from 16 sites with continuous records for 13 years (1995–2007).

The sites selected for analysis are distributed along the primary climatic gradient in northern Alaska (Fig. 1). The sites span the regional spectrum of vegetation and terrain conditions in two dominant physiographic provinces: the Arctic Coastal Plain in the north and the Arctic Foothills in the south (Wahrhaftig 1965).

The elevation of the Arctic Coastal Plain increases gradually from north to south, reaching about 100 m at its southern edge. Poor drainage and low relief create conditions

for development of thaw lakes. Thaw lakes and thaw-lake basins occupy from 20% to 50% of the area. The coastal plain is dominated by wet sedge polygonal tundra on soils associated with windblown loess deposits (Walker et al. 2003).

The Arctic Foothills province extends between the Arctic Coastal Plain and the Brooks Range and is characterized by hills and plateaus divided by river valleys. The area was glaciated during the Pleistocene, and surface deposits are mostly glacial till with discontinuous loess cover (Bockheim et al. 1998). Differences in underlying deposits create distinct geochemical contrast in soils, leading to differences in vegetation species and organic layer thickness (Walker et al. 1998). Based on soil pH, areas of tundra can be subdivided into acidic (pH <5.5) and nonacidic (pH >5.5) classes. Soils in nonacidic tundra have thinner organic horizons, a significantly thicker active layer, and greater cryoturbation than soils of acidic tundra (Bockheim et al. 1998)

The entire study area lies in the zone of continuous permafrost. The only areas possibly without permafrost are occupied by deep bodies of water that fail to freeze to the bottom in winter (Péwé 1975).

Methodology

Of the 16 CALM sites used in the analysis described in the next section, 9 consist of 1-ha plots established to represent relatively homogeneous examples of the landscape categories found in particular physiographic provinces. The selection of landscapes was guided by a regional landcover map derived from Landsat imagery (Auerbach et al. 1996). The map depicts 5 primary landscape units: wet tundra (WET), moist acidic tundra (MAT), moist nonacidic tundra (MNT), shrublands (SHR), and barrens. Characteristics of the 1-ha sites were described by Shiklomanov & Nelson (2003), and Klene et al. (2001b); their geographic distribution is shown in Figure 1. Beginning in 1995, the active layer has been probed at least annually at the 1-ha sites. The procedure involves pushing a metal rod, calibrated in cm, to the point of refusal, interpreted in most cases to be the frost table. Thaw depth measurements at each site were obtained by probing at 5 m intervals along the plot's two perpendicular and one diagonal transect, resulting in 71 points per plot per probing date. Air and soil surface temperature were measured continuously at two-hour intervals over the 1995–2007 period (data are available for the 1996–2006 period) with an array of Onset™ portable data loggers. At each site one logger is mounted on a mast, with thermistors placed approximately 2 m above the ground in a radiation shield. Seven to ten loggers are distributed over each of the 1 ha plots, with thermistors placed at the vegetation/soil interface at locations representative of microtopographic conditions (Klene et al. 2001b, Klene et al. 2008).

Periodic thaw depth measurements were also conducted at 7 surveyed and georeferenced 1-km^2 grids over the period 1995–2007. These sites were established in northern Alaska during the 1980s and 1990s to monitor long-term ecosystem change (Brown et al. 2000). Four grids (Barrow, Atqasuk, Betty Pingo, and West Dock) are situated on the Arctic Coastal Plain, and the remaining three (Happy Valley, Imnavait Creek, and Toolik Lake) are in the Arctic Foothills (Fig. 1). The 1-km^2 grids were selected to represent more generalized conditions found in each physiographic province. Detailed descriptions of the 1-km^2 sites were provided by Hinkel and Nelson (2003). Each grid consists of a square array of surveyed permanent stakes separated by 100 m, yielding an 11 × 11 array of sampling nodes on each grid. Sampling was conducted by manual probing at each stake, yielding a maximum of 121 data points per grid per probing date. The active layer was not measured at locations where grid points intersect rocks or deep water. A significant portion of the Toolik and Imnavait sites are underlain by coarse glacial material that is impenetrable for metal probes. These sections of the Toolik and Imnavait grids were excluded from the analysis.

Each grid is instrumented for air and ground surface temperature measurements using equipment similar to that at the 1-ha sites. In addition, at each 1-km^2 site ground temperature is monitored at hourly intervals at the standard depths of 0, 5, 10, 15, 20, 25, 30, 35, 45, 70, 95, and 120 cm using Campbell Scientific™ and Measurement Research Corporation instrumentation. Periodic, spatially oriented frost heave and thaw subsidence measurements using Differential Global Position System (DGPS) were initialized in 2001 at 2 Coastal Plain 1-km^2 sites and 1 Foothills 1-ha site (Little et al. 2003, Streletskiy et al. 2005). Measurements are performed twice each year at the beginning (June) and the end (August) of the thawing season, using a hierarchical nested sampling design (Nelson et al. 1999). A series of additional sites were instrumented for measuring air and soil surface temperature at locations chosen to facilitate adequate geographic coverage.

Analytical Results

Air temperatures trends

Air temperature trends from individual sites were analyzed using procedures outlined in Shiklomanov & Nelson (2002). In this paper we present monthly air temperatures, integrated over physiographic provinces.

Regionally, air temperature increases from north to south. Mean annual air temperature over the study period varied between -9.2°C and -12.0°C on the Coastal Plain and between -7.3°C and -10.3°C in the Foothills. Mean summer air temperature (June–August) on the Coastal Plain varies between 5.5°C and 8.7°C, while at Foothills it ranges from 6.8°C to 11.7°C. This climatic pattern demonstrates the pronounced influence of the Arctic Ocean during the summer, throughout the Coastal Plain. Province-specific 12-year (1995–2006) records of mean, minimum, and maximum annual air temperature, as observed at CALM sites, are shown in Figure 2. There is a slight decline in mean and maximum annual air temperature for the Coastal Plain and in maximum annual air temperature for the Foothills.

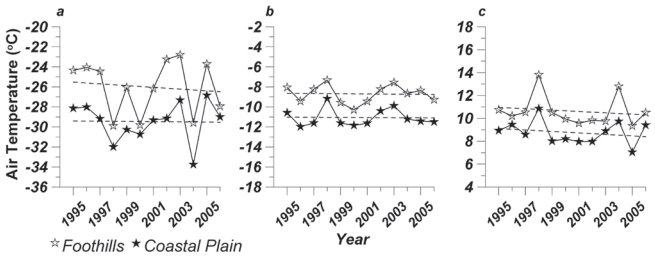

Figure 2. Twelve-year (1995–2006) records of annual minimum (a), mean (b), and maximum (c) monthly air temperature as observed at CALM Coastal Plain and Foothills sites.

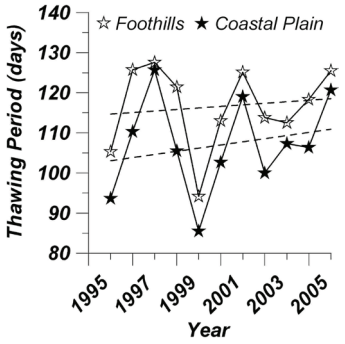

Figure 3. Province-specific 12-year (1995–2006) records of the duration of thawing period, as observed at CALM sites.

Duration of thawing period

The duration of the thawing period was estimated based on analysis of mean daily air temperature at individual sites by counting consecutive days with temperatures above 0.5°C. Results were averaged by physiographic province.

On average, the thawing period on the Coastal Plain is almost 10 days shorter than in the Foothills. However, this difference ranges from 2 to 16 days, depending on the year. Province-specific 12-year records of thaw-period duration, as observed at CALM sites, are shown in Figure 3. Both provinces experienced an increase in the duration of thawing, attributable to both the earlier initiation of the thawing and later freezing.

Effect of vegetation on ground surface temperature

Analysis of ground surface temperature was aimed primarily at evaluating the effects of vegetation and the characteristics of different landscape units on the ground thermal regime. The daily air and soil-surface temperature data obtained at the homogeneous 1-ha sites were used to calculate average differences between surface and air temperature (ΔT) for the warm period (June–August). To evaluate the effect of vegetation on the ground thermal regime further, the landscape-specific values of empirical summer n-factors were calculated. The n-factor, defined operationally as the ratio of the degree-day sum at the soil surface to that in the air (Carlson 1952), has been used in cold regions engineering since the 1950s to estimate soil surface temperature from air temperature records. Estimation of n-factors has been found to be a useful, simple approach for estimating the attenuation of climatic signals by vegetation cover (Klene et al. 2001a, b, Kade et al. 2006). An analysis of winter n-factors for the study sites is presented elsewhere in this volume by Klene et al. (2008).

Table 1. Landscape-specific 12-year (1995-2006) average values of ΔT and n-factors, as estimated from air and ground surface temperature measurements at representative 1-ha CALM sites.

Landscape Unit	Coastal Plain		Foothills	
	ΔT, °C	N-factor	ΔT, °C	N-factor
Barrens	1.0	1.20	1.6	1.22
MNT	-1.2	0.78	-2.6	0.71
MAT			-3.8	0.52
Shrublands			-3.1	0.57
WET	-2.2	0.66	-2.3	0.74

Values of ΔT and n-factors obtained at individual sites were averaged to represent individual landscapes and physiographic provinces. To account for interannual climatic variability, the annual landscape- and province-specific values of ΔT and n-factor were averaged over a 12-year (1995–2006) period and are presented in Table 1.

The vegetated surfaces in both physiographic provinces show negative values of ΔT and n-factor values of less than unity, indicating the cooling influence of vegetation on ground temperature during the warm period. The distinct values of ΔT and n-factor indicate the distinct thermal influence of landcover types characteristic of the Coastal Plain and Foothills physiographic province. The moist acidic tundra (MAT) of the Foothills province has the largest negative value of ΔT (-3.8°C) and the smallest value of n-factor (0.52). The smallest negative ΔT value (-1.2°C) and highest n-factor value (0.78) were found in moist nonacidic tundra (MNT) of the Coastal Plain. Regionally, values of ΔT and n-factor for similar landscape units vary from north to south in response to the increase in density of the vegetation cover. This effect is evident from differences in ΔT and n-factor for moist nonacidic tundra in two physiographic provinces. The thermal influence of MNT is greater in the Foothills than on the Coastal Plain.

Unvegetated surfaces, which consist of sand, gravel, and bedrock along streams and atop hills and mountains, show positive values of ΔT and values of n-factors of more than unity, indicating a warming influence of barren surfaces on ground thermal regime.

Annual thawing propagation

The annual dynamics of thawing were evaluated by analyzing thawing intensity curves for four 1-km^2 sites. The Barrow and Atqasuk sites were selected to represent the Coastal Plain, while Happy Valley and Toolik are representative of the Foothills. The thawing intensity curves were constructed by calculating a daily increase in thaw depth as a portion of the maximum annual active layer value. The daily values of thaw depth for each site were estimated using ground temperature observations from an array of 12 thermistors, distributed vertically from the surface to 1.2 m depth. The daily depth of thaw penetration was assumed to coincide with the interpolated position of the 0°C isotherm. For the silty soils characteristic of northern Alaska, the correspondence between thaw depth, as determined by

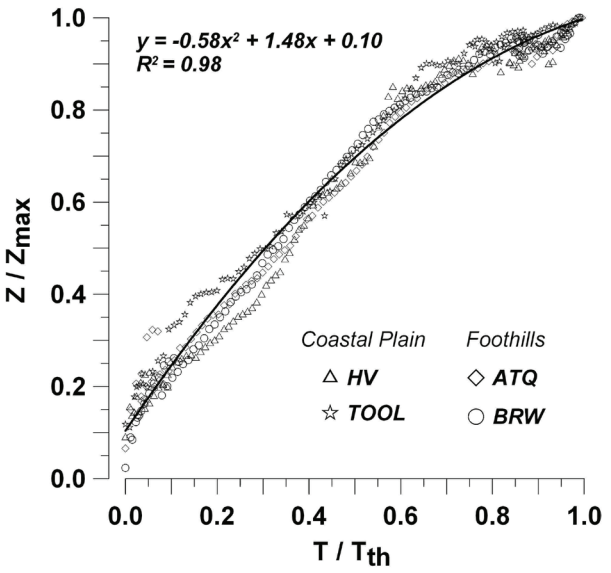

Figure 4. Site-specific 12-year averages of thawing intensity for two coastal plain (Barrow BRW and Atqasuk ATQ) and two foothills (Happy Valley HV and Toolik TOOL) locations. Z is thaw depth at time T and Z_{max} is annual maximum thaw depth achieved over the thaw period $T_{th.}$.

mechanical probing, and the position of the 0°C isotherm is generally quite good (Brown et al. 2000).

The analysis of annual thawing intensity curves indicates that, depending on site and year, 95% to 99% of maximum thaw propagation is reached by mid August, when annual CALM ALT observations by mechanical probing are starting at northern Alaska sites.

To evaluate the physiographic province-specific intensity of annual thaw penetration, independent of interannual variability in climatic conditions, relative increases in thaw depth were plotted as a function of relative time: $Z/Z_{max}=f(T/T_{th})$, where Z is the thaw depth at time T and Z_{max} is the annual maximum thaw depth achieved over thawing period T_{th}. Site-specific 12-year averages of thawing intensity for two coastal plain (Barrow (BRW) and Atqusuk (ATQ)) and two foothills (Happy Valley (HV) and Toolik (Tool)) locations are shown in Figure 4. The thawing intensity curves for all four locations are similar, indicating that the relationship between annual thaw depth propagation and dimensionless time is uniform for different surface, subsurface, and climatic conditions. Figure 4 demonstrates that regardless of location, 44% of annual thaw occurs during the first quarter of the thawing period; during the first half of the thawing period thaw depth reaches 70% of its maximum; after three-quarters of the thawing period, thaw depth is at 88% of its maximum; and that 96% of the active layer has thawed after 90% of the thawing season. These numbers correspond closely to values obtained at three drastically different locations in Russia (Yakutsk, Vorkuta, and Igarka) by Pavlov (1984). The best-fit quadratic equation, presented in Figure 4, can be applied to estimate active layer thickness using thaw depth measurements performed at different times during the summer.

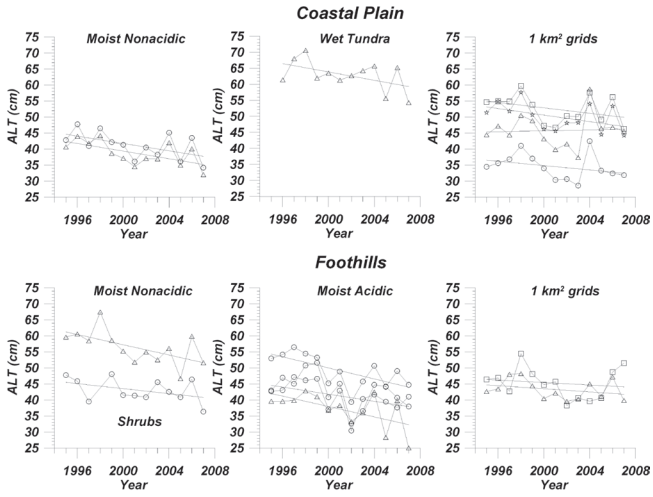

Figure 5. Site-specific 13-year (1995-2007) records of annual active layer thickness. Nine 1-ha sites are grouped by landscape category characteristic of two physiographic provinces. Six 1-km² sites are grouped by physiographic provinces. The Imnavait 1-km² site is not shown due to data quality issues.

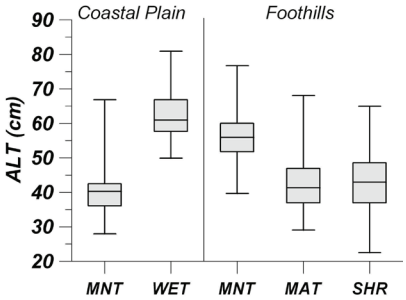

Figure 6. Statistical distribution (box plot) of ALT values for different landscapes characteristic of the two physiographic provinces.

Interannual variability of active layer thickness

The interannual dynamics of active layer thickness were evaluated by analyzing annual, site-specific averages of thaw depth values obtained at the end of the thawing period.

Site-specific 13-year (1995–2007) records of annual active layer thickness for different landscape categories and physiographic provinces are shown in Figure 5. The records indicate a declining active layer trend over the 1995–2007 period for all coastal plain and foothills sites, which generally corresponds to a decline in summer temperature over the same period (Fig. 2c). The maximum values of ALT were recorded in 1998, 2004, and 2006, the years that experienced the warmest summers (Fig. 5). The general agreement between ALT and summer air temperature records stipulates a strong degree of climatic forcing on ALT.

Landscape-specific active layer characteristics

Previous studies, conducted at Alaska CALM sites (Nelson et al. 1998, 1999, Nelson & Hinkel 2003), demonstrated the existence of landscape-specific thermal differences manifested through similar magnitudes of thaw propagation. Although thaw depth can experience significant interannual

Table 2. Landscapes- and province-specific values of active layer thickness.

Landcover categories	Coastal Plain	Foothills
Moist nonacidic tundra	40.0	56.4
Moist acidic tundra		40.5
Moist low shrub tundra		43.0
Wet graminoid tundra	62.9	49.1

variability in response to climatic forcing (Fig. 5), the presence of landform elements shows spatial regularity at the landscape scale and results in landscape-specific thaw depth patterns that repeat on an interannual basis (Nelson et al. 1998, Hinkel & Nelson 2003). Figure 6 shows statistical distributions of ALT, averaged over the 1995–2007 period for different landscapes characteristic of the two physiographic provinces. The landscape- and province-specific mean values of ALT are presented in Table 2.

To evaluate the landscape-specific thermal response to climatic forcing, annual ALT values from representative 1-ha sites were correlated with the square root of degree-days of thawing (DDT), estimated from site-specific air temperature records and accumulated by the date of thaw depth measurements (Shiklomanov & Nelson 2003). A plot of square root of DDT against thaw depth (Fig. 7) yields distinct linear landscape-specific relations, indicating differences in thermal landscape sensitivity to climatic forcing.

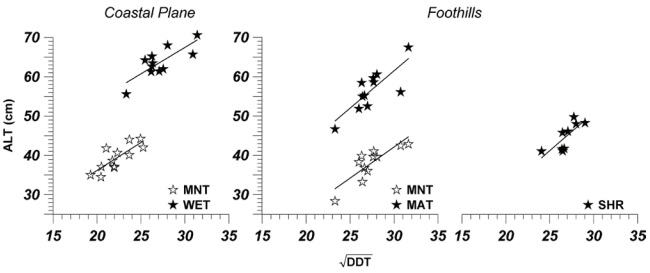

Figure 7. Plot of square root of air DDT against thaw depth for several 1-ha sites characteristic of dominant landscapes in the coastal plain and foothills provinces. Each data point represents annual end-of-thawing season measurements for the 1995–2006 period.

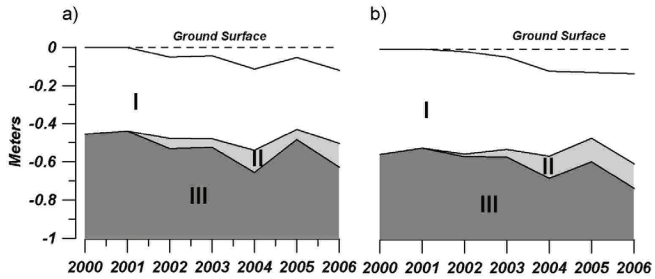

Figure 8. Annual changes in position of ground surface and ALT as measured by mechanical probing for representative Coastal Plain (a) and Foothills (b) CALM sites. I- ALT as measured by probing; II- ALT, corrected for ground subsidence; III-permafrost.

Ground subsidence

Because thaw penetration into an ice-rich layer at the base of the active layer is accompanied by loss of volume (thaw consolidation), straightforward measurement of active layer thickness by such methods as mechanical probing may not always yield accurate estimates of changes in the permafrost system. Periodic thaw subsidence measurements using DGPS technology allowed us to address this problem effectively. Figure 8 shows the results of active layer and ground subsidence measurements over the 2001–2006 period at two locations representative of the coastal plain and foothills physiographic provinces. Total subsidence over the 5-year period was 12 cm at the coastal plain site and 13 cm at the foothills site.

To account for ground subsidence in the active layer record, the annual changes in the position of the ground surface relative to the level in the year 2000 were added to the active layer measurements produced by mechanical probing (Fig. 8). Results from the two sampling locations indicate a monotonic increase in thaw penetration between 2001 and 2006.

Conclusions

The results of 13 years of active layer, air, and ground temperature observations at CALM sites in north-central Alaska indicate that: (1) there is a slight decline in mean and maximum annual air temperature on the Coastal Plain and in maximum annual air temperature in the Foothills. The period of observations was characterized by an increase in the length of the thawing period in both physiographic provinces; (2) the spatially oriented ground surface temperature observations within representative landscapes facilitate evaluation of the effect of ground cover on the ground thermal regime. The distinct values of ΔT and n-factor indicate the distinct thermal influence of landcover types characteristic of the Arctic Coastal Plain and Arctic Foothills physiographic provinces; (3) The results of active layer observations obtained by mechanical probing over 1995–2007 period indicate a pronounced decreasing trend in ALT for all landscape types characteristic of dominant physiographic provinces; (4) Although thaw depth can experience significant interannual variability in response to climatic forcing, the presence of landform elements shows spatial regularity at the landscape scale and results in landscape-specific values of active layer thickness. However, the annual rate of thaw propagation is similar for sites characterized by different surface, subsurface, and climatic conditions; (5) The results of DGPS survey indicate that soil consolidation accompanying penetration of thaw into an ice-rich stratum at the base of the active layer has resulted in subsidence of the surface, accounting for the lack of apparent thickening of the active layer, as traditionally defined.

Acknowledgments

This research was sponsored by the U.S. National Science Foundation grants OPP-9732051, OPP-0352957 and OPP-0352958. We are grateful to M. Walegur, M. Schimek, J. Little, and H. Sandall for their assistance in collecting data, and to VECO Polar Resources and the Barrow Arctic Science

Consortium for providing logistical support. Opinions, findings, conclusions, and recommendations expressed in this paper are those of the authors and do not necessarily reflect the views of the National Science Foundation.

References

Auerbach, N.A., Walker, D.A & Bockheim, J.G. 1996. *Land Cover Map of the Kuparuk River Basin, Alaska.* Institute of Arctic and Alpine Research, University of Colorado, Boulder, CO, USA.

Bockheim, J.G., Walker, D.A., Everett, L.R., Nelson, F.E. & Shiklomanov, N.I. 1998. Soils and cryoturbation in moist nonacidic and acidic tundra in the Kuparuk River Basin, arctic Alaska, U.S.A. *Arctic and Alpine Research* 30(2): 166-174.

Brown, J., Hinkel, K.M. & Nelson, F.E. 2000. The circumpolar active layer monitoring (CALM) program: research designs and initial results, *Polar Geography* 24(3): 165-258.

Carlson, H. 1952. Calculation of depth of thaw in frozen ground. *Frost Action in Soils: A Symposium*. Highway Research Board Special Report 2. Washington, DC: National Research Council.

Ershov, E.D. 2002. *Fundamentals of Geocryology*. Moscow State Univ. Press. 682 pp.

French, H.M. 2007. *The Periglacial Environment*. John Wiley & Sons Ltd., 458 pp.

Hinzman, L.D., Kane, D.L., Gieck, R.E. & Everett, K.R. 1991. Hydrologic and thermal properties of the active layer in the Alaskan Arctic. *Cold Reg. Sci. Technol.* 19(2): 95-110.

Hinkel, K.M. & Nelson, F.E. 2003. Spatial and temporal patterns of active layer thickness at Circumpolar Active Layer Monitoring (CALM) sites in northern Alaska, 1995–2000. *Journal of Geophysical Research* 108(D2): 8168, doi:10.1029/2001JD000927.

Kade, A., Romanovsky, V.E. & Walker, D.A. 2006. The n-factor of nonsorted circles along a climate gradient in arctic Alaska. *Permafrost and Periglacial Processes* 17: 279-289.

Klene, A.E., Nelson, F.E., Shiklomanov, N.I. & Streletskiy D.A. 2008. Interannual variability of winter n-factors in the Kuparuk River Basin, Alaska. *Proceedings of the Ninth International Conference on Permafrost, Fairbanks, Alaska, June 29–July 3, 2008* (this proceedings).

Klene, A.E., Nelson, F.E. & Shiklomanov N.I. 2001. The n-factor as a tool in geocryological mapping: seasonal thaw in the Kuparuk River Basin, Alaska. *Physical Geography* 22: 449-466.

Klene, A.E., Nelson, F.E., Shiklomanov, N.I. & Hinkel, K.M. (2001b). The n-factor in natural landscapes: variability of air and soil-surface temperatures, Kuparuk River Basin, Alaska. *Arctic, Antarctic, and Alpine Research* 33(2): 140-148.

Little, J., Sandall, H., Walegur, M. & Nelson, F.E. 2003. Application of differential GPS to monitor frost heave and thaw settlement in tundra environments. *Permafrost and Periglacial Processes* 14(4): 349-357.

Nelson, F.E., Shiklomanov, N.I., Christiansen, H.H. & Hinkel, K.M. 2004. The circumpolar-active-layer-monitoring (CALM) Workshop: Introduction. *Permafrost and Periglacial Processes* 15: 99-101.

Nelson, F.E., Hinkel, K.M., Shiklomanov, N.I., Mueller G.R., Miller, L.L. & Walker, D.A. 1998. Active-layer thickness in north central Alaska: systematic sampling, scale, and spatial autocorrelation. *Journal of Geophysical Research* 103: 28,963-28,973.

Nelson, F.E., Shiklomanov, N.I. & Mueller, G.R. 1999. Variability of Active-Layer Thickness at Multiple Spatial Scales, North-Central Alaska, U.S.A. *Arctic, Antarctic, and Alpine Research* 31(2): 179-186.

Pavlov, A.V. 1984. *Energy exchange in the Earth landscapes*. Novosibirsk: Nauka, 256 pp. (in Russian).

Péwé, T.L. 1975. *Quaternary Geology of Alaska.* US. Geological Survey Professional Paper 835. 145 pp.

Shiklomanov, N.I., Nelson, F.E., Streletskiy, D.A., Hinkel, K.M. & Brown, J. 2008. The Circumpolar Active Layer Monitoring (CALM) Program: Data Collection, Management, and Dissemination Strategies. *Proceedings of the Ninth International Conference on Permafrost, Fairbanks, Alaska, June 29-July–3, 2008* (this proceedings).

Shiklomanov, N.I. & Nelson, F.E. 2002. Active-layer mapping at regional scales: a 13-year spatial time series for the Kuparuk Region, north-central Alaska. *Permafrost and Periglacial Processes* 13: 219-230.

Shiklomanov, N.I. & Nelson, F.E. 2003. Climatic variability in the Kuparuk region, north-central Alaska: optimizing spatial and temporal interpolation in a sparse observation network. *Arctic* 56: 136-146.

Streletskiy, D.A., Shiklomanov, N.I. & Nelson, F.E. 2005. Monitoring of thaw settlement using a differential global position system approach. In: *Proceedings of the Third Russian Conference on Geocryology*, vol. 2. Moscow: Lomonosov Moscow State University, pp. 163-169.

Wahrhaftig, C. 1965. *Physiographic Divisions of Alaska*, USGS Prof. Pap. 482. Washington, DC: U.S. Govt. Print. Off., 52 pp.

Walker, D.A., Jia, G.J., Epstein, H.E., Raynolds, M.K., Chapin, F.S., Copass, C., Hinzman, L.D., Knudson, J.A., Maier, H.A., Michaelson, G.J., Nelson, F., Ping, C.L., Romanovsky, V.E. & Shiklomanov, N. 2003. Vegetation-soil-thaw-depth relationships along a low-arctic bioclimate gradient, Alaska: Synthesis of information from the ATLAS studies. *Permafrost and Periglacial Processes* 14(2): 103-123.

Walker, D.A., Auerbach, N., Bockheim, J.G., Chapin, F.S. III, Eugster, W., King, J.Y., McFadden, J.P., Michaelson, G.J., Nelson, F.E., Oechel, W.C., Ping, C.L., Reeburgh, W.S., Regli, S., Shiklomanov, N.I. & Vourlitis, G.L. 1998. A major arctic soil pH boundary: implications for energy and trace-gas fluxes. *Nature* 394: 469-472.

Thermal History of Degrading Permafrost in the Source Region of Yellow River, Northeastern Tibet

Tetsuo Sueyoshi
Institute of Low Temperature Science, Hokkaido University, Sapporo, Japan
Atsushi Ikeda
Geoenvironmental Sciences, University of Tsukuba
Norikazu Matsuoka
Geoenvironmental Sciences, University of Tsukuba
Takemasa Ishii
Geological Survey of Japan, National Institute of Advanced Industrial Science and Technology

Abstract

A large part of the source region of the Yellow River (Hunag He) in the northeastern margin of the Tibetan Plateau is underlain by perennially or seasonally frozen ground which has experienced rapid warming in the past decades. Since 2002, we have investigated permafrost distribution in the area to evaluate permafrost degradation and its impacts on groundwater hydrology. It suggested the drastic shrinkage of permafrost area within last the 20 to 30 years, which corresponds to the more than 100 m rise in the lower altitudinal limit of permafrost. This is most likely causing the desertification of the ground surface. In this study, based on the half-century meteorological data from a local observatory, the thermal history of permafrost in the area is investigated by means of a numerical method. The results indicate that some warm permafrost could have existed in the middle of the last century. Considering the time scale of global warming, there is high possibility that the relict permafrost (perennially frozen part beneath the supra-permafrost talik) has widely degraded during the last decades.

Keywords: global warming; numerical modeling; permafrost degradation; Tibet.

Introduction

Recent global warming has raised the temperature of permafrost, which has resulted in the deepening of the active layer and the reversed temperature profile in the high latitudes (e.g., Lachenbruch & Marshall 1986, Harrison 1991, Osterkamp & Romanovsky 1999, Osterkamp 2005, Smith et al. 2005). Warm permafrost in the marginal zone appears to be more sensitive; for instance, the permafrost in Mongolia and the Tibetan (Qinghai-Xizang) Plateau shows rapid thinning in recent decades (e.g., Sharkhuu 1998, Jin et al. 2000).

The source area of the Yellow River (Huang He), located in the northeastern margin of the Tibetan Plateau, appears to be a region broadly underlain by such warm permafrost. Recent studies have reported desertification (degradation of the grassland and meadow vegetation) of the plateau (Wang et al. 2001, Zhang et al. 2004). This has been mainly attributed to the degradation of permafrost (Peng et al. 2003), because there has been no significant change in precipitation during the last half-century (Yang et al. 2004). This study examines this process.

Whereas a few recent reports have indicated rapid degradation of permafrost in the source area of the Yellow River (Zhu et al. 1995, Zhu et al. 1996; Jin et al. 2000, Wang et al. 2000), a large part of the area was considered to have been underlain by permafrost at least until the 1980s (Wang 1987, Wang et al. 1991, Zhou et al. 2000), despite limited evidence. The timescale of the permafrost degradation is therefore of concern to us, to assess the urgency of this environmental change.

In order to verify ongoing degradation of permafrost, we investigated the present geothermal conditions in the source area of the Yellow River (Ikeda et al. 2007, Matsuoka et al. 2004, 2005, 2006), as part of an interdisciplinary research project to model the groundwater circulation and predict near-future water resources of the whole Yellow River basin.

On the basis of the acquired data from field investigations, this paper discusses the ground temperature history of the region using one-dimensional numerical model. The goal of the study is to find a suitable initial condition of the permafrost thickness and to examine its sensitivity to given parameters.

Study Area and Field Study

The fieldwork was undertaken along the R214 road that connects Xining and Yushu in the southeastern part of Qinghai Province (Fig. 1). The elevation varies from 3260–4790 m a.s.l., crossing the boundary between the permafrost and seasonal frost areas (Wang 1987, Zhu et al. 1995). The main study area, Madoi County, is located on an uplifted peneplain composing the northeastern part of the Tibetan Plateau. In this area, valley-fill alluvial plains are widespread between 4200–4300 m a.s.l., and hills rise up to 500 m from the surrounding plains.

The plateau area lies in a transitional zone between

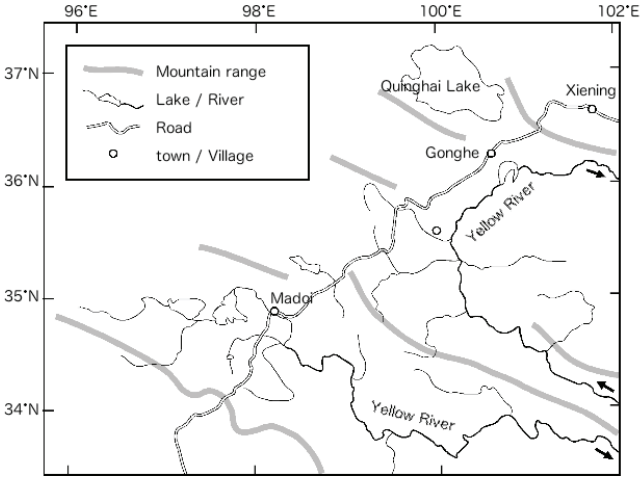

Figure 1. Map of the study area.

Figure 2. Meteorological Station at Madoi borehole site.

discontinuous and sporadic permafrost. Long-term meteorological records at Madoi (98°13′E, 34°55′N, 4273 m a.s.l.; Fig. 1) for 1953–1980 show a cold, dry climate with a mean annual air temperature (MAAT) of -4.1°C, an annual thermal amplitude ranging from -16.8°C in January to 7.5°C in July, and an annual precipitation of 304 mm (Zhou et al. 2000). Decadal mean air temperatures increased by 0.7°C from the 1960s to the 1990s (Yang et al. 2004). More recent records (2001–2005) show further rising MAAT to -2.0°C with an annual thermal amplitude ranging from -13.6°C in January to 9.1°C in July and steady annual precipitation of 304 mm (after WeatherOnline Asia Limited, China). The low precipitation is reflected in shallow winter snow cover (Matsuoka et al. 2005). These conditions favor deep seasonal freezing, whereas the seasonally frozen layer, 2.6 m deep at Madoi, was completely thawed in June 2005 (Matsuoka et al. 2005).

Outcomes from the field study are summarized in previous papers (e.g., Ikeda et al. 2004, Ikeda et al. 2007). Permafrost distribution in the area was examined by ground temperature monitoring and geophysical soundings. Miniature temperature loggers were distributed in the area and recorded year-round ground surface temperatures at hourly intervals. The presence of permafrost was examined from the surface by refraction seismic sounding and one-dimensional (vertical) direct current (DC) resistivity sounding. In addition, a monitoring station was set up at Site Madoi (Fig. 1) with a 8 m-depth borehole for temperature monitoring and meteorological instruments (Fig. 2). During the installation of this borehole, the near-surface stratigraphy of the alluvial plains was directly observed with the recovered cores.

The result suggests that relatively stable permafrost occurs widely above 4300 m a.s.l., that permafrost is mostly absent below 4200 m a.s.l., and that the widespread alluvial plains between 4200–4300 m a.s.l. lack permafrost or have degrading permafrost below a supra-permafrost talik. In contrast, at least until the 1980s, 70%–80% of the plateau surface, that is, the area except for lakes, streams, and nearby swamps, was classified into permafrost terrains (Wang 1987, Wang et al. 1991). Several pits excavated on alluvial plains near Madoi showed that permafrost was generally 15–20 m thick, and the permafrost table lay at about 5 m depth in the early 1980s (Wang 1987). This indicates that permafrost at some places on the plateau began degrading before the 1980s, because the seasonal frost depth rarely exceeds 3 m in the study area (Wang et al. 2000, Matsuoka et al. 2005). From our field study permafrost was completely absent at Site Madoi and its surroundings, indicating that the reported permafrost had considerably disappeared around Madoi after the 1980s, and currently faces a rapid loss of permafrost area, since the elevations mostly belong to a transitional condition between permafrost and seasonal frost environments.

Numerical Modeling

Data

Combining observations and available dataset, the following data were used or referred to for modeling:

(A) data from the borehole (Site Madoi)

(hourly data from 12.08.2004 1500h to 03.08.2006 1000h);

- air temperature, humidity, wind, and snow depth;
- borehole temperature at 7 depths(0.03, 0.3, 1.3, 2.3, 4.3, 6.3 and 7.8 m);
- soil moisture by TDR (0.3, 0.6 and 0.9 m);
- thermal diffusivity, conductivity, heat capacity (0.1 m); and

(B) other dataset

- monthly mean air temperature at the Madoi meteorological station from 1960 to 2006, and
- 2000-year reconstruction of Northern Hemisphere air temperature (from Jones & Mann 2004).

Model settings

As noted above, we conduct numerical experiments to calculate ground temperature history. The system is one-dimensional thermal conduction with phase change driven by one side (ground surface), so we have to solve an inverse problem of diffusion equation to determine initial values.

Though ground surface temperature history (GSTH) has been commonly reconstructed by the inversion of ground temperature profiles (e.g., Cermak 1971, Lachenbruch &

Marshall 1986, Wang 1992), borehole temperatures are only available for the top 7.8 m, with 7 data points at the study site, too shallow for millennia-scale GSTH reconstruction. Instead, we use the permafrost thickness or complete thaw of the permafrost to compare the model output and observation. Here we seek the initial condition of permafrost at the instant of 1960, the condition in which permafrost survived until the 1980s and its condition and thaw by 2006.

Model settings are shown schematically in Figure 3.

For model equation, the formulation of normal one-dimensional heat conduction is used. Ground temperature variation is described by the following heat conduction equation:

$$\frac{\partial T}{\partial t} = \frac{\partial T}{\partial z}\left(\kappa \frac{\partial T}{\partial z}\right)$$

where T is temperature, t is time, z is depth, and κ is thermal diffusivity, which has different values for frozen and unfrozen soil. Latent heat was considered by introducing an apparent heat capacity. During phase change, the heat capacity of the soil increases, reflecting the amount of latent heat of the soil. Phase change is assumed to occur between 0°C and -0.5°C.

As for finite difference equations, the Multi-point Explicit scheme (Saitoh 1974) was used to solve the equations. Since this is an explicit scheme, grid and time spacing should satisfy the stability condition. In this study the spatial grid and the time step were set to 0.2m and 1 hour, respectively.

Soil properties are set basically according to the observed data. Reflecting the low precipitation, soil water content is constantly low and winter snow depth is also shallow (max. 16 cm). Such conditions yield less sensitivity of ground temperature to the soil water conditions. Volumetric soil water content is assumed to be 10% based on TDR measurements on site. The assumed thermal conductivities of frozen and unfrozen soils are shown in Table 1.

Boundary conditions

To drive the model, upper and lower boundary conditions are needed. The lower boundary condition is given as a flux: based on the global heat flow database (Pollack et al. 1993), constant geothermal heat flow 50mW/m^2 is assumed at the bottom of domain for the whole calculated period. This assumption is not extreme because the whole plateau lies on the stable and old continental crust, with no volcanoes. The area is also located well away from local tectonic activities (e.g., fault system), so a standard value of heat flow was taken. The domain of calculations has 500 m in depth, which is deep enough to guarantee the assumption mathematically.

For the upper (i.e., ground surface) condition, hourly temperature dataset is given to the surface grid, reflecting the seasonal variation and long-term climate change. We used 3 cm-depth temperatures in 2005–2006 at the Madoi station, to which long-term temperature anomalies from the annual mean value are added as an offset. Namely, the surface temperature is given as:

T_S(year, date, hour) = $T_{S,P}$(date, hour) + *Anm.*(year),

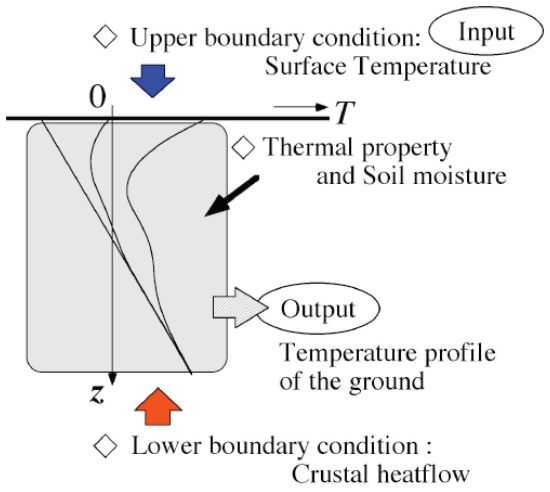

Figure 3. Settings of the one-dimensional model.

Table 1. Thermal conductivities of the soil (Wm^{-1}K^{-1}).

	Depth	Unfrozen	Frozen
Surface	<0.5 m	0.6	0.6
Gravel sediment	<10 m	1.2	1.7
Basement rocks	≥10 m	2.5	3.2

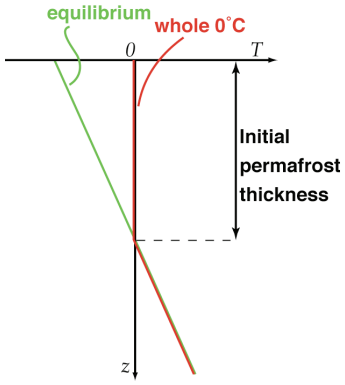

Figure 4. Prescribed initial temperature profile.

where T_S is the ground surface temperature at a certain year/date/hour given to the model, $T_{S,P}$ is the hourly temperature measured on site (i.e., present value), *Anm.* is the anomaly of the annual mean temperature from the present value, for each year. For the period after 1960, monthly mean air temperatures were used to calculate the offset, whereas reconstructed and smoothed data (Jones & Mann 2004) were used for the period before year 1960.

Initial conditions are prepared for two types of runs, illustrated in Figure 4. (1) "Warm permafrost run" is prescribing the initial temperature profile with a certain thickness of warm permafrost at 0°C (i.e., corresponding to the case that the thaw process is in progress). The initial thickness of the warm permafrost is treated as a parameter for this run. (2) "Paleoclimate run" is the long-term calculations based on the reconstructed paleoclimate data for the last 2000 years, which are expected to have reasonable temperature profiles for assumed climate history (see Fig. 5). The offset

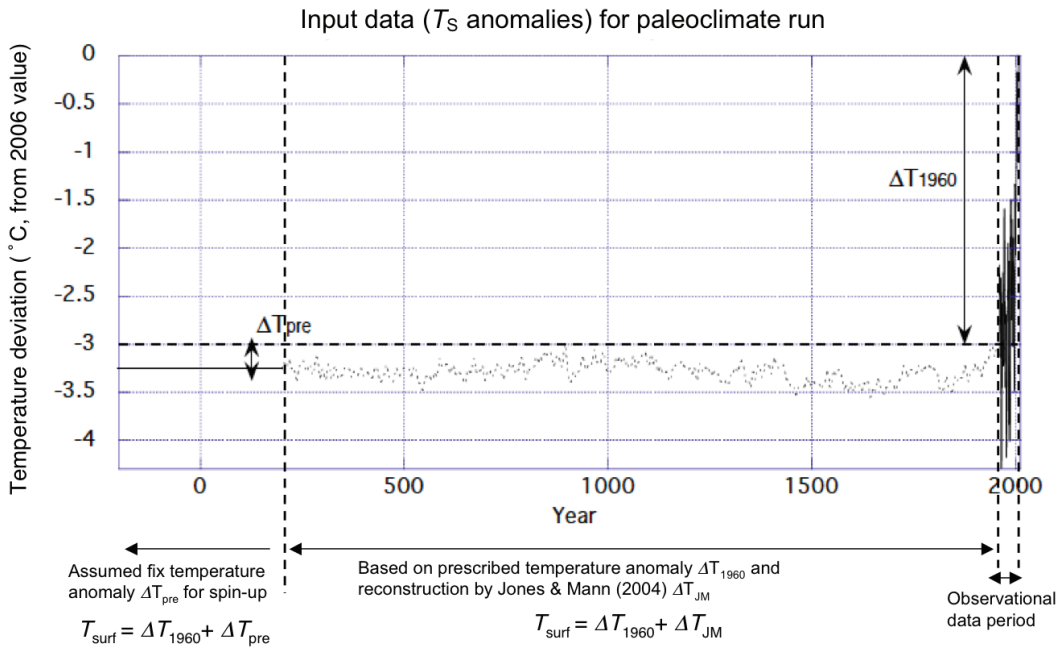

Figure 5. Surface temperature condition for model.

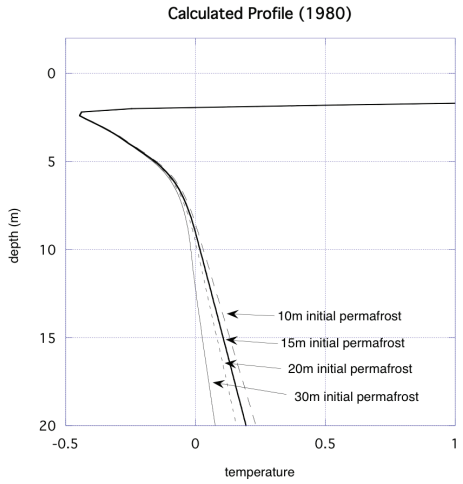

Figure 6. Calculated temperature profiles 1980, starting at warm permafrost conditions.

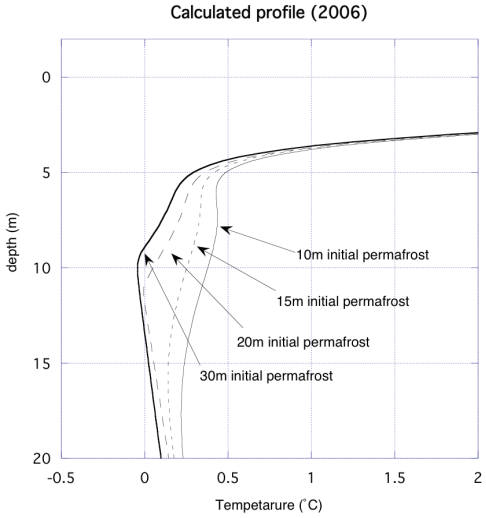

Figure 7. Calculated temperature profiles 2006, starting at warm permafrost conditions.

for the pre-1960 period (ΔT_{1960}) is treated as a parameter to examine the effect of long-term climate, although the 10-year mean (period: 1960–1970) of observed temperature anomaly at Madoi Station can be considered as a standard value.

Soil water content and snow conditions in the paleo-climate runs are assumed to remain unchanged. Recorded precipitation since 1960 was stable in long term, which is partly supports this assumption. The dry condition of the area is considered to be a general geographical setting, mainly due to the blockade of vapor supply by the Himalaya Mountains.

Results

Warm permafrost run

This case is to examine what thickness of warm permafrost can be thawed since 1960. Figures 6 and 7 show the summer temperature profiles in 1980 and 2006 in the model. Permafrost in 2006 can only exist with initial permafrost deeper than 20 m (see Fig. 7).

On the other hand, Figure 6 shows that the permafrost exists for all cases (initial permafrost ≥10 m?) in 1980. Difference in the initial condition produces a slight difference in temperature gradient significantly affects the survival time of permafrost. From this calculation ca. 15 m of permafrost can exist in the 1980s to meet the result of present observations (i.e., it may thaw out by present).

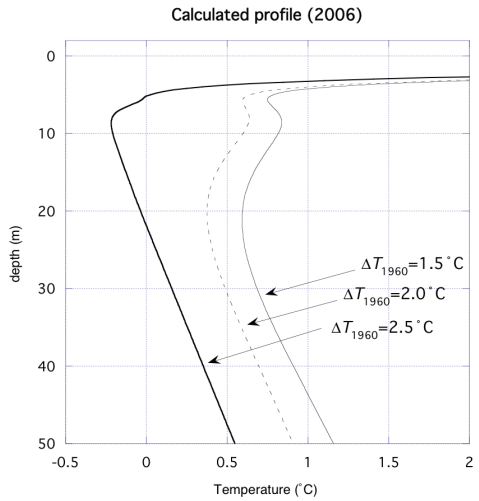

Figure 8. Calculated temperature profiles 2006, under the paleotemperature conditions.

Paleoclimate run

From the parameter study of this run, the effect of pre-1960 climate history to the present condition is examined. Figure 8 shows the temperature profile at 2006 (as before); three profiles correspond to different values of ΔT_{1960}: 1.5°C, 2.0°C, and 2.5°C.

Although the 10-year mean of observed temperature anomaly during the 1960s was 2.5°C, this condition appears to be too cold, leaving thick permafrost (more than 20 m) at 2006. However, as shown in this plot, change in this long-term offset by 0.5°C changes the story completely: the other two cases cannot keep permafrost until the present condition.

In this modeling, the applied trend of paleotemperature is based on the averaged climate for the Northern Hemisphere, which may need reconsideration.

Discussion

Results of this study give a quantitative idea of the timescale of permafrost degradation, which implies that the recent warming climate has played a strong role in causing substantial change in the study area. Although the response of the ground temperature should have delay from the surface (e.g., 10 m-depth temperature lags ca. 10 to 100 years), "Paleoclimate run" shows that the current permafrost condition is strongly affected by the recent climate change. Further accumulation of field and paleoenviroment data would be helpful to discuss more details.

A number of respects have to be improved in modeling. We focus on two topics: thermal properties and paleotemperature input.

One of the uncertainties in modeling lies in thermal properties of the ground. The near-surface layer especially can have a large range of seasonal, and also spatial variation, due to the existence of organic material and differences in the soil water content. In our modeling, the observed values were applied to the near-surface organic layer (Table 1), and they show small seasonal variations through a year, reflecting the dry condition at the observation site. Spatial representativeness of such dry conditions was partly confirmed by the field measurement by portable TDR.

On the contrary, a seasonal difference in thermal conductivity (frozen/unfrozen) appears in wet conditions, which allow more heat flow in winter through the ground surface, compared to summer. This effect cools down the ground temperature effectively in consequence. Therefore, drought of the ground surface can trigger a feedback to cause further thaw of the permafrost.

With respect to the input paleoclimate data, the local paleotemperature history through the last millennia may have significantly larger variability than the reconstruction by Jones and Mann (2004), which was averaged for the whole Northern Hemisphere. Comparing the reconstruction and the recorded temperature since 1960, the hemispherical average has a similar trend with the recorded data, but absolute value of the variation is a few times larger. In general, quantitative paleotemperature data are lacking in the inland continent, but reliable paleoclimate data is essential for further modeling.

Conclusions and Outlook

Ground temperature of the permafrost in the source region of the Yellow River basin was calculated based on the instrumental data, and the response of permafrost to the warming climate was examined quantitatively. The existence of the permafrost in the 1980s, which has been suggested from the previous works, is supported from the modeling results in the case that the permafrost was already the warm (~ 0°C) when it was observed.

It should be noted, however, such a thermal condition of the permafrost is relatively difficult to achieve in dry conditions. If the ground is wet and contains more ice in the permafrost, the thawing process should be slower, and the current distribution of the permafrost, basically lacking up to 4300m, would become hard to explain.

There are still uncertainties in the paleoenvironment of Tibetan plateau, and it is of importance for the prediction of future response of the permafrost to the ongoing climate change. In combination with the paleoclimate study, for example, the reconstruction from lake sediments will be the next step to put the arguments forward. Commencement of deeper borehole temperature measurement, which allows the inversion of surface temperature history (e.g., Pollack & Huang 2000), may also be a candidate of the method to reveal local paleoclimate.

Acknowledgments

We acknowledge Drs. C. Gao, Z. Han, and Mr. J. Ding for logistical help and field assistance. The study was supported by a national program "Sustainable Coexistence of Human Nature and the Earth" founded by the Ministry of Education, Culture, Science, and Technology. We are also thankful for fruitful suggestions by reviewers and the editor.

References

Harrison, W.D. 1991. Permafrost response to surface temperature change and its implications for the 40,000-year surface temperature history at Prudhoe Bay, Alaska. *Journal of Geophysical Research* 96B(1): 683-695.

Ikeda, A., Sueyoshi, T., Matsuoka, N., Ishii, T. & Uchida, Y. 2007. Permafrost sounding (2003–2005) in the source area of the Yellow River, Northeastern Tibet. *Geographical Review of Japan* 80: 259-271.

Ikeda, A., Matsuoka, N. & Sueyoshi, T. 2004. Permafrost survey in the source region of the Yellow River: a preliminary report. *Seppyo* 66: 235-239. (J)

Jin, H., Li, S., Cheng, G., Wang, S. & Li, X. 2000. Permafrost and climatic change in China. *Global and Planetary Change* 26: 387-404.

Jones, P.D. & Mann, M.E. 2004. Climate Over Past Millennia. *Reviews of Geophysics* Vol. 42, No. 2, 6 May 2004.

Lachenbruch, A.H. & Marshall, B.V. 1986. Changing climate: geothermal evidence from permafrost in the Alaskan Arctic. *Science* 234: 689-696.

Liu, S., Lu, A., Ding, Y., Yao, T., Ding, L., Li, G. & Hooke, R.L. 2002. Glacier fluctuations and the inferred climate changes in the A´Nyêmaqên Mountains in the source area of the Yellow River. *Journal of Glaciology and Geocryology* 24: 701-707. (CE)

Lunardini, V.J. 1996. Climatic warming and the degradation of warm permafrost. *Permafrost and Periglacial Processes* 7: 311-320.

Matsuoka N., Ikeda, A., Sueyoshi, T. & Ishii, T. 2004. Permafrost sounding (2003-2004) in the source area of the Yellow River, China. *Annual Report of the Institute of Geoscience, the University of Tsukuba* 30: 33-38.

Matsuoka N., Ikeda, A., Sueyoshi, T., and Ishii, T. 2005. Monitoring frozen ground (2004-2005) at Madoi in the source area of the Yellow River, China. *Tsukuba Geoenvironmental Sciences* 1: 39-44.

Matsuoka, N., Ikeda, A., Sueyoshi, T. & Ishii, T. 2006. Frozen ground monitoring (2004-2006) in the source area of the Yellow River, China. *Tsukuba Geoenvironmental Sciences* 2: 25-30.

Osterkamp, T.E. & Romanovsky, V.E. 1999. Evidence for warming and thawing of discontinuous permafrost in Alaska. *Permafrost and Periglacial Processes* 10: 17-37.

Osterkamp, T.E. 2005. The recent warming of permafrost in Alaska. *Global and Planetary Change* 49: 187202.

Owen, L.A., Finkel, R.C., Haizhou, M., Spencer, J.Q., Derbyshire, E., Barnard, P.L. & Caffee, M.W. 2003. Timing and style of Late Quaternary glaciation in northeastern Tibet. *Geological Society of America Bulletin* 115: 1356-1364.

Peng, X., Wu, Q. & Tian, M. 2003. The effect of groundwater table lowering on ecological environment in the headwaters of the Yellow River. *Journal of Glaciology and Geocryology* 25: 667-671. (CE)

Pollack, H.N. & Huang, S. 2000. Climate Reconstruction from Subsurface Temperatures. *Annual Review of Earth and Planetary Sciences* Vol. 28: 339-365.

Pollack, H.N., Hurter, S.J. & Johnson, J.R. 1993. Heat flow from the Earth's interior: Analysis of the global data set. *Rev. Geophys.* 31: 267-280.

Sharkhuu, N. 1998. Trends of permafrost development in the Selenge River Basin, Mongolia. In: *Proceedings of the Seventh International Conference on Permafrost.* Sainte-Foy: Centre d'études Nordiques, 979-985.

Smith, S.L., Burgess, M.M., Riseborough, D. & Nixon , F.M. 2005. Recent trends from Canadian permafrost thermal monitoring network sites. *Permafrost and Periglac. Process.* 16: 1930.

Wang, G., Qian, J., Cheng, G. & Lai, Y. 2001. Eco-environmental degradation and causal analysis in the source region of the Yellow River. *Environmental Geology* 40: 884-890.

Wang, J. & Derbyshire, E. 1987. Climatic geomorphology of the north-eastern part of the Qinghai-Xizang Plateau, People's Republic of China. *Geographical Journal* 153: 59-71.

Wang, S. 1987. Frozen ground and periglacial features in the southeastern part of Qinghai Province. In: J. Hövermann & W. Wang (eds.), *Reports on the Northeastern Part of the Qinghai-Xizang (Tibet) Plateau by Sino-W. German Scientific Expedition*. Beijing: Science Press, 343-366.

Wang, S., Luo, X. & Guo, P. 1991. The distributive characteristics of frozen ground in the east of Qinghai–Xizang Plateau. *Journal of Glaciology and Geocryology* 13: 131-140. (CE)

Wang, S., Jin, H., Li, S. & Zhao, L. 2000. Permafrost degradation on the Qinghai-Tibet Plateau and its environmental impacts. *Permafrost and Periglacial Processes* 11: 43-53.

WeatherOnline Asia Limited. *WeatherOnline*. http://www.t7online.com (C) (last checked date: November 27, 2006)

Yang, J., Ding, Y., Shen, Y., Liu, S. & Chen, R. 2004. Climatic features of eco-environmental change in the source regions of the Yangtze and Yellow Rivers in recent 40 years. *Journal of Glaciology and Geocryology* 26: 7-16. (CE)

Zhang, S., Wang, Y., Zhao, Y., Huang, Y., Li, Y., Shi, W. & Shang, X. 2004. Permafrost degradation and its environmental sequent in the source regions of the Yellow River. *Journal of Glaciology and Geocryology* 26: 1-6. (CE)

Zhou, Y., Guo, D., Qiu, G. & Cheng, G. 2000. *Geocryology in China.* Beijing: Science Press. (C)

Zhu, L., Wu, Z. & Liu, Y. 1995. Permafrost degeneration in the east of Tibetan Plateau. *Journal of Glaciology and Geocryology* 17: 120-124. (CE)

Zhu, L., Wu, Z., Zang, E., Pan, B., Liu, Y. & Tao, G. 1996. Difference of permafrost degeneration in the east of the Tibetan Plateau. *Journal of Glaciology and Geocryology* 18: 104-110. (CE)

(J): written in Japanese, (C): written in Chinese,
(CE): written in Chinese with English abstract

Permafrost in the *Bibliography on Cold Regions Science and Technology*

Sharon N. Tahirkheli
American Geological Institute, Alexandria, VA, USA

Abstract

The *Bibliography on Cold Regions Science and Technology* has covered approximately 22,000 publications on permafrost and contains an additional 6000 references to the related topic of frozen ground. Permafrost publications are distributed throughout the global scientific literature and are found in peer-reviewed journals, government reports, theses/dissertations, and conference publications. Almost half of the permafrost literature is found in conference proceedings. Coverage of master's theses and doctoral dissertations in the *Bibliography* is limited to a total of two hundred, primarily from U.S. and Canadian institutions. As geographic distribution of permafrost is concentrated in the polar and high-altitude regions of the world, it is no surprise that 9000 publications have been identified in the Russian language. The rest of the literature is published around the globe, including Europe, Canada, the United States, China, and Japan in the north, and Argentina in the south.

Keywords: bibliography; permafrost; publications.

Introduction

The *Bibliography on Cold Regions Science and Technology* is a part of the Cold Regions Bibliography Project (CRBP), jointly sponsored by the U.S. National Science Foundation and the U.S. Army Cold Regions Research and Engineering Laboratory. As part of its scope, the *Bibliography* includes references to publications on all scientific and technical aspects of permafrost including distribution, properties, impacts of current climate change, cold-weather construction, engineering challenges, soil mechanics, hazards, and land use. This paper explores the coverage of permafrost throughout the history of the *Bibliography on Cold Regions Science and Technology* by considering the terminology used, the distributed geographic and linguistic sources of permafrost publications and the variations over time of the frequency of publications.

History of the *Bibliography*

Bibliography on Snow, Ice and Permafrost

The current CRBP evolved from the SIPRE Project. SIPRE stood for the Snow, Ice and Permafrost Research Establishment of the U.S. Army Corps of Engineers and Project was primarily concerned with publishing an annotated bibliography covering snow, ice, and permafrost. Produced at the Library of Congress beginning in 1951 and published as SIPRE Report 12, the *Bibliography on Snow, Ice and Permafrost* was carefully limited to the properties of snow, ice, and permafrost. Only on rare occasions were background materials on peripheral topics included. The objective of the SIPRE Project was to assist SIPRE and other government agencies that were concerned with "various phases of research on the properties of snow, ice and frozen ground." (Library of Congress 1953)

Volumes 16–22 underwent several name and format changes. The SIPRE Report 12 became CRREL Report 12, the *Bibliography on Snow, Ice and Permafrost* became the *Bibliography on Snow, Ice and Frozen Ground* and finally, with Volume 23, the current title, *Bibliography on Cold Regions Science and Technology,* was adopted. With the name changes came an expansion of coverage and an increased emphasis on engineering in a cold environment "including the varied disciplines of engineering and broad coverage of the physical sciences. The disciplines and subject matter remained varied and covered every topic relating to cold regions imaginable" (Liston 2002).

Bibliography on Cold Regions Science and Technology

The CRBP was managed by the Library of Congress until the late 1990s and was published in print as CRREL Report 12 beginning with Volume 23. In 2000, the American Geological Institute (AGI) began compiling the *Bibliography* and producing the current online web-based version of the *Bibliography*. Under the terms of the CRBP Cooperative Agreement between AGI and the U.S. National Science Foundation, all of the publications covered in the CRBP must be obtained and examined. Citations of publications from other bibliographies are helpful in identifying publications for consideration but cannot be used to develop references without access to the original.

The *Bibliography on Cold Regions Science and Technology* now contains more than 218,700 references and is freely available to users via the Internet at http://www.coldregions.org The present-day scope of the *Bibliography* includes "references to scientific and engineering research related to material and operations in a winter battlefield, the nature and impact of cold on facilities and activities, cold-related environmental problems, and the impact of human activity on cold environments" (American Geological Institute 2007).

While permafrost is not explicitly mentioned in the coverage statement, all aspects of permafrost continue to be considered relevant to the *Bibliography* and are included. With the explosion in climate and global change studies, and with the surge in publications expected to result from the International Polar Year 2007–2008, the future expectation

is that the number of permafrost publications will show a marked increase over the next several years.

Finding Permafrost in the *Bibliography*

Terminology

An examination of the original volumes of the *Bibliography* quickly reveals that the subject indexes included "permafrost" and "frozen ground" as entries. As the *Bibliography* evolved to the use of a thesaurus of controlled terms, "permafrost" and "frozen ground" remained consistent in their usage as entry points (Engineers Joint Council 1969). This greatly simplifies the attempt to locate the relevant literature within the online database. To locate references to "permafrost" and/or "frozen ground" in the web-based database of the *Bibliography*, the terms were searched directly as part of the entire bibliographic record. This search included "permafrost" and "frozen ground" as parts of the titles, abstracts, keywords, conference titles, publisher names, or notes.

It is useful to note that the controlled vocabulary used in the production of the *Bibliography* contains the following specific types of permafrost as potential additional identifiers: continuous permafrost; discontinuous permafrost; sporadic permafrost; and subsea permafrost. Processes and concepts related to permafrost can also be directly accessed; for example, permafrost heat balance; permafrost origin; permafrost thickness.

For purposes of this study, only the more general terms were chosen. 27,732 references were retrieved with almost 22,000 references containing "permafrost" and close to 6000 containing "frozen ground." Thus 12.6% of the references in the *Bibliography on Cold Regions Science and Technology* are relevant to "permafrost" or "frozen ground."

Publication Date

Overall distribution by date of publication

Permafrost and frozen ground publications were one of the three primary topics in the earliest volumes of the *Bibliography*. Total publishing numbers, however, were substantially lower. For example, in 1955 only 76 publications on permafrost and/or frozen ground were included in the *Bibliography*. Numbers increased dramatically by the late sixties with 470 publications referenced in 1966, and the totals peaked in 1978 and 1983 with 1111 items in both of those years. The rate of publication in the permafrost field has declined slightly from those highs, but varies between 450 to 750 items per year.

When considered as a percentage of the total number of publications added to the *Bibliography* each year, the permafrost/frozen ground publications have varied from as little as 5.73% in 1995 to as much as 27.55% in 1977 with an overall average of 13.52% based on the publication years 1970–2007. Table 1 presents the dates of permafrost/frozen ground publications as a percentage of the total number of publications added to the *Bibliography on Cold Regions Science and Technology*.

Table 1. Percentage of *Bibliography* by date of publication.

Date of Publication	Percentage total references in the *Bibliography*
1970	10.32%
1974	17.27%
1978	17.42%
1982	20.53%
1986	13.08%
1990	10.16%
1994	7.06%
1998	7.36%
2002	7.92%
2006	12.85%
Average percentage	13.52%

Permafrost/frozen ground publications as a percentage of the total number of publications referenced in the *Bibliography* in a given year. Average percentage based on 1970–2007.

Table 2. Publication type.

Type of Publication	Total Count By Type*
Serial	12,818
Conference	10,925
Book	3,437
Report	1,500
Patent	192
Thesis/Dissertation	160
Map	33

*Total will not equal number of permafrost references because some items have multiple types and others have no type provided.

Publication Type

Overall distribution by type of publication

Permafrost and frozen ground publications are found not only in the peer-reviewed literature, but also in what is often referred to as gray literature—government reports, theses/dissertations, and conference publications. References included in the *Bibliography of Cold Regions Science and Technology* are currently tagged as one or more of the following types: serial, book, conference, report, thesis/dissertation, patent, or map. The earlier volumes of the *Bibliography* that were originally produced for a print publication do not always contain equivalent information; however, procedures were developed to determine whether an item was a journal article, map, patent, monograph, conference paper, or technical report. Out of the total references, 940 items could not be categorized and, while not entirely equivalent, for the purposes of this study, monographs were grouped under books.

An examination of the permafrost references in the *Bibliography of Cold Regions Science and Technology* by type of publication (Table 2) reveals several points of interest.

Primary publication types

The primary type of publication included in the

Bibliography that contains permafrost papers is labeled serial. Serials may be of two types: peer-reviewed journals and monographic serials. While serial is the predominant type, conference publications are a very close second, reflecting the importance of these publications to this discipline. More than one-third of the permafrost/frozen ground publications are drawn from conference proceedings. It is worthwhile to note that the *Bibliography*, with a few rare exceptions, does not include abstracts from meetings—only proceedings.

The International Permafrost Conference proceedings are good examples of the significance of conference papers in the literature. The first International Permafrost Conference was held in 1963 and the proceedings contained 102 papers. With 100 or more papers produced at each meeting, the nine conferences represent a major component of the total permafrost literature.

A random selection of twenty papers from conferences produces items from the following workshops and symposia: International snow science workshop; International Congress of the International Association for Engineering Geology and the Environment; USA/CIS joint conference on Hydrologic issues of the 21st Century; Jahrestagung der Schweizerischen Geomorphologischen Gesellschaft; XI glyatsiologicheskii symposium; and the AGU 2004 fall meeting open Northern Eurasia Earth Science Partnership Initiative science session.

Other publication types

Books and book chapters comprise 12.8% of the total permafrost literature while technical/government reports are a healthy 5.8%. Patents, maps, and thesis/dissertations combined are barely a blip in the totals of types of publications. While this may be appropriate for patents, maps and theses/dissertations seem to be underrepresented in the *Bibliography*. The theses/dissertations that are included are primarily from the United States and Canada—not what would be expected if all theses/dissertations on permafrost and frozen ground were included. Maps were seldom included in the *Bibliography* until the CRBP compilation moved to the American Geological Institute. (Tahirkheli 2004)

Document availability

Because of its history in support of research for SIPRE and the Cold Regions Research and Engineering Laboratory, the CRBP was always concerned with the availability of the documents cited in the Bibliography. The Library of Congress provided a microfiche service that provided copies of uncopyrighted materials to requestors. The need to have the documents immediately available has impacted the coverage of the CRBP. Some types of publications such as maps and thesis/dissertations could have been included more frequently without this requirement. Currently, the bibliographers compiling the *Bibliography* cannot include a thesis/dissertation unless the item is easily accessed by the users of the *Bibliography*. For theses/dissertations, this usually means that the document must be available through a microfiche service. With the wider dispersion of electronic publications, this restriction has been relaxed somewhat, and the inclusion of online theses/dissertations is now possible.

The Permafrost Young Researchers Network web site http://www.pyrn.org/ contains approximately 230 citations under consideration for inclusion in the *Bibliography* in the future, depending on availability of the title.

Country/Language of Publication

Distribution by country

Permafrost and frozen ground publications are widely distributed around the globe. Current serial, book, and conference publications added to the *Bibliography* are tagged with an indicator of the country of publication. The earlier volumes of the *Bibliography* and current theses/dissertations and technical reports do not always contain this information; however, procedures were developed to determine the country of publication whenever possible. Approximately 1100 items could not be assigned to a source country. The rest of the permafrost publications identified in the *Bibliography on Cold Regions Science and Technology* were selected by the country of publication and the results are presented in Table 3.

Primary countries producing permafrost publications

Permafrost publications have been identified from 44 separate countries; however, the Former Soviet Union and Russia are the primary sources with a whopping 44.8% of

Table 3. Country of publication.

Country of Publication	Total Count
Former Soviet Union	11,129
United States	5,658
Canada	2,322
Russia	1,307
China	1,264
United Kingdom	1,233
Netherlands	834
International	735
Norway	515
Germany	463
Japan	385
Sweden	142
Poland	131
Finland	98
France	91
Denmark	71
Switzerland	71
Italy	45
Austria	32
Argentina	24
India	21
New Zealand	20
Belgium	17
Australia	11
21 countries	41

Table 4. Language of text.

Language of Text	Total Count
Russian	14,068
English	12,093
Chinese	858
French	217
Japanese	186
German	173
Polish	40
Norwegian	35
Spanish	26
Swedish	23
Finnish	18
Italian	16
Danish	13
Czech	3
Korean	3
Lithuanian	2
Ukrainian	2
Bulgarian	1
Hungarian	1
Serbian	1

the total. The United States is not even a close second with 20.4% and Canada is a distant third with 8.4%.

While both the geographic distribution of permafrost and the distribution of publishing on the topic of permafrost is concentrated in the polar regions (USSR/Russia, Canada, United States), there are significant numbers of permafrost publications being published in countries with high altitude areas including parts of China, Switzerland, and Italy. There are even scattered publications from India and South Africa.

Distribution by language of publication

Distribution by language of publication for permafrost/frozen ground publications is highly concentrated in three languages: Russian, English, and Chinese, which account for 97% of all publications. This distribution only partially mirrors the distribution of publications by country of publication and emphasizes the dominance of Russian and English for the permafrost literature. The languages of the texts are presented in Table 4 in order of prevalence.

Only twenty languages were identified within the *Bibliography*. The language of the text was determined for every permafrost/frozen ground publication.

CRBP Sources

Or, how does the CRBP obtain the publications cited in the Bibliography?

As indicated by the charts of languages of the texts and countries of publication, many sources are necessary to be as complete in coverage as possible. The CRBP uses many online databases and relevant bibliographies. For permafrost, the *Permafrost and Frozen Ground Bibliography, 1978–2003* (available from the Frozen Ground Data Center at the National Snow and Ice Data Center) is a rich source of potential documents (http://nsidc.org/fgdc/biblio/). Of course, as indicated earlier, the CRBP or one of its partners must actually examine the publications and is further required to digitize any uncopyrighted materials that are included.

The CRBP obtains publications in all of the following ways:

Libraries. Both major government and university library collections are mined for possible relevant publications. Some of the libraries mined regularly include:

- U.S. Army Cold Regions Research and Engineering Laboratory Library
- Institute for Arctic and Alpine Research Information Center
- U. S. Geological Survey Library System
- University of Texas at Austin
- Stanford University

Publishers. Many publishers provide both publications and metadata directly to abstracting and indexing services like the one producing the Bibliography.

Open-access Web publications. Many publications are now appearing on the web and are openly available to all users.

Bibliographic partnerships (where several organizations produce similar bibliographies). Partnerships are often formed to assist in broader access to pertinent publications. The American Geological Institute participates in at least a dozen bibliographic partnerships including a significant collaboration with the Scott Polar Research Institute.

Scientists and authors. Interested researchers provide direct information regarding their publications to the *Bibliography* and either links to full-text as posted on their personal web pages or reprints of their articles.

Current opportunities and challenges in maintaining comprehensive coverage

With the growth of web publishing, CRBP faces both new opportunities and challenges. Information about publications is sometimes easier to obtain, and it may even be freely accessible on the web. Publishers often provide citation information electronically. eliminating the need for expensive and time-consuming data entry. On the other hand, some publications appear on the web today and are gone or moved tomorrow. A publication may be launched and die before the publisher communicates with the community about its existence. Even the definition of what a publication is has become somewhat blurred.

The CRBP is continuously adapting to these changes. Suggestions, as well as notification of new publications, are welcome.

International Polar Year 2007–2008

Plans for the Bibliography on Cold Regions Science and Technology

The International Polar Year Publications Database (IPYPD) is in the process of identifying and indexing any

permafrost/frozen ground publications that result from the International Polar Year 2007–2008 (IPY). A network of five organizations is collaborating to attempt to compile and provide access to all IPY-related publications through a single database. This network includes the Arctic Science and Technology Information System (ASTIS), the Cold Regions Bibliography Project (CRBP), the Scott Polar Research Institute (SPRI) Library, the Discovery and Access of Historic Literature of the IPYs (DAHLI) project, and National Information Services Corporation (NISC). The IPYPD will include publications that result from research as well as publications that relate to outreach and education. The IPYPD, as part of the IPY Data and Information Service (IPYDIS), is attempting to use the IPY Data Policy to require that researchers report their publications to either ASTIS, CRBP or the SPRI library. Each of these organizations will include records for IPY publications in their existing databases, which are part of the Arctic & Antarctic Regions database distributed by NISC.

Of course, the total number of permafrost/frozen ground publications that will result from the IPY is unknown at this time. Based on previous publishing rates from earlier IPYs, the IPYPD expects an estimated 20,000 total publications. If the percentage of permafrost/frozen ground publications remains stable, then we should expect about 12.6% of the total number of publications or about 2500 permafrost publications to be produced.

In an attempt to locate relevant publications, all of the collaborators are trying to contact researchers through conference presentations and web sites. Instructions for reporting publications are available online at http://www.ipy.org

Conclusions

Based on the above estimates of publication rates in the permafrost literature, the CRBP would expect to add upwards of 600 new permafrost publications over the next twelve months. The data on language, country, and type of publication provide a roadmap for focusing future efforts by the CRBP. When considered from the perspective of country and language of texts, the data regarding permafrost/frozen ground publications highlight the immense contribution to the scientific literature by the Former Soviet Union/Russia. Further examination of the Russian literature is warranted to insure continued coverage and access to this information. The CRBP will focus attention on expanding its connections with relevant organizations in this region. In addition, the International Polar Year and the conferences resulting from activities of the IPY should provide a substantial pool of permafrost/frozen ground literature for future consideration for inclusion in the *Bibliography* over the next decade.

Acknowledgments

The Cold Regions Bibliography Project is supported by the U.S. National Science Foundation and the U.S. Army Cold Regions Research and Engineering Laboratory under Grant No. OPP-0440772. The assistance of AGI staff members MaryAnn Theresa Eitler and Lawrence Berg in the compilation of the data for, and the editing of, this paper is appreciated. The International Polar Year Publications Database is part of the IPY Data and Information Service (IPYDIS).

References

American Geological Institute. Cold Regions Bibliography Project. 2007. http://www.coldregions.org

Engineers Joint Council. 1969. *Thesaurus of Engineering and Scientific Terms.*

Library of Congress, Technical Information Division. 1953. *Annotated Bibliography on Snow, Ice and Permafrost*. SIPRE Report 12, Vol. III, v.

Liston, Nancy C. 2002. The Bibliography on Cold Regions Science & Engineering. In: Kirsten Caning & Vibeke Sloth Jakobsen (eds.), *Poles Apart – Poles On-Line; Proceedings of the 19th Polar Libraries Colloquy.* Copenhagen: Danish Polar Center, 58-62.

Tahirkheli, Sharon N. 2004. Distribution of Source Materials for the Antarctic Bibliography and the Bibliography on Cold Regions Science and Technology. In: Barbara E. Kelcey (ed.), *Polar Research: Let Us Share – Amiqqaaluta; Proceedings of the 20th Polar Libraries Colloquy*. Ottawa: Polar Libraries Colloquy, 160-164

Siberian Woolly Mammoths and Studies into Permafrost in the Russian Empire in the 19th Century

Erki Tammiksaar
Centre for Science Studies, Estonian University of Life Sciences
Ken Kalling
Centre for Science Studies, Estonian University of Life Sciences

Abstract

In 1806 an adjunct of St. Petersburg Academy of Sciences, Michael Adams, brought to the Russian capital a fully preserved skeleton of a woolly mammoth. The mammoth issue became central to research made into aspects of permafrost and of the Ice Age, started in Russia in 1837 by a member of the Academy, Karl Ernst von Baer. For the study of permafrost Baer organized in 1842–45 an expedition to Siberia, headed by Alexander Theodor von Middendorff. All the subsequent expeditions to northern Siberia in 1860–1880s (headed by Friedrich Schmidt, Gerhard von Maydell, Alexander von Bunge *jun*., Eduard von Toll) were among other areas of science aimed at the study of palaeontological remains to establish the once widespread range of the woolly mammoth. In addition, these expeditions contributed much to the study of permafrost, laying foundations for the emergence of the outstanding Soviet school of permafrost studies.

Keywords: Baer, Karl Ernst von; Ice Age; Middendorff, Alexander Theodor von; Russian Empire; woolly mammoths.

Introduction

Mammoths, the conditions in which they lived, and their extinction received much interest among the 19th century scientific community. It could even be stated that the finds of these giant mammals from the Siberian permafrost were the main impulse for studies of prehistoric animals, i.e. for the development of vertebrate palaeontology as such. As the remains of the mammoths were mainly found in the northern and Siberian territories of the Russian Empire, it was the Russian scholars (and among others those of Baltic-German origin) who contributed most to the study of mammoths. One of the topics dealt with in connection with mammoths was their preservation in Siberian permafrost. The present article discusses the importance of mammoth studies on the scholarship on permafrost in the Russian Empire.

Information on Mammoths Prior to the 19th Century

In modern times every new discovery of a well-preserved mammoth is an important event both for science and the media. In the 19th century and before that, finds of well-preserved mammoths caused much attention. But due to the low level of development of natural sciences and little public information about Siberia, superstitious theories on the matter tended to prevail. For example, it was possible to believe the legends of the indigenous people of Siberia. According to legends the mammoths lived like moles underground and died if exposed to the daylight. Ideas that mammoths still existed were found in Chinese sources (Baer 1866). Russian colonists in turn believed that mammoths became extinct during the Great Deluge which carried their bodies to Siberia.

The first confirmed information on the Siberian woolly mammoths was taken to European scholars in the 17th century by Dutch traveler Nicolas Witsen, and by a Russian ambassador to Beijing, Ysbrand Ides. The latter brought with him, to confirm his words, a skull and other bones of a mammoth (Baer 1866).

In the 18th century, the geography and nature of Siberia was studied by several foreigners at the request of the Russian authorities. One should mention Daniel Gottlieb Messerschmidt with his companion Philipp Johann Strahlenberg (Tabber), members of Vitus Bering's second Kamtchatka expedition (1734–1744), Johann Georg Gmelin and Gerhard Müller and also Peter Simon Pallas who headed an expedition group from the St. Petersburg Academy of Sciences (1768–1774). These expeditions all secured information concerning mammoths in different parts of Siberia. Gmelin reported also on the Siberian permafrost (Baer 2001), but the two topics—permafrost and mammoths—were not at this stage linked.

In the end of the 18th century, Russian merchants discovered the islands of New Siberia where a lot of mammoth tusks and teeth were found. Subsequent travels, up to the end of the 19th century, to these islands were mainly aiming at collecting this material for profit.

A Mammoth Skeleton Arrives at St. Petersburg

In 1806, the Russian diplomatic mission to China visited Yakutsk. The team included Michael Adams, an adjunct in zoology, St. Petersburg Academy of Sciences. He heard that at the mouth of the Lena River a wholly preserved mammoth had been found. Adams decided to attempt to profit from

this find by going to the site, bringing the mammoth to St. Petersburg, and there placing it on sale. At the site it became evident that the soft tissues of the animal had been lost, partly eaten by scavengers (the mammoth had been discovered in 1799) (Baer 2001). The skeleton of the mammoth was placed in the Zoological Museum of the St. Petersburg Academy of Sciences. In an article published in 1807 in an obscure periodical entitled *Journal du Nord,* data concerning the conditions in which the animal was found were provided by Adams and a local chief named Ossip Schumachow, who had actually made the discovery. The data became more widely known due to a member of the St. Petersburg Academy of Sciences, Wilhelm Gottlob Tilsesius von Tilenau (1815). From him information on the mammoth spread into the works of European scholars, together with a suggestion that mammoths must have been southern animals, the carcasses of which had been carried north by the big Siberian rivers. This idea was supported by a notion that the northern pastures seemed to be too poor for such big animals to feed there. The preservation of the bodies of the animals for a long time was not a matter of concern for the scientists of the day.

The Birth of Permafrost Studies in Russia

At the end of 1837, Karl Ernst von Baer, a natural scientist and member of the St. Petersburg Academy of Sciences in the field of zoology, gave a presentation on the so-called Shergin pit in Yakutsk. This, despite its enormous depth (116 m) did not contain any water due to permafrost. In his presentation Baer analyzed data available to him on the temperature in the pit. He concluded that the observations that had produced these data had to be continued in order to secure more information on this new natural phenomenon in Siberia. Many European scholars (i.e., German geologist Leopold von Buch) were suspicious of Baer's data on the pit stating that in regions in which there was forest and bush growing, the soil could not be permanently frozen, especially if one took into account the theory of a hot core of the Earth (see: Tammiksaar 2002).

Baer in his turn proved that the geothermic observations made in the pit supported current geological theory, proving also that in those geographical regions in which the annual average temperature fell below 0°C the frost entered the soil, causing permafrost (*Boden-Eis*) (Baer 2001).

To defend his arguments, Baer started in 1838 to collect data on this topic not only from literary and archive sources but also from his colleagues who studied the Russian North. As a result he completed by the beginning of 1843 a 218-page manuscript "*Materialine zur Kenntniss des unvergänglichen Boden-Eises in Sibirien.*" This first theoretical study on permafrost remained unpublished for several reasons. In his study von Baer analyzed for the first time the physical characteristics of permafrost and its patterns on the surface and beneath it, characterizing also different formations of ice. Baer also analyzed different landscape formations created by permafrost and tried to fix the distribution of

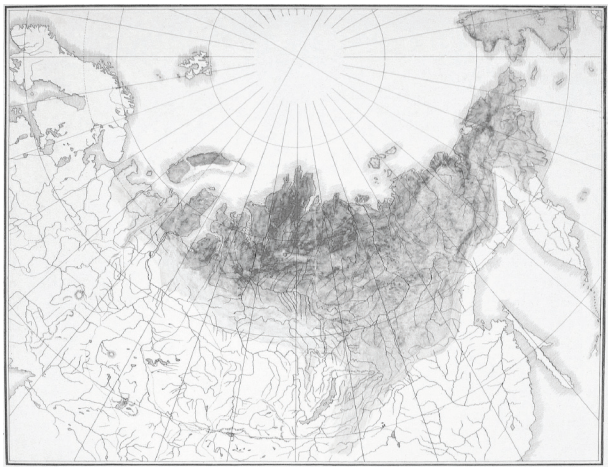

Figure 1. Map of the distribution of the permafrost area in Eurasia compiled by Karl Ernst von Baer (Tammiksaar 2002).

this phenomenon in Siberia and in the whole world (see: Tammiksaar 2001, Tammiksaar 2002). These data were used by Baer in preparing the first map in history of the permafrost areas depicting Eurasia (see Fig. 1). Von Baer also worked out a terminology concerning permafrost. Under *Boden-Eis* he meant permafrost as a physical phenomenon; that is, ice in geological layers. Under *Eis-Boden* he meant the geographic distribution of permafrost (see Baer 2001, Tammiksaar 2002).

Although Baer's manuscript remained unpublished, it was used by his disciple Alexander Theodor von Middendorff. Unfortunately there was no appropriate person in Siberia to run geothermic observations, as Baer had insisted, in the 116 m depth of the Shergin pit. To obtain the necessary data, Baer organised a special expedition with the support of the Academy to study all aspects of permafrost. The leader of the expedition was his countryman Middendorff. The expedition to North Siberia and Far East took place during 1842–1845. Baer gave his manuscript to Middendorff as instruction for the investigation, although many of the arguments set out in it (e.g., the causes of emergence of permafrost-linked surface forms, thickness of ice-cover on the rivers, etc.) still required thorough study (Tammiksaar & Stone 2007). The writings of Middendorff convinced scholars that permafrost really existed and that studies of it were needed. His studies became crucial also for the discipline in Russia, as they served as a starting point for later scholarship on the topic in the region.

Through the studies of Middendorff (Middendorff 1848, 1861) Baer's permafrost terminology spread among European scholars but, due to random and ignorant usage, became corrupted in time, so that a later scholar of permafrost, Eduard von Toll, decided to replace the term *Boden-Eis* with the term *Stein-Eis* (Toll 1895).

Adams' Mammoth, Permafrost, and Ice Age

One of the most important questions to be answered by Middendorff's expedition, according to Baer, was to fix as

exactly as possible the physico-geographic and geologic conditions at the site at which Adams' mammoth had been found, Cape Bykovski in Siberia.

It was Baer's guess that mammoth corpses could survive for several thousands of years but only in permafrost. Baer thus viewed it as highly important to specify the geological and geographical circumstances in which Adams's mammoth had been found. The report by Adams on these conditions was internally contradictory, and its French was poor, leading to confusion. Baer could not understand whether the mammoth had been located on the icebergs/river ice heaped on the shore or whether it had melted out from an ice-wall covered with soil. Baer viewed this as a remnant of the Ice Age. Apparently when Adams had arrived at the site, the ice-wall had melted further and was already 30.5 m (100 ft) from the carcass.

In his manuscript Baer discussed Adams' report on the conditions of the mammoth find, and he devoted 30 pages to this. He tried to compare this data with the materials secured by members of the expedition led by Otto von Kotzebue for the search of the Northeast Passage (1815–1818). These were Johann Friedrich Eschscholtz and Adelbert von Chamisso, who had discovered a buried ice sheet in Eschscholtz-Bay (Baer 2001).

In the 1830s, Louis Agassiz and Jean de Carpentier had founded the theory of glaciation of continents. The theory caused controversy among geologists and other natural scientists. There were arguments for and against it, but only a few scholars collected empirical data to explain the theory. One of the few was Baer who was tending to support the theory. To be convinced, he needed more information on the conditions in which Adams' mammoth had been found. Until this was clear, Baer could not decide whether the carcass had survived intact due to ice surviving from the Ice Age (Tammiksaar 2002). Baer had suggested in his manuscript given to Middendorff that the mammoth must have been found on the heaped sea/river-ice (Baer 2001).

Middendorff searched for witnesses concerning the discovery of Adams' mammoth. In Barnaul he met the mining engineer, Slobin, who stated that the mammoth had not been found on the sea-ice but from the permafrost (Baer, 1866). Middendorff also discovered remnants of another mammoth at Taymyr peninsula (at Nizhnaya-Taymyr River) and described, for the first time in the history of mammoth studies, the particular site. This information suggested (at least for Middendorff) that these animals must have lived in the south, meaning that it had to be the rivers that had carried the bodies northward (Middendorff 1860a, b). Thus the information by Slobin became irrelevant for Baer, and he left the whole issue open.

During his expedition Middendorff could not prove the connections of Adams' mammoth with the Ice Age. He admitted that he could find no evidence for an Ice Age in Siberia. Thus he and Baer remained in a tentative position concerning the glacial theory (Baer 1986, Middendorff 1861).

It is not surprising that both Baer and Middendorff could not give simple answers to such a complicated matter. They were lacking hard empirical evidence upon which to draw accurate conclusions. There was also no theoretical basis for their research as permafrost studies were only in their initial stage and it was, in fact, Baer who had started them. There were also no fieldwork results or theory to distinguish ice formations of different origin (sea- and river-ice, glaciers, buried ice, etc.) as up to then a detailed approach to such phenomena had not been possible. The theory of the Ice Age was also in its initial stage.

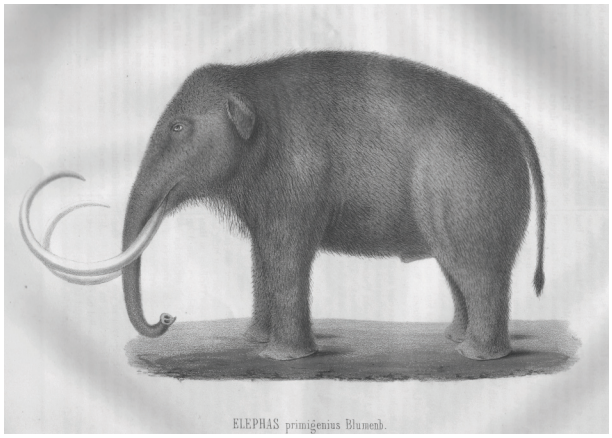

Figure 2. A mammoth drawn by Johann Friedrich Brandt (Brandt 1866a).

On the other hand, the studies of both scholars created a strong basis for future studies of mammoths and permafrost in Russia. It was just a matter of time before a new mammoth find was reported. Middendorff had created, on behalf of the St. Petersburg Academy of Sciences, a prize for those reporting mammoth finds (Middendorff 1860c, Sukhova & Tammiksaar 2005).

Woolly Mammoth as a Northern Species

At the beginning of 1866, Baer received a letter from a mining specialist in Barnaul, Stepan Guliaiev, informing him that near Tazovskaya Guba at the shore of the Arctic Ocean, a wholly preserved mammoth had been discovered. The Academy hurriedly summoned a special commission to organise an expedition to bring the carcass to St. Petersburg. Baer was the head of the commission. He hoped to solve several scientific problems that had remained open after Adams's find had been studied. For Baer it was not the preservation of the soft tissues that was particularly important but the information that might be obtainable from the surviving contents in the animal's digestive tract. He hoped to find remnants of coniferous trees and thus secure support for a theory under which mammoths had been northern animals. Such a find could also give information on the flora in historic times in Siberia (Baer 1866).

In connection with the organisation of the new expedition,Baer published an overview (based on the data of Middendorff (1859, 1860b) and of himself) on all known finds of mammoths in Siberia (Baer 1866). His colleague Johann

Friedrich Brandt, a zoologist, completed an overview on the morphology and living conditions of the extinct animal. In addition Brandt published a drawing to depict a mammoth as understood by him (see Fig. 2) (Brandt 1866a, b). Brandt also stated that mammoths could not have been southern animals but inhabitants of the north, becoming extinct due to climate change and leaving their bodies to survive in the permafrost (Brandt 1866b).

Baer took similar views, but his position was more cautious because of the lack of firm evidence. Baer did not want to rule out the possibility that the mammoths' bodies did not survive only in permafrost but also in ice formed of snow in places not reached by sun. This was possibly confirmed by Adams' case in which there had been ice covered by soil close to where the carcass had been found (Baer 1866).

Friedrich Schmidt, a geologist and later a member in palaeontology of the St. Petersburg Academy of Sciences, was appointed head of the expedition for the search of the mammoth found at Tazovskaya Bay. Arriving at the site, he discovered that the mammoth was not situated at the seashore but on the bank of the Yenissei River. Furthermore the body was badly preserved, and there was no hope of obtaining information on the contents of the digestive tract nor on the physiology of the animal. Yet Schmidt studied thoroughly the place at which the mammoth had been found and concluded that mammoths preserved in permafrost must have been northern mammals (Schmidt 1872). He reported on it to Middendorff (Sukhova & Tammiksaar 2005) and touched on the issue also in the report of his expedition (Schmidt 1869). After that, the scientific community (for example the geologist Count Alexander Keyserling) started to accept the idea that mammoths had not been inhabitants of the southern regions and that the natural conditions of Siberia must have been different in the past (cf. Taube von der Issen 1902, Toll 1895).

The Extinction of Mammoths Becomes Central in Making Broader Conclusions Concerning the Natural Conditions of Siberia

There was, therefore, no doubt that the mammoths had died out due to the chilling of the climate; but how much time the process had taken caused much argument.

In 1871, a member of the St. Petersburg Academy, the geographer Leopold von Schrenck, published a longer article on the issue of the extinction of mammoths based on field studies made by Gerhard von Maydell, a traveler of the Russian Geographical Society, in northeast Siberia studying three mammoth sites between the Indigirka and Kolyma Rivers in 1860–1870s (Schrenck 1871, Maydell 1896).

Schrenck proved that the process of slow ice formation on Siberian rivers, shallow lakes, and swamps during the chilling of the climate was the main reason preventing mammoths from leaving for areas with better conditions, and this finally caused their extinction very quickly. Schrenck also decided that only in very favourable conditions could a mammoth be preserved intact. In most cases bodies would decompose in water or in the atmosphere, and the remnants would be carried by rivers towards the sea in the area between the Indigirka and Lena Rivers. The latter process was still going on (Schrenck 1871).

According to Schrenck, mammoths could remain preserved only if their carcasses fell into the snow beneath the banks which did not melt in summer and finally turned into ice due to temperature changes (Schrenck 1871, Schrenck 1880). Agreeing with Baer in 1860, he considered that the mammoth described by Adams had been preserved in such a way. These two authorities were supported by Alexander von Bunge Jr., who participated in a Russian expedition, dedicated to the International Polar Year (1882–1883), to the delta of the Lena River, and at the request of Schrenck studied the place of Adams' mammoth find (Bunge 1884).

In 1885–1886, during an expedition arranged by the St. Petersburg Academy of Sciences, the region between the Jana and Indigirka Rivers was studied by Bunge and his companion, Eduard von Toll. The main goal of the expedition was to research the New Siberian islands, in which palaeontological finds were abundant (Bunge & Toll 1887). During this expedition the issue of the extinction of mammoths started to interest Toll, especially after seeing the high banks of the Big Lyahhov and Kotelny islands constituted mainly of buried ice/fossil ice (Toll used the term *Stein-Eis*), similar to that described by Adams at the mammoth site at Cape Bykovski. Toll was the first scholar to associate the sites in which mammoths had been found not so much with permafrost as with the occurrence of buried/fossil ice. According to him, the buried/fossil ice was a remnant of the Ice Age in Siberia.

Analysing thoroughly the slightest data on permafrost and traces of the Ice Age between the Lena River and Eschscholtz Bay (the main sources being the works of Baer, Middendorff, Bunge, Schmidt, Maydell, and writings by Erich von Drygalski on the Greenland ice sheet and the results of his two polar expeditions in 1885–1886 and 1893), Toll came to some very important conclusions. He proved that during the Ice Age, one centre of glaciation in Siberia was Cap Sviatoi Nos (east of the Lena River mouth), and this was the reason why after the Ice Age, the New Siberian islands were part of the Asian continent (Toll 1895). Toll named this "mammoth-continent," but this continent was destroyed as a result of gradual melting of the buried ice due to the transgression of the North Polar Sea and the activity of the Siberian rivers (Toll 1899).

Up to then an idea had been dominant (i.e.. Schrenck, Middendorff): the rivers had carried the bodies of the animals to their resting places from the area to the south. Similar conclusions had been made several years earlier by a Russian geologist of Polish origin, Jan Czerski, who had analysed the palaeontological finds and travel reports of Bunge (Tscherski 1893). By the analysis Toll proved that climate in northern Siberia was so warm after the Ice Age that the former continental ice sheet in the "mammoth-continent" was covered with sediments and plants (e.g., Toll found in the same layer bones of mammoth as well as

stems of alder**).** This region was a suitable living place for mammoths and other mammals, but the gradual destruction of the continent and the cooling of the climate made the movement of mammoths and other mammals to the south impossible. As a result, the gradual extinction began. It was not catastrophic, for example, due to flood, a sudden fall of temperature, etc.; rather, the living conditions gradually deteriorated. Thus Toll decided correctly that the remnants of the animals had to be younger than the ice sheet in which the carcasses were preserved (Toll 1895). So, unlike his predecessors (Baer, Middendorff, Schrenck, Schmidt, Bunge), Toll came to the conclusion that the places at which extinct mammals were found in Siberia might be linked to regions with buried ice, either on riverbanks or seashore. If in rivers the buried ice submerged formations typical of the permafrost *taryn* (*Aufeis*), then the buried ice on the seashore had to be regarded as a remnant of the former ice sheet of the Ice Age (Toll 1895).

Besides generalisations made on the reasons of extinction of mammoths, Toll analysed the post Ice Age situation in the area east of the Yenissei River. He explained why Middendorff and others could not find traces supporting the glacial theory during their expeditions. According to Toll, the Arctic Ocean during the post Ice Age transgression had destroyed such traces and former glaciers on the low tundra areas and had disconnected the islands of New Siberia from the continent. Only in some regions, starting from the plateau between the Anabar and Olenyok Rivers to Eschscholtz Bay, survived former glaciers degraded into buried ice. In Toll's opinion, fossil ice was clear evidence that could not be explained differently than a remnant of the Ice Age in Siberia (Toll 1895).

Conclusion

The studies of mammoths by the members of the St. Petersburg Academy of Sciences and the expeditions organised by them in the 19th century reveal how complicated the process of scientific work can be in circumstances in which data for drawing conclusions is almost missing and the only information available is indefinite third person accounts. At the beginning of the 19th century the territory of Siberia had been not studied. In the 1830s fresh data started to emerge but initially they were contradictory. There was a need for more thorough and continual research (i.e. to discuss the relations between the mammoth sites with the essence of permafrost and relics of the Ice Age). There was no theoretical basis to link the gathered material into one entity.

That was the reason why Baer, Middendorff, Schrenck, and Bunge could not solve the question of Adams' mammoth, despite the fact that all of them (with the exception of Schrenck) had personally studied, in different parts of Siberia, both permafrost and other ice formations. Only after studies of Bunge, Maydell, and Czerski had enriched knowledge about the natural conditions in Siberia and the physiology of the extinct mammals was it possible for Toll to bind the earlier scholarship into a new entity. Thus Toll, unlike his predecessors, could explain the reasons why mammoths became extinct, as well as explaining other phenomena in Siberia, which all in turn were connected with matters of permafrost in these territories.

These studies at the end of the 19th century made Russia a leader in the theoretical and practical aspects of permafrost studies and created preconditions for the emergence of a special scientific field concerning the matter (*merzlotovedenie*) in the 20th century.

Acknowledgments

The authors wish to thank Ian Stone and Maie Roos for advice and help in arranging the English of the text. This article has been prepared with support of grant no. 7381 of the Estonian Science Foundation.

References

Baer, K.E. v. 1866. Neue Auffindung eines vollständigen Mammuths, mit der haut und den Weichtheilen, im Eisboden Sibiriens, in der Nähe der Bucht des Tas. *Bulletin de l'Académie Impériale des Sciences de St. Pétersbourg* 10: 230-296, 513-534.

Baer, K.E. v. 1986. *Autobiography of Dr. Karl Ernst von Baer*. Jane M. Oppenheimer (ed.). Science History Publications U.S.A. Canton: Watson, XIV+389 pp.

Baer, K.E. v. 2001. *Materialien zur Kenntniss des unvergänglichen Boden-Eises in Sibirien.* In: L. King, (Hrsg) & K.E. v. Baer (eds.) *Materialien zur Kenntniss des unvergänglichen Boden-Eises in Sibirien. Unveröffentliches Typoskript von 1843 und erste Dauerfrostbodenkunde*. Giessen: Universitätsbibliothek, 234 pp.

Brandt, J.F. 1866a. Mittheilungen über die Gestalt und Unterscheidungsmerkmale des Mammuth oder Mamont (*Elephas primigenius*). *Bulletin de l'Académie Impériale des Sciences de St. Pétersbourg* 10: 93-118.

Brandt, J. F. 1866b. Zur Lebensgeschichte des Mammuth. *Bulletin de l'Académie Impériale des Sciences de St. Pétersbourg* 10: 111-118.

Bunge, A. v. 1884. Naturhistorische Beobachtungen und Fahrten im Lena-Delta. Aus Briefen an den Akademiker L. v. Schrenck. *Bulletin de l'Académie Impériale des Sciences de St. Pétersbourg* 29: 422-476.

Bunge, A. v. & Toll, E. v. 1887. Die von der Kaiserlichen Akademie der Wissenschaften ausgerüstete Expedition nach den Neusibirischen Inseln und dem Jana-Lande. *Beiträge zur Kenntniss des Russischen Reiches und der angränzenden Länder Asiens*. Kaiserliche Akademie der Wissenschaften, Folge III: 2, VIII + 412 pp.

Maydell, G. v. 1896. Reisen und Forschungen im Jakutskischen Gebiet Ostsibiriens in den Jahren 1861–1871. *Beiträge zur Kenntniss des Russischen Reiches und der angränzenden Länder Asiens*. St. Petersburg: Kaiserliche Akademie der Wissenschaften, Folge IV: 2, XXV + 800 pp.

Middendorff, A.T. v. 1848. Geothermische Beobachtungen. In: *Dr. A.Th. v. Middendorff's Reise in den äussersten Norden und Osten Sibiriens*. St. Petersburg: Kaiserliche Akademie der Wissenschaften, 1(1): 85-183.

Middendorff, A.T. v. 1860a. O sibirskikh mamontakh. *Vestnik estestvennykh nauk* 26-27: 843-867.

Middendorff, A.T. v. 1860b. Orographie und Geognosie. In: Middendorff, A.T. v. *Dr. A.Th. v. Middendorff's Sibirische Reise*. Uebersicht der Natur Nord- und ost-Sibiriens. St. Petersburg: Kaiserliche Akademie der Wissenschaften, 4(1), Lief. 2: 201-332.

Middendorff, A.T. v. 1860c. Über die Nothwendigkeit von Vorbereitungen für den Empfang vorweltlicher sibirischer Riesenthiere. *Bulletin de l'Académie Impériale des Sciences de St. Pétersbourg* 1: 557-563.

Middendorff, A.T. v. 1861. Klima. *Dr. A.Th. v. Middendorff's Sibirische Reise*. Uebersicht der Natur Nord- und ost-Sibiriens. St. Petersburg: Kaiserliche Akademie der Wissenschaften, 4(1), Lief. 4, 525-783 + LIV pp.

Schmidt, F. 1869. Vorläufige Mittheilungen über die wissenschaftlichen Resultate der Expedition zur Aufsuchung eines angekündigten Mammuthcadavers. *Bulletin de l'Académie Impériale des Sciences de St.-Pétersbourg* 13: 97-130.

Schmidt, F. 1872. Wissenschaftliche Resultate der zur Aufsuchung eines angekündigten Mammuthcadavers von der Kaiserlichen Akademie der Wissenschaften an den unteren Jenissei ausgesandten Expedition. *Mémoires de l'Académie Impériale des Sciences de St. Pétersbourg.* St. Pétersbourg: l'Academie Impériale des Sciences, VII Série, XVIII(1), VI+168 pp.

Schrenck, L. v. 1871. Bericht über neuerdings im Norden Sibirien's angeblich zum Vorschein gekommene Mammuthe, nach brieflichen Mittheilungen des Hr. Gerh. v. Maydell, nebst Bemerkungen über den Modus der Erhaltung und die vermeintliche Häufigkeit ganzer Mammuthleichen. *Bulletin de l'Académie Impériale des Sciences de St. Pétersbourg* 16: 147-173.

Schrenck, L. v. 1880. Der erste Fund einer Leiche von *Rhinoceros Merckii* Jaeg. *Mémoires de l'Académie Impériale des Sciences de St. Pétersbourg.* St. Pétersbourg: l'Academie Impériale des Sciences, VII Série, XXVII(7), V + 55 pp.

Sukhova, N.G. & Tammiksaar, E. 2005. *Aleksandr Fedorovich Middendorf, 1815-1894*. Moskva: Nauka, 331 pp.

Tammiksaar, E. 2001. «Materialien zur Kenntniss des unvergänglichen Boden-Eises in Sibirien» Die erste «Dauerfrostbodenkunde» von Karl Ernst von Baer. In: L. King (Hrsg.) & K. E. v. Baer. *Materialien zur Kenntniss des unvergänglichen Boden-Eises in Sibirien. Unveröffentliches Typoskript von 1843 und erste Dauerfrostbodenkunde*. Giessen: Universitäts-bibliothek, I–XLIV.

Tammiksaar, E. 2002. The contributions of Karl Ernst von Baer to the investigation of the physical geography of the Arctic in the 1830s–1840s. *Polar Record* 38(205): 121-140.

Tammiksaar, E. & Stone, I.R. 2007. Alexander von Middendorff and his expedition to Siberia (1842–1845). *Polar Record* 43(226): 193-216.

Taube von der Issen, H. 1902. *Graf Alexander Keyserling. Ein Lebensbild aus seinen Briefen und Tagebüchern*. Berlin: Reimer, V + 655 pp.

Tilesius von Tilenau, 1815. De skeleto mammonteo Sibirico ad maris glacialis littora anno 1799, effosso, cui praemissiae elephantini generis specie, sum distinctiones. *Mémoires de l'Académie Impériale des Sciences de St. Pétersbourg* 5: 406-513.

Toll, E. v. 1895. Wissenschaftliche Resultate der von der Kaiserlichen Akademie der Wissenschaften zur Erforschung des Janalandes und der Neusibirischen Inseln in den Jahren 1885 und 1886 ausgesandten Expedition. Abtheilung III: Die fossilen Eislager und ihre Beziehungen zu den Mammutleichen. *Mémoires de l'Académie Impériale des Sciences de St. Pétersbourg.* St. Pétersbourg: L'Academie Impériale des Sciences, VII Série, XLII(13), VII + 87 pp.

Toll, E. v. Ocherk geologii Novosibirskikh ostrovov i vazhneishie zadachi issledovaniia poliarnykh stran. *Mémoires de l'Académie Impériale des Sciences de St. Pétersbourg.* St. Pétersbourg: L'Academie Impériale des Sciences, VIII Série, IX(1), IV + 20 pp.

Tscherski, J.D. 1892. Wissenschaftliche Resultate der von der Kaiserlichen Akademie der Wissenschaften zur Erforschung des Janalandes und der Neusibirischen Inseln in den Jahren 1885 und 1886 ausgesandten Expedition. Abtheilung IV: Beschreibung der Sammlung posttertiären Säugethiere. *Mémoires de l'Académie Impériale des Sciences de St.-Pétersbourg.* St.-Pétersbourg: l'Academie Impériale des Sciences, VII Série, XL(1), V + 511 pp.

Soil Organic Carbon Stocks in the Northern Permafrost Region and Their Role in Climate Change

Charles Tarnocai
Research Branch, Agriculture and Agri-Food Canada, Ottawa, Canada
Gabriele Broll
University of Vechta, Vechta, Germany

Abstract

The soil area of the northern permafrost region is approximately 18,781 × 10^3 km^2, or approximately 14% of the global soil area. Organic soils (peatlands, total depth) and cryoturbated permafrost-affected mineral soils (100 cm) have the highest mean soil organic carbon contents (30–120 kg m^{-2}). Carbon stocks in the northern permafrost region were estimated to be 191 Gt for the 0–30 cm depth and 496 Gt for the 0–100 cm depth. Most of the soil organic carbon stocks occur in permafrost-affected soils, which contain about 70% of the stocks in the 0–100 cm depth. The values calculated here indicate that the organic carbon in soils in the northern permafrost region account for approximately 30% of the global soil organic carbon at the 0–100 cm depth, much of which will be vulnerable to release because of the large temperature increases predicted to result from climate change.

Keywords: carbon content; carbon mass (stocks); climate change; peatlands; permafrost; soils.

Introduction

The importance of permafrost-affected soils in global soil organic carbon stock estimates has been either neglected or poorly handled. This is probably due to the lack of data for these soils and the lack of understanding of the soil-forming processes in permafrost-affected soils. With recognition of the role of cryogenic processes in the genesis of these soils, came an understanding of their function in the sequestration of organic carbon (Van Vliet-Lanoe 1991, Bockheim & Tarnocai 1998, Bockheim 2007). These soils have sequestered carbon for a period of 6–8 thousand years and are still acting as carbon sinks (Tarnocai et al. 2007).

Some estimates of global soil organic carbon stocks are: 1220 Gt (Sombroek et al. 1993), 1395 Gt (Post et al. 1982), 1462 to 1548 Gt (Batjes 1996), and 1576 Gt (Eswaran et al. 1993). Although all of these estimates were based on the 0–100 cm depth, Batjes (1996) did report carbon stocks of 2376–2456 Gt for the 0–200 cm depth.

Post et al. (1982) estimated that the soils in the tundra zone contained, globally, approximately 191.8 Gt of organic carbon. This estimate, however, was based on only 30 samples. Using the, at that time, newly-developed Northern and Mid Latitudes Soil Database, Tarnocai et al. (2003) estimated that the carbon stocks in the 0–100 cm depth of Cryosols (Soil Classification Working Group 1998) in the northern circumpolar region were approximately 268 Gt of organic carbon. In this database, however, coverage of permafrost-affected soils in Eurasia was greatly underestimated.

This paper provides estimates of the organic carbon stocks in both permafrost-affected and nonpermafrost soils in the northern circumpolar permafrost region. The effect of climate change on this carbon is also discussed.

Materials and Methods

Terminology

The U.S. terminology for permafrost-affected (Gelisols) and nonpermafrost soils is used in this paper (Soil Survey Staff 1999).

SOCC (soil organic carbon content) refers to the content of organic carbon in a one meter square soil column. It is expressed as kilograms per square meter (kg m^{-2}).

SOCM refers to the soil organic carbon mass and is expressed as kilograms (kg) or gigatons (Gt).

The northern permafrost region refers to the northern circumpolar permafrost region as outlined by Brown et al. (1997).

The Northern Circumpolar Soil Carbon Database (NCSCD)

This database (Tarnocai et al. 2007) provides the spatial framework and the data needed to determine the organic carbon stocks for soils of the northern permafrost region. The NCSCD contains many thousands of polygons, with each polygon containing one or more named soil or soil taxa that form the basis for determining the carbon stocks.

The North American portion of the NCSCD was compiled from existing soil maps. For remote areas in North America, where more detailed survey maps were unavailable, data from other sources, such as pedon, climate and vegetation data, together with high quality LANDSAT imagery, were used to delineate polygons. The Greenland and Eurasian portion (Russia, Kazakhstan, Mongolia, Scandinavia, Svalbard, and Iceland) was also compiled from small-scale soil maps that had been digitized.

During this process, especially in the case of the Russian maps, the map symbols and classification terms had to be translated into English, and the soil classification terms had to be converted to the US Soil Taxonomy. A special effort was made to harmonize the data and to ensure that no information loss occurred during translation and data conversion, especially for permafrost-affected soils.

Pedon and peatland databases

Data used to calculate soil organic carbon content (kg m^{-2}) were derived from various pedon (soil profile) databases containing numerous pedons and their associated soil attribute data. The Canadian portion of the NCSCD was built up using 3530 pedons. No figures are available for the number of pedons used for the Alaskan portion of the database, but it relies, proportionally, on approximately the same level of supporting data as was used for Canada. Soil data used for the Eurasian portion of the NCSCD is drawn from a number of databases. A pedon database containing information for 253 pedons was developed for the Russian part of the NCSCD. In addition, the West Siberian Lowland Peatland GIS Data Collection, containing data for 90 peat cores (Smith et al. 2000, 2004, Sheng et al. 2004), was also used. Information from Batjes (1996) was also used for Eurasian soils, including Russia, especially where no pedon information was available.

Calculating SOCC and SOCM

Pedons for each soil taxa (Eurasia) or named soil (North America) are selected. These pedons contain all of the data needed to calculate the SOCC. The data for each named soil (North America) are entered into the database and are used to calculate the carbon content of each named soil in the polygon, while data from pedons of each soil taxa (Eurasia) are used to calculate their carbon contents, which are then entered into the database.

The SOCC (kg m^{-2}) was calculated for each named soil (North America) and for the representative pedons for each soil taxa (Eurasia) using the formula:

$$SOCC = C \times BD \times T \times CF \quad (1)$$

where C = organic carbon (% weight), BD = bulk density (g cm^{-3}), T = depth of soil layer (0–30 cm and 0–100 cm), including the surface organic layer, and CF = coarse fragments and/or ice content (% weight). The SOCC data are then stored in the database to be used for further calculations or to generate carbon content maps.

The SOCM was then determined by multiplying the SOCC of the specific soil by the area of each such soil component in the polygon.

Results

Soil area

The total soil area of the northern permafrost region is 18,782 × 10^3 km^2 (Table 1). The Eurasian portion covers approximately 65% of the soil area and the North American portion 35%. Gelisols are the dominant soils in the area, covering approximately 54% of the permafrost region with the remainder of the area (46%) being covered by unfrozen soils. The Continuous Permafrost Zone, the largest of the four permafrost zones, covers 54% of the northern permafrost area while the Discontinuous, Sporadic, and Isolated Patches zones cover the remaining 46% of the area. The distribution of the major soil groups for frozen mineral soils (Turbels and Orthels), peat (Histels and Histosols), and unfrozen mineral soils are shown in Figure 1. Perennially frozen and unfrozen mineral soils cover approximately the same areas (40% frozen, 41% unfrozen). Peat soils cover the remaining 19% of the soil area.

Table 1. Areas of all soils in the various permafrost zones.

Permafrost zones	Area (10^3 km^2)		
	North America*	Eurasia	Total
Continuous	2868	7255	10,123
Discontinuous	1443	1649	3092
Sporadic	1149	1444	2593
Isolated patches	1186	1788	2974
Total	6646	12,136	18,782

* Greenland included in the North America calculation.

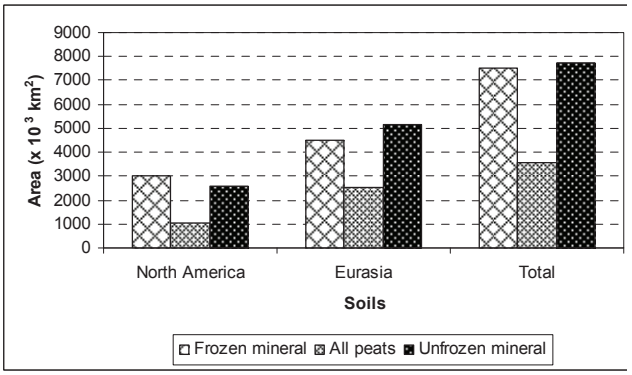

Figure 1. Distribution of major soil groups in the northern permafrost region.

Soil organic carbon content

The mean SOCC values calculated for the northern permafrost region are given in Table 2. Histels (perennially frozen soils) and Histosols (unfrozen peatland soils) have the highest SOCC with average values ranging from 67 to 69 kg m^{-2}. Maximum SOCC values slightly above 100 kg m^{-2} are not uncommon for these soils. The SOCC values for mineral Gelisols (Turbels and Orthels) range from 23 to 32 kg m^{-2}. Turbels have the highest SOCC values, in some cases as much as three times those for unfrozen mineral soils (Table 2).

The standard deviation was greatest (>50) for Histels and Histosols (Table 2). This is probably due to the variability of peat materials, the degree of decomposition, and the mineral (ash) content. Turbels, Orthels, and Spodosols had the second greatest standard deviations (20–27). Their large values were probably due to the various thicknesses of surface organic material associated with these soils and, for Turbels, also to the variability of amounts of cryoturbated organic materials they contained.

Soil organic carbon mass

In the northern permafrost region, the SOCM is approximately 191 Gt in the 0–30 cm depth and 496 Gt in the 0–100 cm depth (Table 3). Approximately 67% of this mass occurs in Eurasia and 33% in North America. The

Table 2. Average carbon contents for soils in the northern permafrost region.

US Taxonomy	Soil organic carbon content (kg m^{-2})		
	Mean	SD	No. of pedons
Gelisols			
Histels	66.6	53.3	87
Turbels	32.2	27.4	256
Orthels	22.6	21.4	131
Histosols	69.6	56.9	417
Andisols	25.4*	–	unknown
Spodosols	24.7	20.2	6
Aqu-suborders	20.1	9.7	531
Inceptisols	15.3	9.4	871
Vertisol	13.5	7.3	11
Entisols	9.9	15.8	198
Mollisols	9.6	8.3	422
Natric-suborders	9.1	7.6	67
Alfisols	8.9	6.9	533
Aridisols	3.0*	–	unknown

* SOCC data from Batjes (1996)

Continuous Permafrost zone contains approximately 60% of the carbon mass; the remaining three zones each contain approximately 13%.

The SOCM for all major soil orders is shown in Figure 2. Gelisols are the major SOCM contributors in the permafrost area. They contain approximately 71% of the SOCM at depths of 0–100 cm in the region. Within the Gelisol soil group, the Turbels contain the largest amount (64%) of SOCM in both the 0–30 cm and 0–100 cm depths (Fig. 3).

Peatlands (Histosols and Histels) contain approximately 48% of the SOCM in the northern permafrost region, with the Histosols containing the second largest soil carbon pool (13% of the SOCM).

When the SOCMs of the major soil groups are compared (Fig. 4), the peat soils and frozen mineral soils are the major contributors of SOCM in both North America and Eurasia. The SOCM in the 0–100 cm depth (for both frozen and unfrozen organic and mineral soils) is approximately 239 Gt for organic soils (peatlands) and approximately 256 Gt for mineral soils. It should be pointed out that, although the SOCM values for these soil groups are similar, peatlands cover only 19% of the soil area of the region.

When soil areas and SOCM values of major soil groups were compared, it was found that, although unfrozen and frozen mineral soils cover about the same area, the SOCM values of frozen mineral soils are approximately twice those of unfrozen mineral soils (Fig. 5). Peat soils (unfrozen and frozen) cover about half as much area as the frozen and unfrozen mineral soils, but they contain about 13% more SOCM than the frozen mineral soils and nearly three times more than the unfrozen mineral soils (Fig. 5).

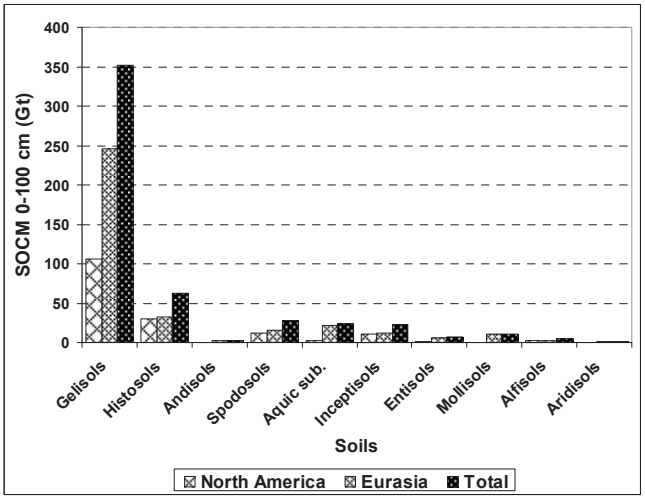

Figure 2. SOCM for the 0–100 cm depth in all soils in the northern permafrost region (SOCM in Vertisols and Natric-suborders is <0.5 Gt).

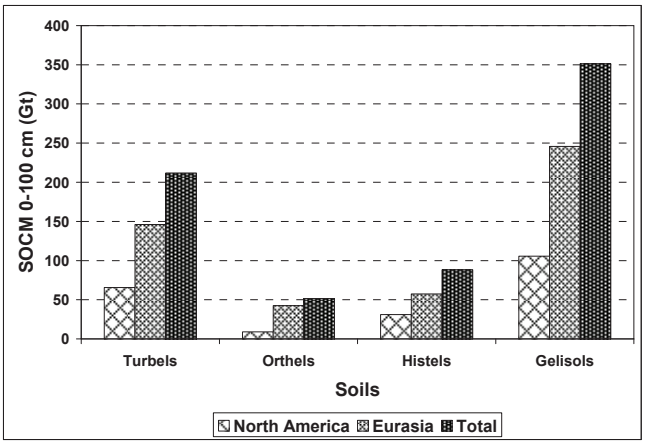

Figure 3. SOCM for the 0–100 cm depth in the three Gelisol suborders and in all Gelisols in the northern permafrost region.

Discussion

Carbon dynamics

The total SOCM at the 0–100 cm depth for soils in the northern permafrost region is approximately 496 Gt, which is about 30% of the global SOCM. The large amount of soil organic carbon in this region is due to the large areas and high carbon content of the peat (organic) soils and cryoturbated mineral soils (Turbels).

Peat soils are composed of organic materials with a high concentration of carbon that has accumulated over a long period of time. Robinson & Moore (1999) found that, in the Sporadic Permafrost Zone, mean carbon accumulation rates in unfrozen bogs (Histosols) and frozen peat mounds (Histels) over the past 100 years were 88.6±4.4 and 78.5±8.8 g m^{-2} per year, respectively. They also found that, in the Discontinuous Permafrost Zone, the mean carbon accumulation rate in peat plateaus (Histels) during the past 1200 years was 13.31±2.20 g m^{-2} per year, while in unfrozen fens and bogs (Histosols) the comparable rates were 20.34±2.86 g m^{-2} and 21.81±3.25 g m^{-2} per year, respectively. Radiocarbon dates from the basal peat (the base of the peat deposit, indicating the beginning of peat deposition) suggest that, in North America, the average basal peat date is 7200 ^{14}Cyr BP in the Arctic, 6200 ^{14}Cyr BP in the Subarctic and 6000 ^{14}Cyr BP in the Boreal (Tarnocai

Table 3. Organic carbon mass in all soils in the permafrost zones.

Permafrost zones	Soil organic carbon mass (Gt)				
	North America*		Eurasia		Total
	0–30 cm	0–100 cm	0–30 cm	0–100 cm	0–100 cm
Continuous	31.17	78.29	79.21	220.46	298.75
Discontinuous	12.23	39.69	13.27	37.75	67.44
Sporadic	10.86	26.27	15.50	36.86	63.13
Isolated Patches	12.65	30.60	16.40	36.50	67.10
Total	66.91	164.84	124.38	331.57	496.42

* Greenland included in the North America calculation.

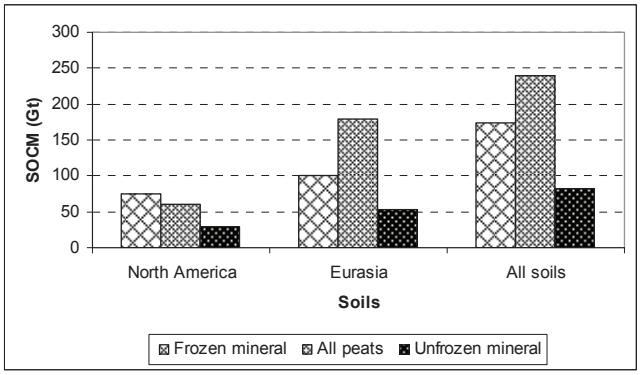

Figure 4. SOCM in major soil groups for the 0–100 cm depth in the northern permafrost region.

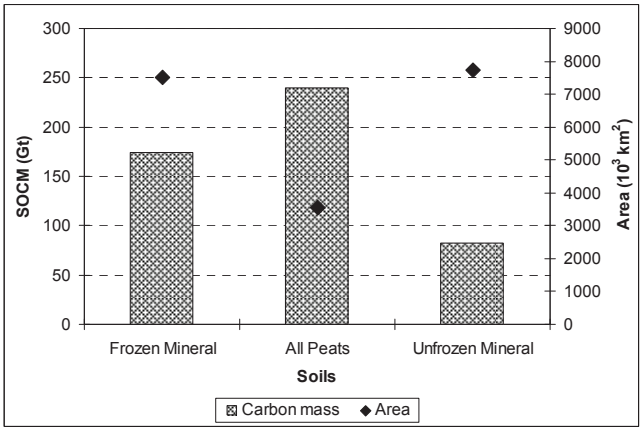

Figure 5. Comparison of the area covered and SOCM in the 0–100 cm depth for the major soil groups.

& Stolbovoy 2006). In Russia, the basal peat dates for the Tundra zone are 2000–3000 ^{14}Cyr BP and for the Taiga zone are 5000–8000 ^{14}Cyr BP (Tarnocai & Stolbovoy 2006).

In mineral soils, Turbels had the highest SOCM, containing approximately 43% of the organic carbon mass occurring in all soils in the northern permafrost region. Cryoturbation, a unique process operating in these soils, is responsible for the high SOCM values. Although the ecosystems in the permafrost region produce much less biomass than do temperate ecosystems, permafrost-affected soils that are subject to cryoturbation (Turbels) have the ability to sequester a portion of this annually-produced biomass and store it for thousands of years. Bockheim (2007) estimated that 55% of the soil organic carbon in the active layer and near-surface permafrost could have resulted from translocation by cryoturbation.

Radiocarbon dates for 50 cryoturbated organic samples from earth hummocks presented by Zoltai et al. (1978) indicate that the dates ranged from 500–11,200 ^{14}Cyr BP. The frequency of dates indicates that the number of samples was constant in the 500–5000 ^{14}Cyr BP range, with a peak occurring in the 3000–3500 ^{14}Cyr BP range. The number of samples decreased in the 5000–11,500 ^{14}Cyr BP range and showed no pattern.

Soluble organic materials also move downward within the soils because of the effects of gravity and the movement of water along the thermal gradient towards the freezing front (Tarnocai 1972, Kokelj & Burn 2005). When these organic materials reach the cold, deep soil layers where very little or no biological decomposition takes place, they may be preserved for many thousands of years.

The SOCC and SOCM values for unfrozen mineral soils in the permafrost region are low because these soils lack a mechanism to move insoluble carbon from the surface into the deeper soil layers. Soluble organic materials, however, may move downward and roots do contribute organic carbon to the subsoil. Trumbore & Harden (1997) reported carbon accumulations of 60–100 g C m^{-2} per year for these soils, but the turnover time, especially because of wildfires, is 500–1000 years. The turnover time for deep carbon, originating mainly from roots, is 100–1600 years (Trumbore & Harden 1997).

Land-use change also has significant effects on soil carbon stocks, especially in northern Europe where large areas are used as pasture (Smith et al. 2005). More research is needed to determine the effect that land-use change will have on northern soils, especially in view of the changing climate and such properties as cryoturbation.

Reliability and uncertainties of carbon data

It is difficult to determine the accuracy of the carbon stocks presented in this paper since no such information has been published for the northern permafrost region.

The North American soil organic carbon estimates were tested by Bhatti et al. (2002), who compared the carbon values generated by both the Carbon Budget Model of the Canadian Forest Sector (CBM-CFS2) and the Boreal Forest Transect Case Study (BFTCS) with the Canadian Soil Organic Carbon Database (CSOCD) (Soil Carbon Database Working Group 1993). They found that the CSOCD generated slightly lower carbon values than the CBM-CFS2 carbon model, but

that there was good agreement between the CSOCD- and BFTCS-generated values.

No SOCM data are available for the permafrost region in Eurasia, but Stolbovoi (2000) estimates that the area of permafrost-affected soils in Russia is 307 million ha. He did point out, however, that this value is much less than the total area of the permafrost zone in Russia, which is more than 1,000 million ha. Stolbovoi (2002) reported that the SOCM in Russia is approximately 297 Gt C for the 0–1 m depth and 373 Gt C for the 0–2 m depth. Estimates of Russian peatland areas and the organic carbon stocks they contain are 1162–2730 × 10^3 km^2 and 94–215 Gt, respectively (Botch et al. 1995, Efremov et al. 1998). Although the peatland area (2730 × 10^3 km^2) given by Efremov et al. (1998) is close to that given in this paper, the carbon mass value (118 Gt) is only half that given here. These large variations occur because of the poor inventory and limited amount of reliable pedon data available for these soils. This supports the statement of Efremov et al. (1998) that: "The accuracy of estimates of peat carbon is ± 10 to 15 percent for the European part of Russia and ± 20 to 30 percent for the Asian part of the country."

Climate warming

It is predicted that the average annual air temperature in the permafrost region of Canada will increase 3–4°C by 2020 and 5–10°C by 2050. Such increases have already been observed at seven northern circumpolar climate stations that tracked temperature changes in winter and spring (NOAA 2007)

Various predictions have been made about the effect this large temperature increase will have on soil carbon. The most commonly predicted effects are melting of ice-rich frozen soil materials, higher frequency of wildfires and shoreline erosion.

It is also predicted that the greatest effects of climate warming on Canadian peatlands will occur in the Subarctic and Boreal zones (Tarnocai 2006). Major concerns are the drying of peatlands and an increase in frequency and extent of wildfires. Richie (1987) found that boreal forests in western Canada have a fire return interval of 50–100 years while Kuhry (1994) indicated that, for Sphagnum bogs, the interval is 400–1700 years.

A study similar to that of Tarnocai (2006) was carried out on mineral soils in the permafrost region of Canada (Tarnocai 1999). This study suggests that 12 Gt of organic carbon in Canadian Cryosols could be severely to extremely severely affected by climate warming. This study also suggests that permafrost-affected soils will cease to exist in the southern part of the permafrost region in Canada, and that cryogenic processes will diminish or disappear in southern regions. In these areas, the mechanism for sequestering carbon would cease to operate and a portion of the soil carbon would be released as carbon dioxide and/or methane.

Bockheim (2007), however, suggests that continued warming of the Arctic could accelerate cryoturbation and, thus, enable the soil to store more soil organic carbon than it can at present. Zoltai et al. (1978) suggest that, based on the higher frequency of carbon dates between 3000 ^{14}Cyr BP and 3500 ^{14}Cyr BP, this period coincided with a time of higher soil moisture and lower temperatures with increased cryoturbation. Relict earth hummocks found in the Mackenzie Valley (Zoltai & Tarnocai 1974) suggest that these hummocks were active during the Little Ice Age, but became dormant and cryoturbation ceased when the climate warmed. The soil horizons in these dormant hummocks showed no signs of cryoturbation, although some fossil cryoturbation features remain in the lower part of the soil.

These contradictory findings indicate that we know very little about the complex interactions between soils and climate in these northern regions.

Acknowledgments

We would like to thank Drs. Peter Kuhry, Galina Mazhitova, and Sergey Goryachkin for providing the Russian pedon data. Special thanks are also due to Dr. David Swanson for translating and digitizing the Russian soil maps, which also included Kazakhstan and Mongolia.

References

Batjes, N.H. 1996. Total carbon and nitrogen in the soils of the world. *European Journal of Soil Science* 47: 151-163.

Bhatti, J.S., Apps, M.J. & Tarnocai, C. 2002. Estimates of soil organic carbon stocks in central Canada using three different approaches. *Canadian Journal of Forest Research* 32: 805-812.

Bockheim, J.G. 2007. Importance of cryoturbation in redistributing organic carbon in permafrost-affected soils. *Soil Science Society of America Journal* 71(4): 1335-1342.

Bockheim, J.G. & Tarnocai, C. 1998. Recognition of cryoturbation for classifying permafrost-affected soils. *Geoderma* 81: 281-293.

Botch M.S., Kobak, K.I., Vinson, T.S. & Kolchugina, T.P. 1995. Carbon pools and accumulation in peatlands of the former Soviet Union. *Global Biogeochemical Cycles* 9(1): 37–46.

Brown, J., Ferrians, O.J. Jr., Heginbottom, J.A. & Melinkov, E.S. 1997. *Circum-Arctic Map of Permafrost and Ground Ice Conditions*. 1:10,000,000. United States Geological Survey, International Permafrost Association.

Efremov, S.P., Efremova, T.T. & Melentyeva, N.V. 1998. Carbon storage in peatland ecosystems. In: V.A. Alexeyev & R.A. Birdsey (eds.), *Carbon Storage in Forests and Peatlands of Russia* (Chapter 10).USDA Forest Service, Northeastern Research Station, General Technical Report NE-244, 69-76.

Eswaran, H., Van den Berg, E. & Reich, P. 1993. Organic carbon in soils of the world. *Soil Science Society of America Journal* 57: 192-194.

Kuhry, G.P. 1994. The role of fire in the development of Sphagnum-dominated peatlands in western boreal Canada. *Journal of Ecology* 82: 899-910.

Kokelj, S.V. & Burn, C.R. 2005. Geochemistry of the active layer and near-surface permafrost, Mackenzie delta region, Northwest Territories, Canada. *Canadian Journal of Earth Sciences* 42: 37-48.

NOAA. 2007. Climate indicators – surface air temperatures. Available at: www.arctic.noaa.gov/detect/climate-temps.shtml. Accessed 03 October 2007.

Post, W.M., Emanuel, W.R., Zinke, P.J. & Stangenberger, A.G. 1982. Soil carbon pools and world life zones. *Nature* 298: 156-159.

Ritchie, J.C. 1987. *Postglacial Vegetation of Canada.* New York, NY: Cambridge University Press, 178 pp.

Robinson, S.D. & Moore, T.R. 1999. Carbon and peat accumulation over the past 1200 years in a landscape with discontinuous permafrost, northwestern Canada. *Global Biogeochemical Cycles* 13: 591-601.

Sheng, Y., Smith, L.C., MacDonald, G.M., Kremenetski, K.V., Frey, K.E., Velichko, A.A., Lee, M., Beilman, D.W. & Dubinin, P. 2004. A high-resolution GIS based inventory of the West Siberian peat carbon pool. *Global Biogeochemical Cycles* 18: GB3004, doi:10.1029/2003GB002190.

Smith, J., Smith, P., Wattenbach, M., Zaehle, S., Hiederer, R., Jones, R.J.A., Montanarella, L., Rounsvelle, M.D.A., Reginster, I. & Ewert, F. 2005. Projected changes in mineral soil carbon of European croplands and grasslands, 1990–2080. *Global Change Biology* 11: 2141-2152.

Smith, L.C., Macdonald, G.M., Velichko, A.A., Beilman, D.W., Borisova, O.K., Frey, K.E., Kremenetski, K.V. & Sheng, Y. 2004. Siberian peatlands: a net carbon sink and global methane source since the Early Holocene. *Science* 303 (5656): 353-356.

Soil Carbon Database Working Group. 1993. Soil Carbon Data for Canadian Soils. Ottawa: Land Resource Research Institute, Agriculture Canada, 187 pp. and maps.

Soil Classification Working Group. 1998. *The Canadian System of Soil Classification. 3rd ed. Publication 1646.* Ottawa: Research Branch, Agriculture and Agri-Food Canada, 187 pp.

Soil Survey Staff. 1999. *Soil Taxonomy, a Basic System of Soil Classification for Making and Interpreting Soil Surveys*, Second Ed. Natural Conservation Service, U.S. Department of Agriculture Handbook No. 436. 869 pp.

Sombroek, W.G., Nachtergaele, F.O. & Hebel, A. 1993. Amounts, dynamics and sequestrations of carbon in tropical and subtropical soils. *Ambio* 22: 417-426.

Stolbovoi, V. 2000. Carbon pools in tundra soils of Russia: Improving data reliability. In: R. Lal, J.M. Kimble & B.A. Stewart (eds.), *Global Climate Change and Cold Regions Ecosystems, Advances in Soil Science*. Washington, DC: Lewis Publishers, 39-58.

Stolbovoi, V. 2002. Carbon in Russian soils. *Climate Change* 55(1-2): 131-156.

Tarnocai, C. 1972. Some characteristics of cryic organic soils in northern Manitoba. *Canadian Journal of Soil Science* 52: 485-496.

Tarnocai, C. 1999. The effect of climate warming on the carbon balance of Cryosols in Canada. In: C. Tarnocai, R. King & S. Smith (eds.), *Cryosols and Cryogenic Environments*, special issue of *Permafrost and Periglacial Processes* 10(3): 251-263.

Tarnocai, C. 2006. The Effect of Climate Change on Carbon in Canadian Peatlands. *Global and Planetary Change* 53: 222-232.

Tarnocai, C. & Stolbovoy, V. 2006. Northern peatlands: their characteristics, development and sensitivity to climate change., In: I.P. Martini, A. Martinez Cortizas & W. Chesworth (eds.), *Peatlands: Evolution and Records of Environmental and Climate Changes* (Chapter 2). Amsterdam, The Netherlands: Elsevier B.V., 17-51.

Tarnocai, C., Kimble, J. & Broll, G. 2003. Determining carbon stocks in Cryosols using the Northern and Mid Latitudes Soil Database. In: M. Philips, S. Springman & L.U. Arenson (eds.), *Permafrost*. Lisse, the Netherlands: A.A. Balkema Publishers, Swets & Zeitlinger, 2: 1129-1134.

Tarnocai, C., Swanson, D., Kimble, J. & Broll, G. 2007. Northern Circumpolar Soil Carbon Database. Research Branch, Agriculture and Agri-Food Canada, Ottawa, Canada (digital database).

Tarnocai, C., Ping, C-L. & Kimble, J. 2007. Carbon Cycles in the Permafrost Region of North America. In: A.W. King, L. Dilling, G.P. Zimmerman, D.M. Fairman, R.A. Houghton, G. Marland, A.Z. Rose & T.J. Wilbanks (eds.), *The First State of the Carbon Cycle Report (SOCCR): The North American Carbon Budget and Implications for the Global Carbon Cycle.* A Report by the U.S. Climate Change Science Program and the Subcommittee on Global Change Research. Asheville, NC, USA: National Oceanic and Atmospheric Administration, National Climatic Data Center, 127-138. Available at: http://cdiac.ornl.gov/SOCCR/pdf/sap2-2-finalall.pdf. Accessed 10 Jan 2008.

Trumbore, S.E. & Harden, J.W. 1997. Accumulation and turnover of carbon in organic and mineral soils of the BOREAS northern study area. *Journal of Geophysical Research* 102(D24): 28, 817-28,830.

van Vliet-Lanoë, B. 1991. Differential frost heave, load casting, and convection: converging mechanisms; a discussion of the origin of cryoturbations. *Permafrost and Periglacial Processes* 2: 123-129.

Zoltai, S.C., Tarnocai, C. & Pettapiece, W.W. 1978. Age of cryoturbated organic material in earth hummocks from the Canadian arctic. *Proceedings of the Third International Conference on Permafrost*, *Edmonton, Alberta*: 325-331.

Zoltai, S.C. & Tarnocai, C. 1974. Soils and vegetation of hummocky terrain. Environmental–Social Committee, Northern Pipelines, Task Force on Northern Oil Development, *Report No. 74–5*, 86 pp.

Thermal Impact of Holocene Lakes on a Permafrost Landscape, Mackenzie Delta, Canada

Alan E. Taylor
ASL Environmental Sciences, Inc., Sidney BC V8L 5Y3, Canada
Scott R. Dallimore
Geological Survey of Canada, Sidney BC V8L 4B2, Canada
J. Frederick Wright
Geological Survey of Canada, Sidney BC V8L 4B2, Canada

Abstract

Canada's Mackenzie Delta has experienced Holocene lake development on a permafrost landscape, exerting significant influence on the sub-lake geothermal regime. Two-dimensional finite element geothermal modeling is used to simulate talik formation beneath lakes of various diameters in sand, clayey-silt, and clay. Forward modeling was initiated from a simplifying assumption of thermal steady state at the end of the Wisconsin, and subsequently incorporated the transient effects of Holocene warming and mid-Holocene lake formation, to the present-day. Thermal taliks (>0°C) quickly developed beneath all lakes. In sands, sediments beneath the taliks remained almost entirely ice-bonded to the present time. In contrast, in fine-grained clayey silt, sediments beneath the taliks developed elevated unfrozen water content that eventually extended to the base of permafrost, thus forming chimney-like structures of partially ice-bonded soils that penetrate thick permafrost beneath larger lakes. This characteristic arises from the strong temperature dependence of unfrozen water content in finer-grained sediments.

Keywords: geothermal; lakes; modeling; permafrost; seeps; talik.

Introduction

Lakes and river channels represent dramatic thermal anomalies in terrestrial permafrost environments. In the arctic, the impact of water bodies on permafrost is accentuated because of the large contrast in mean annual ground surface temperature beneath lakes and rivers (if they do not freeze completely in winter) compared to that of the adjacent sub-aerial terrain. The classic study is the analytic model of Lachenbruch (1957), which demonstrates the steady-state (or equilibrium) impact and simple transient effects of lakes on permafrost. Over 30% of the land area of the Mackenzie Delta is occupied by lakes, and large variations in the subsurface geothermal regime are expected from the contrast of warm lakes (mean annual lakebed temperature about +2°C) superimposed on a cold (-6°C or colder) permafrost landscape. Mackay (1963, sect. 76) calculated the thermal disturbance beneath such lakes and W. Brown et al. (1964) presented early field evidence for the presence of a talik beneath a lake in the Mackenzie region. Numerical studies of talik formation beneath lakes have been made by Ling & Zhang (2003) in northern Alaska, and Burn (2002) in the Mackenzie Delta.

In this paper, we use a two-dimensional finite element model to predict the thermal impact of lake formation (during the Holocene) on thick Pleistocene permafrost typical of the Mackenzie Delta, northwestern Canada. The study focuses on the thermal sensitivity of two typical lithologies (sand and clayey silt) to lake diameter (20 m to 4 km), and to time of lake formation (10 kaBP and 6 kaBP). Model outputs are two-dimensional (horizontal and depth) depictions of ground temperatures and unfrozen water contents through the permafrost, and are presented as contours and summary graphs. The model is not calibrated to observed permafrost temperatures or thicknesses at a particular location. Rather, the intent of the paper is to demonstrate the gross impact of the development of hypothetical lakes on permafrost terrain in terms of changes to the local geothermal regime, subsequent development of taliks, and modification of the properties of underlying sediments. Thermal taliks are unfrozen sediments (temperature >0°C) in association with permafrost, and "geophysical taliks" are defined here as frozen sediments (temperature <0°C) which contain sufficient un-crystallized pore water (herein referred to as unfrozen water) so as to be discriminated by geophysical methods.

Extensive permafrost developed in Quaternary sediments of the Pleistocene Mackenzie Delta (principally the Tuktoyaktuk Peninsula and Richards Island) and today is typically 400–700 m in thickness (Judge 1973, Taylor et al. 1982), consistent with late Wisconsinan and Holocene surface temperatures (Taylor et al. 1996). The glacial history is controversial, but the region was mostly unglaciated during the late Wisconsinan (Dyke & Prest 1987). Maximum development of thermokarst lakes occurred in the early Holocene and most lakes have undergone one or more partial drainage events, attaining their present size by ~6 kaBP (Mackay 1992), and lacustrine sediments bordering many present-day lakes reflect this earlier, more extensive lake cover (Rampton 1988). Numerous tundra polygons and pingos are characteristic of poorly drained areas comprising former lake bottoms (Mackay 1963, §64).

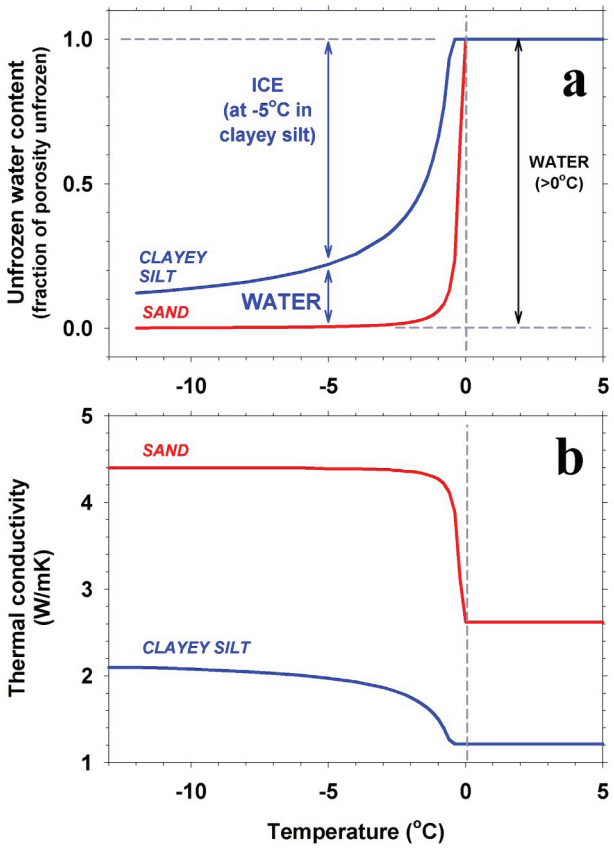

Figure 1. (a) Unfrozen water content and (b) thermal conductivity curves based on laboratory measurements of Mackenzie Delta cores (Dallimore & Matthews 1997) and used in the geothermal modeling.

Model Description

The TEMP/W geothermal modeling software (Geo-Slope International Ltd. 2004) was employed in this work. This two-dimensional finite-element numeric model combines conductive heat transfer and phase-change enthalpies, and accommodates the explicit specification of appropriate geologic properties and temporal boundary conditions. The model has been verified extensively against analytic solutions as well as the pioneering numerical permafrost model of Hwang et al. (1972) and has been used in the permafrost community (e.g., Mottaghy & Rath 2006).

Our problem space extends to a depth of 1000 m along a 14 km hypothetical transect. Lakes of diameter 20 m, 50 m, 100 m, 200 m, 500 m, 1 km, 2 km and 4 km are situated at a spacing that ensures minimal thermal disturbance of adjacent lakes but which is, however, not untypical of the spacing of lakes on Richards Island and the Tuktoyaktuk Peninsula. The goal was to develop, without the advantage of a full 3-dimensional code but with the flexibility of applying quasi-continuous surface boundary conditions, a model that could be applied easily to an actual transect across this region (see Discussion). Water depth in Mackenzie Delta lakes is typically a few meters (Mackay 1963) and is not explicitly

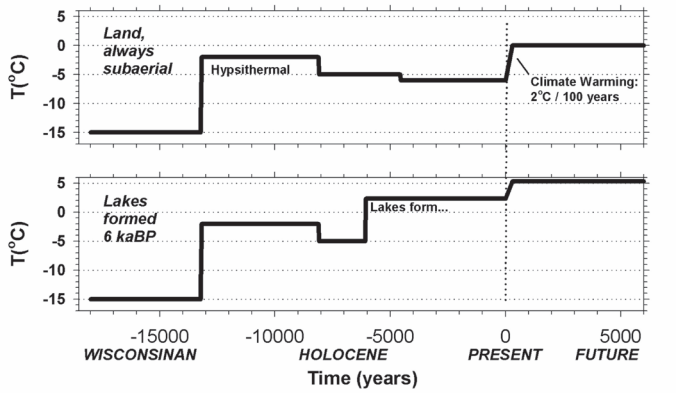

Figure 2. Ground surface/lakebed transient boundary conditions of the model (see Taylor et al. 1996, 63-65; 1999 for development and references).

considered in the model, except that our results apply only to the central basins of sufficient depth that water does not freeze to the bottom in the winter.

Physical properties

Unfrozen water content as a function of sub-0°C temperature (Smith & Tice 1988) is a primary physical property for permafrost modeling, and refers to pore water that remains in the liquid phase even though its temperature is below 0°C. The Geological Survey of Canada has measured unfrozen water content, porosity, salinity, and grain-size distributions for a suite of some 30 subsurface soils from the Mackenzie-Beaufort area (Dallimore & Matthews 1997). Curves of unfrozen water content as a function of sub-0°,C temperature were chosen that are typical of sand, clayey silt and clay (Fig. 1a). Nowhere does clay fully constitute the entire permafrost section in the Delta, but clay was chosen to compare with sand as geologic "end members" of typical Delta soils. Averages of ~ 2000 measured thermal conductivity values (needle probe method), and unfrozen water content curves from previous field programs (Dallimore 1991, 1992) were used to calculate conductivity-temperature profiles for these three lithologies (Fig. 1b). Thermal heat capacity was calculated from the constituent fractions of soil particles, frozen (ice), and unfrozen water. The phase change temperature assumed for pore water is 0°C. Note that as fine-grained sediments freeze or thaw, the latent heat is distributed over a range of temperatures, according to the unfrozen water content curve (Fig. 1a). TEMP/W fully accommodates such a "distributed" latent heat budget of freeze/thaw. The latent heat of the water is 3.38 x $10^8 J \cdot m^{-3}$; hence for soil volumetric latent heat is less, depending on the porosity.

Boundary conditions

Steady state condition. A geothermal heat flux of 69 $mW \cdot m^{-2}$ (Judge 1973, Majorowicz 1996, Fig. 16) was applied at 1 km depth for all models and times.

Initial and transient surface boundary conditions provide the basic constraints under which the geothermal regime is modeled in the forward sense, from ~13 kaBP through the

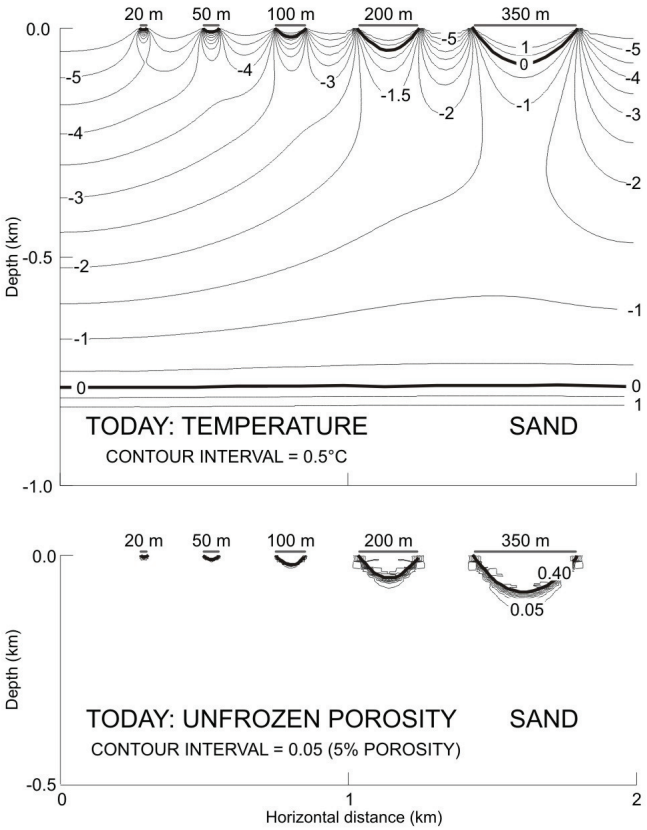

Figure 3a. Modeled present-day temperature vs. depth (upper; contours in °C) and fractional unfrozen volumetric water content (lower) beneath lakes of various sizes (20–350 m diameter) for a sand lithology with volumetric porosity 40%; thus 0.4 designates a totally thawed sand.

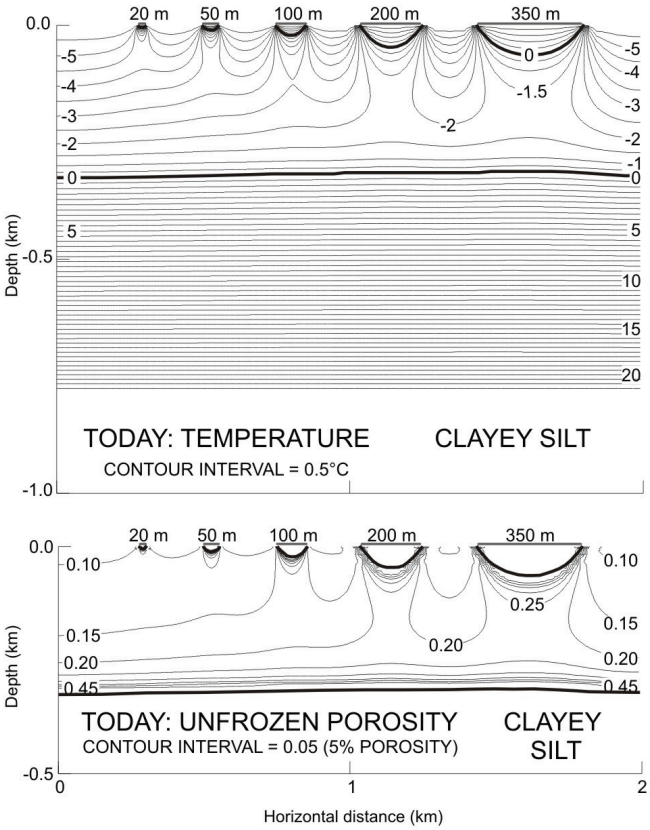

Figure 3b. As above, for a clayey-silt lithology; volumetric porosity 48%; thus, 0.25 indicates sediment in which about half the pore space is unfrozen water.

present to ~13 kaAP (after present). Boundary conditions were developed from the literature for earlier work and were verified through their successful prediction of temperatures measured today (see Taylor et al. 1996 for citations).

Initial conditions provide the geothermal structure at the end of the Wisconsinan from which forward modeling is initiated. Permafrost temperatures at ~13 kaBP were assumed to be in quasi-equilibrium with surface temperatures of -15°C (typical of severe arctic conditions for unglaciated areas) and with the steady state geothermal heat flux.

Transient boundary conditions specify the variation of ground surface temperature through time, forward from the steady state and initial boundary condition at 13 kaBP and at different points along the hypothetical 14-km transect through lakes. Two surface boundary conditions are considered: land that is always subaerial (temperatures variable), and lakes. See Taylor et al. (1996, 63-65) for discussion of subaerial temperatures assumed throughout the Holocene. Lake bottom temperatures were assumed +2.3°C (cf. Burn 2002, +2 to 4°C, 1290). Geological evidence suggests that lakes formed as early as 10,000 to about 6000 years ago (e.g., Mackay 1992); the numerical model applies the subaerial boundary condition prior to those times, and a combination of the subaerial and the lake boundary conditions following lake formation; lakes are assumed to form to full size, a simple "step change" ramped over ~100 years (Fig. 2). The Little Ice Age is not considered. Finally, we invoke a scenario of contemporary climate warming, at 2°C per 100 years for land and half that value for water temperatures for 300 years following the present, thus reaching +0.1°C (land) and +5.3°C (lakes) by 300 aAP. At that time, the transient boundary conditions represent a non-sustainable permafrost environment. Modeling results are saved at frequent time intervals, allowing a depiction of the gross evolution of the two-dimensional ground thermal state.

Model Results

Time slice – present

Figure 3 presents contours of the present transient geothermal regime for lakes formed 6 kaBP in (a) sand, and (b) in clayey silt lithology. The base of permafrost is more than twice as deep in sand due to the effect of higher thermal conductivity (Fig. 1b). Thermal taliks beneath lakes are defined by the upper 0°C isotherm and the base of permafrost is defined by the lower 0°C isotherm. There are two critical observations: (1) Temperature contours are very similar in character for both sand and clayey silt; but (2) the unfrozen water content contours are very different, with <5% volumetric unfrozen water content in sand beneath all lakes regardless of size, whereas >15% unfrozen water content in clayey silt beneath lakes >100 m diameter. The through-

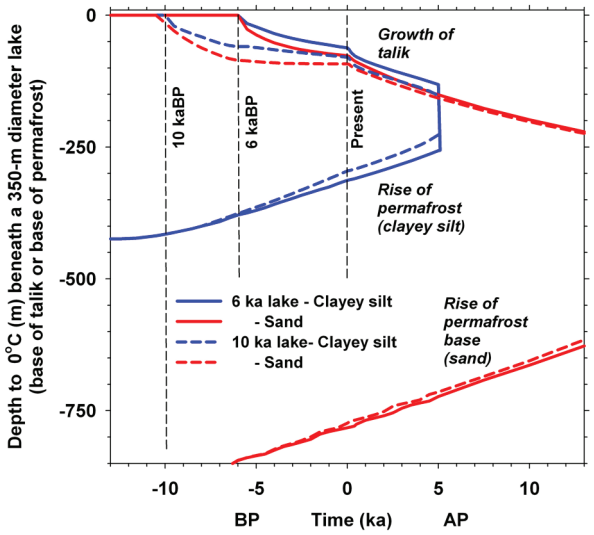

Figure 4. Growth of a talik and rise of permafrost base beneath a 350 m diameter lake, following lake formation at 10 kaBP or 6 kaBP on a permafrost landscape of sand or clayey silt.

going "hourglass" of partially unfrozen soils beneath lakes is absent in sand. These contrasting regimes are directly related to the contrast in unfrozen water content curves in the two lithologies, such that at sub-zero temperatures within a few degrees of 0°C, a comparatively large fraction of pore water remains in the liquid phase in clayey silt compared to sand (Fig. 1a). As a direct result, geophysical taliks (soils having high unfrozen water contents) completely penetrate the permafrost in a clayey silt substrate, while sands underlying lakes of comparable size are almost completely frozen.

Growth of taliks after mid-Holocene lake formation

Figure 4 shows thermal talik development and evolution of permafrost during the Holocene. Today, thermal taliks extend possibly 20 m deeper beneath lakes formed at 10 kaBP than at 6 kaBP. In our model, the 0°C isotherm fully penetrates the permafrost within several hundred years of lake formation on a hypothetical clay lithology (not shown), within ~5 kaAP in clayey silt under contemporary climate warming, and apparently only after several tens of thousand years in sand. The permafrost base rises throughout the Holocene. Many lakes forming ~10 kaBP contracted in size by the mid-Holocene, leaving lacustrine "halos" surrounding some present-day lakes (unit L in Rampton 1988); modeling showed that the geothermal effect at the present time is very small.

Regime beneath lakes and intervening land

Figure 5 depicts the present thermal regime beneath adjacent 100 m and 200 m lakes and the 150 m of land separating them as predicted by the transient model (clayey silt). The expected regime if ground thermal conditions were in equilibrium with today's climate is also shown (lighter

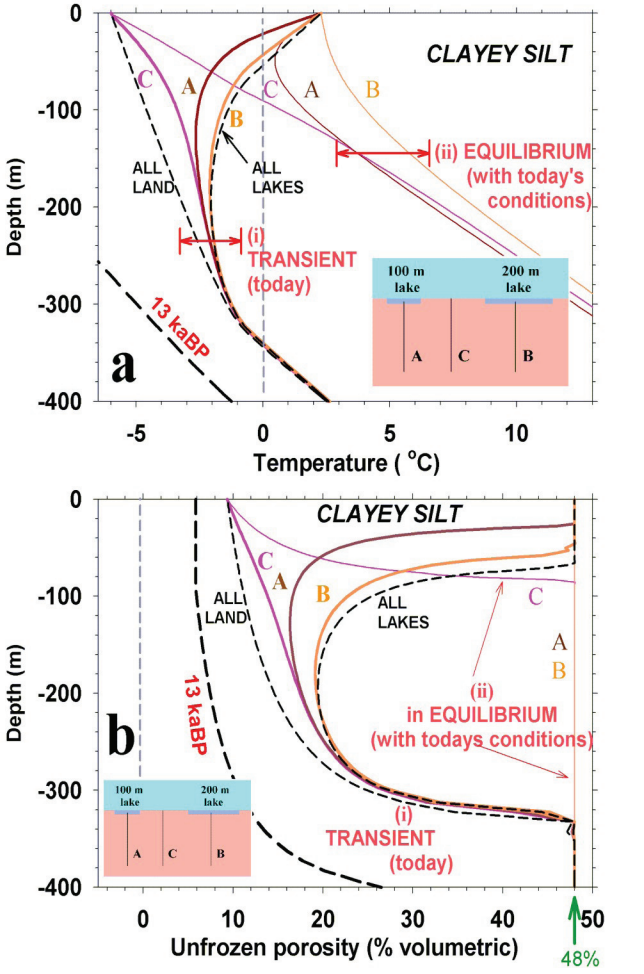

Figure 5. Thermal regime predicted in a clayey silt lithology for today beneath two adjacent lakes (A and B in the insets) and the land separating them (C). (a) transient temperature profiles (i), and equilibrium temperature profiles (ii) for today's surface conditions. (b) volumetric unfrozen water content. Transient profiles labeled "all land" and "all lakes" are bracketing "end member" cases of a landscape that is lake-free or fully inundated.

curves) to demonstrate the fallacy of such an assumption (see "Discussion" for field evidence). Profiles labeled "all land" and "all lake" are the end-member scenarios of the extent of lake coverage and bracket the profiles predicted for a lake-dominated landscape. The temperature profiles beneath lakes 100 m and 200 m in diameter ("A" and "B") contrast to the profile ("C") beneath their shared inter-lake area. Both temperatures and unfrozen water contents deeper than ~300 m appear largely independent of surface conditions (i.e., lakes or land, or Holocene climate change) while at depths less than ~300 m, temperatures reflect the surface environment and Holocene warming. The depth to the base of the sub-lake thermal talik increases from ~ 21 m (100 m diameter lake) to ~40 m (200-m lake, Fig. 5a).

Permafrost with low volumetric unfrozen water content (~6%) underlies all land at 13 kaBP, as predicted by the

unfrozen water curve at –15°C for clayey silt (Fig. 1a) and a soil porosity of 48%. The impact of lakes on the modern landscape is to raise the minimum unfrozen water content to ~10% beneath the intervening land between lakes, and to ~16%–20% beneath lakes >100 m in diameter. Hence, almost half the pore space is unfrozen beneath larger lakes situated on clayey-silt sediments, although ground temperatures remain <0°C. Unfrozen water content, and hence sediment permeability within these geophysical taliks, may be sufficiently high to facilitate vertical transport of water and/or gas from deeper horizons to the surface in these environments (e.g., Williams & Smith 1989, §7.5).

The depth to the base of the thermal talik increases with lake diameter, to a maximum of ~50 m under the largest lakes or an "all lake" landscape (clayey silt) and ~85 m (sand), and at present continues to increases at ~4 m/1000 years at present. In contrast, the permafrost base is rising at ~10 m/1000 years (Fig. 4). The depth to the minimum of the unfrozen water content profile is about 4 to 5 times deeper than the depth to 0°C in clayey silt; and the value of the minimum unfrozen porosity is ~20% in clayey silt and <3% in sand. There is little indication of a "geophysical talik" in sand (Fig. 3a, lower).

Discussion and Conclusions

Our finite element geothermal model demonstrates that the present permafrost geothermal regime is in disequilibrium following the onset of the Holocene, and that for lithologies typical of the Mackenzie Delta, the continuous permafrost is not perforated by through-going thermal taliks (i.e., temperatures >0°C) beneath Holocene lakes of any size. However, '"geophysical taliks"' do penetrate the permafrost beneath lakes due to the substantial unfrozen water content of clayey silts at negative temperatures to about -7°C (Fig. 1a). There is some field evidence in support of our interpretation of modeling results and for the presence of both thermal and geophysical taliks beneath lakes. Pre-drainage temperatures beneath the centre of Illisarvik Lake reach -3°C at 84 m with the sub-lake talik extending to ~32 m (Burgess et al. 1982). Temperatures to ~350 m below seabed in the Amauligak geotechnical hole some 80 km offshore in 32 m of water on the Beaufort Shelf are near isothermal at -2.3°C, a good analogy to the "all lakes" model of Figure 5 (Taylor et al. 1989). Beneath a small island in Parsons Lake, permafrost is >300 m deep, similar to depths at several wells surrounding the lake (Judge et al. 1981). Electromagnetic soundings provide some field evidence of the unfrozen water content of sub-talik sediments (Geophysicon 1983, Todd & Dallimore 1998).

Interpretation of 3-dimensional seismic data by Riedel et al. (2006) provides evidence of seismic blanking beneath shallow lakes in the vicinity of Mallik Bay, Richards Island, possibly due to lower seismic velocities in sub-lake sediments containing significant unfrozen water.

The geology of the Pleistocene Mackenzie Delta is largely sands, silts, and clayey silts, at least through permafrost (Dallimore 1992). Where lithology tends towards finer-grained sediments, our model suggests that geophysical taliks may perforate the permafrost beneath lakes, and the elevated unfrozen water content may have implications for the migration of ground water and/or hydrocarbon gases from below permafrost to the surface. In the case of natural gases such as methane, these conduits may provide physical pathways for the transport of greenhouse gases from deep geological sources (conventional hydrocarbon reservoirs and/or gas hydrate deposits) into the atmosphere.

Our model is meant to be a gross prediction of the thermal regime evolving from the initial formation of lakes in the early to mid-Holocene. The gradual *ab initio* enlargement of lakes (e.g., ~1 m/a at 10 ka or 6 kaBP) is not modeled and may be a negligible effect on the subsurface thermal regime today. An inherent assumption in the 2-D model is the "'third dimension" that extends to infinity. Hence, our model more correctly represents a transverse section across a river. For our model, the result is a moderately enhanced talik development arising from the unconstrained third dimension, especially under smaller lakes. An alternative quasi-3D model could be developed in cylindrical symmetry (e.g., Ling & Zhang 2003), better to model details of the thermal impact of an isolated lake but less appropriate to model transects of the closely-spaced lakes of the Mackenzie Delta where we might expect substantial thermal effect of one lake on another (e.g., Figure 3 predicts permafrost temperature between the lakes is higher than away from the lakes).

To the authors' knowledge, there are no "through-permafrost" temperature profiles with which to constrain our model. The intent here is to present a simple model constrained by the literature and reasonable geological assumptions. Current numerical methods enable almost any detail of lake evolution to be modeled; however, the most significant limitation remains the lack of relevant field measurements to constrain the models.

Acknowledgments

This research was supported by the Program of Energy Research and Development, Natural Resources Canada. Comments of two anonymous reviewers helped clarify the presentation. The authors thank Michelle Côté for assistance with the figures.

References

Brown, W.G., Johnston, G.H. & Brown, R.J.E. 1964. Comparison of observed and calculated ground temperatures with permafrost distribution under a northern lake. *Canadian Geotechnical Journal* 1: 147-154.

Burgess, M.M., Judge, A., Taylor, A. & Allen, V. 1982. Ground temperatures studies of permafrost growth at a drained lake site, Mackenzie Delta. In: H.M.

French (ed.), *Proceedings of the Fourth Canadian Permafrost Conference, Calgary.* Nat. Res. Council of Canada. 3-11.

Burn, C.R. 2002. Tundra lakes and permafrost, Richards Island, western Arctic coast, Canada. *Canadian Journal of Earth Sciences* 39: 1281-1298.

Dallimore, S.R. (compiler) 1991. *Geological, Geotechnical and Geophysical Studies along an Onshore-Offshore Transect of the Beaufort Shelf.* Open File 2408. Geological Survey of Canada.

Dallimore, S.R. (compiler) 1992. *Borehole Logs from Joint GSC-Industry Mackenzie Delta Geology/Permafrost Transect.* Open File 2561. Geological Survey of Canada.

Dallimore, S.R. & Matthews, J.V., Jr. 1997. *The Mackenzie Delta Borehole Project.* Environment Studies Research Funds Report No. 135. Calgary, Canada. 1 CD-ROM.

Dyke, A.S. & Prest, V.K. 1987. *Paleogeography of Northern North America, 18,000–5,000 Years Ago.* Map 1703A. Geological Survey of Canada.

Geophysicon, Ltd. 1983. *Detection of Permafrost Base in Permafrost Areas–Transient Electromagnetic Survey in Mackenzie Delta Area, N.W.T.* Open file 83-17. Earth Physics Branch, EMR Canada.

GeoSlope International Ltd. 2004. *TEMP/W, Software for Finite Element Geothermal Analys., version 6,* Calgary, AB: Geo-Slope International Ltd.

Hwang, C.T., Murray, D.W. & Brooker, E.W. 1972. A thermal analysis for structures on permafrost. *Can. Geotech. J.* 9 (1).

Judge, 1973. The prediction of permafrost thickness. *Can. Geotech. J.* 10: 1-11.

Judge, A.S., Taylor, A.E., Burgess, M.M., & Allen, V.S. 1981. *Canadian Geothermal Data Collection–Northern Wells 1978-80.* Earth Physics Branch, Geothermal Series 12, 190 pp.

Judge, A.S., Pelletier, B.R. & Norquay, I. 1987. Permafrost base and distribution of gas hydrates. In: B.R. Pelletier (ed.), *Marine Science Atlas of the Beaufort Sea: Geology and Geophysics.* Miscellaneous Report 40. Map 39. Geological Survey of Canada.

Lachenbruch, A.H. 1957. Thermal effects of the ocean on permafrost. *Geol. Soc. Am. Bull.* 68: 1515-1530.

Ling, F., & Zhang, T. 2003, Numerical simulation of permafrost thermal regime and talik development under shallow thaw lakes on the Alaskan Arctic Coastal Plain, *J. Geophys. Res.* 108(D16): 4511, doi: 10.1029/2002JD003014.

Mackay, J. Ross. 1963. *The Mackenzie Delta area, N.W.T.* Mem. 8. Geogr. Branch, Ottawa, Ontario (reprinted). Misc. Rep. 23. Ottawa, Ontario: Geological Survey of Canada, 202 pp.

Mackay, J. Ross. 1992. Lake stability in an ice-rich permafrost environment: examples from the western arctic coast. In: R.D. Robarts & M.L. Bothwell (eds.), *Aquatic ecosystems in Semi-Arid Regions: Implications for Resource Management.* NHRI, Environment Canada, Saskatoon, Symposium Series 7: 1-26.

Majorowicz, J.A. 1996. Regional geology and geophysical setting: geothermics. In: J. Dixon, (ed.), *Geological Atlas of the Beaufort-Mackenzie Area.* Miscellaneous Report 59. Maps 15 & 16. Geological Survey of Canada.

Mottaghy, D. & Rath, V. 2006. Latent heat effects in subsurface heat transport modelling and their impact on palaeotemperature reconstructions, *Geophys. J. Int.* 164: 236-245, doi:10.1111/j.1365-246X.2005.02843.

Rampton, V.N. 1988. *Quaternary Geology of the Tuktoyaktuk Coastlands, Northwest Territories.* Memoir 423. Geological Survey of Canada.

Riedel, M., Bellefleur, G., Dallimore, S.R., Taylor, A. & Wright, J.F. 2006. Amplitude and frequency anomalies in regional 3D seismic data surrounding the Mallik 5L-38 research site, Mackenzie Delta, Northwest Territories, Canada, *Geophysic.* 71: B183–B191.

Smith, M.W. & Tice, A.R. 1988. *Measurement of the Unfrozen Water Content of Soils: Comparison of NMR and TDR Methods.* CRREL Report 88-18. U.S. Army Cold Regions Research and Engineering Laboratory, 11 pp.

Taylor, A.E., Burgess, M.M., Judge, A.S., & Allen, V.S. 1982. *Canadian Geothermal Data Collection - Northern Wells 1981.* Earth Physics Branch, Geothermal Series 13: 153 pp.

Taylor, A.E., Judge, A.S. & Allen, V.S. 1989. *Recovery of Precise Offshore Permafrost Temperatures from a Deep Geotechnical Hole, Canadian Beaufort Sea.* Paper 89-1D. Geological Survey of Canada, 119-123.

Taylor, A.E., Dallimore, S.R. & Judge, A.S. 1996. Late Quaternary history of the Mackenzie-Beaufort region, arctic Canada, from modelling of permafrost temperatures: 2. the Mackenzie Delta-Tuktoyaktuk Coastlands. *Canadian Journal of Earth Sciences* 33(1): 62-71.

Todd, B.J. & Dallimore, S.R. 1998. Electromagnetic and geologic transect across permafrost terrain, Mackenzie River delta, Canada. *Geophysics* 63: 1914-1924.

Williams, P.J. & Smith, M.W. 1989. *The Frozen Earth.* Cambridge: Cambridge Univ. Press, 306 pp.

The Impact of Sediments Derived from Thawing Permafrost on Tundra Lake Water Chemistry: An Experimental Approach

M.S. Thompson
Water and Climate Impacts Research Centre, Department of Geography, University of Victoria, Victoria, Canada
S.V. Kokelj
Water Resources Division, Indian and Northern Affairs Canada, Yellowknife, Canada
T.D. Prowse
Water and Climate Impacts Research Centre, Environment Canada, Department of Geography, University of Victoria, Victoria, Canada
F.J. Wrona
Water and Climate Impacts Research Centre, Environment Canada, Department of Geography, University of Victoria, Victoria, Canada

Abstract

Retrogressive thaw slumping can transport ion-rich meltwater and thawing sediment from terrestrial to aquatic systems. Tundra lakes affected by shoreline slumping have elevated ionic concentrations, low dissolved organic matter concentrations, and colour compared to unaffected lakes. To investigate the potential photochemical implications, an in situ microcosm experiment was performed involving the incubation of water from an undisturbed lake with thawed slump sediment. Sediment treatments were 10, 25, and 50% of the total container volume, and containers were incubated in the lake for 52 days during the summer of 2007. Water colour decreased successively with sediment volume, and was highest in the control. Specific conductivity was more than 8 times higher in the 50% sediment treatment water than in the control. Sedimentation of organic matter may explain the low colour in the treatment water. The transportation of thawing permafrost sediment into tundra lakes may rapidly increase water clarity and alter carbon supply.

Keywords: climate change; coloured dissolved organic matter; Mackenzie Delta region; microcosm experiment; retrogressive thaw slumping; tundra lakes.

Introduction

In the uplands east of the Mackenzie Delta, NWT, Canada, thousands of small lakes and ponds are surrounded by terrain underlain by ice-rich permafrost (Mackay 1992, Kokelj et al. 2005). In this region, thawing of the near-surface permafrost commonly leads to the formation of large retrogressive slumps on slopes adjacent to lake shores (Lantz & Kokelj 2008). Solute concentrations in permafrost may be enriched with respect to the overlying active layer (Kokelj & Burn 2003, 2005). The geochemical contrast between the active layer and permafrost is attributed to progressive leaching of soluble materials from seasonally thawed soils and preservation of solutes in underlying frozen sediments, and due to thermally induced migration of water and soluble materials from the base of the active layer into the top of permafrost (Kokelj & Burn 2005). Thaw slumping may release these solutes in the permafrost, with implications for sediment and runoff chemistry (Kokelj & Lewkowicz 1999).

A survey of 298 lakes on five 49 km^2 study plots between Inuvik and the Beaufort Sea indicated that 6 to 17% of the lakes were affected by shoreline slumping (Kokelj et al. 2005). Thaw slumps can be relatively large compared to the size of adjacent lakes. In a sample of 11 first-order upland lakes affected by slumping in the Delta region, the median disturbance area: lake area ratio was 0.48 (Kokelj et al. 2005). The median disturbance size was 1.9 ha, and the median lake size was 4.0 ha. In many cases, disturbance area was almost equivalent to lake area.

Lake chemistry interactions

The water chemistry of small tundra lakes is strongly influenced by lake catchment characteristics, including surficial geology, sediment development, peatland extent, and terrestrial vegetation (Pienitz et al. 1997, Duff et al. 1999, Frey & Smith 2005, Gregory-Eaves et al. 2000, Rühland et al. 2003). In the Mackenzie Delta region, a survey of 22 lakes indicated that those adjacent to retrogressive thaw slumps had elevated ionic concentrations, lower concentrations of dissolved organic carbon (DOC), and were less coloured compared to lake waters in undisturbed areas (Kokelj et al. 2005). Organic carbon supply and related changes in visible and UV light penetration influence the productivity of pelagic algal and bacterial communities (Jones 1992, Teichreb 1999).

Base cations can increase the adsorption and flocculation of coloured dissolved organic matter (CDOM), or humic matter, from the water column (reviewed in Jones 1992, Thomas 1997). Mineral soils, especially clays, that may enter lakes can adsorb humic matter leading to sedimentation (reviewed in Jones 1992, Thomas 1997). This raises the possibility

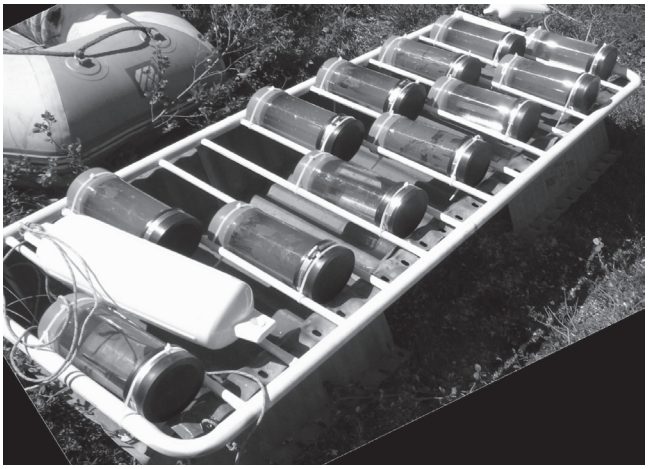

Figure 1. Experimental incubation containers positioned on rack prior to deployment in the lake.

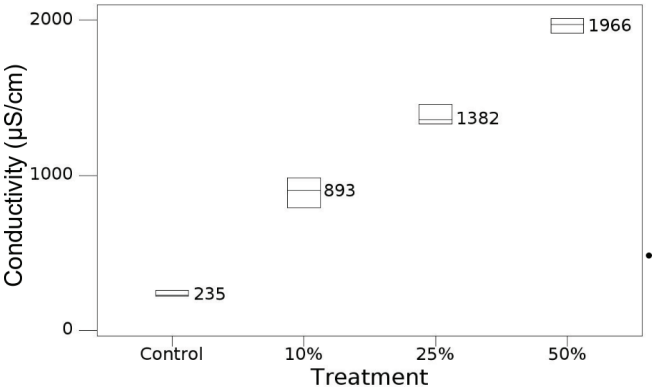

Figure 2. Mean specific conductivity of the incubated lake water in each of the permafrost sediment treatment and control containers (with 95% confidence intervals, mean value provided).

that sediment and soluble ions delivered from terrestrial to aquatic systems by the process of thaw slumping may affect CDOM concentrations and optical properties of water in small tundra lakes.

Here we examine the effects of ion and sediment additions on the colour of lake water by undertaking an incubation experiment. The goal was to test whether exposure of humic lake water to thawed permafrost sediment and associated runoff could produce similar water chemistry conditions characteristic of a "disturbed" lake affected by lake shore thaw slumping.

Methods

Incubation experiment

Recently-thawed sediments and pooled surface runoff were collected on 24 June 2007 from a thaw slump scar located on the shore of a small lake 60 km north of Inuvik. The sediments, comprised of silty clay, were homogenized by mixing with surface water collected from the slump (specific conductivity 2345 µS/cm) to form a saturated slurry. The gravimetric water content of the runoff-sediment mixture was 33% by weight.

The sediment mixture was added to containers constructed from sections of clear acrylic pipe (approximately 10 cm diameter) with a total volume of 2 L. The pipe sections were sealed on one end with a silicone-sealed cap and on the other with a removable rubber "test cap". A spectral scan of the acrylic pipe material indicated that it blocked most UV-B (absorbance at 320 nm = 1.027) and much of the UV-A (absorbance at 380 nm = 0.096) wavelength range. This desirable property of the pipe materials minimized the breakdown of coloured humic substances in lake water by incoming UV radiation (photolysis). The proportion of saturated sediment in each of three replicated container sets was 50, 25 and 10% of the container volume (1.0, 0.5, and 0.2 L respectively).

The incubation containers were installed in a shallow (estimated Z_{max}: 2 m), humic lake within 15 minutes road access of Inuvik, which is unaffected by thaw slumping. Before installation, surface lake water from the same incubation lake site was collected and added to each of these containers, along with a set of replicate control containers, to a total volume of 2 L. The sediment slurry in each container was purposefully not mixed homogeneously with the lake water, since slump materials often enter the lakes as intact blocks. The containers were sealed immediately after the lake water addition, and were attached to a rack apparatus which kept the containers horizontally aligned, approximately 0.75 m below the water surface and elevated approximately 0.75 m above the lake benthos (Fig 1). The containers were installed on 6 July 2007 and were retrieved on 28 August 2007 for a total incubation period of 52 days.

An additional container was filled with distilled and deionized water in order to test the water-tightness of the container seals. Initial specific conductivity of the distilled water was 2 µS/cm; —after incubation it was 20 µS/cm. Specific conductivity in the lake was 219 µS/cm just prior to deployment of the incubation containers.

Analysis

Following retrieval, the containers were removed from the support rack, immediately transported and refrigerated at the Aurora Research Institute lab. Within 3 hours of arrival at the lab, the incubated water was removed from the containers without disturbing the sediment settled at the bottom of each container. Specific conductivity, pH, dissolved oxygen (DO) and oxidation-reduction potential (ORP) of the water was measured using a YSI 556 multiprobe meter (Yellow Springs Instruments, Idaho, USA).

In preparation for measurement of water colour as spectral absorbance, a 125 ml volume of the incubated water was filtered through a 0.45 µm Supor membrane syringe filter (Pall Corporation, NY, USA). Samples were placed in glass containers and kept in a dark refrigerated area until absorbance could be measured. Absorbance was measured across the range 190–900 nm using an Ultrospec 3100 pro spectrophotometer equipped with a 1 cm cuvette (Biochrom, Cambridge, UK). Absorbance measurements at 320 nm (UV-B), 380 nm (UV-A) and 440 nm (PAR, photosynthetically active radiation) were corrected for

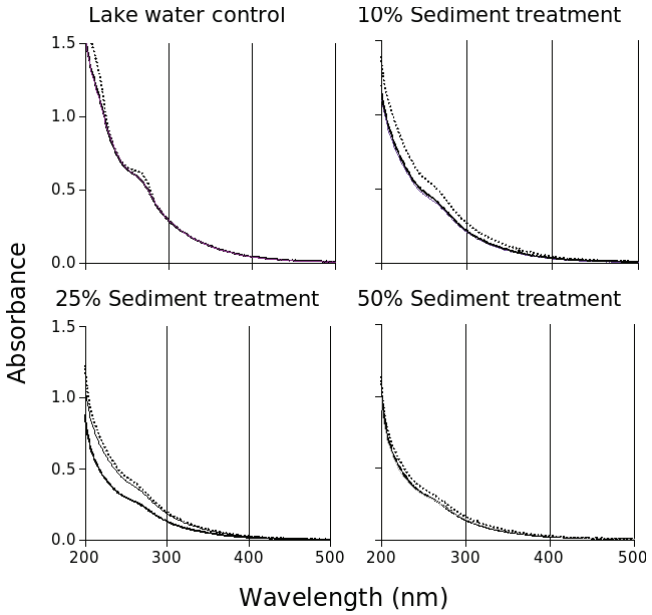

Figure 3. Replicate spectral scans of incubated lake water from the control and each sediment treatment container. For each treatment graph, $n = 3$.

turbidity-related light scattering by subtracting absorbance values at 740 nm. These corrected values were used in statistical analyses.

A one-way analysis of variance (ANOVA) was used to assess the response of the lake water specific conductivity to the sediment treatments. The effect of the sediment treatments on the spectral absorbance of the incubated lake water was tested using a repeated measures ANOVA, including absorbance values at wavelengths in the UV-B (320 nm), UV-A (380 nm) and photosynthetically active radiation (PAR, 440 nm) ranges. Post hoc Tukey tests were used to distinguish between significantly different treatment level. Finally, conductivity and all absorbance measurements were tested for significant Pearson correlations across treatments, with Bonferroni adjusted significance levels. All analyses were completed using SPSS 13.0 (SPSS Inc., Illinois, USA).

Results

Specific conductivity

The measured specific conductivity of the incubated lake water in each of the treatment and control containers are shown in Figure 2. The water at each sediment treatment level and in the control had significantly different mean specific conductivity, with relatively little variation within treatments (one-way ANOVA, $F = 396.23$, $df = 3$, $p < 0.000$). The control and treatment mean specific conductivities were all significantly different from each other (Tukey HSD test).

Water colour

The spectral scan absorbance values for each treatment replicate are shown in Figure 3. Absorbance is generally higher in the control than in all sediment treatments. The greatest difference in the absorbance values between the control and all sediment treatments is apparent in the UV-B and UV-A range (280–320 nm and 320–400 nm, respectively). Differences between the control and treatments in the photosynthetically active radiation range (PAR, 400–700 nm) were lower than observed for the UV range. Relative change in absorbance between the control and treatments for representative wavelengths are provided in Table 1. The change in absorbance across wavelengths in the 25% sediment treatment is somewhat obscured by one low-absorbance replicate (Fig. 3).

Table 1. Relative decrease in mean spectral absorbance at representative wavelengths of lake water after incubation with thaw slump sediment. Change is relative to the untreated control mean. *PAR* is photosynthetically active radiation. *aX* is absorbance at wavelength X.

Sediment treatment	UV-B (a320)	UV-A (a380)	PAR (a440)
50%	49%	43%	27%
25%	43%	44%	44%
10%	20%	22%	13%

The highest correlation occurred with UV-B absorbance ($r = -0.91$), followed by UV-A ($r = -0.85$) and PAR ($r = -0.64$). Absorbance was strongly positively correlated between the three wavelengths ($r > 0.85$).

There was a highly significant effect of sediment treatment on corrected absorbance at all three representative wavelengths (UV-B, UV-A, PAR) (repeated measures ANOVA, $F = 15.156$, $df = 3$, $p = 0.001$). Error variance between treatments for the 320 nm measurements was not homogeneous and could not be remedied via transformation however, and this must be considered when interpreting the ANOVA results. Post hoc tests found no significant difference ($p > 0.05$) between the control, the 10% and 25% sediment treatment, but did indicate a significant difference between the control and 50% treatment (Tukey's HSD test).

Negative correlations (Pearson's r) between incubated lake water specific conductivity and absorbance values in the UV and PAR range were statistically significant with the exception of the correlation with PAR (corrected $p > 0.05$).

Discussion

In the Mackenzie Delta uplands, lakes affected by shoreline thaw slumping contain elevated concentrations of major ions in contrast with lower concentrations in undisturbed lakes (Kokelj et al. 2005). The soluble materials that enrich the lakes are derived from the thawing ion-rich permafrost (Kokelj & Burn 2005). The effect of sediment slurry treatments had a similar effect on lake water specific conductivity in this experiment, as soluble ions were released into solution from the solute-rich slump sediment mixture.

In the natural setting, lakes affected by slumping have clear water in comparison with more coloured water in undisturbed lakes. The experimental response of lake water colour to the sediment treatments suggests that sediment slurry treatments caused the removal of coloured organic materials from the

lake water. This is indicated by the lower spectral absorbance in sediment-incubated lake water compared to the lake water control. High-molecular weight CDOM absorbs UV radiation very effectively (Scully & Lean 1994, Laurion et al. 1997), and the relatively high change in absorbance in the 50% and 10% sediment treatments at the UV-B and UV-A wavelengths compared to the PAR wavelength suggests that it is this type of DOM which has been removed from solution in the incubated water.

The within-treatment variability between replicates was relatively large in the 25% and the 10% sediment treatments. This contributed to the heteroscedasticity in the 320 nm absorbance range and the nonsignificant Tukey test between these treatments. Presence of a slight biofilm on a few of the containers walls, variation in sediment-water interface surface area, and variations in possible photolysis rates may contribute to observed within-treatment differences.

Allochtonous (origin outside the lake, terrestrial) DOM content in lake water is linked to catchment conditions, especially the supply (related to catchment vegetation) and the delivery (related to catchment morphology) of carbon (Rasmussen et al. 1989, Pienitz et al. 1997). Subarctic lakes with catchments underlain by permafrost are typically high in DOM because waters are derived from surface runoff through a thin, often organic-rich active layer (Pienitz et al. 1997). Allochtonous DOM usually has a higher molecular weight and is more highly coloured than autochtonous (origin inside the lake) DOM (Lean 1998, Perdue 1998). Catchment-derived carbon is also generally more reactive with metals and base cations due to its more aromatic structure (Perdue 1998). Adsorption of this humic material to fine-grained clay particles readily occurs. Each of these processes can lead to dissolution and sedimentation of the allochtonous DOM. Field observations in conjunction with our experimental results indicate that degradation of permafrost within the catchment can influence the biological and geochemical availability of DOM within lakes (Kokelj et al. 2005).

Organic matter delivered from the lake catchment may be an important source of energy within the lake. For example, bacteria are known to utilize allochtonous sources of carbon as an energy supply (Jones 1992). DOM may also contain phosphorous, often a limiting nutrient for algal and bacterial production (Jones et al. 1988, Klug 2005). Indeed, uptake of DOM by algae and/or bacteria in the experimental containers used here may have contributed to the observed decrease in absorbance, especially if the slump sediment enhanced biological production by providing limiting nutrients (Hobbie et al. 1999). However, the habitat conditions within the incubation containers were likely not representative of *in situ* conditions, so that conclusions concerning biological activity cannot be made here. In addition to the role of DOM as an energy and nutrient source, allochtonous humic material is generally coloured, and capable of attenuating radiation within the water column. This can limit phytoplankton photosynthesis (Jones 1992, Klug 2002), but can also limit the penetration of damaging UV radiation through the water column (Laurion et al. 1997, Lean 1998).

Humic materials in lakes, therefore, can be involved in many interactions between planktonic biota through their effects on nutrient and light quality and supply. The fact that several of these interactions may be competitive or mutually beneficial, makes the ecological outcome of changes in tundra lake conductivity and DOM concentration difficult to predict. However, such shifts have been linked to the overall heterotrophic or autotrophic nature of lakes in northern/cold regions (Jansson et al. 2000). Certainly a reduction in humic matter content due to addition of ion-rich runoff and sediments derived from slumping permafrost appears to be capable of changing the physical and chemical conditions in the pelagic habitat of tundra lakes.

Acknowledgments

The authors gratefully acknowledge: M. Bothwell for advice regarding study design and analyses; D. Lynch for technical and laboratory assistance; T. Carter, W. Hurst, G. King, and P. Mesquita for field assistance. Support was provided by the Natural Sciences and Engineering Research Council, The Northern Scientific Training Program, the Department of Indian Affairs and Northern Development Canada, and the Aurora Research Institute.

References

DeHaan, H. 1992. Impacts of environmental changes on the biogeochemistry of aquatic humic substances. *Hydrobiologia* 229: 59-71.

Duff, K., Laing, T., Smol, J. & Lean, D. 1999. Limnological characteristics of lakes located across arctic treeline in northern Russia. *Hydrobiologia* 391: 205-222.

Frey, K.E. & Smith, L.C. Amplified carbon release from vast West Siberian peatlands by 2100. *Geophysical Research Letters* 32: L09401.

Gregory-Eaves, I., Smol, J., Finney, B., Lean, D. & Edwards, M. 2000. Characteristics and variation in lakes along a north-south transect in Alaska. *Archiv fur Hydrobiologie* 147: 193-223.

Hobbie, J.E., Peterson, B.J., Bettez, N., Deegan, L., O'Brien, W.J., Kling, G.W., Kipphut, G.W., Bowden, W.B. & Hershey, A.E. 1999. Impact of global change on the biogeochemistry and ecology of an Arctic freshwater system. *Polar Research* 18: 207-214.

Jansson, M., Bergstrom, A.-K., Blomqvist, P. & Drakare, S. 2000. Allochtonous organic carbon and phytoplankton/bacterioplankton production relationships in lakes. *Ecology* 81: 3250-3255.

Jones, R.I. 1992. The influence of humic substances on lacustrine planktonic food webs. *Hydrobiologia* 229: 73-91.

Jones, R.I., Salonen, K. & De Haan, H. 1988. Phosphorous transformations in the epilimnion of humic lakes: abiotic interactions between dissolved humic materials and phosphate. *Freshwater Biology* 19: 357-369.

Klug, J. 2002. Positive and negative effects of allochtonous dissolved organic matter and inorganic nutrients on phytoplankton growth. *Canadian Journal of Fisheries and Aquatic Sciences* 59: 85-95.

Klug, J.L. 2005. Bacterial response to dissolved organic matter affects resource availability for algae. *Canadian Journal of Fisheries and Aquatic Sciences* 62: 472-481.

Kokelj, S. & Burn, C. 2003. Ground ice and soluble cations in near-surface permafrost, Inuvik, Northwest Territories, Canada. *Permafrost and Periglacial Processes* 14: 275-289.

Kokelj, S. & Burn, C. 2005. Geochemistry of the active layer and near-surface permafrost, Mackenzie delta region, Northwest Territories, Canada. *Canadian Journal of Earth Sciences* 42: 37-48.

Kokelj, S.V., Jenkins, R.E., Milburn, D., Burn, C.R. & Snow, N. 2005. The influence of thermokarst disturbance on the water quality of small upland lakes, Mackenzie Delta Region, Northwest Territories, Canada. *Permafrost and Periglacial Processes* 16: 343-353.

Kokelj, S.V. & Lewkowicz, A. 1999. Salinization of permafrost terrain due to natural geomorphic disturbance, Fosheim Peninsula, Ellesmere Island *Arctic* 52: 372-385.

Lantz, T.C. & Kokelj, S.V. 2008. Increasing rates of retrogressive thaw slump activity in the Mackenzie Delta region, N.W.T., Canada. *Geophysical Research Letters* (GL032433, in press).

Laurion, I., Vincent, W. & Lean, D.R.S. 1997. Underwater ultraviolet radiation Development of spectral models for northern high latitude lakes. *Photochemistry and Photobiology* 65: 107-114.

Lean, D.R.S. 1998. Attenuation of solar Radiation in Humic Waters. In: D.O. Hessen & L.J. Tranvik (eds.), *Aquatic Humic Substances: Ecology and Biogeochemistry.* Germany: Springer, 109-124.

Mackay, J.R. 1992. Lake stability in an ice-rich permafrost environment: examples from the western arctic coast. In: R.D. Robarts & M.L Bothwell (eds.), *Aquatic Ecosystems in Semi-Arid Regions: Implications for Resource Management.* Saskatoon: Environment Canada, 1-26.

Pienitz, R., Smol, J. & Lean, D. 1997. Physical and chemical limnology of 59 lakes located between the southern Yukon and the Tuktoyaktuk Peninsula, Northwest Territories (Canada). *Canadian Journal of Fisheries and Aquatic Sciences* 5: 330-346.

Perdue, E.M. 1998. Chemical Composition, Structure, and Metal Binding Properties. In: D.O. Hessen & L.J. Tranvik (eds.), *Aquatic Humic Substances: Ecology and Biogeochemistry.* Germany: Springer, 41-61.

Rasmussen, J., Godbout, L. & Schallenburg, M. 1989. The humic content of lake water and its relationship to watershed and lake morphometry. *Limnology and Oceanography* 34: 1336-1343.

Rühland, K., Smol, J., Wang, X. & Muir, D. 2003. Limnological characteristics of 56 lakes in the Central Canadian Arctic Treeline Region. *Journal of Limnology* 62: 9-27.

Scully, N.M. & Lean, D.R.S. 1994. The attenuation of ultraviolet radiation in temperate lakes. *Ergebnisse der Limnologie* 43: 135-144.

Teichreb, C.J. 1999. *Effects of dissolved organic carbon as a bacterial growth substrate and as an ultraviolet-B radiation sunscreen for aquatic microbial foodwebs in Mackenzie Delta lakes, Northwest Territories*. M.Sc. Thesis. Simon Fraser University.

Thomas, J. 1997. The role of dissolved organic matter, particularly free amino acids and humic substances, in freshwater ecosystems. *Freshwater Biology* 38: 1-36.

Identification of Permafrost Landscape Changes Caused by Climate Variability in Central Siberia

Marina Tishkova
Institute of Environmental Geoscience, Russian Academy of Sciences
Sergey Gorshkov
Moscow State University named after M.V. Lomonosov

Abstract

The functioning of natural and natural/man-made ecosystems is impacted by changes in the duration of seasons more than by rising temperatures. Modeling changes in permafrost conditions caused by climate variability requires identifying the types of permafrost landscapes in terms of their sensitivity to climate changes, as well, as studying transformation rules for specific natural complexes. A large amount of data on changes occurring in the lower reaches of the Stony Tunguska River was gathered during field work of 1999–2007. For further analysis, active processes were classified as short-period and long-period, and as local and regional. Landscapes were classified by sensitivity level. Degradation of permafrost landscapes will occur in the order of sensitivity classes. Study of the most sensitive landscapes will be the most interesting for further research and yield the greatest value for monitoring.

Keywords: permafrost; Central Siberia; climate change; permafrost degradation; sensitivity.

Introduction

Woodwell and Mackenzie (1995) suggest that the Earth's climate is not just changing from one equilibrium to another, but probably is moving towards an unbalanced state, which we may already observe each year in the form of catastrophic climate events (Tchebakova 2006). The area of study (Fig. 1) is the low western edge of the Central Siberian Plateau in the lower reaches of the Podkamennaya Tunguska River. It is located in the periphery of discontinuous permafrost in the middle taiga subzone and thus is in an area vulnerable to climate change. The area presents a prime example of landscape ecotone diversity. Changes in many climate and landscape characteristics are evident, and we have been monitoring them in the course of our multi-year observations. In this paper, we discuss instability while recognizing that it is difficult to predict the patterns and rates of change. In order to predict changes in permafrost conditions in the current climate, it is necessary to identify types of permafrost landscapes in terms of sensitivity to climate change. It also is important to study the rules or mechanisms of transformation, patterns of landscape and climate change, and the individual and collective processes for specific natural complexes.

Methods

The methods that we used can be divided into two main categories: evaluation of meteorological data and collection of field data on terrain characteristics.

Meteorological data were evaluated using a range of applied methods. We used air temperature, precipitation, and snow cover data from the weather stations Bor, Vorogovo, Baikit, Yartsevo, and Bakhta. Data are available mainly from the 1980s on, and in some cases from the late 1960s onward. All these locations have high-quality meteorological stations operated by trained personnel. Annual, monthly, and daily

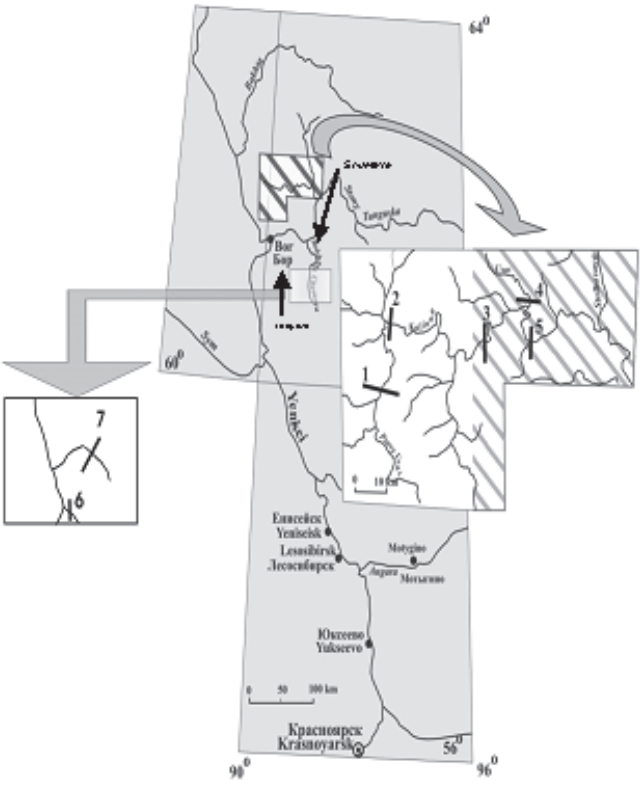

Figure 1. Key areas and transect locations on rivers: (1) Pravy Usas; (2–4) Kulinna; (5) Usas; (6) Bol'shaya Kolonka; (7) Malaya Kolonka; and (8) Bol'shaya Chernaya.

data were analyzed using standard statistics tools, such as differential-integral curves, probability/frequency curves, correlation coefficients, etc.

To evaluate the changes in temperature and precipitation over the last 60 years, their time series were approximated by a linear function of $y = ax + b$ type, where y was the

value of temperature (precipitation); *a* and *b* were empirical coefficients calculated using the least square method; and *x* was the year. The statistical confidence level was calculated by student criterion. A trend was considered to be statistically significant if the significance level (*P*) was equal to or greater than 0.95.

Landscape responses to the changing climate were evaluated through three main stages. First, we performed a preliminary analysis of satellite images for key areas overlaid with geological, forestry, geomorphology, topography, and fire distribution maps. Second, based on the above, we made our prognosis about the sensitivity of particular landscapes. Third, we confirmed our assumptions by actual field observations. This work was performed using ArcGIS software and GPS instrumentation in the field.

An important element of this combinational method was sampling along landscape transects. The sampling included terrain-unit descriptions, identification of reference soil catenas, detailed descriptions of soil, and measurement of active layer thickness and depth to the top of permafrost using a ground auger. Permafrost and non-permafrost landscapes were differentiated through direct observation using various indicators. Special attention was given to studying rock streams (kurums) and blockfields due to their high information value. In active rock streams we counted the abundance of blocks in an unstable position; in inactive blockfields, we studied forest/vegetation covers and the characteristics of tree stands (percentage of trees in non-vertical positions, the character of tree stand abnormalities, etc). Ground-auger measurements sometimes were of reduced quality, because not all of them were made in survey pits (used as control points for building transects) and many were made from the surface, and thus, liable to some error. Most of our survey pits were dug to the top of permafrost. During the latest field season, we also used temperature loggers but they provided clearly wrong data due to installation mistakes, so we did not use any of those data in our analysis.

Results

Climatic changes

As shown in the Synthesis Report on Climate Change 2001 (Watson et al. 2003), 1980 was an inflection point for positive temperature anomalies in relation to the average temperatures for the period of 1961–1990. Analysis of winter and summer temperatures and precipitation in the northern part of the Central Siberian Plateau shows that during 1980–2000, winters became 1°C warmer in comparison to the period prior to 1980. South of latitude 56°N, especially in the mountains, warming was even more significant, up 2–4°C. Summer warming proved to be as significant as the winter warming (1°C) with a high confidence level and the same scale on the south and on the north (Tchebakova 2006).

The linear trend of air temperatures in the area studied is positive for the past 60 years (data from the Bor village, latitude 61°35′N) (Fig. 2). A considerable increase in annual temperatures started in 1980, and in 1995 the anomaly exceeded a record 3°C. The most significant changes

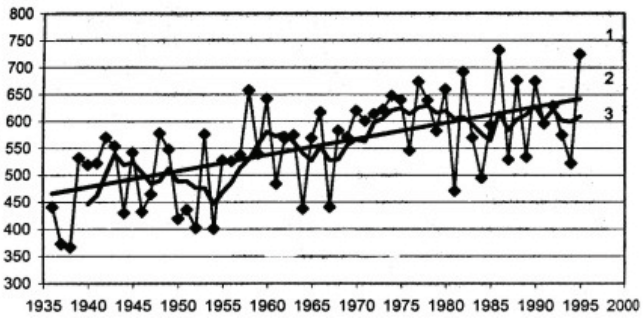

Figure 2. Precipitation at Bor meteorological station: 1 – annual precipitation, 2 – linear trend, 3 – 5-year moving average.

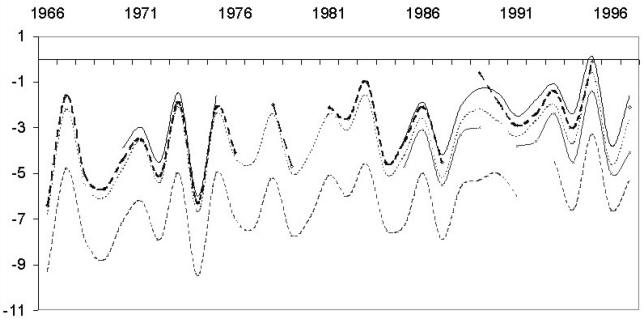

Figure 3. Annual average air temperatures (°C) at Vorogovo, Bor, Bakhta, Baikit, Yartsevo stations.

have occurred during the past 15 years. Analysis of winter (December to March) temperature changes over the past 60 years shows that December temperatures have risen by 3.5°C, and March temperatures have risen by 2.6°C, indicating that winters have become shorter and warmer. Analysis of summer temperature changes also reveals an increase in July and August temperatures. The trend is statistically significant (*P*=0.997 and 0.995 for July and August, respectively). On average, for the time period under consideration, July temperatures rose by 1.9°C, and August temperatures, by 1.1°C. No tendency was observable for June, and May temperatures became somewhat lower. Therefore, winter warming has been more significant than summer warming. A similar situation occurred in the latter half of the 19th century, when contemporaries observed winters becoming essentially less severe, and thawing happened more often (Fedorov 1991).

Annual precipitation for the last 60 years also showed a positive, statistically significant (*P*=0.999) trend, which was even more pronounced than the temperature trend (Fig. 3). The average increase in precipitation was 141 mm. It can be inferred, that this increase was caused by a rise of cyclone activity, especially in the last 20 years of the 20th century. The same process leads to air temperature rises. It should be noted that similar changes of general atmospheric circulation have been traced for the middle latitudes in the European part of Russia (Klimenko 1994). Thus, these changes can be considered global.

Snow accounts for only about 40 per cent of the total annual precipitation (which is 580 mm). There are no apparent trends for changes in snow cover depths.

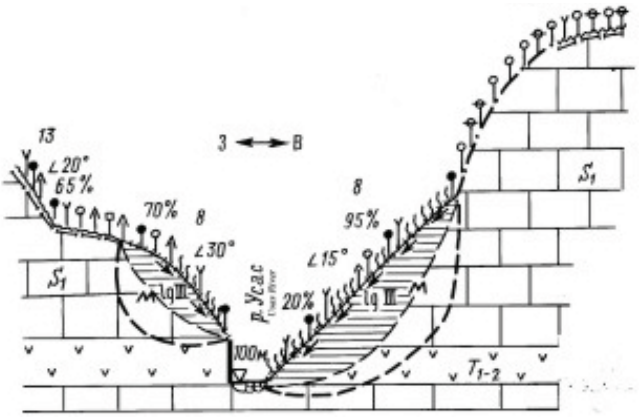

Figure 4. Transect on the Usas River near its mouth.

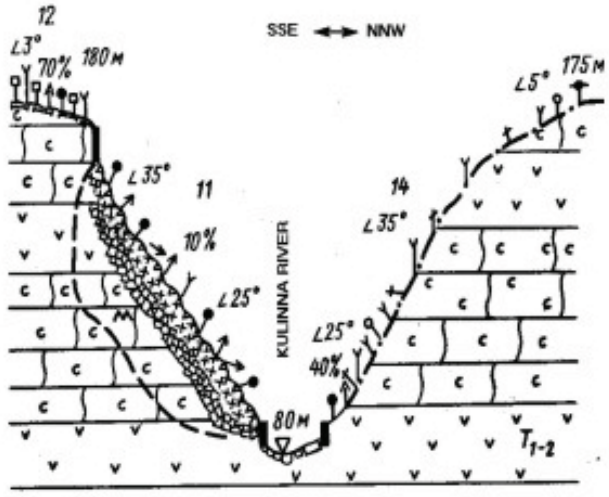

Figure 5. Transect on the Kulinna River near its third line of rapids.

Landscape responses

A large amount of data on changes in Siberian ecosystems was gathered during our field trips between 1999 and 2007. Two representative transects across the valley of the Usas and Kulinna rivers (tributaries of the Bol'shaya Chernaya River), which were sampled during 1999–2003, are shown in Figures 4 and 5.

The Bol'shaya Chernaya River transect crossed the valley with a strongly pronounced hummock swamp under stunted fir-birch taiga with sporadic larch. Hummocks were up to 50 cm in height and covered with true mosses. The depth to the top of permafrost reached 1.05 m under hummocks, and 80 cm under pits, measured from the water surface. This is abnormally deep for such conditions. Evidence of solifluction was abundant on this transect, including at a site by a small creek where soil was probed to a depth of 1.5 m without reaching the top of permafrost.

Observations in rock streams (kurums) on the left bank of the Bol'shaya Lebyazhy'a River about 50 m down from the mouth of the Malaya Lebyazh'a River showed that large rock streams were extremely warm and low in moisture content. At the same time, bi-valley frozen gentle slope deposits (along a zone of a river accumulation that are flooded during the spring floods, and where slope deposits are overlaid with alluvial silts and sands) and hanging bogs kept their permafrost even though it was found at different depths: from the normal depth (0.5–0.7 m) to 1.5 m or deeper. On the whole, data from this and other transects indicate that the top of permafrost has been moving down quite rapidly almost everywhere. Only small areas of bi-valley slope deposits, and hanging peat bogs do not show any signs of permafrost degradation.

During the last observation period, especially recently (in 2006–2007), degradation of cryogenic processes has been clearly tracked in rock streams (kurums). They have been drying out and losing ground ice. In the valley of the Kul'emka River, rock streams have been moving and joining with bottom boulder perluvium, which has a paragenetic connection with rock streams. A similar situation has been observed on the Shumikha River, where a semi-closed rock stream in a birch forest has been joining with an open rock stream on the left cold slope of the river valley.

Systematization of long-term field data shows that with further climate changes, the processes that are already active will only intensify. For further analysis of these processes, we classified them as short-period (fast processes) and long-period (slow), and as local-scale and regional-scale (Table 1).

All these processes manifest an initial response of landscape to climate changes. These primary responses, in turn, will cause secondary changes. For example, the number and the area of forest fires will noticeably increase, vegetation will reorganize, forest/steppe border will shift, the phenological environment will change (which, according to Tchebakova, will affect seed-bearing cycles, cause explosive increases in the numbers of some insects, etc). If the speed of climate change exceeds the adaptive capacity of ecosystems, it will cause a restructuring of all forest hierarchic levels from zonal forests and forest ecosystems to forest forming tree species and populations (Tchebakova et al. 1995, Tchebakova & Parfenova 2003, Tchebakova et al. 2005).

Next Steps

The next steps in our research will include the following:

1) Analyze river run-off data from weather stations and river stations in Bratsk, Boguchany, Motygino, Yeniseisk, Yartsevo, Severoyeniseisk, Vorogovo, Bor, Baikit, Vanavara, Bakhta, Verkhneimbatskoye, Turukhansk, and Tura. These data will be compared with extreme event data, which will make it possible to identify a general rhythmicity of the aggravation and weakening of adverse and catastrophic natural events that reduce the ecological potential of Central Siberia.
2) Evaluate the lowering of the top of the permafrost table and of the process's dependence on particular characteristics of specific terrain units.
3) Select geologic cross-sections with dated syngenetic permafrost structures for detailed documentation and testing. It is necessary to determine the age of permafrost

Table 1. Primary landscape responses to climate warming.

	Short-period	Long-period
Local-Scale	Rock streams (kurums): increase in number of unstable blocks, and increase in number and area of reindeer moss patches left by irrecoverable loss of ice; Rock streams: significant warming of deposit after its water content decreases; Abnormally frequent falls of trees that have creeping root system. Usually it occurs in over-wetted clay soils of visco-plastic consistence and thicknesses of 1.5 m or more; Replacement of solifluction material movements in the lower part of accumulative glacial deposits with local landslide-land creep.	Rock streams : the top of permafrost is going deeper; Rock streams advance towards valley floor as a result of landslide shifts; Solifluction intensifies, especially in areas where slope deposits are in a frozen state and where the thickness of the active layer increases; Drainage improvement on top surfaces and on adjacent gentle slopes (water has disappeared in many pit-ruptures and is often absent in crack-ruptures); General landscape changes with a prevalence of depressive forms which leads to formation of thermokarst lakes; Depletion of underground watercourses under rock streams; Appearance of young fir forests on completely or partially burned out taiga that previously consisted of other tree species.
Regional-Scale	Drying of rock streams. To some degree, drying is also seen in swamped cryogenic-taiga terrain units (e.g., stows, or homogeneous geological and hydrogeological condition).	Thermokarst processes intensify; Wide development of long-frozen rocks which can be evidence of recent permafrost degradation; Solifluction intensifies; The active layer goes down deeper.

(Holocene or Pleistocene) in Central Siberia. This will drive forecasting events resulting from permafrost thawing.

4) Revisit sampling sites.
5) Create a map of permafrost landscapes ranked by sensitivity to climate changes, showing the increased depths to the top of permafrost. This map should also show the estimated times when permafrost will thaw down dozens of meters and cease to impact surface landscapes.
6) Integrate with SEARCH (monitoring of landscape and biological changes as a result of climate change) and TSP (temperature data gathering and evaluation) programs.

Conclusions

Based on the data gathered, landscapes of the region studied can be classified by sensitivity level, where sensitivity is a function of the rate at which landscapes respond to climate change. A slower response indicates a lower sensitivity of the landscape to change.

The *most sensitive* landscapes are terrain units (natural complexes) of "warm" gentle slopes (2–3°) and glacial-related deposits, and low (200–250 m) apical plains, including rock streams. These landscapes are mainly located north of the Podkamennaya Tunguska River. It is an area of Pleistocene moraine and glacio-lacustrine deposits (fine sands, aleurites, loams, and clays). Solifluction in this area is well pronounced. At the end of the summer (1995–1997), the thickness of the active layer did not exceed 0.9–1.0 m; however, during the same period of 2001, the active layer became more than 1.2–1.3 m thick. Thus, there has been a noticeable growth in the depth of the active layer over a few years.

Less sensitive are landscapes of "cold" slopes and slope-related deposits, glacial floodplains, and open rock streams of warm slopes. Mountain and headwater floodplains consisting of slope wash-off material and floodplain alluvial deposits are often swampy, sometimes hummocky, and support dwarf-birch and meadow-bog vegetation growing on alluvial-colluvial bog and meadow-bog cryogenic soils. They are modeled by solifluction and fluvial processes (valley solifluction, alluvial fragment accumulation, bank fragment shifts, and subsiding channel erosion).

The *least sensitive* are multi-factorial permafrost terrain units of cold slopes, including "hanging" peat bogs and forested floodplains of major rivers. "Hanging" bogs are located on moderately steep to steep (25–35°) slopes on hummocky traps and skarns, covered by rock streams and permafrost bogs. Vegetation there consists of scattered trees, alternating with thin cedar pine-spruce-larch forest ("drunken forest"). Our measurements of permafrost depths in "hanging" bogs and floodplains did not show any changes of active layer thickness during the past few years.

We predict that the degradation of permafrost landscapes will occur in the order of the sensitivity classes. The most sensitive landscapes will be the most interesting to study in the course of further research, as they are changing the most rapidly, and their changes will enable us to characterize climate dynamics. The most sensitive landscapes will also yield the highest monitoring value.

Our research showed that it is not annual temperature increases as such, but rather a modification in season durations (changes in intra-annual climate patterns), as well as sharp intra-season fluctuations of temperature and precipitation regimes, which have the greatest impact on the functioning of natural and natural/human-made ecosystems. A rapid downward movement of the permafrost table (5–15 cm/yr) has been occurring since the late 1990s. Permafrost has been moving deeper in most permafrost landscapes. With the depth of the active layer increasing, both solifluction and thermokarst formation have been activated. "Warm" permafrost degrades and rock streams undergo transformation.

Dry and hot weather during the spring season, and followed by severe frosts and different weather fluctuations, which that are not typical for the region with its continental climate, can cause chronic crop setbacks. These in turn influence animal populations. Progressive permafrost degradation can also cause additional emissions of greenhouse gases into the atmosphere and impair biodiversity.

Some of the least sensitive terrain units have not shown any response to climate change yet. However, the processes mentioned, especially solifluction, appear to be a large-scale response to global climate change. It can be considered as a trigger for other natural processes.

If climate change continues at the current rate, it is possible that low-productivity permafrost landscapes will be replaced with highly productive non-permafrost landscapes. With regard to the area of permafrost transition in the zone we studied, this will not cause an ecological disaster, although impacts of such landscape reformation throughout the permafrost zone has not been studied yet.

The work performed is necessary for a comprehensive evaluation of the current and future situation and for the scientifically proven management of natural and natural/man-made systems, consistent with the concept of sustainable development. For the full-fledged and full-scale implementation of what we have intended to do, it is necessary to integrate our research with similar international programs, such as SEARCH and TSP.

Aknowledgments

The research has been performed as part of RFBR Project No. 07-05-00815.

References

Climenko, V.V., Fedorov, M.V., Andreichenko, T.N. & Mikushina, O.V. 1994. Climate on the border between centuries. *Vestnik MEI, N. 3.*

Fedorov, A.N. 1991. *Permafrost landscapes of Yakutia: methods of detection and questions of mapping*. Yakutsk, 140 pp.

Gorshkov, S.P. 2001. First signs of response on the climate warming in periphery of permafrost zone, Central Siberia. *1st European Permafrost Conference, Rome, March 26–28, 2001. Abstracts, 16.*

Gorshkov, S.P. 2006. Prognosis of landscape dynamics in conditions of possible climate change for the lower reaches of the Podkamennaya Tunguska river. In: *Modern Changes in Lithosphere Under the Influence of Natural and Anthropogenic Factors*. Moscow: Nedra, 151-156.

Gorshkov, S.P., Dobrynin, D.V. & Tishkova, M.A. 2001. The resistance of permafrost landscapes to the climate warming in periphery of permafrost zone of Central Siberia. *1st European Permafrost Conference, Rome, March 26–28, 2001. Abstracts:* 24-25.

Gorshkov, S.P, Karrash, H. & Paramonov, A.V. 1998. A geomorphological indication of permafrost and non-permafrost landscapes in the middle taiga in Central Siberia. *Geomorphology* 4.

Gorshkov, S.P. & Tishkova, M.A. 2003. Landscape indication of permafrost degradation in Central Siberia. *Research and New Information*: 43-44.

Gorshkov, S.P. & Tishkova, M.A. 2000. Studying the response of permafrost ecotone to the climate warming (on the example of Central Siberia). *Problems of Regional Geoecology*. Tver, 44-46.

Gorshkov, S.P., Vandenberghe, J., Alexeev, B.A., Mochalova, O. I. & Tishkova, M.A. 2002. *Climate, Permafrost and Landscapes of Middle Yenisei Region*. Scientific edition, Faculty of Geography, Moscow, 96.

Tchebakova, N.M. 2006. *Possible Transformation Of Siberia Vegetation Cover Under Different Scenarios Of Climate Change.* Krasnoyarsk, 60 pp.

Tchebakova, N., Monserud, R., Leemans, R. & Nazimova, D. 1995. Possible vegetation shifts in Siberia under climatic change. In: J. Pernetta, R. Leemans, O. Elder & S. Humphrey (eds.), *Impacts of Climate Change on Ecosystems and Species.* Gland, Switzerland: IUCN, 67-82.

Tchebakova, N. & Parfenova, E.I. 2003. Stand growth and productivity of mountain forests in southern Siberia in a changing climate. In: A. Amaro, D. Reed, and P. Soares (eds.), *Modelling Forest Systems*, Chapter 17.. Wallinford, UK: CAB International, 189-197

Tchebakova, N.M., Rehfeldt, G.E. & Parfenova, E.I. 2005. Impacts of climate change on the distribution of *Larix spp*. and *Pinus sylvestris* and their climatypes in Siberia. Mitigation and Adaptation Stragegies for Global Change. http://dx.doi.org/10.1007/s11027-005-9019-0.

Tchebakova, N.M., Rehfeldt, G.E. & Parfenova, E.I. 2005. Redistribution of vegetation zones and populations of Larix sibirica and Pinus sylvestris in Central Siberia in a warming climate. In: *Proc. of Canadian Tree Improvement Association. 29th Biennal Meeting "Climate Change and Forest Genetics". Eds. G.A. O'Neill and J.D. Simpson. Kelowna, British Columbia. Canada:* 25-42.

Watson, R.T. & the Core Writing Team (eds.). 2003. *Climate Change 2001: Synthesis Report.* Cambridge, UK: University Press, 398 pp.

Woodwell, G.M. & Mackenzie, F.T. (eds.). 1995. *Biotic feedbacks n the global climatic system. Will the warming feed the warming?* 416 pp.

Permafrost in Low Mountains of the Western Chukotka Peninsula

Sergey Titkov
Geological Research Institute for Construction, Moscow, Russia
Vladimir Chernyadyev
Geological Research Institute for Construction, Moscow, Russia
Maria Tsvetkova
Geological Research Institute for Construction, Moscow, Russia

Abstract

The study region is located in the northwest part of the Chukotka Peninsula in the zone of continuous permafrost. Permafrost thickness is from 120–250 m in river valleys and up to 300–350 m on slopes and watersheds. Mean annual ground temperatures are between -4°C and -6.5°C. The ice content of Late Pleistocene-Holocene syncryogenic alluvial, deluvial, eluvial, or solifluction deposits covering the river valleys and slopes is 50%–60%. These types of deposits are characterized by massive fossil ice layers with a typical thickness of 0.5–3.0 m and total area of a separate ice massif up to 30,000 m^2. Thermokarst hollows up to 30 m in diameter are located on sites where the ice surface is less than 1.5 m beneath the ground surface, thus indicating the disposition of the ice body. Frost cracking and frost sorting results in the formation of kurums and patterned ground, such as stone rings and stone stripes that move slowly down slope.

Keywords: continuous mountain permafrost; frozen dam; massive ice layers; patterned grounds; thermal regime of permafrost; thermokarst.

Introduction

A problem of safety in the exploitation of water-engineering systems is especially important in the permafrost zone. The reliability of constructions strongly depends on the consideration of engineering-geological conditions (Biyanov 1983, *Water-Engineering Systems* 2005). Engineering-geocryological investigations in 2007 were carried out in the vicinity of the gold deposit "Mayskoe" at the site of the projected dam for a future water reservoir in order to obtain sufficient data for projecting and construction of the ground dam, pump station, and water pipeline in the zone of continuous permafrost. The study region is widely exploited as a stanniferous and gold-bearing province. Numerous geological expeditions carried out geological exploration in different points of the region (*Engineering Geology of the USSR* 1977*, Geological map of the USSR* 1979, *Chukotka…* 1995*.)*, but it is very poorly investigated by geocryologists. Permafrost researches under similar conditions of low mountains were held in Northern Yakutia (Shur 1988, Kanevskiy 2003).

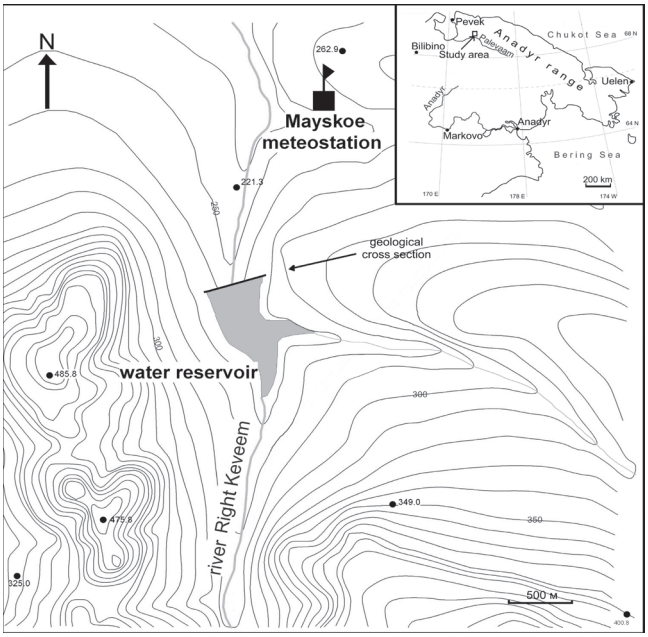

Figure 1. Sketch map of the study area.

Study Area and Methods

The gold ore deposit is located within the Chukotka uplands in the northwest part of the Chukotka Peninsula (68°50′N, 173°40′E) in the northern part of the Anadyr Range, 187 km southeast of the regional center Pevek (Fig. 1).

The study area is situated on a local divide between the rivers Keveem, Pegtymel, and Palevaam, and is characterized by low-mountain relief with gentle slopes and flat watersheds of absolute elevations up to 600 m. Mountain tops rise about 150–250 m above river valley bottoms.

The river valley network is young and has a poorly developed structure. Traces of Late Pleistocene glacial erosion and accumulation are expressed in the presence of exaration and fluvioglacial landforms. The study area is located near the source of the river Right Keveem. The river and its tributaries have fast flow; channels abound with bars and are frequently meandering. The mode of water-flow is extremely changeable in time and depends, basically, on the

precipitation regime. The nearest large waterway is the river Palevaam 20 km south of the deposit. During the winter period, it freezes completely as well as other streams and keeps underground runoff along talik zones.

During the engineering-geocryological research, 57 bore holes 20 and 30 m deep along 6 profiles covering the dam and contour of the future water reservoir were drilled. Geophysical investigations revealed linear zones of fractured bedrock located in the vicinity of the projected dam. Laboratory tests of frozen core samples were held to determine physical, mechanical, and thermal physical properties of loose material and solid rocks. The forecast evaluation of the dam and bed of the reservoir has been carried out. The engineering-geocryological map at a scale of 1:2000 has been compiled based on the results of investigations.

Results

Climate

The climate of the area is determined by its location in the northeast of Asia, in the zone of influence of two oceans with the complex atmospheric circulation differing in cold and warm season. The climate is Arctic, transitive from moderately continental to continental. Mean annual air temperature according to the data of the meteorological station "Mayskoe" (~1,5 km north of the site) for the period of 1982–1991 is -13.7°C. The air temperature absolute maximum is 29.5°C in July, and absolute minimum is -45°C in February. Average temperature of July is 9.3°C, that of January -27.8°C. The annual amplitude of average monthly air temperatures is 37.1°C. Winter is long and cold, with strong snow storms, summer is short and cool, but warmer by 7°C than at the coast of the East-Siberian Sea. The positive average monthly air temperature lasts no more than 3.5 months. The duration of the warm period, both in the air and on the ground surface, is less than 30 days in more than 50% of the years.

The annual precipitation is 262 mm and about 60% of this amount is snow. The average thickness of the snow cover depends on surface relief and does not exceed 0.7 m on flat sites. In the rear parts of cryoplanation terraces, in river valley bottoms, and on leeward slopes the snow cover thickness is 2–3 m and more. The snow cover is established in the middle of September and disappears in the end of May. Snow cover density reaches 0.35 g/cm^3. The wind regime is rigid; the average annual wind speed is 3.5 m/s, with maxima in squalls reaching 40 m/s; the annual number of days with a wind speed higher than 15 m/s is 46.

Geological structure

Loose deposits of interstream areas are comprised of eluvial-deluvial and deluvial-solifluction formations, overlapping slopes, and tops of watersheds with a continuous cover. Loose deposit thickness varies from tens of centimeters on narrow watersheds to up to 15–20 m in places where slopes merge into river valleys. The petrographic structure of these sediments is similar to the bedrock. Gradual transitions of one genetic type to another are marked. All types of deposits were formed during the Holocene period (Q_{IV}), except for the bottom layers of eluvial and alluvial sediments, which are of Late Pleistocene age (Q_{III}). According to the analysis of spores and pollen, the most ancient horizons of deposits were generated in the Late Pleistocene interglacial.

Holocene fluvial sediments (aQ_{IV}) are comprised of alluvium of river beds, flood plains, and the first terraces in rivers and brook valleys of 2–3 orders and consist mainly of blocks of a different degree of roundness (up to boulders), gravel and pebble of different size, sand and a sandy-loam material with lenses of peat and ice. The thickness of alluvial layers is 1.5–3.5 m.

Holocene eluvial-deluvial sediments (edQ_{IV}) are developed most widely on gentle spaces of watersheds and flat (1°–3°) slopes. They consist of rubble from 5% up to 30%-40%, or gruss with a sandy-loamy fill (up to 50%-80%). In the direction towards the central part of valleys, the abundance of rubble is reduced up to 5%–10%. The thickness of eluvial-deluvial deposits is 10–15 m in valley boards and 1–2 m in river bed parts of valleys.

Deluvial (dQ_{IV}) and deluvial-solifluction (dsQ_{IV}) deposits are developed on slopes of watersheds with gradient more than 3°. They are presented by blocks, rubble, or gruss with a sandy-loamy fill. The thickness of deluvial deposits is 1–5 m.

Deluvial-colluvial deposits (dcQ_{IV}) are located on slopes of river terraces and erosive benches having a gradient of more than 10° and comprised of sandy loam and loam with a proportion of rubble and gruss of about 30%–50%. The thickness of deluvial-colluvial deposits is up to 2.5 m.

Eluvial deposits (eQ_{III-IV}) underlay the above listed genetic types everywhere and overlay Triassic sandstones and aleurolites. The thickness of continuous cover eluvial deposits is between 1.5 and 7 m. They are comprised of coarse ground with loam and sandy loam; the rubble content is about 30%–40%, and the gruss content about 10%–20%.

Geocryological conditions

The study area is located in northern geocryological zone and characterized by continuous permafrost. The thickness of permafrost is 120–250 m in river valleys; at transition to slopes it increases up to 300–350 m and more, and reaches the greatest values on watersheds (Geocryology of the USSR 1989). The mean annual ground temperature (MAGT) at the depth of 10–12 m is between -4°C in valley bottoms down to -6.5°C on surrounding slopes. The ground temperature on ridges naturally goes down to 7.5°C–8.0°C. Highest temperatures are characteristic for slopes of a southern exposition and the bottoms of valleys. Outside of talik zones, the snow cover is the most essential influence on MAGT; a thick snow cover results in a rise of ground surface temperature by 5°C–6°C in comparison to snowless sites.

Measurements of temperatures in boreholes 3 and 10 in an axial part of the future dam have demonstrated that the

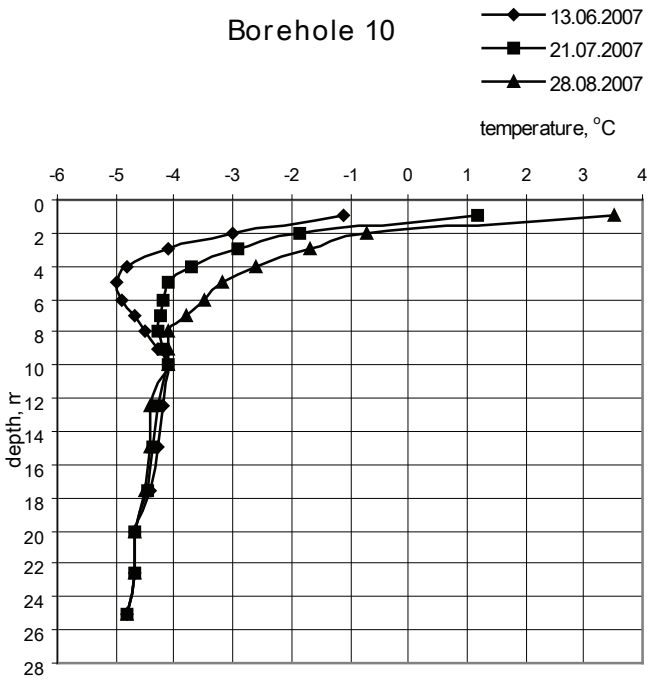

Figure 2. Ground temperature in Borehole 10.

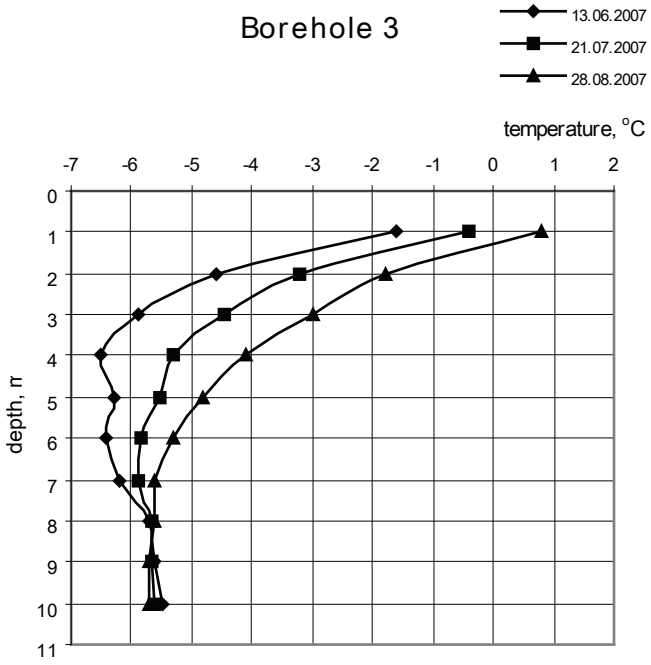

Figure 3. Ground temperature in Borehole 3.

highest MAGT at the depth of 10 m (-4.1°C) is found in the bottom of the river Right Keveem valley in Borehole 10 (Fig. 2).

The ground temperature on the left side of the valley slope was -5.5°C in Borehole 3 (Fig. 3) and -6.5°C on the right side of the valley.

Active layer depth varies from 10–15 cm on sites with thick moss and peat cover to 70–80 cm under swampy areas. At foots of slopes composed of coarse deposits as well as under streamlet beds, active layer thickness is 2–3 m and more.

In a vertical section of frozen ground epigenetic deposits prevail. The characteristic feature of weathered bedrock is its low ice content not exceeding 15%. The average ice content of fissured aleurolites is 5%–6%, decreasing to 1% in monolithic, low-fissured sandstones. The ice content increases up to 10% in strongly fractured aleurolites and argillites where cracks are filled with ice and in sandy-loamy ice-rich ground. Cryogenic structures of the bedrock are massive and crack-like.

Fine-grained deposits contain usually coarse material (up to 30%–40%), and have massive and massive-crust-like cryogenic structures. The ice content does not exceed 10%–15%. Rocks are completely frozen except in separate, localized, fractured, water-saturated zones along tectonic faults.

Late Pleistocene and Holocene deposits are a syncryogenic type of frozen ground formation. These are alluvial, lacustrine, fluvioglacial, swamp, eluvial, deluvial-solifluction and other formations. The ice content often exceeds 50%–60%, and cryogenic structures are lenticular, layered, and recticular.

Loose surface deposits often contain massive ice sheets in the sub-surface. In 2004, drilling in solifluction deposits intersected ice layers that were 1.8–2.0 m thick and had no mineral impurities. The ice sheet was of a layered structure with alternating layers of transparent firm ice and white loose ice 1–2 cm thick. Drilling in 2007 has shown massive ice sheets between 20 cm and 3 m thick occur in an area of about 30,000 m^2 on the left slope of the river Right Keveem valley oriented directly along the axis of a projected dam for a water reservoir (Fig. 4). Ice structure is layered, and the ice contains about 3%–5% fine mineral material.

Massive ice sheets represent, apparently, primary interground ice of segregation-intrusive genesis. They were generated in freezing, water-saturated deposits with constant additional charging by underground water.

Within the limits of the region, permafrost in river valleys has a two-layered structure. In the top part of the section there are friable epigenetic and syngenetic ice-rich and very ice-rich disperse deposits, and in the bottom there is Triassic bedrock frozen epigenetically and having a characteristic, low ice content . The single-layer structure of frozen rock mass is characteristic for epicryogenic bedrock in a mountain part of the region. Cryogenic structures of crack-like type are common for this type of deposit. On highly fissured sites corresponding to zones of constant water saturation before freezing, rocks are characteristic by a high ice content and have crack-vein cryogenic structures. Near the surface, the elevated ice content due to goletz (crust-infiltrated) and segregated ice occurs in most weathered rocks. Crack-like, crust-like, and basal cryogenic structures are most common for this type of deposit.

Numerous cryogenic processes are widely spread in the study area. Frost weathering developed on slopes and watersheds where the snow cover is negligible results in rock destruction and moving of the loose material down slope due

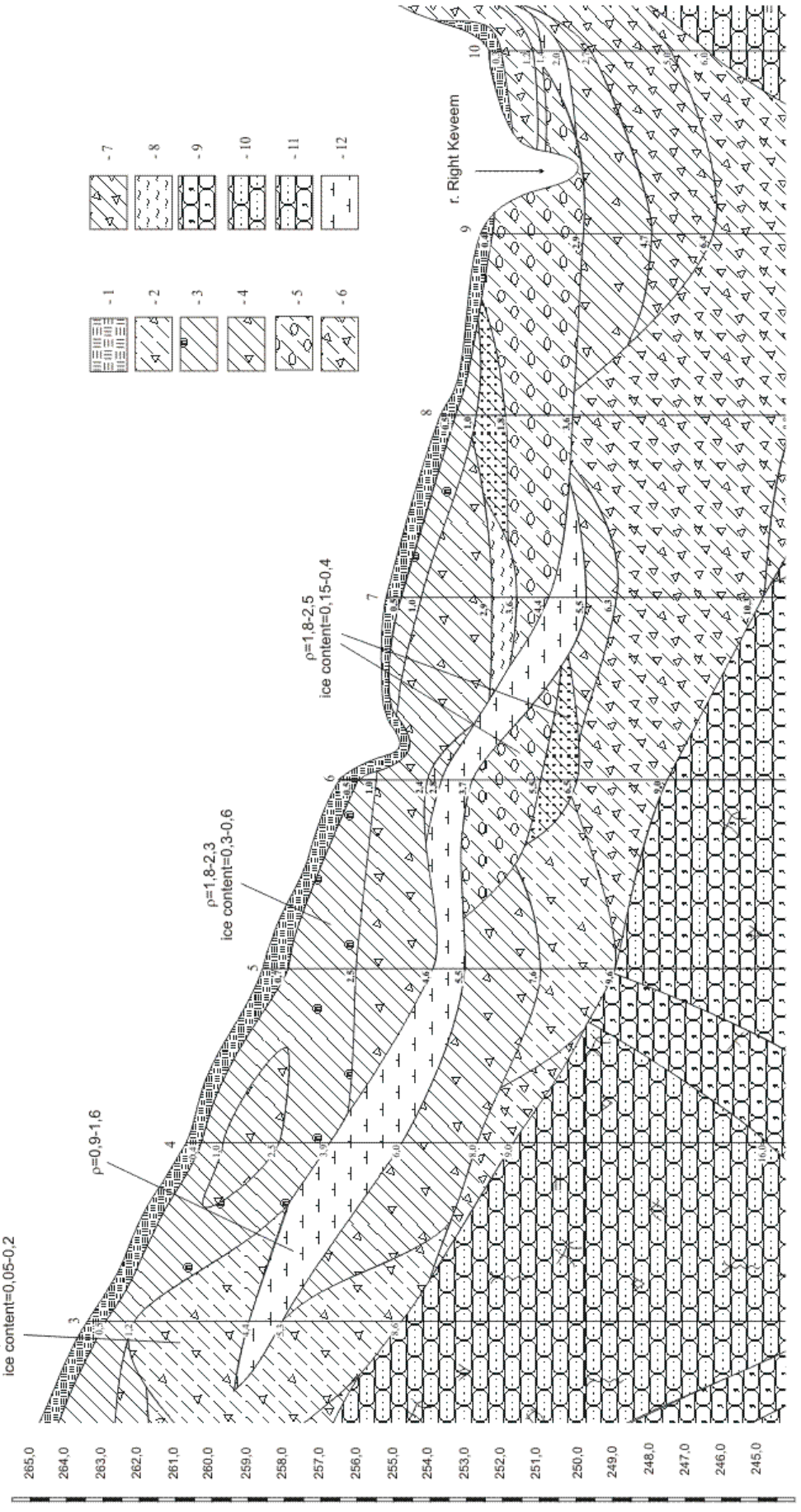

Figure 4. Part of cross section through the left side of the river Right Keveem's valley along the axis of the projected dam. Horizontal and vertical scales in meters. 3… 10 – number of borehole. Lithology: 1 – peat; 2 – sandy-loam with breakstone; 3 – loam; 4 - loam with breakstone; 5 – pebble with sandy-loam; 6 - breakstone with sandy-loam; 7 - breakstone with loam; 8 – silt; 9 – aleurolite; 10 – sandstone; 11 – interleaving of sandstones and aleurolites; 12 – massive ice layer. Ground is frozen from the surface (May 2007).

Figure 5. Stone stripe on the gentle slope surface.

Figure 6. Thermokarst depression – a result of massive ice layer melting.

to active gravitational and deluvial processes. Fine-grained products of the frost weathering accumulate in lower parts of slopes thus forming deluvial and deluvial-solifluction aprons. The surface of slopes is complicated by dells, mud circles, solifluction terraces, and lobes. Dells are the linear hollows 10–12 m wide with flat, swamped bottoms.

On gradual (less than 10°) slopes, solifluction, and deluvial-solifluction slopes, processes of plastic-viscous flow develop. Solifluction occurs in sandy loams and dust-like loams containing sometimes a significant amount of coarse material. The rate of solifluction movement depends on the slope degree, active layer thickness, deposit grain size, etc. Coveral solifluction is a kind of solifluction without surface disturbances when the ground flow is rather uniform and slow. It develops on slopes of 3°–10° and is accompanied by material sorting resulting in the formation of layers of fine and coarse material in longitudinal section.

Frost cracking develops in the active layer and is well defined on the surface in the form of numerous sorted and non-sorted polygons and circles with flat or convex surfaces free of vegetation, 1–3 m in diameter, limited by frost fissures and banks of jacked debris. In non-homogenous friable grounds with a high content of debris (gravel, gruss, pebble), multiple cycles of freezing-thawing result in the frost jacking of coarse material towards the ground surface and its displacement to the fissures located in hollows, thus forming stone rings and polygons. On the slopes, stone rings transform into stone stripes 1.5–2 m wide and 0.4–0.6 m high, divided by convex-plane surfaces covered with turf (Fig. 5).

Thermokarst processes develop by melting out underground ice and ice-rich ground and result in ground subsidence, shallow depressions, and the formation of thermokarst lakes. Thermokarst features are usually closed or semi-closed round-shaped hollows up to several tens of meters in diameter, located predominantly on flat surfaces or gentle slopes. Thermokarst is often caused by the disturbance of natural heat-exchange conditions as a result of technogenic impact or active layer thickness increasing. Thermokarst hollows on the left side of the river Right Keveem valley are connected to the massive ice sheet melting where the ice surface is at a depth of 0.7–1.2 m below the surface (Fig. 6).

The formation of kurums in the study area is a result of a combination of a number of processes. The main factors are cryogenic and gravitational ones. Kurums usually form on deluvial-colluvial slopes of 5°–10° gradient in good conditions of fine-grained material outwash. The thickness of kurums is 1.5–2.5 m, and they consist of clumpy-debris material with sandy-loam fill in the base of the section. This layer is of high ice content, and sometimes lenses of goletz (crust-infiltrated) ice up to 0.5 m thick exist. Kurums move predominantly due to cryogenic creep in the active layer, partly because of plastic deformations of goletz ice in the basal layer.

Discussion

According to the computer modeling, at a constant maximum water level in the future water reservoir, the depth of ground thawing in the upper prism scarp of the dam after one year of operation will be 3.3 m, and by 15 years it will reach 9.9 m. In the seasonal changes of water level in the reservoir assumed by the project, the depth of thawing in the top part of the upper prism scarp will be 1.5 m and should not change during the period of operation while in the bottom part, the depth of thawing will be up to 5.5 m. On the slopes of the lower prism of the dam, the depth of ground thawing during period of operation should remain stable at 1.1–1.5 m.

The depth of frozen ground thawing in the bed of the water basin for 15 years of operation will change from 1.1 m up to 4.9 m. With the presence of ice-rich frozen ground of the relative subsidence 0.2–0.3 (according to engineering-geological researches and laboratory test of frozen ground compressibility in thawing) the total ground subsidence in the water basin bed may be 1.0–1.5 m. It will result in the slipping of the ground of an upper prism and to the

infringement of the dam stability. Therefore, replacement of the ice-rich ground to a depth of 1.5–2.0 m is necessary.

During the process of dam and water reservoir construction, the activation of thermokarst, thermal erosion, cryogenic landslides, frost heaving, and frost cracking should be expected.

The most dangerous process in water basin operation is thermokarst. The tendency of global climate warming may lead to the increase of the active layer thickness and, as a result, to the acceleration of massive ice bodies melting (Fig. 6). Thermal subsidence of ice-rich deposits of the water reservoir bed can be up to 1.0–1.5 m.

The activation of frost heaving and frost cracking on the dam surface with low snow cover is possible. It should promote the development of thermal erosion processes during the warm period. To avoid the activation of these processes, predominantly coarse material should be used in the dam construction.

The thermal effect of water filtration through the dam body should be reduced by using a synthetic diaphragm within the dam. It is preferable to erect the dam in the winter time. Additional ground cooling during dam operation should be provided by the application of two-phase hybrid thermosyphons designed so that the dam can be cooled actively as well as passively. As practice shows, installation of air cooling is less effective. Cooling units should be installed on the crest of the dam close to the head race at a distance of 3 m to a depth of at least 15 m. If the dam will be erected in the summer time, freezing thawed ground in the body of the dam using thermosyphons will take one winter season.

For dam stability maintenance, monitoring of the ground thermal regime should be established.

Conclusions

The projected dam for the water reservoir is located in the zone of continuous permafrost. The presence of ice-rich coarse deposits, massive ice sheets, and numerous cryogenic processes significantly complicate conditions of dam construction. The activation of thermokarst, thermal erosion, cryogenic landslides, frost heaving, and frost cracking should be expected in dam and water basin operation.

The dam should be erected in the winter time and supported in the frozen state by two-phase hybrid thermosyphons installed on the surface of the dam near the head race. The complex monitoring of the ground thermal regime should be carried out to provide for the reliable operation of the dam and water reservoir.

Acknowledgments

The authors are grateful to G.P. Pustovoit (Moscow State University) who carried out the computer modeling of the future frozen dam thermal regime dynamics. We also sincerely thank reviewers for editorial assistance and additional language improvement.

References

Biyanov, G.F. 1983. *Dams in the Permafrost Zone.* Moscow: 175 pp. (in Russian).

Chukotka: Natural and Economical Essay. 1995. Moscow: 370 pp. (in Russian).

Engineering Geology of the USSR. Vol. 4. Far East. 1977. Moscow: 502 pp. (in Russian).

Geocryology of the USSR, Vol. 4. Siberia and Far East. 1988. Moscow: Nedra, 516 pp. (in Russian).

Geological Map of the USSR. Scale 1:200 000. Sheet R-59-XXIX, XXX. Geological description. 1979. Magadan: 90 pp. (in Russian).

Kanevskiy, M. 2003. Cryogenic structure of mountain slope deposits, Northern Russia. *Proceedings of VIII International Conference on Permafrost. Zurich.* Philips, Springman, & Arenson (eds.)*:* 513-518.

Shur, Y.L. 1988. *The Top Horizon of Permafrost Strata and Thermokarst.* Novosibirsk: Nauka, 213 pp. (in Russian).

Water-Engineering Systems of Chukotka: Engineering-Geocryological Conditions. 2005. Magadan: 70 pp. (in Russian).